

Государственное образовательное учреждение
высшего профессионального образования
**«Томский государственный университет
систем управления и радиоэлектроники»**

ТЕМАТИЧЕСКИЙ РЕФЕРАТИВНЫЙ СБОРНИК № 4-2/5

**“Radar Remote Sensing”
(«Дистанционное зондирование в радиолокации»)**

Публикации в трудах конференций

Источник: *Digital Library IEEEExplore*

Язык: *английский*

Глубина поиска: *2001 – 2002 гг.*

Дата формирования: *март 2011 г.*

Составитель: *В.И. Карнышев*

Томск – 2011

ТЕМАТИЧЕСКИЙ РЕФЕРАТИВНЫЙ СБОРНИК № 4-2/5

"Radar Remote Sensing"

(«Дистанционное зондирование в радиолокации»)

Публикации в трудах конференций

"Investigating long-term behavior of Greenland outlet glaciers using high resolution satellite imagery"

High resolution declassified Corona satellite photographs from the 1960s are used to establish baseline velocities for a fast flowing outlet glacier in Greenland. The mathematical model of the camera was developed and position and attitude parameters were estimated using GCPs. To illustrate the procedure, ice velocities were derived from Corona and Landsat-7 images over the Kangerdlugssuaq glacier in SE Greenland. Time series of velocity changes indicate significant increase in ice flow velocity during the last decade, propagating upstream from the calving front. [C5963]

"A wideband radar for mapping internal layers in the polar icesheets for estimating accumulation rate"

Determination of the mass balance of the polar ice sheets requires information on the accumulation rate. Remote sensing methods to determine the accumulation rate are essential in reducing the uncertainty associated with interpolating in situ measurements that are obtained from ice cores and pits. This is essential to reducing the 20% of uncertainty in current accumulation rate maps. Using data from surface-based radar experiments we determined optimum parameters for an airborne radar. We developed an airborne prototype and successfully demonstrated that we can map internal layers with about 1 m resolution to a depth of about 120 m over the Greenland ice sheet. We reported the system design, construction and preliminary experimental results at the 2001 IGARSS meeting. We have developed an operational radar system for routine measurement. This system operates in FM-CW and stepped-frequency pulse modes and it has 20-dB more sensitivity than the prototype radar. We also developed a radar target simulator for testing and evaluating system performance. The target simulator was constructed using fiber optic cables, microwave delay lines and RF/optical transceivers to simulate reflections from the air/snow interface, internal layers and the antenna reflection, which degrades the system's sensitivity. The simulator serves a dual purpose of optimizing the system performance in the laboratory and for internal calibration in the field. We also used a CAD package to design and simulate overall radar performance. The use of CAD package and target simulator reduced cost and time associated with the radar development. In addition, we are also able to obtain an accurate system model to deconvolve the system effects from the received signal. We discuss detailed design, construction and performance of the target simulator and operational radar. We show a comparison of the simulation results and laboratory measurements of the radar system. Also we present analysis of the results from measurements made during the 2001 experiments and preliminary results from planned measurements in May 2002. [C5964]

"A new scattering enhancement scheme for polarimetric SAR images based on covariance matrix"

A new scattering mechanism enhancement scheme has been developed for natural targets based on the eigenvalues and eigenvectors of the covariance matrix in order to identify different scattering events. First, three new vectors were constructed by the eigenvectors of the covariance matrix with some modifications. Then, these modified vectors were weighted by the normalized eigenvalues of the covariance matrix as a weighting function. Thus, three vertices could be obtained in the three-dimensional space. In order to utilize them equally, a triangle was constructed by connecting these three vertices. The shape of the triangle may be changed due to the different scattering mechanisms because the vertices are obtained from the combination of eigenvalues and eigenvectors. The result indicated that different scattering mechanisms can be represented by using an exterior angle which derived from the interior angles of the triangle. [C5965]

"A technique for removing vegetation bias from polarimetric SAR interferometry"

This paper develops a technique for separating the ground and vegetation components from polarimetric interferometric SAR measurements. The objective is to use this technique to remove the vegetation bias in interferometric measurements of elevation in forested terrain. Initial results indicate that the technique is able to

compensate for the vegetation bias and provide improved estimates of the terrain elevation. However, further work is needed to estimate geophysical information about the vegetation canopy. [C5966]

"An extended model for characterizing vegetation canopies using polarimetric SAR interferometry"

Effective exploitation of polarimetric SAR interferometry data over vegetated areas requires the use of a vegetation model of sufficient complexity to capture the underlying scattering processes. The standard Treuhaft model (randomly oriented vegetation + ground) makes a number of assumptions that may not be true in general. This paper presents a two-layer extended model that allows canopy attenuation to be a function of polarization, does not require the canopy to extend all the way to the ground, and allows the ground to be sloped. It is shown that many cases exist in which the two models predict similar coherence region shapes for significantly different structural parameters. It is argued that a minimum of two baselines is required for robust model selection and inversion. [C5967]

"Forest biomass estimation in New Zealand using full-polarisation SAR imagery"

Synthetic aperture radar (SAR) has been proposed as a method for estimating above-ground biomass, and this paper describes a method to estimate biomass over flat or sloping terrain. A theoretical model is used to make a correction for the terrain slope, along with a second model to decompose the backscatter into canopy, trunk and understory layers. The method is semi-analytical, since it uses field-based ground truth information to calibrate the model, yielding canopy and trunk contributions to the above-ground biomass, and a relative indication of biomass contribution due to surface scattering. Qualitative analysis shows that the results generally conform to the model, but that artifacts in the digital elevation model, and limitations of the three-layer model, cause some instability in the solution. Modifications to these steps are under investigation. [C5968]

"Generation of secondary internal waves by the interaction of internal solitary waves with an underwater bank"

The generation of an internal wave packet by the interaction of a large-amplitude internal solitary wave with an underwater bank is studied by using a numerical model and a synthetic aperture radar (SAR) image acquired by the European Remote Sensing satellite ERS-2 over the Andaman Sea. It is shown that, if the internal solitary wave has a sufficiently large amplitude, overturning and wave breaking occurs which gives rise to the generation of a secondary internal wave packet. The results obtained from the model calculations are supported by the ERS-2 SAR observations. [C5969]

"Characterization of forest recovery from fire using Landsat and SAR data"

The Forest fire during May 6-June 4, 1987 in Northeastern China burned 1.14 million hectares of forest and nearly 25 million cubic meters of timber. Landsat (5 and 7) and radar data (ERS and JERS-1) in combination with field measurements, were analyzed in terms of forest destruction and recovery and the results were evaluated. Temporal Landsat data enabled the identification of burned regions and the characterization of forest recovery, but sensitivity after 10 years was gradually lost. While the 1993 (and later) C-band SAR data from ERS cannot identify the fire scars, the 1997 JERS-1 L-band data can be used to characterize the burned area. [C5970]

"Glacier surface velocity measurements from radar interferometry and the principle of mass conservation"

Presents a relation between the three glacier surface velocity components, the surface flux-divergence, glacier thickness and bottom melt and displacement. The relation can be used as an extension to the surface parallel flow assumption often used with interferometric synthetic aperture measurements of glacier velocities. The assumptions for the derivation are described and important limitations high-lighted. [C5971]

"A multi-sensor remote sensing approach for monitoring large wetland complexes in northern Canada"

The Peace-Athabasca Delta is a 3900 km² freshwater wetland complex, located in north-eastern Alberta, Canada. The intricate channel system, the numerous smaller wetland basins and the large shallow lakes of the delta are important habitats for a large number of migrating waterfowl, mammals and insects. The hydrological regime in this remote area is unique as many of the productive wetland are isolated from the channels and require overland floods to be replenished. Recent studies have shown that the delta has experienced a reduced frequency of these large overland floods. Attribution of these changes is complex, however, remote sensing provides a unique opportunity to characterise the spatio-temporal distribution of these changes and to collect

important baseline hydrological information that is too difficult to obtain using traditional methods. This paper focuses on a development of a multi-sensor remote sensing strategy to assess hydrological change in this wetland environment. This includes the use of Radarsat, Landsat, IKONOS and lidar data to derive year to year changes and assist in predicting future outcomes and risks for this ecosystem. [C5972]

"Interpretation of convection cell signatures in radar images of the Greenland Sea"

We present a comprehensive analysis of a convection cell pattern in two SAR images of a site in the Greenland Sea from the satellites ERS-2 and RADARSAT. It is not obvious whether the observed radar signatures can be attributed to oceanic or atmospheric convection phenomena. We show by numerical simulations that they are, on the one hand, not consistent with the theory of oceanic convection features and their radar imaging mechanism, while, on the other hand, they could very well be caused by atmospheric convection cells. The conclusion that the observed features must be atmospheric convection cells is supported by in-situ data and an AVHRR image of the scenario. We discuss the significance of our findings in view of the general problem of discriminating between radar signatures of oceanic and atmospheric phenomena. [C5973]

"Identification of swell zones in the ocean: a remote sensing approach"

This paper presents a feasibility study of using collocated wind speed and significant wave height measurements from simultaneous satellite scatterometer and altimeter to observe the spatial and seasonal pattern of dominant swell zones in the world's oceans. [C5974]

"Multiple sea spike definitions: reducing the clutter"

Multiple definitions of sea spikes have been developed and presented in the literature. This study shows the characteristics of spike populations where absolute cross section ratios are not critical to the spike definition. [C5975]

"Global analysis of ocean wave systems from SAR wave mode data"

One of the major goals of the European Remote Sensing Satellites ERS-1 and ERS-2 were applications in ocean wave research and wave forecasting. For the first time, two-dimensional spectral information on the sea state globally, continuously, and in quasi real time are provided in the so-called SAR wave mode. To use not only the spectral but also the image information of these data, a global set of single look complex (SLC) synthetic aperture radar (SAR) images (imagettes) was processed from ERS-2 wave mode raw data, using the BSAR processor developed at DLR. SAR imagettes are used to analyze recently developed algorithms for wind and wave measurements. As the new European Satellite ENVISAT will provide cross spectra on a global and continuous basis, interest in the described techniques is growing. Two-dimensional ocean wave spectra are derived from SAR imagettes by quasi-linear inversion of the SAR imaging mechanism. Individual wave systems are detected by a so-called partitioning algorithm. The resulting wave parameters are analyzed and compared to model data. To take into account the complete nonlinear SAR imaging mechanisms, wave model spectra are simulated forward into cross spectra and compared to observations. Using this approach cases of significant inconsistencies between SAR and model data can be detected. With our 3 week data base in 1996 (about 30,000 imagettes) statistics are calculated. Finally, we derive daily maps showing areas with significant deviations between simulated and observed cross spectra. [C5976]

"Ambient and breaking roughness of the ocean surface"

Local wind-generated surface roughness can be decomposed into ambient component, surface wave geometric contribution (the mean square slope) and breaking wave contribution (the breaking roughness). Only the last two components can be attributed to local wind condition for remote sensing considerations. The ambient roughness level is estimated to be between 0.01 and 0.02 from altimeter data. The rate of increase of breaking roughness with wind speed is much faster than the counterpart of the mean square slope of wave geometry. In high wind conditions, breaking roughness contribution may exceed the wind-wave geometrical contribution. The data of Cox and Munk (1954) collected in clean and slick conditions, and newer data of filtered surface roughness derived from spaceborne altimeter are analyzed to provide a quantitative description of the breaking roughness. [C5977]

"Polarimetric segmentation using Wishart test statistic"

A newly developed test statistic for equality of two complex covariance matrices following the complex Wishart distribution and an associated asymptotic probability for the test statistic has been used in a segmentation algorithm. The segmentation algorithm is based on the MUM (merge using moments) approach, which is a

merging algorithm for single channel SAR images. The polarimetric version described in this paper uses the above-mentioned test statistic for merging. The segmentation algorithm has been applied to polarimetric SAR data from the Danish dual-frequency, airborne polarimetric SAR, EMISAR. The results show clearly an improved segmentation performance for the full polarimetric algorithm compared to single channel approaches. [C5978]

"Generation of bald Earth digital elevation models as applied to polarimetric SAR interferometry"

In this paper we investigate the comparison of recently proposed schemes to retrieve the bald Earth elevation height of terrain under a vegetation layer, making use of interferometric, fully polarimetric radar remote sensing P-band data. These schemes base on the one hand on an interferometric optimization scheme, which is applied to maximize the separation of scattering phase centers related to the pertinent interferometric coherences, and on the other hand on a nonlinear line fit along these coherences in order to extrapolate the different interferometric phases to those phase values which relate to the bald earth elevation height. A χ^2 -test is performed on the data to estimate the validity of the line fitting in forested areas. Experimental results obtained from P-band fully polarimetric single baseline interferometric data acquired over the Amazon rain forest are used in order to compare the different interferometric bald Earth phases obtained from the proposed approaches. Results are compared against a single polarization channel experiment in HHHH-polarization mode under same experimental conditions to demonstrate the clear superiority of Polarimetric Interferometric Synthetic Aperture Radar (PolInSAR) over single polarization InSAR. [C5979]

"Estimation of basal area from Amazon tropical rain forest using airborne P-band SAR data"

Shows the capacity of P-band polarimetric images to define the space of attributes of primary forest and secondary succession, through the analysis of the relation among backscatter and basal area data. To ensure that different landscapes of Amazon upland forest are represented, a test-site located in the Tapajor's region was selected. Statistical regression model was used to verify the relation between basal area values (37 plots) and backscatter data derived from PHH, PHV and PVV images. An analysis of the spatial configuration of backscatter values for primary forest and secondary succession is made, considering the intrinsic variations of these formations in terms of biometric parameters. For this thematic stratification, a contextual Markovian classification technique (Iterated Conditional Modes CM) was used in polarimetric P-band images, to delineate primary forest and regeneration areas, in association with basal area intervals. The advance that was reached with the treatment of P-band data could improve the regional monitoring process of the land cover change, a process whose speed was accelerated as a result of human action in the Amazon during the last two decades. [C5980]

"Topographic performance evaluation of the RADARSAT-2/3 tandem mission"

The Canadian Space Agency and MacDonald Dettwiler are jointly defining the mission capabilities and the operational performance of a RADARSAT-2/3 tandem interferometric mission. This paper evaluates the expected topographic performance of the mission. This includes a description of the interferometric beam mode, an analysis of suitable baselines and how to achieve them in orbit, and a presentation of relative height accuracy results based on these orbits. Both bistatic and monostatic operation are considered. [C5981]

"A Canadian spaceborne hyperspectral mission"

The increasing use of research and operational airborne hyperspectral imaging systems such as AVIRIS and CASI is establishing the characteristics of an emerging market for imaging spectrometer data. Hyperspectral data are beginning to be used for a wide range of applications in environmental and resource management. The Canadian Space Agency, in close partnership with Canadian industry, is developing technologies and mission concepts leading to an operational hyperspectral mission which may be launched in 2006-2008. Our approach combines the knowledge developed on airborne hyperspectral sensors with the operational experience of the RADARSAT programme. These include options to use the International Space Station or a dedicated small satellite mission as a viewing platform. Product performance characteristics are discussed in conjunction with the design solutions being proposed for each of the mission options. In addition, the exploitation potential of synergy between a Canadian hyperspectral mission and the RADARSAT constellation is discussed. [C5982]

"Estimation of land cover and biomass change from remotely sensed data"

Reports on progress in estimating land cover change, using aerial photography and satellite imagery and biomass change, based on field data, lidar and satellite imagery, in the Fitzroy catchment, Australia. [C5983]

"Ground deformation monitoring exploiting SAR permanent scatterers"

The detection of ground deformation phenomena exhibiting a time non-uniform behavior by means of the

permanent scatterers technique is addressed. Simple but effective models are discussed showing significant results obtained. [C5984]

"Assessing flooding and vegetation structure in forested wetlands using Radarsat SAR imagery"

We used 32 Radarsat SAR images collected between 1996 and 2001 over the Roanoke River floodplain, North Carolina (USA), to assess the utility of C-HH Radarsat SAR for operationally mapping flooding beneath forest canopies. Our objective was to test the sensitivity of standard-beam Radarsat to flooded forests under leaf-on and leaf-off conditions, and at multiple incidence angles (ranging from 10-46°). We found that winter (leaf-off images) could be used to accurately map flooding (>95% accuracy) regardless of incidence angle. Mapping accuracy was acceptable for leaf-on images (>85%) but was nevertheless significantly lower than for leaf-off images. Images at shallow incidence angles (e.g. S6 mode, 41-46°) were especially affected by speckle in the interpretations, whereas images acquired at very steep incidence angles (extended low beam, 10-23°) exhibited a substantial amount of geometric feature displacement that limited their utility for practical applications. For mature forests, forest structure (independent of leaf-on or leaf-off status) did not appear to affect the ability to map flooding; however, separate interpretations were required to delineate flooding in very young, dense successional stands ([C5985]

"Seasonal and spatial variability of surface hydraulic properties"

Monitoring, using remote sensing, of seasonal changes of land surface properties such as: freezing and thawing of wetland, freezing and thawing of soil, as well as soil moisture and snow cover mapping, relies on capabilities to relate physical characteristics of the study area and satellite observations. The water and ice content of soil are very important parameters for determination of the storage capacity and hydraulic properties of the surface. Thus, the objective of this work was to derive indices that would provide link between remote sensing observations and regional/seasonal variability of surface properties. Radiative transfer and radar backscatter models were configured to simulate and analyse the link between surface properties, atmospheric conditions, and the signals measured by active and passive sensors. In this work we present the results of model simulation of microwave backscattering for different land surface types e.g., wetland, forest cover. Several different study sites were selected in Ontario. RADARSAT (Fall, Winter, and Spring) images, at different resolution, were acquired for several different sites in Northern and Southwest Ontario. Two independent transitions corresponding to soil thaw and possible canopy thaw were revealed by the data. Analysis of Radarsat scenes indicates shifts in radar backscatter related to varying environmental conditions during image acquisition, e.g., snow storm. Consequences of such effects on the analysis of surface characteristics can be significant. [C5986]

"Inversion of surface scattering models: comparing criteria and algorithms to estimate bare soil parameters"

Estimates bare soil geophysical parameters (i.e. standard deviation of roughness height s , length of correlation l and soil moisture mv) using polarimetric SAR data. Two direct models have been implemented to simulate the radar measurements and were introduced in an inversion scheme. The methods have been tested on simulated data where speckle effects and model errors were taken into account. A correlation between the roughness parameters, as it can be expected in real measures, has been imposed in the simulation in order to evaluate its effect on the estimation accuracy. Different inversion algorithms based on a Bayesian approach, developed with simple optimization-integration procedures have been compared to neural networks. The comparison has assessed the accuracy achievable by different radar system configurations. Polarimetric data acquired during MAC Europe and SIR-C campaigns, over selected bare soil fields, has been processed to show preliminary estimation results. [C5987]

"Quantitative subsidence monitoring using SAR interferometry"

The paper describes the main characteristics of three procedures to perform subsidence monitoring using SAR interferometry, which are suitable to support quantitative applications, like those related to risk assessment and public safety. The first procedure can be effective even with a single interferogram, while the other ones are suitable to the configurations based on multiple interferograms. [C5988]

"Full exploitation of the ERS archive: multi data set permanent scatterers analysis"

In this paper we start addressing the main advantages and possible applications of carrying out permanent scatterers analyses involving more independent data sets covering the same test area (i.e. data acquired along parallel orbits relative to adjacent tracks as well as data gathered by ascending and descending passes). First interesting results are provided. [C5989]

"Results of processing and analysis of large volumes of repeat-pass InSAR data of Vancouver and Mount Meager (B.C.)"

A large quantity of ERS InSAR data and several scenes of Radarsat InSAR data were used to study historical deformation at Mount Meager in Northern B.C. The Mount Meager Volcanic Complex is a hazardous area showing an anomalously high frequency of catastrophic slope failures. It is also the location of Canada's most recent explosive volcanic eruption (2350 YBP). The primary objective of processing and analysis of the SAR data was to detect and measure small deformation events on the slopes of the mountain. A similarly large number of repeated ERS SAR scenes collected over the urban area of Vancouver between 1992 and 2000 was selected for InSAR processing. The objective of the project was to investigate the potential of detecting and measuring very small deformation rates (better than 1 mm/yr) and deformation events while taking advantage of the large volume of SAR datasets. The following types of deformation were of specific interest: 1. Stability of the Fraser River Delta 2. Tidal loading 3. Subsidence patterns in urban areas 4. Deformation of individual buildings, bridges and infrastructure. This paper provides some information on the processing methodologies that were employed as well as results and interpretation of the results. [C5990]

"Ground uplift in the city of Paris (France) revealed by satellite radar interferometry"

We have analyzed a set of ERS-2 images to investigate centimetric surface deformations within the city of Paris (France) using the radar interferometry technique. We show that a large scale uplift phenomenon occurred during the summer 1998 south of the Saint-Lazare railway station (maximum amplitude of 1.3 cm +/- 0.3 cm). This area corresponds to an important underground working site, which required to lower the piezometric level during 1995 and 1997. The uplift correlates in time with the increase of the underground water level at the end of the construction work. The amplitude of the uplift corresponds to the amplitude of a subsidence which was previously observed in the same area, suggesting that the deformation mechanism is elastic and not simply due to compaction. [C5991]

"Urban subsidence in the city of Prato (Italy) monitored by satellite radar interferometry"

The differential SAR interferometry has been applied to study the displacement field in an urban area. A set of 6 ERS1/2 SAR images has been used to detect, map and quantify the subsidence occurring in the city of Prato near Florence (Italy). Four areas affected by strong subsidence during the period 1993-2000 have been spotted within the city. The analysis of three interferograms processed from images taken two years apart shows that the deformation rate is constant, with a maximum value of about 8.3 cm.yr⁻¹. [C5992]

"Polarmetric SAR data compression using wavelet packets in a block coding scheme"

Previously progress has been made in designing wavelet compression schemes for SAR image data. In this paper, we propose an improvement to the wavelet method based on a subdivision of the image into blocks, so that an optimal bit allocation can be made based on each block's statistics. Unlike single-channel SAR data, polarimetric data have HH, VV and HV channels of radar intensity images, plus the phase differences between them. We examine the information redundancy among these channels, and optimize the block coding scheme across the polarimetric channels and spatial blocks to improve compression performance. Experimental results using SIR-C data show significant improvement in coding efficiency. [C5993]

"Wavelet-based compression of SAR raw data"

In this paper we compare two compression methods for SAR raw data, based on the discrete wavelet transform (DWT). In the former, the data are subject to blockwise normalization prior to being transformed by means of the DWT processor; then, an optimal rate allocation is performed for each subband. The latter employs the well known JPEG 2000 to perform the DWT and the subsequent quantization, rate allocation and coding steps; both the cases of normalized and non normalized data are considered. The performance of the algorithms have been tested on SIR-C/X-SAR data, and FBAQ is employed as the term of comparison for both quality and compression ratio. The obtained results show that if the samples are normalized, the performance of the DWT-based algorithms is more predictable, and less subject to statistical fluctuations related to the characteristics of the input data. [C5994]

"Fractal behavior of sea SAR ERS-1 images"

Fractal dimension of the sea surface is strictly related to its roughness, and may thus be helpful in determining the sea state, or where motion-damping oil spills are located. A possible way to determine the fractal dimension of the sea surface is that of performing a fractal analysis of remote sensing images, in particular satellite images,

which have the advantage of observing a large area at one time. This paper aims to show the utility of fractal analysis of ERS-1 SAR images, and presents the results obtained by three different algorithms. The considered data was sensed by ERS-1 in the Mediterranean Sea at times and locations suitable for comparison with data coming from the Italian "Sistema Ondametrico Nazionale," an environmental measurement system including a number of buoys carrying accelerometers and communications instruments. The experimental results show some accordance between the buoy data and the ERS-1 fractal analysis outcome, but more data are required to provide statistical support to the conclusions. [C5995]

"Remotely sensing bound and free small-scale waves at the edges of monomolecular surface films in a wind-wave tank"

We have carried out wind-wave tank measurements to investigate the small-scale roughness of the water surface at the edges of monomolecular surface films. Small amounts of oleyl alcohol, triolein, and palmitic acid methyl ester were carefully deployed on the water surface at wind speeds between 3 m/s and 9 m/s, thus allowing for wave measurements at either end (i.e., downwind and upwind) of the surface films. Data were acquired using a 10 GHz (X-band) scatterometer, and a two-dimensional laser slope gauge, and a video camera. We found that the effect of slick-edge asymmetry (i.e., a sharp downwind edge and a diffuse upwind edge) depends on both the deployed substance and the wind speed. Due to different states of film compression at the downwind or upwind edges of the surface film, the damping capability of the slick material can vary in these areas. This in turn may cause a varying spectral density of small-scale waves, which are bound to the dominant wind waves, while the slick is drifting by. This effect is shown and interpreted qualitatively using the video data, and quantitatively using the scatterometer and laser gauge data. [C5996]

"Wave tank studies of radar Doppler shifts in the presence of surfactant films on the water surface"

Doppler shifts of Ka-band radar signals backscattered by short wind waves in the presence of organic films have been studied in wave tank experiment at low wind speeds and at different surfactant concentrations. It is shown that phase velocities of mm-scale wind ripples, retrieved from radar Doppler shifts, do not obey the linear dispersion relationship and are determined by the velocities of free gravity-capillary waves and of bound waves-nonlinear harmonics of decimetre-scale dominant waves. A relative intensity of the bound waves as a function of surfactant concentration is estimated. Damping of free and bound waves due to surfactant films has been analysed theoretically and a qualitative explanation of changing of radar Doppler shifts in the presence of films is given. [C5997]

"Assimilation of SAR data to operational hydrological runoff and snow melt forecasting model"

Assimilation of ERS-2 SAR data to the operational hydrological runoff model using a nonlinear Bayesian techniques is demonstrated and tested. The developed assimilation technique combines SAR observations to runoff model by applying a constrained iteration procedure and forward modeling of SAR observations. The aim is to improve river discharge forecasts. The test site is located in the Northern Finland, in river Kemijoki drainage area. The satellite data consists of ERS-2 SAR images from four springs. The results show that inclusion of the satellite data can improve the performance of the discharge forecasting model during the snow melt period. [C5998]

"Analysis of detailed in-situ soil measurements with ERS C-band radar backscattering data"

In order to improve a better quantitative understanding of the effect of soil moisture of bare soils on C-band SAR data, five dedicated "weather" stations with soil moisture probes, rain gauges, and temperature thermometers have been installed through the Flevoland test site (The Netherlands) since April 2000. In addition to the in-situ data, spaceborne SAR data at C-band measured by ERS-2 are also collected (3 images every 70 days), taking advantage that the test site is close-by the locations of the ESA transponders used for calibration of the SAR data. In this paper, the variations of the backscattering coefficient due to soil moisture changes are shown as well as the effect of rain precipitation's on the soil moisture at different depths. Diurnal variations of the soil moisture have been observed during drying periods and soil temperature measurements allow a precise monitoring of this effect. [C5999]

"Comparison of Ku-and C-band backscatter time series over land"

C- and Ku-band scatterometer backscatter time series are analysed and compared to meteorological data for two biomes, the African Steppe and the Scandinavian Boreal Forest. Observed characteristics of large scale scattering are inferred and discussed. [C6000]

"Predictive coding of SAR phase history data"

In this article we evaluate the use of predictive coding for compression of SAR phase history data. We first show that the data are mainly correlated along range lines. Then, we exploit this result to define a new DPCM-based compression algorithm named RDPCM-BAQ. The performance of this algorithm is compared with that of BAQ on SIR-C/X-SAR data, showing a significant improvement in signal-to-noise ratio of up to 2 dB with respect to BAQ. [C6001]

"Data compression for operational SAR missions using entropy-constrained block adaptive quantisation"

Operational SAR satellite missions impose new requirements to on-board data compression such as a higher data reduction ratio, more flexibility, and faster data throughput. A novel approach is Entropy-Constrained Block Adaptive Quantisation (ECBAQ). This method outperforms currently used Block Adaptive Quantisation with respect to Signal-to-Quantisation-Noise-Ratio and equals the performance of more complicated methods such as Vector Quantisation and Trellis Coding variants. The ECBAQ algorithm can be implemented using an architecture that is essentially not more complicated than that of a BAQ encoder and suitable for high-speed implementations. Moreover, the method features bit rate programmability with non-integer rates. This allows the SAR information throughput to be optimised for different types of applications. It is suitable for the application of region-of-interest coding and can be cascaded with frequency filtering to achieve even more data reduction. [C6002]

"Satellite imagery for volcanic hazards mitigation"

As world population and urbanization increase, volcanoes pose an ever greater hazard to life, property, and infrastructure in volcanically active regions. The rise in air traffic world-wide increases the risk of encounters between airborne ash and aircraft, even at great distances from the source. The Committee on Earth Observation Satellites (CEOS), an international association of civilian space agencies, seeks to foster cooperation to increase the usefulness and accessibility of satellite imagery. In February 1997, CEOs initiated the Disaster Management Support Project to assess the present and potential use of satellite-derived information for the mitigation of several hazards, including volcanic hazards. Radar methods are discussed. [C6003]

"Earth observation for ice hazard support"

It is well known that sea ice and icebergs pose a serious hazard to shipping and other maritime activities in the polar regions. The role of Earth observation (EO) data in operational ice monitoring is well documented and has grown in importance over the years. Ice Centers have evaluated the EO data sources currently available to provide emergency response and provide recommendations for improved responsiveness in the future. [C6004]

"High resolution wind retrieval from SeaWinds"

While originally designed for measuring vector winds over the ocean at a nominal resolution of 25 km, data from SeaWinds-on-QuikSCAT can be used to retrieve winds over the ocean at higher resolution with the aid of resolution enhancement reconstruction algorithms. This paper analyzes a technique for retrieving enhanced resolution winds at high resolution from SeaWinds data. Techniques for minimizing the required computation are described. As can be expected the wind estimates are noisier than standard resolution products. Some of the limitations of the approach and resulting products are considered. While validation of this approach to high resolution wind retrieval continues, the results thus far are very encouraging. [C6005]

"Buoy validation of ocean surface wind estimates from the TRMM precipitation radar"

A technique has been developed for retrieving ocean surface winds using surface backscatter measurements from the Precipitation Radar (PR) of the Tropical Rainfall Measuring Mission (TRMM). Though limited by the small incidence angles and the single look capability of the scan geometry, TRMM PR offers a distinct advantage over conventional spaceborne scatterometer systems through the fine scale vertical and horizontal resolution of its normalized radar cross section, σ° . The wind retrieval algorithm developed for TRMM PR makes use of a maximum likelihood estimation technique to compensate for the low σ° sensitivity associated with the PR configuration. The narrow vertical resolution of the PR range bins serves to filter out rain contaminated cells normally integrated into scatterometer surface measurements. The algorithm was developed and validated through remotely measured winds from other spaceborne sensors, namely the TRMM Microwave Imager (TMI) radiometer and the NASA QuikSCAT scatterometer. Further algorithm validation is presented using in-situ observations from oceanographic buoys. All buoy data are acquired from the NOAA National Buoy Data Center. The TRMM PR geophysical model function used in the retrieval process is verified through comparison of PR σ°

measurements and buoy wind measurements. Ocean surface wind speeds derived from the new PR retrieval technique are then compared with collocated buoy winds, revealing excellent agreement in wind speed estimation. [C6006]

"Detecting ocean surface winds using TRMM precipitation radar"

Although designed specifically for the measurement of precipitation in the atmosphere, the Precipitation Radar (PR) onboard the Tropical Rainfall Measuring Mission (TRMM) satellite also measures the normalized radar cross-section at the Earth's surface. As such, this instrument provides an interesting opportunity to explore an alternative radar configuration in the satellite remote sensing of ocean winds. In particular, it can measure the strength of the ocean winds in relatively higher spatial resolution as compared to the conventional scatterometer systems presently in use. The addition of wind sensing capability to precipitation radar also complements its rain profiling capability nicely and allows coincident wind and rain measurements. In this paper, we discuss a new ocean wind algorithm developed specifically for TRMM PR using maximum likelihood estimation. A unique feature of this wind algorithm is its capability to incorporate measurement sensitivity and noise information consistently in both the along-track and cross-track directions. This PR wind algorithm is then tested using data from the TRMM Microwave Imager (TMI) and NASA QuikSCAT scatterometer. Excellent agreement on the retrieved wind strengths is achieved among three sensors. [C6007]

"An advanced FPGA-based processor and controller for the Next-Generation Precipitation Radar"

The Next-Generation Precipitation Radar (PR-2) prototyped by NASA/JPL will depend heavily on high-performance digital processing to collect meaningful rain echo data. Using field-programmable gate arrays (FPGAs), we have developed for the PR-2 a pulse-compression processor and adaptive timing controller that will enable full on-board processing capabilities in a 14 and 36 GHz spaceborne radar. This paper describes some of the new technologies for the on-board processor, including a 404109op/s bit-serial filter attaining -60 dB range sidelobe performance, and an adaptive scanning control and timing unit (CTU) which yields a 7-fold increase in the radar's dwell time over areas of precipitation. [C6008]

"Forest biomass estimation using polarimetric SAR interferometry"

Forest biomass is one of the most important and most unknown parameters for accurate global carbon stock modelling. In this paper we address an alternative methodology for estimating above ground forest biomass from radar remote sensing data, based on forest height estimates from single frequency polarimetric-interferometric SAR data. [C6009]

"Preliminary design of the SWIMSAT radar for the measurement of ocean wave spectra"

The main objective of SWIMSAT is to measure the directional spectra of waves thanks to a space-borne radar. The instrumental concept involves a real-aperture radar using a multi-beam conical scanning, in order to provide measurements of the spectral properties of the wave field, and to estimate the profile of radar cross-section depending on incidence (0° to 10°) and azimuth (0° to 360°). The paper provides an overview of the mission and of the measurement principle, and the status on instrument design. [C6010]

"Earth observation for landslide assessment"

This report provides a summary from the larger CEOS Landslide hazard team report, focusing on EO information requirements for landslide assessment. [C6011]

"Poseidon 2 radar altimeter design and in flight preliminary performances"

Poseidon 2 is the dual frequency, solid state radar altimeter embarked on the CNES/NASA oceanographic satellite JASON 1. This paper gives a brief sum up of the instrument design and some preliminary in flight performances. [C6012]

"Upcoming naval space missions for remote sensing of the oceans, atmosphere and space"

The U.S. Navy is permanently forward-deployed and depends critically on precise knowledge and predictability of global environmental conditions from under the ocean, throughout the atmosphere and into near-Earth space. To satisfy global mission needs, the Navy depends on spaceborne remote sensing platforms to characterize and monitor each of these environments at wavelengths from the microwave to the ultraviolet. In the next five years, the Navy, in partnership with other agencies, will be launching a number of experimental, operational and quasi-operational remote sensing satellite instruments. Traditionally, the Navy has used remote sensing in the

microwave spectrum to characterize the sea surface wind speed, temperature, ice conditions and other land and atmospheric applications. This year the Defense Meteorological Satellite Program (DMSP) will launch the first in a series of operational Special Sensor Microwave Imager/Sounders (SSMISs) aboard their Block 5D3 satellites. Also this year, the Air Force Space Test Program (STP) will launch the WindSat passive microwave polarimeter to test new techniques for determination of the sea surface wind vector. Along with SSMIS the next block of DMSP satellites will include the first of five Special Sensor Ultraviolet Limb Imagers (SSULIs) developed by the Navy for remote sensing of upper atmospheric density profiles and ionospheric electron density profiles. These data will aid the Navy and DoD in tracking objects in Earth orbit and help characterize the radio frequency environment for communication, radar, navigation and other applications. To characterize the littoral regions using hyperspectral imagery, the Navy is developing the Naval EarthMap Observing satellite. [C6013]

"Results from the Crusade ship detection trial: polarimetric SAR"

An experiment was conducted in March 2000 offshore of the Newfoundland, Canada coastline which involved several radar data sets. The objective of the experiment was to assess ship detection capabilities for several radar systems. In particular, image data were collected from RADARSAT, the polarimetric C/X SAR and the High Frequency Surface Wave Radar (HFSWR) at Cape Race, Newfoundland. These data were acquired over a period of ten days while three staged ships remained on site at specified positions. These types of experiments are very rare and hence the results from this experiment will be invaluable for validating ship detection techniques and providing direction for future research and experiments. HH and HV polarizations were found to be optimal for wide area ship detection applications. A moment method and polarimetric decomposition methods provided high ship detection rates. Polarimetric target decomposition results indicate potential capability for recognizing targets and reducing false alarm rates. [C6014]

"The Global Hawk UAV Australian deployment: imaging radar sensor modifications and employment for maritime surveillance"

The Global Hawk system is a high altitude endurance unmanned aerial vehicle developed under the United States Air Force Advanced Concept Demonstrator program primarily as a reconnaissance system for use against fixed and mobile targets. The Global Hawk system deployed to Australia in April 2001 for six weeks and in this period conducted 11 missions with the focus on maritime surveillance. The Australian deployment was the culmination of two years collaboration between the United States and Australia that included modifications to the radar sensor, system control and exploitation to support a surveillance focus. This paper presents aspects of the Australian contribution to the Global Hawk deployment including the rationale behind the sensor modifications and employment that achieved a surveillance capability with a system primarily designed for land reconnaissance. [C6015]

"Possible military requirements and applications of active and passive imaging sensors at micro- and millimeterwave frequencies"

In order to reveal the differences between military and civil applications of remote sensing common military user requirements for the detection, recognition, identification, and revisit time of military targets are discussed. Typical application examples of imaging SAR and radiometer systems are given as well as design examples for advanced sensor systems demonstrating the technological realisation and limits. [C6016]

"U.S. Navy operational sea ice remote sensing"

The National Ice Center provides a variety of sea ice products and services. Most of these products rely heavily upon remotely sensed data. These products are briefly described in this report, with a focus on elucidating the important role that remote sensing plays in the production of these products. [C6017]

"Detection and characterization of diurnal winds using QuikScat data"

Analysis of SeaWinds Scatterometer data show coastal regions exhibiting a greater than 5 m/s wind speed difference between averaged morning (ascending) and evening (descending) observations. This diurnal wind variability is strongest at several Indian Ocean locations including Madagascar, northern Australia, and Sri Lanka, as well as the west coast of South America and on the Pacific Coast of Central America. Two of these regions are discussed here in greater detail. [C6018]

"The ocean surface wind direction signal in passive microwave brightness temperatures"

We analyze the wind direction signal for vertically (v) and horizontally (h) polarized microwave radiation at 37 GHz, 19 GHz and 11 GHz and an Earth incidence angle of 53 deg. We use brightness temperatures from SSM/I

and TMI and wind vectors from buoys and the QUIKSCAT scatterometer. The wind vectors are space and time collocated with the radiometer measurements. Water vapor, cloud water and sea surface temperature are obtained from independent measurements and are uncorrelated with the wind direction. We find a signal that is noticeably smaller at low and moderate wind speeds than a previous analysis had indicated. [C6019]

"The accuracy of high resolution winds from QuikSCAT"

The accuracy of the high resolution QuikSCAT wind product was quantified using spatially and temporally collocated 10 m equivalent neutral stability winds, calculated from selected NOAA NDBC buoy measurements. Only buoys that had sample correlation higher than 1.5 were used in this validation, a total of 5704 records. The validation followed the Freilich nonlinear statistical analysis approach. This analysis of the collocated buoy-scatterometer data set yielded the following statistics for wind speed: deterministic offset -0.25 m/s; linear gain 1.02; standard deviation of component errors 1.9 m/s; and RMS error 2.2 m/s. Wind direction errors were more pronounced for lighter winds, typically for winds up to 5 m/s. The RMS directional error for buoy-QuikSCAT pairs for which $\Delta\theta$ [C6020]

"NOAA CoastWatch RADARSAT-1 SAR coastal monitoring applications demonstrations"

A summary of the interim results of the first two years of the authors' NASA RADARSAT-1 ADRO-2 SAR project is given. The Alaska SAR Demonstration (AKDEMO) is providing winds, vessel positions, and SAR imagery to users in Alaska for evaluation as to their utility to operational government agencies responsible for ocean and weather prediction and fisheries management/enforcement. The AKDEMO applications are maturing and their accuracy has been measured. A new demonstration, the Gulf of Mexico Experiment (GoMEx), is now underway to examine use of SAR data and products in hazardous algal bloom (HAB) and oil spill/seep monitoring. Initial results show correspondence of bloom signatures in ocean color and SAR data in areas of high HAB concentration as measured from ship water samples. In addition to these two applications demonstrations, research is underway in the use of SAR data to study upwelling, river plumes, ocean current boundaries, atmospheric boundary layer processes, and other applications. This research will continue into the third and final year of the ADRO-2 project. [C6021]

"Improving the visualisation of polarimetric response in SAR imagery from pixels to images"

This paper presents a new method for the visualisation of polarimetric response patterns on a synoptic basis. The aim of this approach is to synthesise traditional polarimetric response graphs with the spatial overview provided by standard remote sensing image processing techniques. By doing this, an effective means of exploring phenomenological polarimetric response patterns is achieved, which may prove to be a valuable input for the development of modelling strategies and the application of polarimetry. [C6022]

"SAR geocoding and multi-sensor image registration"

Quantitative analyses of remote sensing data acquired with variable geometries and different sensors are greatly facilitated by geocoding the data to a common geographical reference. Errors in geocoded SAR images are due to inaccuracies in the orbit data, errors in the processing parameters, and DEM errors. Automated terrain geocoding of SAR data is possible using only a single resampling of the native slant-range to the final map geometry after measurement and correction for residual geolocation errors. An accurate adaptive resampling algorithm for the interpolation from the SAR geometry to the map coordinate system is presented. This processing paradigm has been extended to permit combining data from different SAR instruments. [C6023]

"A new maximum likelihood classification technique for multitemporal SAR and multiband optical images"

In this paper we devise a new fusion technique for a sequence of multitemporal single-channel SAR images of a given area with a single multiband optical image. Unlike for SAR, the availability of optical images is largely affected by atmospheric conditions, so that this is a case of practical interest. First, a statistical model for the joint distribution of SAR and optical data is provided. Then the corresponding joint maximum likelihood (ML) classifier is derived, and lower and upper bounds to classification performance are introduced. An optimized technique for ML joint image segmentation and classification is proposed, showing results close to the upper bound. Finally the effectiveness of fusion of SAR and optical images is investigated quantitatively, showing a consistent performance improvement with respect to using either sensor alone. [C6024]

"An outline of fusion and sensor combinational methodologies for disparate, sparse multi-sensor networks for detecting icebergs"

Regions of extensive marine activity, particularly regions that span hundreds of nautical miles, require wide-area, timely, and reliable remotely sensed information to ensure safe and efficient offshore operations. In some areas, such as the western North Atlantic, this issue is exacerbated for one-third of the year when the region can be frequented by icebergs. This paper reports on development of a framework for "fusing" the various sensor data to provide the most accurate and timely "picture" of the region of interest. Available data includes satellite SAR (synthetic aperture radar) imagery, long-range HF (high frequency) radar, airborne radar, conventional and enhanced marine radar from ships and platforms, and human observation. Work to date has focused primarily on developing performance curves for the various sensors based on empirical data collected over the past two years. This paper presents an overview of that work and the parameters to be optimized in combining data from the disparate sensors. [C6025]

"Range antenna pattern measurements of airborne SAR system with arrayed corner reflectors"

To validate antenna elevation patterns of the CRL/NASDA X/L-band airborne synthetic aperture radar, Pi-SAR, corner reflectors (CR) were deployed along the cross-track (range) direction. Six 15-cm trihedrals for the X-band SAR were placed at 5 degree intervals of the incidence angle to cover the entire swath, and also placed were six 70-cm trihedrals for the L-SAR. We computed the reflected power from each CR with slant-range single-look image data in which the antenna gain patterns were already taken. As a result, we found the measured power (of the X-SAR) were 0 to -1 dB different from the calculated one, except at the both edges of the range. Also computed were phase difference between HH and VV channels, to find the. measured one (of the X-SAR) was different as much as 100 degrees from the calculated one when no antenna phase pattern correction was made. [C6026]

"Cornerstones and epilogue of the GRFM Africa project: a gallery of regional scale vegetation maps"

The Global Rain Forest Mapping project (GRFM) is an initiative started by the National Agency for Space Development of Japan (NASDA) in 1996 with the main goal of creating a wall to wall radar map of the tropical belt with homogeneous and consistent characteristics. GRFM Africa-the part of the project related to tropical Africa-has evolved through several years to the stage where significant thematic products have been generated. It is maintained that these products bear relevance to global change studies and to the sustainable management of local resources in the tropics. The objective of this paper is to lend support to this proposition by illustrating through a few examples the results achieved so far. In particular two land cover maps are presented covering respectively the Central Congo basin, and the Gabon country. Validation of these large-scale high-resolution products poses a challenging problem. The method adopted in GRFM Africa is outlined. It is based on comparison with independent thematic information with known error budget, derived from a combination of optical remote sensing observations, national forestry maps and ground surveys. [C6027]

"Ocean wave groupiness from ERS-1/2 and ENVISAT imagerettes"

In this study a global data set of reprocessed synthetic aperture radar (SAR) data acquired by the European Remote Sensing satellite ERS-2 is used to study ocean wave grouping using wavelet based methods. For more than a decade the ERS-1/2 satellites have continuously recorded SAR images of the ocean surface. Operating in wave mode both instruments have acquired about 1400 imagerettes of 1045 km. size (every 200 km along the orbit) each day, which allows to study ocean waves on a global basis. Only coarsely gridded SAR image spectra are available as official wave mode products from the European Space Agency (ESA). As the full image information is required for the present study about 3 weeks of ERS-2 SAR wave mode raw data were reprocessed to 34000 complex SAR images using the BSAR processor from the German Aerospace Center (DLR). ENVISAT satellite, which was successfully launched on February 28, 2002, will provide almost 3000 imagerettes a day due to its higher sampling rate (every 100 km). Applying a wavelet edge detection method on the SAR-amplitude-density image and using a region growing approach for the edgefree areas allows examinations of the wave groupiness on a single image. These examinations include group size and number of large groups. The wavelet coefficient as a measure for edge strength is correlated to both wave height and steepness. The wavelet method is compared with an alternative approach, which is based on the classical Hilbert-transform technique. For the latter method the actual sea surface elevation field has to be known. Therefore a quasilinear inversion scheme is used which estimates the surface elevation from complex SAR data. [C6028]

"Remote sensing of ocean waves and currents using NASA (JPL) AIRSAR along-track interferometry (ATI)"

The along-track interferometry (ATI) SAR measures the Doppler shift of the backscattered signal and thus the

line-of-sight velocity of the scatterers. This interferometric velocity is the sum of the orbital motion of water particles from the swell, phase velocities of the Bragg waves, and ocean surface currents. While the advent of ATI SAR provided us with a potentially powerful technique for ocean current mapping, the surface currents cannot yet be measured exactly from interferometric velocity measurements. In this paper, we will apply a new method of extracting the surface current velocity from multiple-frequency (L- & C-band) ATI SAR data. We have tested ATI SAR data that were collected during the PACRIM-II AIRSAR experiment over the Ulsan coast on the southeastern part of the Korean peninsula. We have investigated the ocean waves and current features and have retrieved dominant ocean wave information. Furthermore, we could differentiate the ocean current and the Bragg wave phase velocities using multiple-frequency (C & L-band) ATI data. [C6029]

"Use of the coherence of synthetic aperture radar cross spectra for ocean wave measurements"

A noise model for synthetic aperture radar (SAR) look cross spectra (LCS) acquired over the ocean is proposed. The study is meant to contribute to the improvement of algorithms for retrieval of two dimensional ocean wave spectra from LCS. Error bars for the LCS phase, which contains information on the ocean wave phase speed and propagation direction are derived. The error estimates depend on the respective LCS coherence and the amount of smoothing applied in the LCS estimation process. A model for the LCS coherence is introduced. The first part of the model describes the dependence of the coherence on system parameters like spatial resolution. The second part is associated with the motion of the imaged ocean wave field. Decorrelation is shown to be caused by the coupling of dispersive ocean wave components in the SAR image formation process. Forward simulations for the cross spectrum coherence are carried out using parameterized swell and wind sea spectra. Coherence is estimated from a global data set of reprocessed ERS-2 wave mode data and compared to theory. [C6030]

"Mixed pixel decomposition of satellite images based on source separation method"

In this paper we propose to prove the importance of the application of blind source separation methods on remote sensing data. Satellite images are represented by radiometric value that can be considered as a mixture of independent sources. To restore the independent sources we use the statistical method of Joint Approximate Diagonalization of Eigen-matrix (JADE). The proposed algorithm generates source images where each one gives a maximum of information specific to a certain type of land cover. These source images do not provide one scalar value per pixel, but rather a vector which components will agree with the radiometric value of the different land cover types present in the pixel. [C6031]

"Radar investigations of breaking water waves at low grazing angles with simultaneous high-speed optical imagery"

Radar scattering experiments were carried out at the wavetank facility at the University of Maryland-College Park. Spilling and plunging breakers were generated by means of a chirped wave packet, and were then imaged with a high-speed camera. Simultaneously, the radar backscatter generated by the breakers at a nominal grazing angle of 12 degrees was measured by an ultrawideband, dual-polarized, X-band radar with a range resolution of approximately 4 cm. This experimental setup also included a moving instrument carriage that allowed the sensors to follow the breakers throughout their entire evolution. In conjunction with numerical simulations, these experiments can guide the development of realistic scattering models by identifying the important wave features and the corresponding scattering mechanisms. [C6032]

"Interferometric phase and coherence of forest estimated by ESPRIT-based polarimetric SAR interferometry"

Polarimetric SAR interferometry has been widely studied for forest observations. The technique utilizes polarization state difference among local scattering centers of the forest to decompose them. Using the method, we can estimate precise forest parameters. We proposed an alternative method based on the ESPRIT algorithm for the estimation. The method can detect as many as 3 local scatterers with fully polarimetric data, and can extract interferometric phase of each local scatterer. In this paper, we verify the availability of the method in 2- and 3-local-scatterer model for forest estimation, and show that forest analysis with 3-local-scatterer improve height estimation accuracy. SIR-C/X-SAR data were used for these verifications. In addition, experimental results of restricted dual-polarization data are also provided to show availability of the method. [C6033]

"Speckle filtering of polarimetric SAR interferometry data"

Polarimetric SAR interferometry has generated much interest for forest applications. In this paper, we study problems associated with interferometric coherence estimation and propose two algorithms to improve the

accuracy in the coherence estimation based on speckle filtering of the 6 Ч 6 polarimetric interferometry matrix. [C6034]

"Interferometric SAR polarimetry using a passive polarimetric microsatellite concept"

Recently, several passive interferometric configurations consisting of two or more receiving only micro-satellites operating in a fully polarimetric mode positioned ahead or behind a master satellite have been proposed as a cost efficient option for future single-pass interferometric spaceborne SAR systems. In this paper the potential performance of such a passive polarimetric and interferometric micro-satellite concept for the estimation of forest structure parameters in terms of polarimetric interferometry is investigated. [C6035]

"Polarimetric interferometry in the Glen Affric project: results & conclusions"

In this paper we summarise the recent results from the Glen Affric radar project, a multi-disciplinary program addressing the potential of polarimetric radar interferometry to provide vegetation structural information of importance in forest mapping and ecology studies. We present a comparison of results from L-band repeat pass SAR imagery with detailed in-situ measurements of forest height and topography. [C6036]

"Forward and inverse modelling of multi-baseline L-band Pol-InSAR E-SAR data"

The objective of this paper is the analysis of forward and inverse modelling of multi-baseline L-band polarimetric SAR interferometry (Pol-InSAR) data. The first part of this study deals with an analysis of the differential phase between interferograms in different polarisation states. It is shown that conventional polarisations in the (h, v)- or Pauli-polarisation basis, while identifying different scattering mechanisms, cannot provide unambiguous interferometric phase centres in vegetation volumes at L-band. On the other hand, the Pol-InSAR optimised singular polarisations provide the largest vertical separability of interferometric phase centres within volume scatterers. The representation of the interferometric coherence in the complex unitary circle as a function of polarisation complements these observations. The second part of the paper concentrates on the forward modelling of Pol-InSAR measurables using a well-known coherent scattering model. The behaviour of the coherence is simulated to provide a more detailed interpretation of the physical meaning of the singular polarisations than was possible in the first part of the paper. Physical parameter ambiguities are emphasised and analysed. In the third part of the paper, Pol-InSAR observables are obtained through inversion of the model mentioned above. The analyses make use of multi-baseline airborne L-band E-SAR data. [C6037]

"A 2-D Fourier domain approach for spotlight SAR raw signal simulation of extended scenes"

In this paper a spotlight SAR raw signal simulator for extended scenes is presented. The proposed procedure has two main advantages: first of all, use is made of efficient FFT codes, thus reducing the computational load with respect to a time-domain simulation; in addition, the procedure is planned taking into account theoretical developments used in an existing stripmap simulator, so that most of the algorithms employed in that simulator can be reused after minor changes. [C6038]

"An advanced airborne real-time SAR processing system"

An advanced airborne real-time SAR processing system has been developed. Some sets of the system are now in operation at several organizations. By implementing all necessary processing functions by software, such as yaw-steering compensation and multi-resolution mode with pre-summing, we are able to eliminate several important hardware components such as mechanical yaw steering system and data reduction filters. This fully digitized and software oriented SAR architecture gives significant flexibility to the system, without compromising its performance. Besides above-mentioned advantages, the system has some new improvements, such as precise target positioning and compatibility of seamless imaging and software yaw steering, which is usually contradictory. [C6039]

"ESTAR experience with RFI at L-band and implications for future passive microwave remote sensing from space"

Although the spectral window at 1.413 GHz (L-band) is protected for passive use, radiometers for remote sensing commonly encounter problems with RFI. Experience with the synthetic aperture radiometer, ESTAR, suggests that airports are one source of this RFI. The existence of RFI at L-band could be a problem for future remote sensing from space. [C6040]

"Polarimetric and interferometric noise modelling"

In this paper, a noise model for the extended six dimensions covariance matrix used in polarimetric synthetic aperture radar (SAR) interferometry is proposed. This noise model is able to interpret interferometric, as well as polarimetric noise characteristics for the diagonal and non-diagonal elements of the covariance matrix. [C6041]

"Robust parameter estimation using dual baseline polarimetric SAR interferometry"

In this paper we employ a two-level polarimetric coherent vegetation scattering model to investigate parameter estimation for dual baseline fully polarimetric radar interferometry. We show that the height and ground phase can be determined without assumptions about the minimum ground to volume scattering ratio and also we investigate the influence of vertical canopy structure on inversion. [C6042]

"The inversion of subsurface VETEM data-theory and practice"

Very early time electromagnetic system (VETEM) is an efficient tool for the detection of buried targets in very lossy medium. In this paper, we will discuss the inversion of VETEM data using a combination of one-dimensional (1D) and three-dimensional (3D) inverse scattering techniques, where the Born iterative method and distorted Born iterative method have been applied. In order to expedite the 3D inversion, an extended Born-type approximation is made in the forward solver, together with FFT acceleration technique. The 1D inversion provides a gross image of the subsurface, but the 3D inversion helps to resolve the subsurface image better. [C6043]

"Advanced classification of buried UXO using a broadband, fully polarimetric ground penetrating radar"

A broadband, fully polarimetric ground penetrating radar (GPR) system has been applied for classification of buried unexploded ordnance (UXO) for the past few years. It utilizes both late-time and early-time signatures extracted from GPR data collected with multiple antenna positions and multiple scan orientations. Various field measurements were conducted from 1999 to 2001 at UXO sites that have quite different environmental conditions. Lessons learned from these tests have led to significant system improvements. [C6044]

"Treatment of broadband and multi-object electromagnetic induction scattering using high frequency approximations"

Wideband electromagnetic induction (EMI) sensing shows increasing capability and promise for characterizing subsurface metallic objects, such as UXO. While EMI has some advantages over radar, such as superior penetration of moist soil, the field problem is still difficult due to the frequent occurrence of multiple targets in close proximity. The numerical modeling problem, even for a single object, is complicated by the fact that transmitted ("primary") fields typically penetrate the target, but will often only do so slightly. In most of the established numerical treatments, the scale of discretization is dominated either by the dimensions of the thin subsurface layer of electrical activity, or, more or less equivalently, by the range over which a Green's function decays, based on the characteristics of the metal. Resolution at this scale is often computationally prohibitive, particularly for magnetic materials, even though external fields of interest have only mild gradients. We approach the problem using the Thin Skin Depth Approximation (TSA). The TSA assumes an exponential form for the internal normal magnetic field component, as a function of distance inwards from the object surface. Despite the fact that it is designed to treat a state of affairs characteristic of relatively high EMI frequencies, results based on the TSA turn out to be accurate across the entire EMI band when the relative permeability of the scatterer material is high (e.g. as for steel). [C6045]

"Study on complex dielectric properties of saline soils"

Using the Vector Microwave Network Analyzer in broad band (from 0.2 to 18 GHz), a controlled laboratory experiment was conducted on artificially prepared wet saline soil samples. The complex dielectric constants of soil samples in a wide range of moisture and salinity contents were measured and the relationship to the moisture and salinity of the soils were analyzed. The experiment results shows that the imaginary part of the dielectric constant of wet soil is more sensitive to the salinity of soils at low frequency range (f [C6046]

"Application of broadband EMI responses to infer buried object's aspect ratio"

A new broadband electromagnetic (EMI) sensor, operating as lows as 10s of Hz and as high as 100s of kHz, has shown significant improvement for classification of buried metallic objects. EMI responses ("secondary" or scattered magnetic field) are characterized by two components, one inphase and another in phase quadrature with the primary field. Numerical and experimental investigations show that the frequency location of the quadrature peak in EMI scattered fields from metallic objects depends strongly on the major axis length ratio and

on the object's orientation relative to the transmitted field. To illustrate potentially useful processing of EMI sensor data, this paper presents results of high fidelity numerical simulations to verify a theory for simple estimation of an object's aspect ratio based on the frequency location of the quadrature peak (permeable case). Results are shown for a permeable cylinder and spheroid. [C6047]

"Multiyear remotely sensed data in support of monitoring, management and protection of the eastern Gulf of Finland coastal zone"

Satellite data sets, obtained from different sensors during 1996-2001 years, are used for coastal zone of the eastern Gulf of Finland study. The effectiveness of using satellite images for study of a change of ecological state of coastal and water environment, features of water dynamics, variability of concentration of total suspended matter, phytoplankton blooming and ice cover characteristics are shown. The results obtained are comparing with previous ones, for period since the middle 70s till the middle 90s. [C6048]

"Control factors of spectral reflectance in tidal flat: a case study in the Gomso Bay, Korea"

The objective of this study is to investigate the control factors of spectral reflectance and microwave scattering in tidal flat. The control factors are generally considered as grain size, soil moisture content, local slope, and creeks. We have carried out field data sampling in the Gomso Bay, Korea, including grain size, soil moisture content and its variation with time, surface roughness, ground levelling, and field spectral reflectance measurement. We have analyzed Landsat TM, EOS-Terra ASTER, RADARSAT, ERS-1/2, and JERS-1 SAR data. L- and C-band radar scattering modelling was also conducted. The results show that tidal condition and remnant surface water are important additional parameters. SWIR is shown to be correlated most with sediment grain size. The grain size of 0.0625 mm has normally been considered as a critical size of mud and sand discrimination. But we propose here that 0.25 mm is more practical grain size criterion in optic remote sensing. The radar scattering modelling show variation of less than 15 dB within the tidal flat, and L-band HV-polarization is turned out to be the best for tidal flat observation. The SAR data is also sensitive to the effective exposed area (EEA) effect. [C6049]

"The role of synergy in developing a marine SAR analysis and interpretation system"

The development of a Marine SAR Analysis and Interpretation System (MARSAIS) for application in the coastal zone is the objective of a current project, funded by the European Union. The system is aimed at the non-expert SAR user and integrates several state-of-the-art algorithms and multiple sensor synergy for quantitative interpretation of SAR data. In this work we focus on the part of the project that is concerned with the combined interpretation of SAR images and data from other sensors, and the ways in which this synergy improves our understanding of SAR monitoring of coastal processes. [C6050]

"A numerical study of the effects of realistic GPR antennas on the scattering characteristics from unexploded ordnances"

The detection and classification of unexploded ordnances (UXOs) is a difficult task, and it is even further complicated by the fact that the ground penetrating radar (GPR) antenna can significantly distort the scattering signal from the UXO. We consider the model of the real antenna which will be used in the numerical study of scattering from UXOs. We consider a rigorous finite difference time domain (FDTD) model of a fully polarimetric horn-fed bowtie (HFB) antenna and study how various modifications of the parameters of the antenna can affect its performance. [C6051]

"The dynamic monitoring and management of coastal zone with SAR remote sensing and fractal approach"

It is known that coastal zone and its environments are the complex and specialized areas. Synthetic aperture radar (SAR) with all weather is the powerful tools for monitoring the dynamic changes of those regions, and fractal approaches may be a good ideal technologies for managements on the unprecedented amount of information from the coastal spatial and temporal processes and remote sensing images etc. database. The needs of coastal dynamic monitoring are introduced at the first. The imaging mechanisms and the technologies as well as the example studies of SAR detecting coastal zone are described in detail. [C6052]

"The Scatterometer Climate Record Pathfinder"

While originally designed for ocean wind measurement, radar scatterometers have proven to be very effective in monitoring land cover and ice conditions and in climate studies. The NASA Scatterometer Climate Record Pathfinder (SCP) project has generated a unique climate data record from the series of historic and ongoing

scatterometer missions. Image data are archived from the Sea-Winds on QuikSCAT instrument, the scatterometer mode of the ERS-1/-2 AMI, the NASA Scatterometer (NSCAT), and the Seasat Scatterometer (SASS). In this paper we describe several SCP data sets and illustrate their application to studies of climate change over Greenland. [C6053]

"Computer vision applications to the study of sea-ice motion in Antarctica"

The motion of sea-ice in Antarctica is studied using QuikSCAT scatterometer imagery using methods from computer vision and image processing such as intensity edges and optical flow (OF). Features are computed as differential invariants based on spatial and temporal derivatives at various scales. The first estimates of the motion vector field obtained through optical flow are used as the starting point for a regularization scheme that imposes constraints that bring the estimate closer to feature tracking results and observed motion. Constraints from fluid dynamics are brought in by separating the motion field into its divergence free and rotational free components with another field obtained through a convex combination of these components. The advantages of this approach are that it produces a dense motion field that can be globally processed and locally adjusted to fit data and a model. This study complements the analysis of sea ice motion by application of wavelet theory. [C6054]

"Accurate classification of water area with fusion of RADARSAT and SPOT satellite imagery"

We fused RADARSAT images and SPOT panchromatic images by a wavelet transform in order to improve the accuracy of classification of water areas. Fused images not only maintained the characteristic of the SAR image (low pixel value) but also had improved boundary information. This leads to an accurate method to classify water areas. [C6055]

"Earth observation and case-based systems for flood risk management"

The case-based approach is presented through two of SERTIT's (Service Régional de Traitement d'Image et de Télédétection) major involvements in flood risk management. The first is operational crisis management action, contracted by ESA on the River Saône March 2001 flood. Archived and scheduled remote sensing data are used, leading to the delivery of rapid flood mapping products to the civil protection authorities. The second consists of research and development actions on well documented historical events. The case definition is based on the analysis of imagery products and environmental data, to both describe flood hazard and vulnerability. This approach stresses the synergy between landscape, its evolution and flood impact. Both optical and radar data are used in these two applications, with specified pre-processing levels. [C6056]

"High-resolution flood mapping from low-resolution passive microwave data"

We have developed a new method for making high-resolution flood extent maps (e.g. at the 30-100 m scale of digital elevation models) in real-time from low-resolution (20-70 km) passive microwave observations. Microwave radiometric measurements are useful for flood monitoring because they sense surface water in clear-or-cloudy conditions and can provide more timely data (e.g. compared to radars) from relatively wide swath widths and an increasing number of available platforms (DMSP, ADEOS-II, Terra, NPOESS). The chief disadvantages for flood mapping are the radiometers' low resolution and the need for local calibration of the relationship between radiances and open-water fraction. We present our method for transforming microwave sensor-scale open water fraction estimates into high-resolution flood extent maps and show several animated examples of the method in action during a retrospective study of the 1993 Great Midwest Flood. The method builds a "flood-potential" database from elevations and historic flood imagery and uses it to create a flood-extent map consistent with the observed open water fraction. We discuss the method's potential improvement through as yet unimplemented algorithm enhancements and expected advancements in microwave radiometry (e.g. improved resolution and atmospheric correction). [C6057]

"An iterative incidence angle normalization algorithm for sea ice SAR images"

For automated interpretation of the sea ice SAR data, the change in backscatter level due to the incidence angle variation should be taken into account. We have studied the statistics of the Radarsat ScanSAR Narrow data for sea ice, and developed an iterative algorithm for normalizing the data for automated interpretation of it. [C6058]

"Polarimetric C-band observations of soil moisture for pasture fields"

Soil moisture information is an important parameter in hydrological modelling, although providing reliable data is difficult due to its spatial variability and dynamic nature. The ability to estimate soil moisture from synthetic aperture radar (SAR) has been the topic of numerous investigations. To date, most of these investigations have

been limited to single or multiple linear polarized configurations. However, Radarsat-2 will be launched in 2004 and will have fully polarimetric C-Band SAR capability. In preparation for a new generation of spaceborne polarimetric SARs, Environment Canada's Convair 580 airborne polarimetric C-band SAR acquired data over an agricultural area west of Ottawa, Canada on September 22, 2000, April 26, 2001 and May 20, 2001. Coincident ground measurements (soil moisture, biomass, and surface roughness) were collected over pasture on all dates and bare fields in the spring of 2001. Analysis includes linear polarizations ($\sigma^{\circ}\text{HH}$, $\sigma^{\circ}\text{VV}$, $\sigma^{\circ}\text{HV}$), circular polarizations ($\sigma^{\circ}\text{RR}$, $\sigma^{\circ}\text{RL}$, $\sigma^{\circ}\text{LL}$), as well as fully polarimetric parameters such as pedestal height, total power, phase difference, and polarimetric signatures. This paper presents preliminary results of the September 22, 2002 data. [C6059]

"Model-based classification of polarimetric SAR sea ice data"

This paper discusses the role of scattering decomposition models in the classification of polarimetric SAR sea ice data. The iterative Wishart classifier was applied to 3-frequency airborne SAR data acquired in the Beaufort Sea, and the scattering models were found to be helpful in interpreting the assigned classes. In addition to using the full data set, reduced data sets based on an eigenvector decomposition were investigated for their potential for classification, as the eigenvectors provided a separation of scattering mechanisms. The surface scattering component was found to be the dominant one for this data set, and yielded a classification similar to the full data set. [C6060]

"Extracting sea ice parameters from SAR imagerettes"

From raw ERS wavemode data, complex SAR images of size 5 km \times 10 km-so called imagerettes-were computed using the BSAR processor at the German Aerospace Center (DLR). Being collected every 200 km along the orbit, imagerettes provide a relatively dense coverage especially over polar oceans up to 84 degrees North. Several statistical measures have been introduced for analysis of imagerettes classifying ice free and ice contaminated imagerettes as well as deriving sea ice parameters such as ice concentration, deformation energy, and ridge frequency. The results are compared to SSM/I data and sea ice model results. In addition, a wavelet-based edge detector is used to examine the ice surface structure. Using the imagerettes in an automatic extraction system can provide global statistics of sea state and sea ice parameters from both upcoming ENVISAT and historic ERS data providing a 10 year dataset. [C6061]

"Incidence angle dependence of the mean C-band HH-polarization backscattering signatures of the Baltic Sea ice"

RADARSAT ScanSAR Narrow images are currently utilized operationally by Finnish Ice Service to monitor Baltic Sea ice conditions. Automatic identification of different ice types and open water in the SAR images is studied by the Finnish Institute of Marine Research (FIMR). Successful implementation of the classification algorithms is complicated due to the significant changes in backscattering level and contrast caused by the large incidence angle variation (up to 20 degrees) in one ScanSAR image. To quantify and to compensate, at least partly, the effects of the incidence angle variation, we determine the incidence angle dependence of the mean backscattering coefficient (σ°) values of various Baltic Sea ice types using helicopter-borne scatterometer data and RADARSAT images. The results are also compared with theoretical backscattering models. [C6062]

"The ONERA RAMSES SAR system"

The ONERA RAMSES system (Radar Aeroporte Multi-spectral d'Etude des Signatures) is a flexible SAR system in constant evolution developed mainly as a test bench for new technologies and to provide specific data for TDMI (Target Detection, Recognition and Identification) algorithm evaluation. It is flown on a Transall C160 platform operated by the CEV (Centre d'Essais en Vol). This paper gives an overview of the system and its recent upgradings. [C6063]

"A phase unwrapping method based on minimum cost flows method in irregular network"

In the process of unwrapping phase images with high noise, traditional algorithms and derivative methods have many problems: for example, the error of noise region is transferred to other regions, and affects the extraction of useful information. In order to resolve this problem, we realize a phase unwrapping method on the minimum cost flows algorithm based on irregular network. This method is that low-quality phases are eliminated from interferogram and only high-quality phases are processed, so it can avoid the effect that low-quality are processed, so it can avoid the effect that low-quality regions make on high-quality ones, and assure phase unwrapping of the high-quality regions, then acquire good results. [C6064]

"High-resolution dual-bands interferometric and polarimetric airborne SAR (Pi-SAR) and its applications"

X- and L-band airborne SAR developed by CRL and NASDA has the capability of high resolution, polarimetry and cross-track interferometry. The radar has been operated since 1995 in the domestic area of Japan aiming at technical capability and validating for various applications. In this paper, we pick up the examples of the volcanic events to show the ability of the Pi-SAR. [C6065]

"MEMPHIS-a fully polarimetric experimental radar"

The MEMPHIS polarimetric SAR is able to operate simultaneously at X-, Ka and W-band. After a detailed technical description, several examples are given to demonstrate its capabilities in the side-looking mode, in forward squinted Doppler beam sharpening (DBS) mode and with across-track interferometry. Of great importance is the polarimetric calibration which is described in some detail. [C6066]

"Coastal imagery from the polarimetric airborne SAR PHARUS"

Polarimetric SAR imagery of a coastal scene is discussed, in terms of polarimetric and kinematic properties of waves on the sea and breaking waves in the surf zone. The coastal zone is a dynamic environment, and there is an increasing demand for monitoring it. Remote sensing can be an economic solution, and this paper explores some possibilities for extracting relevant coastal zone information from polarimetric SAR data. It focuses on the use of polarization for sea wave measurement, coast line determination, and estimation of surf zone parameters. While this work is based on airborne SAR, the results should also pertain to polarimetric satellite systems, especially as a steep incidence angle mode was used. When acquiring polarimetric data, a proper calibration is essential. As the use of dedicated calibration devices in the field is expensive, there is an interest in using scene parameters for calibration. The paper discusses some issues with this approach that arise in coastal areas. [C6067]

"Phase unwrapping by minimizing Kikuchi free energy"

Phase unwrapping in 2-dimensional topologies is an important problem that has several applications in radar and satellite imaging. The sum product algorithm (belief propagation) gives excellent results for the phase unwrapping problem. In this work, we present a gradient smoothing technique that uses higher order surface models to produce very smooth surfaces and report an improvement in the solution obtained. In a recent important work, Yedidia et. al have showed the theoretical connections between belief propagation algorithms and free energy in statistical physics. Based on this, we present a model that uses the Kikuchi technique to compute better posterior marginals than those produced by sum product algorithm. [C6068]

"A three-dimensional phase unwrapping algorithm for processing of multitemporal SAR interferometric measurements"

Phase unwrapping is the problem of reconstructing a function on a grid given its values modulo 2π . This is a key problem in SAR interferometry and in other fields. The typical availability of multiple 2D SAR interferograms of the same scene suggest the possibility of considering the data as samples of a function in a 3D space-time. This helps better reconstructing the right solution, in the same way as 2D phase unwrapping provides more reliable solutions than the 1D (quite trivial) algorithm. However, computational needs result increased in the 3D case. In this work we describe the proposed algorithm for 3D phase unwrapping, and show the results obtained on simulated and real SAR images. [C6069]

"Parameter estimation for the phase statistics in interferometric SAR"

In interferometric SAR applications, the complex coherence between two channels, ρ_{θ} , and the effective number of looks, n , are required to describe the joint channel statistics. Accurate modeling of the statistics is critical in the determination of Ground Moving Target Indication (GMTI) CFAR detection rules in along-track interferometry, and the estimation of topography accuracy in across-track interferometry. In this paper, we propose a method for estimating n and ρ based on the interferometric phase density function. We validate the robust, real-time implementable method with real SAR data in various types of terrain. Particularly, we show how the method can be extended to model the phase distribution even in extremely heterogeneous terrain. We show that the estimation relies only upon the multi-looked interferogram, without reference to the individual channels thereby reducing data storage requirements. [C6070]

"Use of scaling information for stochastic atmospheric absolute phase screen retrieval"

Scaling information is an important tool for the description of natural processes. Many applications of SAR (differential) interferometry lead to a set of sparse phase measurements, e.g. the monitoring of permanent scatterers. In this case, the atmospheric phase screen component of a given SAR image can be estimated over the PS sparse grid. Usually such data have to be unwrapped and then interpolated on a regular grid. We investigate the utility of the scaling information, valid for atmospheric phase screen data, in the process of unwrapping a set of sparse measurements. We show how the power-law behaviour of the data variogram can be used as an a priori constraint for optimization through techniques such as simulated annealing. The results are interpreted in view of operational applications to real data. [C6071]

"Maximum a posteriori height estimation in InSAR imaging"

A multi-frequencies maximum a posteriori (MAP) estimation of height profiles, from InSAR data, is presented in this paper. A quadratic MRF model is adopted to exploit a-priori information about the unknown image; the hyperparameter estimation, performed on a local basis, provides a powerful representation model for realistic height surfaces. The resulting MAP estimation is efficiently performed by a Metropolis version of the simulated annealing algorithm, and is able to reconstruct very discontinuous profiles. [C6072]

"Post-segmentation feature-based classification of synthetic aperture radar data"

Classification is one of the most important image analysis tasks as it provides image data with labels that transform it into information about the real world. In this research, classification of clutter in single and multichannel very high-resolution airborne SAR imagery is achieved by extending several classification methodologies to overcome limitations which exist when applied to SAR data. This is achieved by first pre-processing the data using segmentation techniques, then classifying the resulting regions using a number of features calculated over the regions. By attempting to classify regions as opposed to single pixels we can increase the dimensionality of the feature space even for single channel data, and overcome the problems of speckle and texture inherent in SAR imagery. Both supervised and unsupervised classification methodologies have been adapted to feature-based region classification. The methodology has been extended to multichannel data, specifically polarimetric data. Examples of the application of the proposed method are given for several very high-resolution data sets from the QinetiQ airborne SAR. It is concluded that the proposed approach provides a successful and flexible, sensor independent solution to the problem of classification of very high-resolution SAR data for many different applications. [C6073]

"Impacts of mobile radar and telecommunications systems on Earth remote sensing in the 22-27 GHz range"

The IEEE Geoscience and Remote Sensing Society (GRSS) Technical Committee on Frequency Allocation in Remote Sensing (FARS) is charged with providing recommendations and responses to queries on interference and frequency allocation issues in passive and active microwave remote sensing. In response to questions stemming from proposals to develop ultra-wideband (UWB) vehicular radar systems operating in the 22-27 GHz frequency range a technical assessment on the potential for radio frequency interference to passive Earth remote sensing activities was prepared. The study suggests that interference to the passive services at power levels several orders of magnitude above threshold levels is likely from commercial deployment of vehicular UWB radar and telecommunications systems. [C6074]

"Segmentation and classification of multitemporal data: methodology and results of a modified Gaussian Markov random field model classification system"

Constructive and destructive interference have long been a significant problem for the classification of radar imagery. Several authors have noted the ability of segmentation to work around the problem by incorporation of spatially adaptive filters and fuzzy logic. We present the methodology and results of such a study using multitemporal datasets in the place of multispectral data. For the study 27 standard and ScanSAR images were collected over the region from 1996 to 2001. The majority of the images were S4 ascending, with ScanSAR narrow collected simultaneously. The ScanSAR images allowed us to assess the methodology over a wider swath, yielding results on a regional rather than local scale. Northern Australia exhibits an extremely seasonal climate. The monsoonal nature of this climate means a huge variation in the amount of available water to plant life both on and surrounding the flood plains of the major river systems. Within this area is Kakadu National Park, a heritage listed and Ramsar identified wetland of international significance. Kakadu has a long history of scientific study, and is an ideal site on which to conduct studies such as this. The seasonal nature of this area presents a unique opportunity, that of a worst case scenario for classification schemes, whereby each location on the flood plain undergoes significant change over the seasonal cycle, similar in many respects to the change between bands of a multi-spectral dataset. A modified Gaussian Markov random field model segmentation

routine was used to cluster areas exhibiting similar radar response (both numerical and textural) at each successive date in the time series. For each date cluster statistics were then generated. This allowed the construction of temporal curves due to the fact that as the target material dries the material's dielectric constant decreases. As dielectric constant is significantly dependent on water content, these temporal curves act as a proxy measure for water availability, and hence aid in the discrimination of wetland from non-wetland areas and any change in size and location of these areas throughout the season. The output of the segmentation routine is a series of three bands. The first and second bands are the statistics (mean and standard deviation) of the original image and the third a vector file of the edge locations. By outputting statistical information instead of arbitrary segment number standard classification routines may be used successfully on radar imagery. Classification of the results of the segmentation may be either supervised or unsupervised, however analysis indicated that the Isodata algorithm adequately addressed classification needs. As a combined system the segmentation and classification system used in this paper has shown some excellent results when applied to multi-date radar imagery of Kakadu National Park in Northern Australia. Results for a segmentation of multitemporal radar dataset are presented alongside the results of the subsequent classification. By creating a system that requires minimal user input a wide variety of applications may be addressed. Indeed, the registration of the imagery becomes the most user intensive portion of the process. Automated routines such as this allow for analysis of large areas on a regular basis, an exceptional result for monitoring change and establishing baselines for later comparison. [C6075]

"Shoaling waves produced by offshore winds"

Directional spectra obtained from Doppler shifts mapped by a coherent, X-band, airborne radar show that offshore winds can produce shoaling waves on the same coastline. When wind blows offshore at an angle, the dominant wind wave does not propagate in the wind direction. Combined with refraction, this effect can produce shoaling waves. Data collected by the airborne radar are shown to be in good agreement with the JONSWAP parameterizations of dominant wave period and significant wave height. [C6076]

"Possible generation sites of internal solitary waves observed by ERS SAR in the central region of the Bay of Biscay"

We report on a set of remote sensing observations providing evidence that internal solitary waves (ISWs) observed in the central region of the Bay of Biscay can propagate not only in the NE-SW direction as described in earlier papers, but also in the SW-NE direction, that is, in the opposite direction. Analysis of over 30 ERS SAR images of the Bay of Biscay suggests new possible generation sites for internal waves (in a region comprising 43-46°N, 2-10°W). The investigation of the generation sites is based on maps produced from the SAR imagery and on regions of critical slopes of the local topography. The amplitudes and energies of the ISWs that propagate in the SW-NE direction are comparable with those generated locally in the central Bay (and travelling in the opposite direction) that have been studied before. [C6077]

"DOSAR: a multifrequency polarimetric and interferometric airborne SAR-system"

Presents the operational outlines of the multifrequency polarimetric airborne interferometric SAR system of the EADS/Dornier owned DOSAR. The simultaneous combination of full polarimetric with interferometric data makes it the only SAR system world-wide to collect cadastral information for mapping and land-use classification gathered within a single flight path. The DOSAR system is operational on a wide range of different aircraft. It is suitable for data collection for scientific, commercial and sovereignty as well as military applications. It has displayed its world-wide availability in a number of national flight campaigns in Germany as well as international applications in Austria, Switzerland, Indonesia and Thailand. Examples from these campaigns show the quality of high resolution SAR-data for mapping and classification. [C6078]

"EMISAR: a dual-frequency, polarimetric airborne SAR"

EMISAR is a fully polarimetric, dual frequency (L- and C-band) SAR system designed for remote sensing applications. The data are usually processed to 242 m resolution. The system has the capability of C-band cross-track single-pass interferometry and fully polarimetric repeat-pass interferometry. The SAR is operated at high altitudes on a Gulfstream G-3 jet aircraft. The system is very well calibrated and has low sidelobes and low cross-polar contamination. Digital technology has been utilized to realize a flexible and highly stable radar with variable resolution, swath width, and imaging geometry. Thermal control and several calibration loops have been built into the system to ensure system stability and absolute calibration. Accurately measured antenna gains and radiation patterns are included in the calibration. The processing system is developed to support data calibration, which is the key to most of the current applications. [C6079]

"The SAR-580 facility-system update"

Discusses the Environment Canada SAR-580 system: its capabilities, acquisition hardware upgrades, processing system advances and recent acquisitions. [C6080]

"Multi-channel SAR/MTI system development at FGAN: from AER to PAMIR"

An experimental platform for various investigations on multifunctional SAR and MTI, a four channel airborne X-band SAR with an active phased array antenna has been built up at FGAN, called 'AER' (airborne experimental radar). The system has been operating since 1995 via truck borne experiments and since 1996 via flight experiments. This system was useful in the past for evaluation of scientific work on several areas of signal and image processing. However, the demands to SAR systems increased over the last years. For this reason, FGAN is developing a new SAR system called PAMIR (phased array multifunctional imaging radar) as a successor of AER. PAMIR will offer a finer resolution, a longer range, a large scan flexibility and new modes compared to AER. [C6081]

"Review of the NASA/JPL airborne synthetic aperture radar system"

AIRSAR has served as a test-bed for both imaging radar techniques and radar technologies for over a decade. In fact, the polarimetric, cross-track interferometric, and along-track interferometric radar techniques were all developed using AIRSAR. We present the up-to-date system configuration, the expected performance and data accuracy in the standard radar modes. [C6082]

"Automated methods for atmospheric correction and fusion of multispectral satellite data for national monitoring"

The Earth Observation for Sustainable Development of Canada's forests (EOSD) project monitors Canada's forests from space. Canada contains ten-percent of the world's forests. Initial EOSD products are land cover, forest change, forest biomass, and automated methods. There are more than 500 LANDSAT TM or ETM+ scenes required for a single coverage of Canada's forests. Multi-temporal analysis using satellite data requires automation for conversion of these data to common units of exoatmospheric radiance or ground reflectance. During the next ten years the EOSD project will use a variety of Landsat optical and Radarsat sensors. A diverse set of ancillary and satellite data formats exist which require the development of adaptable data ingest and processing streams. Legacy LANDSAT TM and ETM+ data are available in a number of different formats from several national and US suppliers. In this paper, we present an automated system for managing processing streams for calibration and atmospheric correction of LANDSAT TM and ETM+ data to create data sets ready to analyze for EOSD products. Using known forest attributes from GIS data and field measurements, we validated our results of studies undertaken to assess spectral signal variability using both at-sensor radiance and ground reflectance for LANDSAT TM and ETM+ for a test site on Vancouver Island, BC. We present a strategy for correcting and fusing multi-source and multitemporal satellite data for meeting EOSD requirements. [C6083]

"Automatic registration of SAR and visible band remote sensing images"

Image registration is one of the basic image processing operations in remote sensing. With an increasing number of images collected every day from different sensors, automated registration of multi-sensor/multi-spectral images has become an important issue. A wide range of registration techniques exists for different types of applications and data sources, however no algorithm is known that can accurately register multi-source images consistently. This research addresses this problem by investigating the development of a fully automatic registration system for synthetic aperture radar (SAR) and optical remote sensing images. The development of this new automatic image registration method is based on the extraction and matching of common features that are visible in both images. The algorithm involves the following five steps: noise removal, edge extraction, edge linking pattern extraction and pattern matching. The application of the developed automatic image registration model to SAR and optical image pairs showed that accurate ground control points (GCPs) could be identified automatically. [C6084]

"Model function development for GPS reflection measurements"

Empirical model functions are derived for the retrieval of surface winds from the post-correlation waveform of scattered GPS signals. A geometric optics model is applied to generate model waveforms from the the surface slope probability density function (PDF). Batches of experimentally recorded waveforms are then processed to estimate parameters defining the PDF (ie., up-wind and cross-wind slope variances and the direction of the principal axes). A nonlinear least squares method is used to perform this estimation. Experimentally measured PDFs from this method are then compared with independent measurements of surface wind conditions obtained

from the TOPEX altimeter. Linear and a logarithmic forms are assumed for the functional dependence of apparent slope moments on wind speed. The coefficients of each of these functions are determined by weighted linear least squares. The limitations and uncertainty in these models are discussed. [C6085]

"Fresnel approximation for wave scattering in a random medium"

It is shown that the standard Fraunhofer diffraction approximation cannot be used in the problem of radiowave scattering by a distributed scatterer. The Fresnel approximation is developed for this problem. [C6086]

"Surface roughness estimation from GPS sea reflections"

The research reported in this paper was motivated by a Global Positioning System (GPS) data set collected by researchers at The Johns Hopkins University, Applied Physics Laboratory (JHU/APL) in May 1999. Raw GPS signal data were collected from an aircraft equipped with two downlooking antennas for receiving both left-hand circularly polarized (LHCP) and right-hand circularly-polarized (RHCP) GPS reflections from the ocean surface. Concurrent measurements of the local wind and wave conditions were collected from a nearby research vessel. The measured (LHCP) waveforms were similar to those already reported. The reflected RHCP waveforms were about 10 dB below those from the LHCP antenna. As far as we know, detection of the (depolarized) RHCP waveform has not been previously demonstrated. Models for GPS surface scattering based on geometrical optics or the Kirchhoff approximation predict a very weak depolarized return. We have recently developed a general bistatic scattering model that yields the proper cross section for both the specular and resonant (Bragg) scattering limits and also predicts depolarization for scattering out of the plane of incidence. Comparison of this scattering model with the cross section obtained by exact integration of Maxwell's equations shows good agreement even for relatively rough surfaces. [C6087]

"Bistatic WITTEX: an innovative constellation of radar altimeter satellites"

Describes a bistatic extension to the original WITTEX approach to oceanographic radar altimetry from space. An error analysis of the bistatic link shows that the system timing and height measurement strategy can be designed to retain accuracy comparable to that of nadir-sensing instruments. In a WITTEX constellation, two or more radar altimeter satellites are inserted from one launch vehicle into the same orbit plane. Earth rotation separates their respective surface tracks by distances that are proportional to the along-orbit spacing between the satellites. Monostatic altimeters on n spacecraft together with bistatic altimetric links between adjacent spacecraft generate $(2n-1)$ surface tracks of accurate height data in a bistatic WITTEX constellation. [C6088]

"HYDRO-POL-a spaceborne polarimetric radar-radiometer for land hydrology and ocean salinity"

Microwave sensors are of primary importance in mapping surface states and measuring some significant quantities which affect the hydrological cycle. A space mission aiming at monitoring soil moisture and surface salinity at a global scale is suggested. The mission is based on a combination of polarimetric active and passive microwave sensors. [C6089]

"ALTIKA3: a high-resolution ocean topography mission"

The paper presents the current status of the AltiKa3 mission and performance analysis. It mainly focuses on satellite and instrumental studies as phase B of the payload is currently going on. Apart from the combined altimeter and radiometer, this payload also consists of a DORIS plus LRA (Laser Retroreflector Array) orbitography system that will ensure a high level of accuracy in terms of orbitography and that will ease the connection of historical altimetry series within a common well surveyed geodetic reference frame. Feasibility of accommodating such a payload aboard a microsatellite platform has been shown and will be shortly introduced in the paper. [C6090]

"Interferometric SAR image coregistration based on the Fourier-Mellin invariant descriptor"

The problem of interferometric SAR image coregistration is addressed. For classical images, the application of the Symmetric Phase Only Matching Filtering (SPOMF) to the Fourier-Mellin Invariant (FMI) descriptors allows an accurate and efficient registration of translated, rotated and scaled images. This paper discusses an extension of the technique to cover the FMI descriptors of two interferometric SAR images. This method is tested on two pairs of InSAR data in France and Tunisia. The results are compared with those of classical cross-correlation registration techniques. [C6091]

"SAR images co-registration parallel implementation"

Image co-registration is basilar for interferometry SAR remote sensing applications. This paper describes a parallel implementation based on the Farm skeleton using the MPI library for the co-registration module of SAR Toolbox software. [C6092]

"A least-squares approach for long-term monitoring of deformations with differential SAR interferometry"

A least-squares (LS) approach is presented for the retrieval of a temporal deformation sequence from a database of interferometric SAR images. The method uses a database of interferograms, and by solving all the deformations as a unique least squares problem provides a chronologically ordered sequence, describing the development of the deformation pattern in time. The LS approach is illustrated in detail and discussed with respect to the results of its application on a test site. [C6093]

"Forward-backward iterative method for scattering by dielectric fractal surfaces"

The iterative forward-backward (FB) method is an efficient technique for numerical evaluation of scattering from perfectly conducting 1D rough surfaces. The method has been recently generalised to analyse scattering from dielectric 1D rough surfaces. In this paper the FB method for dielectric surfaces is framed within the theory of iterative methods for the solution of linear systems. In addition, application of the FB method to dielectric band-limited fractional Brownian motion (fBm) fractal surfaces is addressed. [C6094]

"Differential SAR interferometry using corner reflectors"

The differential InSAR technique has the potential for monitoring centimetre-scale ground motion in an accurate and cost-effective manner. Probably the most important limiting factor in the application of InSAR is temporal change in the complex reflectivity of the ground surface during the period between radar acquisitions. This can be due to changes in such parameters as moisture content or vegetation. The stable artificial corner reflectors can be identified from long temporal series of interferometric SAR images even with large baselines and therefore decrease the risk of image decorrelation. In this paper we will discuss the following questions: (1) how to get the true phase of a corner reflector in a SAR complex image; (2) how to co-register the corner reflector pixels, if the coherence of its surrounding area is extremely low; (3) how to computer the interferometric phase of two co-registered corner reflectors without flat Earth term and corners' height contribution. In order to demonstrate the results some practical examples Bonn-Experiment and landslide monitoring in Three Gorges area in China are given. [C6095]

"A new algorithm for monitoring localized deformation phenomena based on small baseline differential SAR interferograms"

This paper presents a new solution for detecting and following the temporal evolution of small scale deformation phenomena; in particular our approach extends the capability of the SBAS technique, presented in P. Berardino et al. (2001), which is mainly focused on investigating large scale deformations with spatial resolutions of about 100 m \times 100 m. The proposed technique relies on small baseline differential SAR (DIFSAR) interferograms only, but it is implemented by using two different sets of data generated at low (multi-look data) and high spatial resolution (single-look data), respectively. The former are used to identify and estimate, via the SBAS technique or O. Mora et al. (2001, 2002), possible atmospheric phase artifacts and large scale deformation patterns; the latter to detect, on the high resolution residual phase components, structures highly coherent in time (buildings, rocks, lava structures, etc.), identified jointly to their heights and displacements. In particular the estimation of the temporal evolution of these local deformations is easily implemented by applying the SVD technique. The presented algorithm has been tested with data acquired by the European Remote Sensing (ERS) satellites relative to the Campania area (Italy). [C6096]

"Blind source separation applied to multitemporal series of differential SAR interferograms"

Introduces the concepts of blind source separation and independent component analysis. We show how they can be applied to the automatic estimation of ground subsidence and atmospheric disturbances on a series of interferograms. Finally we show some results obtained on realistic simulated data which demonstrate the advantages of this approach. [C6097]

"Backscattering behavior of a cloddy soil surface"

This paper presents a numerical computation of backscattering signal over simulated cloddy soil surfaces. A new generation approach of this type of surfaces with Monte Carlo method is proposed. The moment method is used to compute backscattering for these surfaces. The horizontal and vertical polarisation simulation levels and

comparison with IEM model are discussed. [C6098]

"Diffractive analysis of backscatter from wave-crest-like objects"

The backscattering from surface profiles approximating the crests of steep water waves has been modeled using diffraction theory. The diffractive backscattering from rounded-apex wedges is due to diffraction from curvature discontinuities, and can be predicted with apex radii as small as one-third of a wavelength using standard diffraction coefficients provided that heuristic corrections are applied to account for the small radii and finite surface conductivity. The same diffraction theory can also be used to model the backscattering from surfaces that approximate the early formation of a jet on a breaking crest, although accuracy is a bit poorer when the crest-feature radii are one-third wavelength. This confirms that the limitations found in a previous study are due to the limitations of the model itself, and not due to the averaging of surface curvatures that were needed to allow the application of the model. [C6099]

"Bound wave effects in microwave and acoustic backscatter from rough water surfaces"

Simultaneous backscattering measurements with radar and sonar in the large wind wave facility in Marseilles, France shows that bound and free waves coexist on the water surface. By observing the surface from above and below, we were able to show definitively that the bound waves ride on the front face of the dominant wave in the tank. Because of the large width of the tank, we were able to vary the azimuth angle of both the radar and sonar, which viewed a common surface area, and observe the dependence of both free and bound waves on azimuth angle. [C6100]

"Numerical study of frequency and polarimetric dependence of the emissivities and backscattering coefficients of soil based on three dimensional Monte-Carlo simulation of Maxwell equations"

The backscattering coefficient and emissivity of wet soil surface are studied with the 3-dimensional numerical simulations. The study is focused on the angular, frequency, and polarimetric dependence of the scattering and emission. The simulation results are compared with the experimental measurements from real-life soil surface for backscattering coefficients at L and C frequency bands and at the multi-incidence angles. The fairly good agreements are observed for the fixed physical surface roughness parameters at two frequency bands. [C6101]

"Implementation of the higher order small slope approximation for scattering from a Gaussian rough surface"

Computation of the higher-order small slope approximation (SSA) for electromagnetic scattering from a penetrable randomly rough surface is discussed, under the assumption of a Gaussian random process with an isotropic Gaussian correlation function. A simplified form for the first correction to the lowest order SSA theory is presented, and sample results illustrated to investigate the parameter space under which the first correction is appreciable. Reduction of the higher-order SSA to the physical optics approximation limit is also discussed for both perfectly-conducting and dielectric surfaces. [C6102]

"RADARSAT-2; are its technical capabilities expected to provide potential for remote sensing applications ?"

In this paper, we preview and demonstrate how the technical improvements included in RADARSAT-2 will impact the system's potential utility for 32 applications in the fields of agriculture, cartography, disaster management, forestry, geology, hydrology, oceans, and sea and land ice. [C6103]

"The sensitivity of C-band polarimetric SAR to crop condition"

The Canada Centre for Remote Sensing conducted an intensive field campaign in 2000 at an agricultural test site at Indian Head, Saskatchewan (Canada). Airborne C-band fully polarimetric SAR data were acquired over the site. The supporting ground information is being used to establish the sensitivity of several polarimetric parameters to variations in crop condition. Preliminary results suggest that several polarizations are sensitive to variations in crop growth and crop stress, particularly in small grain crops like wheat. Information on crop growth gathered from sensors, like RADARSAT-2, could aid in strategies to better manage nutrient applications on agricultural fields. [C6104]

"RADARSAT-2 antenna calibration using Ground Receivers/Transmitters"

The RADARSAT-2 antenna is an active phased array of 512 T/R modules. In order to characterize the physical distortions and the amplitude and phase errors across the antenna array, it is planned to perform measurements

using the radar in conjunction with a unit on the ground for receiving and recording signals from the satellite, and for generating signals and transmitting them towards the satellite. This unit is referred to as a Ground Receiver/Transmitter. This paper will describe the method of operation of the satellite with the Ground Receiver/Transmitter, the design of the Ground Receiver/Transmitter, and the algorithms to be used to analyze the Ground Receiver/Transmitter data. [C6105]

"Shape preserving edge enhancement in remote sensing imagery"

A novel approach to geometric shape preservation of remote sensing SAR sea ice images is presented in this paper. This approach will complement the existing edge detection schemes. The final edge is evolved by iterations. During each iteration all existing edges are checked for missing link and missing links are found by checking the orientation of the existing edges and by searching for best gradient path. When open edges are reduced considerably, opening of the features that are critical for shape preservation are found by tracing the edges and closing the boundary. [C6106]

"RADARSAT-2 program update"

RADARSAT-2, scheduled for launch in 2004, will be the next Canadian commercial Earth observation SAR satellite. This paper presents an overview of the mission, some featured innovations, and the imaging capabilities. [C6107]

"Radar options for global earthquake monitoring"

Fine temporal sampling is essential for disaster management, e.g. of flooding, fires, landslides, hurricanes, and earthquakes. A powerful technique for mapping such natural hazards is synthetic aperture radar (SAR) interferometry, providing displacement measurements at the subwavelength scale and decorrelation estimates. Pre-seismic deformation, one of the most elusive aspects of earthquakes, will require much finer temporal sampling than present InSAR capabilities provide. Observations taken every few hours could provide time series data of rapidly evolving phenomena, such as pre-eruptive volcano dynamics, leading to major advances in predictive capability, improving the potential for modeling as well as for civil protection. Such radical performance improvements could be attained through large constellations of conventional low Earth orbit (LEO) satellites or small constellations of geosynchronous SARs. The unique capability of a geosynchronous SAR in terms of instantaneously accessible area is contrasted with the requirements for huge electronically steered array (ESA) antennas. The optimal approach is very much dependant on technological developments, in particular geosynchronous SAR depends on the development of affordable very large ESA antennas, but also other technological developments will be required. [C6108]

"Realtime storm surge measurement with a scanning radar altimeter"

The NASA Scanning Radar Altimeter (SRA) was designed primarily to measure the energetic portion of the directional wave spectrum by generating a topographic map of the sea surface. The SRA sweeps a radar beam of 1° (two-way) half-power width across the aircraft ground track over a swath equal to 0.8 of the aircraft height, simultaneously measuring the backscattered power at its 36 GHz (8.3 mm) operating frequency and the range to the sea surface at 64 positions at 0.7 incidence angle intervals. The maximum scan rate was 8 Hz during the Hurricane Bonnie flights, but it is presently 10 Hz. In realtime, the slant ranges are multiplied by the cosine of the off-nadir incidence angles (including the effect of aircraft roll attitude) to determine the vertical distances from the aircraft to the sea surface. These distances are subtracted from the aircraft height to produce a sea-surface elevation map which is displayed on a monitor in the aircraft to enable realtime assessments of data quality and wave properties. On 24 August 1998, the SRA, aboard a NOAA hurricane research aircraft, provided the first documentation of the directional wave spectrum throughout a hurricane in open water when Hurricane Bonnie was about 400 km east of Abaco Island, Bahamas. On 26 August 1998, the SRA provided the first documentation of the directional wave spectrum throughout a hurricane making landfall as Bonnie was approaching Wilmington, North Carolina. [C6109]

"InSAR end-to-end simulation environment"

Describes the concept, design and implementation of the "InSAR-Sim", an end-to-end simulation environment being developed for evaluating InSAR tandem satellite missions at RADARSAT-2 Project Management Office, Canadian Space Agency. [C6110]

"Turning the scientifically possible into the operationally practical: RADARSAT-2 polarimetry applications"

RADARSAT-2, planned for a late 2003 launch, is an advanced SAR satellite. Key features of RADARSAT-2 are high resolution (3 m), polarimetry modes, enhanced ground system providing rapid satellite tasking and near-real time data processing, improved image location accuracy, and on-board solid state recorders. RADARSAT-2 offers three polarimetric modes: (1) selective polarization providing one co-pol channel (HH or VV) and the corresponding cross-pol channel (HV); (2) high resolution (3 m) single pol channel (HH or VV); and (3) a fully polarimetric mode providing both amplitude and phase. The fully polarimetric mode is significant since RADARSAT-2 is the first commercial satellite to offer this mode. The commercial focus of the RADARSAT-2 mission dictates the development of operational applications, and ultimately the extraction of information from the SAR data. [C6111]

"The RADARSAT-2&3 topographic mission: an overview"

The Canadian Space Agency and MacDonald Dettwiler are jointly conducting a study to define the mission capabilities and the operational performance of a RADARSAT-2/3 tandem interferometric mission. The primary objective of the mission is to provide a global digital elevation model of the Earth with quality comparable to the emerging US National Imaging and Mapping Agency High Resolution Terrain Information Level 3 (HRTI-3) specification; approximately 2 m relative height accuracy (90% LE) and 10 m nominal post spacing. The initial phase of the study identified a set of required modifications to the RADARSAT-2 spacecraft to support the tandem interferometric mission. These modifications have already been included in the design of the RADARSAT-2 spacecraft that is currently in Phase C/D of development and is scheduled for launch by the end of 2003. The RADARSAT-3 spacecraft would be a copy of RADARSAT-2 and be launched two years after to maximize the window of opportunity for the tandem mission. The two spacecraft would be flown with a separation of a few kilometres to gather interferometric data in a simultaneous monostatic and bistatic (SiMB-static) mode. At the end of the interferometric mission, the two spacecraft would be set apart to maximize the coverage of the combined system. This paper gives an overview of the tandem mission, and presents a summary of technical investigations carried out by MacDonald Dettwiler on the operating mode, the performance assessment, the orbit definition and the interferometric processing. [C6112]

"LITE aerosol retrievals revisited in support of CALIPSO and GLAS"

The Lidar In-space Technology Experiment (LITE) shuttle mission demonstrated that spaceborne lidar offers an effective means for detecting the spatial features of significant regional aerosol concentrations resulting, for example, from Saharan dust, African and South American biomass burning, urban plumes and the like. Quantitative retrievals of aerosol backscatter and extinction profiles have also been obtained from the LITE 532 nm data using initial LITE calibrations and preliminary assumptions/modeling constraints regarding the aerosol extinction-to-backscatter ratio, S_a , or auxiliary transmittance information. Two upcoming satellite lidar missions, GLAS (Geoscience Laser Altimeter System) and CALIPSO (Cloud-Aerosol Lidar and Infrared Pathfinder Satellite Observations) have provided impetus for continued analysis of LITE data as a testbed for developing and validating improved aerosol retrieval approaches for these satellite missions. This paper presents updated LITE aerosol retrievals, including uncertainty assessments, enabled by revised calibration approaches (including the 1064 nm channel) and techniques/models for reducing the range in S_a values assumed for the retrievals. [C6113]

"High pulse repetition rate, eye safe, visible wavelength lidar systems: Design, results and potential"

In 1993 the first of the eye safe visible wavelength lidar systems known now as Micro Pulse Lidar (MPL) became operational. Since that time there have been several dozen of these systems produced and applied for full time profiling of atmospheric cloud and aerosol structure. There is currently an observational network of MPL sites to support global climate research. In the course of application of these instruments there have been significant improvements in understanding, design and performance of the systems. There are additional potential and applications beyond current practice for the high repetition rate, eye safe designs. The MPL network and the current capability, design and future potential of MPL systems are described. [C6114]

"An overview of the GLAS real-time atmospheric processing algorithms and results from the analysis of simulated GLAS data sets"

A new era in atmospheric remote sensing is about to begin. Global monitoring of clouds and aerosols from space using a backscatter lidar system will greatly add to our knowledge in areas such as polar cloud climatology, aerosol loading and transport, and the planetary boundary layer. The Geoscience Laser Altimeter System (GLAS) will produce nearly 5 GB of data per day. A challenge is to create autonomous algorithms that will analyze the data in near-real time. This paper briefly discusses the algorithms and presents results of testing with simulated GLAS data sets. [C6115]

"Plans for Global Precipitation Measurement ground validation"

This paper introduces plans for ground validation (GV) for the Global Precipitation Measurement. At NASA's request, a Ground Validation Working Group, formed from the meteorological and hydrological communities, is recommending plans to guide the GV program. Ground validation efforts will commence as early as 2003 with the Spring 2003 Pilot Experiment and described herein. The Pilot Experiment is focused on mitigating engineering and scientific risk to the GPM program and, in particular, to the ground validation program. [C6116]

"Cloud Physics Lidar optical measurements during the SAFARI-2000 field campaign"

In this presentation, we will show new optical data processing results from the Cloud Physics Lidar during SAFARI-2000. Retrieved products include aerosol and cloud layer location and identification, layer optical depths, vertical extinction profiles, and extinction-to-backscatter (S) ratios for 532 and 1064 nm. The retrievals will focus on the persistent and smoky planetary boundary layer and occasional elevated aerosol layers found in southern Africa during August and September 2000. [C6117]

"Temporal soil moisture estimation of pastures from Radarsat data for applications in watershed modelling"

Estimating the amount of water stored in a soil profile is essential in most water management projects and for assessing the hydrologic state of a basin. It determines infiltration during a rainfall event and controls evapotranspiration between storms. Rarely, however, are soil moisture data available for model input. In many cases, particularly watershed scale monitoring or modelling, soil moisture is inferred from more easily obtainable hydrologic variables such as rainfall, runoff and temperature. As such, there is a strong need for procedures to estimate soil moisture in a watershed independently from the models. These procedures must provide not only basin average estimates but also the spatial distribution within a basin in order to meet the requirements of emerging distributed models. Active and passive microwave imagery are both candidate sources for these data. Active SAR imagery, with its high resolution, is particularly attractive for use in areas of mixed land cover. This paper addresses the potential of Radarsat to extract information on soil moisture in pastures in a mixed landcover watershed located in eastern Ontario, Canada. A series of 6 Radarsat Standard Beam Mode 1 images covering the watershed for the period of September 2000 through July 2001 were analyzed in relation to ground observations, weather radar and meteorological conditions. A method was then developed to produce soil moisture maps for input to a hydrological model. [C6118]

"Minimum distance texture classification of SAR images using wavelet packets"

A multi-scale texture segmentation algorithm for SAR images based on the discrete wavelet transform is presented. Responses from different sub-bands are used to form a feature vector for each pixel position that is the input to the classification scheme. To further improve the classification results, the tree-structured wavelet packet transform is used to automatically identify a suitable sub-set of elements from the feature vector. Results show that this approach is effective for both the redundant and non-redundant wavelet transforms. [C6119]

"The global soil moisture archive 1992-2000 from ERS scatterometer data: first results"

Soil moisture is a key variable in a number of geophysical and ecological processes. Despite its importance, availability of information on soil moisture is limited. Only recently it could be demonstrated that low resolution radar data in combination with a change detection method can resolve this constraint. Experience gained in a number of successful pilot projects, lead to an initiative, setting up a global soil moisture archive. [C6120]

"Classification of LIDAR data using a lower envelope follower and gradient-based operator"

A new, computationally efficient classification methodology was developed and implemented to classify Light Detection and Ranging (LIDAR) data as ground, vegetation, and man-made features (Weed 2001). The new procedure consists of several components that create ground, vegetation, and building surfaces, which are then used to classify the first and last reflection of each laser pulse. Ground and non-ground data are classified by adapting the concept of a lower envelope follower used to recover information in an amplitude modulated (AM) signal to the problem of extracting the ground surface from the LIDAR signal. The detected ground points include bare surface pixels and locations where the laser was able to penetrate the vegetation canopy, but exclude buildings and vegetation. Buildings are then classified by detecting the extended low gradient regions on their roofs. The first return LIDAR data points are used to accurately detect building edges distorted by multi-path errors in the last return LIDAR data. The combined roof and edge surfaces are then employed to threshold the first and last return LIDAR height values and detect the LIDAR points reflecting from buildings. Once the building

points are classified, the vegetation points are extracted from the remaining LIDAR points using a mask of the regions where there were significant differences in the first and last return of the laser pulse. The technique is robust for classifying LIDAR data acquired over a range of terrains with different vegetation cover and types and sizes of buildings. It requires minimal user intervention for parameter selection. [C6121]

"Modeling lidar and radar returns of forest canopies for data fusion"

Radar backscatter and lidar waveform models, which are based upon a common three-dimensional forest stand structure, are parameterized using realistic forest physical stands to produce a dataset of forest structural parameters and lidar/radar responses. This paper briefly describes some preliminary results in the studies of the sensitivities of models to forest spatial structure, the relationship between radar backscattering and the lidar measurements for various forest stands, and the potential of radar and lidar data fusion for forest structure characterization and biophysical parameter estimation. [C6122]

"Mapping of snow covered area with Radarsat in Norway"

Estimates of snow cover area (SCA) can be obtained from spaceborne SAR sensors such as ERS, Radarsat and Envisat ASAR. A number of algorithms using backscattering images and interferometric coherence have been proposed and documented. It has also been shown that multifrequency and polarization SAR instruments gives enhanced snow mapping capabilities. In this paper we suggest improvements to the Nagler SCA-algorithm and apply them to Radarsat data in the Norwegian mountains. The effect of reduced backscattering due to increased incidence angle is discussed. The effect of mixed pixels (wet snow and other constituents) is addressed, and a sub-pixel method for snow classification is suggested. We also suggest classifying snow on lakes and in forests with different algorithms and separate masks, since the backscattering properties vary from class to class. Finally we try to assess the classification errors by statistical methods. [C6123]

"Monitoring seasonal dynamics of Northern Australian wetlands with multitemporal Radarsat data"

Northern Australia exhibits an extremely seasonal climate and this is reflected in the change in vegetation communities present in a given area of wetland. The monsoonal nature of this climate means a huge variation in the amount of water available to plant life both on and surrounding the floodplains of the major river systems. Kakadu National Park, a heritage listed and Ramsar identified wetland of international significance, has a long history of scientific study an ideal study site on which to conduct studies such as this. Changes within the wetland areas in the park have been noted since the early 1980s, but have been poorly quantified. Many of the changes are related to the timing of the onset of the monsoon, the period of inundation and the location of the major flooding. However neither multispectral or hyperspectral sensors are able to capture information at the onset of the monsoon due to perpetual cloud coverage. Radar has the unique ability to image through cloud and hence 27 Standard and ScanSAR images were collected over the region from 1996 to 2001. The majority of the images were S4 ascending, with ScanSAR narrow collected simultaneously. The images were co-registered allowing comparison of the same geographic location through time. The simultaneous ScanSAR images allowed assessment of the technique over a wider swath, yielding results on a regional rather than local scale. Radar reflection is intimately related to the moisture content of the target due to the influence of moisture upon the dielectric constant. A modified Gaussian Markov Random Field Model Segmentation was used to cluster areas exhibiting similar radar response at each successive date in the time series. The ability to segment and extract reflection statistics for the same geographic location for each image in the series allows the construction of temporal curves, indicating change in the target material's dielectric constant over time. [C6124]

"RADARSAT-1 image quality/continuing success in extended mission"

RADARSAT-1, the first Canadian SAR remote sensing satellite has successfully completed its design lifetime of five and a quarter years. It is in an extended mission operation meeting customer demands. The Image Quality Control program is kept fully operational. Measured results indicate that image quality performance continues to be better than system specification. This paper briefly describes image quality and recalibration work and measured results. [C6125]

"Use of RADARSAT-1 images to map forest fuel moisture over boreal forests"

Our study analyzed eleven RADARSAT-1 images acquired over burned and unburned boreal forests in June 2000 in order to assess their potential to map fire danger variables, like the CFFDRS FWI codes and indices. RADARSAT-1 can acquire images almost daily, but the acquisition is done under different beam modes. Fine beam mode images produced highly variable low radar backscatters. Incidence angles had a predominant effect in the day-to-day σ^0 variations, but these variations were also explained by rain events and by FWI variations. It is suggested that RADARSAT-1 radar backscatters are sensitive to moisture-related variables, but there is

necessary to either correct the images for incidence angle effects or to only consider images acquiring in similar beam modes. [C6126]

"Understanding and responding to earthquake hazards"

Understanding the earthquake cycle and assessing earthquake hazards is a topic of both increasing potential for scientific advancement and social urgency. A large portion of the world's population inhabits seismically-active regions, including the megacities of Los Angeles and Mexico City, and heavily populated regions in Asia. Population growth will exacerbate the potential for huge earthquake-related casualties. However, powerful new tools to observe tectonic deformation have been developed and are being deployed with encouraging results for improving knowledge of fault system behavior and earthquake hazards. In the future, the coupling of complex numerical models and orders of magnitude increase in observing power promises to lead to accurate targeted, short-term earthquake forecasting. Dynamic earthquake hazard assessments resolved for a range of spatial scales (large and small fault systems) and time scales (months to decades) will allow a more systematic approach to prioritizing the retrofitting of vulnerable structures, relocating populations at risk, protecting lifelines, preparing for disasters, and educating the public. The suite of spaceborne observations needed to achieve this vision has been studied, and the derived requirements have defined a set of mission architectures and enabling technologies that will accelerate progress in achieving the goal of improved earthquake hazard assessments.

[C6127]

"RADARSAT-1 Background Mission global coverage"

RADARSAT-1 Background Mission signifies baseline acquisitions of the satellite for building various site, time and application-specific data archives. The archives are to be considered benchmarks for global change studies and can be used in such applications as terrain mapping with radargrammetry and interferometry. These acquisitions were part of several coverage types that were undertaken over the past six years of the satellite operations. The variety of coverage is the result of the satellite's variable imaging modes, such as viewing angle, ground resolution, swath width, etc. Early ScanSAR beam coverage provided snapshots of large surfaces of the Earth. A RADARSAT beam-pair stereo coverage of the world's landmass is nearing completion. Remote oceanic islands were imaged successively to build multi-seasonal and multi-annual data sets for change detection. RADARSAT Fine beam resolution data were collected over most of the major cities of the world. Data acquisitions during the left-looking mode of operations of the satellite focused on the regions considered important in terms of geoscience applications. In the fall of 2000, the Canadian Space Agency improved RADARSAT-1 orbit maintenance for Fine beam interferometry over Antarctica. The opportunity was availed to collect similar data over Canada, Greenland, Iceland and some other ice capped regions of the world. These data acquisition campaigns are referred to in the following account on the status of RADARSAT-1 Background Mission. [C6128]

"RADARSAT ScanSAR roll angle estimation"

Wide-swath SAR imagery obtained by the RADARSAT ScanSAR mode can suffer from radiometric artifacts. These artifacts arise from improper application of Range Dependent Gain Corrections (RDGCs), mainly due to insufficient knowledge of the satellite's roll angle. Specifically, roll angle estimation errors as small as 0.1 degrees can cause noticeable gain errors of 1 dB or more. Beam-stitching techniques exist which can reduce, but not eliminate, these errors in the beam overlap region. Current roll angle estimation algorithms do not consistently provide adequate results. These algorithms are susceptible to RDGC uncertainties in terms of pattern shape and gain offsets. This paper proposes a new data acquisition method, in which signal data is obtained during the beam switchover by transmitting pulses through one beam and receiving them with another beam. This "2-beam data" is then used in a modified algorithm to provide a more accurate and robust roll estimate. The logistics of acquiring 2-beam data are also explored. The effects of various roll angle estimation errors on different beam combinations are simulated. The algorithm results from a current and two proposed algorithms are compared. Algorithms using this 2-beam data can tolerate an overall lower mean scene σ and more RDGC uncertainty than standard data. [C6129]

"SRTM X-SAR DEM of Europe-Results and algorithmic improvements"

In February 2000, the Shuttle Radar Topography Mission acquired a global digital elevation model (DEM) within only 11 days. During the years 2000 and 2001 extensive testing and calibration activities primarily based on ocean surface data took place at DLR. The calibration phase is now finished and the quality of the products analyzed so far met all specifications. The routine processing of the German X-band data at DLR began in November 2001, starting with Europe. Now, that hundreds of image frames over Europe are being processed and mosaicked to a continent-wide DEM, the largescale system stability becomes visible. Our paper reports the

experiences from mosaicking based on self-consistency tests and on comparison with independent reference data. While the overall quality is promising, there are still some outliers to be investigated and compensated. The calibration concept based on the use of ocean data will be presented and discussed. Adaptations and improvements based on self-consistency will be presented, that allow a more robust and automated processing.

[C6130]

"RADARSAT Geophysical Processor System: 2 years of production"

The RADARSAT Geophysical Processing System has been processing geophysical data products at ASF and JPL since 1999. The RGPS data products provide an opportunity to improve our understanding of a myriad of processes that affect climate by generating a range of products over the Arctic at 3- and 6 day intervals. These processes include mass balance, heat transfer and momentum transfer between the Arctic Ocean and atmosphere. The RGPS Team is presently processing data acquired by RADARSAT during the winter of 1998-1999 for the seasonal ice zone and the Barents Sea. Data products from other seasons for the Arctic Basin are currently available on the web. We will summarize the some results from the products generated by the ASF RGPS and describe availability of this data set to the general community. [C6131]

"The use of RADARSAT-1 SAR data for operational wind field retrieval"

A key parameter necessary for interpreting radar images of marine areas is surface wind speed. Knowledge of the wind speed during and after data acquisition can aid significantly with the image interpretation for applications such as oil slick detection and ship detection. In collaboration with PEMEX Exploration and Production, RADARSAT-1 Wide mode images were used to evaluate wind retrieval. The CMOD_IFR2 model was used for wind field extraction. Based on analysis of the six RADARSAT-1 images, the mean difference between the buoy wind speed and the (mean) SAR-derived wind speed is 2.4 m/s and the mean difference between the buoy wind direction and the SAR-derived wind direction is about 50°. PEMEX is planning to use the SAR-derived wind data to aid in SAR-based ship detection and oil slick detection. From an operational perspective, it is important to note that SAR-derived wind fields do not require additional imagery, since the wind information can be extracted from the same set of images that are used for ship and oil spill detection. [C6132]

"Validation of sea ice signatures in radarsat ScanSAR imagery for the Gulf of St. Lawrence"

Sea ice thickness and ice surface roughness profiles were collected over many tens of kilometers in the Gulf of St. Lawrence, Canada with a helicopter-borne electromagnetic (HEM) system containing a laser altimeter. The profiles are compared with RADARSAT ScanSAR Wide images, and digital video images captured in real-time using a downward-looking video camera mounted on the outside of the helicopter. A survey done in early March, 2001 sampled many different ice conditions, including heavily ridged coastal ice, large rough floes, rafted nilas, and brash ice near the ice edge. Near the north coast of PEI in 2001, there were large quantities of thick ice due to ridging of grey-white or thin first-year ice. However, high SAR backscatter was associated with floes that had a rough surface on scales of a few meters or less. [C6133]

"Sensor and data fusion contest: test imagery to compare and combine airborne SAR and optical sensors for mapping"

Presently, a data fusion contest is conducted to compare the potential of airborne SAR with optical sensors for mapping applications. The goal of the test is to answer two questions: (1) Can state-of-the-art airborne SAR compete with optical sensors in the mapping domain? (2) What can be gained when SAR and optical images are used in combination, i.e., when methods for information fusion are applied? The test is organized in the framework of the IEEE GRSS data fusion technical committee (DFC), ISPRS working group III/6 "Multi-Source Vision", which both have strong relations with scientists, active in research on sensor fusion and automation in mapping, and-as the provider of the main organizational framework-the European Organization for Experimental Photogrammetric Research (OEEPE), which is the European research platform of national mapping agencies and other institutions, regarding technology developments to optimize the use of core data in a geoinformation infrastructure context. In the preparatory phase of the test, which has been started on the occasion of IGARSS 2001, test data has been collected and the scope of object extraction for mapping has been defined. The outcome of this phase, i.e. the test imagery to be used in the contest and its potential for mapping is presented in this paper. [C6134]

"Extraction and fusion of street networks from fine resolution SAR data"

This paper deals with a feature fusion technique, especially implemented to characterize street networks extracted from multiple SAR images. The fusion approach may be useful in a number of ways: when applying different road extractors to the same data set, when using different pre-processing algorithms before applying the

same road extractor to the same data set, or finally when applying the same road extractor to more images of the same area. The proposed approach applies "AND" and "OR" rules to the street nets to be compared. These operators are either hard or fuzzy ones, according to the way these networks were obtained. Therefore, the method is able to maintain the fuzzy reliability indicators obtained by fuzzy street extraction algorithms, but also to deal with differently classified segments and paths. We show through some examples how the proposed technique improves the results with respect to the "before fusion" street networks, and we also discuss future developments. [C6135]

"Improving feature extraction in satellite SAR images by an interactive fuzzy fusion of multi-temporal data"

This paper presents a method based on fuzzy fusion to improve feature extraction in satellite SAR images. Two road detectors are applied on SAR images and their output is merged interactively. Experimental results are presented with ERS1/2 SAR images in different configurations including ascending/descending orbits and georeferenced images. [C6136]

"Radar estimation of turbulence eddy dissipation rate in rain"

This paper deals with the algorithm for estimating the turbulence intensity in rain, which is developed on the basis of the model of Doppler-polarimetric spectra of radar signals, reflected from turbulent zones in precipitation. The relationship between the Doppler spectrum width of rain and the eddy dissipation rate is established at two orthogonal polarizations. The approximation of this relationship by Weibull model provides mathematical convenience for further analysis and synthesis. An algorithm for the estimation of turbulence intensity is developed on the basis of modeled and measured Doppler-polarimetric data. This algorithm is researched by statistical simulation. It is shown that the Doppler-polarimetric approach provides an accuracy increase in comparison with the Doppler method without polarization information. [C6137]

"Multiscale fusion of INSAR data for improved topographic mapping"

INSAR data from the ERS-1/2 platforms are combined with multiple sets of data acquired by the NASA/JPL TOPSAR platform to obtain statistically optimal high-resolution estimates of topography over the Finke River Gorge in central Australia. The INSAR data are fused using a multiscale Kalman smoother. The estimated topography preserves the spatial resolution of the TOPSAR data while smoothing noise and providing estimates where there was no TOPSAR coverage. It is shown that the estimation error associated with the multiscale Kalman smoother is smaller than that obtained with a deterministic least squares approach. [C6138]

"Double density wavelet transformation for speckle reduction of SAR images"

Discrete wavelet transformations (DWTs) based on oversampled filter banks, proposed by I. W. Selesnick (2001), are used for speckle reduction of SAR images. The oversampled DWT is called double density DWT (DD-DWT) and is based on a single scaling function (lowpass) and two distinct wavelet functions (highpass). The DD-DWT is useful for speckle reduction through its subband images and the speckle reduction is obtained by thresholding the subband-image coefficients of the digitized SAR images. A thresholding method using non-linear functions which are adapted for each selected subband is used in the paper. The non-linear functions are based on sigmoid functions. The denoising method shows great promise for speckle removal and hence can provide good detection performance for SAR based recognition. [C6139]

"Elimination of false positives in vessels detection and identification by remote sensing"

The article describes how to eliminate the false positives generated by the basic model of an fast automatic algorithm for fishing areas control and vessel detection. [C6140]

"Ship wake detection in SAR images: a segmentation-based approach"

This paper deals with the derivation of a fully automatic and reliable ship wake detector (SWD), which can operate in conjunction with a ship detector scheme (SD) for ship traffic control against non-homogeneous sea background in SAR images. A novel segmentation-based technique is introduced for ship wake detection, which overcomes the drawbacks suffered by standard techniques operating in non-homogeneous background. This is composed of a preliminary segmentation stage to extract context information, followed by a modified wake detector. The new SWD scheme is shown to yield a large performance improvement on both simulated and real SAR data. [C6141]

"Similarity measures for multisensor remote sensing images"

In this paper we will introduce several similarity measures between multisensor images. These measures are based on concepts such as statistical dependence or mutual information. The use of these measures allows for the design of image registration algorithms and automatic change detection techniques. [C6142]

"Detection of targets from electro-optical and SAR data using chaotic predictors and optimal CFAR detectors"

This paper presents a new clutter suppression and target detection technique for locating small land targets in SAR and electro-optical images. The method is based on adaptive nonlinear (chaotic) predictors which provide an estimate of the local SAR and electro-optical clutter and uses this estimate to suppress the clutter and hence increase the signal to clutter power. The residual errors between clutter estimates and actual data correspond to either clutter noise or target signatures. Hence, dedicated models are employed for clutter noise and targets. The modelling is performed using generalized statistical probability density functions. Statistically optimal Constant False Alarm Rate (CFAR) detectors are used to separate the targets from the residual noise. Although, some similarities may be found in the detection process, when multispectral and multipolarized SAR data are employed, the clutter and target statistics are quite different. The paper presents detection approaches that extend those presented in the literature by including threshold statistics, clutter suppression techniques and generalized statistics. Finally, the issue of detection fusion from dissimilar sensors is addressed. For CFAR detection the optimal Order Statistics, Cell averager, Optimal Weibull, Optimal K-pdf and Optimal Generalized Gamma CFAR detectors are employed. The last three have been developed at A.U.G. Signals Ltd. [C6143]

"The application of satellite radar interferometry to subsidence monitoring in the Belridge and Lost Hills fields, California"

Oil production from weak, compactable, and low permeability diatomite oil reservoirs in the Belridge and Lost Hills fields in California has resulted in subsidence. Previous efforts to monitor subsidence in these fields have included the installation of surveyor monuments. These monuments allowed the comparison of repeated elevation measurements at the monument locations and the installation of permanent arrays of tiltmeters to measure the direction of the gravity vector through time. Since late 1998, repeat-pass interferometric synthetic aperture radar (InSAR) data have been operationally acquired from several satellites and evaluated over the Belridge and Lost Hills fields to monitor subsidence. Because of the temporally and spatially dynamic nature of subsidence in these fields, the customer decided to acquire InSAR data sets approximately monthly over both fields to monitor subsidence rate changes caused by field development and operating practices. ERS-2 and Radarsat have been used. It has been possible to measure subsidence rates across each field. InSAR deformation data have been compared to and validated with a series of GPS monument survey measurements. [C6144]

"Ground deformation monitoring in the Ranafjord area of Norway by means of the permanent scatterers technique"

Although Norway is situated along a passive continental margin, it is not devoid of tectonic activity. Several studies have documented significant movements along faults within the last 10-12 ka. Most of such movements probably occurred shortly after deglaciation, when rates of crustal rebound were very high. Nonetheless, current seismicity along the Norwegian coast suggests that crustal deformation is still taking place. Ranafjord, in northern Norway, is a region with higher than average seismic activity. A six-station seismic network installed by NORSAR detected numerous earthquake swarms in the area. In order to retrieve further crustal deformation data relative to Ranafjord it was decided to use differential SAR interferometry (DInSAR). The application of conventional DInSAR is extremely challenging because the expected deformation rates are low (a few mm/yr) and over long time spans phase coherence is not preserved on large portions of the area to be investigated. The Permanent Scatterers (PS) technique overcomes these drawbacks by exploiting long series of ERS data. At Permanent Scatterers, i.e. individual phase stable point-wise radar targets, displacement data can be retrieved with millimetric accuracy. The PS grid can be seen as a high spatial density natural geodetic network. Thirty-seven ERS scenes covering the time span 1992-2000 were involved in a Permanent Scatterers (PS) analysis. [C6145]

"Analysis of landslides in Alpine areas by means of SAR interferometry"

Methods and applications of differential SAR interferometry (DINSAR) for detecting and monitoring slow movements of mountain slopes on the order of centimeters per year were investigated in the Austrian and Swiss Alps, using SAR images from the European ERS-1 and ERS-2 satellites. The DINSAR analysis methods and criteria for selecting SAR image pairs suitable for landslide monitoring are briefly described. Most of the detected

landslides are above the tree line, because on surfaces with sparse vegetation and bare soil or rock the coherence is preserved over long periods. The investigations confirm the operational potential of DINSAR for detecting and monitoring mass movements in high Alpine areas. [C6146]

"Interferometric synthetic aperture radar studies of Alaska volcanoes"

Interferometric synthetic aperture radar (InSAR) imaging is a recently developed geodetic technique capable of measuring ground-surface deformation with centimeter to subcentimeter vertical precision and spatial resolution of tens-of-meter over a relatively large region ($\sim 104\text{km}^2$). The spatial distribution of surface deformation data, derived from InSAR images, enables the construction of detailed mechanical models to enhance the study of magmatic and tectonic processes associated with volcanoes. This paper summarizes our recent InSAR studies of several Alaska volcanoes, which include Okmok, Akutan, Kiska, Augustine, Westdahl, and Peulik volcanoes. [C6147]

"The use of multi-beam RADARSAT-1 satellite imagery for terrain mapping"

Multi-beam RADARSAT-1 satellite imagery has been used as part of a terrain mapping program in Alberta, Canada. Principal components analysis (PCA) has been applied to standard beam modes with incidence angles of $20\text{--}27^\circ$ (S1) and $45\text{--}49^\circ$ (S7) for both ascending and descending passes. The results provide imagery that characterize geomorphology, geologic structure, vegetation differences and a measure of moisture content. These features are highlighted through the interaction of incidence angles and look directions. [C6148]

"Requirements for Global Precipitation Measurement"

The measurement of precipitation on a global basis has many scientific and societal benefits. The National Aeronautics and Space Administration's (NASA's) Tropical Rainfall Measuring Mission (TRMM), developed in cooperation with the National Space Development Agency (NASDA) of Japan, was launched in 1997, and is widely viewed as a highly successful mission. TRMM has successfully addressed many science issues, has identified areas relating to precipitation where additional research is required, and has also demonstrated the value of precipitation measurements to other disciplines, including hydrology and weather forecasting. In response to substantial interest in precipitation measurement, NASA has established a Project Office to begin planning for Global Precipitation Measurement (GPM). This paper will provide a brief overview of the needs for precipitation measurement, identify the top-level requirements, and provide details concerning the spacecraft and instruments that comprise the space segment of the concept mission. [C6149]

"Integral equations for a dual-wavelength radar"

A dual-wavelength spaceborne weather radar is expected to be one of the primary instruments on the proposed Global Precipitation Mission, GPM, satellite. In addition, airborne dual-wavelength weather radar data at (13.6, 35 GHz), (10, 35 GHz), (10, 94 GHz) have been or will be acquired within the next several years. The objective of the paper is to outline some of the techniques for analyzing such data with a focus on an approach that uses integral equations that describe the change in the DSD parameters with radar range. [C6150]

"Validation of a snow water equivalence algorithm over landfast first-year sea ice using RADARSAT-1"

Our understanding of snow distribution (i.e., spatial statistical properties) and magnitude (i.e., snow water equivalent (SWE)) in the polar regions is severely restricted due to the heterogeneity, both in space and time, of this solid precipitate. In this paper we present the theoretical framework for linking microwave scattering from a synthetic aperture radar (SAR) to the thermodynamic and electrical properties of snow on sea ice. We show how the thermophysical properties at the snow/sea ice interface create a change in scattering, which is statistically proportional to the magnitude of SWE over smooth first-year sea ice (FYI). We use in situ data from the 1999 Collaborative-Interdisciplinary Cryospheric Experiment (C-ICE'99) near Resolute Bay, Nunavut to validate RADARSAT-1 derived SWE estimates for a 100-km^2 area of FYI. [C6151]

"New developments and results for snowcover monitoring using RADARSAT and VEGETATION data and the HYDROTEL hydrological model"

The HYDROTEL hydrological model was developed to be compatible as much as possible with remote sensing and GIS data. In parallel, processing procedures to derive snowcover characteristics from RADARSAT and VEGETATION data have been developed for updating purposes in the HYDROTEL model. In the case of RADARSAT data, we are now testing the possibility of using the French CROCUS snowmelt model to derive the snowcover information used in our RADARSAT algorithm. As for VEGETATION data, we have added corrections

for bi-directional effects in the algorithm, using a procedure developed by the Canada Centre for Remote Sensing. We finally explain how we intend to use that information for updating the snowcover as simulated by HYDROTEL. [C6152]

"Radiometric correction of RADARSAT-1 images for mapping the snow water equivalent (SWE) in a mountainous environment"

When trying to monitor the snow characteristics from RADARSAT-1 SAR data in a mountainous environment like the Coast Mountains (B.C. Canada), radiometric corrections must first be applied to correct for the distortions induced by the slant projection of SAR systems and by the highly variable terrain. This paper presents and discusses the results obtained from the implementation of two radiometric slope correction methods on Fine beam RADARSAT-1 images. For slope less than 30°, both algorithms have almost the same effect. But, for very steep slopes, both algorithms are deficient and may not compensate enough. [C6153]

"Calibration and validation of the Shuttle Radar Topography Mission height data for southeastern Michigan"

The Shuttle Radar Topography Mission (SRTM) provided data for detailed topographical maps of about 80% of the Earth's surface. SRTM consisted of single-pass C- and X-band interferometric synthetic aperture radars (INSARs). In order to apply SRTM data to remote sensing applications the data must be calibrated and validated. This paper presents the University of Michigan's SRTM calibration and validation campaign and our results using recently acquired C-band SRTM data of our calibration sites. A calibration array was deployed with the intention of determining the accuracy of INSAR-derived digital elevation maps. The array spanned one of the X-band swaths and stretched from Toledo, Ohio to Lansing, Michigan. Passive and active targets were used. The passive targets included trihedrals and tophats. The locations in latitude, longitude, and elevation of the point targets were determined using differential GPS. The data used in this study are "Principal Investigator Processor" data, which are not the refined final data product. However, we found the data to be of high quality. We report a 6 m to 12 m vertical height offset with a pronounced tilting trend. The average absolute offset is 9 m with a standard deviation of 2 m. This absolute height error is within the stated mission goal of 16 m, even before the final processing to refine the data. In order to calibrate the data, we remove the height offset and find that the resulting absolute height errors are at most 4.2 m in magnitude, with a standard deviation of 1.5 m. [C6154]

"Interferometric calibration with natural distributed targets"

Cross-calibration is a fully automated algorithm for calibration of interferometric synthetic aperture radar (IFSAR) data. It has been developed for single-pass interferometry, but the principles may be applicable to multi-pass interferometry, too. The algorithm is based on natural distributed targets and it excels by neither requiring surveyed ground control points nor dedicated calibration scenes. However, the parameters to be calibrated must be stable during mapping. The algorithm has been applied to data from the Danish airborne SAR, EMISAR, and the performance has been assessed. The algorithm appears to be fairly robust with respect to the terrain type. However, the result of the calibration may deteriorate if the terrain elevation, as measured with the SAR, changes systematically with the incidence angle or the aspect angle. [C6155]

"Filtering of interferometric SRTM X-SAR data"

In February 2000, the Shuttle Radar Topography Mission acquired a global digital elevation model (DEM) within only 11 days. During the years 2000 and 2001, extensive testing and calibration activities followed at DLR. One of the questions during that phase was, which kind of interferogram filtering should be performed. We analyzed different types of filters from the perspective of an operational DEM processing chain. Our paper describes the filters investigated and the arguments that finally led us to the decision to implement a relatively simple Gaussian smoothing in the time domain. This filter performed best in many disciplines and produced the smallest artifacts. [C6156]

"Demonstration of current measurements from space by along-track SAR interferometry with SRTM data"

We present one of the first studies in which interferometric synthetic aperture radar (InSAR) data from the Shuttle Radar Topography Mission (SRTM) are analyzed with regard to the detectability of ocean surface current variations. The InSAR system of SRTM was designed for high-resolution topographic mapping, using two SAR antennas on a Space Shuttle with a cross-track separation of 60 m. For technical reasons, there was an additional along-track antenna separation of 7 m, which results in a time lag of about 0.5 ms between the

acquisitions of images by the two antennas. In theory, this time lag causes additional phase differences, which are proportional to the line-of-sight velocity of moving targets and can thus be exploited, to some extent, for measuring oceanic currents. Indeed, some SRTM images acquired over water exhibit clear signatures of typical flow patterns. We show an example of an X-band phase image of the Dutch Waddenzee and discuss the plausibility of interpreting it in terms of sea surface height or current variations or the effect of waves. We find that only currents can be responsible for phase variations of the observed magnitude on spatial scales of a few 100 meters. We convert the data into a surface current field, which is found to be consistent with the theoretical current field at the time of the SRTM overflight according to a current atlas. Based on this encouraging result and theoretical findings, we discuss the general potential of SAR interferometry from space for oceanic applications.

[C6157]

"Baseline estimation and prediction referring to the SRTM"

The Shuttle Radar Topography Mission (SRTM) radar mapping accuracy is significantly affected by errors in the baseline components. In this paper a baseline estimation method based on tide models is presented. Furthermore, the prediction of the estimated baseline parameters over terrain is considered. The underlying approach enables prediction of error biases. Different methods to correct residual height errors will be considered. [C6158]

"Range resolution limits in multi-pass SAR data processing"

Multiple SAR data sets can be exploited to improve the system range resolution. Obtainable resolution improvement can be impaired by a coherence loss among the different data acquisitions. The effect of different decorrelation factors on the attainable resolution is investigated by numerical simulation. [C6159]

"Characterization of landslide deposits using SAR images"

This paper provides some preliminary results of the use of RADARSAT fine mode image for characterizing the debris size and distribution of a 304106m3 rock avalanche. From the image we were able to classify coarse, medium and fine debris based on their SAR texture. Such simple textural classification will be useful to plan more detail field and aerial surveys on large landslides so as to understand landslide processes, post failure mechanism and mobility. [C6160]

"Space variant filtering of polar format spotlight SAR images for wavefront curvature correction and interferometric processing"

In repeat pass SAR interferometry the scene coherence can be used to detect subtle scene changes that occur in the interval between image collections. In spotlight SAR mode the azimuth resolution of the baseline and repeat pass imagery may be improved by collecting an extended aperture therefore allowing finer resolution estimates of the scene coherence. The formation of the imagery however requires adequate compensation of the wavefront curvature effects which become increasing significant in finer resolution imagery. In N. E. Doren (1997) it is shown that for spotlight SAR imagery, formed using the Polar Format Algorithm (PFA), wavefront curvature effects give rise to residual phase errors that may be removed using an image domain filtering technique. The analysis however is based on the formation of a slant plane image obtained by projection of the scene reflectivity along circular arcs centered on the flight track. In this paper a full 3D imaging geometry is considered to derive an appropriate post PFA image domain filter to form a ground plane image. This allows multipass images to be formed in a common image plane for subsequent interferometric processing. The technique is used to generate a fine resolution coherence map using data collected in a repeat pass SAR experiment using the DSTO Ingara SAR. [C6161]

"Interferometric multi-look techniques for SAR data"

This paper addresses the benefits of the spectral domain multi-look approach for SAR interferometry. A comparison with the wide spread spatial averaging filter is included in the beginning. Next, it is shown that the flexibility of the spectral domain multi-look technique can be used for improved motion compensation and further for precisely updated estimation of azimuth misregistration offsets. This leads finally to the compensation of residual motion errors in case of multi-pass airborne SAR interferometry, e.g. for the E-SAR system of DLR.

[C6162]

"Multi-pass synthetic aperture radar for 3-D focusing"

In the area of tomographic synthetic aperture radar processing we present a new technique that makes use of the singular value decomposition method to improve the resolution limits by including a-priori information about

the radiation penetration depth. [C6163]

"Towards evolutionary optimisation for high resolution bathymetry from sidescan sonars"

The main objective of this paper is to use genetic algorithms in order to improve the quality of the bathymetry derived from sidescan raw data. The optimisation sequence starts with inverse modelling of the phase data, which uniquely corresponds to the characteristics of the coupled system of the sidescan vehicle and the seafloor terrain. These phase data are then compared with phase data actually collected by the sonar, to produce a correlation coefficient as an objective function. Simulation results are reported for the algorithm showing robust convergence towards the optimum value of the objective function. The results indicate that this new approach can be used to avoid difficulties widely encountered during forward processing of phase data to derive bathymetry [C6164]

"Subsurface radar examination of an airstrip"

The increasing intensity of air traffic and growing take-off mass of passenger and cargo civil airplanes leads to the growth of a loading on airstrips, taxiways and aircraft parking places of airports. It results in an increased wear of concrete pavement and requires a continuous monitoring of their state and supporting power with the object of ensuring the flight safety. Subsurface radar can be used as one of the means for non-destructive testing of a reinforced concrete airfield. Taking into account large areas of airfield pavements and their constructive features, the carrying out of these jobs will probably require the creation of dedicated equipment and software. [C6165]

"Combined underwater acoustic and radar instruments for assessing fish near seabed and mapping seabed"

An underwater acoustic and marine radar survey was conducted for the assessment of fish near the seabed and for seabed mapping. For the purpose, an underwater acoustic instrument (split beam echo sounder), and ground penetrating radar (GPR) were used around Seribu Island, Jakarta Bay. Research vessel Mina Jaya (30 GT) and various marine research instruments were employed during the survey. The results show that the fish density near seabed is 0.3 to 35.0 fish/1000 m³ with fish length up to 44.6 cm. Radar has a higher resolution for subbottom detection than high frequency acoustics. [C6166]

"0.25 μ m CMOS and BiCMOS single-chip direct-conversion Doppler radars for remote sensing of vital signs"

Summary form only given. A fully integrated direct conversion Doppler radar that detects heart and respiration movement at a distance of 50 cm is described. The 1.6 GHz transceiver is implemented in both CMOS and BiCMOS technologies, with each chip occupying 14 mm² using a 0.25 μ m silicon processes. The effects on system sensitivity of phase noise at small offset frequencies with range correlation are assessed [C6167]

"0.25 μ m CMOS and BiCMOS single-chip direct-conversion doppler radar for remote sensing of vital signs"

First Page of the Article [C6168]

"A compact low-cost add-on module for Doppler radar sensing of vital signs using a wireless communications terminal"

A simple add-on module that allows the detection of human respiration and heart activity using an unmodified wireless telecommunications terminal is presented here. The module combines an antenna and mixing element to receive direct and back-scattered transmissions from the wireless terminal, and through Doppler radar principles produces an output signal proportional to the motion of the user's heart and chest. This signal can be used to monitor heart and respiration rates, and can potentially be relayed by the wireless terminal to a remote health monitoring facility via the existing telecommunications infrastructure. Module functionality is demonstrated here using a 2.4 GHz cordless telephone [C6169]

"A 94 GHz single-chip FMCW radar module for commercial sensor applications"

A single-chip 94 GHz frequency modulated continuous wave (FMCW) radar module has been developed for high resolution sensing under adverse conditions and environments. The monolithic microwave integrated circuit (MMIC) includes a varactor tuned VCO with injection port, very compact transmit and receive amplifiers and a single-ended resistive mixer. To enable bidirectional operation of a single transmit-receive antenna a

combination of a Wilkinson divider and a Lange coupler was integrated. The circuit features coplanar technology and cascode HEMTs for compact size and low cost. These techniques result in a particularly small over-all chip-size of only 243 mm². The packaged 94 GHz FMCW radar sensor achieved a tuning range of 6 GHz, an output power of 1 mW and a conversion loss of 5 dB. The RF performance of the radar module was successfully verified by real-time monitoring the time flow of a gas-assisted injection molding process [C6170]

"Remote detection of bioparticles in the THz region"

Recent measurements of the electromagnetic transmission through *Bacillus subtilis*, an innocuous anthrax substitute, have revealed absorption resonances in the THz region. A system-level analysis is carried out to show that at least one of the resonances (centered at 14.05 cm⁻¹, or 421 GHz) is located at a frequency of low enough atmospheric absorption to be detectable by an active remote sensor—a differential absorption radar [C6171]

"Development of an ultra-wideband radar system for vehicle detection at railway crossings"

This paper describes an ultra-wideband (UWB) radar system designed to detect motor vehicles such as cars and trucks when they are present in a railway crossing. Once fully developed, the detection performance of the system is to be compared against a video detection system in a test at a crossing in Maywood, Illinois. If the test is successful this system may be further developed and installed at a four-quadrant gate crossing to sense vehicles trapped in the crossing island (i.e. the area bounded by the gate arms). This paper describes the problem at hand and gives details of the radar system development to date. With the current prototype, a pulse width of 3 ns has been achieved, which yields adequate range resolution for this application. [C6172]

"An interactive fuzzy fusion system applied to change detection in SAR images"

The contribution of this paper concerns the detection of changes in multi-temporal satellite SAR (synthetic aperture radar) images by a fuzzy fusion of attributes extracted from the images with a-priori map-based information. The proposed approach is based on a linguistic description of the attributes and of the relations between them that are provided by geophysicists. The fusion system is cooperative thanks to a graphical user interface that allows one to visualize reference areas in the attribute space and to easily adjust some parameters of the attribute fusion (rules, membership functions). Some detection results of small deforested areas are presented [C6173]

"Entropy based phase calibration of antenna arrays for digital beamforming remote sensing radars"

A minimum entropy based calibration algorithm for digitally beamformed imaging radars is presented. The algorithm is derived from work in SAR which corrects phase errors due to platform motion. The performance of the algorithm is compared to traditional techniques through both simulations and data from two imaging radars. The algorithm performs well with similar sidelobe levels for a point target. The results show that the minimum phase entropy algorithm produces a calibration vector without the need for a calibration target or for stringent scene statistics. [C6174]

"Airborne sensor concept to image shallow-buried targets"

This paper develops an airborne sensor concept to detect and image shallow-buried targets with a focus on the remote sensing of landmines. Our ongoing ground-based bistatic ground-penetrating radar (GPR) experiments have demonstrated deep penetration and subwavelength resolution. Simulation software (ground penetrating radar processing-GPRP) was developed and validated using experimental results. Extrapolation of the experimental results to higher frequencies using the simulation software indicates the ability to provide high-quality images of shallow-buried targets. [C6175]

"Application of polarimetric synthetic aperture radar interferometry for land cover classification"

The development of radar polarimetry and radar interferometry is advancing rapidly. The textural fine structure, target orientation, system metrics and material constituents can be recovered with radar polarimetry; while with radar interferometry, the elevation structure of a target can be explored. Polarimetric synthetic aperture radar interferometric (Pol-InSAR) is interferometry between all possible polarization channels at each end of the baseline. Using polarimetric interferometry, the combination of the final structure properties and the spatial information of targets can be implemented. In this paper, we investigate the application of these three approaches to Earth terrain classification with results from the evaluation of fully polarimetric interferometric SIR-C/X-SAR data. The potential of Pol-InSAR for land cover classification has been demonstrated. [C6176]

"A High-Resolution Airborne Radar System for Near Surface Mapping of Internal Layers to Estimate Accumulation Rate"

We developed a 600-90-MHz airborne radar system for high-resolution mapping of the near surface internal layers for estimating accumulation rate of polar ice sheets. Accumulation rate is currently determined by analyzing ice cores and snow pits. Inadequate sampling of the spatial variations in the accumulation of the ice sheet has resulted in accumulation rate uncertainties as large as 24%. Our airborne radar system can provide improved spatial and temporal coverage by mapping a continuous profile of the isochronous layers in the ice sheet. We successfully mapped the internal layers of the Greenland ice sheet with better than 1 m resolution up to a depth of 200 meters. We also developed a radar target simulator to help characterize the system indoors, since we are unable to test the system in the continental USA due to interference from and to wireless communication devices that operate in the UHF band. [C6177]

"A new solution to polarimetric radar discrimination problem"

A new solution is proposed for polarimetric radar discrimination problem by using cross-entropy to measure the difference between two scatterers. Two cross-entropy measures in favor of one scatterer over another are obtained for two independent probability mass functions that indicate the average scattering mechanism and the scattering randomness, respectively. These probability mass functions are formed by the modified similarity parameters and the eigenvalues of target coherency matrix. The cross-entropy measures utilize the polarimetric information efficiently to show the difference between scatterers. The advantage of using cross-entropy for solving polarimetric radar discrimination problem is demonstrated by the simulation results. [C6178]

"Gyro-amplifiers for high power millimeter wave radar"

Summary form only given. Over the past several years there has been a concerted effort within the US to develop millimeter wave gyro-amplifiers for high-power millimeter wave radar. Efforts have been carried out by a number of researchers at both Ka- and W-bands. These efforts have culminated in the successful integration of a high-average-power W-band gyro-klystron into the NRL WARLOC radar. The author reviews gyro-amplifier research and development at both Ka- and W-bands, as well as the completed integration into the NRL W-band radar. [C6179]

"Laser frequency converters for Universal Lidar system"

We present phase-matching conditions and widths, results on estimations of frequency conversion efficiencies, and other potential characteristics of frequency converters [C6180]

"Optimal classification of polarimetric SAR images using segmentation"

The paper presents an optimised polarimetric segmentation technique for synthetic aperture radar (SAR) images, based on a generalised maximum likelihood approach. A full theoretical derivation is presented, together with a closed form analytical performance evaluation. The technique is compared to other known polarimetric segmentation schemes by application to a polarimetric SAR image of agricultural areas. A complete characterisation of the technique is provided in terms of polarimetric sensitivity and memory requirements. [C6181]

"Radar breadboard for DSP scatterometer"

The design and test results for the radio frequency (RF) portion of a breadboard polarimetric scatterometer operating at 13.402 GHz are presented. To evaluate the feasibility of a programmable digital signal processing (DSP) approach for a follow-on scatterometer similar to SeaWinds an integrated breadboard has been developed at the Jet Propulsion Laboratory (JPL). Early breadboards of this type have been identified as valuable assets in developing effective subsystem requirements for the eventual flight instrument. Many compatibility and partitioning issues between the RF and DSP hardware are addressed with empirical results derived from the aforementioned breadboard. The RF portion of the breadboard consists of a dual channel receiver, heterodyning the received signal of 13.402 GHz down to an IF of 37 MHz and a single channel transmitter, that converts the I/Q baseband transmit waveform up to Ku band. The breadboard makes provision for emulating capabilities such as programmable attenuators, loop-back calibration, and saturation effects in an actual instrument's power amplifier. It also provides control interfaces to allow early verification of software control algorithms. [C6182]

"Subsurface radar investigation of arched wall aperture"

A subsurface holographic radar using a monochromatic signal has been developed. It is intended for surveying

building structures and works. The characteristic feature of this device is the possibility of obtaining in a sounding plan the microwave images featuring a high resolution attaining 2...3 cm. The main application of this device includes the survey of building constructions to reveal their internal structure and defects. An arched aperture in a brick wall was studied with help of the radar to search metallic beams. The goal of investigation was evaluation of the load-carrying ability of the wall. [C6183]

"Influence of two media interface on the frequency characteristics of a two dipole antenna system"

Radar remote sensing methods for exploration of different dielectric media may be highly efficient for obtaining the necessary information on media properties. In many practical cases, the operation of such systems is carried out either directly on the surface of the investigated media or for elevated antennas at some height (comparable with the wavelength) above the surface. In these cases it is necessary to take into account the influence of dielectric properties of the medium on the impedance characteristics of the transmit-receive antennas. The results of theoretical and experimental investigations concerning the influence of the dielectric properties on the parameters of dipole antennas situated near the surface are analysed. The possibility to determine the dielectric medium properties by means of a two-dipole antenna system is evaluated. [C6184]

"Specular multipath analysis for a coherent ultrawideband random noise radar"

First Page of the Article [C6185]

"Airborne weather radar as an instrument for automatic mapping"

The classification of navigational radar landmarks and the principles of their display at automatic radar mapping are proposed. Selection algorithms of each type of navigational landmarks are developed. The priority of navigational landmark classes is established, and the scheme of the combining different channels is designed. The automated recognition of landmarks and radar mapping is implemented in a new airborne weather radar. [C6186]

"Statistical modeling of scattering matrix elements"

Attention is paid to distribution laws describing the statistical characteristics of scattering matrix elements. Taking into account the many mathematical difficulties to set up an analytical approach, it is shown how to use numerical methods as a promising alternative. The probability density functions of the real and imaginary parts of the measured scattering matrix elements, as well as modules and phase values are determined. They are used in the process of statistical modeling and lead towards distribution laws, which are in good agreement with the measured statistics. A search of best-fitted distribution laws has been carried out on the basis of generalized Pearson curve classes. [C6187]

"Methods for solving inverse problems in radar remote sensing"

A general approach to solve inverse problems in polarimetric radar remote sensing is considered. Starting from the general statement of ill-posed problems in the mathematical sense the special case of inverse scattering problems in polarimetric radar is formulated. Regularization methods to handle inverse problems are described and an illustration leading to an inverse classification problem for determination of the soil humidity using radar measurements is given. [C6188]

"2002 IEEE International Geoscience and Remote Sensing Symposium. 24th Canadian Symposium on Remote Sensing. Proceedings (Cat. No.02CH37380)"

First Page of the Article [C6189]

"GCOM mission concept"

Global Change Observation Mission (GCOM) is a follow on mission of ADEOS, ADEOS2 and TRMM. It is under phase A study in NASDA. GCOM is not a series of satellites but a mission and its concept is to continuously monitor geophysical parameters which are critical to understand global change phenomena, especially phenomena related to climate change. Those parameters include, but not limited to, optical thickness of aerosols and clouds, water and energy fluxes, carbon fluxes, sink and source of greenhouse gases, atmospheric constituents, etc. The measurements of geophysical parameters will continue more than 15 years after the launch of ADEOS2. The first generation satellites of GCOM after ADEOS2 is now composed of 3 satellites, i.e. GCOM-A1, GCOM-B1, and GPM core satellite. The follow on satellites of ADEOS2 is divided into 2 satellites, i.e. GCOM-A1 and GCOM-B1. The target of GCOM-A1 is to monitor stratospheric and upper tropospheric

greenhouse gases distribution and ozone as well as ozone related constituents. The target of GCOM-B1 is to measure geophysical parameters which are uncertain in the today's climate models. GPM core satellite is a follow on of TRMM and the target of GPM core satellite is to measure precipitation. GCOM-A1 will carry 3 instruments, i.e. OPUS (Ozone and Pollution Ultra-violet Sounder: TOMS follow on), SOFIS (Solar Occultation Fourier Interferometric Sounder: ILAS follow on), and SWIFT (Stratospheric Wind Interferometer: stratospheric wind sensor). GCOM-B1 will carry three core instruments, i.e. SGLI (GLI follow on), AMSR2 (AMSR follow on), alpha-Scat (SeaWinds follow on). GPM core satellite will carry 2 instruments, i.e. DPR (Dual Precipitation Radar: PR follow on) and a microwave radiometer. [C6190]

"Mapping of land mines using air borne radars"

The detection of land mines using an air borne radar is investigated. The relation between the height of the radar and the separation distance between regular linear distributed mines is obtained. Bistatic and monostatic radars are employed with different operating frequencies to detect the number of mines and their locations. An E-plane or H-plane horn antenna can be used during the simulation. [C6191]

"A wavelet galerkin scattering approach for improved radar detection models"

First Page of the Article [C6192]

"Voting fusion adaptation for landmine detection"

This paper presents a voting fusion application for use with a remotely controlled multisensor vehicle platform for antitank landmine detection. Data from three landmine detection sensors mounted at the front of the vehicle enhance the probability of detection and, when combined via data fusion, limit the false alarm density to practical levels. The performance of the voting fusion scheme presented in this paper is contrasted with a heuristic data fusion approach developed by General Dynamics Canada. [C6193]

"The Mueller matrix solution for polarimetric scattering from inhomogeneous random media of non-spherical scatterers under a pulse incidence"

Polarimetric scattering from inhomogeneous random media of non-spherical scatterers under a pulse incidence is studied. The time-dependent Mueller matrix solution of vector radiative transfer for layering random media is derived. Co-polarized and cross-polarized, bistatic and back scattering are numerically calculated. The shape and intensity of polarized echoes well depict the inhomogeneous fraction profile of random scatterers. Its functional dependence upon the fraction profile, layering thickness, and other parameters is discussed. This technique is applicable to reconstruction of the inhomogeneous fraction profile and inversion of the media thickness. [C6194]

"The synthesis of offset dual reflector antennas by genetic algorithms"

Reflector antennas have various applications in radar, microwave telecommunication, remote sensing and radio-astronomy systems. Although there are applications in which shaped reflector antennas are used, most applications use the classical parabolic reflectors. Therefore, the design of an optimized reflector is of great importance. We present a new method for the far field pattern synthesis of parabolic reflector antennas that can virtually optimize all major design parameters simultaneously. The direct problem is formulated using the equivalent paraboloid technique with the far field pattern computed based on high frequency geometrical optics (GO) and/or physical optics (PO) approximations, depending on the desired speed and accuracy. The inverse problem is formulated based on an optimization of the geometrical parameters of the antenna using a simple genetic algorithm (see Goldberg, D., 1989). The proposed design method optimizes the gain and the cross-polarization of the radiation pattern of the reflector antenna. It also satisfies the FCC standard limits on the sidelobe level envelope. [C6195]

"A study of bit planes for the compression of raw synthetic aperture radar data"

The compression of raw SAR data has been a topic of interest to researchers for many years. The goal of such compression is to transmit the highest fidelity data from the radar satellite within the downlink bandwidth constraints. The necessity of new compression techniques is further emphasized as advances in the design of radar technologies are close to surpassing the capabilities of current compression techniques. Developing only a theoretical compression technique is not a complete solution to the problem as the technique must be realizable in the hardware available for placement on the radar satellite. The implementation must not only be low in computational complexity, but must also be able to handle the ever increasing throughput demands of the radar. Bit-planes have been used successfully with several other compression techniques, and are extremely amenable

to hardware due to their inherent parallelism. This paper shows that bit-plane segmentation and simple coding transformation of raw SAR data can reduce the entropy of a single plane by 59%. [C6196]

"IEEE CCECE2002. Canadian Conference on Electrical and Computer Engineering. Conference Proceedings (Cat. No.02CH37373)"

First Page of the Article [C6197]

"Research of possible improvement of lidar potential performance"

A possibility to reduce the influence of the turbulent atmosphere on the potential performance of lidar instruments is studied. It is shown that the improvement can be achieved by using adaptive telescopes, which compensate the turbulent distortions of optical signals in each sensing cycle. This facilitates an increase of the signal to noise ratio in the output of the photoreceiver, and, therefore, an improvement in the instrument performance. [C6198]

"Classification of objects by radar remote sensing"

At present radar object classification by means of radar remote sensing making use of the appropriate received information is widely based on the Bayesian approach. However, this does not take into account that certain parameters (attributes) of sensed objects (and derived from measured data) have a certain degree of uncertainty. This uncertainty consideration necessitates a modification in the Bayesian approach. This modified variant of the Bayesian approach to be used for classification of sensed radar objects is described in this paper. [C6199]

"Determination of polarization invariants of asymmetric scattering matrix"

Polarization invariants of the backscattering matrix in HV-basis are estimated for the case of an arbitrary non-reciprocal object. Two additional polarization invariants, which describe non-reciprocal properties of the object itself, are introduced supplemented to the well known Huynen-Euler invariants. Supposing the simultaneous measurement of all 8 quadratures of the scattering matrix's elements in the monostatic radar case, closed form expressions for calculation of 8 polarization invariants are found. The given approach can be used for research of various polarization effects in remote radar sensing of artificial and natural objects. [C6200]

"Frequency-swept microwave imaging using multi-source illumination"

The principle and experimental results of bistatic frequency-swept microwave imaging of continuous shape and discrete line conducting objects using simultaneous multi-source illumination are presented. Images of scattering objects reconstructed from the experimental data measured in the frequency range 7.5 GHz to 12.5 GHz are in good agreement with the scattering object geometries. The experimental results show that using multi-source illumination can provide a cost-effective approach for a wider imaging viewing angle and higher resolution of the scattering object. [C6201]

"Accurate antenna models in ground penetrating radar diffraction tomography"

Linear inversion schemes based on the concept of diffraction tomography have proven successful for ground penetrating radar (GPR) imaging. In many GPR surveys, the antennas of the GPR are located close to the air-soil interface and, therefore, it is important to incorporate the presence of this interface in the inversion scheme (see Hansen, T.B. and Meincke Johansen, P., IEEE Trans. Geoscience and Remote Sensing, vol.38, p.496-506, 2000). Hansen and Meincke Johansen modeled the antennas as ideal (Hertzian) electric dipoles. Since practical GPR antennas are not ideal, it is of interest to investigate the validity of this model. We extend that formulation to hold for arbitrary antennas. For simplicity, the 2.5D case is considered, that is, it is assumed that the scattering object in the soil is invariant in one direction, which, for instance, is the case for a pipe. The arbitrary antennas are modeled by their plane-wave receiving and transmitting spectra. We find these spectra numerically for a resistively loaded dipole using the method of moments. Also, we illustrate, through a numerical example, the importance of taking into account the correct antenna pattern in GPR diffraction tomography. [C6202]

"Modelling and simulating SAR raw signals of oil-covered sea"

Remote sensing has proved to be a powerful tool for studying ocean dynamics and detection of oil spills. In particular, synthetic aperture radar (SAR) systems have been shown to be very useful. The main effect of oil on the ocean surface consists of dampening the capillary waves: this reduces electromagnetic backscattering from areas where oil is present, generating darker zones in the SAR image. Dark areas in SAR images can be caused by several other phenomena, causing possible ambiguities in oil spill detection. A SAR raw signal

simulator is a powerful tool for devising algorithms for oil slick detection. Besides, a good simulation can be an important step in identifying the nature of the slick. Modelling and simulation of SAR raw signals corresponding to a sea surface covered by an oil film are presented. The proposed SAR simulator is based on an ocean model and an oil slick model. Meaningful simulation experiments are presented and discussed, elucidating the role of pollutants, oil thickness, wind speed and direction, incident wavelength and angle and other radar parameters. Validation of the simulator is also presented by comparison with experimental data. [C6203]

"The role of HF radar within operational forecasting systems of the ocean"

Operational forecasting of current and wave fields in coastal regions got more and more important in the last decades, both for coastal management and for security aspects. One of the key tools in this context are high-resolution numerical models, which however require accurate forcing and handling of the boundary conditions to give results which are close to nature. HF radar remotely sensed current and wave fields can significantly increase the data quality of the models, if these on-line measurements are assimilated. In some cases, when the oceanographic processes induce high local variability, such as mesoscale eddies and fronts, this approach might be the only way to get reliable now- and forecasts. In Europe, the European Radar Ocean Sensing (EuroROSE) project has demonstrated the feasibility and performance of an HF radar based ocean monitoring system in support of safe navigation in port approach areas and otherwise densely operated sea areas. Two demonstrations were carried out off the Norwegian coast north of Bergen, and at the North Spanish coast near Gijon. During each of these demonstrations, WERA (Wellen Radar) HF radars of the University of Hamburg were deployed. WERA measured surface currents within an area of about 40 km by 40 km with a spatial resolution of about 1 km and with a temporal sampling of 10 minutes. [C6204]

"The availability and accuracy of HF radar wave measurements"

The possibility of measuring the ocean wave directional spectrum in real time at up to 350 locations every 10 minutes was demonstrated in the EuroROSE experiments at Fedje, Norway and Gijon, Spain in 2000. These experiments used the WERA HF radar which, at the operating frequency used, had a maximum range for wave measurements of about 20 km. Trials of the PISCES HF radar are currently underway in the UK with a view to providing real-time wave measurements to over 100 km. These and earlier experiments have clarified the main limitations to the accuracy of the wave measurements (scattering theory used, noise levels and antenna sidelobes) and the temporal variability in spatial coverage (noise levels, antenna sidelobes, waveheight and surface current variability). In this paper the accuracy and limitations will be discussed with examples given from the above mentioned experiments and also from the EU-funded SCAWVEX experiments and the ONR-funded SHOWEX experiment. Work in progress directed at solving or minimising their impact on wave measurement accuracy will be described. [C6205]

"A comparison of decision tree and backpropagation neural network classifiers for land use classification"

Decision tree classification techniques have been used for a wide range of classification problems and becoming an increasingly important tool for classification of remotely sensed data. These techniques have substantial advantages for land use classification problems because of their flexibility, nonparametric nature, and ability to handle nonlinear relations between features and classes. This paper compares classification results obtained by using a backpropagation neural network and decision tree classifier. It is shown by a number of studies that neural classifiers depends on a range of user defined factors, that ultimately limits their use. This study show that there are fewer number of user defined factor affecting the accuracy of a decision tree classifier. Further, this study highlight that training a decision tree classifier is much faster and these classifiers are easy to read and interpret as compared to a neural classifier which is a "black box". The performance of these two classification system is compared using ETM+ and interferometric SAR data. [C6206]

"Evaluation of RADARSAT-1 for monitoring and mapping land use/land cover in Thailand"

A project was designed to evaluate the applicability of RADARSAT-1 multitemporal and multiangle data for the discrimination and mapping of tropical landuse/landcover. Five fine beam mode images were acquired over the summer of 2001 for F1, F4, and F5 angles. Principal Component and texture analysis were applied to backscatter images. The results indicate that the texture (mean vector) images spanning the growing season yielded the best discrimination potential. In addition multiangle texture images were combined to highlight raised berms surrounding individual shrimp ponds. [C6207]

"On the optimisation of RBF-based radar rainmap prediction"

The problem of analysing and forecasting the motion of rain structures sensed by weather radar is mostly faced

using approaches based on correlation of rain intensity values. Some approaches, however, consider rain structures as a base for the analysis. Of such approaches we considered a neural RBF-based one, of which we recently presented an improved version. The method we develop shows advantages over a linear prediction, while on the other side it is heavy and thus requires some tuning of the parameters to avoid exceedingly long processing times. In this paper we present some facts we discovered about time-saving compromises in tuning parameters and provide some rule-of-thumb guidelines for selecting their values. [C6208]

"Calibration and early results of the ASAR on ENVISAT"

This paper presents the approach for the in-flight calibration of the ENVISAT-1 ASAR and the verification of the ground processing facility PF-ASAR during the commissioning phase. The philosophy presented is a logical progression from the experience gained during calibration of the ERS SARs. The ASAR has a comprehensive internal calibration loop, which is described distinctly from the external calibration and characterisation. The antenna patterns of the various beams have been fully measured during on-ground flight-model testing and have been used for initial performance predictions. In-flight characterisation of the main beams is performed over the South American rainforest. As for ERS, absolute gain calibration is achieved using three fixed and one transportable precision calibration transponders situated in the Netherlands. These transponders are also capable of recording the azimuth beam patterns and supporting the external characterisation mode of ASAR. [C6209]

"RA-2/MWR in-flight performance-preliminary results"

The EnviSat-1 satellite embarks an innovative radar altimeter, the RA-2, which represents a new generation of radar altimeters compared the earlier ERS altimeters and TOPEX/Poseidon. This is due to its use of many advanced features such as autonomous resolution selection a robust "model free" tracker and its ability to telemeter individual echo samples. EnviSat also embarks a radiometer, the MWR which provides the altimeter with the tropospheric correction. Before the measurements from the RA-2 are exploited the instrument and the data processing system will be commissioned and a verification activity will be performed. During this activity the operation of the instrument in-flight operation will be verified and its functionality optimised. The measurement performance of the instrument and the overall system will also be evaluated, including verification of the instrument auxiliary data retrieval and correct use of these data in the ground processing algorithms. Finally, calibration and validation of the data products are performed such that, at the end of the commissioning phase, the data may be fully released for scientific exploitation. In this paper we will outline the strategy and procedures adopted to tune the parameters used on-board and in the on-ground processing. We show results before and after the optimisation activities as well as comparison with pre-flight simulations. Also, we will show the RA-2 measurement performance of range and sigma-0 as well as the performance of its tracker. In particular the tuning of the autonomous range resolution selection logic is a challenging task and we will show the results of this activity. Finally we will show the status of the in-flight calibration of the Range and Sigma-0. [C6210]

"Active optical remote sensing of dense clouds with diffusing light: early results, present implementations, and the challenges ahead"

We survey the rapid progress of "off-beam" cloud lidar, from inception to validation via laboratory-scale simulations. Cloud observations from ground, aircraft and even space are covered. Finally, we describe future work in this instrument development effort born out of pure theory in the mid-1990s. [C6211]

"Some fundamental statistics associated with ocean surface current measurement using a dual station, long-range, high-frequency ground wave radar system"

Raytheon Systems Canada Limited, in association with Northern Radar Inc (NRI), have designed and built two long-range High Frequency Ground Wave Radar (HFGWR) facilities at Cape Race and Cape Bonavista, NF, Canada. Even though these systems can routinely monitor offshore target activity, the data stream for target detection can also be used to generate surface currents. Since each station is capable of providing estimates of the radial components of the surface current field, the vector current field can be reconstructed from the radial data via geometric considerations. To explore this possibility, sample datasets from both stations were collected in June of 2000 and subjected to a dual station analysis scheme. The treatment presented here will discuss some of the statistics associated with the radial current data as well as the dual station technique used to generate the surface current field. Finally, the radar current estimates will be compared with current meter data collected near the Hibernia platform. [C6212]

"A perspective on two decades of fundamental and applied research in electromagnetic scattering"

and high frequency ground wave radar on the Canadian East Coast"

While a vast amount of literature, dating back at least six decades, exists on the problem of the scattering of electromagnetic (e-m) radiation from randomly rough surfaces, important advances have been made within the Canadian context over the last twenty years. A new theory for dealing with rough-surface scattering problems has evolved from the work of researchers at Memorial University of Newfoundland. Primary incentives for the work lie in its relevance to remote sensing in the harsh environment of coastal and offshore resource development as well as the surveillance of Canadian interests within the "200-mile limit". Several applications of the theory to ground wave radar operations on Canada's East Coast have resulted. Some of the most significant theoretical and applied developments are briefly summarized here. [C6213]

"Global millimeter-wave observations of precipitation using AMSU on the NOAA-15 satellite"

This paper extends prior work on estimating instantaneous rain rates using data from the NASA Advanced Microwave Sounding Unit (AMSU) aboard the NOAA-15 satellite (Staelin and Chen, IEEE TGARS, vol. 38, pp. 2322-32, 2000) by utilizing more AMSU channels, training orbits, and seasons of the year, and by 1) inferring 15-km perturbations for the 50-km resolution channels, 2) adapting the algorithm to include cold dry atmospheres, 3) training using only the most reliable NOAA NEXRAD 3-GHz radar data, 4) applying the method to snowfall rate retrievals, and 5) preliminary global testing of the resulting algorithm over land and sea. The 15- and 50-km resolution algorithms were tested at AMSU rain rates up to 160 and 100 mm/h, respectively. [C6214]

"Elastic-wave scattering from a solid circular cylinder embedded in an elastic half-space"

An analytical solution is presented for the elastic-wave scattering from an infinitely long, solid circular cylinder embedded in an elastic half-space. The solution utilizes the spectral (plane-wave) representation of the fields and accounts for all the multiple interactions between the interface and the buried cylinder. Compressional and shear waves are allowed in both the half-space medium and the cylinder. A buried line-source is used for excitation and several cases are considered to examine the interaction of the incident elastic waves with the buried cylinder. The solution presented here is derived in the frequency-domain but is efficient enough to provide useful time-domain results through Fourier transform techniques. Using an incident Gaussian pulse in the time-domain, simulation results demonstrate the wave components (compressional, shear, Rayleigh) on the surface of the half-space and show the effect of burial depth on the scattered wave displacement. The analytical solution is general and not limited to buried object detection but can be used in other areas, such as non-destructive evaluation of composite materials or dynamical effect studies of composites. [C6215]

"Power budget study for passive target detection and imaging using secondary applications of GPS signals in bistatic radar systems"

Signals from satellite systems like GPS, IRIDUM and Globalstar that are reflected from moving or stationary objects are utilised for their detection in a synthetic aperture bistatic radar system (SAR). The movements of the satellite and its position at different coordinates with respect to time can serve as a base for a synthetic aperture. This paper focuses on the development of a system based on the analysis of indirect signals, in particular GPS signals. The main concern in this study is the low power of the GPS signal at the earth's surface (typically about -160 dB). Due to the nature of the reflector/target, some power will be absorbed, and hence result in a further reduction in signal strength reflected by the target. However, the other equally important concern here is the ground and sea clutter, which is 18-22 dB stronger than the direct signal level. Here we present theoretical results of both the maximum detection range and land clutter contributions of the air target detection by bistatic SAR that utilizes the existing GPS satellite as the transmitting signal source. [C6216]

"Bistatic radar scattering experiments of parallel wire grids"

The continued interest in bistatic polarimetric radar, particularly for SAR applications, has resulted in the requirement for additional simple, well characterized targets for external calibration. These targets must enable both bistatic and polarimetric radar modes to be calibrated, often to a precision of less than 1 dB. Previous research has shown that the use of wire grid structures could be a suitable bistatic calibration reference. In this paper we investigate the far-field bistatic scattering from a grid of parallel thin wires of different grid spacings. Experiments are conducted using the European Microwave Signature Laboratory (EMSL) over a frequency range of between 5 to 15 GHz for bistatic angles from 5 degrees to 150 degrees. The data was calibrated and compared to a Method of Moments (MOM) theoretical solution. [C6217]

"Could bistatic observations contribute to forest biomass monitoring?"

This contribution discusses some relevant features of bistatic scattering from vegetation. Based on a simulation

analysis using a theoretical model developed at Tor Vergata, it is shown that specular scattering of coniferous forests present a better sensitivity to biomass with respect to monostatic case. The performances of a non-specular bistatic radar are also simulated. [C6218]

"Analysis of temporal backscatter of rice: A comparison of RADARSAT observations with modeling results"

In this study, an established microwave backscatter model is used to predict the radar backscatter behavior of rice and to understand the interaction between backscatter and the rice canopy during its growth cycle. The emphasis of this study is to understand the effect of physical plant parameters on the backscatter signatures as a function of polarization and how these signatures vary during a complete growth cycle of rice. Inputs to the backscatter model included the physical parameters of rice as obtained through field measurements. These measurements were acquired within a few days of multiple RADARSAT acquisitions of the Zhaoqing test site in southern China. RADARSAT observations and the modeling results were then compared and analyzed. The results show that the interaction mechanisms change during the rice growth cycle and that polarimetric and/or multi-polarization measurements at C-band will contribute to rice monitoring programs. [C6219]

"Wheat cycle monitoring using radar data and a neural network trained by a model"

An algorithm, based on an electromagnetic model and a neural network, aimed at monitoring the multitemporal evolution of wheat fields, is described. Three different sites are used to validate the model, provide reference ground data, and test the algorithm. [C6220]

"Automatic rice-crop mapping using maximum likelihood SAR segmentation and Gaussian expectation maximisation"

Accurate, large scale crop monitoring requires the use of weather-independent sensors such as SAR. Rice is the staple food in many parts of Asia and knowledge of rice growth provides valuable economic and environmental information. Extensive pixel accuracy ground truth from an area of Kojima, Japan is used to compare the accuracy of unsupervised mapping algorithms. An acceptable classification is achieved by Gaussian expectation maximisation applied to existing maximum-likelihood (ML) based segmentation methods. Using a Bayesian extension of the ML segmentation scheme gives a dramatic improvement in accuracy which results in a pixel classification accuracy of 86% (68% kappa) and an essentially exact estimate of rice coverage within a 1000 hectare area. [C6221]

"Physics-based simulation of high-resolution polarimetric SAR images of forested areas"

In this paper, we present a comprehensive simulation of high-resolution, polarimetric synthetic aperture radar (SAR) images of forested areas. We model forest stands using realistic fractal trees over a lossy ground. The total response of the stand is calculated by coherently summing the responses of all the individual scattering components of the fractal trees, similar to the approach in Y.-C. Lin (1997, 1999). The major advantages of our simulation method are twofold: its potential high fidelity, since it employs a physics-based forest scattering model, and its ability to model high-resolution SAR response. We introduce our simulation method beginning with a description of our fractal mathematical models of trees. Next, we consider the polarimetric formulation of the received SAR signal from a forest of fractal trees. We describe methods of more efficiently calculating the received SAR signal and present a simple example of the efficiency of the simulation. [C6222]

"Joint application of altimeter and radiometer data for sea surface microwave signatures' detection and classification"

A concept for combining of data of altimeter and down looking or slight tilted radiometer observations is presented. Microwave, combined active-passive method for detection and identification of sea surface anomalous formations (signatures) is described, originated due to separate changes of various parameters, such as: the wind speed, the sea state in the form of swell or long wave spectrum characteristics, air and water temperatures, characteristics of foam formations, etc. [C6223]

"A study of radar backscattering on multi-scale bi-dimensional rough surfaces"

The principal objective of the present work is to find an adequate description of natural rough surfaces in order to study backscattering from these surfaces and try in a future work to retrieve soil characteristic parameters. Previous work has shown the inadequacy of the classical description which considered rough surfaces as stationary random Gaussian processes. They proposed a multi-scale surface description considering one-dimensional surfaces and incorporated it into the integral equation model (IEM). We extend this multi-scale

description to the bi-dimensional case using the Mallat algorithm and we investigate its impact on radar backscattering. [C6224]

"Application of IEM and radiative transfer formulations for bistatic scattering of rough surfaces"

Systematic characterization of scattering behavior of natural and man-made rough surfaces is required in many radar applications. In general, the overall scattering response of such surfaces is composed of surface and volume scattering components. In this paper integral equation method (IEM) is outlined to work out the surface scattering and the radiative transfer theory is applied to model the volume scattering. [C6225]

"Electromagnetic field simulation of target detection by high-resolution radar"

The electromagnetic field simulation of the target detection by high-resolution radar is performed by incorporating the asymptotic waveform evaluation (AWE) technique and the compression technique of a chirp signal. The electromagnetic field simulation is very helpful for revealing the multi-scattering mechanism of wide-band radar signal between targets or within a target. Our current simulation involves three major steps, in the first step, AWE technique is used to calculate the scattering far field over a wideband at which a radar is operated; in the second step, the frequency response of scattering field is multiplied by the spectrum of the chirp signal transmitted by radar to get the frequency response of radar system; in the third step, the system response is multiplied by the conjugate of the spectrum of the chirp signal and then transformed into time domain by inverse FFT. In this way the target detection by chirp radar can be accurately simulated using electromagnetic field. Numerical examples are presented. [C6226]

"Performance analysis for bistatic interferometric SAR configurations"

The results of an interferometric performance analysis for spaceborne parasitic SAR configurations are presented. The analysis includes errors due to limited SNR, block adaptive quantization, range and azimuth ambiguities, and geometric decorrelation for both flat surfaces and random volumes. Relative height accuracies for three spaceborne configurations with PALSAR, ASAR and TerraSAR-X as illuminators are derived and compared. [C6227]

"Comparison of microwave scattering models for leaf"

The Generalized Rayleigh-Gans (GRG) approach is used for the scattering cross section computation of leaves at low frequencies, while the Physical Optics (PO) approach is employed at high frequencies. In this paper, the magnitude of the scattering amplitude of the leaf is calculated using the two analytical methods (GRG PO) at different frequencies (i.e., L, C and X bands) and with different leaf shapes (circular and elliptical). In general, the difference between these models is of the order of several dB. [C6228]

"New designs or modes for flexible space borne SAR"

In a first step we recall the key constraints in spaceborne SAR and propose a new sizing typology for optimum trading around. The swath over azimuth resolution ratio, which is here called merit factor, has a strong impact on antenna area and power. A critical sizing is defined as giving the maximum merit factor at given antenna area. Then we introduce (or recall) different modes or designs for circumventing these constraints and we evaluate them with respect to the critical sizing reference. The DATS mode (doubling aperture by timing saturation) significantly reduces the power sensitivity to merit factor. The SETS mode (swath extension by timing saturation) doubles the swath at unchanged merit factor and antenna length and without the drawbacks of Scansar mode. Still at unchanged antenna area but at a price of some extra complexity in terms of antenna control (beam agility) or architecture (multi-antenna array), other modes improve the merit factor by up to 3.2. Echo tracking and steering are two possible modes for improving the merit on swath domain while DPCA (displacement phase centre) does it on resolution. To go further in merit factor and in reconfigurability needs radically different architectures with DBF (digital beam forming) possibly coupled with DPCA. We identify the limitations of all these modes/designs and particularly the matters of the timing and the nadir echo rejection. Rejection by beam notching is the only solution with standard SAR geometry while the vertical antenna geometry provides a natural nadir echo blocking and helps to reconcile antenna simplicity and reconfigurability. Finally we recall the ROSE concept (Radar Observation on Systematic and Economical way) that implements DBF (+ optionally DPCA) with vertical antenna and combines huge merit factor and design simplicity. [C6229]

"An evaluation of performance parameters of reconfigurable SAR systems"

The rapid progression in digital hardware systems and signal processing capabilities is increasingly advantageous for the development of radar systems. The trend is to move the digital hardware towards the

antenna front-end replacing, whenever possible, RF-hardware. Based on software codes these digital systems are more flexible and easier to reconfigure than RF-hardware. This paper investigates capabilities and limitations of synthetic aperture radar systems utilising digital beamforming. [C6230]

"SAR++: a multi-channel scalable and reconfigurable SAR system"

SAR++ is a technology program aiming at developing know-how and technology needed to design the next generation civilian SAR systems. Technology has reached a state, which allows major parts of the digital subsystem to be built using custom-off-the-shelf (COTS) components. A design goal is to design a modular, scalable and reconfigurable SAR system using such components, in order to ensure maximum flexibility for the users of the actual system and for future system updates. Having these aspects in mind the SAR++ system is presented with focus on the digital subsystem architecture and the analog to digital interface. [C6231]

"Synthetic aperture characterization of radar satellite constellations"

The concept of radar satellite constellations, or clusters, for SAR and other radar modes has been proposed and is currently under research. These systems are composed of multiple, formation-flying satellites with each satellite having its own, coherent receiver. Increased swathwidth compared to that of traditional SAR is attainable by processing the spatial data obtained from multiple satellites. The multi-channel system can also be scanned both forward and backward. The size and orientation of a such a system's resolution cell can change dramatically, however, depending on the number of satellites in the constellation, the size of the constellation, the look geometry, and the subset of data that is coherently processed. In addition, any of these parameters can be varied on demand according to mission requirements. The constellation itself forms an array that is sparsely populated and irregularly spaced. Furthermore, if the constellation is of extremely wide extent, then the width of its array pattern determines resolution rather than system bandwidth and coherent integration length. The problem of predicting system resolution is further exacerbated by forward- and backward-looking scenarios. In order to aid in the design, analysis, and signal processing of radar satellite constellations, we present a method of characterizing the resolution of such systems. We derive two eigensensors that can be interpreted as the dimensions of a two-dimensional synthetic aperture. Then, the synthetic aperture expression is used to derive resolution; simulations are presented to verify the theory. [C6232]

"Multi-channel airborne radar"

This paper examines two applications of a multi-channel airborne radar system, or an array-based synthetic aperture radar (SAR). The first mode involves a stripmap SAR array whose electronically-steered beam patterns are exploited to achieved the azimuth resolution of its single element while maintaining a relatively high radar power; this system has applications in foliage penetrating (FOPEN) SAR. The second array-based SAR utilizes two or more elements in the along-track domain to detect moving targets. Signal processing issues associated with these two array-based SAR systems are discussed. [C6233]

"Polarimetry based on one transmitting and two receiving polarizations: the $\pi/4$ mode"

The purpose of this study is to assess what can be learnt from polarization duality in reception for a SAR which transmits only one polarization. We focus here on a configuration where the two linear receiving polarizations are oriented at $\pi/4$ of each side of the unique transmitted linear polarization. A procedure to estimate a full polarimetric (fp) information over extended targets from this design (hereafter called the $\pi/4$ mode) is proposed, when the ity of complex correlation between co- and x-polarized terms is assumed. The behavior of point targets is subsequently considered. The performance assessment (based on SIR-C L band image analysis) relates to the level of information preserved comparatively to fp, but also to the concurrent space segment complexity, in terms of working pulse repetition frequency (PRF), processed swath and down link features. [C6234]

"Incidence angle dependence of the L-band POL-IN-SAR sensitivity at forestry region-ALOS PALSAR study using the Pi-SAR"

Forest biomass is one of the key parameters that indicate temporal change of the global continental carbon volumes, and its global estimation is required as described in the Kyoto protocol. NASDA's ALOS science project strongly intends its estimation either solely by SAR or in conjunction with the other optical sensors and the ground truth data. There have been (or are being) developed SAR based methods to estimate the forest biomass, which utilize the relationship between sigma-zero and biomass quantity, those based on coherence of one day separated C band data and L band radar intensity, and those based on forest tree heights and biomass quantities, etc. For the third category, it is expected that Pol-In-SAR might relate the interferometric phase difference at different polarizations to the tree structures and heights, and two-frequency interferometry relates to the phase center difference to the tree height. [C6235]

"Eigenvector analysis of polarimetric SAR data"

Fully polarimetric SAR data analysis has found wide application for terrain classification, land-use, soil moisture and ground cover classification. New methods and algorithms continue to be developed and tested. One method that has gained great popularity is the Cloude-Pottier eigenvalue/eigenvector decomposition of coherency matrices (Cloude and Pottier 1996). The eigenvalue spectrum uniquely describes the scattering entropy, anisotropy and span (total power). The eigenvectors are employed in the calculation of averaged quantities. Typically though the eigenvector components have not been analyzed in much detail. Here we present a general analysis of the eigenvectors based on an earlier observation (Cloude 2001) that the eigenvectors may be parameterized by a set of rotations. [C6236]

"A new method for radiometric calibration of spaceborne SAR and its global monitoring"

To calibrate synthetic aperture radar (SAR) images to normalized radar cross sections (NRCS) a calibration constant is required. Usually the calibration constant is determined by analyzing measurements of corner reflectors. However, due to the high costs there are only a very limited number of corner reflectors available. In this paper a new method for estimating the calibration constant on the basis of a few days of SAR data is introduced. The method is based on knowledge of the dependency of the NRCS on the ocean surface wind, which is described by well-tested empirical C-band models, e.g., CMOD4 and CMOD IFR2. Given the mean wind vector at each SAR wave mode image both models enable to derive the mean NRCS of the image. Application of the method is demonstrated and validated utilizing a total of 34000 SAR imageries and co-located winds from the European Centre for Medium range Weather Forecast and the ERS-2 scatterometer. The SAR imageries were processed to ENVISAT ASAR-like single look complex SAR images using three weeks of SAR wave mode data. It is shown that the method is an ideal tool for retrieving the SAR calibration constant and is capable to monitor and estimate variations of the calibration constant, e.g., due to saturation of the SAR analogue to digital convertor or gain drifts. [C6237]

"Multi-resolution analysis of polarimetric SAR data using wavelets"

An analysis technique is presented for quantifying statistically and under a unified framework non-stationarity in polarimetric SAR imagery. The unified framework is provided by a multi-resolution analysis (MRA) based on a particular wavelet frame that works like a differential operator. The wavelet MRA provides local estimates of a statistics called structure function, that in turn can characterize two types of non-stationary behavior: smoothed singularities (e.g. edges, point targets); self-similar processes with stationary increments (e.g. fractional Brownian motion). In the polarimetric case we are interested in the combined dependencies on scale and polarization state. To the purpose an extension of the wavelet MRA is introduced for deriving wavelet representations of an intensity image synthesized at any polarization state (pol-MRA). A novel formalism called the polarimetric structure signature condenses in graphical form the properties of points of discontinuity with respect to scale and polarization transformations. A test case illustrates the application of the pol-MRA technique to the analysis of weak but polarimetrically diverse linear features embedded in clutter. [C6238]

"On the relationship between polarimetric parameters and soil moisture"

Rough surface scattering depends on both roughness and dielectric constant of a surface. Therefore, a polarimetric measurement is useful for estimating soil moisture since we can remove the surface roughness effect using multiple scattering components from a polarimetric measurement. In this paper, we examine the relationship between polarimetric parameters and soil moisture. For example, the co-polarization ratio is independent of surface roughness to the first order of the small perturbation approximation. As surface roughness increases, it can be shown that both co- and cross-polarization ratios depend on the surface slope under the tilted Bragg approximation. The effects of the surface roughness to these ratios are theoretically investigated. An algorithm is proposed to estimate soil moisture from both co- and cross-polarization ratios. We will also study other polarimetric parameters such as the average alpha angle and eigenvalues to understand their relationship with soil moisture. [C6239]

"Estimate relative soil moisture change with multi-temporal L-band radar measurements"

First Page of the Article [C6240]

"A new parameter for soil moisture estimation"

In this paper we introduce a new ratio of polarimetric scattering coefficients that we suggest is sensitive to surface moisture content and insensitive to roughness variations. The parameter is first derived from the

extended Bragg surface model and then validated using wide band chamber measurements of surface backscatter collected at the European Microwave Scattering Laboratory (EMSL). [C6241]

"Classification and interpretation of polarimetric interferometric SAR data"

In this paper is introduced an approach to the classification and interpretation of SAR data using the complementary polarimetric and interferometric information. An unsupervised polarimetric segmentation is applied to one of the separate interferometric dataset. The use of pertinent polarimetric indicators permits to give an interpretation of each resulting cluster scattering mechanism and to classify the observed scene into three canonical scattering types. The interpretation and the segmentation of an optimized interferometric coherency spectrum is applied, for each type of scattering, to initialize an unsupervised statistical interferometric classification procedure. [C6242]

"Polarimetric SAR measurements of slope distribution and coherence changes due to internal waves and current fronts"

Studies have shown that polarimetric SAR may be used to measure terrain slopes and surface roughness. These measurement concepts have been extended here to study slope distributions generated by surface manifestations of internal waves, as well as, by convergent current fronts. Measurements/modeling of these ocean features are generally done using backscatter intensity modulations. In this work, internal wave induced changes in the polarimetric orientation angle are measured. These changes are then used to estimate those perturbations in the ambient wave slope distribution and coherence that are directly caused by the internal wave. [C6243]

"Model-based principal component techniques for detection of buried landmines in multiframe synthetic aperture radar images"

Here we consider the use of model-based methods for the detection of buried objects from a sequence of synthetic aperture images obtained by a radar sensor moving linearly down a track. The scattering physics of the underlying sensing modality cause the relevant target signatures to change in a complex yet predictable manner from one image to the next. To arrive at a tractable processing scheme that exploits these motion-induced changes, we develop a flexible parametric model capable of capturing the full variation of these signatures. A detection scheme based on a principal components analysis of estimated model vectors is then derived. Results are demonstrated using field data from a forward-looking sensor. [C6244]

"Optimization of migration method to locate buried object in lossy medium"

We present an optimized frequency-wavenumber (F-K) migration method to localize buried objects such as landmines in lossy medium. F-K migration has been proposed to find the location of a buried object using ground penetrating radar (GPR) data. This approach makes use of a wave equation in the Fourier domain to back-propagate the received wavefield. For GPR applications however, standard F-K migration assumes that the ground surface is flat and the medium is loss-free which are not true in reality. When implemented in the Fourier domain, the wave equation becomes the Helmholtz equation. It is then straightforward to incorporate a complex index of refraction in the Helmholtz equation to describe wave phenomenon in lossy medium. We generalize F-K migration to the case of rough ground surface and lossy medium. In the framework of Tikhonov regularization, we develop an algorithm that optimally alters the wave propagation velocity and the complex index of refraction to take into account of the ground roughness and lossy medium. In the process of searching the optimal velocity and complex index of refraction, the algorithm is constrained to produce an image of minimum entropy. By minimizing the entropy of the resulting image, better results are obtained in terms of enhanced mainlobe, suppressed sidelobes, and reduced noise. We use examples from field data to demonstrate the performance of our method. [C6245]

"Multistatic GPR data acquisition and imaging"

This paper proposes multistatic measurements to increase the information content of ground penetrating radar data. Three different acquisition strategies are distinguished. To obtain measurement data, a flexible setup has been realized. Tomographic backpropagation and the nonlinearized factorization method are discussed with regard to their applicability to multistatic data. [C6246]

"Despeckling SAR images using a low-complexity wavelet denoising process"

Most existing wavelet denoising techniques are developed for additive white Gaussian noise. In their applications to speckle reduction in SAR imagery, the traditional approach is to first perform a logarithmic transformation to

convert the multiplicative noise model to an additive model, and then after wavelet denoising is performed on the log-transformed image, an exponential operation has to be implemented for radiometric preservation. In this paper, we introduce a low-complexity wavelet-based SAR speckle reduction algorithm which omits both the log-transform and the exponential transform operations. We decompose the multiplicative speckle model into an additive model with signal-dependent noise. Then, in the wavelet domain, we derive the shrinkage factor for each wavelet coefficient by applying the Minimum Mean Square Error (MMSE) estimation procedure. Simulated SAR images are used to evaluate the denoising performance of our proposed algorithm along with another wavelet-based denoising algorithm that involves the log-transform and exponential operation, as well as the refined Lee speckle filter. Experimental results show that the proposed filter outperforms the other filters in most cases. [C6247]

"Stand off detection of buried anti-personnel landmines"

A small, low powered, ultra wideband radar using a picosecond switching system has demonstrated the ability to produce radar images of surface laid landmines using an experimental rail SAR setup at a stand off range of 30 feet. [C6248]

"A super-resolution locationing algorithm for ultra-wideband phased-array radars"

Super-resolution direction finding algorithms such as MUSIC or ESPRIT methods inherently assume narrow-band signals, which are not applicable to ultra-wideband radars such as GPR (ground penetration radar). We developed a time-domain algorithm to determine the time and direction of arrival pulses with an order higher resolutions than the nominal resolution determined by the aperture size. The received signal waveform at each array element is first analyzed by the recursive nonorthogonal decomposition using a dictionary of basic waveforms. After the delay time of the echoes in each element of the receiving array is determined, the number of targets and their locations are determined by analyzing variation of the delay time over the array with the aid of a Hough transform. The robustness of the proposed algorithm is confirmed by numerical simulations. [C6249]

"The afternoon constellation: a formation of Earth observing systems for the atmosphere and hydrosphere"

Two of the large EOS observatories, Aqua (formerly EOS-PM) and Aura (formerly EOS-CHEM) will orbit in nearly the same inclination with 1:30 PM ± 15 min ascending node equatorial crossing times. Between Aura and Aqua a series of smaller satellites will be stationed: Cloudsat, CALIPSO (formerly PICASSO/CENA), and PARASOL. This constellation of low Earth orbit satellites will provide an unprecedented opportunity to make atmospheric cloud observations. This paper provides details of the science opportunity and describes the sensor types for the afternoon constellation. [C6250]

"Ground water migration monitoring by GPR"

In order to understand the capability of monitoring ground water movement by ground penetrating radar (GPR), we carried out a field survey in Mongolia. We controlled water production at a ground water source area and the change of ground water level at about 5 m in depth could be detected by GPR. The change of the ground water level was observed more than 15 m in the radial distance from the pumping well. The change of the vertical water content was also evaluated by GPR. [C6251]

"Optimized GPR signal deconvolution using an adaptative conjugate gradient method"

Presents a signal processing method to improve the identification of interface between different layered media, using a deconvolution process. Our methodological approach is based on an inverse problem algorithm, called conjugate gradient method. The emitted pulse is assumed to be known, and the convolution is considered as a linear operator that must be inverted. We take into account the distortion of the signal and the noise of the recorded signal. [C6252]

"On the use of surface impedance in the detection of buried objects"

A method to detect and locate the objects buried in a half-space is presented. The method is based on the reconstruction of the appearing surface impedance of the half-space through remote field measurements of scattered field for a single plane wave illumination. The existence of the objects causes surface impedance to be a function of location and by observing its variation along the surface one can achieve the detection. The method is applied to several examples to show its efficiency and accuracy. Effects of different parameters on the solution are also demonstrated. [C6253]

"Performance of scanning millimeter-wave radar in a tropical environment"

The minimum detectable radar reflectivity (dBZ_{min}) is computed for the University of Massachusetts' 33 GHz/95 GHz Cloud Profiling Radar System (CPRS) under humid tropical conditions. Extinction by water vapor and oxygen are calculated for a horizontally stratified atmosphere as a function of range and scan angle for both radar frequencies. Combined radiosonde and dual-frequency microwave radiometer measurements are used to model radar signal extinction for the Maritime Continent Thunderstorm Experiment (MCTEX), which was conducted in northern Australia. These data are compared with CPRS radar measurements to evaluate the performance of both frequencies for sensing clouds and precipitation versus elevation angle. [C6254]

"Estimating TRMM spacecraft attitude errors using the precipitation radar"

Results are presented from analysis of the Tropical Rainfall Measuring Mission (TRMM) Precipitation Radar (PR) data for the purpose of estimating satellite attitude information. Deviations from nominal roll are detected using the surface echo distances measured by the PR. This technique has been used for continued monitoring of attitude anomalies that occurred shortly after the TRMM satellite altitude increase and for historical data. [C6255]

"Rainfall observations by the airborne dual-frequency precipitation radar during CAMEX-4"

The 2nd Generation Precipitation Radar is a new design for a dual-frequency (13.4 and 35.6 GHz) spaceborne precipitation radar. An airborne PR-2 simulator has been developed to demonstrate key technologies. This airborne system was flown on the NASA DC-8 aircraft during the 4th Convection and Moisture Experiment in 2001. Data were acquired in Tropical Storms Chantal and Gabrielle, Hurricane Humberto, and in several more localized convective systems. The authors discuss the design of the PR-2 airborne radar and show observations from CAMEX-4. Overall, the observations validated the design of PR-2 and provide an extensive data set for scientific analyses. [C6256]

"Polarimetric radar rainfall algorithms at S and X bands"

This paper presents a comparison of S- and X-band algorithms for rainfall estimate. This topic is fairly extensive and only limited results are presented for brevity. The results demonstrate that $R(Kdp)$ at X-band can be useful at much lower rainrates compared to S-band. [C6257]

"Bright-band modeling of air/space-borne microwave radars"

In simulating the radar echo in the melting layer of stratiform rain, a melting snowflake is modeled as a spherical non-uniform mixture, prescribed as a stratified-sphere in that the fractional water content is given as a function of the radius of sphere. Combined with the melting layer model that depicts the melting fractions and fall velocities of hydrometeors, the radar profiles are produced and then compared with the measurements of TRMM PR and the dual-wavelength airborne radar. [C6258]

"Speckle reduction of SAR images in the curvelet domain"

Curvelet transform (CT), proposed by E. Candes et al. (1999), is used for speckle reduction of SAR images. The CT is useful for speckle reduction through its subband images and the speckle reduction is obtained by thresholding the subband-image coefficients of the digitized SAR images. Two thresholding methods are used; hard thresholding and soft thresholding. The denoising method shows great promise for speckle removal and hence provides good detection performance for SAR based recognition. [C6259]

"Heterogeneity-sensitive adaptive speckle reduction in a translation-invariant wavelet domain"

In this paper, LLMMSE filtering is performed in the undecimated wavelet domain by means of an adaptive rescaling of detail coefficients. The amplitude of each coefficient is divided by the variance ratio of the noisy coefficient to the noise-free one. All the above quantities are analytically calculated from the speckled image, the speckle variance, and the wavelet filters only, without assuming any model to describe the underlying backscatter. Empirical criteria based on distributions of multiresolution C_v calculated in the undecimated wavelet domain are introduced to mitigate the rescaling of coefficients in highly heterogeneous areas where the speckle is not fully developed, to definitely avoid the slight blurring noticed in some textures and the perceivable smearing of point targets. Experiments carried out on SAR images demonstrate that the visual quality of results is excellent in terms of both background smoothing and preservation of edge sharpness, textures, and point targets. The absence of decimation in the wavelet decomposition avoids the typical impairments produced by critically-sampled wavelet-based denoising. [C6260]

"Enhanced polarimetric radar signatures above the melting level in a supercell storm"

The dataset analyzed is the first simultaneous in-situ and radar survey of phenomena associated with observed "columns" of differential reflectivity Z_{dr} and specific differential phase K_{dp} in a supercell storm. Further, no in situ measurements in regions of such enhanced Z_{dr} and K_{dp} have ever been reported. The measurements were made in an Oklahoma convective storm that formed in Kingfisher County, on May 17, 1995. Parcel and environmental freezing temperatures were near the 600 mb level (3.5 km AGL). Official observations of 2.5 cm hail were reported as well as a 40 m s⁻¹ wind gust. Dual-polarization radar measurements were obtained with the NSSL's Cimarron radar. The in situ measurements are provided by the T-28 aircraft at a height of between 4.9 and 5.2 km (near 500 mb; about -5° C). These include temperature, vertical velocity and liquid water content (LWC), as well as hydrometeor size and concentration from the hail spectrometer and a foil impactor. [C6261]

"Evaluation of TRMM PR attenuation correction using ground radar estimations of the raindrop size distribution along the PR beam"

Estimation of the raindrop size distribution (RSD) is made along the beam-path of the Tropical Rainfall Measuring Mission (TRMM) Precipitation Radar (PR). The PR is a nadir-pointing spaceborne radar that operates at 13.8 GHz frequency. It is currently being used, along with other instruments aboard the TRMM satellite, for meteorological research. Short wavelength systems are used to reduce cost while maintaining the resolution near the Earth's surface required for meteorological sampling. The limitations are the high signal degradation of the return signal caused by scattering and absorption of the precipitating medium that it is intended to probe. Correction of the TRMM PR return echo is based on a single-frequency technique, which is evaluated using ground-based polarimetric radar observations. Quantitative estimation of a 3-parameter gamma model is made of the RSD along the PR beam. PR attenuation correction is compared to the median values of the RSD parameters. In particular, variations of the median drop size diameter (DO) and normalized intercept parameter (Nw) with PR correction is made along the PR vertical profile in the rain layer. Data collected during the TEXAS and FLORIDA UNDERFLIGHTS (TEFLUN-B) experiment and TRMM Large Biosphere-Atmosphere experiment in Amazonia (LBA) field campaign is used in the evaluation. [C6262]

"Global mapping of attenuation at X-band and higher frequencies"

The propagation of radio waves for Earth/space slant path at C-band and higher frequencies are dominated by precipitation in the atmosphere. At a given frequency, attenuation depends on the length of the radio path, the size distribution and the phase state of the hydrometeor profile. Using the observations from the TRMM spaceborne Ku-band (13.8 GHz) radar at Low Earth Orbit of 350 km above Earth, global attenuation maps are produced at the Ku-band frequency. A simple precipitation microphysical model developed using hydrometeor size distributions and phase state is used to scale this observed attenuation to Ka-band (35 GHz) where numerous high bandwidth satellite applications are being planned including the next generation space based radar for the Global Precipitation Mission (GPM). In this study, three layers of precipitation that consist of aggregate, dry graupel and rain are considered. Using this precipitation model the attenuation and backscatter reflectivity relations between Ka- and Ku-band frequencies are developed for scaling the specific attenuation and backscatter reflectivity along the observation path. The results show substantial attenuation variation in a 12-month period at both Ku- and Ka-bands over the various regions of the globe. These results can help in the design and development criteria for satellite applications at Ka-band. [C6263]

"L-band polarimetric AIR/Pi-SAR images around Niigata City"

Pacific Rim Campaign has been successfully carried out in 2000. The well known AIRSAR system by JPL flew over Niigata Area, Japan, on Oct. 2, 2000, which brought us the L-band fully polarimetric data set. On the other hand, Pi-SAR, developed by CRL and NASDA, Japan, simultaneously (2 hours in advance) flew the same path taking the same area data in the L-band. It became possible for us to carry out comparative analyses using the same area data. Since the resolution and incidence angle of each SAR are different, we examined the difference in the two POL-SAR images using correlation coefficient in the Right-Left Circular (RL) polarization basis, polarimetric entropy, and three component scattering power ratio. [C6264]

"Extraction of surface parameters from multi-frequency and polarimetric SAR data"

The aim of this paper is to analyse the information contained in multi-frequency and polarimetric SAR data for an accurate retrieval of surface geophysical parameters. A two-scale surface scattering model is presented with the aim to develop an inversion algorithm. This model is represented by projection into a three-dimensional space defined by the H-A- α parameters, which permits, for each observation frequency value, to obtain distinct curves with respect to the soil moisture content and large-scale roughness. Then, a comparison between multi-

frequency and polarimetric data from the JRC laboratory and the two-scale surface polarimetric response is carried out. At last, two different multi-frequency parameter inversion methods based on artificial neural networks schemes are proposed. [C6265]

"Surface parameter estimation using interferometric and polarimetric SAR"

In this work the potential of using the interferometric coherence at different polarisations over surface scatterers in order to extract information about surface parameters is investigated. The sensitivity of the individual coherence contributions to surface roughness and moisture conditions is discussed and simulated using a polarimetric surface scattering model. Finally, experimental airborne SAR data are used to demonstrate the discussed effects. [C6266]

"Characterization of symmetric scattering using polarimetric SARs"

Cameron's coherent target decomposition (CTD) and classification are discussed in the context of SAR, and the limitations of Cameron's classification are examined. It is shown that these methods may lead to a coarse and misleading scattering segmentation because of the large radiometric dispersion tolerated in each of the elemental scatterer classes, as well as the implicit assumption on the coherence nature of target scattering. A new method, named the symmetric scattering characterization method (SSCM), is introduced to better exploit the information provided by the largest target symmetric scattering component, under coherent conditions. The SSCM, which expressed the symmetric scattering in term of the Poincare sphere angles, permits a better characterization of target symmetric scattering and the generation of coherent scattering segmentation of much higher resolution, in comparison with Cameron's segmentation. [C6267]

"Scene characterization using sub-aperture polarimetric SAR data analysis"

In this paper is introduced a fully polarimetric sub-aperture analysis method. A deconvolution technique is developed in order to decompose synthesized SAR images into sub-aperture data sets which correspond to the scene global response observed under different azimuthal look angles. A polarimetric variation analysis is achieved, using pertinent parameters, to determine the nature of the non-stationary scattering mechanisms. A statistical analysis of the polarimetric parameters permits to clearly discriminate the media showing a varying behavior during the SAR integration. Decomposition and analysis techniques are applied to data acquired by the DLR airborne E-SAR sensor at L band. [C6268]

"Passive bistatic radar sensing with LEOS based transmitters"

In this paper we describe the concept of a bistatic SAR system which involves a purpose built stationary ground based receiver but which utilizes existing or proposed low earth orbit satellite (LEOS) communication systems, such as Globalstar or ICO as the transmitting signal sources. In general, such a system has a 3-D configuration (in contrast to the 2-D bistatic SAR systems examined previously in the literature). We analyse this system. With earth observation applications in mind, we characterize quantitatively the 2-D resolving capability within the ground plane. This is demonstrated via a meaningful simulation. [C6269]

"A comparison between IEM-based surface bistatic scattering models"

The original IEM surface scattering model used a simplified surface current estimate leading to relatively simple but accurate results for forward and backscattering configurations. Since then other estimates of the surface current based upon the same set of integral equations have appeared in the literature. A major reason for considering a more complex estimate is because in the original IEM model the phase in the Green's function was not included in the integration process over the surface current to find the scattered field. Thus, it is not applicable to multiple scattering calculations. Currently, there are three different modifications suggested by different investigators: (1) use of the phase factor in the Green's function of the upper medium for integration over surface current, (2) use of the phases in the Green's function in both the upper and lower medium for integration over surface current, and (3) in addition to (2) further modify the Fresnel reflection coefficient to be the sum of reflection coefficients evaluated at the incident and scattering angles divided by two. In this paper we want to compare model predictions based on the use of the above surface current estimates under backscattering and bistatic conditions. [C6270]

"The interferometric cartwheel: a multi-purpose formation of passive radar microsattellites"

The interferometric cartwheel (CNES patent) is composed of three passive identical microsattellites set in a particular orbital geometry and flying behind or ahead of an active synthetic aperture radar (SAR) satellite. This satellite illuminates a ground swath and the reflected signals are received by the microsattellites with specific

viewing configurations. The obtained data are mainly used for the computation of a Digital Elevation Model (DEM). This paper details first the across-track interferometry principle specific to the cartwheel geometry. General system and satellite characteristics are then presented as well as their main constraints. Finally, a performance budget based on a typical satellite configuration is carried out and leads to the topographic accuracy of the DEM. [C6271]

"Polarimetric mapping of ship wakes"

This paper addresses the problem of ship wake detection and analysis at low grazing angles. Specifically, we examine the spatial distribution of the characteristic polarimetric signatures of the sea surface in and around the wakes of a pilot boat. The received signals were range-processed and polarimetrically decomposed to yield the characteristic polarisation states. Inspection of the locations of these states revealed that the polarisation signatures were highly non-uniformly distributed in the spatial domain, as expected, with interesting features attributable to nonlinear effects. Focusing on the cross-polar s , we found that the corresponding eigenvector distribution made a strong transition as one moved from the wake region to the surrounding sea. By defining appropriate scalar quantities we were able to identify wake and clutter regions. The results suggest that exploitation of the coherent polarisation domain may significantly enhance wake feature extraction and discrimination. [C6272]

"Modulation of polarimetric coherence by ocean features"

Fully-polarimetric SAR images from two scenes from the west coast are analyzed to study the modulation of polarimetric coherence by ocean features. Co-polarized and circularly polarized coherences are calculated for ocean surface waves, a weather front, a coastal plume and a ship wake. The study concludes that changes in short scale surface roughness did not modulate the co-polarized coherence. But changes in the dielectric constant did affect this coherence. [C6273]

"Feasibility study on polarimetric use and calibration of ALOS/PALSAR"

Calibration and application of polarimetric synthetic aperture radar (SAR) onboard the Advanced Land Observing Satellite (ALOS) is discussed using airborne L-band SAR data. We find that even a simple calibration is useful for polarimetric classification, if the system has a small cross-talk and good channel balance. [C6274]

"Development of a retrodirective PARC for ALOS/PALSAR calibration"

A novel PARC of Van Atta array design is developed for polarimetric calibration of PALSAR onboard the ALOS satellite. The PARC consists of four dual-polarized 343-cross-dipole subarrays. The Van Atta array configuration combining with dual-polarized nature of the subarrays provides the PARC the depolarizing and retrodirective characteristics simultaneously. [C6275]

"Calibration and validation of PALSAR"

This paper introduces preliminary CAL/VAL of the Phased Array type of L-band Synthetic Aperture Radar (PALSAR) onboard the Advanced Land Observing Satellite (ALOS) in terms of the antenna pattern error distribution and the image correlation using the PALSAR parameters. More CAL VAL will be conducted to ensure the applicable potential of PALSAR to the Earth environmental monitoring, e.g., the disaster, forest (biomass), land surface classification, DEM generation capability, and so on. [C6276]

"Needs for communications and onboard processing in the vision era"

The NASA New Millennium Program (NMP), in conjunction with the Earth Science Enterprise Technology Office, has examined the capability needs of future NASA Earth Science missions and defined a set of high priority technologies that offer broad benefits to future missions, which would benefit from validation in space before their use in a science mission. In the area of spacecraft communications, the need for high and ultra-high data rates is driving development of communications technologies. This paper describes the current vision and roadmaps of the NMP for the technology needed to support ultra-high data rate downlink to Earth. Hyperspectral land imaging, radar imaging and multi-instrument platforms represent the most demanding classes of instruments in which large data flows place limitations upon the performance of the instrument and systems. The existing and prospective data distribution (DD) modes employ various types of links, such as DD from low-Earth-orbit (LEO) spacecraft direct to the ground, DD from geosynchronous (GEO) spacecraft, LEO to GEO relays, multi-spacecraft links, and sensor webs. Depending on the type of link, the current data rate requirements vary from 2 Mbps (LEO to GEO relay) to 150 Mbps (DD from LEO spacecraft). It is expected that in the 20-year timeframe, the link data rates may increase to 100 Gbps. To ensure such capabilities, the aggressive development of

communication technologies in the optical frequency region is necessary. Current technology readiness levels (TRL) of the technology components for the space segment of communications hardware varies from 3 (proof of concept) to 5 (validation in relevant environment). Development of onboard processing represents another area driven by increasing data rates of spaceborne experiments. The technologies that need further development include data compression, event recognition and response, as well as specific hyperspectral and radar data processing. Aspects of onboard processing technologies requiring flight validation include: fault-tolerant computing and processor stability, autonomous event detection and response, situation-based data compression and processing. The required technology validation missions can be divided in two categories: hardware-related missions and software-related missions. Objectives of the first kind of missions include radiation-tolerant processors and radiation-tolerant package switching communications node/network interface. Objectives of the second kind of missions include autonomous spacecraft operations and payload (instrument-specific) system operations. [C6277]

"ALOS-PALSAR image simulation in various polarization bases"

The ALOS-PALSAR is the first L-band space-borne SAR in the world equipped with a fully polarimetric data taking function. For the data utilization purpose, the authors have examined the polarimetric performance (scattering matrix and resultant images) over the Toyano area, Niigata City, Japan, using the airborne Pi-SAR radar. Since the resolution will be 20 m by 20 m on the ground surface by PALSAR, the Pi-SAR data (3 m by 3 m) are ensemble to be an equivalent size for ALOS-PALSAR image simulation. The polarimetric characteristics of terrain including paddy-fields, grass-fields, residential areas, etc., were examined to show the difference in the right-left polarization handedness basis and coherency vector, three-component scattering model, and polarimetric entropy. [C6278]

"Advances in extra wide-band multi-modal air/space-borne radar polarimetry, POL-IN-SAR imaging and its applications"

Radar Polarimetry, Radar Interferometry and Polarimetric SAR Interferometry represent the current culmination in 'Microwave Remote Sensing' technology, but we still need to progress very considerably in order to reach the limits of physical realizability. Whereas with radar polarimetry the textural fine-structure, target orientation, symmetries and material constituents can be recovered with considerable improvement above that of standard 'amplitude-only' radar; by implementing 'radar interferometry' the spatial (in depth) structure can be explored. With Polarimetric Interferometric Synthetic Aperture Radar (POL-IN-SAR) imaging, it is possible to recover such co-registered textural and spatial information from POL-IN-SAR digital image data sets simultaneously, including the extraction of Digital Elevation Maps (DEM) from either Polarimetric (scattering matrix) or Interferometric (dual antenna) SAR systems. Simultaneous Polarimetric-plus-Interferometric SAR Imaging offers the additional benefit of obtaining co-registered textural-plus-spatial three-dimensional POL-IN-DEM information, which when applied to Repeat-Pass Image-Overlay Interferometry provides differential background validation and environmental stress-change information with highly improved accuracy. Then, by either designing multiple dual polarization antenna POL-IN-SAR systems or by applying advanced POL-IN-SAR image compression techniques, will result in 'POL-arimetric TOMO-graphic' (Multi-Interferometric) SAR or POL-TOMO-SAR imaging. [C6279]

"Helicity in radar remote sensing"

In this paper we investigate the use of radar polarimetry and polarimetric radar interferometry for measuring the properties of random chiral particle clouds. Helicity is an established concept in radar polarimetry but to date it has been restricted to coherent scattering mechanisms. Here we show how it can be used for random media studies and conclude as to its potential impact in the radar remote sensing of vegetation. [C6280]

"Preparation of multi-stage remote sensing for monitoring sea ice in the Okhotsk Sea with ALOS sensors"

In order to develop and/or improve algorithms of extracting various sea ice parameters, such as sea ice concentration, sea ice thickness, and sea ice types from ALOS data, it is necessary to prepare certain data set for verification. This paper describes about the preparation of multi-stage remote sensing for obtaining a series of remotely sensed data of sea ice in the Okhotsk Sea. [C6281]

"Study of environmental issues with ALOS PALSAR data"

The Advanced Land Observing Satellite (ALOS) will carry three advanced sensors for addressing many environmental issues, such as vegetation change, water resource management, disaster and earthquake mitigation, and cryosphere monitoring, in a broad range of earth science disciplines. PALSAR has many unique

features in its L-band, multi-imaging mode (high-resolution, ScanSAR, and polarimetric), varying incident angles, and multi-polarization, compared to other SAR satellites operating in the orbit now or in the past. In our research proposal for ALOS research announcement, we focus on the use of PALSAR data in flood management and surface change monitoring for the Yangtze River, detection of surface subsidence in oil field, monitoring of coastal expansion and land cover changes in the Yellow River estuary, and study for surface deformation related to potential volcanic activities, palaeo-environment evolution, and snow and ice etc. Although the launch of ALOS in 2003 makes us unable to give a report of research result with ALOS data, we will present our research plan and expectation with PALSAR and other sensor data, and give some results of our study using other SAR data in relation to the issues being addressed in our research with ALOS data. [C6282]

"Study on air-sea-land interaction in the coastal seas using ALOS data"

The coastal surface wind is complicated due to deformation by the land topography and influence through land-sea thermal and roughness differences. ALOS has a high potential in observations for coastal seas because of its high-resolution sensors, i.e., Phased Array type L-band Synthetic Aperture Radar (PALSAR) and Advanced Visible and Near Infrared Radiometer type 2 (AVNIR2). We present research and operational prospects of ALOS for air-sea-land interaction in the coastal seas. [C6283]

"Anisotropic diffusion filtering and phase unwrapping for interferometric SAR"

This paper describes a novel variational optimization model with anisotropic diffusion for interferometric synthetic aperture radar (SAR) phase unwrapping, which is derived with the use of a global cost function to minimize the phase discontinuities in the unwrapped phase map and reduce noise. Numerical results proved that our phase unwrapping algorithm is robust and reliable on high noisy phase data with discontinuation. [C6284]

"PURSUIT: an automatic classification tool for remote sensing data"

PURSUIT (Projection Understanding and Recognition from a SUite of intelligent Tools) has been under development at the Naval Research Laboratory for a number of years. It is a versatile software tool designed to address the problem of automatic feature extraction and classification from remote sensing data. Although the tool can be applied to a variety of applications outside of the field of remote sensing, it is particularly useful for automated remote sensing imagery analysis. To date, the package has been applied to imagery from a variety of different sensor types including: multispectral, hyperspectral, synthetic aperture radar (SAR), and multi-sensor data. Because of its modular design, PURSUIT is re-configurable and the suite of algorithms that comprise it can be flexibly combined to address new applications as they arise. As such, new algorithms can be easily added. Algorithms included in the present corpus consist of a variety of in-house algorithms, as well as standard algorithms derived from many areas of the statistical pattern recognition literature, including adaptive vector quantization, unsupervised and supervised feature extraction and classification, and neural networks. Each module contains a number of different preprocessing and post-processing options, and the input data may be spectral, spatial, or spatial-spectral. The modular design of the package allows data from multiple sources to be combined in the same overall automatic classification model. [C6285]

"A spectral analysis algorithm for the estimation of sea SAR image fractal dimension"

This paper proposes a spectral analysis algorithm for sea SAR image fractal dimension estimation. The power spectral density of the sea SAR image is obtained through the periodogram approach and by decomposing the spectrum into sub-bands according to a dyadic scale. The fractal dimension of the image is obtained by a linear regression of the absolute maxima of each sub-band. This method can be applied globally or locally to have a single value or a map of the image fractal dimension. Examples on simulated and real data are reported. [C6286]

"GoMEx-an experimental GIS system for the Gulf of Mexico region using SAR and additional satellite and ancillary data"

The National Oceanic and Atmospheric Administration (NOAA) National Environmental Satellite, Data, and Information Service (NESDIS) is in the third year of the Alaska SAR Demonstration (AKDEMO), an applications project using RADARSAT-1 synthetic aperture radar (SAR) and derived products. The success of this demonstration in providing near real-time SAR data, derived products, and other ancillary data to federal and state agencies, has motivated the development of a similar experimental multi-sensor data fusion system for the Gulf of Mexico and Caribbean region called GoMEx. Unlike the AKDEMO system which focused on near-real time data, this project will begin by using archived data from diverse remote sensing sensors such as RADARSAT-1 SAR, GOES imagers, SeaWiFS, MODIS, AVHRR, scatterometers, as well as data from moored buoy measurements and numerical weather models to study issues and phenomena unique to the region. Other

agencies that will contribute and use this system include the National Ocean Service (NOS), Louisiana State University, National Marine Fisheries Service and the University of Maryland. Sample applications of this system are presented including detection of algal blooms, coral reefs off of Belize, oil slicks and rigs off of Louisiana, and fishery applications. [C6287]

"Data fusion of multiple polarimetric SAR images using discrete wavelet transform (DWT)"

Data fusion is a very effective technique which can be applied to many remote sensing areas such as classification, monitoring of environmental surveillance and man-made target tracking. In this paper, we tested fusion of multiple frequency (C-, and L-band), multiple polarization (HH, HV and VV) and multiresolution data sets. One can obtain a polarimetric SAR data after enhancing spatial resolution through the image fusion process. In order to fuse multiple SAR data and high spatial resolution data, they have to be geometrically co-registered over the same target area and have the same pixel size (spatial registrations). At this stage, we used the nearest neighbor resampling to avoid spectral distortion by interpolation. Multiresolution polarimetric SAR image fusion was performed using the multiscale image fusion technique-discrete wavelet transform after spatial registrations. To evaluate the spectral fidelity of fused polarimetric SAR data, spectral dissimilarity was calculated at each wavelet decomposition level. The resulting classification map based on polarimetric feature vectors shows better class separation after application of fusion processing than without fusion. The polarimetric SAR data over the Gong-ju areas, tested in this research, were acquired during NASA/JPL AIRSAR PACRIM-II experiment in 2000. [C6288]

"Geospatial data integration for applications in flood prediction and management in the Red River Basin"

Following the 1997 flood, the Red River Basin Task Force recommended the development of an international geospatial database. This database will consist of remotely sensed and GIS data that will eventually be implemented in the decision support system, to improve forecasting and modelling of the Red River basin. This project demonstrates the cross border issues and challenges encountered in the process of merging roads and hydrography vectors from Canadian and US federal governments. The major differences in the datasets between countries are: classification systems, details of attributes, validation dates, and mapping scales. Discrepancies include: horizontal offsets, feature density variations, feature discontinuities, and attribute discontinuities at the border. Flood extent vectors were extracted from RADARSAT images to provide an overview of flood extent at specific time within the Red River basin. [C6289]

"Path processing and block bundle adjustment with RADARSAT-1 SAR images"

A spatio-triangulation process is applied to 15 RADARSAT-SAR fine mode images (5 paths by 3 rows). The paths were acquired over the Rocky Mountains, Canada, from different look angles (F1 and F4), creating a weak 6° intersection geometry. A precise geometric correction model and algorithms developed at CCRS were used. Results over 3-image paths and 5-path block gave errors of 20 m and 25-35 m, respectively. These final errors are mainly due to the weak 6°-intersection geometry, but also include the map errors. For better accuracy, the adjacent paths should have 8° minimum difference in the look angles. [C6290]

"Adaptive difference of Gaussians to improve subsurface imagery"

In detection of landmines using ground penetrating radar (GPR), the most significant interference is the specular reflection. Compared with the specular reflection, landmine scattered signals are of small amplitude and difficult to observe. Better detection results can be obtained if the specular reflection can be well separated from the landmine scattered signals. Difference of Gaussians (DOG) is an operation that generates a sharp image from an original image, i.e. in the case of a GPR image, it keeps the specular reflection intact. Therefore by subtracting the DOG output from an original GPR image, we are able to remove the specular reflection and enhance the landmine scattered signals. The DOG takes the difference between two Gaussian curves of zero means and different standard deviations and convolves with the original image. One advantage of the DOG is that the two standard deviations can be chosen properly to suit different applications. We develop an adaptive DOG (ADOG) to process GPR images to improve detection of buried landmines. In the ADOG, the two standard deviations of Gaussians are computed adaptively as a GPR image is scanned from the top to the bottom row. At each row, two windows are used to calculate the two standard deviations and the current row is convolved with the DOG. The output has an unchanged specular reflection while there is a reduced landmine scattered signal. The final image is obtained by subtracting the ADOG output from the original image to remove the specular reflection. The landmine scattered signal is greatly enhanced, allowing more accurate detection. [C6291]

"Automatic extraction of rivers in tropical rain forests from JERS-1 SAR images using spectral and

spatial information"

A fully automated method of extracting narrow rivers in tropical rain forests from JERS-1 SAR images was implemented using both spectral and spatial information. The system was divided into extraction of narrow rivers that appear as a series of line-like blobs and extraction of wide rivers that appear as dark continuous line-like features. The method was assessed by comparing the results from optical JERS-1 VNIR data and by applying 21 scenes in other areas in Amazon basin and Congo basin. [C6292]

"A new maximum likelihood generalized gamma CFAR detector"

The Generalized Gamma Model has as special cases the Rayleigh, Weibull and Lognormal models. It also closely approximates the K-pdf model. Radar Clutter is often approximated in one of these forms. It is therefore quite useful to develop CFAR (Constant False Alarm Rate) detectors that perform well under this clutter model. In this paper, a Maximum Likelihood Generalized Gamma (MLGG) CFAR detector has been developed. This MLGG detector uses the Maximum Likelihood Equations, both locally and globally, in order to estimate the parameters of the Generalized Gamma clutter. These estimated parameters are then used to estimate the local mean of the detector. The mean of the local CFAR window is then taken as the first moment of the Generalized Gamma distribution evaluated with the estimated parameters. In the examples it is shown that in homogeneous Generalized Gamma clutter, with point targets, the MLGG detector outperforms our standard test detectors, Cell Averager, Ordered Statistic and Optimized Weibull. [C6293]

"A new multiscale edge detection technique [Cfor synthetic aperture radar images]"

An effective algorithm using the multiscale technique for detecting edges in synthetic aperture radar (SAR) images is presented utilizing the empirical mode decomposition (EMD). Since EMD is a one-dimensional data processing method, EMD is employed to image in two directions: horizontally (0°) and vertically (90°) to obtain two directionally smoothed images at different scales. In this way, different scales of image data were obtained. In order to obtain edge points of single pixel width, the grad of different image scales is computed. The edge map is extracted from different image scales based on a uniform space condition. Application of this method to SAR images has shown that the effectiveness of the method is quite satisfactory. [C6294]

"Environmental change detection in prairie landscapes with simulated Radarsat 2 imagery"

For the past decade, we have been using Landsat TM imagery to monitor changes in the area and distribution of ecosystems in a relatively undisturbed natural region in southwestern Manitoba, Canada. The 40,000 hectares of Canadian Forces Base Shilo are protected from urbanisation, commercialisation and agriculture, and are disturbed only by modest and controlled amounts of military training. A significant problem with the use of TM imagery for this study is that some of the more sensitive indicators of environmental change, such as the infestation of disturbed grassland by leafy spurge, are very difficult to identify and delineate in the visible and near-IR bands. A fully polarized SAR that is sensitive to vegetation morphology may not have the same difficulty. C band radars, such as that being constructed for Radarsat 2, are known to have difficulty differentiating vegetation types in regions of dense foliage, but, in a prairie ecosystem such as the one under study here, even the densest foliage should be sparse enough to yield a unique polarisation signature. In order to test this hypothesis we have simulated Radarsat 2 HH, HV and VV images, using several TM images of the area, polarisation ratios extracted from the literature for vegetation types similar to those found in the area, and a Radarsat 1 HH image of the area collected almost simultaneously with one of the TM images. Comparison of synthesized imagery from different years shows sufficient differences to imply that Radarsat 2 imagery will likely be a useful tool for continuing our prairie ecosystem monitoring and assessment. [C6295]

"Land cover classification using RADARSAT data in a mountainous area of southern Argentina"

In this paper, a new procedure is proposed for land cover classification in a mountainous area using data derived from a stereo pair of RADARSAT images. Land cover classifications using the RADARSAT tonal and textural information and ancillary terrain data were evaluated. All the derived data were from the same source of the stereo pair of the RADARSAT images. An artificial neural networks (ANN) classifier is applied. The performance of the proposed method was evaluated over a mountainous study area in Southern Argentina. The results showed that the extra information, texture and DEM, extracted from the RADARSAT images can greatly improve the accuracy of classification using ANN. It can be concluded that RADARSAT images and terrain data derived from the RADARSAT images are valuable data sources for land cover mapping, especially in the mountainous areas where optical satellite data and DEM data are not always available. [C6296]

"Monostatic CW radar system for microwave attenuation measurements for atmospheric water"

vapor estimate"

In this paper we report the first simulation-based results concerning the potential of a CW radar system for differential attenuation measurements around 19 GHz. The objective is the estimate of the columnar water vapor from a LEO satellite or from airplanes carrying a nadir pointing radar system. Simulations are based on a microwave propagation model for atmosphere, radiosonde data, and ground backscattering cross section models. The correlation between the radar output and the columnar water vapor is shown. [C6297]

"Feasibility study of using small satellite synthetic aperture radar for global 3D imaging"

This paper deals with the feasibility study of using small satellite constellation to perform Interferometric Synthetic Aperture Radar (InSAR) global 3D imaging. A scheme in which three exactly identical small satellites make up a constellation is given. Two of them flying along parallel orbits with a little different ascending nodes observe the same area and make interferometry without any time decorrelation. The third flies along another orbit with a certain angular separation behind the two satellites, and observes the same area in a short revisit time. These three satellites together can form differential interferometry, which is of great benefit to observe surface changes with short time baseline. Simulation is conducted in this paper to perform a mission study. The results show the potentiality of the system for accurate global three-dimensional measurements. [C6298]

"COSMO-SkyMed SAR processing parallel implementation"

COSMO-SkyMed constellation will acquire data from its four SAR satellites in several image modes, and will generate focused data products. As images will be acquired at fine geometric resolution and will cover medium sized swath, the SAR processing involved will result well suited to parallel programming implementation. [C6299]

"Fuzzy coded space frequency quantization"

In this paper we propose a new image coding technique, which consists of the space frequency quantization (SFQ), and a fuzzy context based modeling. The space frequency quantization (SFQ) is an effective coding technique, which uses a zerotree pruning of wavelet coefficients. After the space frequency quantization is applied to the wavelet coefficients the non-pruned coefficients are quantized using context modeling. The context based quantization technique uses the partitioning proposed by the trellis coded quantization and fuzzy logic to predict the next TCQ state from the context. Quantized indices are entropy coded using an arithmetic coder. The probability estimation is based on the observation of the past coded bits. The results of the proposed compression scheme showed that the proposed coder outperforms the state-of-the-art coders in the RD sense for the SAR data compression. [C6300]

"The advantage of segmentation in SAR image compression"

SAR images are severely degraded by speckle, and filtering is therefore a common practice. Filtering is especially useful before compression, to avoid spending valuable resources to represent noise; unfortunately, it also degrades important image features, like region boundaries. To overcome this problem, one can resort to a segmentation-based compression scheme, which allows one to preserve region boundaries, carry out intense denoising, and improve overall performance. In this work we assess the potential of segmentation-based compression through controlled experiments on synthetic SAR images. Numerical results seem to confirm the validity of this approach. [C6301]

"Examining vegetation phenological change in South America using reconstructed SeaWinds data: grasslands and savanna"

This research reports the use of NASA SeaWinds data to measure phenological change in equatorial South America through a growing season. The SeaWinds data was reconstructed to a resolution of 8 km and studied on a monthly basis. Vertically and horizontally polarized data were examined in the context of monthly NDVI composites as well as monthly weather variables. Thirty-nine vegetation physiognomic classes and transition types were studied using data collected in the year 2000. Only the preliminary results for equatorial savannas of northern South America are discussed in this paper. Backscatter in these savannas is correlated primarily with NDVI and precipitation totals. Backscatter difference (HH-VV) is likewise very strongly correlated with monthly precipitation. We hypothesize that backscatter from the top of the canopy and multiple-bounce backscatter from wet soils are the key components explaining seasonal SeaWinds backscatter change within this class. [C6302]

"Lineament extraction from Landsat TM, JERS-1 SAR, and DEM for geological applications"

The Hough transform is an efficient numerical method for extracting lineaments or linear features from 2-D

geological and geophysical data, including satellite images. Analysis of lineaments has also been widely carried out in geological research, and Landsat TM data have been used most extensively for geological lineament investigations. However, there has been less geological application research carried out in the lineament extraction from synthetic aperture radar (SAR) data. This research has tested several spatial data including Landsat TM, JERS-1 SAR and DEM data for automatic geological lineament analyses. The Hough transform technique is applied here for the extraction of lineaments from preprocessed binary spatial data. The multiresolution method is tested to extract lineaments efficiently, because geological lineaments usually appear in various length scales. The Kyungsang Basin in the southeastern part of the Korean peninsula was selected as the test site in this research. The lineaments are extracted from JERS-1 SAR, Landsat TM, and DEM data using both manual and the automatic Hough transform method. The results of lineament extraction indicate that the predominant direction is the NNE direction of azimuth angle 0° - 30° , and the second dominant directions are the NNW, NE, and WNW directions. The results obtained in this research agree well with the regional trends and also with the local geological maps. [C6303]

"Monitoring of forest fire damage by using JERS-1 InSAR"

The authors investigated on the applicability of interferometric SAR (InSAR) for monitoring forest fire damage. We attempted to use the coherence information obtained through interferometric SAR (InSAR) to detect and monitor damaged areas by forest fire. The test site is the forest around Tamano City in Okayama Prefecture, where a relatively big forest fire occurred in August, 1994, and a total area of 359 ha was burnt. We used several interferometric data pairs by JERS-1 SAR acquired before and after the forest fire. The multilook intensity images and the coherence images were created in the test site and both of intensity and coherence changes due to the fire in damaged forest areas were extracted and they were compared with those in non-damaged forest areas. The result indicated that intensity decreased slightly after the fire, however, the change was not big enough to interpret and extract damaged forest areas clearly. On the other hand, coherence increased significantly in damaged areas after the fire and it was much easier to interpret and extract damaged areas compared with intensity. The experimental result in this study supports that InSAR is effective for detecting and monitoring land cover changes by a forest fire as well as deforestation, for which InSAR has been already verified to use effectively. [C6304]

"A new method for SAR speckle reduction"

A new method derived from the Frost filter kernel for SAR (synthetic aperture radar) image speckle reduction is introduced. In the speckle reduction procedure, both the statistical information of the central pixel in the filter window and that of the neighborhood pixels are used. The experimental results on ERS-1 PRI images demonstrate the efficiency of the proposed method compared to other common filters. [C6305]

"Characterization of local 3D rough surfaces using UWB near-range phase-based GPR signatures from wide-beamwidth antennas"

This paper pertains to further investigations on using an ultra wideband (UWB) multistatic coherent ground-penetrating radar (GPR) technique for precise profiling of the rough surfaces in three-dimensional space. The method is essentially based on the phase processing of the sliced layers of three-dimensional rough surfaces with multiple sub-frequency bands. The data acquired in the near range by a UWB stepped-frequency continuous-wave GPR with wide-beam antennas over a compound surface are used to verify the method. It was found that in the near-range measurements the range side-lobe interference effects and the reflections from the measurement surroundings sometimes have a significant influence on the target phase and amplitude responses, and consequently degrade the localization of the targets. The present study on this issue shows that within the ultra wideband, some sub-frequency bands are less sensitive to the measurement surroundings, but still sensitive to the target area. With the selected sub-frequency bands the image of the compound surface reconstructed in the surface height domain shows good agreement with the practical geometry of the rough surfaces. [C6306]

"On the use of contrast stretch and adaptive filter to enhance ground penetrating radar imagery"

We propose using an adaptive filter to enhance ground penetrating radar (GPR) images. It is well known that GPR images are usually dominated by the specular ground reflection. The specular reflection makes the object scattered signals difficult to observe, so it first must be removed before more refined detection and classification processing can be employed. To remove the specular reflection, the biggest challenge is that, due to ground roughness, the reflection cannot be satisfactorily subtracted by some simple methods such as a moving-average filter. Using contrast stretch we can enhance the object reflect signal and then use standard background removal method to eliminate most of the specular reflection. During the contrast stretch, the GPR images may have

"streaky" artifacts because of the background removal. To overcome this side-effect, we apply an adaptive filter to remove "streaky" artifacts. Using field data, we show that images of higher quality can be obtained by our method. [C6307]

"Field experiments of a surface-penetrating radar for Mars"

Using ground-penetrating radars to investigate the subsurface of Mars will be a key scientific objective over the next several years, especially in light of the large possibility that water could exist within the planet. Radars operating from a few megahertz up to a gigahertz will be able to provide valuable information concerning the subsurface electrical structure at resolutions ranging from a few centimeters near the surface to a few tens of meters at greater depths. One of the major goals of the work presented was to develop a lightweight, low-power, frequency-modulated radar system that could be used to detect subsurface deposits of ice and water. An inexpensive prototype system was developed using off-the-shelf connectorized components and evaluation boards. To verify the operation of this prototype system, a preliminary experiment was conducted in Lawrence, Kansas. Next, experiments were conducted over locations containing permafrost and ice in Fairbanks, Alaska. Results from these experiments are presented. [C6308]

"Generalized refractive mixing dielectric model for moist soils"

In this paper, a technique for estimating the maximum bound water content and complex dielectric constants for both the bound and the free water in soil is presented. The thus attained dielectric properties for the water in soil, are used to derive the Debye spectroscopic parameters for both types of water. Empirical data sets for the soil complex dielectric constant as a function of moisture measured only at two frequencies are sufficient for applying this technique. As a result the model for predicting soil complex dielectric constant in the microwave band is proposed and validated. [C6309]

"The Mueller matrix solution for polarimetric scattering from inhomogeneous random media of non-spherical scatterers under a pulse incidence"

Polarimetric scattering from inhomogeneous random media of non-spherical scatterers under a pulse incidence is studied. The time-dependent Muller matrix solution of vector radiative transfer for layering random media is derived. Co-polarized and cross-polarized bistatic and backscattering are numerically calculated. The shape and intensity of polarized echoes well depict the inhomogeneous fraction profile of random scatterers. Its functional dependence upon the fraction profile, layering thickness, and other parameters are discussed. This technique is applicable to the reconstruction of inhomogeneous fraction profile and inversion of the media thickness. [C6310]

"Measurement of snowfall parameters by radar and optical lidar"

A new system to measure physical snowfall parameters using a microwave radar, an optical lidar (laser radar) and an image processing technique is proposed. A high accuracy electrical balance is also used to obtain reference data. The radar, the imaging system and the balance recorded snowfall on the ground level, while the optical lidar recorded an atmospheric profile up to 7500 m. Z-R relations obtained from simultaneous measurement of radar reflectivity factor at X band and snowfall rate are compared to the snow parameters measured directly on the ground by the video camera and the optical lidar. [C6311]

"Automated Geophysical Observatory (AGO) Lidar-post Antarctic deployment performance"

A ground-based, autonomous, low-power atmospheric lidar instrument developed at NASA Goddard Space Flight Center has been returned from an extended period on the Antarctic polar plateau. We report on the pre- and post-deployment performance of the AGO Lidar, compare the instrument performance with lidar models, and compare results with the anticipated performance of the new Automatic Weather Station (AWS) Lidar. [C6312]

"Development of a 3-D scanning 1.5 μm portable aerosol lidar"

The design, testing and field measurements with a portable, eye-safe, 85 mJ, 15 Hz, 1.5 μm 3-D scanning aerosol lidar system is presented. [C6313]

"Test results from a 1319-nm laser radar with RF pulse compression"

We report the results of a three-year, NASA-funded project at The University of Kansas Radar Systems and Remote Sensing Laboratory on the development of a laser radar that uses RF pulse compression to significantly improve system performance. Receiver sensitivities of less than -90 dBm have been demonstrated by applying heterodyne optical downconversion and RF pulse compression. With the improved sensitivity, the required

transmit power is significantly reduced. This system approach also permits multi-kilohertz pulse-repetition frequencies that enable spatially dense range measurements. Compared to lidars like GLAS and MOLA, this sensor requires a lower peak transmit power while providing orders of magnitude more measurements per second. In the receiver design, we have evaluated two detection schemes: envelope detection and direct downconversion. Envelope detection provides the benefit of discarding the effects of optical phase variations on the detected signal consequently avoiding many temporal correlation issues, however it is less efficient in terms of the resulting signal-to-noise ratio (SNR). Direct downconversion to baseband is more SNR efficient, however the baseband signal contains the effects optical phase variations, which include laser phase noise, effects of atmospheric turbulence, and frequency shifting due to Doppler effects. We have demonstrated the feasibility of using a linear array of optical fibers in the telescope's focal plane to launch and receive the optical signals. Using separate fibers for transmit and receive while sharing telescope optics, we have achieved the required transmitter-receiver isolation of a bistatic system without the accompanying alignment difficulties. With our breadboard system ranging measurements from both man-made and natural extended targets have been made and the results are presented. These results support the feasibility of a satellite-based altimeter (600 km altitude), capable of making more than 4000 range measurements per second with 10 cm accuracy using less than 10 W peak transmit power. While the present breadboard operates at 1319 nm, the overall concept is wavelength independent. Benefits of this development may include increased system reliability, reduced power requirements, smaller sensor mass and volume, improved eye-safety, and lower probability of signal detection.

[C6314]

"Establishing analytical criteria for selection of sites for calibration of spaceborne laser altimeters"

The expected launch of spaceborne laser altimeters and the accuracy demands of derived products raise the need for post-launch calibration/validation to verify the measurements and the performance of the instruments. In addition to deriving adequate procedures for calibrating the system it is necessary to identify suitable sites over which calibration parameters can be estimated in an optimal way. Although it is clear that the surface topography should have a direct influence on the estimated parameters it is not clear what exactly the effect is, and how it can be generalized into a rule for evaluating a site. Indeed, the option of using trial and error methods always exists but it is inefficient and does not generalize, especially when several sites should be evaluated. Analytical criteria that enable direct evaluation of a site are established. Results of several sites that were evaluated for the calibration of the Geoscience Laser Altimeter System (GLAS) demonstrate the application of this method.

[C6315]

"The relative and absolute geometric algorithm for the ERS baseline estimation"

Two fundamental parameters in synthetic aperture radar (SAR) interferometry are baseline orientation and baseline length, which are the key elements of the interferometric geometry. These parameters control how topography is mapped into interferogram phase, and affect the accuracy of the DEM directly. Without ephemeris or the accuracy parameters in it, how to estimate more accurate baseline parameters is an important question. It is an important way to make use of the ground target position in the sub-satellite track, the relative information in the image and other correlative information. In fact, it can estimate the fundamental parameters with the position of the satellite, the difference of two homonymic points' position, the spatial resolution. etc. Considering the ERS characteristics, the correlative information in the two complex images, and the position of the reference points to the sea level, this paper presents the relative and absolute geometric algorithm to estimate the two parameters. The algorithm is simple in computing, and facile in actualizing. The estimation accuracy is more precise by tests using the ERS data for interferometry. [C6316]

"SAR interferogram MAP filtering based on stationary wavelet transform"

Strong speckle noise of SAR interferogram is a great obstacle to phase unwrapping. In this article, we propose to filter this noise with a multiresolution analysis of the interferogram, the real part and the imaginary part of the interferogram are processed respectively. Several different probability density functions are modeled with the Pearson system of distributions, then the wavelet coefficients of the noiseless data are estimated with a Bayesian model, maximizing the a posteriori probability density function. The result is compared to that of another method and shows that the proposed method is powerful to interferogram speckle noise reduction.

[C6317]

"A piece-wise polynomial fitting method to filter the interferogram phase noise [CInSAR]"

Among many important factors for the whole interferometric processing, the interferometric phase quality affects the phase unwrapping and the accuracy of the DEM directly. The noise, which exists in the single complex image, affects the judgment of the image. After the interferogram phase (IP) is taken out from the complex

images, the distribution of the phase noise is complicated. To get the high quality IP, the IP noise, which always exists, must be eliminated. The IP noise should be distributed continuously in one period and disconnected from one period to another. The polynomial fitting method can eliminate the phase noise in the continuous interval, but it can also add noise in the discontinuous interval, especially in the whole phase interval. This paper brings forward the piece-wise polynomial fitting (PWPF) method that can eliminate the IP noise. The PWPF can be obtained from the range and azimuth director respectively in the whole IP image. The experiment shows this method has a better IP noise eliminating effect. [C6318]

"Amplitude-driven coherence filtering in complex interferograms"

Presents a new method for filtering the coherence image issued from an interferometric pair. The basic idea is to determine for each pixel an adaptive neighborhood with respect to the amplitude information. Then, complex averaging is performed using values of pixels in the determined neighborhood to derive the filtered coherence value. It is shown that the proposed technique performs better than the standard fixed-neighborhood filtering technique, both objectively and subjectively. [C6319]

"The Alaska DEM project: repeat-geometry approach for generating accurate InSAR DEMs"

In recent years the rapidly growing field of SAR interferometry (InSAR) has showed its potential to provide high quality three-dimensional information in the form of digital elevation models (DEMs). Especially during the ERS tandem mission, a large number of valuable data sets were acquired. The Alaska DEM project was initiated to demonstrate the capability of SAR interferometric data to meet the topographic needs of the State of Alaska. For the high-priority areas identified by the Department of Natural Resources, a large number of data sets from the ERS tandem mission are available providing multiple coverage of the same area in ascending and descending orbits. A processing strategy for calculating the most accurate result in this repeat geometry has been developed. An iterative approach processing image pairs from the smallest to the longest baseline is used to obtain higher accurately InSAR DEMs. A statistical evaluation of results helps to identify and to remove outliers before the individual results are mosaicked together in a final result. Layover and shadow masks are derived from orbital data to identify areas of poor data quality. For quality control the results are compared to high-resolution airborne data and a point target analysis for corner reflectors is carried out. The paper describes the processing strategy in detail and shows examples of one of the high-priority areas. [C6320]

"Scattering from wet snow by applying strong fluctuation theory"

In this study, the strong fluctuation theory is applied to calculate the scattering from a half space of wet snow. The first and second moments of the fields are calculated, respectively, by using the bilocal and the distorted Born approximations, and the low frequency limit is taken. The singularity of the dyadic Green's function is taken into account. The effective permittivity of wet snow is calculated by the two-phase model with non-symmetrical inclusions. In the two-phase model, wet snow is assumed to consist of dry snow (host) and liquid water (inclusions). Numerical results for the backscattering coefficients of wet snow are illustrated for random media with isotropic and anisotropic correlation functions. The three-phase strong fluctuation theory model with symmetrical inclusions is also presented for theoretical comparison. In the three-phase model, wet snow is assumed to consist of air (host), ice (inclusions) and water (inclusions) and the shape of the inclusions are spherical. [C6321]

"Estimation of EM radiation source in ELF band"

Our goal is to locate anomalous electromagnetic (EM) source caused by seismic activity for earthquake prediction. For the purpose, we have been measured EM wave of 223 Hz at 35 sites in Japan. This paper analyses relation between EM power attenuation and distance from its source. The relation is necessary to estimate the source location. [C6322]

"The application of analysis techniques based on DEM and GIS in airborne radar signal simulation"

Airborne radar altimetry sometimes records abnormal phenomenon. In this case, information of real terrain must be incorporated to analyze the abnormality region. This paper applies terrain information of a test area organized by a spatial geographical information system (GIS) to the radar signal analysis. With the support of Global Positioning System (GPS) and Inertial Navigation System (INS), we can simulate the radar altimeter data by organizing and analyzing three-dimensional terrain information inside of the radar beam. [C6323]

"Polarimetric SAR data classification method using the self-organizing map"

In this paper, we introduce a supervised classification method, which differentiates polarimetric SAR data into

three categories using a self-organizing map (SOM) and a counter propagation learning approach after identifying the appropriate scattering classes. This classifier produces category maps corresponding to the Kohonen layers using training data for each scattering class. The SAR data are classified by inputting both like- and cross-polarization power elements into the learned SOM. In the experiment, PI-SAR data are employed since the resolution of aerial SAR data is higher than that of SAR data obtained from space. The proposed method yields higher-accuracy classifications than do conventional methods. [C6324]

"Rainfall estimation from vertical profiles of reflectivity using neural networks"

The neural network is a nonparametric method for representing the relationship between radar measurements and rainfall rate. Recent research had demonstrated that neural network techniques can be successfully used for ground rainfall estimation from radar measurements. An adaptive neural network has been developed to estimate rainfall rate from vertical profiles of reflectivity that gradually adapts itself over time, without retraining from the beginning. Such a network is also computationally stable. The performance of the neural network is evaluated by conducting tests on data sets using WSR-88D over Melbourne, FL and surface gage network data during 1998, 1999. The results show that the adaptive neural network can estimate rainfall fairly accurately and consistently. [C6325]

"Left- and right-looking RADARSAT-2 data for mosaics of ancient supercontinents"

The Pangaea supercontinent began its break-up some 200 Ma ago, during which time the ancient cratons of West Africa and San Francisco-Congo of Gondwana were rifted apart. These older parts of the continental crust now reside in the African and South American shields, but share a common geological past. Geological maps of reconstructed Pangaea aid geologists to understand the tectonic history of the evolving Earth, the global distribution of rock units and ore deposits. It follows that radar and other remotely sensed images of Earth can be mosaicked in the same fashion to provide supplementary information in support of such investigation. In our radar mosaic for part of Gondwana, left-looking RADARSAT-1 data of west Africa acquired on ascending passes during the Antarctic Mapping Mission and normal mode (right-looking) data of South America from descending passes were first seamed together separately. The two continental image maps were then rotated into their pre-breakup configuration to create a radar mosaic with a relatively consistent westward radar look. This critical aspect of the mosaic would not be possible from a SAR system without left- and right-looking capability. A consistent look direction is of great importance when landform interpretations are made. The left and right pointing of the RADARSAT-2 antenna will enable routine data collection of this kind for similar studies. [C6326]

"Comparison of SAR and optical images of the rainforests of Borneo, Malaysia with field data"

Preliminary results are described on the comparison of the optical and radar images of the rainforests of Sarawak, Malaysia, with the ground-truth data collected from the field survey. The test sites are the mangrove and adjacent virgin forests, and oil-palm plantation areas. Visible and infrared images acquired by the MOS-1b have shown their capability of extracting deforestation areas, but their applications to mangrove forests are limited. Operating at L-band with longer penetration depth, the JERS-1 SAR is superior to the ERS-2 C-band SAR for differentiating the mangrove from virgin forests, although both forests have biomass similar and well above the saturation range of the L-band RCS. The field data show that the mean tree diameter is about a half the radar wavelength in both the forests, indicating that the L-band microwave is "semi-transparent" in these forests. It is, thus, concluded that the lower (about 6 dB) RCS in the mangrove is due to specular reflection beneath the forests; while in the virgin forests there is a substantial amount of diffuse scattering by undergrowth. This hypothesis is supported by the difference in image intensity between the dry and wet seasons. [C6327]

"Relationships among airborne scanning LiDAR, high resolution multispectral imagery, and ground-based inventory data in a ponderosa pine forest"

Estimating forest structure and stand density using remotely sensed data is important for a wide range of scientific and management goals, including assessing biogeochemical budgets (e.g. aboveground carbon storage) and determining the susceptibility of an area to catastrophic fires. The objective of this study is to determine relationships among ground-collected forest structure data, high resolution IKONOS imagery, and airborne scanning LiDAR collected at a ponderosa pine (*Pinus ponderosa*) dominated site in the Black Hills of South Dakota. Ground data were collected in the summer of 2001 along four 104140 meter belt transects. IKONOS imagery was obtained over the site on July 28, 2000, and airborne scanning discrete-return LiDAR was acquired at a nominal 2 meter post spacing (56 cm beam footprint diameter) on October 26, 2001. No thinning or fire activity occurred at the site between data collection dates. Transect data were subdivided into 10410 meter plots and co-registered with the IKONOS and LiDAR data for analyses. A combination of IKONOS multispectral and panchromatic data was used to select image endmembers (i.e. spectrally "pure" components) of bare soil,

open grass, and tree/shade. In 80% of the plots, LiDAR-derived first return canopy height agreed with field-measured maximum tree height to within 20%. On average, LiDAR-derived first return canopy height underestimated field measured maximum tree height by 3.7%. Effective tree canopy leaf area index (LAI_e, a measure of canopy cover fraction) ranged from 0.3 to 2.5 among the plots. The fraction of LiDAR tree canopy returns were significantly correlated with LAI_e at the plot level ($r=0.55$; $p(r) = 0.76$; p [C6328])

"Multi-temporal JERS coherence for observation of Siberian forest"

This paper presents the first results from a study of multi-temporal JERS repeat pass coherence. Two test areas in a forest region north of Krasnoyarsk in Siberia have been used to investigate if L-band coherence with a 44-day temporal baseline can be used for estimations of growing stock volume in boreal forest. The available data show promising results for winter images, but for the summer scenes the standard deviations are too large to give reliable results. A comparison with ERS tandem coherence has also been done. [C6329]

"Rapidly assessing the flood disaster by using remote sensing and GIS"

The method of rapidly assessing the flood disaster is discussed here by using the technologies of remote sensing and geographic information system (GIS). The method included four steps. Firstly, satellite SAR image such as Radarsat SAR or ERS SAR is geometrically corrected and matched with the data from the GIS database such as landuse or the geometrical-corrected Landsat TM image. Secondly, the flood extent can be extracted from SAR images by visual interpretation or automatic extraction with support of DEM or Landsat TM. Thirdly, the flood extent can be overlaid with the data such as landuse data from GIS database or Landsat TM. Fourthly, the results such as map and table can be obtained by using GIS. The case of assessing the large flood disaster of P.R. China in 1998 showed that the technologies are very useful tools for assessing the flood disaster, which provides the government with very important information for alleviating the flood damage.

[C6330]

"The wetland conservation atlas of the St. Lawrence valley produced from decision tree classifications of RADARSAT and Landsat images"

The Canadian Wildlife Service, Quebec region, has initiated a project oriented toward the production of a wetland atlas covering agricultural landscapes of the St. Lawrence Valley, Quebec. A classification method that integrates a series of RADARSAT ortho-images, Landsat Thematic Mapper-5 decorrelated images and digital elevation model has been developed. Several reference plots on wetlands were used to build the classification tree model. Classification accuracy was evaluated at 85% using 190 independent sites evenly distributed over the study area. The classification results, reported on a vector format, constitute the Wetland Conservation Atlas designed to provide guidance to each regional county municipality in the production of their conservation action plans.

[C6331]

"Development of an algorithm for estimating snow hydrological parameters in wet snow regions using combined C- and L-band satellite-based SAR data"

Develops an algorithm for estimating snow parameter distributions using synthetic aperture radar (SAR) images. The study area is a part of the Hokuriku District of Japan that is well known for having wet snow from the beginning of the winter season. We develop an algorithm to estimate snow density and roughness distributions using RADARSAT images acquired in February. Furthermore, we show the possibility of inferring snow depths from combined parameters estimated with an L-band SAR image. [C6332]

"Application of RADARSAT-1 in mineral potential evaluation, Lac Grandin area, NWT: identifying geologic features/processes associated with mineralization"

The purpose of using RADARSAT-1 for this mineral potential evaluation was to provide a means for acquiring quick and relatively inexpensive information about the study area. The problems faced in carrying out the mineral potential evaluation of this area were two-fold: (1) very limited geologic information exists to base a mineral assessment on and (2) the rocks with the greatest mineral potential are overlain by younger flat-lying sedimentary rocks. The Lac Grandin area has never been flown by regional or industry geophysics, it has only seen very limited reconnaissance geological mapping, no geochemical data exists and no mineral exploration has been carried out over the area. Flat-lying sedimentary rocks of the Phanerozoic Interior Platform underlie the Lac Grandin area. The Great Bear magmatic zone (GBMZ) of the Proterozoic Bear Geological province outcrops 30-50 km to the east and underlies the Phanerozoic sedimentary cover rocks of the Lac Grandin area. Depth to Proterozoic crystalline basement (GBMZ) rocks in the study area has been determined to be less than 200 m. The GBMZ is known to host significant mineral deposits and some past producing mines. An industry

aeromagnetic survey exists for the area immediately adjacent to the study area and was flown to fill in a gap in the regional geophysical database. It was hoped that structural patterns recognized from the aeromagnetic data could be extrapolated into the study area using the RADARSAT-1 images. The RADARSAT-1 images acquired were Fine Mode, Beam 1 descending (f1d) and Standard Mode, Beam 4 descending (s4d), which partially overlap the study area and the adjacent area with industry aeromagnetic coverage. The images proved very effective in demonstrating that basement feature lineaments could be recognized through the sedimentary cover rock and continued beyond the aeromagnetic coverage area into the study area. The RADARSAT-1 images proved very effective as an ancillary tool to the aeromag maps by aiding in locating and identifying structures thought to be important to the determination of areas of high mineral potential. [C6333]

"Estimating the morphological changes in fluvial beds by means of differential SAR interferometry"

We investigate the potentialities of differential SAR interferometry (DInSAR) to estimate the morphological changes of the channel bed induced by processes of erosion and deposition. The Cellina stream (North-East Italy) has been chosen as a test site. The stream has a braided channel morphology with a gravel bed. A set of ERS-1/2 SAR images acquired in this area has been interferometrically processed. The DInSAR analysis enabled areas of erosion and sedimentation to be mapped. [C6334]

"Monitoring the Tessina landslide by a ground-based SAR interferometer and assessment of the system accuracy"

This work concerns the application of groundbased SAR interferometry (GB-InSAR) for the monitoring of the Tessina landslide, using the LISA (Linear SAR) system developed at the JRC. This landslide is continuously monitored by a topographic system. For this reason it has been chosen as a test site to fully confirm the accuracy of the, GB-InSAR. The GB-InSAR-derived ground displacements have been compared with those obtained by a set of topographic benchmarks placed in the unstable areas. [C6335]

"Classification of landslide surfaces using fully polarimetric SAR: examples from Taiwan"

Landslides typically denude forested hillsides, changing dominant scattering from multiple- to single-bounce. SAR polarimetry can be used to determine the dominant scattering mechanism of the terrain on a per pixel basis. Thus, hillslopes affected by landslides may be distinguished easily from adjacent, unaffected hillslopes. Based on the polarimetric eigenvalue decomposition and the relative amplitudes of scattering matrix terms, dominant scattering mechanisms can be determined. These mechanisms-odd- or single-bounce (bare surface), double- or even-bounce, and volume (diffuse) scattering-describe the total radar returns for each pixel. The modified approach of Kim and van Zyl (2001) include the radar vegetation index, pedestal height and entropy, all representative of forest. Our analysis follows Kim and van Zyl to reveal that at L-band, the landslide scar areas of the Tsaolong and Mt. Jou-Feng-Err mega-slides are dominated by single-bounce scattering and the surrounding forested regions are dominated by volume scattering. In addition, fully polarimetric SAR is sensitive to reforestation in tropical jungle environments as demonstrated by comparison with a panchromatic Indian Remote Sensing (IRS) image. Inversion of SAR polarimetry for terrain scattering mechanisms offers a new approach for landslide mapping that has significant operational advantages over traditional methods that rely on optical sensors for rapid response to and management of landslide disasters. [C6336]

"Using multiparameter data to calibrate polarimetric weather radars in the presence of a partial beam blockage"

The paper describes a technique to calibrate dual-polarization weather radar in the presence of a partial beam blockage. Radar reflectivity factor Z and differential reflectivity ZDR can be calibrated using an idea of self-consistency among Z , ZDR , and specific differential phase KDP for rain medium and polarization properties of dry snow and light rain. [C6337]

"Recognition of hail areas with polarimetric radar by the method of potential functions"

In this paper the method of potential functions is proposed and developed for the recognition of hail areas in weather objects. The method can be applied to the processing of fields of any informative parameters of microwave remote sensing or fields of meteorological elements. [C6338]

"Triple-wavelength radar for cloud and precipitation microphysics research"

The University of Massachusetts, Colorado State University and the National Center for Atmospheric Research are collaborating to develop an advanced Multi-Frequency Radar (MFR) system for studying clouds and precipitation, which should become operational in 2004. This highly portable radar consists of three polarimetric

Doppler subsystems operating at Ku-band (13.8 GHz), Ka-band (33 GHz) and W-band (95 GHz), a programmable scanning pedestal, and a unique single aperture antenna that generates co-located matched beams at each wavelength. This combination of wavelengths allows measurement of a wide range of atmospheric targets including weakly reflecting clouds and precipitation. [C6339]

"Ground-based radiometric retrieval of cloud liquid"

Considers the retrieval of cloud liquid from the brightness temperature measurements taken by a ground-based multifrequency microwave radiometer using a neural network-based inversion algorithm. Comparisons between the retrieved quantity and the atmospheric information provided by active instruments such as a 94-GHz radar and a lidar ceilometer, co-located on the RAL Chilbolton Observatory site (UK), are carried out. [C6340]

"Cross-calibration of ground and space radar"

Presents results from comparing space radar and ground radar to cross-calibrate the Kwajalein polarimetric radar (KPOL) with the spaceborne TRMM Precipitation Radar (PR). Use of self-consistency of polarimetric measurements is implemented to check the absolute calibration of KPOL and is checked against the cross-calibration results of PR and KPOL. Differential reflectivity (Zdr) calibration is also done and compared with vertical looking scans through rain. [C6341]

"Efficient flood monitoring based on RADARSAT-1 images data and information fusion with object-oriented technology"

RADARSAT-1 delivers SAR imagery well suited for monitoring and mapping of natural risks and hazards. Current methods are either based on human interpretation and are extremely time consuming, or they are automatic pixel based approaches, which have limitations for many applications. Here, we propose a new object-oriented strategy to monitor flooding using three RADARSAT-1 data sets with different acquisition times during a flood event shortly after the monsoon. A flexible strategy for the fusion of SAR and optical data is proposed. Using the synergy of data fusion enhances the usefulness of each individual sensor. [C6342]

"Detection of flood damaged areas in the entire Chao Phraya River Basin from JERS-1/SAR images with a help of spatial information"

The water surfaces detected by a conventional intensity based method from JERS-1 SAR images do not always coincide with the flood-damaged areas especially existing paddy fields. The authors propose morphological methods as spatial information. The result roughly agree with the reported flood-inundated areas. We concluded that this kind of methods has an advantage of the disaster monitoring using SAR satellite. [C6343]

"Damage estimation model using temporal coherence ratio"

This paper presents a damage estimation model suitable for evaluating earthquake damage using coherence images derived from interferometric SAR data. The damage degree is estimated through temporal decorrelation by employing a coherence ratio which is defined by dividing a post-event coherence image by a pre-event image. The temporal coherence ratio is confirmed to be closely correlated with the probability of the damage degree. As a result of applying both C and L bands SAR data for evaluating the damage of the 1995 Hyogoken-Nanbu Earthquake in Japan, the cumulative probability of the damage degree can be approximated by a linear function of the coherence ratio. [C6344]

"A comparative analysis of Landsat TM and radarsat SAR signatures in restricted tidal channels"

In this study we examine and comparatively analyze synthetic aperture radar and near infrared Thematic Mapper signatures observed in the restricted tidal channel of a shallow lagoonal estuary. Both imaging systems show coherent structures, identified as longitudinal convergence zones, that appear as bright and dark bands aligned parallel with the axis of the tidal channel in question. This result indicates that Doppler shifting is not the mechanism responsible for the observed SAR signatures. Furthermore, modulation of relative intensity shows similar trends in location and magnitude of peak intensity with respect to tidal phase. Background variances from the unperturbed regions also show similarities between the two sensor systems. Finally, TM imagery, in the context employed here, is limited by the solar illumination cycle with the optimal period from May through August for the northern latitude site examined here. [C6345]

"Polarised TOPSAR operational model of internal wave generation mechanism"

The generation mechanism of internal waves can be investigated by polarised SAR data. The integration

between digital elevation model and Canny algorithm will be more useful for automatic detection of internal waves. The aim of this paper is to understand the generation mechanism of internal waves in shallow water of Malaysian coastal waters. The continuous wavelet transform is used to estimate energy and wavelengths within solution peaks from the detect internal wave. The Doppler radar was used to model the speed of internal wave. This study shows that the polarized PHHband is more suitable for internal wave detection compared to LHHband Cvvbands. It can be concluded that polarised SAR data could be used to understand the generation mechanism of internal waves. It can said that internal waves on the shallow waters of Malaysia are generated by strong tidal current flow over the irregular bottom topography. [C6346]

"Microwave, optical and IR combined studies of the sea surface perturbations caused by underwater gas bubble plume"

In connection with extensive world-wide development of transporting gas networks the problem of the gas leakage detection on the underwater gas pipes becomes rather actual. The present paper is devoted to the solution of the problem of underwater gas plume detection by microwave remote sensing methods. [C6347]

"Use of Radarsat F5 images for detection and positioning of fish cages"

We have investigated whether synthetic aperture radar images can be used to observe and position the fish farms and polymer type fish cages along the Norwegian coast. In order to maximize sea-object backscatter difference, the images selected are Radarsat F5 with 10 m/10 m resolution, 45-48° incidence angle and HH-polarization. We found that it was possible to detect and position all fish cages within the study area, even single ones of polymer-type. It was also possible to determine the overall shape of larger collections of fish cages, and count the number of fish cages within the collections. The wind condition was favorable during the satellite pass (less than 5 m/s). It is concluded that Radarsat F5 images are well suited to detect and position fish farms. [C6348]

"Joint field experiment of microwave and visible sensors for bare soil and vegetation and preliminary analysis"

A joint field experiment was carried out using microwave and visible sensors for bare soil and vegetation in Shunyi of Beijing in May 2001. The sensors include a microwave radiometer, microwave scatterometer and visible and infrared spectrometer. The microwave radiometer operates in the L, C and K band with H and V polarizations. The microwave scatterometer operates in the C band with HH, HV, VH, VV polarizations. The microwave brightness temperature, backscatter coefficients and reflectivity of bare soil, winter wheat and alfalfa were measured at various incidence angles. Meanwhile, ground surface parameters such as soil surface roughness, soil moisture and temperature of various depths, LAI of winter wheat and alfalfa were measured at the same time. The measured data were analyzed and an algorithm based on synergistic use of all these data is put forward to estimate soil moisture. [C6349]

"SAR sea-ice texture classification using discrete wavelet transform based methods"

Texture finds important application in SAR sea ice description and classification. The wavelet transform is an efficient tool for texture analysis because of its multi-resolution nature. This paper presents a study of SAR sea ice classification based on the discrete wavelet transform (DWT). Two kinds of approaches, the traditional DWT based classifier and the tree-structured wavelet packet (TSW) based classifier, have been applied to SAR sea ice textures as well as to the well-known Brodatz textures. The results show that both methods are efficient in interpreting SAR sea ice textures. [C6350]

"A comparison of sea ice field observations in the Barents Sea marginal ice zone with satellite SAR data"

Routine sea ice observations of ice type, concentration and thickness were carried out during a microwave remote sensing validation campaign in the Barents Sea aboard the US Coast Guard icebreaker Healy during October-November 2001. Ice near the edge was generally a near equal mixture of small to medium floes of thin first-year ice and approximately 2 meters thick multiyear ice, with large floes occurring deeper in the ice pack. These data are compared to estimates of ice concentration from several radarsat and SSM/I images to validate routine operational ice analysis performed at the National/Naval Ice Center in Washington, D.C. Observations of several different ice regimes observed in the field are compared to observed SAR backscatter characteristics. Results show that while some distinction between ice types can be made within the pack, near the ice edge unambiguous determination is difficult from SAR data alone. For the most accurate analysis of ice conditions from SAR in the marginal ice zone, the day to day evolution of the ice drift and growth should be monitored.

[C6351]

"ERS-2 SAR image analysis for sea ice classification in the marginal ice zone"

The possibility to distinguish between different sea ice types in the marginal ice zone in the Greenland Sea using ERS-2 SAR is investigated. Statistical, textural and spectral features derived from ERS-2 SAR images and ice concentrations from 85 GHz SSM/I data are analyzed using learning vector quantization. The proposed method is useful for resolving ambiguities arising from frost flowers or pancake ice with very high backscatter values similar to the wind roughened sea surface. [C6352]

"Passive calibration of the backscattering coefficient of the ENVISAT RA-2: evaluation of radiative models for sea and land"

The passive calibration of the radar altimeter consists in characterising the receiver by observing natural surfaces with known emission in the so-called noise-sensing mode. The paper focuses on the general approach undertaken to simulate the brightness temperature at the top of the atmosphere observed by the Envisat Radar Altimeter (RA-2). It is based on emissivity models for land and sea as well as atmospheric radiation models supported by a continuous flow of on-line data used as model inputs. [C6353]

"Radar remote sensing of Great Lakes ice cover"

Summary form only given, as follows. Remote sensing of Great Lakes ice cover uses various classes of radars including scatterometer, polarimetric Synthetic Aperture Radar (SAR), and interferometric SAR. Satellite wide-swath scatterometers provide large areal coverage with high temporal resolution data to map Great Lakes ice cover. They compliment the high spatial but lower temporal resolution of satellite SAR data. The approach is to use in-situ and ground truth measurements from our 1997 Great Lakes winter experiments (GLAWEX 1997) in conjunction with concurrent satellite SAR data from ERS-2 and RADARSAT-1 and scatterometer data from NSCAT to determine scatterometer backscatter signatures of lake ice. The backscatter signatures are used as a library to develop an ice mapping algorithm using first the NSCAT data acquired during GLAWEX 1997 and then SeaWinds data (currently operational on the QuikSCAT satellite). Verification of the ice mapping results are carried out with in-situ observations from US Coast Guard (USCG) icebreaker vessels operating on the Great Lakes under the jurisdiction of the Ninth Coast Guard District. In addition, we installed a web camera to monitor ice cover over an area in Lake Superior to verify time-series scatterometer results obtained from QuikSCAT data. Moreover, polarimetric radar backscatter measurements from a USCG icebreaker acquired during GLAWEX 1997 reveal that multi-polarization backscatter data for the typical snow-covered snow ice on lake ice in the Great Lakes can be used to map ice and open water without the ambiguity encountered in single polarization data due to variations in wind speed over water. During our 2002 winter experiment (GLAWEX 2002) NASA AIRSAR C-band and L-band polarimetric and interferometric measurements are collected over Lake Superior, Green Bay and northern Lake Michigan, and the North Channel together with in-situ field observations. Polarimetric C-band SAR data obtained from GLAWEX 1997 (shipborne radar) and GLAWEX 2002 (airborne SAR) are used to develop multi-polarization algorithms in view of ENVISAT and RADARSAT-2 multi-polarization SAR applications to lake ice mapping. Furthermore, interferometric SAR data acquired during GLAWEX 2002 are used to evaluate the utility of interferometric SAR data for three-dimensional mapping for lake ice including aerial coverage and thickness. Because lake ice, unlike sea ice, has no salinity content, microwaves can propagate into lake ice unless the surface is wet due to melting. GLAWEX 2002 is a large-scale experiment including in-situ observations by webcam with all azimuth coverage, in-situ measurements from ship, air reconnaissance from helicopter, polarimetric and interferometric SAR from the NASA DC-8 aircraft, satellite scatterometer data from QuikSCAT/SeaWinds, and satellite SAR data from RADARSAT. [C6354]

"The CryoSat space segment: definition, design and predicted performance"

CryoSat is the first of the ESA Earth Explorer Opportunity Missions. It will allow an accurate determination of the marine and land ice mass fluxes at a global scale. This paper gives a brief overview on the CryoSat space segment, which is currently under development by an industrial consortium with Astrium as prime contractor. [C6355]

"Measuring soil moisture change with vegetation cover using passive and active microwave data"

Two basic microwave approaches are used to measure soil moisture, one is passive which is based on radiometry and the other is active and uses radar. Both approaches utilize the large contrast between the dielectric constant of dry soil and water. A total backscattering amount for a vegetated surface include volume, surface, and surface-volume interaction scattering terms. The backscattering model here is based on without surface-volume interaction scattering terms. In attempt to use active microwave remote sensors in estimation of

soil moisture, two major problems, effects of surface roughness and vegetation cover, are faced. For a given sensor, we assume the roughness under the condition of no change during data acquisitions. The main problem for retrieval of surface dielectric properties is separate the volume scattering item from total backscattering. With the time-serial soil moisture map from L band passive microwave radiometry, the Electronically Scanned Thinned Array Radiometer (ESTAR) at Southern Great Plains 1997 (SGP97), we calculated the surface reflectivity with 800 m resolution. The volume scattering items at 800 m resolution can be derived using multi-temporal resample calibration Radarsat SAR and surface reflectivity data. Weighting the ratio of NDVI at different resolution from NOAA/AVHRR and TM, the surface reflectivity change with 50 m resolution can be estimated according to the total backscattering and volume scattering, then soil moisture change be mapped at 50 m resolution. [C6356]

"Concept and realization of an Airborne SAR/Interferometric Radar Altimeter System (ASIRAS)"

Cryosat is an approved ESA mission. Its objective is to determine fluctuations in the Earth's land mass and marine ice fields. The mission utilizes a completely new SAR/interferometric altimeter concept, which combines a nadir-looking configuration with pulse-limited altimetry. The concept has been verified by simulations, but no dedicated experimental validation has been performed so far. For this reason, an Airborne SAR/Interferometric Radar Altimeter System (ASIRAS) is currently under development in the frame of an ESA contract. Due to the large bandwidth of the system, several components, i.e. the chirp generator, are critical and therefore require innovative solutions. A dedicated software performs SAR- and interferometric radar data processing and, in addition, supports internal instrument calibration. ASIRAS is intended to be tested, verified and optimized on a DO 228/100 aircraft carrier during a measurement campaign scheduled fall 2002 in the area of Fram Street north of Greenland. The paper presents mission objectives, the instrument concept of ASIRAS, and critical building blocks. [C6357]

"South China Sea internal wave analysis using radar imagery"

Some results of analysis conclude that the internal wave can affect the sea wind-generated wave crucially, so that the spectrum accounts for the interactions between the two kinds of sea water masses. These backscattering coefficients of the internal wave sea surface of the South China Sea are calculated using some existing models and the results are compared with the calculations of SIR-C/X-SAR data. Different results among the radar bands exist and are affected by sea surface roughness. The ocean wave spectrum is derived from the X-SAR image. Finally, we point out that the tidal current is the main factor that causes the internal waves. [C6358]

"Further numerical studies of backscattering from time evolving non-linear sea surfaces"

Previous studies have demonstrated that the West et al. (1987) model for non-linear hydrodynamic evolution of a sea surface realization produces significant features in calculated L-band backscattered Doppler spectra compared to a linear sea surface evolution model. Previous comparisons, however, were limited to a maximum wind speed of 2 m/s due to failure of the West et al. algorithm when steep short-wave features formed in the surface. In this paper, L-band Doppler spectra with the West et al. model are reported for wind speeds up to 4 m/s through the use of a suppression filter to reduce steep short-wave features. Results again show significant effects on Doppler spectra, including a strong polarization sensitivity at 80° observation angle. [C6359]

"SAR manifestations of sea fronts and vortex streets in the Bering Strait"

The analysis of ERS-1/2 SAR data of the Bering Strait, obtained in summer 1995, 1998 and 2000 has allowed us to observe many important oceanic processes. These include meandering fronts and vortex activity (well pronounced in the eastern part of the Strait), a strong jet current at the Prince Wales Cape, and intrusions of the cold Chukchi Sea water (extensions of the Siberian Coastal Current) in the western part of the Strait. These images demonstrate some interesting diversions from the northward current typical for the Bering Strait. The flow direction in the central part of the Bering Strait can be revealed from prominent wake features. Also, generation of internal waves on fronts can be detected in some images. Especially impressive is the large variety of surface manifestations of vortex streets north of the Fairway Rock due to high variability of the incident flow. The asymmetry of the Rock causes a special form of the Ka'rma'n vortex street consisting of a row of single vortices. [C6360]

"Anormal Doppler shifts of radar signals backscattered from marine slicks"

Results of field experiments on remote sensing of organic slicks on the sea surface using Ka-band radar are presented. Slicks of different surfactants with the film elasticity values ranging from some mN/m to some tens of mN/m were studied. It is shown that the radar Doppler shifts can change strongly in slicks, depending on the film

elasticity, while the depression of radar backscatter in slicks is nearly the same for the different substances. A physical explanation of the effect is given assuming different contributions of free capillary-gravity waves and "bound waves"-nonlinear harmonics of longer surface waves in the spectrum of cm- to mm-scale wind waves. A simple theory of wave damping in slicks is used to explain qualitatively the dependence of the Doppler shifts on film elasticity. [C6361]

"The property of sea surface scattering in millimeter wave \$satellite-borne cloud profiling radar calibration"

For calibrating a satellite-borne cloud radar, widely distributed natural targets are necessary because of the difficulty of antenna beam pointing. Sea surface scattering is considered as one good target. The problem is that the sea surface scattering property in mm waves (95 GHz) has not been reported. The authors have measured the sea surface scattering by a CRL airborne cloud radar (SPIDER) performed around the Japan Sea area or the Pacific Ocean. The sea surface property measured from this experiment is similar to that measured in a microwave scatterometer. [C6362]

"A multidecadal study of the number of Antarctic icebergs using scatterometer data"

Tabular Antarctic icebergs are regularly formed by the separation of massive sections of ice from ice shelves and glaciers. The National Ice Center (NIC) uses a variety of satellite sensors to track large Antarctic icebergs and reports iceberg position,. According to the NIC database, the number of large Antarctic icebergs has been increasing in recent years. A long term analysis of Antarctic iceberg activity based on scatterometer and radiometer data is presented. Our analysis suggests this increase is largely due to improved resources and technological advancements for iceberg tracking. Recent calving events may represent natural variability in iceberg activity. This study identifies some of the advantages and limitations of tracking icebergs using scatterometer data. [C6363]

"Evaluating the use of QuikSCAT data for operational sea ice monitoring"

Near-real time QuikSCAT image products are evaluated for ice mapping from the perspective of the Canadian Ice Services Operational Environment. [C6364]

"A microwave sensor for agricultural implements"

For soil preparation, the concept of precision agriculture requires real time measurements of soil characteristics and cultivator behavior. The microwave sensor presented in this paper overcomes the limitations of sensors based on optical or ultrasound devices towards agricultural environment (dust, rain, etc.). The sensor uses the principle of frequency-modulated continuous wave (FM-CW) radar, low cost technology well intended for short range applications. First laboratory results of two major applications are presented. The first one is the distance measurement applied to the control of working depth. Soil-implement distances are computed with the measurement of a beat frequency: a maximum positioning error of ± 5 mm is obtained for distances between 0.7 and 1 m. The second one is the evaluation of soil roughness in order to control seedbed quality. The backscattered coefficient, measured at normal incidence with samples of dry soil, is correlated with the rms height. [C6365]

"Global ocean wind fields from SAR data using scatterometer models and neural networks"

Three weeks of ERS-2 SAR wave mode data, representing a total of 34000 SAR images of 5 km Ч 10 km size, were utilized to verify wind retrieval algorithms on a global basis. Wind speeds are retrieved from calibrated SAR normalized radar cross section (NRCS) as well as uncalibrated SAR intensity images. In case of the calibrated NRCS the well-tested empirical C-band scatterometer (SCAT) model CMOD4 is used, which describes the dependency of the NRCS on wind. Therefore the SAR data are calibrated, which is performed by utilizing a subset of co-located ERS-2 SCAT data. SAR derived wind speeds are compared to co-located winds from the ERS-2 SCAT and model results of the European Centre for Medium-range Weather Forecast (ECMWF). The comparison to ERS-2 SCAT results in a correlation of 0.95 with a bias of -0.01 ms⁻¹ and a root mean square error of 1.0 ms⁻¹. In case of SAR intensities a Neural Network (NN) is used that allows to retrieve wind speeds from uncalibrated SAR images. Comparison of NN retrieved SAR wind speeds to ERS-2 SCAT wind speeds result in a correlation of 0.96 with a bias of -0.04 ms⁻¹ and a root mean square error of 0.93 ms⁻¹. [C6366]

"Measurement of the sea surface wind vector by an airborne altimeter"

A pilot needs operational information about wind over sea as well as wave height to provide safety of hydroplane landing on water. Near-surface wind speed and direction can be obtained with an airborne microwave

scatterometer, radar designed for measuring the scatter characteristics of a surface. Mostly narrow-beam antennas are applied for such wind measurement. Unfortunately, a microwave narrow-beam antenna has considerable size that hampers its placing on flying apparatus. In this connection, a possibility to apply a conventional airborne radar altimeter as a scatterometer with a nadir-looking wide-beam antenna in conjunction with Doppler filtering for recovering the wind vector over sea is discussed, and a measuring algorithm of sea surface wind speed and direction is proposed. The obtained results can be used for creation an airborne radar system for operational measurement of the sea roughness characteristics and for safe landing of a hydroplane on water. [C6367]

"Method of spectral function in the problem of Doppler lidar sensing in the stratified atmosphere"

The equation for the estimation of the Doppler shift is derived for the spectral function method. The measurement accuracy is analyzed for the mean and actual wind profiles at different atmospheric stratification. [C6368]

"Texture feature neural classifier for remote sensing image retrieval systems"

Texture information is useful for image data browsing and retrieval. The goal of this paper is to present a texture classification system for remote sensing images aimed at the administration of large collections of those images. The proposed classifier is a hybrid system composed by an unsupervised neural network and a supervised one. Starting from a small portion of the image (pattern) the system should recognize the most similar class to a pattern in a database as well as to identify images that contain similar patterns. The texture feature vectors used to characterize the patterns are obtained from the images processed by a bank of Gabor filters. Experimental results using textures of the Brodatz album, multi-spectral and radar images are presented. [C6369]

"Linear features detection in SAR images for urban analysis"

This work is concerned with extracting straight lines in SAR image areas for application of urban analysis. The methodology combines the Hough transform and line detector algorithms proposed by Tupin et al. (1998) to extract the main axes in road networks. A real SAR image is used to test the proposed algorithm. [C6370]

"Recognition of drift ice using synthetic aperture radar images"

In recent years, observation of a wide variety in the Earth surface can be done by improvement of the remote sensing technology. The purpose in this paper is to recognize a drift ice using synthetic aperture radar (SAR) images. The recognition of the drift ice is achieved by using neural networks. The neural networks used include: a BP trained neural network and a self-organizing map. The training data are image features extracted from SAR images. The two methods used of extracting the features are: Fourier transform and high-order autocorrelation function. Furthermore, false colors are given to the SAR image. Features are extracted from that image and are recognized by the neural networks. [C6371]

"Automatic indexing system for atmospheric laser radar data"

The purpose of this paper is to design a new method for an automatic indexing system with unsupervised conditions. In this paper, the method of a self-organizing clustering network is adopted. It is used to classify and index a large amount of real atmospheric laser radar data. Initially, the parameters of each cluster will start with random initial values and are adapted with the algorithm. In this paper, six groups are clustered from the given data. It is also shown that some of these indicate quite important atmospheric condition characteristics. [C6372]

"Microwave photonic source for coherent Doppler LIDAR system operating at 1550 nm"

We present theoretical and experimental results for a microwave photonic oscillator (MPO) that provides a microwave signal and a modulated optical wave simultaneously, and which can be used as a local oscillator for a coherent Doppler LIDAR operating at 1550 nm. [C6373]

"Low frequency radar phenomenology study in equatorial vegetation \$preliminary results"

This paper presents a study based on field measurements on several equatorial foliage penetration phenomena in Singapore. The study includes short-range back scattering and propagation measurements in a very wide frequency band from 100 MHz to 1 GHz. The measurement setup and the data analysis are presented. [C6374]

"An HF-radar test deployment amidst an ADCP array on the West Florida Shelf"

For 11 days in January 2002, the Conrad Blucher Institute for Surveying and Science, Texas A&M University-Corpus Christi, in collaboration with the College of Marine Science, University of South Florida, deployed a pair of 25-MHz CODAR Ocean Systems HF-radars on the West Florida Shelf over an array of six acoustic Doppler current profilers. The radar footprint had a maximum range of 60 km offshore, and it included mooring locations between the 10 m to 30 m isobaths. We examine, using a variety of metrics, the correlation between the surface currents measured remotely by the HF-radar and the subsurface currents measured by the ADCPs, which were either bottom- or surface buoy-mounted. Qualitative comparisons are generally good for this inner-shelf environment where the wind-driven current magnitudes were less than about 40 cm/s. The scalar regression analysis shows correlation coefficients (R) of 0.8 to 0.9 for the alongshelf components but 0.6 or less for the cross-shelf components. Complex vector correlation produces correlation values of 0.76 to 0.90 and a consistently clockwise veering from the radar-measured currents to the ADCP-measured ones ranging from 1.3 to 5.2°. The alongshelf surface currents measured by the radar are about 30% larger than those of the ADCPs measured 2 to 3 m below the surface according to standard deviations and linear regression slopes. [C6375]

"Robust mapping of tropical cyclone wave fields using HF skywave radar"

The prospect of obtaining real-time measurements of oceanographic and meteorological conditions over vast areas of the Earth's oceans by means of HF skywave ('over-the-horizon') radar has been the subject of many investigations over the past three decades. The remote sensing information is obtained by interpretation of echoes from the sea surface, whose time-varying geometry imposes a complex modulation on the radar signals. Depending on radar design and ionospheric conditions, a map spanning several million square kilometres may be acquired on a grid with resolution typically 10-20 km in less than 30 minutes. We describe methods developed in the Defence Science and Technology Organisation (DSTO) to overcome, or at least minimise, the deleterious effects of radio interference, disturbed ionospheric propagation conditions, scattering from very rough seas and the intrinsic complications of wave fields generated by intense weather systems. The goal is the integration of these various measures into a fully automated cyclone mapping system. [C6376]

"Space-surface bistatic synthetic aperture radar-prospective and problems"

The paper introduced a feasibility analysis of a synthetic aperture radar (SAR) with novel architecture. Two essential peculiarities are discussed: the system configuration with a moving transmitter when the receiver is stationary and noncooperative transmitters utilization for the system. The system is named space-surface BSAR or S-SBSAR. The system analysis confirms its feasibility. S-S SAR could find numerous applications where an observation area of 20-30 km relevant to the receiver is acceptable. S-SBSAR space resolution corresponds to the general approach to BSAR when the resolution degradation due to a non-optimal satellite-targets-receiver geometrical position could be resolved using the satellites diversity. [C6377]

"Complete coastal mapping with airborne lidar"

Eight years of SHOALS (Scanning Hydrographic Operational Airborne Ladar Survey) operations have proven that airborne lidar is an ideal tool for rapidly measuring shallow water depths and nearshore land elevations. SHOALS has produced high-density measurements of the coastal zone, enabling coastal engineers and scientists to quantify volumes of navigation channel shoaling, track movement of sand placed for beach nourishment, aid in coral reef mapping, and provide depths and navigation hazard locations for nautical charting. SHOALS success in producing valuable data for an ever-widening range of coastal applications has culminated in the development of the next-generation of airborne lidar sensors. SHOALS-1000 will be an integrated system including a bathymetric lidar component, a topographic lidar component, and a digital imagery capability. The bathymetric component will operate at a rate of 1,000 Hz, while the topographic component will operate at 10,000 Hz. SHOALS-1000 will collect data exceeding IHO Order 1 requirements and will easily mobilize in most photogrammetric aircraft of opportunity. Current SHOALS data processing schemes are automated for the system based on the expertise gained through eight years of evaluating lidar returns from the SHOALS system. [C6378]

"WARLOC: a high-power millimeter-wave radar"

A high-power, coherent, W-band (94 GHz) millimeter-wave radar has been developed at the Naval Research Laboratory. The radar employs a 100 kW peak power, 10 kW average power gyrokystron as the final power amplifier, an overmoded transmission line system, and a quasioptical duplexer, together with a 6 foot Cassegrain antenna, a four-channel receiver, and state-of-the-art signal processing. Developed as a research radar for the investigation of tactical Navy radar applications in the millimeter wave band, additional radar measurement studies include cloud physics, propagation, and forward and backscatter studies. [C6379]

"Comparison between surface impulse ground penetrating radar signals and ultrasonic time-of-flight diffraction signals"

Surface impulse ground-penetrating radar (GPR) and ultrasonic time-of-flight diffraction (TOFD) are recent innovations in the respective geophysical remote sensing and non-destructive testing industries. Both techniques have proved highly versatile and valuable applications. This paper provides a brief description of the time-of-flight diffraction (TOFD) signals and the surface impulse ground penetrating radar (GPR) signals. The similarities between the two techniques are highlighted and it is shown how processing techniques developed for GPR data processing may be adapted for use with TOFD data. [C6380]

"Toward the detection of bioparticles by radar in the THz region"

A first-pass analysis is carried out of a 421 GHz coherent radar to detect the presence of a bioparticle cloud at a stand-off of 1 km. Compared to the incoherent radar performance under identical field conditions, the coherent system achieves a post-demodulator signal-to-noise ratio roughly 300 times higher and far superior probabilities of detection and false alarm. [C6381]

"Real-time integrity monitoring of stored geo-spatial data using forward-looking remote sensing technology [Caircraft navigation/displays]"

Terrain awareness and warning systems (TAWS) and synthetic vision systems (SVS) provide pilots with displays of stored geo-spatial data (e.g. terrain, obstacles, and/or features). As comprehensive validation is impractical, these databases typically have no quantifiable level of integrity. This lack of a quantifiable integrity level is one of the constraints that has limited certification and operational approval of TAWS/SVS to "advisory-only" systems for civil aviation. Previous work demonstrated the feasibility of using a real-time monitor to bound database integrity by using downward-looking remote sensing technology (i.e. radar altimeters). This paper describes an extension of the integrity monitor concept to include a forward-looking sensor to cover additional classes of terrain database faults and to reduce the exposure time associated with integrity threats. An operational concept is presented that combines established feature extraction techniques with a statistical assessment of similarity measures between the sensed and stored features using principles from classical detection theory. Finally, an implementation is presented that uses existing commercial-off-the-shelf weather radar sensor technology. [C6382]

"Helicopter in-flight tracking system (HITS) for the Gulf of Mexico"

Helicopters and other low-altitude air traffic over the Gulf of Mexico operate without the benefit of radar surveillance due to the location and range of existing onshore radar installations. The NASA Ames Research Center (ARC) is sponsoring deployment and testing of a prototype helicopter in-flight tracking system (HITS) in a portion of the Gulf of Mexico offshore area. Using multilateration principles, HITS determines the location and altitude of all transponder-equipped aircraft without requiring changes to current mode A, C or S transponders. In addition to multilateration, HITS provides surveillance reports for aircraft equipped for automatic dependent surveillance broadcast (ADS-B). This paper describes the HITS project-specifically, the system equipment (architecture, remote sensors, central processing site, and communications equipment) and system performance (accuracy, coverage, and reliability). [C6383]

"Parameters optimization for synthesizing aperture method at practical use of continuous radiation underground radar"

A modification of the aperture synthesizing method aimed at improving the resolution of a subsurface radar is proposed. The results of data processing by this method are presented. The input data had been obtained with the use of a prototype of the step-frequency subsurface radar developed in the Institute of Applied Physics. [C6384]

"Conference Proceedings. 2002 International Conference on Mathematical Methods in Electromagnetic Theory. MMET 02 (Cat. No.02EX554)"

First Page of the Article [C6385]

"Drift ice recognition using remote sensing data by neural networks"

In recent years, observation of a wide variety in the Earth's surface can be done by improvement of remote sensing technology. The purpose of the paper is to recognize a drift ice as thick ice, thin ice, and sea using synthetic aperture radar (SAR) images. The recognition of the drift ice is achieved by using neural networks

(NN). The neural network applies two methods, a BP trained neural network and a self-organizing map. Training data are image features extracted from SAR images. There are three methods for extracting the features: Fourier transform, high-order autocorrelation function (HACF), and image features based on a run length method. We carry out a comparative experiment, and demonstrate their effectiveness by means of computer simulation.

[C6386]

"Nonparametric algorithm for a detection of random process disorder in the signals of radar remote sensing"

A new nonparametric algorithm of radar signal disorder detection is considered. The algorithm is based on spectral estimation of a few signal samples of some close windows and application of a nonparametric Wilcoxon's test to compare them. The algorithm can be used for radar signal detection specifically in the tasks of turbulence detection in clouds and precipitation as well as for moving target detection. The efficiency of the new algorithm is analyzed. [C6387]

"Doppler-polarimetric retrieval of rain rate and turbulence intensity in precipitation"

This paper deals with mathematical modeling and simulation of echo-signals of microwave remote sensing of precipitation in both the frequency and time domains. It establishes some important relationships between Doppler-polarimetric observables and the weather object under observation. [C6388]

"Combined active and passive microwave sensing of ocean surface wind vector from TRMM"

This paper presents a new ocean wind vector measurement technique that uses the combined passive and active microwave measurements respectively from the Tropical Rainfall Measuring Mission (TRMM) Microwave Imager (TMI) and the Precipitation Radar (PR). The wind speed is inferred by TMI over a wide swath that includes the narrower PR swath. The PR scans cross-track $\pm 18^\circ$; and near the swath edges, where the radar backscatter responds to both the magnitude and direction of the surface wind, we use the microwave radiometer estimate of wind speed and the measured σ_0 at incidence angles greater than 15 degrees to derive wind direction. Because the PR provides only a single azimuth look, multiple possible wind direction solutions exist. The ability to select the proper (single) direction is beyond the scope of this paper; but comparisons are presented between the "closest" retrieved TRMM wind vectors and near-simultaneous wind vectors measured by the QuikSCAT satellite scatterometer to demonstrate the potential for measuring ocean surface vector winds.

[C6389]

"Delay compensation of stretching signal in OTHR"

In the stretch processing system of linear FM (chirp modulation), the time delay of the return is converted into frequency. The frequency and time delay are proportional to the target range. Each intermediate frequency (IF) pulse occupies a different time interval, indicating the variation in time delay as a function of range. It results in a high sidelobe when proceeding with a uniform weight in the whole time width. The paper describes the delay compensation technology by a subband filter group which can reduce the sidelobe level of the weighted signal greatly after the synthesis of multiple channels. [C6390]

"Despeckling and detection of high reflectance regions from SAR images"

A speckle reduction method for synthetic aperture radar (SAR) images is presented here. This method can be considered as a first step for the extraction of other important information. The second one is the detection of high reflectance regions which yields an important step to continue the segmentation of the total image. We have worked in 3-look simulated and real ERS-1 amplitude images. The iterative filter is based on a membrane model Markov random field (MRF) approximation optimized by a synchronous local iterative method (SLIM). The final form of restoration gives a total sum preserving regularization (TSPPR). [C6391]

"A novel speckle filtering technique for SAR image"

A new technique using an adaptive window for filtering SAR images is proposed. It is based on developing a mechanism of speckle whose lever varies with the reflectivity property of the scene. Taking account of such scene heterogeneity, the proposed scheme to search homogeneous areas with increasing window and different thresholds works as perfectly as expected in edge preservation and texture restoration of SAR images. The comparison between this new method and some well-known filters is also shown. [C6392]

"TCP-friendly congestion control mechanism for an UDP-based high speed radar application and

characterization of fairness"

The transfer of digitized radar data over the Next Generation Internet at data rates ranging from 64 Mbps to 384 Mbps, is an emerging real-time, high-bandwidth application using the UDP transport protocol. We propose the TCP-friendly Rate Adaptation Based on Loss (TRABOL) algorithm that relies on relevant QoS parameters feedback from the receiver to the source to control the transmission rate for congestion control. We also characterize the fairness of the system of UDP-based and TCP-based flows sharing a single bottleneck link bandwidth, using a throughput-based fairness index and show by experiments that the congestion-controlled radar application is TCP-friendly. [C6393]

"An architecture for sensor data fusion target tracking"

Many geographic target tracking scenarios provide difficult geospatial environments for collecting reliable sensor data. As a result, multiple sensor data sources must be integrated to provide a reliable estimate of an object's position as it moves through various environments. We describe MTI-Net, a geospatial database dedicated to providing reliable sensor data for an object moving through various geospatial environments by integrating multiple sensor data sources together in a Web-based environment. MTI-Net is an integration of database and signal processing resources. [C6394]

"Performance evaluation of maximum likelihood SAR segmentation for multi-temporal rice crop mapping"

Optimal (maximum likelihood) processing for a SAR image comprised of discrete regions of constant radar cross section is now well known. This scheme considerably improves upon windowed and iterative schemes by merging regions on an individual pixel basis. In theory, rigorous expressions for 'false alarm rate' can be defined but they are perhaps too sensitive to the underlying assumptions of independence and homogeneity. Images can be visually improved by a restraint on the 'surface tension' of the segmented regions but, to avoid subjective judgement, performance is assessed using pixel-accuracy ground truth from a rice growing area in central Japan based on multi-temporal, 8 m resolution Radarsat data. Gaussian expectation maximisation is used to achieve accurate, fully-unsupervised classification of the area without fixed-value thresholding. This large scale backscatter information is then used in a Bayesian merging scheme to give a significant improvement in performance. [C6395]

"Radar payload design and its performance characteristics for spaceborne small platform remote sensing system"

The spaceborne imaging radar mission and system requirement is analysed with the key performance characterized by the small satellite system. Based on the various imaging modes and the system requirement model, the X-band imaging radar payload is designed and the major results are presented with the key performance characteristics. [C6396]

"Evaluation of P-band foliage penetration through polarimetric high resolution SAR imaging with the RAMSES radar"

ONERA in association with DGA, CNES and several laboratories, conducted an experiment of P-band (435 MHz) imaging at high resolution (2 m) with full polarimetric capability. The test site is a cultivated pine forest in south west France. It is populated with appropriately scattered and oriented dihedrals and corner reflectors. Under-covered reflectors and vehicles are also included. Measures of the under cover reflector returns showed that attenuation in horizontal polarisation depends on the angle of view (more than in vertical polarisation). The wide antenna illumination pattern ($\pm 30^\circ$) allows one to image up to aircraft nadir, thus confirming an important penetration through foliage on its vertical profile. [C6397]

"Modern synthetic aperture radar systems"

Synthetic Aperture Radar (SAR) is a side looking airborne radar sensor that provides high-resolution microwave images of selected ground areas. It is an all weather day and night sensor. Additional features include stand-off capabilities (long range) and fast coverage rate. Stationary ground targets are clearly visible upon a SAR image and can also automatically be detected. SAR sensors are used for reconnaissance and remote sensing applications. In this article a new generation of advanced SAR systems is presented. It features high performance reconnaissance and Zooming SAR modes as well as dedicated modes for display overlay of moving targets upon SAR images. It processes the radar raw data on-board and transmits SAR images via data-link. That on board processing capability greatly reduces the data link bandwidth. Those advanced systems operate upon fighter and transport aircrafts and upon unmanned vehicles (RPV's). A derivative of SAR for

airborne fire control radars and for airborne maritime patrol applications is also presented. [C6398]

"Statistical modeling of multipolarization and multifrequency SAR images of the sea surface"

A statistical analysis of polarimetric and multifrequency SAR images of the sea surface is presented. The analysis is carried out resorting to binary hypotheses tests aimed at verifying to what extent the texture value is shared between pixels of the same image in spatial proximity to each other, measurements of the same pixel acquired at different polarizations but in the same band, and measurements of the same pixel at different frequencies but with the same polarization. The data under test were acquired during a SIR-C/X-SAR mission in 1994. It is shown that cells in spatial proximity share the same value of the texture over sub-images of certain dimensions; moreover, while the HH and VV measurements of the same pixel possess a common value of the texture both in the L- and the C-band, the texture generally varies from the L- to the C-band (for both the HH and the VV channel). [C6399]

"Oceans 2002 Conference and Exhibition. Conference Proceedings (Cat. No.02CH37362)"

First Page of the Article [C6400]

"A resolution enhancement method for SAR images with adaptive speckle reduction"

Due to the capability of producing a high-resolution image under all weather conditions, SAR (synthetic aperture radar) is a very powerful and attractive tool for remote sensing. Since SAR systems generate images by coherent processing of the scattered signals, they are susceptible to speckle noise. Speckle noise is multiplicative so the presence of speckle noise hinders a human observer from analyzing features of SAR images. Also, speckle noise makes automatic interpretation of SAR images extremely difficult. Various methods have been proposed to suppress speckle noise. Although conventional speckle filtering algorithms can effectively reduce speckle noise, but also smear edges and blur images to some degree. Because SAR system has a limited bandwidth, even if no speckle suppression filter is applied for obtaining fine-detail images, there still exist slow responses to sudden changes, i.e. sidelobes. We propose a new SAR image enhancement method, which reduces sidelobes in fine details as well as suppresses speckle noise effectively in homogeneous areas. To verify the efficacy of the proposed method we apply it to an ERS-1 SAR image. The resulting image shows that the proposed method suppresses speckle noise effectively without any blurs or sidelobes in fine detail areas. [C6401]

"The New Jersey Shelf Observing System"

The New Jersey Shelf Observing System is a coastal ocean observatory whose primary goal is supporting collaborative interdisciplinary oceanographic research. The observatory has both a sustained component designed to provide spatial datasets year-round, and a process study component for more intensive measurements during short-term scientific experiments. The sustained component consists of tracking stations for the international constellation of ocean color and IR satellites, multi-frequency multistatic CODAR HF radars, and long-duration subsurface glider AUVs. The processes study component uses numerous platforms that include aircraft, ships, propeller-driven AUVs and relocatable mooring arrays. Process studies focused on recurrent coastal upwelling centers and their biological impacts from 1998-2001, and are planned to focus on the Hudson River plume, chemical contaminants, and their biological impacts from 2003-2007. Despite being a research-oriented observatory run by the scientists for the scientists, it maintains a significant societal impact through its Website (marine.rutgers.edu/cool), receiving an average of over 60,000 hits/day during the busy summer months. [C6402]

"Improved hurricane wind speed algorithm for the seawinds satellite scatterometer"

Satellite microwave scatterometer wind retrievals, given in the standard product (e.g., QuikSCAT L2B), badly underestimate the peak wind speed in tropical cyclones. One important reason is that the effects of precipitation on the normalized radar cross section σ_0 are neglected in the processing algorithms. This paper presents results of a first attempt to provide σ_0 corrections, which account for the atmospheric attenuation of the rain. Atmospheric transmissivity is derived from the QuikSCAT Radiometer (QRAD) excess brightness temperatures taken simultaneously with σ_0 measurements. When applied, retrieved wind speeds show improved agreement with numerical hurricane models (PSU/NCAR MM5) where there is moderate to high rainfall. [C6403]

"Measuring sea surface salinity from an airborne SAR in the Gironde region, France"

Radar is being developed in many work fields essentially in coastal areas and mounted on satellites (ERS,

Seasat). Only a few experiments have been made these last decades in order to study sea surface salinity from microwave radiation (Miller et al., 1998). It has become a real key in coastal area remote sensing. The tool we are working with is a P-band airborne synthetic aperture radar (SAR) called RAMSES made by the ONERA (Paillou et al., 2001). It is a multiband frequency radar which works for all four-polarizations. The active P-band challenge is that such an airborne radar has never been experimented before this day for the study of salinity. This is particularly surprising because of its rising sensibility with salinity gradient. The major aim is to discuss how we can discern bathymetry effects in the Gironde mouth from salinity response into the radar signal. Adding to the radar data, simulations of salinity fields (MARS 3D model from IFREMER) over the Atlantic platform were run for this date contributing to ensure what we suppose with the radar signal. Then we modeled the intensity of the radar (σ_0) found on a dielectric constant model (Klein & Swift, 1977) and on Bragg diffusion theory from sea surface. The model simulates a variability of less than 1 dB with the signal intensity for a 1% gradient considering a P-band radar and three time less for a L-band one. This range is ten times less than what is observed from the data. From a qualitative point of view, the intensity of the retrodiffusion globally increases along the saline gradient from low to high salinities. Moreover, the VV polarization is getting more dependent to salinity with higher incidence angles. The study of the saline plume with chlorophyll and suspended matter has permitted to make coincided the 10 to 20 dB drop in the signal with the turbidity limit and phytoplanktonic bloom.

[C6404]

"A 3-D imaging method using cross-traverse data for ground-penetrating radar"

To save ground-penetrating radar computer time, this paper presents a 3D imaging method using cross-traverse data, which is based on focusing and correlation techniques. Experimental result shows the method is effective.

[C6405]

"An algorithm of bridge detection in radar sensing images based on fractal"

This paper presents a new method to detect bridges in Synthetic Aperture Radar (SAR) images based on fractals. In this method, the gray surface of an SAR image is modelled as a DFBR (Discrete Fractional Brownian Random) field. In the homogenous region of SAR image, the H (Hurst) exponent of the DFBR is about the same; but in the sharply changing region such as the boundaries of a bridge, the H occurs singularity. According by this characteristic, the bridge can be detected and extracted. In order to alleviate the influence of the speckle of SAR image, the concept of mean was introduced into this algorithm. Experiment results show this algorithm is very effective and superior to other classical edge detection operators.

[C6406]

"Analyzing on phase error for single pass interferometric SAR"

The height error induced by phase errors is decisive for the final performance of interferometric synthetic aperture radar (InSAR) systems. The principle reasons associated with the phase errors are illustrated in this paper, including SNR, baseline length, number of looks, etc. The derived models are applied to a practical example.

[C6407]

"Image fusion for uninhabited airborne vehicles"

In image fusion, information from a set of images is extracted and then combined intelligently to form a new composite image with extended information content. The original data may come from different viewing conditions (bracketed focus or exposure) or various sensors (visible and infrared or a cat scan and magnetic resonance imagery). Uninhabited Airborne Vehicles (UAVs) often have visible, infrared and synthetic aperture radar imaging sensors, so image fusion is an appropriate onboard processing task for UAVs. Some forms of image fusion are computationally intensive tasks, but like many other image processing applications are naturally suited to acceleration in hardware. This potential for hardware acceleration, and the ability to reconfigure the UAV to implement new algorithms as it moves towards objects of interest make reconfigurable computing a natural route for a hardware implementation. In this paper we present what we believe is the first implementation of image fusion on a reconfigurable platform alone, and the first investigation of adaptive image fusion which makes use of dynamic reconfiguration to change the fusion algorithm as the UAV approaches an object of interest.

[C6408]

"Polarimetric scattering from inhomogeneous random media under a pulse incidence"

Polarimetric scattering from inhomogeneous random media of non-spherical scatterers under a pulse incidence is studied. The time-dependent Muller matrix solution of the vector radiative transfer for layered random media is derived. Co-polarized and cross-polarized bistatic and back-scattering are numerically calculated. The shape and intensity of polarized echoes depict well the inhomogeneous fraction profile of random scatterers. Its functional dependence upon the fraction profile, layer thickness, and other parameters are discussed. This technique is

applicable to the reconstruction of inhomogeneous fraction profile and inversion of the media thickness. [C6409]

"Edge and line detection in polarimetric SAR images"

A scheme for detecting edges and lines in multichannel SAR images is proposed. The line detector is constructed from the edge detector. The latter is based on multivariate statistical hypothesis tests applied to log-intensity SAR images. The raw results are vectorized by a traditional bright line extraction process. The scheme is illustrated by extracting dark linear structures on various full-polarimetric SAR images. [C6410]

"Design on return signal simulator of scatterometer and method of generating its signal"

The return signal simulator (RSS) of the Chinese spaceborne scatterometer is designed in order to compensate for the insufficiency of the common test and calibration device. The RSS can calibrate and test conveniently the transfer function and signal processing function of the scatterometer in ground-based tests. It employs the principle of pulse reconstruction. The characteristics of the return signal are generated by a digital method. The accurate round trip path delay of the radio-frequency signal, pulse width modulation and Doppler frequency shift are simulated. Also the phase difference shift is improved. By using the RSS, the testing and calibrating experiments for the scatterometer are implemented, which indicate that the generated return signal not only can fully express the statistics of the real return signal, but also can meet the requirements of testing and calibrating the scatterometer. This method of generated return signal can be realized easily and the results are correct, so it will provide a reference for future RSSs. [C6411]

"A super resolution SAR imaging method based on CSA"

Available conventional super resolution SAR imaging methods are based on complex images obtained by SAR imaging algorithms, and form super resolution SAR images via 2-D spectral estimation methods. A super resolution SAR imaging method combined with the chirp scaling algorithm (CSA) is presented in this paper. The new method forms a super resolution image by performing the range and the azimuth processing independently. This method can reduce the effects of phase errors on super resolution processing. The method is suitable for practical application since it does not require heavy computation. Experimental results show the effectiveness of the presented method. [C6412]

"Development of return signal simulator for Chinese satellite altimeter test and calibration"

The prelaunch performance assessment and function modes assurance of Chinese first satellite altimeter, developed by the Center for Space Science and Applied Research, must be subjected to a rigorous test and calibration program. As an important part of this program, an ocean Return Signal Simulator (RSS) is developed. This paper describes the principles of the RSS with its means of testing and calibrating the satellite altimeter. By employing a chirp regeneration technique, a full de-ramp technique, an ocean return spectrum digitally synthesizing technique and a high speed DSP technique, a full signal RSS is successfully developed for the Chinese satellite altimeter test and calibration, full range of time delay and full sea state simulation is achieved. Time delay precision is 0.2 ns, significant wave height simulation precision is 0.5 m and backscattered coefficient precision is 1 dB. By using the RSS, the full system testing and calibrating experiment to the Chinese satellite altimeter are implemented, and the dynamic performance of the altimeter is validated by the obtained results. [C6413]

"The design of China spaceborne radar altimeter control system"

The control system plays a key role in the spaceborne radar altimeter, such as it should implement track function to provide the height from the satellite to the sea surface, the significant wave height (SWH) and the backscatter coefficient. In this paper, the design of the China spaceborne radar altimeter control system (RACS), which is one part of Multi-mode Microwave Remote Sensor (M3RS), is discussed in detail. RACS can realize the function of noise-bias measurement, inner calibration, return wave acquisition-track process, and data transfer. A new algorithm to implement the IF simulation signal is brought forward, and an IF simulator is developed to test RACS. RACS is also successfully tested in the airborne flight experiment. [C6414]

"Automated calibration of multi-temporal ERS SAR data"

Quantitative analysis of multi-temporal SAR datasets requires accurate radiometric calibration. This can usually be achieved by considering a number of multiplicative factors, to be applied to statistically-homogeneous areas on each image to be calibrated. We propose an automated procedure to easily obtain a relative radiometric calibration of a stack of an arbitrary number of ERS SAR images, all coregistered to a unique master. The procedure relies upon the theoretical invariance of both system and scene parameters for targets whose

amplitude values are statistically correlated with each other. In practice, with the above-mentioned assumptions, the only varying quantity to take into account is the temporal variation of the calibration factor. We show, based on experiments on two multi-temporal datasets, that the ERS-1 calibration constant exhibits practically no variations except for the expected statistical fluctuations of about ± 1 dB. This observation is consistent with the reports on the operations of the ERS-2 satellite, published by ESA. The proposed procedure then consists in applying the full absolute calibration procedure only to the master image, and then relatively correct all other images in the stack by the method described. [C6415]

"Ground-based aviation weather radar research at the Rutherford Appleton Laboratory and University College London"

We present an overview of recent collaborative research, involving RAL and UCL, in the field of ground-based meteorological radar systems for weather assessment at, and in the terminal manoeuvring area (TMA) surrounding, civil airports. Three projects are briefly described. Firstly, we present the results from a design study intended to develop the specifications for a dedicated C-band weather surveillance radar covering an airport TMA. Secondly, we discuss the design of, and present some measured data from, a recently installed S-band weather radar system located at St. Andrews in Scotland. This low-cost radar uses a small antenna and low transmitted power, but is capable of providing a high-resolution display of significant precipitation within a coverage area extending to 60 km range. High sensitivity is achieved by coherent signal processing techniques. This system demonstrates that relatively inexpensive TMA weather surveillance using radar techniques is a practical proposition. Finally, we illustrate the potential of a vertically pointing millimetre-wave radar to remotely sense the height-distribution of cloud above an airport runway. Design details of a 94 GHz cloud-profiling radar system are presented, and examples of measured data from this instrument are used to show its capabilities for automatic detection of cloud-base height and cloud depth. [C6416]

"A portable eye-safe scanning aerosol lidar of the Hampton University Center for Lidar and Atmospheric Sciences Students"

Hampton University Center for Lidar and Atmospheric Sciences Students (CLASS) team and ITT's Advanced Engineering & Sciences Division have worked together to develop a portable, eyesafe and scanning aerosol lidar system, the system is based on a 1.5 micron, 125 mJ, 20 Hz eye-safe optical parametric oscillator (OPO). Its purpose is to remotely detect aerosols, clouds, and pollution in the lower atmosphere. [C6417]

"Unsupervised learning rules for POLSAR images analysis"

It has been shown (see Chitroub, S. et al., Signal Processing, vol.82, no.1, p.69-92, 2002) that the model for POLSAR (polarimetric synthetic aperture radar) images is a mixture model that results from the product of two distributions, one characterizes the target response and the other characterizes the speckle phenomenon. For scene interpretation purpose, it is desirable to separate between the target response and the speckle information. We propose here to use some unsupervised learning rules for POLSAR images analysis via a PCA-ICA neural network model. Based on its rigorous statistical formulation (see Chitroub et al., Intelligent Data Analysis International Journal, vol.6, no.2, 2002), a neuronal PCA approach for the simultaneous diagonalization of the signal and noise covariance matrices is proposed. The goal is to provide PC images that are uncorrelated and have an improved SNR. Speckle is a non-Gaussian multiplicative noise, and the higher order statistics contain additional information about it. ICA is used to separate the speckle from the PC images and providing new IC images that have an improved contrast. The method has been applied on real POLSAR images. The extracted features are quite effective for scene interpretation. [C6418]

"Analysis of radial velocity effect on synthetic range profile of stepped-frequency waveform"

The stepped-frequency waveform is able to obtain large effective bandwidth by sequentially changing the carrier frequency in steps over pulses. However, this waveform is very sensitive to the radial velocity between the radar and the target. In this paper, the effect of the radial velocity on the synthetic range profile is discussed first, and then the range spread in terms of the processed range bin is defined differently from others, which is validated by the simulation. Furthermore, the relation between the processed range bin and the range resolution is also discussed. [C6419]

"Development of an ultra-wideband radar system for vehicle detection at railway crossings"

This paper describes an ultra-wideband (UWB) radar system designed to detect motor vehicles such as cars and trucks when they are present at a railway crossing. Once fully developed, the detection performance of the system is to be compared against a video detection system in a test at a crossing in Maywood, Illinois. If the test

is successful this system may be further developed and installed at a four-quadrant gate crossing to sense vehicles trapped at the crossing island (i.e. the area bounded by the gate arms). This paper describes the problem at hand and gives details of the radar system development to date. With the current prototype, a pulse width of 3 ns has been achieved, which yields adequate range resolution for this application. [C6420]

"Assessment of digital elevation models obtained in Brazilian Amazon based on P and X band airborne interferometric data"

An airborne campaign in September of 2000 over Tapajor's National Forest, which is a region of Brazilian Amazon, Parar' State, has acquired P and X band interferometric data over a region which comprises primary forest, secondary forest in several stages of regrowth, pasture, crop plantations, bare soil, water and other classes. The AeS-1 polarimetric system, from AeroSensing Radarsysteme GmbH, Germany, provided P band polarimetric data for two-pass interferometry and X band single polarization, single-pass interferometric data. During the radar mission, a ground survey was carried out for target identification and collection of tri-dimensional differential GPS data for P and X band corner reflectors and other characteristic points. Georeferenced Digital Elevation Models (DEMs), with spatial resolution of 2.5 m, were generated considering X and P band interferograms. The X band DEM generally shows higher altitude than the P band DEM, especially over forested areas, because the considerably higher penetration of P band towards the forest floor, while X band DEM reflects the canopy altitude. X band DEM is called a Digital Surface Model (DSM), because it is related mainly with the top of the land cover. The difference between the DSM and the DEM (P band) potentially gives the forest height. The actual internal height of the forest was estimated, in the field, in transects opened in the primary and secondary forest and compared with the DSM-DEM difference. The results showed that the DSM-DEM difference tends to underestimate the forest height under secondary forest, probably due to higher volume scattering of P band emission. The DSM-DEM difference over primary forest is closely related to the average height, in the transects, standing between the global average tree height and the average height of the upper storey trees of the forest transects. [C6421]

"A comparison of radar altimetry and repeat pass interferometry as methods of producing digital terrain elevation models"

Two methods used to produce digital terrain elevation models (DTEMs) are considered: radar altimetry and repeat-pass interferometry. In the case of the radar altimetry-derived DTEM, elevation values are obtained by subtracting aircraft altimeter measurements from GPS measurements of absolute aircraft height. Discrete elevation values are interpolated to form a continuous surface. Repeat-pass interferometry with RADARSAT-1 data is used to produce the second DTEM, which has then been georeferenced by means of ground control points. The two models are compared in terms of positional accuracy of terrain features and resolution of small-scale landforms. The interferometry-derived model is of higher resolution than the altimetry-derived model; this is expected based on the method of data collection. Positional discrepancies between terrain features are also identified. These discrepancies are attributed to the incidence angle of the RADARSAT-1 satellite relative to feature orientation. Georeferencing using control points is essential to the success of producing terrain models using repeat-pass interferometry. [C6422]

"Evidence for a peculiar style of ground deformation at Vesuvius volcano revealed by 10 years of ERS mission"

We present results obtained via an innovative spaceborne SAR interferometry algorithm showing that, despite its quiescent stage, the Somma-Vesuvius volcanic complex is subject to a particular deformation process. This is characterized by a rather continuous subsidence effect, revealed by both ERS satellite data and levelling surveys, between 1992 and 2000. These deformations are mainly localized in two zones involving the Vesuvius cone and a narrow discontinuous annular area that extends around the base of the Somma edifice. A likely explanation of subsidence at both sites involves the joint effect of gravitational sliding and extensional tectonic stress occurring at the contact between different lithological units. [C6423]

"The enhancement of lidar backscattering by horizontally oriented ice crystal plates in cirrus clouds"

The backscattering of radiation at 0.532 and 1.064 μm wavelengths by quasi-horizontally oriented hexagonal ice plates is investigated. The geometric optics ray tracing method is not applicable to the scattering problem associated with oriented ice crystals (in particular, in backscattering direction) because of the singularity of the ray-tracing technique. In the present study, we solve the scattered field of quasi-horizontally oriented ice plates using an approach based on electromagnetic wave theory. The effect of side faces of a plate on the internal field inside the particle is ignored. This is a reasonable approximation under the condition that the ratio of particle diameter to its length is large or the tilt of the particle symmetric axis from the zenith is small. Preliminary results

show very strong resonant oscillations of backscattering cross section versus size parameter. The bulk backscattering intensity has been calculated by including size distribution and a random tilt of particle symmetric axis within a small angular region (2°). [C6424]

"DTM error minimization via adaptive smoothing [CLIDAR forest measurements]"

Airborne light detection and ranging (LIDAR) is emerging as a tool to provide accurate digital terrain models (DTMs) of forest areas since it can measure bare earth beneath the canopy. In an attempt to minimize the error in generating DTMs, an adaptive smoothing technique is presented. The results indicate that DTM error can be minimized through the adaptive process. [C6425]

"A monostatic solid state W-band FM-CW Doppler profiler"

The Institute for Tropospheric Research (IfT) in Leipzig, Germany, operates a number of airborne in situ probes for cloud microphysical properties, and ground based and airborne radiation measurement tools. To enhance information about clouds for radiative transfer calculation and research, IfT decided to add a cloud radar to its equipment. In the final state, this radar system will be applicable for dual purpose operation in ground based and airborne modes. This requirement defined a number of constraints concerning size, weight, and power supply. [C6426]

"Motion compensation of wideband synthetic aperture radar with a new transponder technique"

A high resolution synthetic aperture radar (SAR) system called phased array multifunctional imaging radar (PAMIR) is currently under development at FGAN. This system uses a very high bandwidth and performs a coherent integration along a large synthetic aperture. Problems in the area of calibration and motion compensation arise which can't be solved using common tools like corner reflectors. This paper describes the construction of active transponders which modulate and re-radiate radar pulses, discusses the advantages for calibration and shows how the echoes can be used for motion compensation in the SAR processing. [C6427]

"Alpine landslide periodical survey"

Potential and limitations of differential SAR interferometry for the periodical survey of Alpine displacements are investigated. For the Alpine territory, which is characterized by low vegetation, C-band differential SAR interferometry shows a relatively high coherence during the snow-free season permitting the detection and monitoring of unstable slopes on a regular basis. Limitations to the spatial coverage arise from decorrelation over forested and snow covered areas and from layover and shadowing caused by the very rugged topography. Significant results in the Swiss Alps using ERS-1/2 SAR data are used as support to our investigations. [C6428]

"Coherence loss minimization in SAR interferometric registration"

A comparative study regarding the interpolation of stochastic electromagnetic band-limited signals in synthetic aperture radar (SAR) interferometry is detailed. It is shown that the most appropriate interpolation scheme to minimize the coherence losses is the one based on the Knab Sampling Window kernel. [C6429]

"Optimum interpolation and resampling for PSC identification"

The first basic step in the permanent scatterers analysis technique is the location of the stable reflectors. For this purpose, an inter-image amplitude analysis, on a pixel-by-pixel basis, is performed, and the scatterers showing stable amplitude response are named Permanent Scatterer Candidates (PSC). The effects of the interpolation of the SLC (Single Look Complex) images are considered, with particular attention to the oversampling factor and to the interpolation kernels. Finally, experimental results are shown to confirm the PSC theory and the interpolation analysis. [C6430]

"Solid-state lasers for space-based applications"

Summary form only given. Solid-state lasers have been in use in the space program from the early stages. These lasers are discussed in the context of their missions and the architectural choices made in the architectures due to operation in the space environment. [C6431]

"An ultra-wideband radar for vehicle detection in railroad crossings"

This paper describes an ultra-wideband (UWB) radar system designed to detect motor vehicles such as cars and trucks when they are present in a railway crossing. Once fully developed, the detection performance of the

system is to be compared against a video detection system in a test at a crossing in Maywood, Illinois. If the test is successful this system may be further developed and installed at a four-quadrant gate crossing to sense vehicles trapped in the crossing island (i.e. the area bounded by the gate arms). This paper describes the problem at hand and gives details of the radar system development to date. With the current prototype, a pulse width of 3 ns has been achieved which yields adequate range resolution for this application. [C6432]

"Fusion of radiometry and textural information for SIR-C image classification"

We consider the problem of multi-channel image classification. We take into account not only the radiometric information but also some textural information. The proposed algorithm is a particular case of a fission-fusion scheme. The fission step consists of defining some textural parameters and extracting them from the different channels. The fusion between the texture channels and the original radiometric channels is performed in a second step. We consider a supervised scheme in which some training areas are given. These training areas allow us to define the class parameters and to drive the fusion process. Some results are given on SIR-C images. [C6433]

"A robust mm wave radar sensor for underground applications"

This paper outlines some of the issues that were considered during the development of a sensor for an underground range measurement application. These include a description of the working environment that drives the selection of a particular technology and some of the tradeoffs that were made to accommodate manufacturing and reliability issues. It concludes with a brief overview of the sensor and its performance. [C6434]

"Developing a remote staring sensor for optimizing successful boost phase intercept"

Interception of large missile systems during their boost phase has been a goal of the United States Defense industry for quite some time. Due to a variety of technical obstacles, however, defense scientists have focused their energy upon developing systems that are capable of intercepting the missiles in mid-course; so the boost phase interception (BPI) objective has, until recently, remained on the sidelines. Shortly following the change in Administration in January, 2001, it was announced that the Ballistic Missile Defense Organization (BMDO) would begin actively developing BPI capabilities. Although, perhaps, this change in agenda is primarily attributable to the different priorities of the respective Administrations, it may also be due in part to recent advances in remote sensing technologies. In this paper, we describe a theoretical space-based sensor that will be capable of cueing retaliatory forces in time for successful BPI. The specifications for the sensor in this theoretical system are developed using modeled missile signatures and scene data from the LANDSAT 7 sensor. [C6435]

"Testbed for development of a DSP-based signal processing subsystem for an earth-orbiting radar scatterometer"

A testbed for evaluation of general-purpose digital signal processors in earth-orbiting radar scatterometers is discussed. Because general purpose DSP represents a departure from previous radar signal processing techniques used on scatterometers, there was a need to demonstrate key elements of the system to verify feasibility for potential future scatterometer instruments. Construction of the testbed also facilitated identification of an appropriate software development environment and the skills mix necessary to perform the work. A testbed was constructed with three Astrum MCMDSPs, based on the Temic TSC 21020 general purpose DSP. Commercial data conversion hardware and high-speed serial communication hardware was interfaced to the MCMDSPs to allow demonstration of the key interfaces between subsystem elements: DSP program loading, synchronization and communication between multiple DSPs, interface to the scatterometer radio frequency subsystem, commanding, and science data delivery to the instrument data handling subsystem. A baseline set of requirements for the radar signal processing subsystem was established. From these requirements, signal processing algorithms such as digital filters and FFTs were developed using a combination of standard library functions and custom software. A software framework was developed to coordinate execution of the periodic signal acquisition and processing routines with asynchronous commanding and timekeeping functions. Emphasis was placed on developing modular software that would be applicable to a number of potential future instruments. Performance of the DSP subsystem was evaluated in terms of measured vs. theoretical execution speed, timing accuracy, power consumption, and computational accuracy. [C6436]

"Entropy optimized contrast stretch to enhance remote sensing imagery"

This paper presents a contrast stretch (CS) method based on minimum entropy constraint to enhance images obtained in remote sensing applications such as ground penetrating radar (GPR), synthetic aperture radar, and infra-red imagery. The CS enhances contrast of the low-contrast part of an image. In remote sensing, it is

usually the desirable signals that are of low contrast while interference of high contrast. The CS modifies the original image such that pixel values above and below preset boundaries are set to Zero and the maximum possible pixel value and the pixel values falling between the boundaries are stretched out to enhance the contrast of the image. Using the CS we can enhance the contrast of desirable signals from, for example, a buried landmine or an object obscured by some interference. On the other hand, the CS inevitably enhances other parts of a remote sensing images, such as clutter and measurement noise. Therefore there is a trade-off in using the CS. It is beneficial to find the correct "cut-off" boundaries in the CS in some optimal sense. We propose using minimum entropy as a criterion of looking for the optimal CS parameter Using field data from GPR application, we show that improved image can be obtained which makes further processing such as detection more accurate. [C6437]

"Relational graph labelling using learning techniques and Markov random fields"

This paper introduces an approach for handling complex labelling problems driven by local constraints. The purpose is illustrated by two applications: detection of the road network on radar satellite images, and recognition of the cortical sulci on MRI images. Features must be initially extracted from the data to build a "feature graph" with structural relations. The goal is to endow each feature with a label representing either a specific object (recognition), or a class of objects (detection). Some contextual constraints have to be respected during this labelling. They are modelled by Markovian potentials assigned to the labellings of "feature clusters". The solution of the labelling problem is the minimum of the energy defined by the sum of the local potentials. This paper develops a method for learning these local potentials using "congregation" of neural networks and supervised learning. [C6438]

"Robust detection of buildings in digital surface models"

There is growing interest in the automatic interpretation of range data acquired by airborne laser scanners. Huge volumes of data involved in land use analysis and building reconstruction applications necessitate a preliminary step to focus attention on interesting areas. We present a technique to detect and discriminate buildings and vegetation in dense digital surface models (DSM) by combining curvature based features and edge information. Our results demonstrate the effectiveness of differential geometric properties in the analysis of range data. [C6439]

"An iterative dynamic programming approach to 2-D phase unwrapping"

We propose a novel Bayesian approach to 2-D phase unwrapping. Modeled as a first-order Gaussian Markov random field, the unwrapped phase is estimated according to a maximum a posteriori (MAP) rule. The estimate is made through a form of 2-D dynamic programming, using a series of row-by-row or column-by-column 1-D dynamic programming optimizations. Increasing the number of states in the dynamic system can improve the unwrapping performance, but also increases the computational complexity. Due to this trade-off, a structured iterated conditional mode (SICM) is used to achieve good performance without examining a large number of states in each iteration. A row-by-row followed by column-by-column raster scan takes previous estimates into account through a weighting. Other raster scans are also possible. The approach can be implemented efficiently in terms of memory usage due to the recyclable memory of dynamic programming. An example of the approach with seven states is given. Experimental results are compared to other algorithms including the least-squares method, the branch-cut method and Flynn's method, using interferometric SAR data. The new SICM algorithm is seen to be superior. [C6440]

"A target detection method in range-Doppler domain from SAR echo data"

The direct evidence of radar target recognition is the backscatter energy and its distribution of objects, which is concluded by the imaging process of synthetic aperture radar (SAR) in a two-dimension image domain. Thus, the issues about automatic target recognition of SAR are often a "post-process" following SAR imaging. A method of target detection in the state of non-imaging based on analyzing the features of all kinds of targets on SAR echo data is presented in this paper, where the targets are detected in range-Doppler domain (RDD). Based on the analysis of target features in RDD, an algorithm of target detection in a RDD image is developed. The experimental results indicate the validity of the algorithm for special kinds of target detection. The algorithm is simple, able to recurrent, easy for real-time processing and hardware implementation. It can also be applied to getting target alarm with real-time SAR data for the pre-selected targets and do the imaging process selectively at the same time. [C6441]

"Technological spin-offs of the PMST program of the Italian. Space agency (ASI)"

ASI Small ("Piccole") Missions for Science and Technology (PMST) have been running full speed ahead for four

years already. The program is one of Italy's responses to the general call, by the Space Agencies, for challenging science missions that are also a good opportunity for new advancements in space technology and in the related technology transfer. Both research institutes and industries are asked to cooperate in the program. Another goal of the program is to demonstrate ASI's capability of launching a scientific/technological satellite every two years with the objective of doubling launching frequency by 2005. Currently ASI has two PMST already approved and in advanced development phases: AGILE and DAVID. The former is a γ -ray observatory, which uses innovative photon detectors developed in Italian centers; the latter a dedicated TLC program operating at very high frequencies: 80-100 GHz. A third PMST, for Earth observation science, will be selected by the end of the year, out of five preselected proposals which have been funded for Phase A study. [C6442]

"The BISSAT mission: A bistatic SAR operating in formation with COSMO/SkyMed X-band radar"

BISSAT mission has been funded by the Italian Space Agency for a competitive Phase-A study along with five other missions. Its concept consists in flying a passive SAR on board a small satellite, which observes the area illuminated by an active SAR, operating on an already existing large platform. To this end, two quite different satellites must fly in formation in order to guarantee bistatic coverage within the range of latitude 65.2°S - 66.2°N . In particular, the orbit selection for the passive satellite leads to the same orbit as for the primary radar with a difference in the ascending node right ascension and in the time of the passage on the ascending node. The main critical aim, consisting of superimposition of passive and active radar swaths, is achieved by ad-hoc steering radar antennas along the orbit. Design is critical because two existing buses, which have been developed for different purposes, are used. [C6443]

"Design and performance of the vegetation canopy Lidar (VCL) laser transmitter"

Design details of the vegetation canopy laser (VCL) for the NASA multi beam laser altimeter (MBLA) earth orbit mission are presented. The laser is a Nd:YAG Q-switched, diode side-pumped, zig-zag slab design producing 10 ns, 15 mJ pulses at 1064 nm. It employs an unstable resonator as well as a graded reflectivity output coupler with a Gaussian reflectivity profile. A cylindrical lens of undoped YAG collimates the 809 nm pump diode radiation and focuses it into a region 1.5 mm wide down the 100 mm long Nd:YAG slab. In order to conserve power, a conductively cooled design is employed. The laser is designed to operate over a range of 25°C without active thermal control. Passive cooling is achieved with a large thermal radiator panel consisting of heat-pipes and a change-of-state element. The laser is equipped with a 154 beam expander to limit the output divergence to less than $60\text{ }\mu\text{rad}$. One discussion will explain the compensation of the thermal lens created in the side-pumped slab and the different treatments of the x and y portions of the z-directed beam in order to obtain an output beam of near circular symmetry. Paraxia modeling was used along with performance data to determine the optimum location of the thermal compensating lens, and how the slab's thermal lens changed with temperature. This is due to the change in inversion density resulting from the varying overlap of the pump radiation spectral profile with the location of the Nd:YAG pump bands. Performance data as a function of temperature are given. The total number of shots to date and any change in performance as a function of shot count are presented. [C6444]

"Seed laser for space borne LIDAR applications"

A space qualified single frequency laser has been presented recently. Such oscillators will be utilized in scientific programs as well as in commercial intersatellite communication links. One particular application is to serve as a source for LIDAR measurements (global wind fields, atmospheric dynamics). We present the development and tests of the Tesat-Spacecom seeder laser unit (SLU) used in a ESA Doppler wind LIDAR project study. [C6445]

"Performance of a breadboard lidar receiver at 1570 nm for remotely sensing atmospheric CO₂ concentration"

Summary form only given. We are developing a differential absorption lidar technique to remotely measure the atmosphere CO₂ concentration from aircraft. It uses two alternating multi-kilohertz pulsed lasers, one "on-line" at a CO₂ absorption wavelength about 1570 nm and one "off-line" at a nearby wavelength. The two lasers are co-aligned and pointed at the ground. The receiver detects the ground echoes from both lasers and measure the ratio of the echo pulses energies to determine the absorption due to the CO₂ in the column along the optical path. The goal is to achieve a signal to noise ratio (SNR) of 500 to 1000 in each measurement after averaging over a few tens of seconds for detecting CO₂ concentration to a few parts per million. [C6446]

"The Europa Orbiter radar sounder: Innovative radar design for a challenging mission"

Recent observations of the surface of the Jovian moon Europa indicates the possibility of the presence of a vast ocean beneath the icy surface. Currently the NASA mission Europa Orbiter plans to place several instruments,

including a radar sounder, in a 150 km circular orbit around this moon. The science objectives of the EO Mission are: to understand the surface composition, especially compounds of interest to prebiotic chemistry; map the distribution of important constituents of the surface and characterize subsurface interfaces; and characterize the radiation environment in order to reduce the uncertainties for future missions, especially landers. To support these science objectives, the Europa Orbiter will have the following instruments: an ice-penetrating radar; a laser altimeter and an IR-visual imager. [C6447]

"Subsurface water search by TEM [Con Mars]"

This paper presents the project TESEO (TEM sounding for Geophysical Exploration) for planetary TEM (Time Electromagnetic Methods) survey, focused on the main issue of the search for water on Mars. The project aims to extend the TEM (largely and successfully employed on the Earth) to the planetary environment, where the many unknown variables (above all the background EM noise and the subsoil composition), together with the limited resources availability (mission constraints in mass, time and power) pose a formidable obstacle to performing operations and measurements. In such a context, we first investigated the opportunity for a TEM system to be housed as a payload in a future mission with special attention given to those ones deploying a network of carrier (landers, rovers, robots). Secondly, we evaluated the sounding capability of a TEM for a simple case study verifying the role played by the system and survey parameters. [C6448]

"Mapping the world in 3-D"

Summary form only given. Remember when the world was flat? Not any more. In February, 2000 NASA, using six astronauts aboard the Space Shuttle Endeavor, spent 11 days gathering data for the first complete three-dimensional global map of the planet as part of the Shuttle Radar Topography Mission. The 12 terabytes they collected will revolutionize knowledge of the Earth, and have applications in fields as disparate as geologic mapping and petroleum exploration, flight training and navigation, siting cell phone transmitters, water drainage modeling and disaster planning. The author describes how it was done!. [C6449]

"The wide swath ocean altimeter: radar interferometry for global ocean mapping with centimetric accuracy"

The recent Shuttle Radar Topography Mission (SRTM) has demonstrated the capability for global interferometric topographic mapping with meter level accuracy and 30 meter spatial resolution. The next challenge in radar interferometry is the measurement of ocean topography: the global characterization of ocean mesoscale eddies requires global coverage every 10 days, with centimetric height accuracy, and a spatial resolution of 10-20 km. We have developed an instrument concept that combines a conventional nadir altimeter with a radar interferometer to meet the above requirements. In this paper, we describe the overall mission concept and the interferometric radar design. We also describe several new technology developments that facilitate the inclusion of this instrument on a small, inexpensive spacecraft bus. These include ultralight, deployable reflectarray antennas for the radar interferometer; a novel five frequency feed horn for the radiometer and altimeter; a lightweight, low power integrated three frequency radiometer; and a field programmable gate array-based onboard data processor. Finally, we discuss recent algorithm developments for the onboard data processing, and present the expected instrument performance improvements over previously reported results. [C6450]

"Ku-band receiver and transmitter for breadboard DSP scatterometer"

The design and test results for the Radio Frequency (RF) portion of a breadboard polarimetric scatterometer operating at 13.402 GHz are presented. An integrated breadboard has been developed at the Jet Propulsion Laboratory (JPL) to evaluate the feasibility of a programmable Digital Signal Processing (DSP) approach for a follow-on scatterometer similar to SeaWinds (scheduled for launch in winter 2002). Early breadboards of an integrated system have been identified as valuable assets in developing effective subsystem requirements for the eventual flight instrument. Many compatibility and partitioning issues between the RF and DSP hardware are addressed with empirical results derived from the aforementioned breadboard. The RF portion of the breadboard consists of a dual channel receiver, heterodyning the received signal of 13.402 GHz down to an IF of 37 MHz prior to the analog to digital conversion, and a single channel transmitter, that converts the I/Q baseband transmit waveform up to Ku band. The breadboard makes provision for emulating capabilities such as programmable attenuators, loop-back calibration, and saturation effects in an actual instrument's power amplifier. It also provides control interfaces to allow early verification of software control algorithms. [C6451]

"Identification of cloud ice crystals using a 95 GHz polarimetric radar"

The identification of various ice crystal types within a cloud, as well as the estimation of their ice water content

are important goals with applications to cloud microphysical studies and to understanding the effect of clouds on the Earth's radiation budget. Millimetre wave polarimetric radars have the potential for accomplishing both of these goals. There are several millimetre wave radars operating at 95 GHz for the remote sensing of ice clouds from ground-based and airborne platforms. This paper brings together observations from experiments and modeling studies, and focuses on 95 GHz polarimetric radar signatures of ice crystals including pristine crystals such as columns, plates, and stellar crystals, as well as dendrites, ice crystal aggregates, and graupel. Results from simulations and from experimental data for several polarimetric radar observables are combined to generate different ranges of values for each observable corresponding to different crystal types. A simple fuzzy logic classification scheme is presented for identifying crystal types based on these ranges. Suggestions for further development and refinement of this scheme are given. [C6452]

"Detection and imaging of small buried 3D non-metallic objects with multistatic phase-based GPR signatures"

In this paper the bistatic and monostatic phase-based ground-penetrating radar (GPR) technique for ingenious detection of poor-contrast scattering objects hidden just beneath the air-ground interface is discussed. This technique neither requires a priori knowledge about the background medium nor needs any pure background measurement. It was developed to deal with one of the worst-case scenarios in terms of landmine detection. The method was tested with the data measured from the L-band and S-band stepped-frequency continuous-wave GPR over the compound soil where small non-metallic mines are shallowly buried. The results demonstrate that it is feasible to detect small buried poor-contrast objects by using coherent phase processing and imaging. [C6453]

"Integration of high resolution optical satellite imagery and geophysical survey for archaeological prospection in Hierapolis (Turkey)"

An in-depth analysis of the site of Hierapolis (Turkey) has been carried out using high resolution remotely sensed imagery integrated with geophysical survey and direct field data in order to detect evidence of archaeological features and environmental setting. High resolution panchromatic and multispectral images acquired by different satellites were used in this study. These images, acquired also in stereoscopic configuration, were digitally processed and visually interpreted. Geophysical data were collected in some areas of interest using different surveying methodologies (electric, radar). Besides the important scientific implications, the integration of remote sensing and geophysics in archaeology provided a useful tool for the optimization of landscape and cultural heritage management. All data collected were integrated in a Geographic Information System (GIS) to produce comprehensive maps of the site depicting archaeological and environmental features. [C6454]

"Refining electromagnetic bias estimation [Csea surface height measurement]"

Sea surface height measurements using remote sensing instruments have become increasingly accurate as satellite altimetry technology has matured. Early satellite missions had altimetry errors on the order of tens of centimetres. As these errors have been eliminated, the electromagnetic (EM) bias has become increasingly significant. The latest satellite missions, TOPEX/Poseidon and Jason-1, have EM bias error budgets of 4.2 cm and 2.5 cm, respectively. The purpose of our research has been to investigate methods to reduce the EM bias estimation errors to the sub-cm level. Most current EM bias models create estimates from geophysical properties that can be measured remotely. Typically these parameters are wind speed and significant wave height. The current operational model for the TOPEX/Poseidon and Jason-1 satellite missions is of this type. The operational model uses nonparametric methods to improve the accuracy of the estimates. In addition to improving the bias estimates, the latest operational model has shown a stronger agreement between satellite and tower EM bias models. Combining nonparametric techniques with the wind speed and significant wave height has created the most accurate empirical models to date. However, the amount of variance in the bias requires new methods to improve bias estimates. We made a preliminary study based on the angular dependence of the EM bias. Theoretical scattering models indicate that the bias is dependent on incidence angle, which may allow improved operational correction of the bias using a wide-swath altimeter. [C6455]

"Wind field retrieval from SAR images using the continuous wavelet transform"

Describes the results of a method, based on the two dimensional wavelet technique, to retrieve the wind field from synthetic aperture radar (SAR) images without any external information about the wind direction. This method works well when backscatter structures formed by wind rolls are shown by SAR images. An ERS-2 SAR image has been analysed with this technique. The result has been compared with the ADEOS-1 NSCAT scatterometer wind field obtained in the same area 15 minutes after the ERS-2 passage. The SAR and NSCAT wind fields are very consistent in direction (mean difference is 15°), but the NSCAT wind velocities are higher

than the SAR ones by 3.5 m s⁻¹. [C6456]

"Evidence of a threshold wind speed in tower-mounted scatterometer data"

The normalized radar backscatter (σ_0) in scatterometer measurements over water is theorized to go to zero below a threshold wind speed due to insufficient friction between the wind and water to create capillary waves from which the radar signal scatters. Evidence of the threshold wind speed and a hysteresis effect have been observed in airship and wave tank data. There is additional evidence for a threshold wind speed in tower-mounted scatterometer data in an uncontrolled marine environment. In situ wind measurements and corresponding σ_0 values obtained from YSCAT, an ultra-wideband scatterometer deployed on the Canada Centre for Inland Waters research tower at Lake Ontario, are used to detect and estimate the threshold wind speed. There is evidence for a detectable threshold in approximately half of the observations. The observed threshold wind speeds correspond well to theoretical threshold wind speeds. [C6457]

"Variations in the convective rain fraction observed by the Tropical Rainfall Measuring Mission (TRMM) Precipitation Radar (PR)"

Using a data clustering method, monthly statistics are calculated from rain rate estimates of the TRMM Precipitation Radar. The statistics show how the following variables change with the size of a rain event: convective rain rate, total rain rate, and convective rain fraction. On average, the convective rain fraction is found to be greatest for small mesoscale events covering 103 km², while rain rate increases monotonically with the size of the rain event. [C6458]

"Cirrus spectral optical depths retrieved from solar transmittance measurements"

Current multi-channel solar radiometers now allow for near-simultaneous collection of transmitted solar radiation in multiple spectral bands. Such simultaneous measurements are necessary for understanding the spectral nature of highly temporal phenomena such as cirrus clouds. Measurements of spectral optical depth from several locations in the desert southwest have been made by the University of Arizona for more than 10 years under both clear and cloudy conditions. Studies of the data collected under cirrus conditions indicate, as expected, that the transmittance through cirrus is nearly spectrally flat over a range of optical thicknesses. A recent data set collected at Ivanpah Playa, Nevada included measurements through a layer of cirrus clouds of varying thickness for a period of nearly three hours. These data were preceded by a two hour period of cloudless conditions with relatively stable atmospheric aerosol loading. Results from this data set indicate that the cirrus optical depth is spectrally flat to better than 6% over a range of optical depths from 0.10 to 0.30. Because of the spectrally flat nature of the cloud radiative properties, it is possible to use these clouds as hand-to-hand radiometric calibration targets for multichannel radiometers and two-channel lidar systems. The possible accuracy of such calibrations is presented based on the historical measurements of cirrus cloud transmittance. [C6459]

"Relationships between rainfall rate, attenuation, and reflectivity at 14 and 35 GHz frequencies"

The specific attenuation and reflectivity factors are simulated at 14, and 35 GHz frequencies from disdrometer measured raindrop spectra. Scatter plots showing their relationships with the simulated rainfall rates are presented. Power fits to these relationships are also presented for drop size distributions measured at three different geographical locations around the world. [C6460]

"SAR observations of dryland moisture-towards monitoring outbreak areas of the Brown Locust in South Africa"

RadarSat and ERS-2 images acquired over a Brown Locust breeding site in Southern Africa were analysed with a view to estimating soil moisture levels, which are important for determining locust egg development. Predictions from the IEM model using data from field measurements were compared with the backscatter responses from the satellites. The results confirm the potential of SAR imagery in pest management applications. [C6461]

"The use of ERS2 SAR for assessment of changes in dry herbaceous biomass"

Changes and spatial pattern of dry herbaceous biomass was monitored using backscatter coefficients in a time series of ERS-2 SAR images of the semi-arid savanna in Senegal, West Africa. The results were compared to in situ measurements of dry biomass. It has been demonstrated, that the overall spatial and temporal change in SAR backscatter correspond to the changes in biomass, however, the quantitative relation remains to be established. [C6462]

"An analytical and numerical framework for interpretation of SAR images of urban areas"

Electromagnetic modeling and its use in SAR raw signal simulation constitute powerful instruments for the interpretation of SAR images. As far as the urban environment is concerned, the need of such instruments is higher, for the complexity of the mechanisms that contributes to the formation of the scattered field. We present an analytical model for the scattering from typical elements of the urban environment. The obtained closed form solution is then employed in a SAR raw signal simulator. Simulated images well match with the expected characteristics. [C6463]

"Monitoring of new-ice in Greenland waters"

In the sea ice covered waters of Greenland the active polarisation ratio (APR) of QuikSCAT SeaWinds Ku-band (13 GHz) scatterometer measurements and the passive polarisation ratio (PPR) of DMSP-SSM/I 19 GHz radiometer measurements are used in combination to classify new-ice and older ice from 1999 to 2001. In particular, the two regions where new-ice is covering large areas: (1) Baffin Bay (64°W, 72°N) during the yearly freeze-up in autumn, and (2) the formation of the 'Odden' in the Greenland Sea (8°W, 75°N) in late winter, were used in the study. The results of the surface cover classification in the Greenland Sea and in Baffin Bay were validated against 19 Radarsat ScanSAR wide scenes from the same period. In our study new-ice is defined according to its backscatter and radiative properties and our results show that the transformation to older ice usually occurs within one week. Further, the formation of new-ice and its transformation to older ice or the destruction of an ice cover occur on a daily time scale. The detection of new-ice using the above method is consistent with Radarsat data for areas >50 km both in Baffin Bay and the Greenland Sea. Furthermore, it was found that large areas are covered by new-ice during the freeze up of the Baffin Bay in October and November. In the Greenland Sea the new-ice appears in March as an ice peninsula appended to the belt of older ice drifting along the east coast of Greenland. These results have been confirmed by Radarsat observations. However the algorithm was found to mis-classify the surface cover in the following cases: (1) open water into sea ice at high surface wind speeds (>15 m/s), and (2) regions of grease ice into open water or other ice types. [C6464]

"Using cross-entropy for polarimetric SAR image classification"

In this paper, the concept of cross-entropy is introduced for measuring the difference between two scatterers in polarimetric SAR image classification. The difference between two scatterers is composed of three parts, i.e., the difference of average scattering mechanism, the difference of scattering randomness and the difference of the two spans of scattering matrices. The minimum cross-entropy principle is adopted to make the classification decision. The capability of this method is demonstrated by the experimental results. [C6465]

"Exploiting the polarimetric information for the detection of ship targets in non-homogeneous SAR images"

Ship detection in polarimetric SAR images of non-homogeneous sea areas is considered. We demonstrate the impact of non-homogeneous sea features on the false alarm rate and the need of extracting the image structure. We thus introduce polarimetric segmentation procedures that cooperate with high-resolution polarimetric detection features for the control of the false alarms. Different polarimetric segmentation-plus-detection procedures are tested over real data to devise the appropriate method to exploit the polarimetric information. [C6466]

"Sea ice classification using multi-frequency polarimetric SAR data"

This paper discusses the capability of the complex Wishart classifier for sea ice and classification using multifrequency, fully polarimetric SAR data. C-, L-, and P-band data acquired by the JPL AIRSAR in the Beaufort Sea was used. Classification using the unsupervised Wishart classifier is a two-stage process. An initial classification is required to seed the algorithm and can be derived using other classification methods. The Wishart classifier then used in iterations where the class means are updated after every step. The convergence of this approach is investigated. The Wishart classifier was found to be extremely dominant so that the classification result after a few iterations depends not necessarily on the initial classification used to derive the first class means. Even an initial classification derived with a random number generator leads to a good result after a few iterations. [C6467]

"The principles of positioning with space-borne SAR images"

The researchers of surveying and mapping have paid much attention to SAR radar because of its capabilities of observing the Earth by all weather and all-time. With the development of science and technology, especially with the improvement of SAR resolution and orbital positioning accuracy, the application of SAR to surveying and

mapping field has been broadened. The principles and methods proposed in this paper are aimed to realizing (a) mapping with single SAR image; (b) generating SAR orthophotomap; and (c) mapping with SAR stereo-image provided that orbital parameters are already known in the digital photogrammetric system. Finally the principles have been successfully applied to automatic generation of DEM through image matching by using ERS-1 and RADARSAT1 images to construct image pairs. [C6468]

"Land use classification of SIR-C imagery based on a published database of multi-polarization backscattering"

Land use classification of polarimetric SAR imagery is carried out by referring not to training area data within the image but to a published database consisting of independently measured backscattering data. The results are reasonable when the appropriate radar parameters are chosen in the measurement. [C6469]

"Nonparametric classification of SAR data based on a modified iterated nearest-mean reclustering of pixel features"

This work describes a nonparametric algorithm suitable for scene classification, either supervised or not, starting from a number of pixel features derived from SAR observations. Pixel vectors composed by simple features derived from the backscatter coefficients of one or more bands and/or polarizations are iteratively clustered into dynamically upgraded classes. Possible "a priori" knowledge coming from ground truth data may be used to initialize the procedure, but is not mandatory. Experiments on MAC-91 NASA/JPL AIRSAR data on the Montespertoli test site show that seven features derived from each of L-HV and P-HV observations are capable to discriminate seven agricultural cover classes with an overall pixel accuracy of 60%, when the algorithm learns from 10% of the truth data and classifies the remaining 90%. [C6470]

"Two ice concentration algorithms benefitting from 85 GHz Special Sensor Microwave/Imager data: a comparison"

Sea ice concentration maps retrieved from spaceborne passive microwave sensor data such as from the Special Sensor Microwave Imager (SSM/I) often suffer from the coarse spatial resolution compared to synthetic aperture radar (SAR) data. However, SAR images are still difficult to interpret and therefore there is a need to improve the spatial resolution of the above-mentioned sea ice concentration maps. Under certain circumstances this can be achieved using 85 GHz SSM/I data together with the SEALION and the ASI sea ice algorithms. [C6471]

"Microwave sensing implied sea ice distribution in the Weddell Sea, Antarctica"

We investigated the distributions of sea ice using various microwave remote sensing techniques in the part of Drake passage, Antarctica, between the area 45-75°W and 55-66°S. We used TOPEX/Poseidon (T/P) radar altimeter, ERS-1 altimeter, ERS-2 scatterometer, Nimbus-7 Scanning Multichannel Microwave Radiometer (SMMR), and DMSP Special Sensor Microwave/Imager (SSM/I) data. The sea ice distributions were estimated between May and June 1995 and October and November 1998. The two altimeter measurements (T/P and ERS-1) showed good coherence with the results from the radiometer data in the given period when the ice concentration of 20% and greater was selected. The scatterometer data also showed good correlation with the altimetry-implied sea ice surface. The maximum and minimum values of sea ice distribution appeared in August and February, respectively. In general, the sea ice distributions estimated from radar altimeter, radiometer, and scatterometer are well correlated. [C6472]

"Radarsat Lagrangian flow effects on oil spill spreading"

This paper presents work done utilizing Radarsat fine mode data to model the Lagrangian effects on oil spill trajectory model. The input for the model is current field derived from a 2 D hydrodynamic model. The correlation statistical model was applied to modulate the Radarsat water movements with current field by applying Doppler frequency shift model. The study shows that current movements are the main effect on oil spill spreading compared to wind speed and direction. Verification of simulation results with those of tidal current model shows a good agreement in the direction of the oil spill movements. In conclusion, Radarsat data has good potential for oil spills detection and mapping. Radarsat data could be used to model the Lagrangian effects on oil spill trajectory model. The main effect on the oil spill movements in Malacca Straits is the tidal current flow. [C6473]

"Ocean wind fields retrieved from radar-image sequences"

An algorithm is presented for retrieving wind vectors from radar-image sequences acquired by a standard nautical radar near at near grazing incidence. The radar operates at X-band (9.5 GHz) with horizontal and vertical polarization in transmit and receive. The algorithm consists of two parts, one for wind direction and

another for wind speed retrieval. Wind directions are locally extracted from wind induced streaks, which are approximately in line with the mean wind direction. The algorithm assumes wind direction as normal to the gradient of the amplitude image, which is approximated by finite differences over an appropriate length. The resulting wind direction is taken as normal to the retrieved local gradients. Wind speeds are derived from the radar cross section, by parameterization of its dependency on the wind vector using a neural network. The algorithm was tested and validated using data from a radar mounted in the North Sea. The applicability of nautical radars for wind retrieval is shown for both tower based and ship borne (moving) instruments. [C6474]

"A study of surface winds in tropical storms using modified near real-time processing of QuikSCAT measurements"

Performance of the NOAA/NESDIS near realtime QuikSCAT wind retrieval algorithm was assessed in the case of tropical cyclone IRIS, that occurred in Northern Atlantic, in October 2001. For this storm, the estimated wind field failed to produce a circular structure characteristic of tropical cyclones. We established that the Aviation Forecasting Field that was used to initialize ambiguity removal process was the primary cause of error, since it completely missed this feature. We proposed an initialization process that uses the information available from backscatter data to estimate possible regions of tropical cyclones. The proposed procedure allows estimation of wind fields that are less influenced by an external field. However, in the case of tropical storm IRIS the wind retrieval algorithm failed to generate solutions that would allow ambiguity removal to close circulation even when clustered errors in the initial field were broken by the new initialization procedure. [C6475]

"Nowcast of surface currents from blending HF radar: inverse model, application to Monterey Bay"

We formulate an approach to reconstruct surface circulation from a high-frequency (HF) radar data in open boundary areas. The approach uses flow decomposition through two scalar potentials, the self-consistent open boundary conditions, the cost function (penalty) for the validation of free model input and selective filter. The nowcast skill is enhanced through an ensemble averaging technique. The current nowcast in Monterey Bay was realized through the approach for August 1994. We demonstrate it has weak sensitivity to level of noise in the observations. The nowcast gives better understanding of inshore circulation, eddy activities and upwelling processes. [C6476]

"Ocean current estimation using ScanSAR data"

It is possible to estimate the radial velocity of a target by comparing the Doppler centroid, as estimated from the return from the target, with a "reference" Doppler centroid. Of particular interest is the estimation of one component of an ocean current, where the target is an area of ocean a few square kilometres in extent. Studies using single beam SAR products have shown this technique to be effective in estimating the location of the Gulf Stream and the Loop Current in the Gulf of Mexico, but the size of these features means that a swath width of greater than 100 km would be desirable. This immediately suggests working with ScanSAR data, where a wider swath is formed by combining several beams. However, adapting the technique to such data presents a number of difficulties. The spectral information needed for Doppler estimation is not available from standard products, thus custom processing of raw data is necessary. For each beam we have burst mode rather than continuous data, which complicates the spectral shape of the target return but this problem can be avoided by the appropriate choice of azimuth patch size. Combining estimates from several beams involves problems with independent errors and beam edge corruption. The "reference" Doppler centroid must be estimated over a large range and azimuth extent. This estimation is accomplished by fitting a quasi-physical model, involving orbital information, satellite attitude and information about the satellite antenna. The fitting problem is examined, with specific reference to RADARSAT and ENVISAT. Examples of ocean current estimation using RADARSAT ScanSAR data are shown. [C6477]

"Capability of Radarsat-1 for estimation of ocean surface current on the Scotian Shelf"

Doppler shifts in space-based synthetic aperture radar (SAR) data are due to movement of objects in the image area. These frequency shifts are most obvious in fast moving point targets such as ships. However, an area target such as the sea surface can also cause a measurable Doppler shift from which ocean surface currents can be estimated. We compare surface currents derived from three standard mode Radarsat-1 scenes over the Scotian Shelf to in situ currents measured with 21 self-locating datum marker buoys (SLDMBs). The SLDMBs drift with the local surface current, and their locations, obtained every 30 minutes via Argos satellite, are used to calculate the current. Three Radarsat-1 scenes were processed by Atlantis Scientific of Ottawa, Canada, to obtain the component of the surface current vector perpendicular to the path of the satellite. The results show that the noise in the derived Doppler shift was comparable to the Doppler shift expected from the relatively low surface currents prevalent on the Scotian Shelf. While it was concluded that present space-based SAR

technology cannot provide accurate surface current data for Scotian Shelf conditions, the methodology and results provide a useful metric by which future SAR systems can be evaluated. [C6478]

"Mars meter-scale roughness: Goldstone Solar System Radar delay-Doppler database"

The entire fourteen-year database of Goldstone Solar System Radar Mars near-nadir radar scattering model fits is being revised using the latest topography from the Mars Global Surveyor Mars Orbiter Laser Altimeter instrument. The improved radar dataset will better serve the Mars exploration community for landing site selection and characterization. [C6479]

"Sea ice microstructural characteristics in the Barents Sea in autumn: relevance to microwave remote sensing"

The microstructural characteristics of sea ice during autumn freeze-up in the Barents Sea were measured during a microwave remote sensing validation campaign aboard the US Coast Guard icebreaker Healy during October-November 2001. Ice samples were obtained from 16 ice floes and digital images of the thin and thick sections were taken to examine the characteristics of the brine and void structure. Due to the dynamic nature of the marginal ice zone, brine structure in first-year or thin ice was highly variable. Although brine pockets were typically elongated and tube-like, they could either be randomly oriented or aligned vertically, and may form either well-connected network or relatively isolated pockets. Some samples contained a significant fraction of air bubbles. Multi-year ice was typically very porous. Void diameters ranged from less than 0.1 mm to several centimeters and were often nonspherical. Of particular importance for microwave scattering, the larger voids may have contained either brine or air, depending on the fluid permeability of individual cores. A wide range of void fractions were observed in the upper, salt-free layers of the ice, which could account in part for the range of backscatter values observed for multi-year ice. [C6480]

"Venus radar for subsurface and ionosphere sounding (VENSIS)"

As a subsurface sounder, VENSIS would obtain fundamentally different kinds of geologic information than Magellan. Mapping of interfaces of geologic units (e.g. tessera, plains, lava flows, impact debris) could be extended into the third dimension. Reflectivity variations recorded at the surface by Magellan are likely to extend into subsurface, providing dielectric contrast at interfaces. The VENSIS sounder would also show detailed characterization of the Venus ionosphere using active sounding in a frequency range of 100 kHz to 6.5 MHz. In a passive mode, VENSIS can be used to detect lightning the presence of which remains both controversial and critical to understanding the behavior of the atmosphere and the possibility of present day volcanism. In this paper the Scientific Objectives are described and the system performance is analyzed. [C6481]

"A parametric scheme for ocean wave spectra retrieval from complex SAR data using prior information"

A parametric inversion scheme for the retrieval of two dimensional ocean wave spectra from look cross spectra (LCS) acquired by spaceborne synthetic aperture radar (SAR) is presented. The scheme takes information about the spectral shape of different wave systems from a prior wave spectrum, while estimates for wavelength, waveheight and wave propagation direction are extracted from SAR cross spectra. The Partition Rescaling and Shift Algorithm (PARSA) is based on a partitioning of a prior wave spectrum, e.g. taken from ocean wave models. For each ocean wave system a stochastic model is set up, which defines the probability that the propagation direction, the wavelength or the energy of the different wave systems deviate from the prior knowledge. The prescribed probabilities thereby quantify the confidence into the prior wave spectrum. Based on the probability models for the prior wave spectrum and the measured cross spectrum an optimal ocean wave spectrum is estimated using a maximum a posteriori approach. To solve the corresponding minimization problem the prior model is approximated with a multivariate Gaussian model. The optimization problem is solved with a Gauss-Newton method. The scheme is tested using both simulated cross spectra and reprocessed wave mode data acquired by the ERS-2 SAR. The reprocessed data are similar to the products, which will be available from the ENVISAT satellite launched in March 2002. [C6482]

"Mars high resolution Shallow Radar (SHARAD) for the MRO 2005 mission"

The search for water is a primary focus of Mars exploration. At the surface of Mars, water is present as ice in the polar ice caps and in trace quantities in the atmosphere. To detect liquid water on Mars today probably requires searching below the surface. As noted in the MRO SDT Report, the unambiguous detection of liquid water in the upper crust of Mars and the profiling of ice in the subsurface, particularly within one kilometer of the surface, would be major discoveries in the exploration of Mars. To that end, the MRO SDT recommended that

flight of a subsurface sounding radar be considered for MRO, if the radar could confidently detect liquid water and profile ice in the topmost 1 km of subsurface with approximately 10 m in vertical resolution. In response to this recommendation a team of Italian researchers, sponsored by the Italian Space Agency (ASI), has proposed a Shallow Radar sounder (SHARAD). In this paper the main features of the SHARAD (to be complementary to MARSIS) in terms of the expected penetration performance according to proposed models of the martian crust composition and surface scattering are described. [C6483]

"Forest parameter retrieval with JPL Airsar P-, L- and C-band data: a plot level analysis for slash pine stands in Georgia"

During an EOAP-SAR project, Airsar P-, L- and C-Band data were used to test the capability of SAR to predict biometric parameters which are frequently used by timber managers as inputs to growth, harvest and yield models. The test site was a commercially managed area in Jesup, south-east Georgia, with stands owned by The Timber Company (TTC). Field campaigns provided an extensive plot-level georeferenced ground data set of four slash pine stands which was used to determine the correlation with the Airsar data. Additionally, 18 stands were surveyed and stand level summaries of biometric variables height, basal area, and volume were obtained. A statistical model was used to test all possible scenarios of polarimetric and frequency combinations. The best models were chosen to develop inversion models for basal area. These model results were applied to stands which are owned by a different timber company (Rayonier), and which were located in the Airsar strip. Within the TTC land holdings, R² correlation coefficients for volume prediction from SAR were 0.85. The correlation between predicted basal area and stand age on 65 Rayonier stands resulted in the an adjusted R² of 0.86. [C6484]

"Regrowth biomass estimation in the amazon using JERS-1/RADARSAT SAR composites"

Synthetic Aperture Radar (SAR) is known to have a response that is directly related to the amount of living material that it interacts with. It is this property that our research seeks to exploit in order to better understand carbon dynamics in the Amazon. The vegetation density causes the radar response to saturate such that vegetation that is more dense than some threshold is indistinguishable from each other. However, the areas of regrowth are likely to have a low enough biomass during the first 10 years of regrowth to be accurately assessed using radar. Our efforts involve obtaining appropriate pairs of radar images at L and C bands from different sites and for both seasons. These data are then orthorectified to allow accurate calibration and incidence angle correction. The seasonality of the data is used to deal with the moisture sensitivity of the data, and the different frequency data is used to help classify the data into several classes for use in class-specific biomass estimates. We have chosen 2 sites in Brazil for our study. we use the JERS-1 (L-band) and RADARSAT (C-band) data to create a 2-channel composite. These data are then classified into the following classes: flat area (water, bare soil), short vegetation, regrowth, and trees. We report on the accuracy of both our classification and biomass estimation efforts. [C6485]

"Assessment of operational radar satellite for monitoring land cover change in Amazonia"

The objective of this paper is to verify the viability of using existing radar satellite (ERS and RADARSAT), as an operational tool for monitoring land cover in Amazonia. It is well known that C band radar data are not adequate for land applications, but as cloud cover in Amazonia is a constant problem, particularly in certain areas, radar data can help, as complimentary information, for change monitoring. In this paper ERS and RADARSAT images are classified using texture measures, in several classes of land use, and then the adequacy of using these classes for change detection is analyzed. Progressive sequential feature selection, using the Kappa coefficient of agreement as a selection criterion, chooses a subset of the texture layers that maximizes that coefficient. It was observed that even for the best feature set, the Kappa coefficient was considered too low and unsuitable to be used for change detection. However, it is shown that this coefficient progressively increases when classes are merged sequentially. When only two classes are considered, identified as forest/non-forest, the overall accuracy is higher than 85%, which was considered adequate for change detection. The classifications of the 1992, 1993 and 1996 ERS1/2 images over the Tapajor's National Forest, Brazil, were performed using the iterative contextual mode (ICM) classifier. Deforestation was detected for those points changing from forest in one year to non-forest in other year, with very good agreement with the results obtained with optical imagery sequence. Similar results were obtained using RADARSAT imagery for the year 1996. [C6486]

"Application of the damage detection method using SAR intensity images to recent earthquakes"

One of the remarkable characteristics of synthetic aperture radar (SAR) is to record physical value called the backscattering coefficient of the Earth's surface not depending on weather conditions and Sun illumination. Therefore, SAR could be a powerful tool and be used to develop a universal method for grasping damaged

areas by disasters such as earthquakes, forest fires and floods. Detailed ground truth data for building damage due to the 1995 Kobe earthquake provided us the opportunity to investigate the relationship between the backscattering property from SAR images and the degree of damage. From the above analysis we have already developed a method to detect areas of building damage. In this paper, we applied this method to the images taken over the area hit by the 1999 Kocaeli, Turkey and the 2001 Gujarat, India earthquakes, and then the accuracy of the proposed method was examined by comparing the results of the analyses with those from the damage surveys. [C6487]

"Urban damage detection using decorrelation of SAR interferometric data"

We investigate decreasing interferometric correlation of SAR data caused by building damages in urban area. We analyze JERS-1 SAR data pairs straddling the occurrence of the 1995 Hyogoken-nanbu earthquake. The distribution patterns of the pixels which indicated interferometric decorrelation correspond well with the building damaged area reported by the ground survey. The degree of decorrelation shows obvious correlation with the damaged building ratio on the area in each block and measured seismic intensity from strong motion data. The result of this study indicates a fact that the building damage causes the interferometric decorrelation. We also try to extract the urban area damaged by the 2001 Gujrat (western India) earthquake using Radarsat data. For practical use of interferometric decorrelation to detect the urban damage, effect of building type and urban concentration should be examined. These results show the applicability for interferometric analysis of SAR data to urban disaster management. [C6488]

"Greenland snowmelt estimation using multi-spectral passive and active microwave observations"

Principal component analysis (PCA) has previously been used to characterize snowmelt on the Greenland ice sheet using all seven SSM/I channels. Three extensions to this algorithm are presented in this work. First, a location dependent thresholding technique is developed that facilitates improved sensitivity in snowmelt detection as compared to prior studies. Second, an adapted PCA algorithm is formulated that is able to link key physical processes with vectors in the SSM/I data eigenspace. Finally, the inclusion of active scatterometer data in the PCA implementation is shown to offer additional information that assists in snowmelt estimation. [C6489]

"Integrating active and passive satellite-based technologies to improve European fisheries monitoring and control"

The European Commission Joint Research Centre's studies so far have shown that ScanSAR Narrow imagery can be used for fisheries control as it combines large coverage of fishing grounds and resolution sufficient to distinguish vessels subject to the VMS (Vessel Monitoring System). Studies were performed in typical fishing grounds such as Flemish Cap, the North Sea etc. [C6490]

"Interferometry SAR in Antarctic Grove Mountains"

Grove Mountains locates to the southwest of Princess Elizabeth Land, inland areas of east Antarctica. Field Work in Grove Mountains is very difficult. Interferometric SAR is a powerful tool in DEM generation, vertical change detection and determining the velocities and directions of ice streams. After the field GPS/RTK surveying work in Grove Mountains during the 1999/2000 summer season, we got the topographical map. Further research about Grove Mountains is ongoing. With the tandem radar image of ERS-1/2 in 1996.2, we generated DEM of this region. [C6491]

"Utility of SARs for mapping forest disturbance in Siberia"

Radar backscatter data from multiple SAR satellites were acquired and analyzed for two sites subject to the forest disturbances in Western Siberia, Russia. The backscatter from disturbed and non-disturbed sites were analyzed and the individual and combined capabilities of ERS, JERS, and Radarsat evaluated. JERS was the single most useful radar for this analysis. The combination of radars improved the results. [C6492]

"Forest stem volume estimation using high-resolution lidar and SAR data"

Presents a comparison of remote sensing of forests using two complementary, high-resolution sensors; namely the TopEye lidar and CARABAS VHF SAR systems. The lidar data are from a small footprint configuration, allowing discrimination between pulses reflected from the tree crowns, and those penetrating through gaps in the canopy. From these data, measurements of tree height and crown size can be made for individual trees, and the tree volume calculated through empirical relationships. The CARABAS VHF SAR provides a more direct measurement of tree volume, since the long wavelengths penetrate the forest canopy and are scattered by the trunk-ground dihedral. Results of stem volume retrieval for individual trees using data from the two systems are

presented, and the possibility of using the complementary measurements discussed. [C6493]

"Direct estimation of vegetation parameters from covariance data in polarimetric SAR interferometry"

Polarimetric SAR interferometry (POLINSAR) is an emerging technique for the characterization of volumetric scattering processes. Each pixel of a POLINSAR interferogram is a 646 matrix of complex sample covariances among the polarimetric channels in the image pair. A model of polarimetric scattering from vegetation specifies the expected covariance matrix as a function of the vegetation parameters. The data matrix obeys a complex Wishart probability distribution that depends on the expected covariance. Using this, one can find the maximum-likelihood estimate of the parameters from the data matrix. This paper presents the formula for the expected covariance matrix, as predicted by the model of Treuhaft and Siqueira for a random canopy over flat ground. An algorithm for computing the maximum-likelihood parameter estimate is derived. We test the algorithm on simulated data and compare its results to estimates derived from coherence samples. We conclude by discussing the extension of the direct estimation technique to more general POLINSAR scattering models. [C6494]

"Estimation of boreal forest biomass from multi-temporal INSAR data by inverting an empirical backscattering-coherence model"

The applicability of INSAR coherence observations for stem volume (biomass) retrieval is investigated by applying coherence data from 14 ERS-1 and ERS-2 C-band SAR image pairs. A novel technique for stem volume retrieval is developed based on the inversion of a non-linear empirical forest coherence model. The seasonal behavior of interferometric coherence, the accuracy of coherence modeling as well as the performance of stem volume retrieval is tested. The data set enables the study of stem volume retrieval performance under varying conditions and as a function of the number of images. The results indicate that the applicability of winter images with snow-covered terrain is superior to that of images obtained under summer conditions. The highest correlation coefficient between the estimated stem volume and the ground truth stem volume shows values as high as $r=0.89$ (obtained with two optimum images using separate training and testing data sets) and a percentage RMSE level of 48%. [C6495]

"Forest biomass retrieval using L-band polarimetric measurements"

Airborne L-band fully polarimetric SAR measurements over a boreal forest were analysed as a function of forest biomass. The HV backscattering coefficient was selected for inversion up to 70 m³/ha. HH appears to have information for stem volumes above 70 m³/ha. An inversion scheme was developed from this boreal forest and applied on a temperate forest site. [C6496]

"Evaluating integrated multi-scale frameworks for strategic forest inventory and monitoring in Australian heterogeneous woodlands"

Evaluates the use of multi-scale sampling frameworks for improved forest and woodland inventory. The representative sampling strategy integrating field and remotely sensed data provided more detailed information than is currently available, allowing improved understanding of forest and woodland composition and structure, and improved biomass estimations. [C6497]

"Improving temporal and spatial consistency of forest biomass data by integrating forest yield tables and satellite radar data"

Biomass information is needed by research activities relating to natural resources sustainability, carbon cycle, and forest fire fuel loading. Yet, spatially and temporally consistent biomass data distribution over large scales is often not available. In this study, we explore the potential of developing such a forest biomass data sets by integrating traditional yield tables and satellite data. [C6498]

"Multi-spectral analysis of the Amazon basin using SeaWinds, ERS, Seasat scatterometers, TRMM-PR and SSM/I"

The Amazon basin represents a vast geographical zone containing large proportion of global biomass. We use the SeaWinds scatterometer (QSCAT), ERS-1/-2 scatterometer (ESCAT), NASA scatterometer (NSCAT) Seasat scatterometer (SASS), Tropical Rain Measuring Mission Precipitation Radar (TRMM-PR) and Special Sensor Microwave/Imager (SSM/I) data to study the multi-spectral microwave response of Amazon vegetation. Incidence angle signatures of combined backscatter measurements (σ_0) from the scatterometers and precipitation radar

indicate a good inter-calibration of the sensors. The multi-frequency signatures of both σ^0 and radiometric temperature measurements (T_b) from SSM/I are also studied. Temporal variability of the Amazon basin is studied using C-band ERS data and a Ku-band time series formed by SASS, NSCAT and QSCAT data. ESCAT data reveals a possible mismatch in the calibration of scatterometers between ERS-1 and ERS-2. Although the central Amazon forest represents an area of very stable radar backscatter measurements, portions of the southern region exhibit backscatter changes over the past two decades. [C6499]

"Adaptive FIR filtering of range sidelobes for air and spaceborne rain mapping"

This paper describes an adaptive finite-impulse response (FIR) filtering technique to reduce the range sidelobes due to surface return inherent in a pulse-compression radar used for air or spaceborne rain mapping. Its sidelobe suppression performance exceeds traditional windowing methods without a reduction in range resolution. [C6500]

"Probability distribution of surface wave slope derived using Sun glitter images from geostationary meteorological satellite and surface vector winds from scatterometers"

Probability distribution of the sea surface slope is estimated using sun glitter images derived from visible radiometer on Geostationary Meteorological satellite (GMS) and surface vector winds observed by spaceborne scatterometers. [C6501]

"A mean based algorithm for the multi-temporal SAR image filtering"

Any despeckling method for SAR images is a trade-off between speckle reduction level and preservation of image resolution. The Time-Space Filter (TSF) proposed by Coltuc et al. (2000), despeckles the multi-temporal SAR images while preserving the radar reflectivity, the textures and the edge contrast. The price paid for this feature integrity is a non-uniform despeckling: the speckle is reduced only in the homogenous areas, whereas the edge vicinities and the textured areas remain noisy. We propose a new version of the TSF, the Mean based Time-Space Filter (M-TSF), which reduces everywhere the speckle, disregarding the image content. The residual noise in the images filtered by M-TSF remains multiplicative and stationary. This latter property makes M-TSF appropriate for pre-treatment in automatic edge detection. A comparison between M-TSF and the Lee et al. (1991) filter for multipolarization SAR images leads to an interesting conclusion: M-TSF is a frequential version of the Lee et al. filter. [C6502]

"Detection of thinning cuttings using CARABAS-II VHF SAR data"

Thinning cuttings constitute a considerable part of the annually harvested forest stem volume in Scandinavia. The interest to detect thinning cuttings is in the areas of global biomass monitoring in accordance with international treaties, annual local scale measurements of thinnings, forestry law enforcement, and commercial planning of the forest resource. This paper presents results from a study using the airborne CARABAS-II VHF SAR system for detection of thinning cuttings in coniferous forest stands. SAR data were acquired prior to and after thinning cuttings over 25 stands located at a test site in the southwest of Sweden. For the analysis another 24 stands were selected for reference measurements. The results from the statistical analysis show a significant difference between the reference stands and the thinning cuttings for one out of three flight paths examined. A decrease in backscatter due to thinning was found for all image pairs analyzed. Factors influencing the results such as variations in radio frequency environment, image noise variations, and removal of image artifacts have to be further investigated. Nevertheless, the proposed change detection method indicates a possibility to map thinning cuttings using CARABAS-II VHF SAR data. [C6503]

"Peatland ecosystem characterization employing L-band SAR"

Peat swamp forests are very important sources of carbon among the terrestrial forest ecosystems. Large areas of peat swamp forests have been deforested in the recent past. A time series of L-band SAR data has been employed to detect the deforestation that has occurred in the central Kalimantan region, Indonesia, between 1994 and 1998. Large areas that have been deforested have been converted into cultivated lands but agricultural crops have miserably failed to grow on these soils because of the adverse water and soil chemistry. Furthermore, the L-band SAR has been able to detect the flooded conditions in these forests, particularly in short pole and riverside vegetation types where the transmissivity of the L-band SAR signals are quite significant. In case of very dense forests, the inundation could not be detected because of very high attenuation and thus low penetration of L-band radar. The information about these two phenomena viz., deforestation and inundation would be used for estimation of the carbon and trace gases exchange in these forests. [C6504]

"Airborne lidar measurements for Cryosat validation"

Airborne laser measurements provide a detailed capability to measure the geometry of an ice surface with an accuracy of 5-25 cm over a large range of spatial scales (1 m to 100's of km), either as along-track profiles or scanning lidar swath mapping transects, thus providing a useful calibration and validation tool for Cryosat measurements. The lidar measurements are based on precise GPS positioning and inertial attitude data, with accuracy currently limited by long-range kinematic GPS performance. Over marine areas measured sea-ice topography may be converted into ice thickness using models of sea-surface height (geoid) variations and equilibrium assumptions. Over glaciers and ice sheets the varying radar penetration into the snow and ice complicates understanding of radar satellite data, and similarly snow thickness and snow density provides uncertainty in recovering ocean ice thickness from ice free-board measurements. We describe in the paper some recent campaigns using single-profile and scanning lasers to map sea-ice in the Arctic Ocean north of Greenland, as well as some results of comparing radar measurements to laser data in selected areas over the Greenland ice sheet. [C6505]

"Design of the CryoSat system"

CryoSat, as the first Earth Explorer Opportunity Mission, is characterised by a clear focus on science within a very limited financial budget and a short development time. CryoSat is now well into its development and will be launched in 2004. The entire mission is designed in support of specific scientific objectives and this has enabled very clear trade-offs to be made in all the key technical aspects. The selection of the orbit, the payload and the services provided by the satellite subsystems have all been optimised. The primary instrument is a state-of-the-art radar altimeter with additional SAR and interferometric capabilities to improve its spatial resolution. The CryoSat orbit has an inclination of 92 degrees, to optimise the satellite measurements over polar regions. A single ground station, at Kiruna, will be used for all operations. The CryoSat mission has the promise of addressing a well-formulated scientific question, affordably, and within a realistic timescale. [C6506]

"Validation of CryoSat sea-ice products: instruments and methods"

Sea-ice properties like ice and snow density, freeboard, thickness, roughness, and their measurement are described in the context of ground-truth studies for the validation of CryoSat measurements. Both ground-based and airborne methods are presented. [C6507]

"Tropospheric heterogeneities corrections in differential radar interferometry"

Differential radar interferometry (DInSAR) has been used more and more widely to monitor crustal deformations due to underground mining and oil extraction, earthquakes, volcanoes, landslides, and so on. However, tropospheric heterogeneities have been identified as one of the major errors in DInSAR, which can be up to 40 cm as derived from dual-frequency GPS measurements in the example given in this paper. Therefore, it is crucial to correct the tropospheric heterogeneities in the DInSAR results for monitoring crustal deformation. These corrections from several GPS stations in the radar imaging area can be interpolated and applied to the DInSAR results. The discussions are based on data from the Tower Colliery test site southwest Sydney, Australia. [C6508]

"CryoSat: a mission to determine fluctuations in the Earth's ice fields"

This paper provides an overview of the CryoSat satellite mission, the first of the European Space Agency 'Opportunity' Missions. It is aimed at measuring fluctuations in Earth's land and marine ice fields. The mission objectives, instrument system and measurement principles, mission operation and the approach to the calibration and validation of the measurements are described. [C6509]

"Fusion of optical and SAR data for forestry applications in the Sierra Nevada of California"

Ecologists and forest managers commonly emphasize the description of forest structural features because these elements often serve as indicators of organisms and surrogates for processes that may be difficult to observe or measure directly, such as wildlife habitat suitability and the dynamics of forest ecosystems. As used here, the term structure refers to the numbers, sizes, and shapes of the vegetative components in a forest ecosystem and their spatial distribution. Key attributes of forest structure include above-ground biomass, canopy cover, tree height, large tree density, and three-dimensional structural complexity. Remote sensing is a particularly attractive alternative to ground-based measurements because data can be acquired repeatedly and across broad geographic areas that might otherwise be inaccessible. Mapped estimates of forest structural attributes are therefore considered critical to ongoing monitoring efforts requiring reliable inventories of forest resources and accurate assessments of species status and trend. Two pilot study areas were established in the Sierra Nevada

mountain range of California for the purposes of characterizing the three-dimensional structure of selected Sierran forest vegetation types. Field measurements are being used to calibrate and validate estimates of forest structural attributes derived using remote-sensing techniques. Study area locations were selected to represent the pronounced elevational (hi/low) and latitudinal (north/south) gradients that distinguish the Sierra Nevada range. One study area, representing the southern Sierra, was established on the Sierra National Forest and includes the 60,000-ha King s River Sustainable Forest Ecosystem Project and the 1300-ha Teakettle Creek Experimental Forest. The second study area, representing the northern Sierra, was located on the Plumas National Forest. Within each study area, a stratified-random sampling scheme was used. A 3% sample resulted in a total of 500 1-ha sample plots. [C6510]

"The evaluation of different sensors and techniques for the detection of storm damages in forests"

After each disastrous storm event quick and reliable information of the extent of forest damage is required. This study investigates different remote sensing data and analysis methods for their possible fields of application to detect blowdowns. Therefore both optical satellite sensors and synthetic aperture radar data in various frequencies were evaluated. Obligatory aspects under consideration were the operational usage, the heterogeneity of the Swiss landscape, the effects of topography and season in Alpine regions and last but not least the financial conditions. Classification results were compared to aerial images which were interpreted manually on an stereoscopic base. The pros and cons of the sensors and the analysis techniques are very heterogeneous. In order to assign the appropriate data with the most suitable classification method, the primary objective of the classification must be set up. [C6511]

"SIRAL: the radar altimeter for CryoSat mission, under development"

SIRAL (SAR Interferometer Radar Altimeter) is the new spaceborne altimeter designed for CryoSat mission. The instrument is currently in the development phase, in ALCATEL SPACE, which encompasses an Engineering Model and a Flight Model. This ESA mission, planned for 2004, will be used to estimate-on a global scale-the fluctuations in mass of sea-ice and land-ice. This paper discusses the flexibility of the instrument and in particular its capability to operate in various modes (conventional altimeter, SAR and interferometer modes), and gives main results from the pre-developments and breadboard activities. [C6512]

"CryoSat level 1b processing algorithms and simulation results"

The CryoSat synthetic interferometric altimeter (SIRAL) has been designed to extend the coverage of conventional pulse-limited altimeters to allow the measurement of sea ice thickness and the elevation of the marginal regions of ice sheets. The science data acquired by the instrument is of a more complex nature than the conventional radar altimeter and is in one of three forms each of which are described in the paper. Examination of simulated echoes from each of these 3 modes provides a useful insight into how the CryoSat mission will tackle its primary objectives, and how an improvement in elevation measurement will be made over its conventional satellite borne counterpart. [C6513]

"An airborne CryoSat prototype: the D2P radar altimeter"

Through airborne flight tests over the ocean and the ice of southern Greenland, we have successfully demonstrated the technical viability and waveform characteristics of an innovative radar altimeter concept (D2P), the first of its kind. The D2P takes advantage of range-curvature-corrected, multi-look Doppler processing along-track, and interferometric angle measurement across-track. The radar's performance met or exceeded expectations. The D2P radar serves as an airborne prototype of CryoSat. [C6514]

"Validation of QuikSCAT Radiometer rain rates using the TRMM microwave radiometer"

The primary mission of the SeaWinds scatterometer on the QuikSCAT satellite is to infer surface wind vector from ocean backscatter measurements. Occasionally the backscatter measurements are contaminated by the presence of rain; therefore a reliable method of identifying rain is needed. Fortunately, the SeaWinds scatterometer simultaneously obtains active (scattering) and passive (emission) measurements of the ocean; thus, the QuikSCAT Radiometer (QRad) measured brightness temperatures can be used to infer rain rate within the scatterometer antenna field-of-view. This paper describes a new QuikSCAT Level-2B science product of rain rate over oceans. The principal use of this product for quality control purposes to provide a quantitative rain flag associated with QuikSCAT wind vector cells. The QRad rain rate algorithm is described and the characteristics of the rain rates product are presented. This product has been validated by near-simultaneous comparisons with rain rate measurements from the Tropical Rainfall Measuring Mission (TRMM) Microwave Imager (TMI). An example of QuikSCAT retrieved winds in the presence of rain is presented with collocated QRad rain measurements. Results demonstrate that the QRad rain rate product provides a reliable, quantitative wind vector

quality flag. [C6515]

"Wind-direction dependence of quasi-2D SAR signatures"

Documents the typical variations in quasi-two dimensional marine atmospheric boundary layer SAR signature orientation with respect to the near-surface mean wind direction, making it of practical interest to those researchers using such techniques to infer wind speed from SAR imagery. [C6516]

"SAR and MODIS images of atmospheric solitary waves generated by upstream blocking in flow over St. Lawrence Island Bering Sea"

A group of atmospheric solitons is identified on a RADARSAT-1 synthetic aperture radar (SAR) image and a Moderate Resolution Imaging Spectroradiometer (MODIS) image taken about 4.5 hours later on June 6, 2001. On both images, this group of solitons is showed as dark-bright linear features. The atmospheric solitons are generated at St. Lawrence Island in Bering Sea and propagate against the airflow in the upstream direction. On the first SAR image, there are only three wave crests. However, on the second MODIS image, the wave train propagates further upstream and seven wave crests can be identified. The basic properties of this group of solitons are measured and derived. Radiosonde data show that the Froude number is close to unity. Therefore, theoretically, this phenomenon can be described by the classic "flow over bump" model and analyzed using the classic KdV equation. [C6517]

"L-band SAR wind-retrieval model function and its application for studies of coastal surface winds and wind waves"

An L-band geophysical model function (GMF) is developed using Japanese Earth Resources Satellite-1 (JERS-1) SAR data. This GMF describes the relationship among L-band NRCS and ocean surface wind speed and direction. It enables us to convert JERS-1 SAR image into a wind-speed map. Using retrieved SAR wind, a high-resolution wave prediction model, SWAN (Simulating WAVes Nearshore) was derived to demonstrate SAR high-resolutions winds. [C6518]

"High resolution wind fields retrieved from SAR in comparison to numerical models"

An algorithm is introduced, which is designed to retrieve high-resolution wind fields from C-band synthetic aperture radars (SARs) operating at vertical or horizontal polarization. Wind directions are extracted from wind-induced streaks, which are approximately in line with the mean wind direction near to the ocean surface. Wind speeds are derived from the normalized radar cross section (NRCS) and image geometry of the calibrated SAR data, together with the prior retrieved wind direction. Therefore the semi empirical C-band model CMOD4, which describes the dependency of the NRCS on wind and image geometry, is used. CMOD4 was originally developed for the scatterometer of the European remote sensing satellites ERS-1 and ERS-2 operating at C-band with vertical polarization. Consequently CMOD4 requires modification for horizontal polarization, which is performed by considering the polarization ratio. To verify the algorithm, wind fields were computed from 159 ERS SAR and 20 RADARSAT-1 ScanSAR images and compared to co-located results from the numerical models REMO and HIRLAM. [C6519]

"Implications of QuikSCAT and RADARSAT wind comparisons for SAR wind speed model functions"

Active microwave scatterometers such as the SeaWinds scatterometer on QuikSCAT measure wind speed and direction over the world's oceans at 25 km resolution. This resolution does not capture much of the wind field spatial variability in coastal regions. High-resolution synthetic aperture radar (SAR) can measure normalized radar cross section at sub-km resolution. The RADARSAT SAR has been effectively used to measure high-resolution wind fields. This paper systematically compares QuikSCAT scatterometer and RADARSAT SAR winds over the years 2000 and 2001. The results obtained thus far demonstrate that modest changes in the SAR to NRCS model function can improve the SAR wind speed retrievals. [C6520]

"Results of a bistatic HF radar surface wave sea scatter experiment"

We describe a set of HF radar sea scatter experiments that test a new digital receiver in both monostatic and bistatic modes. The University of Miami's OSCAR HF radar system was used as a transmitter signal source, and sea echoes were received with both receive systems using different receive antenna arrays. Independent GPS time-coupled rubidium clocks were used to maintain site-pair coherence, and Bragg spectral purity was used as a measure. Expected first order Bragg line characteristics are first discussed that are based on a model (Trizna, 2000): predicted Bragg line NRCS and Doppler shift. With a monostatic transmitter and receive array and a

single bistatic transmitter, two different aspects onto the same ocean surface area allows one to estimate current vectors. [C6521]

"Phenomenological models of Doppler-polarimetric microwave remote sensing of clouds and precipitation"

This paper deals with mathematical modeling and simulation of echo-signals in both frequency and time domains. It establishes some important relationships between Doppler-polarimetric observables and weather object under observation. [C6522]

"Measurement of wind speed and direction using multifrequency HF radar"

HF radar has become an important tool for mapping surface currents in the coastal ocean. It is well known that HF radars are capable of measuring wind direction by using the relative strength of the echoes from the approaching and receding ocean waves at the Bragg resonant wavelengths. Here we examine the ability of multifrequency HF radar to measure wind speed as well as direction. In this study we use data collected over Monterey Bay, California in the late summer of 2000. At that time there were two buoys in the radar's observational area that were capable of measuring wind speed and direction one near the Bay mouth and one nearer the shore. We investigate the relationship between the wind speed and the near surface currents and Bragg line ratios as measured by two multifrequency HF radars near Santa Cruz and Moss Landing, California. These radars operated at 4.8, 6.8, 13.4 and 21.8 MHz, measuring currents at effective depths of 2.5, 1.8, 0.9 and 0.6 m respectively. The method of partial least squares is used with results for speed of a standard error of prediction (SEP) of ≈ 1 m/s, a bias of ≈ 0.5 m/s and an R^2 of ≈ 0.8 . For direction the SEP $\approx 40^\circ$, the bias $\approx 4^\circ$ and R^2 of ≈ 0.45 . These preliminary results suggest that wind speed as well as direction can be estimated from multifrequency HF radar data. [C6523]

"Detection of extreme waves using synthetic aperture radar images"

Within the last years a considerable number of large ships have been lost due to severe sea state conditions. The cause of accidents are in many cases believed to be rogue waves, which are individual waves of exceptional wave height or abnormal shape. In particular steep breaking waves can be fatal for smaller ships. Damage is sometimes can also be caused by unusual grouping of waves, which can lead to dangerous ship motion. In situ measurements of extreme waves are sparse with most observations reported by ship masters after the encounter. In this paper a global data set of 5 Ч 10 km sized synthetic aperture radar (SAR) images acquired by the European Remote Sensing satellite ERS-2 every 200 km along the track is used to analyse extreme ocean wave events. As the European Space Agency (ESA) does not provide this dataset as a standard product wave mode raw data were reprocessed to complex SAR images using the processor BSAR developed at the German Aerospace Center (DLR). About 1000 globally distributed SAR wave mode images are available every day. Two dimensional ocean wave fields are derived from SAR images by inversion of the SAR imaging mechanism. Individual high waves are detected in the derived wave fields using a matched filter technique. The inhomogeneity of ocean wave fields is analysed using a parameter, which describes the shift invariance of the wave spectrum. [C6524]

"Root-MUSIC direction finding applied to multifrequency coastal radar"

Recently several authors have examined the theoretical performance of the Root-MUSIC algorithm, which is a variation of the popular MUSIC algorithm applicable to a linear array of uniformly-spaced, identical elements (or a uniform circular array). It is thus more restricted than conventional MUSIC, but simulation studies indicate that Root-MUSIC (and related algorithms, such as ESPRIT) have performance advantages over ordinary MUSIC for such linear arrays. The receiving array of the University of Michigan's Multifrequency Coastal Radar (MCR) is a linear array of 8 identical loops and thus is a good candidate for experimental study. Four-frequency data recorded during the COPE-3 experiment at Chesapeake Bay, Virginia during 1997 have been processed with Root-MUSIC as well as ordinary MUSIC and beam formation. Directional estimates for a calibration transponder at known locations processed with MUSIC and Root-MUSIC are compared. Root-MUSIC and MUSIC appear to give very similar results. [C6525]

"Detection of extreme waves using radar-image sequences"

A method is presented to localize wave groups spatially and spatio-temporally utilizing synthetic aperture radar (SAR) images and nautical radar-image sequences of the ocean surface. Extreme waves can grow in space and time as a result of wave group evolution. These wave groups have to be taken into account for instance for the design of offshore platforms, breakwaters or ships, because they can cause severe damage on those structures.

To detect extreme waves, dominant wave groups are selected from SAR images and radar-image sequences by considering the wave envelope. A radar-image sequence is transformed into the wave-number frequency domain using a 3D Fourier transform where the signal of the ocean gravity waves is filtered using a band pass filter based on the dispersion relation for linear surface gravity waves. Thereafter, a 3D Hilbert transform is applied to the filtered complex Fourier coefficients, which are then transformed back into the spatio-temporal domain applying an inverse 3D Fourier transform. The resulting spatio-temporal complex envelope of the wave field is investigated for the dominant wave groups, by considering the amplitude of the complex envelope. With slight changes the algorithm can also be applied to single radar images. To test and verify the algorithm, several radar image sequences were acquired with the wave monitoring system WaMoS-II, which is based on a nautical radar operating in the X-band (9.5 GHz) near grazing incidence. The instrument was operated on towers in the North Sea. All these data sets are exploited with respect to the localization of extreme waves and wave groups.

[C6526]

"Systematic discrepancies between altimeter and scatterometer wind speed measurements"

A collocated TOPEX/NSCAT/ECMWF dataset is compiled to investigate the systematic discrepancies among the three kinds of wind estimates. It is found that the discrepancy between TOPEX and NSCAT winds is characterized by a significant "phase opposition" with respect to latitude, season and wind intensity. [C6527]

"Simulation of SeaWinds measurements in the presence of rain using collocated TRMM PR data"

The scatterometer SeaWinds on QuikSCAT measures ocean winds via the relationship between the wind and the normalized radar backscatter cross-section (σ°) from the ocean surface. Scattering and attenuation from falling rain droplets along with ocean surface perturbations due to rain change the backscatter signature of the waves induced by near-surface winds. A Simple model incorporates the effects of rain on ocean σ° . Colocated data from the precipitation radar (PR) aboard the Tropical Rainfall Measuring Mission (TRMM) satellite is used to simulate the effects of rain as seen by SeaWinds. PR-derived backscatter, atmospheric rain attenuation, and rain rates are averaged over the SeaWinds footprint. The enhancement in backscatter from rain striking the ocean surface is estimated as a function of rain rate using a least-squares technique. QuikSCAT σ° values are simulated from the PR-derived parameters and numerical weather prediction wind data using the simple backscatter model. The simple model estimates 90% of the observed rain-contaminated QuikSCAT σ° values to within 3 dB. [C6528]

"Validation of current and bathymetry measurements in the German Bight by airborne along-track interferometric SAR"

We present final results of the German research project EUroPAK, whose main objective was the development of a remote sensing technique for surface current fields and underwater bathymetry on the basis of conventional and interferometric synthetic aperture radar (SAR and InSAR). In May 2001, the second of two field experiments with an airborne along-track InSAR was carried out over a test site in the North Sea, where scientists of the GKSS Research Center performed simultaneous in-situ measurements with a variety of instruments within the framework of another project. We describe data processing procedures, show examples of measured current fields and bathymetric maps, and discuss the quality of our results and the potential of the INSAR technique for operational services such as routine monitoring of bathymetric changes. [C6529]

"W-band radar backscattering at low grazing angles measured in a wave tank at various wind speeds"

W-band backscatter experiments have been performed at the wind-wave tank of the University of Hamburg. The aim of the experiments is to study the backscatter mechanisms under shallow incidence angles and to compare the results with previous ones obtained with an X-band scatterometer. The measurements were performed at three grazing angles, 7.5°, 10°, and 20°, and at VV-, HH-, and VH-polarization. The wind speed ranged from 2 to 10 ms⁻¹ and was increased in steps of 1 ms⁻¹. The analysis of the acquired radar Doppler spectra shows that Bragg scattering from both bound and freely propagating Bragg waves is the dominant backscattering mechanism at all deployed wind speeds. In particular, at low wind speeds (up to 4 ms⁻¹), when the overall backscatter is small, bound waves are the dominating scatterers, whereas at higher wind speeds (5 ms⁻¹ and above) the acquired signal is mainly caused by freely propagating Bragg waves. This is in qualitative agreement with similar findings, which have been made earlier with an X-band scatterometer working at moderate incidence angles. [C6530]

"Inversion techniques for ground-based microwave radiometric retrieval of precipitation columnar contents and path attenuation"

Nonlinear inversion algorithms are developed to invert ground-based radiometric measurements for different sets of frequency channels and precipitation regimes. Both statistical regression estimators and feedforward neural networks are applied and compared using synthetic data sets from 6 to 50 GHz. An experimental validation is carried out using data collected by the ITALSAT ground-station (near Rome, Italy) equipped with 3 beacons at 19.7, 39.6, and 49.5 GHz together with a multi-channel radiometer at 13.0, 23.8, and 31.6 GHz. Results in terms of comparison between measurements and predictions for a rain event are finally discussed. [C6531]

"Rain rate measurement with an airborne scanning radar altimeter"

The NASA Scanning Radar Altimeter (SRA) sweeps a radar beam of 1° half-power width (two-way) across the aircraft ground track within $\pm 22^\circ$ of nadir, simultaneously measuring the backscattered power at its 36 GHz (8.3 mm) operating frequency and the range to the sea surface at 64 points spaced across the swath at 0.7° incidence angle intervals. Flights were made into Hurricane Humberto on 23 and 24 September 2001, aboard a WP-3D hurricane research aircraft of the NOAA Aircraft Operations Center. The ranges produce raster lines of sea surface topography at a 10 Hz rate. The SRA was primarily designed to produce sea surface directional wave spectra, but the backscattered power measurements can be used to determine path integrated rain rate below the aircraft. [C6532]

"Rain rate retrieval using airborne imaging radiometry during CAMEX3/TEFLUN-B"

A multiband Polarimetric Scanning Radiometer (PSR) was integrated onto the NASA DC-8 aircraft (N717NA) and flown from August through September of 1998 during the third Convection and Moisture Experiment (CAMEX3) and Texas-Florida Under-flight (TEFLUN-B) campaign. The PSR is a unique conically-scanned imaging radiometer with channels at 10.7, 18.7, 21.5, 37.0 and 89.0 GHz, measuring both vertical and horizontal polarizations at each of these frequencies. These channels correspond to several key bands of the DMSP (Defense Meteorological Satellite Program) SSM/I (Special Sensor Microwave Imager) and the NASA TRMM (Tropical Rainfall Measuring Mission) TMI (TRMM Microwave Imager). The PSR was developed by Georgia Institute of Technology and the NOAA Environmental Technology Laboratory. It is the first airborne imaging radiometer to provide a research quality set of high spatial resolution multiband polarimetric microwave imagery within and around a hurricane. A nonlinear statistical emission algorithm was developed for rain rate retrieval, similar to that described by Skofronick-Jackson and Gasiewski (1995). We use the PSR/A 10.7 GHz channels of horizontal and vertical polarization because of their predominantly monotonic response to near-surface rain rate from 0 to 50 mm/hr. An initial comparison of the PSR retrieved rain rate to coincidentally observed rain rate retrieved using NASA JPL's Airborne Rain Mapping Radar (ARMAR) shows favorable agreement over at least an order of magnitude in rain rate intensity. Discrepancies are within the standard deviations of the PSR retrieval algorithm and can be explained by differences in the observation geometries of the sensors and by differences in the physical measurement principals between the two instruments. Further comparison of the PSR rain rate retrieval with the TMI level 2A12 rain rate product is similarly favorable. Some discrepancies can be explained by the differences in spatial resolution of the two passive microwave instruments and the different nature of the two retrieval algorithms. Despite these differences, the correlation coefficient between the TMI and the PSR coincidentally observed rain rates is 0.92 and 0.91 for PSR horizontal and vertical channels (respectively), for rain rates from -1 to 16 mm/hr. [C6533]

"Measurement of the ocean surface in low to moderate winds at C-band"

Several research flights were conducted over the Gulf of Alaska using a NOAA WP-3D aircraft to study the radar backscatter and radiative emission behavior of the ocean surface under a variety of meteorological conditions in an experiment called the Alaska Rain and Ocean Backscatter Experiment (AROBEX). Particular use was made of the University of Massachusetts C-band scatterometer (CSCAT) and multifrequency C-band radiometer aboard the WP-3D to examine microwave remote sensing techniques for the retrieval of ocean surface winds. A plethora of instrumentation onboard the aircraft was used for simultaneous measurements of surrounding environmental conditions, including a C-Band lower fuselage radar, an X-band tail Doppler radar, and GPS dropsondes. Additionally, flights were planned to take coincident measurements with the RADARSAT satellite, providing collocated synthetic aperture radar measurements of the ocean surface. An examination of these data is presented with particular emphasis on passive microwave retrieval capabilities in the low to moderate wind regime and in the presence of precipitation. GPS dropsonde profiles provide the fine tuning and ground truth information needed for a direct comparison of C-band scatterometer measurements of the ocean surface scattering and multi-frequency C-band radiometer measurements of ocean surface and atmospheric column precipitation emissions. Variability within the multi-frequency radiometer footprint is also examined through comparisons with the high resolution surface roughness measurements of simultaneous RADARSAT passes. The implications of these comparisons to remotely sensed ocean surface winds are discussed, particularly with regard to the use of satellite based passive and active microwave instrumentation. [C6534]

"Study of the variability in the rain drop size distribution over a 2.3 km path"

In an effort to study the drop size distribution (DSD) a state-of-the-art instrument arrangement was deployed on Wallops Island, VA. The instrumentation consisted of a 2.3-km multi-frequency microwave link, three impact disdrometers, and a network of optical and tipping bucket raingauges. A dual-frequency inversion technique was implemented with the link measurements of attenuations at 25 GHz and 38 GHz to estimate the path-average DSD. Concurrently, an X-band, dual-polarization radar, located in the vicinity, collected polarization and reflectivity measurements over the link path. The evaluation of the estimates and measurements generated some preliminary results. [C6535]

"Polarimetric remote sensing of sea ice-from theory to practice"

The employment of radars in remote sensing monitoring of polar regions is well known and largely proven practice today. In general the sea ice controls the heat transfer and mass-balance between the ocean-and the atmosphere. To interpret ice polarimetric signatures a composite microwave model is studied. The model relates the electromagnetic scattering from sea ice to its geophysical properties. [C6536]

"High altitude compact solid state 95 GHz cloud radar"

The study of high altitude clouds has motivated the development of new airborne and space-borne millimeter-wave cloud radars. Airborne millimeter-wave radars can offer better spatial resolution and sensitivity than ground-based counterparts, by avoiding water vapor attenuation in the lower atmosphere and spatial resolution degradation due to beam spreading. Furthermore, aircraft can cover large geographic areas and simulate satellite geometry. A next generation 95 GHz Compact Millimeter-wave radar (CMR) is currently under development. Incorporation of pulse compression will provide sensitivity comparable to larger klystron tube-based transmitters traditionally used in ground based 95 GHz radars. The CPU-bases signal processor will be replaced with a stand alone processor bases on re-configurable Field Programmable Gate Array Logic (FPGA). The new processor digitizes the IF signal, performs digital-in phase and quadrature phase detection, and applies the pulse-pair algorithm. [C6537]

"A multiwavelength airborne polarimetric lidar for vegetation remote sensing: instrumentation and preliminary test results"

Several spaceborne and airborne lidar systems have been launched for vegetation canopy studies. Previous research has shown that lidars are useful tools for remote sensing of vegetation architecture. To support its Airborne Remote Sensing Program, the University of Nebraska has developed a multiwavelength airborne polarimetric lidar system. This system employs a Nd:YAG laser which emits radiation at two wavelengths: the fundamental at 1064 nm and the frequency-doubled at 532 nm. Both laser beams are highly linearly polarized (100:1 extinction ratio) and have a beam divergence angle of 4 mrad. The receiver consists of four channels, which enable dual-wavelength and dual-polarization detection. In addition to the polarimetric information that could be gathered, this lidar system also has ranging capability and is able to record the whole lidar waveform. Thus, our lidar is capable of performing studies of vegetation canopy structure as well as characterization of vegetation depolarization. The system has been packaged to fly aboard a Piper Saratoga aircraft from a height of 1000 m. In this paper, we will present the details of the lidar system design, instrumentation, the system alignment and preliminary ground test results. [C6538]

"An airborne low-cost SAR for remote sensing: hardware design and development"

An airborne low-cost synthetic aperture radar (SAR) is under development at the University of Nebraska-Lincoln. The SAR system is an X-band, stepped-chirp frequency modulation (SCFM) radar system. One of its unique features is that the waveform generation consists of a timing-controlled D/A converter and VCO arrangement to synthesize the SCFM signal, whereby allowing for less design complexity and a much lower overall system cost. In this paper, we present a brief description of the system and some computer simulation results. [C6539]

"Research on ground based microwave signature measurement technology for spaceborne SAR applications"

The article proposed a novel method to resolve the quantitative application of the SAR images. It is to develop new ground-based spectrum measure instrument to get the normalized radar cross section under the same conditions with the SAR. The ground-based scatterometer uses a pulse as a measuring signal that is matched with the spaceborne SAR. It has more merit than the FM-CW scatterometer in the back scatter measurement. The characters of the pulse ground-based scatterometer are analyzed and the system has been realized.

[C6540]

"Polarimetric borehole radar and its applications"

We introduce applications of radar polarimetry in borehole radar. One example is classification of subsurface fractures, where we estimate the water permeability of each fracture by radar polarimetry. Then polarimetric borehole radar was then used for cross-hole radar measurement. Transmitted signal between boreholes having a 20 m separation was measured, and we could show that the polarization information can be used for estimation of the orientation of a subsurface cavity. [C6541]

"Using SHOALS LIDAR system to detect bottom material change"

Bathymetric lidar systems, e.g., the Scanning Hydrographic Operational Airborne Lidar Survey (SHOALS) have a proven capability to measure water depth accurately. Although the system is optimized for depth retrieval, there is much more than depth information since the data stream (waveform) includes backscatter from the water surface and water column as well as the bottom return. This paper uses the amplitude of the bottom return signal to characterize the illuminated bottom materials. It is found that, while there are changes in the bottom return that clearly correlate with changes in bottom type, the bottom slope and surface waves have significant effects on the bottom return. These factors can distort the recorded waveforms and alter the apparent reflectance of illuminated materials, and must be accounted for if changes in bottom type are to be detected. [C6542]

"Differential SAR interferometry for the study of slope instability at Maratea, Italy"

In this paper we explore the use of differential synthetic aperture radar interferometry to improve our knowledge of the slope instability of a well investigated area (the Maratea Valley) affected by continuous slow movements. In particular, by using this technique we analyse the time evolution of terrain movements from 1997 to 2000, a time interval already explored using distancemeter (EDM) and GPS measurements. Results obtained by means of different techniques have been compared, and all the acquired data turn out to be consistent. [C6543]

"Doppler lidar using aerosol backscatter and a frequency agile laser transmitter for profiling atmospheric winds in the planetary boundary layer"

A cost effective, miniature, Doppler wind lidar system based on atmospheric scattering from aerosols is presented. The initial design and theory of this instrument will be discussed. A method for minimizing the systematic error resulting from the component of the return signal that is backscattered by the atmospheric molecular constituents is also briefly described. [C6544]

"An airborne multi-mode microwave sensor and flight experiments"

An airborne multi-mode microwave sensor has been developed in order to verify the design and performance of future Chinese spaceborne multi-mode microwave sensor. Like spaceborne system, the airborne system also includes altimetry, scatterometry and radiometry functions. There are five frequency channels in radiometry mode. Altimetry mode, scatterometry mode and one of radiometry channels operate at the same Ku band. Flight experiments have been conducted on southern sea of China. The results show that future Chinese spaceborne multi-mode microwave sensor is practicable. In this paper, the principle of spaceborne and airborne multi-mode microwave sensor is briefly introduced. Flight experimental details and results are described. [C6545]

"JZM-Ku1 pulse-modulated scanning air-borne scatterometer"

JZM-Ku1 airborne scatterometer works in the Ku-band with a pulse-modulated transmitting probe, conically scanning pencil beam and dual-polarization antennas. Digital signal processing is employed in this instrument to improve the measurement stability, accuracy and speed. This scatterometer is very suitable for backscatter coefficient measurements over land and sea. In the second part, some of the experimental results of sea surface wind were presented. Compared with the actual wind (synchronously collected by weather and hydrology survey instruments on ship), the wind direction deviation is less than 12 degree, and the wind speed deviation is less than 10%. This radar is also suitable for observation of forests, crops and soil moisture and salinity. [C6546]

"Modeling of microwave dielectric properties of rice growth stages in Zhaoqing test site of Southern China"

This paper presents the modeling results of dielectric constants from different rice growth stages in Zhaoqing test site using Debye-Cole dual-dispersion model of vegetation. In the test site, two crops of early season rice and late season rice are planted in 1997 and 1996, and the growing period of rice crop is divided into five major

stages: transplant, seedling developing, ear differentiation, heading and mature period. Based on the results, the paper discussed the influences from microwave frequency, gravimetric moisture content of rice, temperature, salinity and bulk density of dry vegetation materials on dielectric constant. The rice crops of different growth stages have the various dielectric constants, and the dielectric constants of early and late season rice crops show the diverse changes. The parameters, including in microwave frequency, gravimetric moisture content of rice, temperature and bulk density of dry vegetation materials, made the influence on dielectric constant, but salinity had no effect on the dielectric constant. [C6547]

"BISSAT: a bistatic SAR for Earth observation"

This paper summarizes scientific rationale and technical approach for a bistatic synthetic aperture radar (SAR) mission (BISSAT). The study has been funded by the Italian Space Agency for a competitive Phase-A study along with other five missions. Its concept consists in flying a passive SAR on board a small satellite, which observes the area illuminated by an active SAR, operating on an already existing large platform. [C6548]

"Frequency dependence of scattering by dense media of small particles based on Monte Carlo simulation of Maxwell's equations"

The frequency dependence of scattering by geophysical media at microwave frequencies is an important issue because multi-frequency measurements are useful for remote sensing applications. Classically, the independent scattering theory states that if the particles are small, scattering is proportional to the fourth power in 3-D scattering and the third power in 2-D scattering. In this paper, we study rigorously the frequency dependence of scattering by dense media by Monte Carlo simulations of the solutions of both 2- and 3-dimensional Maxwell's equations. The particle positions are generated by deposition and bonding techniques. The sparse-matrix canonical-grid method has been applied to speed up the simulation of scattering by 2D small particles. Numerical solutions of Maxwell's equations indicate that the frequency dependence of densely packed sticky small particles is much weaker than that of independent scattering. The results are illustrated using parameters of snow in microwave remote sensing. [C6549]

"Polarimetric SAR interferometry for vegetable vertical structure parameters extraction"

Polarimetric SAR interferometry is much more sensitive to the distribution of oriented objects in a vegetated land surface than either polarimetric or interferometry alone. In this paper, we propose a polarimetric SAR interferometry technique for the estimation of parameters characterizing the vertical structure vegetated land surfaces. Based on simple physical model, we use SIR-C/X-SAR full polarimetric data to calculate the optimized interferometric coherences. The test site is Tianshan and its surrounding area, where pine trees are planted and the characteristics are well known. As a result, we could estimate the tree height distribution, and the quantitative evaluation is presented to relate the phase center differences and the tree types and the polarization combinations. [C6550]

"Clustering of EM radiation source based on eigenvector"

Our goal is to locate anomalous electromagnetic (EM) sources caused by seismic activity for earthquake prediction. For the purpose, we have measured the EM wave of 223Hz at 35 sites in Japan. The measured signal contains much noise caused by lightning around the equator, human activity, near field lightning and so on. EM noises from far sources can be eliminated by using correlation in multi-point observation. But near-field noise is not easy to eliminate. This paper shows that the principal component analysis methods for covariance matrices of measured signals are effective for clustering signals and separating each source. It is shown that a result to estimate thunder lightning location in near field agrees with real thundercloud observed by radar system. And results of estimation of sources of anomalous EM radiation occurred before and after earthquake are also shown. [C6551]

"An empirical calibration of the integral equation model based on SAR data and soil parameters measurements"

The retrieval of surface parameters demands the use of well calibrated models and unfortunately, none of the existing models provide consistently good agreement with the measured data. The overall objective of this paper is to propose a semi-empirical calibration of the Integral Equation Model (IEM) so as to better reproduce the backscattering coefficient measured from SAR images over bare soils. As correlation length is not only the least accurate parameter but also the most difficult to measure, we propose its empirical estimation from an experimental data set of SAR images and soil parameter measurements. Based on a first data set, relationships between optimal correlation length and rms height were found for each radar configuration. The IEM was then

tested on another set of measured data in order to validate the calibration procedure. The new calibrated version of the IEM, corresponding to the original IEM (Fung, 1994) with a coupling of the empirical function of correlation length, shows a very good agreement with the backscattering measurements provided by spaceborne SAR systems. [C6552]

"SAR polarimetry for permafrost active layer freeze/thaw processes"

In this paper, a feasibility study is conducted in regard to using SAR for the freeze/thaw processes monitoring. The backscatter polarimetry parameter defined as a proportion of the statistically averaged HH backscatter to the VV one is calculated through solving the Maxwell equations in the small perturbation method approximation. In order to provide for the soil complex dielectric constant dependencies on moisture, texture, frequency, and temperature the generalized refractive mixing dielectric model is used. The polarimetry parameter size of changing, due to seasonal soil temperature profile deviations, soil moisture variations, and the radar look angle alterations have been analyzed in detail. The outcomes of the performed analysis intend for planning SAR observations and data processing in the experiments on active permafrost layer monitoring. [C6553]

"Estimation of the object depth accurately with GPR"

In this paper, we propose an automatic algorithm for estimating objects depth using f-k migration and velocity scanning method for the homogeneous medium. Experimental results show that the relative estimating error of depth is as low as 10%. [C6554]

"Analysis of backscattering enhancement for partially convex targets in random media for plane and beam wave incidences"

Fields due to electromagnetic waves propagating in continuous random media are calculated efficiently, by a method that uses a current generator, M. Tateiba et al. (1992). This method solves the problem of wave scattering from targets in random media as a boundary value and this technique of solution is important for radar detection of a target of finite size. This method uses two operators: the current generator that transforms the incident wave falling on the target into the surface current and Green's function in the random medium. In earlier investigation, Z. Q. Meng et al. (1996), numerical results for radar cross-section (RCS) of conducting convex bodies such as circular and elliptic cylinders have elucidated that the spatial coherence length (SCL) of incident waves around a target is one of the key parameters for the clarification of random media effects on the RCS. The shape of the target is one of the parameters that constitute an important factor in the radar detection problem. Recently we have presented numerical results for the backscattering enhancement in RCS of conducting cylinder with a concave-convex cross-section. It has been found that the target configuration together with the SCL of the incident wave around the target play a leading role in determination of the RCS of partially convex targets. To render a satisfactory understanding of the backscattering enhancement behavior for the concave-convex targets in random media, we analyze the scattering problems for plane wave propagating in continuous random media and beam waves in free space for vertical polarization. [C6555]

"Scattering from randomly distributed dielectric cylinders: experiment and modeling results"

An experiment aiming at studying the scattering properties of a collection of dielectric cylinders placed on a reflecting plane has been performed by using the EMSL of the JRC of Ispra Italy. Experimental data have been compared with simulations performed with a coherent electromagnetic model. [C6556]

"Generation of deformation maps at low resolution using differential interferometric SAR data"

In this paper, an advanced technique for the generation of deformation maps using SAR data is presented. The input data is a set of low resolution Differential Interferograms (multi-looked data) and their associated coherence images. An important advantage of this algorithm is that it can work with a reduced number of SAR images with a diversity of spatial baselines. The algorithm takes advantage of those pixels presenting a good coherence level in the whole set of interferograms, avoiding the rest affected by temporal decorrelation. All pixels accomplishing the selection criteria are related using a Delaunay triangulation. The subsidence velocity map over the scene is obtained adjusting an interferometric phase model, which also considers the error on the DEM used to remove the topography from the interferogram set, to the pixel phase increments. If the density of quality pixels is high enough over the scene, an interpolation of the areas with no information can be performed to obtain a complete deformation map of the zone. Otherwise, the information can be presented only on those zones with enough pixel density. This algorithm has been tested with ERS data from an area of Catalonia (Spain) and validated with precise levelling measurements. [C6557]

"High performance artificial SAR raw data generation algorithms for remote-sensed imaging applications"

This on going seminal work presents a new methodology for the design and implementation of high performance artificial raw data generation algorithms for remote-sensed imaging applications. Special attention is given in this work to synthetic aperture radar (SAR) system modeling and simulation imaging applications in the geosciences. Of particular importance are processes such as soil moisture content, backscattering from crops, nearshore ocean surface currents, and subsurface imaging in hyperarid regions. Our computing approach is based on the successful use of cross-ambiguity functions, in a Weyl-Heisenberg computational framework, as surface point target response functions for nonlinearly modulated, time-frequency structured, artificially created transmitted signals for our SAR system raw data modeling and simulation efforts. The functions are correlated with prescribed target reflectivity density functions to produce the desired results. [C6558]

"A multi DSP board for real time SAR processing using the HiPAR-DSP 16"

At the University of Hannover a fully programmable DSP, the HiPAR-DSP 16, was developed. This HiPAR-DSP 16 contains 16 parallel datapaths and a 2-dimensional memory adapted to image processing algorithms. For real time SAR processing high computational power is required. Therefore a multi DSP board with 6 HiPAR-DSP 16 is developed. The high performance of up to 28 GOPS enables a SAR processing in real time. The calculation time for the wk-algorithm running on this board was estimated. For blocks of 4096 lines with 4096 8 bit complex samples real time processing is possible to a pulse repetition frequency (PRF) of 1200 Hz. Due to a low power consumption and the small size of 160x230 mm² of this board the use in on-board systems is predestinated. [C6559]

"Pre-processing compensation for saturation power loss in SAR data"

In this paper, we describe a method for compensating data for saturation power loss due to the analog to digital converter (ADC) in spaceborne synthetic aperture radar (SAR) instruments. The algorithm counts the number of saturated points in a block of raw signal data and adjusts the data to regain the lost power. The algorithm compensates well for lost power, showing a correction of up to 7 dB, and agreeing within 1 dB with unsaturated data. If care is not taken in the compensation sort order image artifacts can occur. We describe the methods used and discuss limitations in the application of the algorithm. [C6560]

"SAR/MTI radar mapping from ships and ground based vehicles"

In this paper, the performance of MTI/SAR radar in ships and ground vehicle applications is analysed. If a single antenna beam scans a sector, significant degradations in MTI sensitivity and SAR resolution occurs due to the reduced dwell time on target. Full performance can be achieved by using an ESA antenna with multiple beam generation, or high speed scanning. SAR needs accurate phase error compensation by inertial measurements or auto-focusing due to the non-linear movement path of the antenna. [C6561]

"Techniques of blind SAR processing: theory and practical applications"

Some ideas of blind SAR processing are discussed. The non-stationary model of the SAR images is studied. Autofocusing is also studied. The methods can be used for imaging in transionospheric low frequency SAR, estimation of quality of the SAR images, range processing in UWB SAR, motion compensation in airborne SAR and others. [C6562]

"Azimuth modulation of backscatter from SeaWinds and ERS scatterometers over the Saharo-Arabian deserts"

Saharo-Arabian deserts includes large expanses of sand dunes called ergs. These dunes are formed and constantly reshaped by prevailing winds. We use backscatter (σ_0) measurements observed at various azimuth angles from SeaWinds scatterometer (QSCAT) and ERS scatterometer (ESCAT) to determine the σ_0 azimuthal modulation over the sand dunes. A second order harmonic equation is used to model the σ_0 measurements as a function of azimuth angle and provides similar results for both sensors. Images of the magnitudes of the model harmonics show many small-scale linear features corresponding to the large dune fields in the ergs. The images of the phases of the two harmonics are coherent with the large scale topography of the area. Most ergs exhibit isophase related to the general orientation of large- and small-scale features of the sand surface. [C6563]

"A study of low level jet characteristics using a sodar-RASS profiling system"

The development and characteristics of low level jets (LLJs) over the western site of a knife edge mountain in

the Greater Athens area, Greece, is presented. The data were collected for a five-month period, with a commercial sodar-RASS profiling system that was placed at the foot of Mount Hymettus (1026 m) which is located on the north-south axis of the eastern side of the city of Athens. The LLJ cases were classified into three main categories according to the possible forcing mechanism. The classification was based on the background flow, the diurnal course of solar radiation and cloudiness and the atmospheric stability. In order to reveal the mechanism that is responsible for the LLJ occurrences, the non-Coriolis forcing at LLJ heights has been calculated. A simple arithmetic model was applied and the results were compared with experimental findings.

[C6564]

"Processing algorithms for COSMO-SkyMed SAR sensor"

The COSMO-SkyMed (Constellation of Small satellites for the Mediterranean basin Observation) constellation is a project of the Italian Space Agency (ASI) tailored for risk management, coastal zone monitoring and sea pollution in a dual use approach (military and civil applications). The COSMO-SkyMed payload is constituted of a fixed antenna with electronic scanning capabilities in both the azimuth and the elevation planes. It has been designed to implement three different operation modes in order to acquire the images at the required resolution: Spotlight mode, Stripmap mode and ScanSAR mode. This paper describes the algorithms implemented to focus images acquired in the above three different modes together with the first results obtained using simulated and real data. Telespazio, in cooperation with Consorzio Innova and Digimat, is the prime-contractor of the COSMO-SkyMed CREDO project, in which is foreseen the development of a SAR ground processing chain. [C6565]

"ISAR imaging in strong ground clutter by using a new stepped-frequency signal mode"

In this paper we have presented a new mode of stepped-frequency signal. By using this signal, which transmits two pulses of the same carrier frequency at each burst and with this carrier frequency stepped up a Δf in each subsequent burst, the ground clutter can be cancelled by using simple first-order cancellation. A computer simulation is given to illustrate the effectiveness of the proposed method. [C6566]

"Robustness of wavelet-based stereo matching for variable acquisition geometries using simulated SAR images"

It has been shown that digital surface models (DSMs) generated using stereo SAR can be used to ease the phase-unwrapping process during interferometric height model generation. In addition, wider availability of combined stereoscopic and interferometric coverage generated by air- and spaceborne sensors makes the combined use of the two techniques more feasible. This paper describes a series of experiments whereby different stereo acquisition geometries were simulated for an airborne X-band SAR sensor. The product of such a simulation, taking the topography, flight geometry, and local illuminated area into account, is a pair of amplitude images in slant range geometry. The use of such simulations allows rigorous control of error sources. A phase-based, multi-resolution image-matching technique built on the discrete wavelet transform is used to measure the parallax field between simulated image pairs, and a geocoded height map is generated in each case. The robustness of the matching algorithm across variable sensor configurations is thereby determined. Same-side stereo geometry is assumed, as is a typical airborne flight height of 2.8 km. Matching accuracy and the subsequent height accuracy of the DSMs are evaluated by varying the sensor incidence angles and stereo intersection angle. The optimal flight geometry for a test area in Switzerland is determined. [C6567]

"Polarimetric scattering indexes and information entropy of the SAR imagery for surface classification"

The Mueller matrix solution and eigen-analysis of the coherency matrix for completely polarimetric scattering have been applied to analysis of the SAR (synthetic aperture radar) imagery. Usually, the polarization index is defined as a parameter to classify the difference between co-polarized scattering signatures from the terrain surfaces. In this paper, the eigen-values of the coherency matrix and information entropy are derived to directly relate with co-polarized and cross-polarized indexes. Thus, it combines the Mueller matrix simulation, the information entropy of the coherence matrix, and two polarization indexes to yield an overall theory for quantitative understanding of the SAR imagery. This theory is applied to the AirSAR images. [C6568]

"Simulation of polarimetric SAR vessel signatures for satellite fisheries monitoring"

This paper presents a tool able to realistically simulate the SAR raw data recorded by an orbital sensor while imaging a vessel. The simulator is based on a RCS prediction code developed at the UPC, but modified in order to take into account the characteristics of the chirp radar signal and the orbit of the satellite. The vessel models can be generated with commercial computer-aided-design packages with a high degree of detail and fidelity.

The simulator is able to calculate the full-polarimetric raw data and will be used to develop vessel classification algorithms based on polarimetric decompositions. Existing or new sensors can be simulated to study its limitations and suggest new configurations to improve its applicability to the problem. [C6569]

"Generation and error analysis of DEM using spaceborne polarimetric SAR interferometry data"

From the SIR-C polarimetric L-band data of Hotan, China, on 9 and 10 October 1994, the DEM of polarimetric SAR interferometry (Pol-InSAR) and the conventional L-band HH-HH interferometric pair are extracted. The difference of DEM generation using Pol-InSAR and conventional InSAR is discussed in detail. Based on the result of comparison and analysis of two DEM, it is concluded that the accuracy of DEM generated from the polarimetric SAR Interferometry data is significantly improved, especially for the area covered by rich vegetation with enough high coherence, the error less than 10 m. Finally, error sources of DEM generated by polarimetric SAR interferometry are further analyzed. [C6570]

"Quantitative assessment of interferometric SAR images registration accuracy"

Accurate registration of images is very important for interferometric SAR topography mapping. The interferogram (phase pattern) extracted from the conjugate product of two complex images registered with different registration algorithms will be slightly different too. In this paper, we investigate the theoretical relationship between registration accuracy and probability of residue. Based on the derived model, we present that the number of residues can be used as a criterion to judge the registration accuracy and select the optimal interferogram. A pair of ERS1/2 SAR images has been used to illustrate the effectiveness of this means. [C6571]

"The DEM generation of a volcano using airborne SAR interferometry"

The airborne interferometric SAR technique enables us to generate a digital elevation model (DEM). However, in the mountainous area with steep terrain, we cannot obtain some DEM data because of radar shadowing, layover, etc. To generate the complete DEM of the observed area, it is necessary to observe with different incident angles and directions, and compound some DEMs obtained from the data of different incident angles and directions. In addition, if we use a light airplane, which is much affected by turbulence, the generated DEM contains large height errors caused by the intense body motion. Therefore, in case of the map projection, location errors are caused. As a result, it is very difficult to compound the DEM with accuracy. The volcanic eruption of Miyake Island in Japan occurred in July 2000, caused large-scale cave-in. We observed the crater by airborne interferometric SAR with two different incident angles from four directions in order to generate the DEM of the inside of the crater. After data acquisition, we tried to improve the accuracy of the DEM. The method is to iterate the following process, namely motion compensation considered to the rough target height in the azimuth compression in time domain and the interferometric SAR processing. Then, we were able to generate a comparatively accurate DEM, which covers the whole of Miyake Island with the inside height information of the crater. [C6572]

"Digital terrain elevation models produced using radar altimetry and GPS data"

Acquisition of any airborne geophysical data set involves two parameters: measurement of the actual signal being sought and definition of the position where each data observation is acquired. GPS provides accurate estimates of the location of the sensor position relative to a defined ellipsoid. If at the same time one measures the distance from the observation platform to the surface of the Earth, using a radar altimeter, it is then possible to obtain an estimate of the elevation of the Earth's surface at that point. By generating a grid image of discrete elevation data it is possible to produce a digital terrain elevation model (DTEM) of the survey area. Most aeromagnetic surveys comprise a series of flight lines and orthogonal tie-lines. With ideal data a second pass over the same location (either on the tie-line versus the flight-line, or even on a subsequent survey) should give the same elevation. However, attributes of the source data and characteristics of the terrain being modeled can significantly affect the accuracy of results. Comparing elevation data generated from two aeromagnetic surveys of the same area in Southern Alberta shows it is necessary to apply a series of corrections to elevation data just as one might with aeromagnetic data. [C6573]

"Empirical determination of thermal noise levels in synthetic aperture radar"

Thermal noise in synthetic aperture radar can be significant when working with dark targets. This paper outlines an empirical method of determining thermal noise levels for Radarsat beam modes ST 5, ST 6 and ST 7. Calm water bodies are the reference targets that are used in the empirical analysis. The backscatter from these targets is assumed to be very close to the noise floor. This empirical method is compared to a theoretical calculation based on nominal values from the Canadian Space Agency. Using the theoretical method the user is responsible to determine additional processing parameters applied to the data during processing and subtract those back out

from the image. This method may not account for all the possible contributing factors to thermal noise levels. [C6574]

"Velocity estimates from fully polarimetric SAR"

Fully polarimetric SAR data provides sufficient information so that some level of feature attribute classification, is usually possible for signatures found in these images. In particular, polarimetric analysis can provide structural information from SAR image signatures for some target types. Additionally, although not commonly recognized, there is evidence that polarimetric SAR data collected from systems similar to the C/X SAR (and the future RADARSAT 2) can also provide velocity information. This velocity information is not an attribute of the polarimetric ellipse information, but rather a consequence of the system's data acquisition method and the provision that the reciprocity relationship is assumed. Here, an example is presented which indicates that this velocity information is likely available in polarimetric data. This capability has great potential for classification purposes, since both velocity and structural properties of an imaged feature may be deduced from the same data acquisition. While the velocity estimates may have some limitations compared to Along-Track InSAR systems, this information is readily available from fully polarimetric SAR systems, such as the future RADARSAT 2. [C6575]

"Seasonal and diurnal changes of polarimetric parameters from crops derived by the Cloude decomposition theorem at L-band"

The objective of this study is to analyse and interpret the seasonal and diurnal changes of polarimetric parameters derived by the Cloude decomposition theorem. The investigations were carried out on polarimetric E-SAR data at L-band. The seasonal scattering behaviour of cereals strongly depends on the local incidence angle. Mainly surface scattering and double bounce processes contribute to the radar backscatter. Broad-leaf crops are characterised by a pronounced contribution of all scattering processes to the radar signal. With respect to diurnal variations of the polarimetric parameters due to dew and interception no significant changes could be determined. Nevertheless, the changes of the σ^0 -values indicate an increase in volume scattering with moisture for all crops, whereby the contribution of the other mechanisms decreases for wet plant surfaces. [C6576]

"A synoptic visualisation of fully polarimetric SAR data-an annotated example icon"

This paper explores an example SAR data set that has been displayed using a new method of visualising polarimetric data. It is based on an iconic representation of information within a pixel, which allows for the complete polarisation response to be viewed simultaneously across the image. An example from a test site in Sweden is presented, with a detailed description of how such an image can be interpreted. This will be through particular examples of polarimetric responses correlated with features in the landscape. [C6577]

"Matching criteria for radargrammetry"

The aim of this paper is to study the use of cross-correlation for radargrammetric applications. Two other criteria derived from the mean square error analysis are proposed. These three criteria are studied first through their distributions computed using simulated data, and secondly when applied on synthetic and real SAR images. Besides, the influence of the use of logarithm or averaged data is studied. [C6578]

"Mars electromagnetic environment: insights from field analysis at Earth analogs"

Active and passive low frequency electromagnetic sounding may be very useful to monitor Mars subsurface conductivity in order to detect the presence of water. However, without knowing more about the electromagnetic noise levels, the above possibilities remain uncertain. The paper presents a research activity aimed at the characterization of Martian electromagnetic environments using Earth's analogues. The scientific basis of the research and some preliminary tests on implemented instrumentation are described. [C6579]

"A study on the surface temperature distribution and the urban structure in Tokyo with ASTER and LIDAR data"

The purpose of this paper is to understand the relationship between the surface temperature distribution and urban structure in Tokyo metropolitan area. ASTER data and LIDAR data both are used for this analysis. The daytime (2001.9.24 at 10:39 JST) and night (2001.9.22 at 21:54 JST) scenes of ASTER TIR are used for the surface temperature in daytime and night. The same daytime scene of ASTER VNIR is also used for the land-cover. LIDAR data, 3D point clouds from the remote airborne mapping system, is used for the building height. As results, the distribution of the surface temperature is high at residential areas and low at business centers and main roads in daytime, and then it is reversed in night. The correlation between the surface temperature and the

urban structure shows 1) green areas have a good impact on the urban heat environment and these areas are not enough, and 2) tall buildings make shadows and fall the surface temperature in daytime, but raise it for obstructing winds in night. [C6580]

"Ocean Observer SAR requirements and instrument characteristics"

This paper is a brief summary of the synthetic aperture radar (SAR) user requirements, satellite requirements, and instrument requirements for the proposed, but yet unfunded, U.S. Ocean Observer satellite. [C6581]

"ENVISAT ASAR in disaster management and humanitarian relief"

Space-borne SAR has a good potential to support disaster management and humanitarian relief projects thanks to its all-weather capability, its capabilities for change detection, the large existing data archives, and, of course, the geometric and thematic information content of the images. Basic processing techniques, including precision image co-registration, multi-temporal analysis, terrain corrected geocoding, interferometry, and radargrammetry, are well developed and operational. This contribution is an assessment of possible roles of space-borne SAR and in particular ENVISAT ASAR in disaster management and humanitarian relief projects. Relevant additional functionality of ASAR as compared to ERS-1/2 comes from the beam-steering, multipolarization, larger incidence angle, wide-angle, and scan-SAR capability. [C6582]

"An aerosol lidar model program used for the Center for Lidar and Atmospheric Sciences Students lidar system"

A portable, eyesafe, 3-D scanning aerosol lidar system designed and operated by the Hampton University Center for Lidar and Atmospheric Sciences Students (CLASS) is introduced. A mathematical lidar model program wrote using MathCAD software being developed and used by the student lidar team in CLASS is presented. [C6583]

"On the homomorphic filtering by channels' summation"

A simple method to reduce the speckle in the multichannel SAR images consists in channel summation. Developed, originally, for the multi-look treatment, this method may be used also for other multi-channel images, if features' integrity is not a first concern. In the case of the multi-temporal sets, the channel summation leads, usually, to a non-uniform speckle reduction. This nonstationarity of the residual noise is a negative effect since it excludes a series of speckle specific treatments that could be applied subsequently. Our paper shows that this drawback can be removed if the summation is realised in the homomorphic space. More precisely, by taking the logarithm of the images, before summation, and the exponential, subsequently, we obtain a uniformly denoised image, disregarding the channels' content. We give the mathematical support for the calculation of the coefficient of variation of the residual noise in the case of the homomorphic summation, and we test our result by comparing this theoretical value with the coefficient measured with the radial sector method. [C6584]

"System for automatic registration of remote sensing images"

Describes a system for automatic and semi-automatic registration/mosaic of remote sensing images. Information provided by the user can be used to speed up processing or to avoid mismatched control points. A statistical procedure is used to characterize good and bad registrations. Based on this "good fit-bad fit" statistical test the user can stop, modify the parameters, or continue the processing. Several tests have been performed by registering optical, radar, multi-sensor, high-resolution images and video sequences. We have included very difficult image registration examples in order to show the strengths and limits of our system. An online registration system demo containing several examples can be executed using a Web browser. [C6585]

"Polar Stratospheric Cloud (PSC) classification using LIDAR measurements from the recent SAGE III Ozone Loss and Validation Experiment (SOLVE)"

Lidar measurements from the recent SAGE III Ozone Loss and Validation Experiment (SOLVE) have been used to identify the number of classes of Polar Stratospheric Clouds (PSCs) and their corresponding characteristics. The backscatter lidar, flown aboard a DC8 aircraft, measures profiles of backscatter at 532 nm and 1064 nm, and depolarization at 532 nm. These data along with the color ratio were used to categorize PSCs using a clustering algorithm. For each group or cluster, the central values or medoids describe the optical characteristics of the clouds. For this preliminary study, five such groups were determined with medoid scattering ratios of 1.13, 11.90, 47.68, 71.07, and, 88.96 at 532 nm. The mean quality index of 0.82 for the five groups shows that the clusters are sufficiently distinct from each other. [C6586]

"Comparison of InSAR capability for land subsidence detection between C-band and L-band SAR"

Investigates the capability of interferometric SAR (InSAR) using C-band (ERS) and L-band (JERS-1) SAR data for land subsidence detection in urban and rural areas. The Kanto Plains and the Saga Plains were selected as the test site. In the Kanto Plains, several continuous land subsidence areas are found both in urban and rural areas, while in the Saga Plains, they are located only in rural areas. We used several data pairs with different time intervals from two to five years from ERS and JERS-1 SAR data, in which observation periods nearly correspond with each other. The land deformation patterns were compared with each other in the data pairs of corresponding observation periods. In the Kanto Plains, the subsidence amounts in urban areas detected by JERS-1 were smaller than those detected by ERS, which might be due to the difference of minimum detectable subsidence. However, JERS-1 could detect major subsidence areas in rural areas, while ERS could hardly detect them. In the Saga Plains, ERS could not detect any subsidence in rural areas, while JERS-1 succeeded in detecting a significant one even by using the data pair with a five-year interval. These results verify that L-band InSAR will be a practical tool for land subsidence monitoring of the Japanese Islands, especially by using ALOS/PALSAR to be launched by Japan in 2004. [C6587]

"Microwave and optical remote sensing study of Boone County, Missouri"

Integration of synthetic-aperture radar data with spaceborne optical data offers potential for improving land-use classification for local and state government applications. Remote sensing techniques using optical sensor data are well established for local and state government applications. As commercial SAR products become available at lower costs, local government applications using optical based classification can incorporate SAR sensor data into their processing. For this study, we orthorectified and analyzed Radarsat SAR data and Landsat TM data that covers Boone County, Missouri. Optical and SAR sensor data are co-registered for data fusion and classification process. Training data from sites throughout the study area are used to verify and validate the classification of five classes: crops, water, built-up, forest and grass. We present preliminary results of our study. [C6588]

"C-band radar for soil moisture estimation under agricultural conditions"

A time series of space-borne ERS-2 SAR satellite data is used for the temporal monitoring of the soil moisture in Sukhothai area, Thailand. The backscattering coefficient σ_0 from the SAR data has shown reasonable correlation and sensitivity to the observed volumetric soil moisture at 5 cm depth in Thailand at the field scale. A tandem coincidence of the ERS-2 and Radarsat missions, with two different polarizations, over the area provided an opportunity to estimate soil moisture over a large area by inverting a semi-empirical backscattering model. The estimates were validated with the field observations over a small area and are in good agreement. Furthermore, the soil moisture at a point was simulated using three hydrological models and compared with the radar backscattering and the point observations. There are large variations in the responses of these approaches. [C6589]

"Estimation of soil water content in the Negev Desert open areas using archived ERS SAR images"

This paper presents a study that was conducted using ERS SAR archived images to assess the soil water-content of open desert areas containing two different soil types (loess and sand). For this purpose we used the different look directions model proposed by Blumberg and Freilikhher. The results show that the soil moisture predictions are almost equal to those known as typical for these soil types at the equivalent seasons. [C6590]

"Synthetic aperture radar for DEM generation in snow-covered mountain terrain"

Digital elevation model (DEM) generation has mainly been based on optical imagery and photogrammetric techniques. However, in recent years there has been a growing interest in the use of synthetic aperture radar (SAR) for this purpose. It is mainly two techniques that are used, SAR interferometry and stereoSAR. We have studied the influence of the snow cover on the accuracy of SAR derived DEMs. Three different Interferometric ERS1/2 tandem acquisitions are investigated, a dry-snow case, a wet-snow case and a no-snow case. It is found that with wet-snow the InSAR DEM has lowest accuracy. The dry-snow DEM is less accurate than the no-snow DEM, even though the coherence is higher. This is explained by a redistribution of dry snow that can degrade the accuracy of interferometric DEM but still maintain high coherence. Six different Radarsat s2-s7 stereo pair combinations covering dry-snow/dry-snow, wet-snow/wet-snow, partly-snow/partly-snow, no-snow/no-snow, dry-snow/no-snow and wet-snow/no-snow situations are considered. With stereoSAR it is observed that the type of snow cover has no significant influence on the DEM accuracy. This is even the case for dry-snow/no-snow and wet-snow/no-snow stereopairs, even though these DEMs are less accurate than those originating from data with the same snow cover. [C6591]

"Potential of RADARSAT-2 for sea ice classification"

Polarimetric data acquired by the CCRS CV-580 airborne SAR are used to assess the capability of RADARSAT-2 for operational sea ice classification. The information content of the polarimetric data is illustrated by showing how specific scattering mechanisms are portrayed by the entropy, anisotropy and α -angle features. Ice type classes are derived from the full polarimetric data set using a complex Wishart classifier. The classes are then mapped into 2-D scatterplots to compare the information content between dual and fully polarimetric data. While dual polarimetric data are an improvement over single channel data, it is found that fully polarimetric data are needed to provide accurate ice classification performance. [C6592]

"Radar measurements of ice sheet thickness of outlet glaciers in Greenland"

We have conducted airborne measurements over the Greenland ice sheet from the NASA P-3B aircraft using a 150-MHz coherent radar depth sounder to obtain extensive ice sheet thickness measurements. Simultaneous measurements of ice sheet elevation were also made using a laser altimeter. In outlet glacier areas along the ice sheet margin, the ice surface is characterized by a very rough, crevassed surface near the calving front. The rough ice surface generates signal clutter, which can mask the bottom echo. We are developing a technique to remove the surface clutter component from the signal to reveal the bottom echo, providing a complete ice thickness survey to the calving front of outlet glaciers. This technique makes use of a dense array of ice surface elevation measurements provided by the laser altimeter to characterize surface roughness. Surface roughness parameters are then used in a backscatter model to characterize the clutter waveform, which can be subsequently removed from the radar signal. [C6593]

"RADARSAT-1 synthetic aperture radar iceberg detection performance ADRO-2 A223"

Since the initial Canadian Space Agency (CSA) ADRO-1 program in 1997, C-CORE has been investigating the capabilities of the RADARSAT synthetic aperture radar (SAR) satellite for the detection of icebergs. This multiyear program has received support from a variety of sources including the CSA's ADRO-1 and ADRO-2 programs, the Canadian Ice Service, and a consortium of oil and gas companies operating on the east coast of Newfoundland. During this program, various RADARSAT modes, including Wide2, Wide3 and ScanSAR Narrow-B have been validated. Threshold and probability of detection curves were generated for small, medium and large sized icebergs in various wind conditions. For these curves, the radar cross-section values from ocean clutter were modeled using the CMOD4 wind model and verified with point source wind measurements. The performance curves show a reasonable success rate for detecting icebergs whose size is on the order of the resolution cell, despite the significant effect of wind speed on detection. [C6594]

"Third party encroachment monitoring using RADARSAT-1, IKONOS, EROS-A1 and simulated RADARSAT-2 imagery"

Third party mechanical damage is the principal cause of on-land pipeline failure and is related to such activities as road construction, cable laying, farming and residential and commercial land development. Earth observation data with wide area coverage offers an alternative to the high cost of aerial patrol on large pipeline networks. In order to demonstrate the feasibility of using satellite imagery to detect third party encroachment upon pipeline rights-of-way, two field experiments were carried out in 2000 and 2001. These experiments were conducted at test sites in Alberta and Ontario, Canada. Satellite imagery evaluated during these trials included IKONOS and EROS-A1 optical imagery, RADARSAT-1 fine beam imagery and simulated RADARSAT-2 imagery. Both IKONOS and EROS-A1 imagery were effective in detecting a range of vehicles in areas free of cloud cover. RADARSAT-1 images were effective in the detection of larger vehicles independent of atmospheric conditions. Using simulated RADARSAT-2 it was possible to detect smaller vehicles not previously detected with RADARSAT-1 imagery. [C6595]

"An update in the evolution of Radarsat1 azimuth Doppler for differential interferometry purposes"

Clarifies the use of interferometry on Radarsat-1 in mid- and long-term intervals between two acquisitions, taking into account changes in the evolution of the azimuth Doppler since April 1999 to maximize coherence and signal to noise ratio. This study is based on fine mode acquisition over Piton de la Fournaise volcano (La Reunion island) and shows examples of displacement fields of the July 1999 eruption. [C6596]

"A new empirical model to inverse soil moisture and roughness using two radar configurations"

A new empirical model for the retrieval, at a field scale, of the bare soil moisture content and the surface roughness characteristics from radar measurements is proposed. The derivation of the algorithm is based on the results of 3 experimental radar campaigns conducted under natural conditions over agricultural areas. Radar

data were acquired by means of several C-band space borne (SIR-C, RADARSAT) or helicopter borne (ERASME) sensors. This algorithm is more specifically developed using the radar cross-section σ_0 (HH polarization and 39° incidence angle off nadir), namely, σ_0 (HH,39), and the differential (HH polarization) radar cross-section $\Delta\sigma_0 = \sigma_0,23^\circ - \sigma_0,39^\circ$ in terms of an original roughness parameter, Zs, and Mv. An inversion technique is proposed to retrieve Zs and Mv from radar measurements. [C6597]

"Moose Mountain Virtual Explorer: A learning and ground-truthing tool to explore high-resolution remote sensing and geoscience data in mountainous area"

The objective of the Moose Mountain Virtual Explorer system (MMVE <http://www.cgq-qgc.ca/geoide/>) is to provide access, through an efficient web interface, to a geologically-rich digital library to remote sensing and geoscience researchers, resource explorationists and students. Data sets are all geographically located within a rugged area of the Rocky Mountain Foothills of Alberta. The library collection was acquired through field campaigns, and airborne and satellite acquisitions, over the course of a 3-year canadian GEOIDE Network of Excellence project (Moose Mountain project, Lebel et al. 2001). High-resolution aerial orthoimages, oblique aerial and terrestrial photographs, radar imagery, geological data, maps and cross-sections constitute the database content. The project is nearing completion and aims to promote the integration of geoscientific, photogrammetric and remote sensing data as a guide for oil and gas exploration in mountain fold and thrust belts. Moose Mountain was selected because it represents a surface analogue of complexly faulted carbonate rock formations that host a gas field at depth. MMVE can thus be used to explore the complex relationships that exist between rock properties and hydrocarbon reservoir favourability within the context of small and subtle gas plays that are being explored in the deep subsurface of the Canadian Cordilleran Foothills. [C6598]

"Automatic registration of radar imagery"

Registering radar imagery is not an easy task since the images may be heavily contaminated with noise. Strong speckle noise can produce artifacts that mimic good control points and may produce low precision or even wrong registration. This article presents an automatic registration method that tries to overcome these problems. The method was originally developed for optical images and adapted for radar images. [C6599]

"Range interferometry technique to determine radial wind"

Presents a range interferometry technique to determine radial wind. The wind velocity is obtained by the ratio of range cross-correlation function at positive and negative lags. The feasibility of the method is studied through error analysis. The standard error of the estimated radial wind is derived and its sensitivity to range resolution, sample time and turbulence is analyzed. [C6600]

"Hierarchical segmentation of polarimetric SAR images"

A hierarchical stepwise optimization process is used for polarimetric SAR image segmentation. The process starts with small sets of pixels as segments and then sequentially merges the segment pair that minimises a stepwise criterion. The polarimetric information could be represented by a covariance matrix. The proposed criterion is based upon the testing of the equality of covariance matrices of adjacent regions. The segmentation of SAR images is greatly complicated by the presence of coherent speckle. We are using spatial constraints and contour shapes in order to improve the segmentation results. [C6601]

"Phase noise countermeasures for synthetic interferogram generation"

During synthetic interferogram generation (whereby a DEM and platform positions are used to calculate expected fringes), an interpolation step is necessary during the transformation from map geometry into the slant-range geometry of the radar image. Particularly in hilly terrain, assumptions made during the interpolation step can have an impact on the accuracy of the simulation. We investigate differences between simulations made using differing assumptions and interpolation methods, and provide algorithm recommendations. We show results both from one-pass methods (where no knowledge of each radar geometry grid location's neighbouring slopes is assumed) and a two-pass method (improved accuracy at the price of increased computational cost). In the latter method, after the initial pass through the DEM, a second-pass range-sorted traversal is made (allowing knowledge of each point's immediate neighbours, even in hilly terrain) before the final interpolation for each point. We highlight the effects of differing algorithms for various terrain types, and discuss how assumptions about the extent of topography within a scene can be used to accelerate generation of the synthetic image products. We demonstrate the differences using simulated ASAR imagery produced using ERS data. [C6602]

"The new curvature methods of image fine registration for synthetic aperture radar interferometry"

The image fine co-registration whose accuracy has a direct influence on DEM accuracy, is more important for synthetic aperture radar interferometry (INSAR). The co-registration based on intensity values is easy to implement and computationally efficient but the least accurate. To get better accuracy, we must consider the characteristics of the complex images intensity, the geometrical characteristics of the distributed targets, and the correlative characteristics between the two characteristics. This paper presents the curvature method for fine co-registration of the images. It makes use of not only the intensity value of the pixel, but also the geometric distributing of the group of pixels. At the same time, the characteristic surface is built by combining the two characteristics. The curvatures of some curves in surface show the geometric characteristics of the surface, which have no relation with the surface flexibility and its coordinate position. The characteristic of the registration objects is obvious when using the curvature of surface as the fine co-registration object. This method is feasible and easy to be implemented. Detailed theoretical deduction and practical research is done in this paper. The experiment result shows that the registration accuracy is better than that of traditional methods. [C6603]

"Determination of the rheology of Arctic glaciers using multi-temporal ERS1/2 SAR interferograms combined in a least squares adjustment"

We propose a general method to separate topography- and displacement-related phase components in repeat-pass interferograms based on adjustment theory. The method is exemplarily demonstrated for the analysis of rheology of Arctic glaciers. More than two multitemporal interferometric data sets are combined in a least squares adjustment based on a Gauss-Markov model. Within the adjustment algorithm glacier flow is modeled by a polynomial function. This technique on the one hand allows us to improve the separation of topography- and displacement-related phase components and on the other hand provides glaciological information about the flow characteristics of observed glaciers. [C6604]

"Land cover classification of polarimetric synthetic aperture radar (POLSAR) data based on scattering mechanisms and complex Wishart distribution"

The use of C- and L-band polarimetric synthetic aperture radar (POLSAR) data for classifying land cover features in a tropical area is investigated in this study. The POLSAR data were acquired during the NASA/JPL PACRIM-1 mission over the northern part of Peninsular Malaysia on 3rd December 1996. Prior to classification, the Lee polarimetric filter was applied to the complex covariance matrix for speckle suppression. In unsupervised classification, the scattering mechanism of each pixel in the speckle-suppressed images was analyzed and grouped into one of the three categories: (1) odd-bounce, (2) even-bounce, or (3) diffuse scattering. Training samples were then generated from the outputs of the unsupervised classification, to be used in subsequent supervised classifications of various frequency and polarization combinations. The Kappa statistics computed for classification using single-frequency fully polarized C- and L-band data were 0.69 and 0.73, respectively. An improvement to 0.79 was achieved by using the dual-frequency (combined C and L bands), fully polarized data in the classification. [C6605]

"Polarimetric target decomposition and physical interpretation of NASA (JPL) AIRSAR data in mountainous terrain"

Two types of polarimetric Target Decomposition (TD) theories were used to investigate the effects of surface slopes on the physical scattering mechanisms over mountainous scattering surfaces. This study is implemented with the L- & P-band NASA (JPL) airborne SAR (AIRSAR) data, which was acquired during PACRIM-II Korea campaign in September 2000. Although the dominant scattering mechanism of mountainous forest area is volume scattering in pine forest scattering surface, detailed scattering mechanism varies with respect to the local incidence angle variations due to the local topography and wavelength. [C6606]

"Unsupervised approach for polarimetric SAR image classification using support vector machines"

In the previous works S. Fukuda et al. (2001), we developed the classification method of land cover from polarimetric SAR data using support vector machines (SVMs). As the extended study of the SVM-based classification method, an unsupervised approach is presented in this paper. Since SVM, originally a technique for pattern recognition, can not be applied to unsupervised classification straightforwardly, we propose the automatic selection scheme of representative training areas based on the number of the closest training samples to the separating hyperplane in the feature space; such samples are called the support vectors. In the experiment for a part of the AIRSAR Flevoland data including five classes of agricultural crops, the scheme performs successful classification, which can bear comparison with the supervised result. [C6607]

"Multiband SAR classification using contextual analysis: annealing segmentation vs. a neural"

kernel-based approach"

In this paper we derive two techniques for the classification of multipolarimetric/multifrequency SAR images, based respectively on a statistical and on a neural approach. Both techniques are especially designed to exploit of the spatial structure of the observed scene, thus identifying homogeneous regions that can be jointly classified. Such techniques are useful when looking at medium to large scale features, like the boundaries between urban and non-urban areas. They are applied to a set of multipolarimetric/multifrequency SIRC images of a urban area, to test their effectiveness in the identification of built up areas. A quantitative comparison of the results achievable with the two techniques is carried out, showing a similar behavior, even if the statistical approach tends to achieve better performance. [C6608]

"Coherence region shape extraction for vegetation parameter estimation in polarimetric SAR interferometry"

Polarimetric SAR interferometry (POLINSAR) provides volumetric information about electromagnetic scattering processes, whereas standard INSAR assumes that only surface scattering is present. Instead of a single complex interferometric coherence for each pixel, POLINSAR observes a polarization-dependent coherence function whose range is called the coherence region. To estimate canopy parameters, the shape of this region must be matched to predictions from scattering models. For computational efficiency, the region must be represented by a small number of samples. Current sampling methods find the stationary points of coherence magnitude or phase; it is questionable whether the coherence region can be characterized adequately with so few samples. We have developed an algorithm for sampling the outer boundary of the coherence region. We formulate the problem of finding the minimum and maximum real part of the coherence as an eigenvalue problem. The solutions specify two points on the boundary. Other points are found by applying a phase shift to the POLINSAR cross-correlation matrix. The mathematical literature shows that the coherence region is convex, and hence the algorithm finds the entire boundary. We present a comparison of boundary sampling to standard methods on L-band POLINSAR data from the SIR-C platform. It is evident that boundary sampling describes the shape of the coherence region more thoroughly than other methods. [C6609]

"SAR image matching using the edge strength map"

Based on the principle of stereovision, radargrammetry uses the parallax between a couple of SAR images to reconstruct the 3D information of the scene. In the radargrammetric process, the matching step is the most problematic one, due to speckle noise. In this paper, we present our radargrammetric chain, and then, focus on the matching module we are developing, which includes an edge detection to improve the reconstruction. [C6610]

"Simulation on the extraction of ships' images embedded in speckle using cross-correlation of multilook SAR images and applications to Radarsat data"

Preliminary results are reported on the simulation of ship detection and applications to Radarsat data using coherence images computed from cross-correlating multilook SAR images. The traditional techniques of ship detection by radars such as CFAR (Constant False Alarm Rate) rely on the amplitude data, and therefore the detection tends to become difficult when the amplitudes of ships images are at similar level as the mean amplitude of surrounding sea clutter. The proposed method utilizes the property that the multilook images of ships are correlated, while those of sea surface are covered by uncorrelated speckle. Thus, cross-correlation of multilook images yields the different degrees of coherence between the images of ships and water. The ability of the technique has been illustrated in the previous reports using Radarsat data, where the images of ships are clearly visible. In the present article, we examine the technique when the ships' images are embedded in the surrounding sea clutter. [C6611]

"Gamma mixture modeled with "second kind statistics": application to SAR image processing"

SAR images are classically analyzed with the help of Goodman approach and multiplicative noise. By this way, speckle is modeled by a Gamma law (for intensity images). A new approach based on "second kind statistics", J. M. Nicolas et al., (2000), identifies multiplicative noise as a "Mellin convolution", J. M. Nicolas et al., (1998), yielding oversimple expression when texture is not homogeneous. In this article, we propose to use this new approach for solving the problem of binary additive mixture of Gamma law, J. M. Nicolas (2001), and to apply the results to SAR image processing. [C6612]

"Edge preservation evaluation of digital speckle filters"

This paper makes three contributions. It clarifies the definition of edge preservation in SAR images. The

definition of edge preservation is important for edge preservation evaluation of digital speckle filters. Only if the definition of edge preservation is reasonable, can the edge preservation evaluation be successfully performed. Second, an algorithm to evaluate edge preservation of digital speckle filters is proposed. Third, we analyze the reason why the enhanced Lee, enhanced Frost, gamma, and Kuan filters cannot effectively preserve edges. The main contribution in this paper is that we clarified the difference between edge preservation and edge point preservation. It is important to develop new methods to reduce speckle in SAR images, which can successfully preserve edges in smoothed images. [C6613]

"From Gaussian to inverse Gaussian statistics in SAR imagery"

Among the family of exponential distributions the normal or Gaussian distribution plays a fundamental role in natural environments-above all-due to its symmetrical properties. In distributed terrain the size, position and orientation of scatterers within the ground resolution cell of a SAR system is Gaussian distributed as well as their backscatter over a series of radar pulses; particularly when the size of scatterers is of similar magnitude as the radar wavelength and their number is greater than 10. Now, the motion of the SAR system influences the statistics of backscatter in such a way that its symmetrical properties are lost to asymmetry. The more the structure of terrain changes from homogeneous to heterogeneous (from pasture to forest) and from heterogeneous to extremely heterogeneous (from forest to urban) the more the statistics of SAR backscatter deviates from Gaussian. Hence, another distribution, the inverse Gaussian, arises most naturally for backscatter of distributed targets under the assumption that the single scatter cell keeps its Gaussian behavior. (The term inverse refers to the cumulant generating function of this distribution being the inverse of the Gaussian one.). [C6614]

"MAP-MRF filtering of SAR interferometric phase fields"

Presents a new technique, based on a MAP (maximum a posteriori probability) approach, for filtering interferometric phase images. To describe prior knowledge about the unknown image, a MRF/Gibbs model is adopted, and its energy function is defined so as to impose two desirable constraints on the solution: the absence of residues (which leads to unambiguous phase unwrapping) and the smoothness of the phase field (which reduces noise). MAP estimation is carried out by simulated annealing, obtaining accurate results even for low values of the coherence. [C6615]

"Phase unwrapping of SAR interferogram based on dyadic wavelets"

A new phase unwrapping algorithm based on fringe line detection is presented. Dyadic wavelet theory is used to extract the multi-scale edge of an SAR interferogram. The phase characteristic of the interferogram are derived utilizing an active contour algorithm of the gradient vector flow. [C6616]

"Balancing rewrapping error and smoothness in two dimensional phase unwrapping problems"

Describes two classes of two-dimensional phase unwrapping algorithms. It is shown that combining advantages from each of these classes is useful in improving phase-unwrapping solutions. [C6617]

"Signal operator cores for SAR real time processing hardware"

This work deals with the mathematical formulation and hardware implementation of computing methods for the action of one and two-dimensional operators on discrete, finite length signals representing real time synthetic aperture radar (SAR) image formation data. We give emphasis to modular and scalable computing methods. The complex Hilbert spaces $l_2(\mathbb{Z}N)$ and $l_2(\mathbb{Z}R\mathbb{Z}S)$ are used to represent signals of very large size. These spaces are converted into algebras using circular convolution and cyclic Hadamard signal operations. The operators themselves are also represented as being part of matrix algebras for computational studies and algorithm development. Special attention is given to unitary operators, such as the discrete Fourier transform (DFT), and to finite impulse response (FIR) operators. For FIR operators, we concentrate on the study of properties of convolutional algebras and present new mathematical formulations of filtering theories. [C6618]

"Image classification in complex spaces"

Addresses issues related to classification of images in complex spaces. The image is represented in terms of phase and amplitude components. The classifier optimizes functions of joint real and imaginary conditional probability density functions. A bound on the total probability of errors in terms of Rayleigh quotient is derived and compared to the cases where a non-complex amplitude-only signal is used. Examples of application of the proposed approach on polarimetric radar imagery indicate several orders of magnitude improvement in performance. [C6619]

"Automatic multi-sensor image registration by edge matching using genetic algorithms"

Automatic registration of images from different sensors is often needed in near-real-time applications. In this paper we describe a method for performing this task. SAR and SPOT images are discussed [C6620]

"A compact real-time SAR processing system using the highly parallel HiPAR-DSP 16"

At the Laboratorium für Informationstechnologie the HiPAR-DSP 16, a parallel digital signal processor (DSP) optimized for image processing algorithms, has been developed. We present a design of a compact multi-DSP board utilizing the HiPAR-DSP 16. Two boards were implemented: an application development board with a PCI interface and a board for SAR processing. With a computational power of up to 15 GOPS this board is suitable for real-time SAR processing, as an estimation for an wk algorithm (range line length of 4096 samples, PRF of 600) shows. A volume of 1604230420 mm³ and a power consumption of less than 20 W enables on-board integration. The first version of the board is used for filtering of SAR data to show the capabilities of the system [C6621]

"Super-resolution of polarimetric SAR images of a ship"

This paper deals with the application of modern spectral analysis (SPECAN) techniques to polarimetric Synthetic Aperture Radar (SAR) data. The purpose is to use all the information provided by images of the same SAR scene at the different polarimetric channels (HH-VV-HV-VH) in order to improve the geometrical resolution with respect to the resolution corresponding to the transmitted bandwidth and the synthetic aperture length. One practical motivation for this work is to improve radar image quality so that subsequent classification procedures will have greater chance of success [C6622]

"Reduction of cardinal effects in SAR imagery of densely populated urban areas by suppressing strong multiple returns"

In SAR imagery, strong returns from a group of man-made reflectors obscure adjacent target areas leading to a significant loss of information. The wide dynamic range of response levels from urban area is the source to degrade the SAR image characteristic. In this paper, we explore a way to interpret this problem in SAR imaging and propose a waveform design technique to improve target detection performance [C6623]

"SAR images filtering and segmentation: a multiresolution and contextual approach"

In this work we present a mixed contextual algorithm for segmenting SAR-ERS 1 images (© ESA). The first step was to pre-process the original SAR image by means of a polynomial transform based filter in order to decrease the effect of speckle. Segmentation stage was performed as follows: cluster centers were obtained using a non-contextual algorithm; then, based on a Bayes classifier we achieved a first segmentation step, but defining a 'reject class'; finally, rejected pixels were re-classified via a Markovian model. Results obtained show segmented images exhibiting homogeneous regions and a minimal presence of isolated pixels. As well, they evidence that combined use of polynomial transform and Markov random field theory does not introduce a noticeable degradation of edges in segmented regions [C6624]

"Superresolution ISAR imaging by 2-D complex asymmetric half-plane lattice predictors"

An efficient algorithm to obtain high resolution ISAR images in the case of limited frequency band and small angular section is presented. The method is based on the 2-D autoregressive asymmetric half-plane modeling of the backscattered data using a 2-D complex lattice predictor. The locations of the scattering centers are determined by the zeroes of the transfer function of the prediction error filter. A simulation example is included to show the performance of the algorithm [C6625]

"A comparative study of coherence information by L-band and C-band SAR for detecting deforestation in tropical rain forest"

The author studied the applicability of coherence information by C-band SAR from ERS-1 and 2 together with by L-band SAR from JERS-1 for the purpose of monitoring the changes of tropical rain forest due to deforestation. The test site was a southern part of Sumatra Island with 50 by 50 kilometers coverage. The results of this study indicated that the coherence obtained from a repeat-pass pair by C-band SAR was almost useless due to its extremely poor quality. On the other hand, the coherence obtained from a repeat-pass pair by L-band SAR was proved to be useful for identifying the deforested areas together with the coherence obtained from a tandem pair by ERS-1/2. This result suggests the usefulness and the importance of repeat-pass interferometry by L-band

SAR like ALOS/PALSAR for the purpose of monitoring tropical rain forest changes [C6626]

"A multifractal approach for auto-segmentation of SAR images"

A multifractal spectrum, which gives a complete statistical description of images, can be used to characterize radar images. In this paper, a new method based on multifractal analysis is proposed to segment the SAR image into regions and to highlight their boundaries. A computation experiment shows that the segmentation result is encouraging [C6627]

"InSAR coherence estimation for temporal analysis and phase unwrapping applications"

In SAR interferometry, coherence between data acquisitions is potential information on the accuracy of interferograms. In this paper, a new coherence estimation approach is investigated. Our study is based on a binary mixture modelisation of coherence images. A Bayesian criteria is so used to discriminate between the two statistical mixed laws. It is shown that empirical coherence is biased and depends on the number of pixels averaged. The results of this paper can be applied to the estimation of the interferogram noise in interferometric SAR [C6628]

"The effect of free vegetation water on the multi-frequency and polarimetric radar backscatter-first results from the TerraDew 2000 campaign"

This paper presents the first results of the TerraDew research project about the effects of free vegetation water on the radar backscatter signal. The investigations are based on intensive SAR and field measurements of diurnal free vegetation water changes in different vegetation types. The results show a systematic backscatter influence in dependence of the investigated backscatter features (wavelength, polarization, vegetation structure, amount of free vegetation water). The highest backscatter increase is found at C-VV and for grassland (up to 4.5 dB), no significant backscatter change is indicated for L-VV and forested areas. The further investigations will focus on the physical description and simulation of these effects to include them in backscatter models and the evaluation of the impacts for thematic SAR data analysis [C6629]

"Radar remote sensing of a forest at VHF frequencies: a two dimensional full wave approach"

A two dimensional model of forest based on a full wave approach, is developed to describe the interaction between a finite number of rows of trees and a VHF plane wave (20 MHz to 90 MHz). The trees are placed on a ground represented by a lossy medium. The evolution of the scattered electric field with respect to the geometrical parameters of the scene is analyzed, and the results are compared with those retrieved from a simple interferometric model. The case of an object hidden by the trees is also considered in view of detection applications [C6630]

"Small scale properties of the radar backscatter from the sea surface at off nadir angles"

Analyses coherent radar backscatter data from the sea surface at C-band and VV polarization, sampled at 300 Hz. The aim is to understand their usefulness in the investigation of the sea surface properties. The variability of the backscatter intensity I_{bk} at frequencies close to the Bragg frequency suggested a Bragg-like mechanism in the formation of the radar backscatter from patches of Bragg waves randomly distributed in the radar footprint. This led us to consider that both I_{bk} and the associated Doppler frequency f_d have to be computed over time intervals of $O(0.1)$ s, the periodicity of the Bragg waves at C-band and 45 degree of incidence. Shorter time intervals would produce unrealistic estimates. This sets the lowest limit of data sampling for further research [C6631]

"LGA scattering from measured breaking water waves: extension to jetting surfaces"

A numerical electromagnetic technique is used to find the low grazing angle (LGA) microwave backscattering from a series of surface profiles giving the measured time evolution of the crest of a breaking water wave generated in a wave tank. Surfactant was added to the water prior to the generation of the wave, giving more energetic breaking than in previous waves similarly considered. In particular, two well-defined, fairly large jets form during the breaking. The horizontally polarized backscatter exceeds the vertically polarized backscatter as the jets form, giving brief, but large magnitude super events (or "sea spikes"). These events occur although front face of the modeled wave is truncated, eliminating the large-scale multipath to which super events are usually attributed. The Doppler shifts of the backscattering at the two polarizations are also quite different, with the strongest VV signal appearing at the shift associated with the maximum velocity of the jetting, while the strongest HH signals are at lower Doppler shifts associated with the formation of the jets. The shifts from the distributed-surface roughness of the turbulent "Scar" remaining after breaker are that expected from the orbital

motion of the wave [C6632]

"Fractal and multifractal analysis of sea SAR clutter data"

The goal of this work is to investigate on the fractality of the sea clutter collected by SAR systems like the existing ERS1-2 SAR. The analysis of data generated by simulation is performed by using two kind of techniques: 1) Multiscale fractal analysis; 2) Multifractal analysis. The results show that sea clutter retains a few fractal features of the sea. This study is very interesting for applications in the field of sea remote sensing like classification and target recognition [C6633]

"Lava-flow textural trends using SAR: the Virunga Volcanic Chain, East Africa"

Multi-frequency polarimetric Shuttle Imaging Radar-C (SIR-C) data acquired in October 1994 were analyzed for the Virunga Volcanic Chain, East Africa. The synthetic aperture radar (SAR) data can be used to define the roughness, texture, orientation, and dielectric properties of scattering elements of volcanic surfaces. SIR-C acquired C- and L-band SAR in two polarizations, horizontal transmit and receive (HH), and horizontal transmit and vertical receive (HV). The SAR backscatter from the volcanoes is mainly controlled by roughness and vegetation cover, as there is a correlation between radar intensity parameters and age of lava-flow. This is best illustrated by the ratio of C-HV/C-HH, and to some extent, L-HV/L-HH, which show positive linear relationships with age of flow until a threshold age of ~30 years (~12000 days) is reached. The H-polarized incident energy is converted to significant amounts of V-polarized backscatter, so that the cross-polarized backscatter intensity increases with flow age. For flows older than ~30 years, the backscatter signature is from volume scattering due to vegetation cover. The vegetation signature threshold with time can serve as an age proxy to determine recent flank eruption frequency [C6634]

"Speckle reduction of SAR images in the complex wavelet domain"

Dual tree complex wavelet transformation (CWT), proposed by N. G. Kingsbury (1999), is used for speckle reduction of SAR images. The CWT is useful for speckle reduction through its subband images and the speckle reduction is obtained by thresholding the subband-image coefficients of the digitized SAR images. Two thresholding methods are used; soft thresholding and thresholding using non-linear functions which are adapted for each of selected subband and is based on sigmoid functions. The denoising method shows great promise for speckle removal and hence should provide good detection performance for SAR based recognition [C6635]

"The Kirchhoff analysis from one- and two-dimensional random surface with the statistical shadowing function"

In this paper, the bistatic scattering coefficient from one- and two-dimensional random surfaces using the Kirchhoff approximation (KA) with shadowing effect is investigated. The originality of this paper is to include the statistical shadowing function in the average of the scattered field. Although the statistical shadowing function and the scattered field depend on the surface slopes and heights, they are assumed to be statistically independent. Consequently, the shadowed scattering coefficient obtained from averaging the scattered field multiplied by its conjugate, is computed by using the unshadowed scattered field multiplied by the statistical shadowing function. This new model involves an accurate behavior of the scattering coefficient for grazing incidence angles. The model is compared with experimental data from a one-dimensional perfectly-conducting Gaussian rough surface and applied to a two-dimensional sea surface [C6636]

"Application of differential SAR interferometry over the Baegdu stratovolcanic mountain"

Mt. Baegdu, a Cenozoic stratovolcano, was studied using twenty-three JERS-1 SAR and two ERS-2 SAR data sets. We investigated surface changes for 6 years from 1992 to 1998 using three approaches: (i) interferograms of large altitude of ambiguity, (ii) the 2-pass, and (iii) 3-pass DInSAR technique. After analyzing 11 differential interferograms having various time intervals, we suggest that several tens of kilometres of surfaces are subsiding centered around the southwest part of Mt. Baegdu. When the observed displacement is assumed to be only in the vertical direction, the rate of surface subsidence is about 9 cm/year. Although these results are not conclusive due to lack of ground truthing, they must be very useful as background information for long-term monitoring [C6637]

"Estimation of spatial and temporal evolution of vegetation and surface moisture from ERS2 radar in a semi-arid region"

In this paper, a simple model is proposed for retrieving the vegetation cover over soil surfaces from radar signals acquired in semi-arid regions. In Tunisia, vegetation is characterized by the presence of clumps which partially

cover the soil surface. The proposed model describes the relationship between the percentage of covered surface and the measured radar signal. Model simulations compared with actual ERS2 radar data show a very good agreement. A map of the whole studied site (in Tunisia) is then derived combining classification approach and previous modeling [C6638]

"Multi-parameter airborne SAR remote sensing of soil moisture in agricultural area"

This study investigates issues and problems in soil moisture radar remote sensing in agricultural areas as part of the International Surface Parameter Retrieval Collaboration (SPARC). The analysis is based on multi-parameter E-SAR data and intensive field measurements of soil moisture and surface roughness. The analysis of multi-frequency, polarimetric and interferometric backscatter shows the dominance of the roughness signal compared to the variations in soil moisture. Problems on soil moisture mapping were described and discussed in a spatial error evaluation and in a physical backscatter modeling [C6639]

"Detection of seasonal water level changes in Amazon forests from JERS-1 SAR images using isolated strong scatterers"

A new method of detecting and visualizing narrow open-water rivers from JERS-1 SAR images was applied to a series of twenty continuous scenes of Amazon forests observed in May, August, and October, 1996 and February, 1997. The tributaries observed during high water seasons were longer and wider than those observed during low water level seasons. Comparing the 30 year-average of monthly precipitation and the change in the river width, the estimate water retention period of the part of the Amazon forests is about 1~2 months [C6640]

"Applications of Tropical Rainfall Measuring Mission (TRMM) data"

Since the launch of TRMM, over three years of data have been collected. In addition to the archival and distribution of TRMM data, GDISC provides data subsets, and search, access and visualization services. Prototype GIS compatible data sets are created to facilitate wide dissemination to the application users [C6641]

"Retrieval of soil moisture content with the use of neural network-scattering model"

This research is a part of the PacRim-II AIRSAR experiment carried out over Korean peninsula in September 2000 and consists of two parts. One is the analysis of surface roughness characteristics and spatial distribution of soil moisture contents of the test site, acquired as a part of the ground truth survey in Jeju island. The other is the test of neural network-scattering model based estimator for the surface parameter retrieval from polarimetric SAR data. At the time of preparing this paper, we have not received the actual polarimetric SAR data yet and this paper discusses the research approach and research plans. It was tested that when backscatter coefficients of surface are represented as fuzzy numbers, the physical surface parameters are also estimated as fuzzy membership functions [C6642]

"Vehicle-borne laser mapping system (VLMS) for 3-D GIS"

We have developed a vehicle-borne laser mapping system (VLMS), which consists of Laser Scanners, Line Cameras, GPS and INS. The system uses range data, scanned by the laser scanners as the main source of 3D data. In this paper, we present about the development of VLMS, which includes the system architecture, calibration and geo-referencing of sensors and positioning devices. Next, we present the extraction of some basic features like building surfaces, road surfaces (man made features) and trees (natural features). Finally, we will show how these features can be used to build 3D urban GIS database, which will assist in various applications as mentioned above. Besides, we will also discuss about the capabilities and difficulties of such a system [C6643]

"Extracting digital terrain models in forestry using lidar data"

Airborne light detection and ranging (LIDAR) is emerging as a tool to provide an accurate digital terrain model (DTM) of forest areas since it can even penetrate beneath the canopy. However, the determination of DTM in dense forest areas is still a difficult task and in an early stage of development. In this paper, an adaptive prediction technique based on the least mean squares (LMS) algorithm is presented. Results for LIDAR data, taken in 1999 at the Bellingham, WV site, are considered to illustrate the applicability of the presented technique [C6644]

"Backscattering behavior and simulation comparison over bare soil using helicopterborne radar data (the Alpilles-ReSeDA project)"

In the framework of the Alpilles-ReSeDA (Remote Sensing Data Assimilation) project, a consistent and comprehensive helicopterborne C-X band radar data set has been acquired during a complete vegetation cycle. General behavior of the data in terms of the season, the soil moisture and the soil roughness are presented here [C6645]

"GPR SAR simulation and image reconstruction"

Subsurface object detection has mainly been carried out using conventional ground penetrating radar (GPR) techniques which use a single receiving antenna from which a number of range profiles (known as "A Scope" images) are assembled to form a two-dimensional data field (known as a "B Scope" image). These GPR system have difficulties with high clutter level, surface reflections, limited ground penetration and the required fine resolution. The resolution in the across track and along track directions is limited by the physical aperture in these directions. This paper describes an imaging technique, which uses a single transmitting/receiving antenna to synthesize a two-dimensional planar aperture. Thus a three-dimensional reflectivity image of a scene is generated. The resolution in the across and along track directions is achieved via a SAR aperture synthesis technique. The depth/range resolution is achieved via the transmission of narrowband stepped frequency continuous wave (SFCW) signals [C6646]

"Dynamic monitoring of land cover changes in Yellow River delta of China using multi-sources remote sensing data"

The Yellow River delta of China is the youngest land in China formed by deposition of sands along the Yellow River. The delta expends 40,000 ha of land every year into the sea. The second largest oilfield "Shenli Oilfield" and the largest national wetland natural conservancy in China are located in the area. And over 100 ha saline land, which hampers agricultural development, in the area needs treatment and makes use of it. Nowadays the delta area is one of the rapidly changing places in China. The Chinese government has listed the development of the Yellow River delta area as the first priority project in "China's 21st Century Agenda". Thus, this study uses Radarsat data acquired in 1997 and 2000, ERS-1 SAR data acquired in 1995, and Landsat MSS and TM data acquired in 1976, 1980, 1995, 1996 and 1999, for dynamic monitoring of land cover changes in the Yellow River delta, which provides valuable information about the historical evolution of the delta area and water-course changes. The results show that significant changes have happened, noticeably the expending of land into the sea and water-course changes, as well as land use status changes because of oil field development and regional economic development [C6647]

"Integration of aerial photography, hyperspectral and SAR data for mangrove characterization"

In previous studies the use of time-series of stereo black and white and colour aerial photographs for establishing baseline datasets of mangrove extent and height against which to monitor long-term changes was demonstrated. In this research, our analysis was extended using NASA JPL MODIS-ASTER simulator (MASTER) data to discriminate and map dominant mangrove communities. With the provision of datasets describing the extent, height and species composition of mangroves, related allometric equations and field-based assessments of tree density, fine spatial resolution datasets of total above ground and component biomass can potentially be generated. Such datasets provide a basis for the interpretation of POLSAR backscatter data acquired at different wavelengths and polarisations [C6648]

"Influence of the microscopic fractal dimension on the statistical characterization of natural surfaces"

A popular model describing the statistics of remote sensed data is based on the decomposition of the area illuminated by the sensor into several facets which act as elementary scatterers. We investigate whether significant changes in the received electromagnetic field statistics may be induced by a modification of the microscopic details of the surface. Here microscopic means a scale length shorter than the typical dimension of a facet. We show that the overall field statistical characterization is very weakly dependent on the microscopic fractal dimension of the illuminated surface [C6649]

"Mapping the African rift valley in northern Uganda with SAR interferometry"

Cartographic mapping of the western arm of the great African rift valley near Lake Albert in Northern Uganda using ERS SAR tandem data was performed. Elevation information were generated from the interferometric SAR (InSAR) data and height values in the range of 540 m to 610 m deep were measured along the 42 km long depression region identified in the SAR image. The results do quite agree with reported data in the geographic literature [C6650]

"An advanced point-wise ambiguity selection algorithm: application to SeaWinds"

The scatterometer wind estimation process results in several possible wind vectors (ambiguities) at each resolution cell. The current ambiguity selection technique applied to SeaWinds on QuikSCAT data requires outside data as part of the initialization. An advanced ambiguity selection algorithm known as BYU point-wise does not use nudging data; rather, it utilizes a low-order Karhunen Loeve (KL) wind field model to promote self-consistency. In application to a subset of SeaWinds data, BYU point-wise selects 93% of the same ambiguities as the JPL method. On a set of non-storm error regions, BYU point-wise performed subjectively better in 55% of regions and subjectively worse in only 11% of regions. In cyclonic-storm cases, BYU pointwise performed subjectively better in 11% of regions while performing worse in 23% of regions. Thus, BYU point-wise generally produces more consistent results in non-storm regions without the aid of external nudging data [C6651]

"Sampling effects on radar measurements and rain rate estimation"

In this paper, we have studied sampling effects on radar measurements and on parameter retrievals. A two-level DSD model is proposed and illustrated for calculating statistical moments. The numerical results show that variations of DSD contribute to the over-estimation of statistical moments and biases the parameter retrieval. A range correction has been applied to radar estimated rain rate for accurate rain rate estimation based on the two-level Gamma DSD model. Although the two-level DSD model is proposed to include the DSD variation, the effects due to incomplete beam filling can also be compensated, since incomplete beam filling will alter DSD and hence the parameters of DSD. The model and numerical results have been applied to radar rain estimation with a range correction. In this study, we randomize DSD parameters to include sampling effects while their fluctuations are assumed to be independent random variables. Some of the observations show that DSD parameters may be mutually dependent, but the fluctuations in DSD parameters are less correlated. So, the independence among the fluctuations of DSD parameters can be a valid assumption for some cases. Even if the correlation among the fluctuations of DSD parameters is found, the two-level model does not lose its generality [C6652]

"Seasonal water level changes in tropical forests in New Guinea detected from JERS-1 SAR images"

A method for detecting and visualizing narrow open-water rivers using very strong scatterers was applied to a series of JERS-1 SAR images of tropical forests in New Guinea. These images were observed in November and December, 1995 and February and March, 1996. The results indicate that the narrow river water levels on the Pacific side of the major mountain range stayed relatively constant during this period, while the water levels on the Australian side were low in November, highest during February and March and slightly lower in December [C6653]

"High resolution wind retrieval from SeaWinds"

SeaWinds is a Ku-band pencil-beam scatterometer launched in 1999 on the QuikSCAT mission. It is designed to make nominally 25 km resolution observations of vector winds over the ocean. However, by taking advantage of resolution enhancement and its dense sampling characteristics, the wind can be retrieved at much higher resolution, albeit with greater noise. Winds with resolutions as fine as 2.5-5 km can be retrieved. Such wind data can support a variety of applications including hurricane monitoring and studying submesoscale wind phenomenology. While validation of this high resolution wind measurement capability is in progress, initial results are very encouraging [C6654]

"Temporal analysis of synthetic aperture radar signatures in a back bay-barrier island system"

We examine a 3-year sequence of SAR Imagery consisting of 30 RADARSAT frames and find a relationship between radar cross section and tide stage and bathymetry. Most notably, we observe that SAR signal intensity switches between banks within tidal channels on tide reversal [C6655]

"Evolution of upwelling-associated biological features in the Middle Atlantic Bight as captured by SAR, SST, and ocean color sensors"

Seasonal upwelling in the Middle Atlantic Bight (MAB) occurs during the summer months as a result of episodic wind forcing generally from the south. A wind-generated Ekman divergent surface flow is compensated by an onshore deeper flow that brings nutrient-rich colder waters to the surface. Colder upwelled waters are readily detectable using spaceborne sea surface temperature (SST) observations while increased productivity associated with the enhanced nutrient availability can be imaged by ocean color observations. Low backscatter patterns

imaged by synthetic aperture radar (SAR) match closely upwelling patterns observed in the SST data. An abundance of slick filaments also indicated by SAR is consistent with-enhanced biological activity associated with the upwelling regime NOAA AVHRR SST, SeaWiFS ocean color (i.e., Chl-a), and Radarsat-1 SAR imagery of upwelling conditions in the MAB during 1998 were reviewed. The data indicate the development of upwelling centers along the MAB coast. The offshore extension of upwelling-associated filaments as well as offshore blooms is observed in the data. The ability and limitations of these diverse datasets to complement each other in the detection, interpretation, and monitoring of upwelling-associated biological features are explored [C6656]

"Feature extraction in the Hankel transform domain"

Parameter estimation for the class of compound Gaussian random variables is considered in the more natural domain of the Hankel transform, where the expression of the probability density function appears generally more manageable. The estimation algorithm, based on the minimization of the integrated mean squared error between empirical and theoretical Hankel transform, has been tested for the case of K-distributed data using Monte Carlo simulation and some guidelines for the algorithm setup are derived [C6657]

"Bias correction and speckle reduction in time-space filtering of multi-temporal SAR images"

This paper extends the work on time-space filtering of multi-temporal SAR images presented in Coltuc et al. (2000), by providing theoretical support for bias correction and noise reduction evaluation. The bias value and a lower bound of the coefficient of variation for the residual noise are derived from the speckle probability density function. Theoretical results are compared with experimental measures obtained on multi-temporal SAR images from satellites ERS 1/2 [C6658]

"Comparing GPS, optical leveling and permanent scatterers"

The subject of this paper is the comparison of the results obtained exploiting the permanent scatterers (PS) technique on ERS DInSAR data with displacement measurements carried out by means of optical leveling and GPS [C6659]

"Applications of AIRSAR data acquired during PACRIM-II in Taiwan"

The Taiwan sites, organized by the Center for Space and Remote Sensing Research of National Central University, were planned as four sites: West Taiwan, South Taiwan, 921 quake, and Ken Ting. The West Taiwan site and South Taiwan site were selected for the study of land cover, ship detection, and coastal mapping using 40 MHz POLSAR and 80 MHz HiSAR, respectively. There are various types of agricultural crops and vegetation in the West Taiwan site. The HiSAR data of the South Taiwan site acquisition was centred on Kao, Hsiung Harbor for the study of ship detection. The other two sites, the 921 quake site and the Ken Ting site were selected for generating a digital elevation model using XT11 ping pong TOPSAR mode and XT12 ping pong TOPSAR mode, respectively. The terrain was strongly deformed by the 921 great quake (Chi-Chi quake) in Sep. 21, 1999. The purpose of the 921 quake site is to generate digital elevation model of disaster area of 921 quake and to study the land deformation by comparing with historical data and GPS survey. Finally, the Ken Ting site was planned in part as verification site for SRTM and PACRIM I. The ground truths over these sites were also collected by a field trip from Sep. 26 to Sep. 28, 2000 with the aid of unmanned remote helicopter sensing. There are a total of five sets of ground truth: 1) Hsin-Chu, an important wetland area located in north-west Taiwan. 2) Coastal lines of West Taiwan. 3) Kao-Hsiung Harbor, in which types and locations of ships entering and leaving the harbor were recorded by means of coastal radar. 4) Tai-Chung Harbor, where the land covers inside, and outside of the harbor were recorded by photography. 5) Au-Ku Farm Field, which is an agricultural field and is cultivated with sugar cane and rice. The cultivating area is arranged regularly and shaped as a rectangle. The land cover of each cultivation area was recorded. The fishpond outside the field was photographed by a remote helicopter. Besides, overpass remote sensing sensor data from SPOT and Radarsat were also acquired during the campaign. This paper outlines the applications of POLSAR and TOPSAR data in the area of coastal monitoring, land subsidence and deformation, and terrain cover classification. It is hoped that these demonstration will lead to future operational use of SAR data in these study areas [C6660]

"Data fusion approach for change detection in multi-temporal ERS-SAR images"

This paper presents a new method to detect changes in multi-temporal satellite SAR images. The proposed approach consists in an extraction step-specific change measures reveal the presence of changing features-followed by a fusion step where these measures and a priori information such as geographical map are merged to detect changes. The method is applied to the detection of deforested areas in tropical rain forest of French Guiana. Results obtained with SAR images from satellites ERS 1/2 are presented at two different scales: on a macroscopic scale for the detection of zones presenting a strong deforestation probability and on a microscopic

scale for a segmentation of the main deforested parcels [C6661]

"RADARSAT-2 mission update"

RADARSAT-2, scheduled for launch in 2003, will be the next Canadian commercial Earth Observation SAR satellite. The past few years have seen a dramatically different evolution of the RADARSAT-2 program from the original proposal in both the baseline design and primary sub-contractors. This paper presents an overview of the mission, summarizes the changes that occurred, and presents the new baseline that has resulted and lists the revised sub-contractors line-up [C6662]

"Development of a virtual radar environment"

The CSU-CHILL radar facility has embarked on an initiative to enable the real time operation of the radar over the Internet called VCHILL or Virtual CHILL. The concept of operation over the Internet can be implemented at several levels. The simplest one is to make the routine CHILL images available on the Internet as soon as the scans are completed. This type of data dissemination has been available with CSU-CHILL over 5 years. However such images are clearly not sufficient for aircraft coordination or actively conducting coordinated scans with rapid updates. The VCHILL initiative has a more ambitious goal of providing the same quality of service (QoS) at remote locations as at the radar site. In addition, the goal of the VCHILL initiative is to provide the educational experience of polarimetric radar at a remote location, without compromising on features of an on-site radar console. This paper describes some progresses and plans of the VCHILL initiative [C6663]

"Applications of RADARSAT-2-polarimetric data"

Expected applications improvements provided by dual- and quad-polarised data from Radarsat-2 are identified. Dual-polarised data is expected to have a wide range of applications. More detailed information is provided by quad-polarised data but here applications are limited by the narrow swath width. A specific study on sea ice monitoring is focussed on as an example application. The effect of system noise on polarimetric data analysis is considered as is the potential for polarimetric interferometry. The latter will be limited by temporal decorrelation [C6664]

"CFAR detection of extended objects in high resolution SAR images"

Presents a processing scheme for the constant false alarm rate (CFAR) detection of extended objects embedded in non-Gaussian disturbance. The proposed receiver exploits some relevant properties of the location-scale distributions for ensuring constant false alarm against Weibull clutter. The system has been specifically conceived for operating on high-resolution SAR images where space processing (but not time processing) is allowed [C6665]

"Evaluation of the potential cartographic accuracy of Radarsat and JERS-1 data"

Synthetic aperture radar images reveal geometric distortions, which are caused by different sources. The aim of this study is to quantify the geometric quality of some of these images-SGF product type (path image), standard beam mode, beam positions S2 and S3 Radarsat and JERS-1 level 2.1 images, acquired in the region of Ariqueemes-RO. A set of control points were acquired by using a GPS receiver in the area of study and differentially corrected. The planimetric and altimetric errors of these points are about 1,11 and 2,19 meters, respectively. These points were used as ground truth and compared with geometric properties (linear distances and angles) measured over the images. The uncorrected images presented relative scale and rotation errors of about 2 pixels. The images were geometrically corrected (geocoded and ortho-rectified) and had their geometric characteristics analyzed. The reduction of the relative scale and rotation errors obtained with the processes of geometric correction of the images were of 1/3 of pixel (4,17 meters). Visual inspection of an overlay of the SAR images and a GPS collected road network indicated a reasonable degree of coincidence. Results obtained with the calculation of the absolute accuracy of the geocoded and ortho-rectified images showed errors of absolute localization smaller than a pixel, varying from 5,42 meters to 12,24 meters to geocoded images and from 5,62 meters to 11,72 meters to the ortho-rectified ones. The images with viewing angles ranging from 24° in the near range to 31° in the far range (Radarsat S2), 30° in the near range to 37° in the far range (Radarsat S3) and 32° in the near range to 38° in the far range (JERS-1), acquired in regions with moderate altimetric variation (the area of study presents altimetric variations from 100 to 376 meters), presented geometric errors acceptable for mapping at 1:40000, 1:25000 or 1:20000 scales depending on the class of the mapping product to be obtained [C6666]

"Ultra high resolution spaceborne SAR processing with EETF4"

The performance of the EETF4 (extended exact transfer function 4th order) SAR processing algorithm is investigated. 1-D ETF analysis is used to show that the spaceborne SAR processing approach has to be used when the resolution is less than 1 m, especially with increasing squint angles. Phase differences for a spaceborne INSAR are estimated and used as input to the inverse-EETF4 and then the simulated raw data are processed with EETF4 using 1 block with squint 20 degrees and 0.3 m resolution. Point targets are processed with 40 degrees squint for one block of size 1100 range pixels. It is indicated that multi-block processing with block size 565 range pixels at extreme Doppler centroid variation works properly up to 10 degrees squint. Point targets with resolution 0.3 m were also processed with an erroneous satellite speed of 0.07 m/s, which causes visible degradation [C6667]

"Stochastic modelling of atmospheric effects in SAR differential interferometry"

A stochastic model for the atmospheric disturbance in DInSAR images is presented. Using a ray-propagation approach, the random path between two points in a turbulent atmosphere is modeled as a three dimensional random walk. First and second-order probability density functions of the differential phase of the atmospheric disturbance are derived and the model is experimentally validated by comparison between the characteristic function of real data and that predicted from the theoretical model [C6668]

"Model-based Doppler estimation for frame-based SAR processing"

Presents a new method of Doppler centroid estimation whereby estimates are made over small blocks of data covering a whole frame of data, and examined for strong SNR and lack of bias. Poor estimates are rejected, and the remaining estimates are used to fit a surface model of the Doppler centroid versus range and azimuth. The method is applied to both the fractional and integer PRF part of the centroid. A geometric model is used to constrain the model to allowable roll, pitch and yaw values of satellite attitude. The method is tested with RADARSAT-1 and SRTM/X-SAR data [C6669]

"A space-time analysis technique for monitoring terrain displacements from SAR differential interferometric measurements"

Synthetic aperture radar (SAR) differential interferometry is a powerful technique that allows to measure very small movements of the terrain that occurred between two data acquisitions. In previous works we demonstrated how to overcome the main limitations of the technique (i.e. decorrelation noise and atmospheric artifacts) by means of a method for unwrapping sparse phase data and by performing a temporal analysis of successive acquisitions. In this work we explore the possibility of considering together the space and time properties of the studied signal. The two steps mentioned above (i.e., sparse phase unwrapping and temporal analysis) act in the space and in the time domains separately. A significant advance can be obtained by considering the data as samples of a function in a three-dimensional (3D) space-time, and by exploiting this structure in the processing. The 3D structure of the data makes the processing more complex but can help both phase unwrapping and atmospheric (and other) artifact filtering [C6670]

"Change detection in polarimetric SAR data and the complex Wishart distribution"

When working with multi-look fully polarimetric synthetic aperture radar (SAR) data an appropriate way of representing the backscattered signal consists of the so-called covariance matrix. For each pixel this is a 3x3 Hermitian, positive definite matrix which follows a complex Wishart distribution. Based on this distribution a test statistic for equality of two such matrices and an associated asymptotic probability for obtaining a smaller value of the test statistic are given and applied to change detection in polarimetric SAR data. In a case study EMISAR L-band data from 17 April 1998 and 20 May 1998 covering agricultural fields near Foulum, Denmark are used. The derived test statistic can be applied as a line or edge detector in fully polarimetric SAR data also [C6671]

"Multidimensional cloud images retrieval from dual-frequency millimeter-wave radar"

In order to obtain a better understanding of the dynamics of heat transfer in the Earth's atmosphere, we need to develop better and more accurate climate models for the hydrometeor distribution within clouds. A better insight into the microphysical structure of clouds will be helpful to several meteorological and climate prediction models. In this work, stratus clouds are studied using dual-frequency radar. Liquid stratus clouds are found in the lower part of the atmosphere and have a profound impact on the Earth's radiative budget because of their high albedo and large global coverage. These clouds are difficult to study and quantify with visible and IR remote sensors due to their high optical extinction rate. We retrieve stratus cloud properties in two dimensions using a dual-frequency mm-wave radar. This work is a joint project between University of Massachusetts and University of Puerto Rico, Mayagüez [C6672]

"Analysis and correction of artifacts on differential SAR interferometry for the study of subsidence phenomena"

This paper deals with the analysis and correction of artifacts on differential synthetic aperture radar (SAR) interferometry. Particularly, we concentrate on those artifacts arising from the use in interferometric processing of low accuracy acquisition geometry data. To remove these artifacts, we propose a new algorithm able to estimate the acquisition geometry parameters with high accuracy directly from the SAR data. The application of the proposed technique to the study of the subsidence phenomena in Bologna (Italy) and the surrounding area is also presented to validate the new algorithm [C6673]

"Convective/stratiform classification from TRMM Precipitation Radar"

TRMM Precipitation Radar (PR) provides three dimensional reflectivity observations from space. A technique to distinguish between convective and stratiform regions in storms using reflectivity profiles is developed using the multiresolution analysis by the use of wavelet transform. The wavelet transform of radar signals are used to conduct scale analysis, spatial variability, and subsequently to distinguish between the convective and stratiform regions. The convective/stratiform separations obtained using this method are compared against current method used [Awaka et al. 1998] in the TRMM operational algorithms. The results are also compared against ground radar observations. The data analysis shows that the technique presented in this paper works fairly well convective/stratiform separation [C6674]

"Automation of the DEM reconstruction from ERS Tandem pairs"

The difficulties related to InSAR DEM reconstruction and the computational burden necessary to get the final result strongly depend on the topography of the area of interest and accuracy requirements. Whenever high quality results are requested, a multi-interferogram approach is strongly recommended, especially for repeat-pass interferometric data, such as ERS Tandem acquisitions. In this paper we recall the rationale of the multi-baseline strategy for DEM reconstruction and we propose a new phase unwrapping algorithm. In fact, phase unwrapping is the major obstacle to be overcome in the processing chain for InSAR DEM reconstruction, and often cannot be performed in a totally automatic way. Our attempt is to develop a robust processing chain that does not require user interaction and where possible prior information can be easily exploited. Preliminary results obtained by this algorithm are indeed very promising [C6675]

"On the relationship between the Mueller and the scattering matrices"

Radar polarimetry has gained more and more popularity in microwave remote sensing of the environment due to the progresses made on the technological and physical sides. In this paper a study on the relationship between the Mueller matrix and the scattering matrix is presented. The study is based on the group theory approach [C6676]

"A new estimator of the sea state bias using a three frequency radar altimeter"

This work deals with the estimation of the sea state bias (SSB). We performed a method to compute an altimeter return waveform from a deterministic sea surface [Amarouche et al. 2000]. To simulate the SSB, the sea surface characteristics and the electromagnetic model have been modified in agreement with statistical and physical theories and observations [Amarouche et al. 2000]. The conclusions of this study allow us to propose an estimator of the SSB using three frequency bands. Our simulator is tested using the performance budgets of Poseidon-2 (C and Ku bands) and AltiKa (Ka band) radar altimeters. The SSB is estimated with a bias of the order of about one millimeter and a noise of the same order of magnitude as the height estimation noise. The importance of the significant wave height estimation in determining the SSB, led us to propose a method to improve this estimation by studying the point target impulse response approximation by a Gaussian shape in the waveform model [C6677]

"Integrating multi-source remote sensing data for soil mapping in Victoria"

Mapping of soils at paddock level is being undertaken at 3 selected sites in Victoria by using remote sensing data from a variety of sources. The three sites represent different agricultural practices in high and low rainfall zones across Victoria. The project work is divided into 4 stages: (1) soil analysis at sample points, (2) analysis and integration of remotely sensed information, (3) exploring relationships between soil properties and remotely sensed variables, and (4) extrapolating soil mapping to a wider area using relationships established at stage 3. Detailed soil surveys were initially conducted to characterise the soils of each site at the sub-paddock scale to obtain information on the physical and chemical properties of the soil, particularly those relating to limiting factors such as salinity, toxicity (boron, aluminium), acidity, alkalinity and soil moisture regimes. To achieve this,

exploratory soil cores were collected across the site from locations representing different soil types and landform patterns. Soil pits (ranging between 4-10 per site) were then dug. Chemical and physical analyses were also completed for each pit to assist in understanding the soil characteristics across each site and down the soil profile. This site specific soil information is then used to aid soil feature extraction from the remotely sensed data sets. High resolution remote sensing information acquired for this study includes airborne synthetic aperture radar (PACRIM 2 AIRSAR), Landsat 7 ETM+, conductivity measurements from EM38 and EM31, and ground penetrating radar data sets. All data sets are integrated into raster format. The sets of remotely sensed data are treated as explanatory variables with soil properties as response variables. The integrated approach enables a number of space, air and ground borne data sets to be evaluated in terms of their potential to be able to identify soil components both on the surface and at depth. The differences in the resolution of these sensors also allow evaluation on the type of soil information that can be obtained at varying scales, from the sub-paddock to catchment [C6678]

"View of French Guyana by ERS SAR presented on an interactive CD-ROM"

The aim of the described CD-ROM is to introduce the main properties of synthetic aperture radar (SAR) images provided by remote sensing satellites. We have also included some concrete examples of how such radar data can be used. This presentation relies mainly on data provided by the European Remote Sensing (ERS) 1&2 satellites over the territory of French Guyana, from where those satellites were launched in 1991 and 1995 from the Space Center at Kourou [C6679]

"Influence of stone cover over bare soil on backscattering"

Identifies the potential of radar signal to characterise the stone cover over bare soil surfaces. A high correlation was observed between radar measurements and stone cover percentage. Numerical moment method based on integral equations of backscattering has been used to study the influence of the stone cover percentage on simulated radar signal. Simulations are validated with measurements acquired in two arid sites. A good agreement is demonstrated between numerical simulations and radar ERS2 measurements. An empirical model is then proposed to inverse radar measurements and retrieve stone cover percentage [C6680]

"A Kalman filter-based approach to detect landmines from metal detector data"

Metal detectors play a significant role in landmine detection. Automatic sensor fusion is required to improve the performance of ground penetrating radar (GPR)-metal detector multi-sensor systems. The existing version of the Kalman filter-based detection algorithm has been adapted for automatic detection and discrimination of landmines in metal detector data. In this algorithm, multi-channel metal detector output data are fused to produce a distribution of probabilities of the presence or absence of a target. Performance of this algorithm has been assessed using data obtained by burying a number of simulant landmines, canonical targets and shrapnel in different soil types [C6681]

"EuroROSE: a project to support shipping in port approaches"

The European Radar Ocean Sensing (EuroROSE) project is presented. The project was designed to monitor and forecast sea state conditions in coastal areas, in particular port approaches. The aim was to provide area-covering information to traffic managers and search and rescue organizations, using ground based radar and numerical models in combination with data assimilation techniques [C6682]

"Mars surface models and subsurface detection performance in MARSIS"

The MARSIS (Mars Advanced Radar for Subsurface and Ionosphere Sounding) instrument is a multi-spectral, low frequency, nadir looking pulse limited radar sounder and altimeter with ground penetration capability. Moreover the detection of a subsurface interface will be possible only if the following conditions are met: -the level of the subsurface reflection is higher than the noise floor -the surface/subsurface dynamic is included in the system dynamic range -the subsurface reflection is higher than the corresponding surface clutter reflection For MARSIS the noise floor has been evaluated to be about 60 dB below the fully coherent surface echo, so that an overall 60 dB dynamic range will be allowed if sidelobes and nonlinearities are controlled and reduced down to the noise level with a proper design. In this case we can assess that the penetration depth can be defined as that depth where the subsurface power is equal to the surface clutter power. In this paper the subsurface to surface clutter ratio will be evaluated, taking also into account the results related to the new fractal models of the structure of the planet's surface and in particular the new MARS surface models obtained from the MGS/MOLA data [C6683]

"Adaptive compensation of Mars ionosphere dispersion in the MARSIS experiment"

MARSIS (Mars Advanced Radar for Subsurface Ionosphere Sounding), selected as scientific payload of the ESA mission Mars Express, is a low-frequency nadir-looking pulse limited radar sounder and altimeter with ground penetration capabilities, which uses synthetic aperture techniques and a secondary receiving antenna to isolate subsurface reflections. In order to maximize the penetration capabilities of the transmitted pulse MARSIS must operate at a frequency as low as possible (few MHz). Moreover the requirement for fine range resolution calls for a relatively large transmitted bandwidth (1 MHz) so that MARSIS will operate with a very high fractional bandwidth and very close to the expected Martian ionosphere plasma frequency. This will result in a generally large phase distortion across the spectrum of the received pulses (due to either the antenna frequency response or the propagation through the ionosphere) which will cause severe degradation of the matched filter performance in terms of SNR, pulse spreading and sidelobe level. This paper deals with the definition and implementation of an adaptive range compression algorithm, which makes use of the contrast maximization technique to estimate the phase dispersion spectrum, in order to perform a matched filtering of radar sounder echoes in the presence of phase distortions across the signal bandwidth [C6684]

"Polarimetric SAR interferometry as applied to fully polarimetric rain forest data"

The scope of this paper is to establish a polarimetric SAR interferometry approach to estimate interferometrically observable forest and ground parameters. Three optimized interferometric coherences can be found through a properly weighted superposition of all the interferometric coherences available from a fully polarimetric single baseline experimental set-up in repeat-pass mode. These proper weights can be found by solving an eigenvalue problem for each resolution cell [Cloude and Papathanassiou 1998]. The result serves as the right hand side of a least square optimization problem which makes use of a scattering model based on a randomly oriented volume over an impenetrable surface [Treuhaft and Siqueira 2000] to estimate a set of physical forest parameters transformed through this model. A conjugate direction set iteration scheme is used to minimize the cost function of the optimization problem and to solve for the pertinent candidate parameters, which are the forest volume thickness, the volume extinction coefficient, the interferometric phase related to the underlying topography, and the effective ground-to-volume amplitude ratios of the related interferometric coherences. Due to the non-uniqueness of this inversion problem an additional constraint is introduced via a Tikhonov regularization scheme. The results of the presented schemes are shown for the first time on P-band data taken acquired over tropical rain forest in Brazil [C6685]

"A performance analysis of several bistatic calibration techniques"

Several popular bistatic calibration techniques are evaluated, and comparisons are made between the relative merits of various calibration objects. This analysis considers the following: sensitivity to object alignment error, sensitivity to polarization impurity, and ease of implementation. Both theoretical concepts and practical considerations are discussed, based on measurements accomplished at the European Microwave Signature Laboratory (EMSL) of the Joint Research Centre (JRC) in Ispra, Italy. This facility has the capability to produce far-field, fully polarimetric, bistatic measurements with an approximately 30 cm diameter quiet zone, with the necessary precision for comparing different calibration methods [C6686]

"ERS-1/2 SAR and IFSAR for Antarctica"

In this paper we present a work conducted under the PNRA (Progetto Nazionale Ricerche in Antartide) project aimed at assessing the capability of synthetic aperture radar (SAR) and interferometric SAR (IFSAR) in providing useful geophysical information in the study of Antarctica. The study is concentrated over the Ross Sea-Terra Nova bay area wherein the Italian base is located. This study uses a limited remotely sensed data set and ground truth data. Notwithstanding, the study is capable of meaningful results [C6687]

"An adaptive filter for removal of noise in interferometrically derived digital elevation models"

A low-pass filter that chooses the window size depending on the degree of smoothing required by detecting isolated as well as clustered noise in the DEM is developed and tested. In the noise-free case, the standard deviation of the values of the pixels inside a window increases as the size of the window increases, due to the inclusion of height values that are either lower or higher than the central pixel value. If the standard deviation of the window pixels decreases as the size of the filter window increases then the presence of noise, either isolated or clustered, is indicated. Changes in the value of the standard deviation of the window pixels as the window size is increased can thus be used to fix an appropriate window size. Given a specific window size, the 'sigma operator' (Lee, 1983) is used to produce a 'noise-free' estimate of the central pixel value. In this operation, the values of pixels within the window that lie between an upper and a lower limit are averaged. The median is preferred as the measure of central tendency in determining the lower and the upper limit, because the value of

the median is less affected by the presence of a minority of aberrant pixel values, whereas the mean value is computed from the values of all pixels in the window, including noise pixels. Hence the smoothing operation employed in this study is called the 'modified sigma operator'. The performance of the modified sigma operator is compared with that of a median filter in removing noise present in InSAR DEM. The performance of the filter was evaluated by comparing the distribution of root mean square (RMS) error against percentage of pixels (Balan and Mather, 2000), for unfiltered and filtered DEMs. The results show that the adaptive lowpass filter is more effective in reducing noise in the DEM [C6688]

"Electromagnetic aspects for sub-surface sounding of planets"

Some aspects of satellite-based planetary subsurface sensing are outlined. One constraint has to do with the fact that at very low frequencies, needed to penetrate the ground, it is difficult or impossible to achieve a narrow antenna beam-width and therefore a large area is illuminated, creating backscatter which interferes with the wanted signal. Another issue is the propagation through the planet's atmosphere and particularly through the ionosphere [C6689]

"A new approach for analyzing the temporal evolution of Earth surface deformations based on the combination of DIFSAR interferograms"

We present a new approach for the evaluation of the Earth surface deformation evolution based on the combination of several differential interferograms spanning a time interval of interest. In particular we present a method that extends the least squares combination technique presented by S. Usai et al. (2000) by applying the singular value decomposition (SVD) method. Experiments carried out on ERS data validate the proposed approach [C6690]

"A mosaic technique for the generation of wide-area DEMs with interferometric SAR data"

We propose and evaluate an operational algorithm, capable of obtaining a mosaic DEM from a wide area from several interferometric data sets [C6691]

"Borehole Interferometric SAR: A preliminary study"

The objective of borehole radar interferometry is to reconstruct subsurface structures (such as an orebody) in three dimensions, which in turn, will help in optimizing the design of mines. Synthetic aperture radar technology uses the reflected data from two or more antenna tracks and to convert interferogram phase difference to the corresponding height values. To study the potential of SAR technology in borehole environment we have considered the reflection between a homogeneous ($\epsilon_r=9$) host rock and a perfectly reflecting surface such as a conductive orebody. Taking into consideration practical exploration borehole geometries and the high attenuation of RP signals in host rock, the boreholes are made non-parallel and the master antenna is kept 100 metre away from near the reflecting surface. The coherence value in slant range, simulated and expected DEM in both slant range and ground range, the error between simulated and expected values in slant range have been calculated. Future work involves the use of 3D vector model to convert the phase values into corresponding height values, multiple boreholes and layered medium EM wave propagation to reconstruct the subsurface [C6692]

"A super-fast scanning technique study for an on-airport weather radar"

We assess the prospects for detecting a dry microburst core in the vicinity of an airport using a super-fast scanning (SFS) technique. In particular we propose a 20-beam SFS radar system and develop a system specification delivering a similar performance to a conventional mechanical scanning terminal Doppler weather radar (CMS-TDWR). The performance is compared in terms of the accuracy by which the three spectral moments can be estimated. These parameters were calculated using the signal models generally accepted by the industry for a microburst, for both scanning systems, and sampling at the same range intervals. The simulated results show that a 20-beam SFS X-band radar could update the weather information at twenty times the rate of the CMS-TDWR, but the radar would need a peak power of 45 kW. Whilst this peak power requirement is considerably less than the CMS-TDWR radar, this may be difficult to achieve for an electronically scanned array. The research emphasis is on developing and analysing the potential of the SFS technique, and this technique can be applied to improve the weather radar scanning rate once phased array radars of adequate peak power are feasible [C6693]

"Localization of target tracking and navigation by correcting atmospheric effects"

For any type of target tracking and navigation, the localization is critical for tracking/navigation missions. The

real-time localization error correction for the atmospheric refraction can be achieved through the ray bending compensation by the refractivity profiles or ray-tracing. Ray-tracing can be computed through the real-time weather data (surface temperature, pressure, and relative humidity or dewpoint) from daily/hourly, local meteorology, or global climatology data. Operational results of this new technique indicate that the time difference of arrival (TDOA) of radio-waves vary dynamically in hours, days, months, seasons and geographically. Errors for the low elevation angles less than 10 degrees are much higher than expected for higher frequencies above 300 MHz, and it should be calibrated or corrected in tactical operation and strategic system implementation. The localization of tracking and navigation mission can be achieved within a couple of hundred meters if the integrity of measured tactical data is well within the confidence boundary [C6694]

"Can geometric optics fully describe radar images of the sea surface at grazing incidence?"

It is possible to estimate the significant wave height of the ocean surface using shadowing statistics computed from grazing incidence radar imagery. The theoretical basis for this estimation is a geometric optics view of a gaussian surface. In practice it is necessary to apply an empirical correction based on the intensity of the radar backscatter in order to produce a wide range of verifiable wave heights. To explore the reasons for this correction, we have conducted a one-dimensional Monte-Carlo simulation of the sea surface at a wide range of significant wave heights, and have observed it with a ray trace program from several source heights and configurations. We conclude that, although the finite amplitude effects simulated in this experiment partially explain the results observed at sea, some electromagnetic interaction unaccounted for in geometric optics must also be responsible for the result. We suggest that increased local incidence angle is a possible source of the difference between observations and our simulation [C6695]

"On the fractal behavior of SAR images of ocean sea surface"

The fractal properties of SAR images of the sea surface are currently studied by many researchers, but definite results have not been derived. We investigate the fractal behavior of SAR images of the sea surface by analyzing both real ERS-1 images and synthesized sea-surface images. These sea surfaces are obtained from a 2D fractal model using model parameters derived from real data measurements from buoys, acquired at the same locations and at the same dates of the ERS-1 passes. The analysis of fractal images is performed by two different fractal approaches and by an algorithm of multifractal analysis. Experimental results and comparisons are presented in terms of fractal dimension estimated both from sea spectra computed from 'in situ' measurements, and from the corresponding true ERS-1 SAR images [C6696]

"Observing abnormal wind features of the tropical Pacific Ocean during the 1997-98 El Niño"

The 1997-98 El Niño, the strongest in recorded history, manifested itself with unusual features associated with the Pacific wind system. These features include: (1) an annual cycle of an east-west migration of a weakened wind speed zone between 2°N-9°N; and (2) an asymmetric seesaw process of trade wind variations between the two hemispheres in terms of relative intensity and central position. These features, revealed by the multi-year TOPEX altimeter data, may serve as new clues to improve our understanding of El Niño formation, and may also contribute to its future prediction [C6697]

"The Glen Affric project: forest mapping using polarimetric radar interferometry"

We describe the Glen Affric radar project, a multi-disciplinary program addressing the ability of polarimetric radar interferometry to provide quantitative vegetation structural information of importance in forest mapping and ecology studies [C6698]

"A low-cost polarimetric response tool using spreadsheets"

This paper describes a spreadsheet based low-cost tool for displaying polarimetric response graphs. It describes the actual implementation in detail and shows examples of the polarimetric signatures of various types of terrain that have been computed using the tool. These signatures are interpreted in relation to the geophysical characteristics of the ground features they represent. The tool can be found on the Canadian Space Agency website at www.space.gc.ca/csa_sectors/earth_environment/radarsat2/ [C6699]

"Estimation of comprehensive forest variable sets from multiparameter SAR data over a large area with diverse species"

Polarimetric and multifrequency data from the NASA/JPL airborne synthetic aperture radar (AIRSAR) have been used in a multitier estimation algorithm to calculate a comprehensive set of forest canopy properties including branch layer moisture and thickness, trunk density, trunk water content and diameter, trunk height, and

subcanopy soil moisture. The estimation algorithm takes advantage of species-specific allometric relations, and is applied to a 100 km \times 100 km area in the Canadian boreal region containing many different vegetation species types. The results show very good agreement with ground measurements taken at several focused and auxiliary study sites. This paper expands on the results reported in Moghaddam and Saatchi (2000) and applies the algorithm on the regional scale [C6700]

"A pilot experiment for stem volume retrieval based on VHF SAR data"

In Swedish forestry, reliable forest parameters are needed for both short and long term planning. The traditional methods used for acquiring forest data at reasonable accuracy are very expensive and labour intensive. Therefore, new cost-effective methods for data collection must be used to meet the requirements being imposed on timber supplies and environment conservation. Based on promising results obtained earlier in relating VHF SAR data to forest stand parameters a pilot project has been defined. The objective is to develop a fully integrated system for retrieval of forest parameters using VHF SAR images. A representative data set covering 625 km² of predominantly conifer-forested terrain was collected with the CARABAS-II sensor in November 2000 as an initial step [C6701]

"Monitoring big river estuaries using SAR images"

Since the launch of the ERS-1/2 Satellites in 1991 and 1995 respectively, synthetic aperture radar (SAR) images of coastal regions have been acquired and processed at the receiving station of the German Aerospace Center at Neustrelitz on an operational basis in near real time. These data are used to monitor large river estuaries of the German Bight which are morphodynamically very active, i.e. the bottom topography underlies a continuous change due to sediment transport, with strong impact on the main waterways of the river. Because of their all weather, day and night capability radar images are ideally suited to investigate these morphodynamics by monitoring the land-water boundary of the mud flats. Edge detection is a demanding task for radar images as they are contaminated by speckle noise. The water-line is extracted using edge detection methods based on a combination of blocktracing, wavelet-edge detection, and a snake algorithm resulting in the final coastline. The detected shorelines are transformed into isolines of bottom topography by combining them with available tide gauge information. Longer time series of such water lines are used for monitoring changes of topography over the years by comparing images taken at a similar tidal situation. The examples given, range from coastline monitoring, bottom topography control to sediment transport measurements. The areas investigated are the large estuaries of the German rivers at the North Sea (i.e. Ems, Weser, Elbe and Eider) and the Canadian Mackenzie delta [C6702]

"Wavenumber correlation analysis of Topex/Poseidon and tide-gauge sea surface heights in the East Sea (Japan Sea)"

Sea surface height (SSH) was extracted from the Topex/Poseidon MGRD radar altimeter data in the East Sea (Japan Sea) and compared with the SSH estimated from in-situ tide-gauges at Ulleungdo, Pohang, and Sockcho/Mucko sites. Selection criteria such as wet/dry troposphere, ionosphere, and ocean tide were used to enhance the accuracy of SSH. For time series analysis, the one-hour interval tide-gauge SSHs were resampled at 10-day interval of the satellite SSHs. The ocean tide model applied in the altimeter data processing showed periodic aliasings of about 175, 88, 62, 58, 49, and 47 days, and, hence, the 200-day filtering was applied to reduce all these spectral noises. The SSH features showing direct, inverse, and no correlations between the two independent measurements were separated by applying filters in the wavenumber domain of the data sets. The correlation filter passes or rejects wavenumbers as given by the cosine of their phase difference. The original correlation coefficients (CCs) between the satellite and tide-gauge SSHs were 0.46, 0.26, and 0.25, respectively [C6703]

"Simulation of SAR raw signal relevant to oil slicks in ocean scenes"

In this paper we present a SAR raw signal simulator of ocean scenes, polluted by the presence of an oil layer. We investigate how oil influences both the physical behaviour of the ocean and the electromagnetic mechanisms that govern the scattering from the ocean surface. Significant simulations are presented [C6704]

"Comparison of RADARSAT SAR-derived wind speeds with buoy and QuikSCAT measurements"

The radar cross section (RCS) of the ocean surface depends on both wind speed and direction. By using estimates of the wind direction from an atmospheric model plus RCS measurements from the RADARSAT-1 synthetic aperture radar (SAR), we processed over 3000 wide-swath SAR RCS images into wind speed fields. We have validated these wind fields against both buoy and QuikSCAT scatterometer measurements. The standard deviation of SAR wind speeds with respect to buoy or QuikSCAT wind speeds is less than 2 m/s. If the

QuikSCAT wind directions are used rather than the model directions for the SAR wind speed retrieval, the agreement between SAR and QuikSCAT wind improves to a standard deviation of 1.5 m/s [C6705]

"Coastal high resolution wind fields retrieved from RADARSAT-1 ScanSAR"

An algorithm is presented for retrieving high resolution wind fields from the scanning synthetic aperture radar (ScanSAR) data acquired aboard the Canadian satellite RADARSAT-1. The wind directions are extracted from wind induced streaks, e.g. from boundary layer rolls, Langmuir cells, or wind shadowing, which are approximately in line with the mean wind direction. The wind speeds are derived from the normalized radar cross section (NRCS) and image geometry of the calibrated ScanSAR images, together with the local wind direction. Therefore the semi-empirical C-band model CMOD4, which describes the dependency of the NRCS on wind and image geometry, is inverted. CMOD4 was originally developed for the scatterometer operating at C-band with vertical polarization and has to be modified for horizontal polarization, which is performed by considering the polarization ratio according to Kirchhoff scattering. To verify the algorithm, wind fields were computed from several RADARSAT-1 ScanSAR images and compared to collocated results from the Danish high resolution limited area model. To estimate relative errors of wind speed due to uncertainties in wind direction and NRCS, sensitivity studies were performed [C6706]

"The relationship between time series sea surface slope and El Nino event from satellite altimetry: a potential indicator"

China suffered a serious flooding in the summer of 1998, which is regarded as initiated by the 1997/1998 El Nino. From previous investigators we know that the sea water transportation across Takara Strait is closely related with the occurrence of El Nino event. As the geostrophic current Kuroshio flows almost perpendicularly across the Takara Strait, the net volume transportation at this site may be well described by the sea surface slope. In the present study, decadal monthly averaged sea surface slope across Takara Strait are derived and presented combining the ERS-1,2/ALT measurements of 35-day repeat and the TOPEX/Posidon data of 10 day repeat. It is found that an abnormally high peak takes place in the October of 1996, i.e., one year prior to the 1997/1998 El Nino. To further test the feasibility of the method, the time series sea surface slope across PN section were also examined through which the Kuroshio in the East China Sea goes perpendicularly as well. It is revealed that an abnormally low peak appears exactly in the October of 1996. This is just the opposite to what happens in Takara Strait during the same period. However, the geostrophic transport at PN section is out-of-phase with that at Takara Strait on the basis of field investigations, which shows the two results are virtually in support of each other. Our preliminary results demonstrate the sea surface slope at Takara Strait may be regarded as an index for the upcoming El Nino event. Relevant dynamic mechanisms are discussed [C6707]

"Structures of marine wind variability at four selected sites derived from TOPEX altimeter data"

As the largest source of momentum for the ocean surface, wind affects the full range of oceanic motion-from individual surface waves to complete current systems. The marine surface wind is among the critical geophysical parameters which determine the most fundamental aspects of the ocean. Using six years of TOPEX altimeter data with unprecedented accuracy and continuity, a detailed investigation on the structures of marine wind variability at four selected sites is carried out in this study [C6708]

"Wave tank modelling of strong modulation of radar backscatter due to long waves"

Modulation of radar backscatter due to long wind waves for Ka-band radar has been studied in wave tank experiments at different wind velocities and fetches. The modulation transfer function (MTF) was analysed, and it is shown that the mechanisms of tilt modulation, hydrodynamic straining and modulation of wind stress strongly underestimate the effect when compared with experiment. Radar Doppler shifts were measured and they were shown to be larger than those, connected with free gravity-capillary Bragg waves, and smaller than for bound waves, generated by decimetre-scale dominant wind waves and propagating with their phase velocities. It is shown that the contribution of the bound waves in the short wind-wave spectrum, estimated from the measured Doppler shifts is significant so that these waves can give strong modulation of radar backscatter [C6709]

"The scattering polarimetric response contrast between two wind-generated rough sea surfaces"

Polarimetry for SAR applications is an excellent technological method to extract more information about wind-generated rough sea surface according to the scattering mechanisms. With the use of the scatter matrix, i.e. Mueller matrix, and Stokes vector operator, the paper describes a comparison between the polarimetric responses of two types of wind-generated sea surface offshore Baogang, Hainan Province. It gives representative results for the polarimetric response of backscattering electromagnetic field from the rough sea

surface and the characteristics of Mueller matrices' traces. The long wavelength sea surface and the short one can be determined by their polarimetric responses. The traces and determinant values of scattering matrices are related to the wind conditions. Some heuristic conclusions are given upon the results [C6710]

"Precise orbit determination of meteors using a radar and an optical sensor"

Impacts of meteors with spacecraft are among the major sources of possible problems in the space environment. Although the average mass of meteor bodies is much less than artificial space debris, the relative velocity of high-speed meteors against the Earth reaches 72 km/s, which far exceeds that of artificial objects. It is thus very important to establish the statistics of meteors, especially those of the mass and velocity, along the Earth's orbit around the Sun in order to make a reliable data base for designing large scale spacecraft such as space stations. Radar with the help of an optical camera are most suited for this purpose. The purpose of the present paper is to develop a high- sensitivity combined radar-optical system consisting of a high-power VHF Doppler radar and an ICCD video camera for the purpose of studying the velocity and mass distributions of faint meteors. A description of the systems and their performance evaluations are given. Preliminary results of the mass estimates and the relations of the radar echo power and the absolute visual magnitude derived from test experiments are also presented [C6711]

"Multiplier-free filters for wideband SAR"

This paper derives a set of parameters to be optimized when designing filters for digital demodulation and range prefiltering in SAR systems. Aiming at an implementation in field programmable gate arrays (FPGAs), an approach for the design of multiplier-free filters is outlined. Design results are presented in terms of filter complexity and performance. One filter has been coded in VHDL and preliminary results indicate that the filter can meet a 2 GHz input sample rate [C6712]

"Improved timing calibration of QuikSCAT"

Since being launched in June 1999, QuikSCAT has successfully and accurately measured ocean wind vectors. Current research is attempting to increase performance beyond the original design parameters in order to increase the utility of the data. Timing calibration is critical to this effort. Timing information is used to determine instrument performance as well as to calculate the location of each measurement on the Earth's surface. This paper reports a method of obtaining high-precision time validation measurements through the use of the QuikSCAT Calibration Ground Station (CGS). The QuikSCAT CGS passively records satellite transmissions as it passes overhead. Analysis of CGS data can determine the arrival time of each QuikSCAT pulse to within microseconds. Utilizing the high stability of the onboard pulse repetition interval clock, along with CGS observations, precise instrument timing can be determined during a portion of the orbit, which enables more precise determination of the timing throughout the entire orbit. The improved timing is able to support the requirements of advanced data applications [C6713]

"Pointing angle and timing calibration/validation of the Geoscience Laser Altimeter with a ground-based detection system"

The scientific goals of the laser altimeter carried on ICES at require that the laser pointing direction should be known to an accuracy of 1.5 arcseconds and the time tag of the altitude measurement should have an accuracy of 0.1 millisecond. In order to verify that the satellite altimetry instrumentation is properly characterized, the laser spot position and time tag should be independently verified. One independent approach uses a ground-based electro-optical detector array. Operation of many devices over an area will enable detection of the laser footprints when they illuminate the ground. With the coordinates of the captured spot obtained from the detector array, the laser spot position determination is compared to the position inferred from the data collected onboard ICESat. A small subset of these detectors will also be used to time-tag the footprint for further verification. These timing detectors will be hardwired to a central timing station that uses a GPS receiver to time stamp the laser pulse time of arrival. The detectors used only for positioning are designed for autonomous operation [C6714]

"Observations from space of meteorological fields on the scale of numerical weather forecasting models"

In this paper we report the results of some preliminary studies concerning the use of a weather radar from a polar orbiting space platform for the direct observation of meteorological fields (rain and large-scale small-value vertical velocity) at horizontal resolutions which are useful in the initialisation-diagnosis of numerical limited area models (LAMs). The studies have been performed with specific reference to the "Cassini" radar from the International Space Station (ISS) [C6715]

"Global wind speed retrieval from complex SAR data using scatterometer models and neural networks"

The global availability of synthetic aperture radar (SAR) wave mode data from the European remote sensing satellite ERS-2 allows to investigate the wind field over the ocean on a global and continuous basis. For this purpose 27 days of ERS-2 SAR wave mode data were processed to single look complex SAR images, representing a total of 34310 images of size 5 km⁴10 km, available every 200 km along the satellite track. In this paper two methods for retrieving wind speeds from SAR images are presented and validated, showing the applicability of both methods for global ocean wind retrieval. The first method is based on the well tested empirical C-band scatterometer (SCAT) models which describe the dependency of the normalized radar cross section (NRCS) on wind speed and direction. To apply C-band models to SAR data the NRCS has to be accurately calibrated. This is achieved by a new simple but effective method using a subset of collocated ERS-2 SCAT and model winds from the European Center for Medium Range Weather Forecast (ECMWF). SAR derived wind speeds are compared to the entire set of collocated ERS-2 SCAT and ECMWF model data. Comparison to ERS-2 SCAT results in a correlation of 0.94 with a bias of -0.45 m s⁻¹ and a root mean square error of 1.21 m s⁻¹. The second approach is based on neural network algorithms allowing one to retrieve wind speeds from uncalibrated SAR images. For this purpose a neural network is trained using ERS-2 SAR data and collocated wind data from ERS-2 SCAT and the ECMWF atmospheric model. Validation of the neural network retrieved SAR wind speeds to ERS-2 SCAT and ECMWF model wind data is performed. A correlation of 0.95 with a bias of -0.1 m s⁻¹ and a root mean square error of 1.03 m s⁻¹ is achieved in comparison to ERS-2 SCAT [C6716]

"Coastline detection in SAR images using texture analysis in textural or geometrical multi-resolution"

A new method is proposed in this paper for coastline extraction which uses the SAR amplitude images, or if available, the interferometric coherence images. This method uses texture analysis based on textural multi-resolution (TMR) or geometrical multi-resolution (GMR), for a fine analysis of coastline. First order texture measures (TM) have been used. In TMR, a series of TM are generated at various textural scales from the original image. In GMR case, a wavelet transform produces a low-resolution approximation of the original image. Consequently, TM are also generated at a suitable low-resolution approximation. A selection of the suitable TM in one or another multi-resolution approach, leads to a good separation of sea and coastal area and reveals coastline. A detection of discontinuities allows then easy extraction of coastline. The obtained results are promising and show a good detection, and a good continuity of coastline. A proposed method has been tested on ERS SAR amplitude and coherence coastal region images of Cameroon, Mauritania and Guyana [C6717]

"Polarimetric measurements of microwave emission from capillary waves"

The results of polarimetric microwave measurements of thermal emission from a water surface with artificial periodic structure are presented. The structure in a water tank was produced by a set of parallel threads raised a little over a surface. The measurements of the three Stokes parameters of the emission were carried out with the Ka-band polarimeter. The experimental setup allowed measurements over a wide range of elevation (from near-nadir to 70 degrees) and azimuth (over 300 degrees) angles. The experimental data show the existence of the resonant peak in the Stokes parameters predicted by the model. This result is evidence of the important role the short gravity-capillary waves play in the sea-surface polarized microwave emission [C6718]

"Polarimetric radar remote sensing of ocean surface wind"

Experimental data are presented to support the development of a new concept for ocean wind velocity measurement (speed and direction) with the polarimetric microwave radar technology. This new concept has strong potential for improving the wind velocity measurement accuracy and for extending the useful swath width by up to 35 percent for follow-on spaceborne scatterometers to NASA SeaWinds missions. The key issue is whether there is a relationship between the polarization state of ocean backscatter and ocean wind velocity at NASA scatterometer frequencies (13 GHz). A set of aircraft flights indicated clear and repeatable wind direction signals in polarimetric Ku-band scatterometer observations of sea surfaces at 10 m/s wind speed [C6719]

"The information content of multiple receive aperture SAR systems"

For SAR to perform correctly, the number of unique measurements obtained by the radar (i.e., the rank of the received signal's covariance matrix) must be greater than the number of pixels illuminated. For a single aperture SAR, the coherent processing interval (CPI) and bandwidth determine the number of independent measurements collected; therefore, the received time-bandwidth product limits the maximum unambiguous illumination area, or swathwidth. For a multiple aperture SAR (MSAR), however, the rank of the received signal is not as easy to

determine. When the array is large, its beamwidth determines resolution rather than the radar's bandwidth and CPI length. Furthermore, redundant lags in the space-time-frequency co-array reduce the amount of unique information collected. This paper generalizes the theory behind determining the rank of a signal received from stationary targets. Resolution is determined by all radar parameters including CPI length, bandwidth, and array extent. The co-array concept for antenna arrays, which is a measure of the lags sampled in the array's spatial covariance matrix, is extended and applied. A hybrid coarray is derived that indicates lags sampled in the hybrid spacetime-frequency space. The hybrid co-array is then applied to signals received by MSAR to show that the number of unique lags in the hybrid co-array limits the number of unique samples collected. The results provide important analysis tools for MSAR systems that are likely in the future, especially sparse, constellation-flying satellite systems [C6720]

"Velocity estimation of fast moving targets using undersampled SAR raw-data"

The paper presents a new methodology to retrieve slant-range velocity estimates for moving targets which induce a Doppler-shift beyond the Nyquist limit determined by the Pulse Repetition Frequency (PRF). The proposed scheme takes advantage of the fact that the range velocity of a moving target induces a Doppler-shift in the azimuth spectra which depends linearly on the fast-time frequency. We present results that take real and simulated SAR data [C6721]

"Statistical properties of L-band sea clutter measured with a polarimetric synthetic aperture radar"

The limiting factor affecting the performance of most airborne radar systems in detecting targets on or near the surface of the sea is return echoes from the sea surface or sea clutter. The objective of this paper is to provide an analysis of the statistics of Australian sea clutter for an L-band VV-polarised airborne radar system from sampled measured values. Polarimetric synthetic aperture radar (POL SAR) image of the North-West region of Australia, acquired in 1996 by the Jet Propulsion Laboratory (JPL) was used to study, the backscattered statistics of the sea surface. Using this POL SAR image, a number of different candidate distribution functions have been investigated, and their goodness-of-fit have been carried out using the Kolmogorov Smirnov goodness-of-fit test. The log-normal, Weibull and K-distributions have been applied to model the statistical properties of multi-look polarimetric SAR sea clutter. The K-distribution has been found to have good agreement with the observed sea clutter intensity distributions [C6722]

"Application of inverse chirp-z transform in wideband radar"

Pulse stepped frequency radar is a kind of wideband radar technique. It can obtain high range resolution by correct signal processing methods. One of most important methods is the inverse Fourier transform method. This method can realize pulse compression by the coherent sum of a series of echoes. Although the inverse Fourier transform method is very useful, the number of echo series limits the sampling resolution. In order to improve the sampling resolution at a fixed number of echo series, a special inverse chirp-z transform method is presented in this paper. This special inverse chirp-z transform method has all the features of the inverse Fourier transform method. It can compress a series of pulse signals and increase sampling resolution within a range profile window [C6723]

"A novel algorithm for reconstructing three-dimensional target shapes using sequential radar images"

Inverse synthetic aperture radar (ISAR) is one of the radar techniques used to observe two dimensional images of a remotely based target using radio waves. Since the "cross range" vector is ambiguous, estimating the three-dimensional shape of the target is difficult. However, it is possible to estimate the three-dimensional shape using moving pictures taken by a video camera, if the relative movement between the camera and the target is known. In this paper we propose an algorithm for reconstructing three-dimensional shape of the target by applying a similar technique to the ISAR images. The theory and the required condition of the proposed method are described and some results obtained by the computer simulations are shown [C6724]

"SARIS: synthetic aperture radar instrument simulator"

An application specific synthetic aperture radar (SAR) instrument simulator (SARIS) is presented. SARIS is initiated by the technical and economical requirements to simplify the instrument hardware and to reduce by this way the cost. The simulators structure is based on a system-theoretical modeling of the processes within a SAR system and results in the modular description of components and subassemblies. Contrary to known simulators, with SARIS the influence of imperfect hardware behavior will be calculated by adding realistic error functions to every component of the instrument assembly. The developed simulation model is turned into a MATLAB code. First simulation results are presented and illustrated [C6725]

"On the performance of curved SAR-mapping"

Normally SAR-mapping is performed along a straight path. A curved path might increase the mapping rate significantly, however. Drawbacks are more complex signal processing and that defocusing may occur. In this paper, curved SAR-mapping is analysed in more detail including forward look geometry. Relationships are shown how resolution performance and mapping rate are influenced by the curved SAR-path. Examples are also presented showing how the phase error depends on side acceleration and scene geometry [C6726]

"Estimating X-band synthetic aperture radar detection of objects obscured by foliage using the DSTO Ingara airborne imaging radar"

Estimating the Probability of Detection (Pd) of synthetic aperture radar (SAR) imagery of foliage-obscured objects requires a knowledge of the object backscatter and the obscuration properties of the foliage. At X-band frequencies minimal penetration of the foliage occurs and as such the assumption that the object is visible only through gaps in the foliage can be made. Given this assumption this paper discusses the use of Hemispherical Canopy Photographs (HCPs) and SAR imagery of unobscured objects to estimate the Pd of obscured objects. These estimates are compared with Pds measured directly from imagery of obscured objects. The results of this comparison show good agreement between the estimated and measured Pd values, indicating that a knowledge of the particular object backscatter and the HCP of a particular obscuration scenario is sufficient to predict the Pd without the need to image the obscured object directly [C6727]

"Autofocus of multi-band, shallow-water synthetic aperture sonar imagery using shear-averaging"

A significant problem with Synthetic Aperture Sonar (SAS) imaging is the compensation of compensating for unknown errors in the sonar path trajectory. Unknown path errors in SAS have the effect of blurring and smearing the sea-floor image. Inertial navigation systems as used in Synthetic Aperture Radar (SAR), are not accurate enough for use in SAS. To deal with this problem, techniques for estimating and compensating the path errors from the gathered data (autofocus algorithms) have been developed. In this paper we present enhancements to an existing sonar autofocus algorithm presented in 1995 by Johnston et al. These enhancements help prevent the autofocus being biased by strong targets. Improvement in autofocus is significant and more apparent whenever an extended prominent target is far stronger than the surrounding seafloor clutter signal. We have tested both algorithms using and simulated data and the results are presented in this paper. In addition, we demonstrate the advantage of using single pass multiband imagery to improve the autofocus result [C6728]

"2 GHz self-aligning tandem A/D converter for SAR"

A new generation of the Danish synthetic aperture radar system (EMISAR) is under development targeting a bandwidth of 800 MHz and a corresponding range resolution of around 25 cm. Two alternative approaches to achieve the wide bandwidth are considered. One is to use analog I/Q demodulation before digitizing, and the other is to digitize the signal before digital I/Q demodulation. In both cases the digitizing may be performed by a digital front end (DFE) with two parallel analog-to-digital-converters (ADCs) sampling at 1 GHz in phase or in anti-phase respectively, provided the analog bandwidth of the ADC is sufficient. In the first case each ADC has to digitize a 0-400 MHz signal, and in the second case both ADCs have to digitize a 100-900 MHz signal. In both cases the sampling time alignment is a critical parameter. The paper addresses some aspects of ADC alignment in the implementation of a DFE for the EMISAR system [C6729]

"Overview of the performances and tracking design of the SIRAL altimeter for the CryoSat mission"

This paper presents the principle of the measurements, the main system features and the basic ground processing of SIRAL. Simulations of the main performances in the different modes are also discussed including the bidimensional impulse response (range and azimuth). A major scientific requirement is to ensure the continuity of the measurements. This is particularly challenging for the on-board tracker over the steepest parts of the Antarctica. As a consequence a new tracking algorithm has been designed for SIRAL with the expertise of CNES. The algorithm has been derived from the analysis of simulated echoes using an Antarctica DEM and a radar echo simulator. The tracking design and performance are briefly described [C6730]

"SRTM X-SAR motion compensation: concept and first assessment of the interferometric observation geometry"

The space shuttle Endeavour that flew from 11 until 22 February carried the radar systems for the Shuttle Radar Topography Mission (SRTM). In the course of this project the first space born single pass interferometer has

mapped the Earth's topography. Two different radar systems operated on board of the space shuttle: the C-band radar of the American NASA/JPL and the X-band radar of the German DLR and the Italian ASI. It is the objective of this mission to generate a digital elevation model (DEM) of the Earth with an accuracy that has never been reached before on this global scale. The inevitable technically caused oscillation of the secondary antenna turns this task into a scientific and technological challenge. The Synthetic Aperture Radar (SAR) observation is influenced by a resulting sensor motion in the line of sight. The consequence of this effect on the secondary SAR scene and subsequently on the DEM is described in this paper. To obtain the requested height accuracy in spite of the antenna oscillation, the principle of motion compensation is applied. The concept of this key algorithm in the X-SAR SRTM project is explained in detail. The essential parameters of the interferometric observation geometry were recorded by the Attitude and Orbit Determination Avionics (AODA) system of the JPL. These AODA data are employed to investigate the movement of the secondary antenna [C6731]

"SAR instrument using stable active front-end technologies"

The next generation of synthetic aperture radar (SAR) for high resolution will utilize active front-ends with the capability of beam-steering. The challenge for the DESA technology program for an active front-end was to control several hundreds of transmit/receive modules (T/R modules) independently with high speed from pulse to pulse, and to maintain the phase and amplitudes constant over -20°C to +60°C. Also for interferometry the stability of the RF front-end and electronics plays a dominant role. In this context the X-SAR/SRTM hardware is presented. The ambitious measurement of the phase variations in the instrument channels is essential for the instrument calibration and picture quality [C6732]

"ERS-1 multitemporal backscatter analysis of different types of land cover in Brazilian Amazonia"

Three ERS-1 images acquired in 1992, 1993 and 1996 respectively, over the Tapajos National Forest, Brazilian Amazonia, were used and the results show that the pasture areas backscatter had a random behavior in all three images. Agricultural areas also had a random behavior in the three images, however their average backscatter was higher than the pasture average backscatter. The behaviors of regrowth at age ranged from 1 to 8 years affected by fire and regrowth at the same age but not affected by fire were different. Three different types of regrowth whose ages ranged from 9 to 15 years showed three different behaviors. Regrowths whose age vary from 18 to 22 years old showed behavior according to their previous land use. Three different types of primary forests also were analyzed and three different behaviors were found. This study shows that the previous land use can interfere in the multitemporal backscatter behavior of the land cover, and it was also inferred that multitemporal analysis can be useful for the building of automatic radar images classifiers, once different types of land covers present different behaviors [C6733]

"Suppressed ambiguity in range by phase-coded waveforms"

In Doppler radar for surveillance and remote sensing, the ambiguities in range/Doppler are usually solved by varying the pulse repetition frequency. In this paper, two alternative methods are discussed based on phase-coding and orthogonal waveforms. The first one distributes a phase code over a pulse sequence with only one phase step per pulse. The received pulses are correlated with the phase code sequence, and by varying the delay of the phase code, the subintervals in range are scanned and reflector responses outside the focused range interval become highly suppressed. The alternative method that was studied applies a set of near-orthogonal phase codes, which modulate the pulses transmitted. In the receiver, the different subintervals in range are scanned, or detected in parallel, by correlating the signal from the scene by the delayed code sequence of the pulse transmitted. Because orthogonal codes are used, a strong suppression is achieved for signals originating outside the focused subinterval in range [C6734]

"Noise radar for range/Doppler processing and digital beamforming using binary ADC"

Presently, there is an increasing interest in noise modulated radar. Wide-band signal processing with high range resolution, reduced ambiguities and high ECCM performance can be achieved. The processing involved correlates the received signal and the delayed reference. Range/Doppler processing and digital beamforming can be performed with surprisingly good results even for binary or a few bits ADC, if a second noise signal is added before [C6735]

"A high-resolution Imaging Wind and Rain Airborne Profiler for tropical cyclones"

The Microwave Remote Sensing Laboratory (MIRSL) at the University of Massachusetts (UMass) has developed the Imaging Wind and Rain Airborne Profiler (IWRAP) to improve the ability to nowcast and forecast extreme weather-events. This novel instrument is devoted to improve our knowledge in both the atmospheric boundary layer perturbances as well as the ocean surface winds, by providing both reflectivity and Doppler profiles

simultaneously at C and Ku-band and at four incidence angles [C6736]

"Use of an adapted marine radar for the short-range detection and tracking of small birds in flight"

As part of a project to develop an inexpensive songbird tracking and identification system, we have modified the antenna system of a standard marine radar to estimate the three dimensional position of point targets. Although the radar formally gives only two coordinate parameters, we show how the Incorporation of other information about the targets allows estimation of the full three dimensional position. We present two independent methods for this estimation. We have used this system in several field experiments at Prince Edward Point, Picton County, Ontario, Canada, where we have tracked various targets including a C-130 Hercules aircraft (RCS = 11 m²) and 10-40g birds (RCS = 7-22 cm²). Target locations were verified using an array of acoustic receivers to provide an independent measure of location [C6737]

"Major conclusions relating to the Katse Dam differential InSAR study"

The Katse Dam in Lesotho, which was completed in 1997, is the deepest dam on the African continent (180 m). Lithological modelling prior to the dam's construction had indicated that the loading effect of the reservoir on the Earth's crust would be well within the imaging capabilities of ERS InSAR, both in terms of vertical surface movement and lateral extent. A study, funded by The South African Water Research Commission, was started in 1996, the aim of which was to derive the crustal deformation field by differential InSAR, and to compare this with hypothesised models of the Lesotho lithosphere, thereby improving the models used for seismic risk assessments in the Lesotho Highlands Water Scheme. The lack of independent height data and the alpine terrain made the removal of the topographic phase component from interferograms very difficult. Fortunately however, surprisingly good phase coherence as well as a short baseline between images acquired as far apart as three years, meant that a conclusion could be reached in spite of the topographic problems, albeit a negative one. In a short baseline (21m) interferogram generated from a pair of ERS images acquired before and after the first filling of the Katse reservoir, no clear evidence of differential movement was apparent. Conventional geodetic levelling conducted at the dam showed that the actual vertical deformation was an order of magnitude less than that anticipated through the modelling. The basic implication here being that the flexural thickness of the Lesotho crust is greater than previously thought [C6738]

"Correction of atmospheric excess path delay appeared in repeat-pass SAR interferometry using objective analysis data"

In this study, we evaluated the robustness of a method to correct the atmospheric excess path delay component in the repeat-pass SAR interferometry using the typical objective analysis data, i.e., the Global Analysis Data (GANAL) and ECMWF [C6739]

"A SAR interferogram filter based on the empirical mode decomposition method"

In order to obtain a more accurate topographic model, a noise filtering step must be performed before the unwrapping of phase. In this article, a filter for suppressing speckle in SAR interferogram is proposed. The filter is based on the empirical mode decomposition (EMD) method which can separate the information to parts with different scale, when the parts related to the speckle is subtracted from the original interferogram, the speckle noise is reduced. The result is compared to that of two other methods and shows that EMD method is powerful to interferogram speckle noise reduction, as well as it can preserve fine details in the interferogram that are directly related to the ground topography and maintain phase values distribution [C6740]

"Topographic mapping with multiple antenna SAR interferometry: a Bayesian model-based approach"

Multiple-antenna SAR interferometry involves the use of three or more antennas to reduce the overall phase ambiguities and phase noise in interferometric data. This paper presents a Bayesian approach to topographic mapping with multiple-antenna SAR interferometry. Topographic reconstruction is formulated as a parameter estimation problem in the model-based Bayesian inference framework. An InSAR simulator based on a forward model is developed for simulating SAR data from multiple-antenna InSAR for evaluating the Bayesian topographic reconstruction algorithms. A Bayesian point position algorithm is developed to estimate the height of a point in the image. A measure of the uncertainty in estimated position and height is also defined in terms of the spread of the dominant mode of the posterior distribution. An example demonstrating the performance of the algorithm for a three-antenna InSAR system is reported, and conclusions are drawn regarding the performance and improvements are proposed [C6741]

"Effect of tropospheric range delay corrections on differential SAR interferograms"

The tropospheric range delay is estimated from meteorological data or GPS data, and then is used to correct JERS-1 SAR differential interferograms. Topography of the concerned area is considered in mapping the delay [C6742]

"Interferometric DEMs in rugged terrain"

Interferometric DEMs in steep mountains are a challenge even for high coherent single pass sensors like SRTM. This work compares shadow and lay-over problems for SRTM and ERS and shows how multiple interferometric observations could be used to compute a consistent DEM of an alpine region [C6743]

"Satellite radar interferometry reveals mining induced seismic deformation in South Africa"

Shortly after midnight on April 23rd 1999, the South African mining town of Welkom was shaken by a magnitude (local) 4.5 earthquake. Because of resulting power failures and substantial damage to the Eland shaft of Matjhabeng mine, two mine-workers were killed and hundreds of others were temporarily trapped more than a kilometre underground. Although seismicity due to rockbursts in the deep (>2 km) South African gold mines is relatively common, the consequences are not usually as serious as those resulting from the April 1999 event. By means of ERS SAR interferometry, we have successfully derived a map of the surface deformation resulting from the April 1999 event, and our result is being used in rockburst characterisation models. The location and magnitude of the deformation coincides well with that expected, given the epicentre location and the subsurface geological structure. The deformation feature is a 5 km long elliptical depression centred on the Eland Shaft of Matjhabeng mine. Its depth at the centre is 9 cm. Our result is significant not only because of our success in imaging the effects of a seismic event two orders of magnitude smaller than most of those previously imaged by interferometry, but also because it demonstrates the potential that the interferometric technique offers in providing critical information for rockburst amelioration studies [C6744]

"Progress report on the NASA/JPL airborne synthetic aperture radar system"

AIRSAR has served as a test-bed for both imaging radar techniques and radar technologies for over a decade. In fact, the polarimetric, cross-track interferometric, and along-track interferometric radar techniques were all developed using AIRSAR. In this paper, we present the up-to-date system configuration and expected performance in the standard radar modes. In addition, we describe the various experimental modes available to researchers. Finally, we discuss on-going improvements with AIRSAR and future direction of the program [C6745]

"MCF-homomorphisms of cost functions for minimum cost flow InSAR phase unwrapping"

Branchcut methods represent an important class of phase unwrapping (PU) approaches in SAR interferometry (InSAR). Their main idea is to circumvent the problem of path dependency for the integration of the wrapped gradient of the wrapped interferometric phase by placing suitable barriers (branchcuts) to the possible integration paths in the image. In 1996 M. Costantini proposed to transform the problem of InSAR PU to a minimum cost flow (MCF) problem. The critical point of this new approach is to generate cost functions which represent the a priori knowledge necessary for phase unwrapping. Since many algorithms for generating cost functions from a priori knowledge have been proposed in the last years, it has become important to decide whether two given methods of computing cost functions lead to the same branchcut system on every interferogram. A formal tool to treat this problem mathematically are universal MCF-homomorphisms. Any mapping α from the space of cost functions into itself is called an universal MCF-homomorphism if every cost function c and its image $\alpha(c)$ have the same MCF solution and if α can be defined separately for each arc. This paper presents the proof of the following mathematical theorem: The only existing universal MCF-homomorphisms are the componentwise multiplications with a fixed positive scalar [C6746]

"Validation of a CFAR vessel detection algorithm using known vessel locations"

The National Oceanic and Atmospheric Administration (NOAA)/National Environmental Satellite, Data, And Information Service (NESDIS) is in the second year of a two-year demonstration of Synthetic Aperture Radar (SAR) derived products called the Alaska SAR Demonstration (AKDEMO). This demonstration provides near real-time SAR data and derived products, including wind images and vectors, hard target locations, along with ancillary data, to specific users in the government community. One of the derived products are vessel positions obtained from a constant false alarm rate (CFAR) vessel detection algorithm developed by Veridian ERIM. This algorithm has been tested and validated to maximize the number of ships found while minimizing the number or false alarms on one SAR image of the Red King Crab fishery in Bristol Bay on October 18, 1999. This resulted

in using a detection statistic threshold of about 5.5, depending on image resolution used. Until now, this validation has been done with only general knowledge of fishing fleet size and location, but no in situ vessel information. This paper presents the results of a validation of the SAR vessel detection algorithm using observer reported vessel positions along with information on vessel size and local wind speed [C6747]

"Derivation of spatial distribution of snow precipitation using interferometric SAR technique"

Accurate knowledge of spatial variation of snow precipitation in an area is important because it provides information of an initial condition that has significant impact on subsequent processes. However, such information is difficult to obtain because (1) snow gauges are sparsely distributed, and (2) snow gauges are notoriously inaccurate for snow measurement. The sparsity of snow gauges is especially severe in Alaska because of its remoteness. We applied satellite interferometric SAR (InSAR) technique to investigate spatial variation of snow precipitation on the Alaskan North Slope. SAR images acquired during the ERS-1 second ice phase in early 1994 were processed to form interferograms at a study site near Franklin Bluffs. Because new snow accumulation would increase radar path length, a pattern of spatial variation in snow precipitation might be derived from the phase pattern seen on the interferograms. A new snow precipitation of 7 cm on February 5, 1994 was reported for the area. An interferogram constructed from ERS-1 SAR images acquired on February 4 and 7 spanned this snow event. The terrain effects were removed using another interferogram that was constructed from a pair of SAR images acquired before the snow event. The resulting interferometric phase pattern is interpreted as a thickness variation of 8 cm in the new snow precipitation [C6748]

"Volcanic ash size distribution determined by weather radar"

A Doppler weather radar has been observing routinely the backscatter from ash emitted by a volcano on top of Mt. Oyama on Miyake Island-south east of Tokyo. The purpose of this paper is to show that the time dependent size distribution $N(D,t)$ of ash particles can be obtained from the time dependence of the reflectivity factor $Z(t)$ in the radar's resolution volume V_6 (Doviak and Zrnic 1993) advecting with the wind. It is assumed that $Z(t)$ is controlled by the different times required for ash particles of different diameters D and terminal velocities to empty V_6 [C6749]

"Detection of ships using cross-correlation of split-look SAR images"

One of the main problems in ship detection is the presence of sea clutter inherent to coherent imagery. A traditional approach to differentiate a target embedded in noise is to utilize the statistical property of the clutter with some success. In this paper, we propose a new technique of ship detection based on cross-correlating split-look SAR images. If the inter-look images consist of the correlated images of a ship and clutter, the degree of mutual correlation increases, and from the difference in correlation, the ship can be identified. Applying the present method to RADARSAT (Standard 1) images, we have found the minimum detectable size of ships is 62.6 m. The SAR data used in this application were acquired under fairly calm sea states, such that the ships can be identified by the naked eye. Thus, the method has not been tested in an extreme limit of high sea states, and remains as a further study [C6750]

"Satellite altimetry-implied sea ice distribution in the Weddell Sea, Antarctica"

We investigated the distribution of sea ice using Topex/Poseidon(T/P) and ERS-1 radar altimeter data in the northwest Weddell Sea, Antarctica, between the area 45-75°W and 55-66°S. Using the Geo_Bad_1 flag of the Merged GDR of Topex/Poseidon, we classified the surface into ocean, land, and sea ice based on the return waveforms. A total of 257 cycles of altimeter measurements between Oct. 1992 and Sep. 1999 (for nearly 2570 days) were analyzed to visualize the distribution of sea ice. We then calculated the surface area of ice coverage using SUTM20 map projection to quantify the periodic variations. Each year, the maximum and minimum coverages of sea ice were found in early October and March in the study area, respectively. We also studied the sea ice distribution using ERS-1 altimeter data between 45-75°W and 55-81.5°S. Using the valid/invalid flag of the ocean product, we studied the sea ice distribution between March and August of 1995, which showed very good coherence with the T/P measurements [C6751]

"Snow and ice characterization studies using a radar altimeter"

A Ku-band radar altimeter has been deployed above a layer of snow to explore the effectiveness of a new method for snow depth measurement. This method takes advantage of the effect of the reflection coefficient of the snow layer on the transmitted chirped pulse to determine the snow depth. The snow layer and the ground are modeled as dielectric layers. The magnitude of the reflection coefficient from such a model varies with the frequency of the transmitted signal, and that variation changes in frequency as the depth of the dielectric layer changes. This is used to determine the depth of the snow. Experimental data is used to support the method

[C6752]

"Global distribution of sea surface features from SAR wave mode data"

A global set of single look complex (SLC) synthetic aperture radar (SAR) images is processed, from wave mode raw data using the B-SAR processor developed at Deutsches Zentrum für Luft und Raumfahrt (DLR). Multilook methods are used to reduce speckle or to analyze the time evolution of the ocean surface cross section during SAR Integration time. Using imagerettes instead of image power spectra allows to study ocean surface features caused by natural slicks, sea ice or atmospheric processes. Different automatic image analysis methods are used to detect and classify these features. About 200 imagerettes are acquired over the Arctic every day, from these data sea ice parameters are derived [C6753]

"Azimuth variation in microwave backscatter over the Greenland Ice Sheet"

Scatterometer backscatter measurements are becoming an important tool for monitoring the dynamic behavior of the Greenland Ice Sheet. However, most Greenland studies assume constant backscatter for varying azimuth angles. Detailed analysis of scatterometer data sets show non-negligible (1-2 dB) azimuth modulation. The magnitude and orientation of the azimuth modulation observed by SeaWinds, NSCAT, and ERS are documented herein. The dominant factor is second order azimuth modulation, which is largest for C-band (ERS). For SeaWinds, the h-pol azimuth modulation is larger than for v-pol [C6754]

"On shape, orientation and structure of atmospheric cells inside wind rolls in SAR images"

SAR images of sea surface often show roll-vortex structures, which have multiscale character. The present work investigates this aspect, using the two dimensional continuous wavelet transform (CWT2), which appears suitable to extract quantitative information about the structures present in SAR images. CWT2 analysis has been applied to ERS SAR images showing wind rolls, to evaluate the horizontal and vertical scales of the highest backscatter cells. The possibility to produce a SAR-like image at given scale lengths has permitted to evidence the backscatter cells. They have been characterised in terms of the orientation, size of their principal axes, area as well as of the spatial structure of the probability density function. The results may be used to study the inner structure of the atmospheric wind rolls [C6755]

"Reconstruction of 3D urban model using range image and aerial image"

This paper introduces a method that utilizes airborne laser range images and aerial images for the 3D reconstruction of urban models. The method consists of three procedures: object extraction and object modeling using range images, and texture mapping using aerial images. Objects are extracted from range images by edge analysis and classification through the use of vertical geometric patterns. Our approach also uses the automatic registration of images onto 3D models for texture mapping. The method is based on edge pair extraction as matching features and displacement determination by voting. Experimental results show that 3D reconstruction in a test area is generally successful [C6756]

"OSCAR-object oriented segmentation and classification of advanced radar allow automated information extraction"

DEFiNiENS is a new innovation oriented German company which developed a powerful image analysis software, eCognition. One of the current research projects within the company is to expand the capabilities of eCognition for SAR information extraction. These developments will help remote sensing on its way from a research oriented to an operational technology with commercial benefit. To support this development, the German Aerospace Center (DLR) co-funds the project ProSmart II and therein the sub-project OSCAR (object oriented segmentation and classification of advanced SAR data). In OSCAR, DEFiNiENS improves the suitability of eCognition for automatic information extraction and validates the results together with ProSmart II partners on exemplary applications [C6757]

"Case-based lightning flash forecast support system taking account of range of thundercloud"

In order to prevent the damage caused by natural phenomena, such as rain, cloud, lightning and squall, we use meteorological radars for the observation. Demand has been increasing for more accurate information for natural phenomena, since it is becoming more important to analyze the observation data for the forecast. We have been applying a case-based retrieval algorithm to forecast lightning flashes. However, since the proposed method considers the partial local region in retrieving the similar case, a number of dissimilar cases may be retrieved. In order to solve this problem, we propose a new retrieval scheme which takes account of the range of the thundercloud. We show that this scheme is efficient by means of an example of the application [C6758]

"Measurement of Z-R relations using a small Doppler radar and image data of snow particles"

Presents a new system to measure physical snowfall parameters using image processing techniques. It is possible to calculate the snowfall rate from the mass and volume of each snow particle. Using image data, it is also possible to calculate the radar reflectivity Z, assuming Rayleigh scattering and discrete data. The relationship between X-band wave attenuation, Z and snowfall rate was investigated and compared to the characteristics of snow particles. It was suggested that the power spectrum is related with the content of ice crystals [C6759]

"The use of airborne P-band radar data for land use and land cover mapping in Brazilian Amazonia"

The aim of this work was to analyze the potentiality of polarimetric P-band data for land use and land cover mapping in a site of the Brazilian Amazonia. These data are the first P-band image set gathered in the Brazilian Amazonia, so they represent a unique opportunity of analyzing the potentiality of this frequency for classification purposes. The stratification of land use/land cover classes was performed using a classification system specially developed for polarimetric data. Results showed that P-band data were able to discriminate forest and regeneration areas from crop, pasture and bare soil areas. Moreover, regeneration areas (older than 12 years) were successfully distinguished from primary forest and other regeneration stages [C6760]

"Parallel SAR processor using PVM on a Beowulf cluster"

Beowulf cluster computers (often called a "pile of PCs") have become common place, since they offer significant processing power at a fraction of the cost of custom, massively parallel machines. The processing needs of SAR naturally seem to point to a Beowulf cluster. However, as with all parallel computing, task granularity is a governing factor in the choice of compute node (processor, memory) and the interconnection (network technology and switch). This paper examines some of these issues in the design and testing of a SAR processor for a non real-time airborne radar. The system presented was constrained to fit to an existing, small Beowulf cluster [C6761]

"Non-uniform azimuth image shift caused by the pitching motion of ships observed in Radarsat images"

Non-uniform azimuth image shift of a rigid body is observed, for the first time, in the Radarsat images of moving ships in pitching motion. The pitching velocity is estimated from the SAR image of a known ship, and compared with that computed using a numerical model with the meteorological and ship's data; further comparison is made with the wave orbital velocity. The results are shown to be all in excellent agreement. Comparisons are also made between the pitching velocities of unknown ships with the wave orbital velocity, and a reasonable agreement is obtained [C6762]

"Sea ice segmentation using Markov random fields"

Tools are required to assist the identification of pertinent classes in SAR sea ice imagery. Texture models offer a means of performing this task. The texture information in SAR sea ice imagery can be characterized by two Markov random field models: the Gauss model for conditional distribution of the observed intensity image and the discrete model for the underlying texture label image. The segmentation can be implemented as an optimization process of maximizing a posteriori distribution in a Bayesian framework [C6763]

"Effects of time series imagery on automated classification of coastal wetland environments using projection pursuit methods"

Using a time series of Radarsat SAR and Landsat TM imagery, we developed automated classification models for coastal land-cover in Northampton County, VA. The database consisted of three pairs of images from each sensor taken within one week of each other. We compared the results of models based on data from one set with the results based on data from all three sets for Radarsat only, Landsat only and both sensors combined. For Radarsat only, there is an increase on the order of 23-30% in the overall classification score for the three-date set compared to the one-date set. This is consistent with previous results based on different classification methods. We found a smaller increase, on the order of 1-5%, for the Landsat only. For combined sensor cases, three-date inputs did not improve results when compared with single-date inputs. For the feature extraction stage, we compared a projection pursuit method with principal component analysis. In the final classifier stage, we compared a vector quantization algorithm, LVQ, and the backward propagation of error model with a cross-entropy cost function. The differences given above for one-date versus three-date results hold for all the

methods studied. Best model agreement with a National Wetlands Inventory (NWI) map was found for three-date atmospherically corrected Landsat inputs, for which generalization performance was 80.5% of pixels correct, with 86.4% obtained on the cross-validation set used to find a stopping point for model optimization, and 87.9% for the training set [C6764]

"A comparison study of the surface scattering models and numerical model"

This paper describes a comparison study of surface scattering models and a numerical model for dielectric surfaces. Two surface scattering models namely the integral equation model (IEM) and the small slope approximation (SSA) model are used to calculate the backscattering coefficients of rough surfaces and the results are compared with numerical simulations based on the moment method (MoM). Analysis of the results obtained is also presented [C6765]

"Performances of the POSEIDON-1 radar altimeter"

This paper describes the results of the performance analysis of the French radar altimeter, POSEIDON-1 (also called SSALT for Solid State Altimeter), flying on board the TOPEX/POSEIDON satellite. The results we present are issued from the analysis of eight years of data (from 1992 to 2000). They range from operation performance (availability, coverage...) to altimetric system performance (cross-over analysis, sea level analysis...) going through instrumental performances. It is shown that POSEIDON-1 is behaving well within its specification. Comparisons of the data set issued from POSEIDON-1 and TOPEX have been performed. Mutual benefits in term of data quality and characterizations are illustrated. The TOPEX/POSEIDON follow-on mission called JASON-1 will embark the dual frequency (Ku and C bands) POSEIDON-2 altimeter which inherits from POSEIDON-1 [C6766]

"Simulation study on optimal conditions for internal wave observation by SAR"

A simulation model for internal wave observation by synthetic aperture radar (SAR) has been developed based on the radar imaging mechanism of internal waves. The model consists of the Korteweg-de Vries (KdV) equation, the action balance equation and the radar backscattering model. The results of the simulation model have been used to study the image characteristics of internal waves, the optimal SAR parameters (frequency, polarization, incidence angle and look direction) for observing internal waves and the relationship between internal wave related parameters (amplitude, pycnocline depth, density variation of pycnocline) and SAR observation of internal waves [C6767]

"Application of recent satellite remote sensing technology in earthquake disaster reduction"

It has been proven that InSAR technology has special advantages in the measurement of coseismic displacement and evaluation of earthquake damage. It will provide a powerful vehicle for effective earthquake emergency response. This paper discusses the necessity, feasibility and related scientific-technical issues of satellite remote sensing technology applied in earthquake disaster reduction [C6768]

"The seismic fault parameters retrieval of Zhangbei earthquake"

Using the interferometric fringes generated by the phase difference among three SAR images acquired by the ERS-1/2 satellite, based on a standard elastic dislocation formation for coseismic displacement, the seismic fault parameters of Zhangbei-Shangyi earthquake are estimated. It is suggested that the seismic fault of Zhangbei-Shangyi earthquake is a thrust fault dipping SW with a large right-lateral displacement component. The strike, dip are 95°, 30°, respectively on a fault patch 12 km long by 14 km wide. Its hypocenter is located at N40°58', E114°21', 7.5 km depth. The estimated slip vector is 0.728 m with a rake of 105.95° the trend of slip is NW13.26° [C6769]

"Depth and amplitude estimation of internal waves from SAR imagery"

Imagery from ERS-1 synthetic aperture radar (SAR) has been used to estimate the depth and amplitude of internal waves in the China seas. It is assumed that the observed groups of internal wave packets on SAR imagery are generated by local semidiurnal tides. The mean distance between the leading crest of two successive wave packets has been used to derive the group velocity of the internal waves. The depth and amplitude of internal waves have been calculated from a model which consists of the KdV equation, action balance equation and Bragg scattering model. Results show a good agreement with in situ measurements [C6770]

"Study on soil moisture with ground-based scatterometer and IEM model"

A FM-CW ground base C-band scatterometer is used to measure the bare soil surface. The measurement was conducted at different incident angles and for two soil moisture conditions. In-situ measurement is also arranged simultaneously in order to verify the retrieved moisture. During the moisture retrieval, the integration equation method (IEM) is used. The results show that the method could be used to build up the soil moisture database and could then be used for satellite data applications [C6771]

"Potential and methodology of satellite based SAR for hazard mapping"

SAR and InSAR data have a high potential for change detection due to their "all weather" capability and the day/night access of the sensors. Here we investigate the potential and methodology for forest storm, flood, and avalanche mapping with ERS1/2 data. In our methodology process models are used to describe the targets before, during and/or after the hazard event. Very important are the good relative calibration and accurate coregistration of the different information layers. The presented results demonstrate the good potential of multitemporal SAR and InSAR data for hazard mapping [C6772]

"Detection of flood-inundated area and relation between the area and micro-geomorphology using SAR and GIS"

A flood-inundated area can be detected using JERS-1/SAR data in the central plain of Thailand. The area is related with micro-geomorphology. It has the possibility that agricultural damage by flood can be estimated using both SAR data and geomorphological maps [C6773]

"Radar rainfall estimation from vertical reflectivity profile using neural network"

An adaptive radial basis function (RBF) neural network to estimate the ground rainfall from a vertical profile of reflectivity factor (Z) is presented in this paper. This RBF network was applied to two months of WSR-88D radar data to estimate rainfall. Results show that the adaptive RBF developed here can estimate rainfall fairly well. Results were also compared with the WSR-88D, Z-R relationship and the Z-R algorithm derived from previous day observations [C6774]

"Extracting the flood extent from satellite SAR image with the support of topographic data"

A satellite SAR image is broadly used in monitoring and evaluating flood disasters. It is difficult to automatically extract the flood extent from RADARSAT SAR images because of the confusion of the gray value between the flood and shade in imagery gray. Therefore, extracting the flood extent from satellite SAR image with the support of digital topographic data is explored here. It included several steps as follows. Firstly, RADARSAT SAR imagery was filtered by enhanced frost filter with window size of 7 pixels by 7 pixels, and geo-registered to the topographic map. Secondly, flood extent was primarily extracted from RADARSAT SAR imagery. Thirdly, DEM was created from the digital topographic data by using GIS software. Fourthly, simulated SAR imagery was created from DEM. Finally, the simulated SAR imagery was registered to RADARSAT SAR imagery, and the shade from the simulated SAR image was used to mask the mislabeled flood extent from RADARSAT SAR due to its shadow influence. It is shown that the flood extent can be accurately, semiautomatically extracted from RADARSAT SAR by the method. It also is shown that the method is not only suitable for RADARSAT SAR imagery, but also suitable for other satellite SAR imagery with the different imaging mode, especially for SAR image covering mountainous area [C6775]

"The application of SLAR image in surveying fossil river course"

Keliya River is in the hinterland of the Taklamakan desert. Revealing the distribution of the lower reaches of the fossil river has important significance for its ecological construction and groundwater source surveying. Using an X-band SLAR image as an important information source, and combining this with the field investigation, the fundamental principle and imagery feature of the river course in the airborne SLAR image are studied and analyzed. The study indicated that the X-band of the SLAR image could pass through 14.6 cm depth in the background desert, and 10.34 cm depth in the fossil riverbed [C6776]

"Extraction of DEM from single SAR based on radargrammetry"

Topographic information is important in many geographic applications. Synthetic aperture radar (SAR) is a kind of imaging radar capable of producing high-resolution images in all weather and all-day conditions. But it is usually needs image pair or more images to generate DEM from SAR imagery, such as interferometric SAR (InSAR) and radargrammetry. The imaging conditions (look-angle, space baseline, for acquiring the image pair)

sometimes are very difficult. SAR is a side-looking imaging mode and its image is very sensitive to the terrain shape. The undulation of the terrain may induce the change of the image gray distribution and/or the texture characteristics. In this paper, the radarclinometry for extracting the earth elevation from only single SAR image is investigated, which is based on the shape-from-shading principle developed in computer vision. Firstly, the approaches for generation of the digital terrain elevation from the SAR image data are discussed. Secondly the method of radarclinometry is briefly described. The elevation reconstruction relies on a Lambertian assumption for the terrain backscatter model. Then a single-line integral process is applied to calculate each pixel altitude, but it is still contaminated by noise. Finally the multi-line integral processing with various directions and the simulated annealing algorithm are respectively introduced to improve the single-line integral processing result. The presented experiment results promising in many geographic applications [C6777]

"SAR ocean wave imaging spectra simulation"

The main object of the article is to simulate the two-dimensional image spectrum from raw synthetic aperture radar data. The quasi-linear imaging model for simulating synthetic aperture radar (SAR) images of ocean spectra is explored in this article. Wave height spectra measured by the National Data Buoy Center (NDBC), US are used as inputs to the quasi-linear model. Additional parametric variations are presented to illustrate the imaging process [C6778]

"Data fusion of multi-sensor for petroleum geological exploration"

Integrating different remote sensing data to obtain the geological information as much as possible for petroleum geological exploration is the main object of this research project. Radar images have very different characteristics from visible/infrared satellite remote sensing images in both physical properties and image mechanization. Data fusion technology is used to merge Landsat TM data and Radarsat SAR data, and several methods of image fusion and information extraction are tried to compare their results. The result images show that the different detail can be highlighted by different approach, and the method of image multiplication followed by PCA transform obtains good effects by analyzing carefully the each character if these two images. The integrated images give some new understand for the geological structure of the area and reveal some buried structures and faults through comprehensive geological interpretation [C6779]

"The collection of GPS signal scattered off a wind-driven ocean with a down-looking GPS receiver: polarization properties versus wind speed and direction"

A GPS transmitter-receiver pair form a bistatic radar for ocean remote sensing when the receiving platform carries a downlooking antenna capable of collecting the GPS signal scattered off the ocean surface. The aggregate GPS signal scattered by the ocean and received in a general bistatic configuration has been calculated for representative geometries and a variety of wind speeds and directions, using the integral equation method (IEM) combined with a realistic ocean correlation function (spectrum). The role of polarization of the reflected signal is investigated and its dependence on wind speed and direction is analyzed to assess its suitability as a detector of the wind vector. The complexity of the scattering calculations is handled by an efficient integration scheme based on combining Gaussian quadrature with a local interpolation of the surface correlation function. Additionally, since a large number of scattering contributions are required the code has been parallelized for efficiency. Some relevant features of the parallelization scheme are outlined [C6780]

"Coherence time and statistical properties of the GPS signal scattered off the ocean surface and their impact on the accuracy of remote sensing of sea surface topography and winds"

A GPS transmitter-receiver pair forms a bistatic radar for ocean remote sensing when the receiving platform carries a down-looking antenna capable of collecting the GPS signal scattered off the ocean surface. The average received power versus time is derived as a function of viewing geometry, system parameters and ocean state. This waveform is crucial for the derivation of the sea surface topography (from its leading edge) or wind speed and direction (from its trailing edge). In predicting the accuracy of either measurement it is important to understand how accurately the average power can be determined in practical situations. This starts with the determination of the coherence time of the scattering, over which the received signal can be integrated for optimal signal to noise ratio. Additionally, the real signal is affected by self-noise which introduces variability from one sample to another. This work examines the coherence properties of the modeled received power as a function of sea state and scattering geometry. In particular the coherence time variability between leading and trailing edges is addressed, and its impact on the accuracy of either sea surface topography or wind speed and direction measurements is addressed. In particular, having determined the integration time necessary to produce independent samples, the incoherent summation time required for a given measurement accuracy is derived. Furthermore, the lag-to-lag correlation is addressed, leading to a covariance analysis formulation for the formal

error in height retrieval [C6781]

"Remote sensing technique and prognosis of sandstone type uranium deposit"

This paper is firstly aimed at discussing how to utilize different types of remote sensing data and image enhancement, information extraction and multi-source data (TM, JERS-SAR, and geophysical, geochemical data) fusion processing to acquire information related to uranium mineralization. Then, how to interpret structures (including faults and folds) which controlled uranium deposit distribution, lithology and stratigraphy, and how to interpret ore controlling factors have been elaborated. Based on the analysis of metallogenic environment and condition, the metallogenic prognosis procedure has been established and finally, a favorable section has been predicted. The practice has indicated that application of remote sensing techniques to uranium reconnaissance, exploration and prognosis has potential prospects [C6782]

"The scanning mathematic models of a sensor with three freedoms of rotation"

There are various sensors based on surveying distance and/or recording spectrum. Many of these sensors, including remote sensing sensors, normally have 1-2 degrees of freedom of rotation in their optical and mechanical parts. This paper introduces scanning mathematic models of a sensor with three degrees of freedom of rotation for the sensor designers. It is advantageous to use the scanning equations of the mathematic models in various forms and directions in overcoming dead corner and offering arbitrary location scanning. The mathematic models have been successfully used in a structure-light industrial surveying system based on a laser theodolite with three degrees of freedom of rotation, which was researched by author [C6783]

"Investigations on anti-personnel mine detection using microwave radiometers"

Many million anti-personnel mines are polluting the environment in about 60 countries and cause a considerable limitation of the living space for agricultural purposes. The present mine clearance operations are much slower than the mine laying operations. Therefore the principal goals of a mine detection system designer must be focused on the following key requirements: 1) The system should be capable of detecting small surface and subsurface plastic mines with very low metal content under most environmental conditions, 2) the detection probability should be maximised and the false alarm rate minimised, 3) the hardware expense should be as most cost-effective as possible. The optimum solution is the use of multiple sensors, e.g. metal detectors, ground penetrating radars, microwave radiometers, based on different physical phenomena and on data fusion. In this paper we give an overview on relevant physical phenomenology and on our past work in investigating passive microwave sensors for mine detection purposes as a possible contribution to a multi-sensor system. We present experimental equipment and corresponding illustrative measurements results [C6784]

"Multi-baseline airborne Pol-InSAR measurements for the estimation of scattering processes within vegetation media"

Interferometric decomposition permits the identification of arbitrary scattering mechanisms in two interferometric SAR images and the optimisation of the interferometric coherence, using mathematically independent phase centres related to these scattering mechanisms. Polarimetric SAR interferometry (Pol-InSAR) is sensitive to the distribution of oriented objects in vegetation layers. It has been demonstrated that the calculated scattering mechanisms have different vertical loci that can be related to certain vegetation structures. Additionally, theoretical models allow for the reconstruction of the quasi-three-dimensional spatial distribution of such scattering mechanisms within multi-layer morphologies and the derivation of vegetation-related physical parameters. The paper presents an evaluation of a coherent Pol-InSAR scattering model using simulations based on the configuration of a real airborne experiment. This experiment provides multi-baseline L-band scattering matrices acquired by the DLR experimental SAR system (E-SAR) [C6785]

"The Poseidon-2 altimeter simulator of performances"

Presents the simulator of performances of the Poseidon-2 altimeter embarked onboard JASON-1 oceanographic mission to be launched during 2001. This simulator is a key tool used during the whole life of the Poseidon-2 altimeter, from feasibility studies, definitions, specifications and development phases to "expertise" tasks on the behavior of the instrument during the operating phase. It has been developed by Centre National d'Etudes Spatiales and Collecte Localisation Satellites teams [C6786]

"Robust inversion of vegetation structure parameters from low-frequency, polarimetric interferometric SAR"

The Cloude model provides an approach to estimating vegetation structure parameters, such as bald Earth

elevation, tree height, and canopy attenuation, using polarimetric interferometry techniques. We show that the model contains a degeneracy that allows the bald Earth elevation to be solved for reliably, but prevents accurate estimation of the other model parameters unless simplifying assumptions are made. We present results using UWB UHF data from the P-3 FOPEN sensor [C6787]

"Barrier Reef Airborne Gravity Survey (BRAGS'99)"

Support from the Australian Hydrographic Office made it possible to install and operate a gravimeter in their Fokker F-27 aircraft which carries their Laser Airborne Depth Sounding (LADS) system. The LADS system operated in the Great Barrier Reef region, northeast Australia, at that time. This shallow water area is a major gravimetric data void, and thus degrades the gravimetric geoid models in and around the area. The aim of the airborne gravity measurements was both to gather new data in the area to improve the geoid and to examine the feasibility of combined airborne bathymetry and gravity surveys. The system performance is validated by internal crossover analysis and comparison to existing data. The contribution of the newly acquired data to geoid modelling is examined [C6788]

"Efficient geolocation and image simulation for extended SAR strip maps"

We introduce a more efficient method for implementing backward geocoding. For grid locations sparsely spaced along the extended swath, forward geocoding is used to calculate map coordinates corresponding to near and far-range locations (at a single nominal height). A buffer extends the near and far range positions to account for differences between nominal and true (DEM) heights. All map co-ordinate locations outside these boundaries are marked apriorias "no data" positions (no radar data available there). Within the confines of these boundaries, geolocation proceeds normally. We document the run-time improvement provided, and show how the increase in efficiency provided by geolocation confinement grows quadratically with the length of the swath. We demonstrate significantly improved run times for image simulation using simulated ENVISAT products generated with ERS data [C6789]

"Polarimetric edge detector based on the complex Wishart distribution"

A new edge detector for polarimetric SAR data has been developed. The edge detector is based on a newly developed test statistic for equality of two complex covariance matrices following the complex Wishart distribution and an associated asymptotic probability for the test statistic. The new polarimetric edge detector provides a constant false alarm rate and it utilizes the full polarimetric information. The edge detector has been applied to polarimetric SAR data from the Danish dual-frequency, airborne polarimetric SAR, EMISAR. The results show clearly an improved edge detection performance for the full polarimetric detector compared to single channel approaches [C6790]

"Validation of the ENVISAT RA2/MWR Level 2 ocean reference processor using real TOPEX data"

CLS (Collecte Localisation Satellite) was contracted by ESA (European Space Agency) to develop the ocean geophysical reference processor of the ENVISAT radar altimeter. After briefly describing the different main processes, this paper presents the validation of this reference processor with real data from the TOPEX/Poseidon mission [C6791]

"CARABAS measurements of coniferous forest stem volume on sloping terrain"

Low frequency SAR has shown good results for the retrieval of stem volume in coniferous forests, where the scattering strength is directly related to the volume of the trunk. However, since the scattering is dominated by the trunk-ground dihedral mechanism, it is also sensitive to the topography (i.e. angle between trunk and ground). Using data from CARABAS, we show how the backscattering is sensitive to the topography and radar viewing geometry. However, unlike higher frequencies, the VHF scattering from trees on moderate slopes is still dominated by the trunk-ground interaction [C6792]

"Polarimetric radiometer sensing of sea surface winds using SHOWEX data to determine the Stokes harmonic coefficients"

This research utilizes the analysis of data acquired from microwave remote sensing instruments deployed on the Twin-Otter aircraft during the Shoaling Waves Experiment (SHOWEX 99) between November 11 to December 4, 1999. The principal data comes from the NOAA/ETL 37 GHz polarimetric radiometer and APL/UW coherent real-aperture radar (CORAR), a dual polarized X-band radar (which for the purposes of this investigation is being used as an incoherent scatterometer) A principal focus is the study of the magnitude and variance of the harmonic coefficients of the Stokes parameters (mainly the Fourier coefficients, "Q2" and "U2") at a variety of

incidence angles, as a function of wind speed and friction velocity. An examination of the azimuthal variation of the polarimetric radiometer (PR) data from seven different flight days during SHOWEX (with winds ranging from 7 to 12 m/s) showed that the Stokes parameters (Q & U) increase with wind speed consistent with results obtained during the COPE Experiment in 1995. However, the variability observed at higher incidence angles increases the likelihood of errors in applications [C6793]

"ERS differential SAR interferometry for urban subsidence monitoring of Suzhou, Eastern China"

Since the 1980s excessive ground water exploitation in a lot of cities has resulted in significant land subsidence that has damaged buildings, roads, and pipelines. It has also changed the areas affected by flooding. And in recent years the subsidence of the megalopolis has been increasingly serious. Differential SAR interferometry (D-InSAR) with ERS-1/2 SAR data has a high potential for surface displacement mapping in the mm to m range. In this paper the potential of ERS-1/2 SAR interferometry for mapping of subtle land subsidence has been investigated. Our measurements were taken in Suzhou city, Jiangsu province, China. We collected a time series of ERS-1/2 SAR data from February 1993 to February 2000, Eight ERS-1/2 SAR images were used to create seven interferograms, three differential interferograms were produced using three-pass method, which clearly showed the spatial extent of subsidence. The D-InSAR deformation maps were validated by leveling surveys. The correlation between D-INSAR observations and leveling observations was 0.943 and standard error was 0.1706. Based on seven benchmarks, the subsidence rates were estimated the overall trend were in close agreement with D-InSAR results. We concluded that for the mapping of land subsidence in urban environments D-InSAR had a strong potential with regard to cost effectiveness, resolution and accuracy. In many other cities affected by subsidence, D-InSAR should be operationally applied [C6794]

"SDRS: software-defined radar sensors"

This paper presents a new system idea for SAR, in which the key functions are software defined. This means they can be changed during a mission either by control of stored software or by downloading the new functions. The operation modes may be very flexible including side-looking and forward-looking modes. Multiple antennas arranged across track or along track are used for receive, depending on the application. The spatial resolution is achieved by phase comparison, Doppler and/or bandwidth compression. The system configuration becomes extremely simple and modular. Ground-based and airborne high resolution can be achieved. Digital beam forming on receive only can be implemented. These SAR sensors are also suitable for bistatic operation or for operation with transmitters of opportunity [C6795]

"Complimentary measurement of geophysical deformation using repeat-pass SAR"

Differential radar interferometry has proven to be an excellent method to measure displacements associated with geophysical phenomena such as glacier flow, subsidence, tectonic plate motion, and earthquake displacement. Since the technique utilizes the interferometric phase, it is limited in cases where large displacements in the slant range direction result in complete decorrelation. Similarly, if the surface deformation causes rotation of the scene or other disturbances the interferometric signal will be lost. The geophysical displacement field can also be measured via incoherent or coherent cross-correlation of small image chips. This method has the advantages that it does not require phase unwrapping. In cases where there is some degree of interferometric coherence between data acquisitions, the single-look complex image speckles themselves become features that can be accurately tracked. This method is complimentary to the phase-based approach since it works well with the large displacements. Examples for the successful application of the two techniques are found in the mapping of the velocity fields of surging glaciers and displacement fields of major earthquakes. Furthermore, image cross-correlation measurements yield the two-dimensional displacement field while measurements of the phase yield deformation only along the line-of-sight. Accuracy of the cross-correlation method is dependent on the scene content, correlation, and image chip size [C6796]

"Air-sea interaction observed by HF radar on Monterey Bay"

Monterey Bay provides an interesting location for studying air-sea interaction under a cyclic, land-sea breeze, circulation in the atmosphere above the bay. The strong diurnal cycle allows investigation of the response of near-surface currents to large, periodic wind fluctuations. The observations used in this analysis were collected in the summers of 1997 and 2000. During both summers an air-sea measurement buoy M1 was active in the mouth of Monterey Bay and in 2000 a specially instrumented 'flux buoy', FB, was also deployed in the east-central portion of Monterey Bay. Two multifrequency coastal radars (MCRs) operating at 4.8, 6.8, 13.4 and 21.8 MHz were sited at Moss Landing and Santa Cruz, California, collecting current maps at hourly intervals. We present observations and analyses in two areas: the center of the bay mouth (near the M1 mooring) and 8 km off the northeast shore of the bay (near the flux buoy FB mooring). These observations occurred during periods

of strong land-sea breeze circulation in June of 1997 and Aug./Sept. of 2000. At the two buoy sites we study correlation between the surface wind vector and the current vectors at effective depths of about 0.5, 1, 2 and 3 m as sensed by the different radar frequencies. We find the strongest correlation between the wind and the currents nearest the surface and that the surface currents are rotated about 40° clockwise (as seen from above) with respect to the wind vector, i.e. in the same sense as the Ekman spiral. We also study the spatial coherence of the surface current response to the surface winds [C6797]

"Statistical and phenomenological recognition in polarimetric SAR imaging"

The maximum likelihood classifiers are of large interest because they allow one to simulate, quantify and compare easily the rate of correct recognition for various cases of partial polarimetries and symmetries hypothesis. In this paper, they are used within the framework of natural surfaces recognition from SAR polarimetric images. The purpose is to advise the choice of the more suitable partial polarimetry for a remote sensing satellite. The results of this work infer some questions about the validity of some properties often supposed in the analysis of SAR images and in the radar calibration method [C6798]

"Interpretation and analysis of polarimetric L-band E-SAR-data for the derivation of hydrologic land surface parameters"

Evaluates the use of polarimetric L-band synthetic aperture radar (SAR) information for applied derivation of important hydrologic parameters. In most cases empirical relationships between SAR-data and water cycle components are investigated as a first step towards hydrological information extraction. The use of polarimetric parameters for hydrological modelling is analysed. Furthermore, the dependency of the polarimetric parameters from the local incidence angle is investigated [C6799]

"Preparing the Joint Multi-sensor Mine-signatures project database for data fusion"

The Joint Multi-sensor Mine-signatures (MsMs) project was started in the year 2000 and has as its main goal to organize and execute an experimental campaign for collecting data of buried land-mines with multiple sensors. These data sets are being made widely available to researchers and developers working amongst else on sensor fusion, and signal processing for improved detection and identification of land-mines. The outdoor test facility (6480 m) of the Joint Research Centre (JRC) of the European Commission, located at Ispra (Italy), houses the test minefield. Six test strips of 646 m consisting of different soil types (cluttered grassy terrain, loamy soil, sandy soil, clay soil, soil with high content of organic matter and ferromagnetic soil) are complemented with one reference test strip of 646 m consisting of pure sand. The list of objects buried in the minefield includes mine simulants of three different dimensions with either a low or a high metal content, reference targets for position referencing and calibration checking, and clutter objects including empty bullet cartridges, metal cans, barbed wire, stones, wood, plastic boxes, etc. This test minefield is going to be left intact for a long period, in order to be able to perform multiple runs on it. For the test campaign of the year 2000, the core sensors were a metal detector a ground penetrating radar, a microwave radiometer and several thermal infrared imagers. The first data sets are in the process of being released right now. This paper aims to prepare the first results to be obtained by fusing the data coming from these different sensors, by presenting the available datasets [C6800]

"Operational coastal map re-actualization by RADAR SAR images, examples in French Guiana, Mauritania and Cameroon"

The French Hydrographic Office has to publish information for navigation security in its responsible zones (French territories, West African coasts (with agreements between these countries and France), Djibouti, Viet-Nam, etc.). Nautical charts on African coasts are old and had often been established in the 1950s. Local geodetic reference systems used are not well known, so maps are not in accordance with GPS navigation. In French Guiana, coastal evolution is so important that nautical charts are obsolete. Sedimentation and erosion of mangrovia vegetation can reach one kilometre per year. We study the contribution of RADAR SAR imagery for nautical chart updates. Our interests are coastline, intertidal zone delimitation, harbour structures and bathymetry (<20 metres). We present solutions for different problems. First, for cartographic applications, we reference geographically our ERS images in a global geodetic reference system without ground points, we use precise orbitographic products, differences between geoid and global ellipsoid and ERS annotation files: precision estimation of this step was made by GPS measurements and also comparison between images acquired in ascending and descending mode. Second, ground interpretations permit first in Mauritania and French Guiana to follow coastal evolution and particularly coastline erosion and flood risk zones, and last in Cameroon to understand high and low vegetation distribution in mangrovia and in Wouri estuary, to follow sand banks which obstruct the Douala city channel. We propose a methodology for ERS RADAR SAR use including interferometry, the speckle reduction process and automatic detection tools. Third, we present new coastal cartographic

documents for regions with strong changes and a low map update frequency [C6801]

"Markov random fields for digital terrain model extraction"

This paper deals with the automatic extraction of the ground elevation or digital terrain model (DTM) from the global digital elevation model (DEM). The proposed method is divided into two main steps: first, the road network and the cross-roads are extracted, and the elevation of the cross-roads is estimated on the DEM; secondly, the height of the cross-roads is regularized using some contextual knowledge. The second step is performed inside a Markovian framework based on the natural graph of the roads. Results on interferometric SAR data and optical images are presented [C6802]

"Building extraction from LIDAR data"

A strategy for building reconstruction relying on LIDAR data only is presented. Roofs are modeled as plane surfaces, connected along ridges and bordered by the eaves lines. Edge pixels and plane surfaces are detected and labelled as roof slopes based on gradient orientation and plane fitting by RANSAC; a similar procedure applies to eaves lines. Based on geometric reasoning, the topology of the roof slopes and walls is reconstructed, deriving also roof ridges and roof corners. Constraints to be enforced in order to obtain a building shape consistent with the geometric evidence are established. The final reconstruction is performed by a global l.s. adjustment where all raw data contribute to a determination of the building faces while the constraints are satisfied. Preliminary results from a laser scanning survey with a ground resolution of 1 m are presented [C6803]

"Classification of polarimetric SAR images of suburban areas using joint annealed segmentation and "H/A/ α " decomposition"

A joint segmentation-based classification technique is proposed for fully polarimetric SAR images of suburban areas. This is based on the joint use of the H/A/ α decomposition and a multivariate annealed segmentation. This allows us to exploit the information available in the noisy estimate of the anisotropy parameter, retaining the highest possible spatial resolution. Specifically, the anisotropy is processed in conjunction with entropy and α angle, so that it is regularized by their more stable values. The application of the proposed technique to an AIRSAR image of suburban areas shows its practical effectiveness [C6804]

"Detection of urban areas in multispectral data"

During various campaigns, multispectral data have been gathered with airborne sensors over typical urban environments. For each of these scenes passive IR-systems, as well as laser-scanners, mm-wave radars under different operating modes, forward-looking with beam scanning antennas, side-looking SAR and interferometric SAR for 3D-imaging, have been employed. For these sample scenarios advanced image based pattern recognition algorithms have been validated and the features of each sensor have been studied to allow to choose the optimum sensor combination for a specific application. The contribution describes the different sensors and gives an overview over the image material for the sample scenes. Methods of image discrimination for the urban environment are discussed [C6805]

"Building footprint extraction and 3-D reconstruction from LIDAR data"

Building information is extremely important for many applications within the urban environment. Automated techniques and user-friendly tools for information extraction from remotely sensed imagery are urgently needed. This paper presents an automatic approach for building footprint extraction and 3-D reconstruction from airborne light detection and ranging (LIDAR) data. First a digital surface model (DSM) is generated from the LIDAR point data. The approach then extracts objects higher than the ground surface. Based on general knowledge about building geometric characteristics such as size, height and shape, buildings are separated from other objects (trees, etc.). The extracted building footprints are then simplified using an orthogonal algorithm to obtain better cartographic quality. Watershed analysis is conducted to extract the ridgelines of building roofs. The ridgelines as well as slope information are used to classify building roof types. The buildings are reconstructed using three basic parametric building models (flat, gabled, hipped) common to the study area. Finally, the results of extraction are compared with manually digitized building reference data to conduct an accuracy assessment [C6806]

"Bayesian model based city reconstruction from high resolution ISAR data"

We present Bayesian information extraction methods for feature extraction from metric resolution interferometric radar data. The extracted information is naturally related to a three-dimensional environment. We consider this

information for the reconstruction of complex urban settlement areas. We target the higher complexity of the scene that is captured by the high resolution of the sensors by using hierarchical models of the data. Their stochastic nature allows us to deal with the uncertainties that are inherent in both the acquisition process and in the data themselves. We present results of the application of the described concept to the separation and characterization of typical man-made objects appearing in urban areas [C6807]

"Optimal combination of multiple SAR differential interferometric measurements for monitoring terrain displacements"

Synthetic aperture radar (SAR) differential interferometry is a powerful technique that allows to measure very small movements of the terrain happened between two data acquisitions. In previous works we demonstrated how to overcome the main limitations of the technique (i.e. decorrelation noise and atmospheric artifacts) by means of a method for unwrapping sparse phase data and by performing a temporal analysis of successive acquisitions. In this work we explore the possibility of considering together the space and time properties of the studied signal. The two steps mentioned above (i.e., sparse phase unwrapping and temporal analysis) act in the space and in the time domains separately. A significant advance can be obtained by considering the data as samples of a function in a three-dimensional (3D) space-time, and by exploiting this structure in the processing. The 3D structure of the data makes the processing more complex but can help both phase unwrapping and atmospheric (and other) artifact filtering [C6808]

"Analysis of coherence images over urban areas in the extraction of buildings heights"

In this paper we show how ERS coherence imagery can be useful to extract information about building heights in urban areas. The first part analyses the causes of decorrelation over urban areas. Spatial decorrelation is partially offset by spectral shift filtering, while thermal and processor decorrelation can be neglected. In order to extract building heights, we use tandem coherence only, so that temporal coherence can be set equal to one. Hence, the estimated coherence over built-up areas coincides with volume scattering decorrelation. Using the Van Cittert Zernike theorem, we introduce a model for the backscatter coefficient of urban areas. This model links volume decorrelation to a height variable so that theoretical coherence values can be obtained for varying heights. At this stage, it is possible to compare theoretical and experimental values of tandem coherence and mean heights of buildings can be extracted. To test the procedure, four sites in Italy, have been considered. For one area, results show that in situ measurements are in agreement with values of building heights obtained from coherence comparison. For two areas, results seem to agree with local observations. For the fourth area, discrepancies occur, probably due to weather effects. Hence, the described procedure seems to be promising and more accurate results may be achieved using fine resolution coherence images. However, the effects of weather on tandem coherence in urban areas should be investigated and taken into account [C6809]

"Potential and limits of InSAR data for the reconstruction of buildings"

The automatic reconstruction of buildings for the generation of city models is of great interest for different tasks. 3D information can be directly obtained from both, laser (LIDAR) and radar (InSAR) measurements. The data acquisition by SAR is described, with emphasis on the special properties of the interferometric SAR principle. A segmentation approach for building reconstruction is proposed. In the case of InSAR, special effects are taken into account, which are caused by the side-looking illumination. The estimation of the signal noise is considered in the segmentation process. Besides the elevation, the intensity information is exploited to detect building areas. The results show that building reconstruction is possible from InSAR, but the achievable level of detail cannot be compared with LIDAR. Inherent geometric constraints which limit the reconstruction of buildings from SAR data of dense urban areas are discussed [C6810]

"Interpretation of InSAR mapping for geometrical structures"

In this paper we present a methodology to detect large geometrical structures from interferometric synthetic aperture radar (InSAR) measurements. The ortho-rectification of synthetic aperture radar imagery which is a part of interferometric SAR processing can be a many-pixels to one-pixel mapping. This mapping is used for automatic detection of geometrical structures which are large compared to the SAR resolution [C6811]

"Correction of artifacts on differential SAR interferometry for the study of subsidence phenomena in urban and suburban areas"

This paper deals with the analysis and correction of artifacts on differential synthetic aperture radar (SAR) interferometry applied for monitoring urban and suburban areas. Particularly, those artifacts arising from the use in interferometric processing of low accuracy acquisition geometry data are considered. To remove these

artifacts, we propose a new algorithm able to estimate the acquisition geometry parameters relevant to the interferometric processing with high accuracy directly from the SAR data. In order to validate the proposed algorithm, the results obtained by applying the new technique to the study of the subsidence phenomena in Bologna (Italy) and the surrounding area are presented and compared to the results obtained by using in the interferometric processing the precise orbit data provided by the Delft Institute for Earth Oriented Space Research (DEOS) [C6812]

"Investigation of multirate techniques for digital generation of transmitter signals for TIGER radar"

Research has been carried out on possible methods for the digital generation of signals for the TIGER (Tasman International Geospace Environment Radar) transmitter. Simulation results have shown that the polyphase network provide better performance compared to an FIR filter. The lower sampling rate of polyphase filters make them good candidates for applications with high throughput requirements. Implementation of an FIR filter is addressed with a technique which is less sensitive to hardware utilization. A hardware prototype has been constructed using an Altera Flex 10k20 device. Results demonstrate the feasibility of using FPGA devices for the complete implementation of a digital TIGER transmitter. [C6813]

"Fully 3D and joint 2D/3D segmentation of InSAR data over urban environments"

Reliable extraction of buildings from InSAR images is made tricky by the many disturbance factors that affect the measurement process, especially in urban areas where the proximity of many different buildings aggravates the problem of multiple reflections. In this paper we propose and discuss two different approaches to segmentation for building extraction [C6814]

"Texture analysis of urban areas in ERS SAR imagery for map updating"

In single-band and single-polarized SAR image classification, textural information is important, both for pixel and segment based classification schemes. To study the map updating capabilities of such sensors in urban areas, several texture measures were studied. Among them are statistical measures, wavelet energy, fractal dimension, lacunarity, and semivariogram. The latter was chosen as an alternative for the well known gray-level co-occurrence family of features. Two urban areas were studied using ERS1/2 data, one of which is reported: the conurbation around Rotterdam and The Hague in The Netherlands. The area can be characterized as a well-planned dispersed urban area with residential areas, industry, greenhouses, pasture, arable land, and some forest. The digital map is a 1:250,000 vector map (VMapl). The texture measures that gave the best landcover separability for this area are: mean intensity, variance, skew, weighted-rank fill ratio, semivariograms (or alternatively wavelet energy measures), and lacunarity. The latter is preferred to be included in case more than one man-made landcover class is involved, which is often the case in urban environments [C6815]

"Evaluation of COSMO/SkyMed SAR data for urban area characterization"

In this work we present some preliminary results of a feasibility study about urban applications of the COSMO/SkyMed SAR sensor data. We investigate the capability of the different imaging modes of the satellites of this constellation to characterize an urban area, using a data set of satellite SAR measurements. We show that medium resolution data (25 m) is indeed sufficient to have a first, rough definition of the urban area, as well as of its principal features, like large roads, and textural characteristics. The latter may be used, for instance, to extract different building density areas [C6816]

"IEEE/ISPRS Joint Workshop on Remote Sensing and Data Fusion over Urban Areas (Cat. No.01EX482)"

The following topics were dealt with: urban areas remote sensing; detection and classification; interferometric SAR; data fusion; decision making and planning; urban reconstruction [C6817]

"Fusion of SAR/optical images to detect urban areas"

We explore the idea of combining images from optical and SAR (synthetic aperture radar) sensors relative to the same scene on the Earth's surface with special emphasis on applications to urban areas detection. Indeed the images obtained with the two sensors are complementary and an effective image fusion approach may provide a useful tool to achieve a better understanding of the observed scene. The underlying basic assumptions of the proposed fusion approach are: the images to be fused refer to the same scene and are coregistered, moreover the images change in the same locations in the scene, and, consequently, have similar "structures". The idea is to fuse the two images (optical and SAR) defining an objective function that quantifies the difference in "structure" between the two unknowns that represent the two "fused" images and that contains a penalization

term to establish a relation between the unknowns and the measured data, and minimizing this objective function using a proper numerical algorithm. The urban detection algorithm used is very simple and corresponds to recognize brilliant areas in the images. Some numerical results obtained using real data with the proposed fusion and urban areas detection procedures are presented. The numerical results show that the proposed SAR/optical data fusion procedure facilitates the detection of urban areas [C6818]

"Automatic mapping of linear structures in 3-dimensional space from ground-penetrating radar data"

Non-invasive geophysical techniques such as ground-penetrating radar allow rapid and low-cost investigation of the shallow subsurface for the detection of such features as utilities and plant. This paper presents a pattern recognition approach based on the 3-dimensional Hough transform for the detection of extended linear targets in ground-penetrating radar data. By transforming spatially extended patterns into spatially compact features in parameter space, a difficult global detection problem in data space becomes a more easily solved local peak detection problem in parameter space. Due to the sparseness and variability of the data, the accumulator peak detection stage is replaced by a novel algorithm called the adaptive non-accumulated Hough transform (ANHT) 3-dimensional clustering algorithm. This technique allows the combination of qualitative site information and ground truth in order to increase the accuracy of the final result. The user is presented with a 3-dimensional site survey report detailing the length, depth and orientations (azimuth and zenith) of any pipes, cables or the like. The ANHT performs substantially superior to the standard Hough transform implementation in computer memory requirement. Our experimental results on the artificial 3-dimensional linear objects indicate that method works quite well under various background conditions. The automatic mapping of linear structures in 3-dimensional space from ground-penetrating radar data is achieved by implementing the ANHT in the detection of linear targets in ground penetrating radar data [C6819]

"3D surface-penetrating radar "Defectoscope""

A surface-penetrating radar, called "Defectoscope", is described. It is intended to investigate various media and, in particular, to detect defects in building constructions. One of the characteristic features of the radar, designed on the basis of a portable computer, is the availability of an ultrasonic exact positioning system that allows automatic collection of radar data for three-dimensional imagery of the volume under the investigated surface. Results of sensing of a concrete wall with armature and placed behind it metal and plastic objects are presented. Results of experiments on the polarization recognition of subsurface objects are discussed [C6820]

"Bistatic matched illumination radar involving synthetic aperture and synthetic pulse for signal to clutter enhancement and target characterization"

The "Radar Fence" is a bistatic multi frequency radar system. Based on the principles of frequency coding, time coding and space diversity we detect and characterize objects and geophysical phenomena. The system's capability is illustrated with results from detection of internal wave wake produced by a submerged vehicle. and aircraft identification [C6821]

"The influence of the lower atmospheric refraction on measurements of down-looking radar"

According to the Snell refraction law of spherically stratified atmosphere, a radar with down-looking mode is different from one working with an up-looking mode. A down-looking radar is limited by the critical depression angle, which is related to the radar height and profile of the atmospheric refraction index. The difference between measurements of the down-looking radar and up-looking ones is analyzed statistically by using some measured profiles of the atmospheric refraction index [C6822]

"An analysis method research of radar measuring precision"

An analysis method used to evaluate the random error of radar measuring data has been researched according to radar precision analysis theory and the characteristics of the radar system. The analysis method, which is based on an improved method of variable difference, has been applied to evaluate satellite measuring data, with perfect results [C6823]

"Fusion of radar images: state of art and perspective"

Image fusion refers to the acquisition, processing and synergistic combination of information provided by various sensors or by the same sensor in many measuring contexts. The aim of this survey paper is to describe three typical applications of data fusion in remote sensing. The first study case considers the problem of the Synthetic Aperture Radar (SAR) Interferometry, where a pair of antennas are used to obtain an elevation map of the

observed scene; the second one refers to the fusion of multisensor and multitemporal (Landsat Thematic Mapper and SAR) images of the same site acquired at a different time, by using neural networks; the third one presents a processor to fuse multifrequency, multipolarization and multiresolution SAR images, based on the wavelet transform and multiscale Kalman filter. Each study case presents also results carried out by the proposed techniques applied to real data [C6824]

"2001 International Conferences on Info-Tech and Info-Net. Proceedings (Cat. No.01EX479)"

The following topics are dealt with: digital Earth; remote sensing for geology, water resources, agriculture and land; SAR technology; GIS technology; data and image processing; telecommunication traffic control and engineering; network operation and management; high speed switching and routing; 3G and beyond; advanced optical communications; broadband access networks; MAC and scheduling issues; resource management and QoS control; multicasting; smart antennas and propagation; modeling and performance of communication networks; mobile communication systems; signal processing in communication systems; modulation and coding; intelligent networks; information retrieval; data mining; network computing; agent technology; neural networks; computer vision; self-organization maps and intelligent systems; multi-agent systems and hybrid controls; intelligent transport systems; fuzzy systems; intelligent control systems; variable control systems and robust control; blind separation and object identification; intelligent automation in Internet environment; nonlinear control systems; evolutionary computation; robot control systems; fuzzy control; information security and network security; Web technology; information network management, architecture and protocols; Internet engineering and applications; computer supported cooperative working; wireless computing networks; e-commerce; network-based learning and education; intranets and enterprises automation [C6825]

"Research on GIS-oriented radar background clutter database"

In this paper, a geographic information system (GIS) technique is applied for the collection and analysis of radar clutter signals to acquire the information of clutter background corresponding to each scanning area. All factors related to the features of radar echo are combined to a database according to their situation in space; functions of the database include organizing, managing, examining, analyzing and assisting decision output [C6826]

"Remote detection of biomolecules in the THz region"

Summary form only given. Recent measurements of the electromagnetic transmission through certain bioparticles such as bacillus subtilis (BS), have revealed absorption resonances in the THz region. The physical origin of these resonances, be it nucleic acids, proteins or other biomolecules embedded in the particle, is not yet clear. But the resonances are repeatable and strong enough that one can estimate their detectability in a remote sensor. This paper summarizes calculations of the detectability of BS by four sensor modalities, including (1) passive incoherent (i.e., direct detection), (2) passive coherent (i.e., heterodyne radiometry), (3) active incoherent differential absorption spectroscopy, and (4) active coherent radar. Because of the small absorption cross section of the typical THz resonance ($\sim 10^{-11} \text{ cm}^2$), the small concentrations expected in the environment ($\ll 10^5 \text{ cm}^{-3}$), and the large background temperature at THz frequencies, passive techniques lack the sensitivity, even when implementing liquid-helium-cooled electronics. An active differential absorption spectrometer (DAS) is more promising using either a monostatic (i.e., retrodirective mirror) or bistatic (i.e., opposed transmitter Tx and receiver Rx) architecture. For example, a two-frequency DAS sensor operating at the absorption center (20.65 cm-1 or 619.5 GHz) and the absorption edge (20.0 cm-1 or 600 GHz) with 1 mW of transmit power and a room-temperature direct detector can obtain a receiver-noise-limited S/N ratio of unity through a 20-m cloud containing 10^5 bioparticles/cm³ (minimum detectable concentration MDC) at a Tx-Rx separation of 1 km and Tx/Rx apertures of 100 cm² [C6827]

"Concurrent polarization operation mode of location system"

Equipment for active location with optical and radar wave bands receives information on the object from the formation of sounding signals and the analysis of scattered signal. Radar systems are successfully used in monitoring environment, remote sensing of polarization characteristics, measurement of hydrometeor characteristics. Laser locators (lidars), on the basis of polarization measurements, allow one to estimate the characteristics of atmospheric aerosols, to control for atmospheric pollution. The high frequency of laser radiation provides very narrow diagrams of lidar direction, the formation of impulse sounding signals of short duration and the following peculiarities: great time of the operating region review; strong weakening by atmosphere of the sounding laser radiations and those reflected from the target; most of the targets are spatially distributed. Superposition of radar and optical channels in a complex location system (CLS) allows one to avoid the limitation of each of the systems. The paper describes the concurrent polarization operation mode of a CLS system [C6828]

"An electromagnetic model for SAR raw signal simulation of urban areas"

Synthetic aperture radar (SAR) techniques can provide powerful instruments for many fields of research related with the urban environment. In order to fully exploit the potentiality of such instruments it is necessary to reliably model the interaction of the electromagnetic waves with urban settlements. In this paper, an electromagnetic model of scattering of a plane wave from typical element of urban structure is presented. The proposed analytical procedure leads to the evaluation of the scattered field in closed form in terms of the geometric and dielectric building parameters. obtained results provide useful indications for the comprehension of the SAR raw signal formation phenomena and for the development of proper simulation tools [C6829]

"Vehicle-borne Laser Mapping System (VLMS)-a new observation system for 3-D mapping of urban areas"

We have developed a new observation system for mapping urban areas in three dimensions. This. system is called Vehicle-borne Laser Mapping System (VLMS). The system consists of three laser scanners and six line cameras for data acquisition. GPS, INS and Odometer are used for position data. Laser scanners are used as primary data source for building 3-D spatial data. Line camera images are used only for texture. In this paper, we present system architecture, accuracy analysis of the system and feature extraction from range data. Features are basically categorized as man-made features (buildings, roads, utility facilities, tunnels etc), natural features (trees, plants etc) and dynamic/static features (parked vehicle, moving vehicles, pedestrians) [C6830]

"Radar permanent scatterers identification in urban areas: target characterization and sub-pixel analysis"

Summary form only given, as follows. The permanent scatterers (PS) technique, developed by the authors during the last three years, allows the identification of radar targets particularly suitable for SAR interferometric measurements. In fact, despite its remarkable potential, spaceborne SAR differential interferometry (DInSAR) has not been fully exploited as a reference tool for ground deformation monitoring, due to the presence of atmospheric artifacts as well as geometrical and temporal phase decorrelation. Both drawbacks are overcome by using a multi-image framework of interferometric data (>30 images) in order to properly identify and exploit the subset of image pixels corresponding to coherent reflectors (PS). Whenever the sparse grid of PS is dense enough (more than 3-4 PS/km², constraint always satisfied in urban areas); accurate phase measurements carried out on the sparse PS grid allow one to compensate data for the atmospheric phase contributions. Average ground deformation rate as well as full displacement time series (both along the satellite line of sight, LOS) are estimated with millimetric accuracy on individual PS locations, fully exploiting the long temporal series of SAR, data available in the ESA ERS-1/2 archive. Therefore, the PS subset of image pixels can be seen as a high-density (100-300 PS/km², in urban areas) "natural" geodetic network. In this paper, we present some new results concerning the statistical characterization of the PS, both in terms of amplitude and phase returns. Moreover, it is shown how PS density can be significantly increased, in urban areas, by adopting a second-order model. Here, two individual scatterers per resolution cell are considered. Available data are then used to recover their reflectivity, elevation and LOS velocity. Problems related to over-fitting and model parameters estimation will be addressed. Results obtained processing 64 SAR images (ESA-ERS archive) acquired over Milan are shown. Finally, we present how PS can be exploited to carry out interferometric measurements using ERS-2 images acquired when the sensor was in emergency back-up mode (EBM). Both theoretical (signal processing) and practical issues are considered. First results obtained over Paris are discussed [C6831]

"Scene understanding for settlements from metric resolution imagery"

Summary for only given, as follows. Satellite and airborne remote sensing has reached a new level of sophistication, but available interpretation methodologies cannot cope with the huge amounts of acquired data. At the same time, the new generations of metric resolution sensors, e.g: Ikonos, and the huge potential of synthetic aperture radar SAR have opened up the perspective on novel applications related to the understanding of high complexity settlement scenes. At meter resolution, mainly for man-made scenes, the complexity of the scene structures and of imaging phenomenology can be very high. This is reflected in the complexity of the observed images. New methods are needed for their interpretation, both for 2- and 3- dimensional analysis. The present article proposes methods of 2-dimensional information extraction from SAR and optical metric resolution observations. The presented methods are based on several assumptions: 1) the most compact encoding of the data is by the probabilistic model that describes it best, 2) a large number of sources of information coexist within the same observation data set, 3) the understanding of a scene requires complementary or multisensor observations. Thus, the concept developed aims at a description of the scene using data and information fusion. The primitive features, signal parameters, are extracted using model based methods such to obtain a quasi complete description of image content, i.e. radiometric/polarimetric attributes, structural information, geometric

features, analysis at multiple scales. A hierarchic Bayesian modeling and learning paradigm is used for data and information fusion and for interactive exploration of the scene identity. The article presents the image formation phenomenology relevant for metric resolution observations, a concept for quasi-complete image content characterization, methods for supervised learning for scene classification by information fusion, and examples using X-SAR, E-SAR (X band, and L band polarimetric) and Ikonos images [C6832]

"Statistical characterization of scattering signals from vegetation at frequency above X-band by numerical simulations"

Since the wave scattering from a vegetated canopy is due to scattering from different vegetation components (leaves, branches, stems, etc.) within the volume enclosed by the transmitting and receiving antenna beams, it is necessary to understand the role played by each component on the total radar return from the whole canopy. To meet the objective of this study, dielectric non-spherical scatterers are used to model the vegetation components. Circular disks are used to model deciduous leaves, needles to model coniferous leaves, and finite cylinders to model branches or trunk scatterers. The radar return from disc or needle has been evaluated by applying the Generalized Rayleigh Gans approximation for a disc or needle scatterers. As for the signal return from a finite cylinder, it has been calculated by using the inner field inside similar cylinder of infinite length. Then the scattered field from the canopy is formulated in terms of the scattered field from each forest component through the first-order radiative transfer theory. By means of computer simulation, the samples of signal returns from such vegetation components are obtained and the signal probability density is estimated from these samples. The goodness of fit procedure is then applied to fit the simulated data to known statistical models. [C6833]

"Shuttle radar topography mission (SRTM): experience with the X-band SAR interferometer"

The X-SAR single pass SAR interferometer as part of the Shuttle radar topography mission (SRTM), its measuring principle and configuration, as well as the operation of the system during the mission in February 2000 is shortly described. The experience with the system was, that it was well designed and manufactured, it had very good monitoring capabilities and its performance was excellent and the preliminary results are very promising. The calibration activities post mission deal with the Shuttle and mast motions which as well as the phase errors due to temperature variation have to be compensated [C6834]

"Polarimetric classification of trees"

Since scattering matrix acquisition capability will be equipped with space-borne radar systems such as ALOS PALSAR to be launched in 2003, radar polarimetry is now an indispensable tool for monitoring the Earth's cover. The advantage of using the vector nature of electromagnetic waves is the information on the amplitude, phase and their relations pertaining to target. In this paper, we retrieve a useful index for classifying broad leaf trees and conifer (needle like leaf) trees based on the scattering characteristics of tree canopies. The index used is the polarimetric correlation coefficient derived by the elements of the Sinclair scattering matrix. It is shown that correlation coefficient defined in the circular polarization basis serves to distinguish conifer tree and broadleaf tree [C6835]

"The geometric distortion correction in SAR motion compensation"

This paper presents the geometric distortion correction in SAR motion compensation and discusses the sources of the distortion. The autofocus technique only solves the defocusing of the image; after a phase correction, the geometric distortion can be removed. Also the simulation is given [C6836]

"Analysis and simulation of spaceborne SAR interferometric baseline"

In this paper, the baseline's effect on spaceborne SAR (synthetic aperture radar) interferometry is discussed. The existence of critical baselines and optimal spatial baselines are analyzed and the formulas to determine them are presented. The simulation method from baseline design to phase unwrapping is presented and the results from it are given to illustrate the baseline's effect on interferometric SAR [C6837]

"Surface currents imaged with hybrid along and cross track interferometry"

Radar interferometry is known to be a useful technique for mapping terrain heights and surface currents. Several studies on along track or cross track interferometry provided highly accurate results. In the case of coastal applications a simultaneous measurement of topography and surface currents is beneficial. Therefore an approach for airborne interferometric measurements with a baseline consisting of an along and cross track component is presented. Analysis of experimental airborne interferometric data shows good results. The final accuracy is highly dependent on the accuracy of the navigation data of the aircraft [C6838]

"Quality assessment of digital surface models derived from the Shuttle Radar Topography Mission (SRTM)"

In February 2000 the Shuttle Radar Topography Mission (SRTM) was flown on board the Space Shuttle Endeavour. The aim of the mission was to survey about sixty percent of the complete landmasses of the Earth's surface. During the mission a US C-band antenna and a German/Italian X-band antenna were installed on board the Shuttle. The main result of the mission will be a three-dimensional digital surface model (DSM) obtained from single-pass interferometry. During the validation process the SRTM elevation data will be analysed by comparing them to reference data of a well-known test site. This paper describes and investigates an algorithm for this task which was developed at the Institute for Photogrammetry and Engineering Surveys (IPI) of the University of Hannover. It is based on a spatial similarity transformation which matches the SRTM data onto reference data of higher accuracy. The algorithm is comparable to the absolute orientation of a photogrammetric block by means of a DTM. Any detected transformation parameters which differ from the identity transformation point to potentially existing systematic errors of the SRTM data, the standard deviation of the remaining height differences represents the accuracy of the SRTM data. The algorithms was successfully tested using simulated and real data, the obtained results are reported in this paper [C6839]

"Synthetic aperture radar (SAR) images classification using speckle filtering and texture information"

Synthetic aperture radar (SAR) is a very efficient instrument for obtaining remotely sensed images of the Earth's surface. However, SAR images are degraded by a form of multiplicative noise known as speckle, which is a result of the illumination by the coherent radar. Hence speckle reduction is a necessary procedure before automatic image classification can be performed. This paper deals with the supervised classification of SAR images. Our approach consists in the speckle filtering before the clustering. But the only knowing of the filtered intensity image is not sufficient because of the high noise level. The other possible information to help the clustering is the texture, thus our approach is based on these two criteria [C6840]

"Multi-sensor data classification in remote sensing using MRF regional growing algorithm"

This paper studies a multi-stage method using hierarchical clustering for unsupervised image classification to classify the land-cover using remotely-sensed data from multiple sensors. The multi-stage method performs region-growing segmentation using a hierarchical clustering procedure which makes use of the spatial contextual information by characterizing geophysical connectedness of digital image structure with Markov random field [C6841]

"Snow monitoring using interferometric TOPSAR data"

We have investigated the usability of simultaneous interferometric C- and L-band SAR data to retrieve the snow layer volume during the snow melt. The wetness in the snow layer causes scattering to be mainly due to the snow-air interface and, therefore, makes it possible to use simultaneous interferometric SAR and DEM to estimate the depth of the snow layer. Our results show that (1) most of the areas covered by wet snow can be identified from the SAR images and (2) the use differential interferometry gives a fair estimate to the snow layer depth. As a result we have produced a map showing the areal extent and depth of the snow layer on the Emerald lake test site [C6842]

"The bistatic scattering from the natural rough surfaces in X and Ku bands"

The scattering of waves by random rough surfaces has important applications in remote sensing of oceans and land. At low grazing angles and ranges involved, the existing data base is quite limited. The problem of developing a model for rough surfaces is a very difficult one, since, at best, the scattering coefficient σ_0 is dependent upon (at least) radar frequency, geometrical and physical parameters, incident and observation angles, as well as polarization. In this paper, the development of a theoretical two-scale model describing bistatic reflectivity is presented. The author also gives the numerical results computed for the bistatic radar cross-section from random rough surfaces, especially from the sea surface [C6843]

"SAR interferogram phase filtering based on the Von Mises distribution"

We propose the use of the Von Mises distribution for circular data to model interferometric phase images. Based on the kappa parameter of the Von Mises distribution a locally adaptive phase filter is developed. A two-sided confidence interval on the kappa values is constructed, and only phase measurements where kappa values fall inside this interval are input to the filter. We additionally put more importance to spatially closer pixels than to

pixels further away from the pixel in question. The latter idea is achieved by narrowing the confidence interval depending on the distance from the central pixel [C6844]

"Road extraction from high-resolution airborne SAR using operator fusion"

Extraction of roads from high-resolution airborne X-band SAR data is described. The method employs identification of regions of interest, followed by fusion of basic road feature detectors and is complemented by a higher level road model. Identification of regions of interest employs a significance test for the local coefficient of variation. In regions of interest a road feature detector provides a road score through fusion of functions for road edge presence and road center continuity. Finally, an active contour model which is optimized by a genetic algorithm is applied to the fused image [C6845]

"Strategies for non-linear deformation estimation from interferometric stacks"

A testing procedure is presented to estimate topography and deformation parameters from an interferometric stack (a number of reference phase corrected interferograms w.r.t. the same master image). A subset of pixels exhibit coherent phase in time, and a time series of phase differences between pairs of these pixels allows to set up a system of equations. A null hypothesis of zero deformation can be tested against alternative hypotheses, specifying linear and non-linear deformation. The covariance matrix of the phase differences accounts for phase noise, atmospheric effects, and orbit inaccuracies [C6846]

"Wake detection in polarimetric SAR images"

Investigates wake signature in polarimetric imagery using the Radon transform. This paper describes two methods for the wake-shape detection: the first method reduces the dimension of the polarimetric data to a single channel image and the second method conserves the polarimetric information until the peak detection process. Results obtained from polarimetric C-band image data are presented [C6847]

"A new AR-based technique to exploit SAR image correlation properties for rain forest classification"

In this paper we develop a detector that exploits both variance and correlation properties of SAR images for the discrimination between regions with different characteristics. This detector is based on the generalized maximum likelihood approach applied to an autoregressive (AR) correlation model for the pixels of a homogeneous region. The application of the newly derived detector to C-band SAREX images of the Brazilian rain forest shows improved performance in the discrimination of clearings from forest [C6848]

"A joint classification technique based on multivariate annealing segmentation and $H/A/\alpha$ decomposition for fully polarimetric SAR images of suburban areas"

A joint classification technique is proposed for fully polarimetric SAR images of suburban areas. The technique is based on the joint use of $H/A/\alpha$ decomposition and multivariate annealing segmentation. This allows one to exploit the information available in the noisy estimate of the anisotropy parameter, retaining the highest possible spatial resolution. This is obtained by jointly processing the anisotropy with entropy and α , angle, so that it is regularized by their more stable values. The application of the proposed technique to a AIRSAR image of suburban areas shows its practical effectiveness [C6849]

"Methods of estimating ridging of Antarctic sea ice"

Estimating the sea ice thickness surrounding Antarctica is important for determining the ocean-atmosphere heat fluxes, the salt flux to the ocean and for verifying global climate models. A widespread method of estimating ice thickness in the Antarctic is the use of ice observation data. These data are collected by ship-based observers who estimate the sea ice and snow properties hourly as the ship transects the pack. This is a relatively low-cost method of collecting data on ice properties, and data can be collected in all weather conditions, both day and night. However, it is limited to the region of the pack immediately around the ship, and consequently to ice regimes that the ship transects. The largest uncertainty in estimating the total ice volume is from the estimates of the ridging properties (average ridge height and percent ridging). To help quantify this error, we compared the ice observation data to ridge distribution data collected using aerial photography. The number of ridges, and the volume of ice contained in these ridges are estimated using 505 aerial photographs. Using a ridge cut-off height of 0.4 m, 0.8 m and 1.0 m, the ridge frequency is 60 km⁻¹, 12 km⁻¹ and 6 km⁻¹, respectively. Using the same cut-off heights, these ridges are estimated to add 0.7 m, 0.4 m, and 0.3 m to the area-averaged, undeformed ice thickness. Different ridging regimes are also compared to backscatter values obtained from synthetic aperture radar (SAR) data collected from RADARSAT-1 [C6850]

"Noise filtering of SAR interferometric phase based on wavelet transform"

Presents a new technique to remove phase noise from SAR interferograms. This new technique is based on the wavelet transform. The algorithm adapts to the quantity of noise, but does not process low coherence areas thereby avoiding the creation of artifacts or false information in these areas [C6851]

"Application of InSAR on the research of Mani strong earthquake"

InSAR is an advanced technology for measurement of crustal deformation with high precision. This paper deals with measurement of the crustal deformation one year before, and the coseismic displacement in, the 7.4 Ms earthquake in Mani, Tibet on November 9, 1997. Five image pairs composed of five scenes of ERS-1/2 data are selected within the range of 50 km⁴50 km around the earthquake center, which form two D-InSAR image pairs, respectively denoting crustal deformation one year before the earthquake and the coseismic displacement. The InSAR technology is then used to process these image data and ideal results are achieved. On the D-InSAR image of coseismic displacement, the effects of the earthquake faults are clearly seen. In the diagonal direction, deformations up to 0.5 m can be detected, which shows the special advantage and prospect of InSAR technology on quantitative study on coseismic displacement and quake faults [C6852]

"On the scattering from natural surfaces: the IEM and the improved IEM"

A comparative study regarding the scattering from natural surfaces is conducted by means of real measurements and the integral equation model (IEM) and the improved integral equation model (I-IEM). A large set of experiments have been conducted and hereafter illustrated [C6853]

"SAR Interferometry coherence analysis for snow mapping"

For climatological and hydrological investigations, the areas covered by snow and their spatial variability are important parameters, particularly in alpine regions. A interferometric SAR technique not only can produce a high-resolution digital elevation models but also can detect the changes in the surface. By comparing four ERS-1/2 repeat pass SAR image in the Tibet Plateau test area, we find that the coherence measurements from the bare soil, bare rock and the short vegetation are significantly high, and lake and snow cover have very low coherence. On other way, the entire target may show very low coherence if there are great decorrelations due to other parameters, such as spatial baseline, rotation and temporal. We will demonstrate the method and result for snow mapping by using both backscattering and coherence measurements with repeat passes ERS-1 image data at the Kunlunshan Mountain, the Tibetan plateau (36°03'N, 91°00'E). An accuracy of better than 82% can be achieved if we consider the classification result from TM imagery as the ground truth. The results showed that the coherence measurements provide an effective way to map snow-covered area [C6854]

"Another surface scattering model for bistatic scattering"

In the development of the IEM model for surface single scattering a simplifying assumption was applied to the phase of the Green's function in the average power calculation leading to a surface scattering model in algebraic form. We remove this assumption yielding a more complex model but still in algebraic form. We show that the simplifying assumption used in the past does not cause an appreciable difference in forward and backscattering directions. However, for different incident and scatter directions there is a noticeable difference especially when the surface roughness is small and scattering is weak. For surfaces with large root mean square height the difference between the original IEM and the new IEM is generally small [C6855]

"A 50 MHz logarithmic amplifier for use in lidar measurements"

We have demonstrated that a logarithmic amplifier can dramatically improve the range of an existing lidar system. In addition, it provides the needed amplification for photomultiplier tubes and avalanche photo-diodes detectors without saturating the ADCs. We conclude that such an amplifier should be an essential component of an analog lidar system [C6856]

"Mapping of wind-thrown forests using CARABAS-II VHF SAR image data"

Heavy storms are causing severe damage worldwide to forested land every year. The devastating storms that struck central Europe in late 1999 destroyed the equivalent of several years of normal forest harvesting, amounting to very large economical sums. Therefore, rapid mapping of damaged areas is of major importance for assessment of short-term actions as well as for long-term reforestation purposes. In this paper, the use of airborne CARABAS-II VHF (20-90 MHz) SAR imagery for high spatial resolution mapping of wind-thrown forests

has been investigated and evaluated. The investigation was performed at a test site located in southern Sweden, dominated by Norway spruce forests. A regression model predicting forest stem volume from radar backscattering amplitude was used to retrieve stem volume for storm-damaged areas. Finally, the predicted volumes were compared with subjectively inventoried stem volumes. Unexpectedly, the results indicate that the backscattering amplitude is considerably higher for wind-thrown forests in comparison with backscattering from unaffected forests. Nevertheless, this finding implies that VHF SAR imagery has potential for mapping wind-thrown forests, preferably using change detection techniques of images acquired prior to and after storm-fellings [C6857]

"Resolution improvement via multipass SAR imaging"

We investigate the possibility to exploit coherent SAR multi-acquisition to improve the system range resolution. The problem is formulated in the signal statistical estimation framework, where the space invariant and space variant case are addressed. Numerical experiments on simulated data are shown [C6858]

"Context based SAR data compression using fuzzy logic"

In this paper we propose a new image coding technique based on context modeling of wavelet coefficients using fuzzy logic. The scalar codebook was partitioned into four disjointed subsets. A fuzzy logic was used to predict the current subset using previous subsets and the values of the wavelet coefficients in the context. We designed the fuzzy logic using fuzzy rules and membership functions in order to achieve minimal mean square error. The proposed context-based modeling of wavelet coefficients outperforms the trellis quantization in the rate distortion sense by 0.2 dB in SNR [C6859]

"Refractivity-from-clutter using global environmental parameters"

This paper examines the sensitivity of radar clutter returns to variations in parameters used to describe the refractive environment that is associated with surface-based ducts. This supports determining efficient parameters so as to minimize the search space required in the inverse problem of inferring the refractivity environment from observations of radar sea clutter. First, the sensitivity of replica fields to variations in range-independent parameters are considered. Next, variations in the parameters with range are modeled as a Markov processes. It is seen that either source of variation could explain variations in radar clutter observations obtained during a surface-based ducting event with the 3.0 GHz Space Range Radar (SPANDAR) at Wallops Island, VA. We then use the Simulated Annealing/Genetic Algorithm (SAGA) general purpose inversion code to infer refractivity parameters from observed clutter. SAGA is configured to use an embedded parabolic equation electromagnetic propagation model, a four-parameter model for atmospheric refractivity, and a linear least-squares objective function. The mismatch between (a) the optimal replica field and the observed clutter and (b) the inferred refractivity profile and the range-dependent refractivity structure obtained by in situ measurements, is discussed [C6860]

"Multistatic GPR for antipersonnel mine detection"

Today's ground penetrating radar (GPR) systems encounter a variety of difficulties when applied to the detection of buried antipersonnel mines, e.g., a high clutter level and strong surface scattering. Angular diversity or "multistatic" data acquisition promises for the cost of additional hard- and processing effort high potential to overcome some of the problems. The paper explains the basic idea, illustrates a hardware realization and processing strategies and presents first results [C6861]

"Reconstruction parameters of underground objects based on FDTD and optimization method"

The inverse of the parameters of underground targets is still highly in expectation in ground penetrating radar (GPR) applications. In this paper, the FDTD method and time-domain optimization algorithm have been used to reconstruct the permittivities of underground multiple targets. An iterative optimization algorithm has been put forward. The forward scattering data are also calculated by a 2.5 D-FDTD algorithm in order to better simulate the practical GPR situation. The relationship between the convergent rates of the inverse algorithm and the initialization values are studied [C6862]

"Instantaneous parameters calculation and analysis of impulse ground penetrating radar (GPR) data"

We use the wavelet transform (WT) method to analyse impulse GPR signals received from anti-personnel (AP) plastic mines. The mine radar echoes examined in this work are characterized by an average low amplitude and low signal-to-noise ratio (SNR). We focus on the use of WT to extract such weak transients from the noisy

background. In particular, we calculate the instantaneous parameters of the radar signals by means of the WT. Instantaneous wavelet power and energy spectra allow enhanced identification of plastic mines echoes in low SNR. We further propose a novel non-linear transform method to process the results after WT in order to increase the energy difference between the mine signal and the clutter [C6863]

"Unsupervised classification and analysis of natural scenes from polarimetric interferometric SAR data"

In this paper is introduced a classification approach for polarimetric interferometric SAR data sets, based on the analysis of an interferometric (646) polarimetric coherency matrix properties. From the Wishart probability density function of this polarimetric representation, is defined a maximum likelihood decision rule to perform an iterative adaptive classification. Another classification scheme based on the derivation of the conditional probability of the cross-correlation between both data sets is presented [C6864]

"Multi-baseline polarimetric SAR data classification using the complex Wishart distribution and principal component analysis"

In this paper is introduced a classification approach for multi-baseline polarimetric interferometric SAR data sets, based on a principal component analysis of coherent scattering vectors. From the Wishart probability density function of a restricted data set, is defined a maximum likelihood decision rule to perform an iterative adaptive classification [C6865]

"Fuzzy clustering and interpretation of fully polarimetric SAR data"

Classification of Earth terrain components using fully polarimetric synthetic aperture radar (SAR) data sets is an important application of radar remote sensing. For the operational application some demands, besides the accuracy requirements, must be fulfilled. In order to make the handling of the classification easy for users, the algorithms have to be data set independent and the handling must be possible without aprioriknowledge. The ultimate aim is an unsupervised algorithm which is suitable for automation. In this treatment we propose an approach applying an unsupervised automatic clustering of the $H/A/\alpha/\lambda^1$ space. From the resulting clusters rules are derived for a fuzzy rule based classification. The resulting clusters can then be assigned to the desired object classes by the user. The approach enables us to combine the wide range of information contained in polarimetric SAR data with the robust and still flexible strategy of fuzzy rule based classifiers and with a high degree of automation. The effectiveness of this approach is demonstrated using fully-polarimetric L-band airborne SAR data acquired with the E-SAR system of the DLR at the well know test site of Oberpfaffenhofen, Germany [C6866]

"Removal of additive noise in polarimetric eigenvalue processing"

This paper concerns with the problem of additive noise in fully polarimetric SAR data. Two approaches-the first one based on conventional four-channel polarimetry and the second one based on polarimetric interferometric data-for estimating and removing additive noise level are presented and discussed. The performance of the proposed approaches is demonstrated using experimental fully polarimetric P-band data acquired by the experimental airborne SAR system (E-SAR) of DLR [C6867]

"Shallow water bathymetric surveys by spaceborne synthetic aperture radar"

A numerical model for shallow water bathymetric surveys by spaceborne synthetic aperture radar (SAR) and its calculation procedure have been developed based on the SAR imaging mechanism of sea bottom topography. Water depths of the Xiaoyinsha sandwave off the east coast of Jingsu province have been calculated from the ERS-1 SAR imagery. The results have been compared with the sea chart. It is shown that the agreement between the image-calculated bathymetric pattern and that in the chart is excellent. A root mean square difference accuracy of 0.42 m has been achieved [C6868]

"Sensor and data fusion contest: information for mapping from airborne SAR and optical imagery"

The concept of a sensor and data fusion contest on topographic mapping from SAR and optical imagery is presented. The image data to be used in the test will have a spatial resolution of approximately 1 m or better. The SAR data will be multi-frequency polarimetric INSAR data, the optical data will be multispectral. The goal of processing is the extraction of topographic objects which are commonly subject of mapping projects, e.g. roads, built-up areas and other land cover/land use classes. The final scope of the test will be defined after interaction with potential participants of the test. Besides the image data, digital reference maps will be compiled for the test sites. For this task, contributions from e.g. official mapping authorities would be very valuable. The data fusion

contest will be organized in the framework of the IEEE GRSS data fusion technical committee (DFC), the ISPRS working group III/6 "Multi-Source Vision" which both have strong relations with scientists active in research on multi-sensor fusion and automation in mapping, and-as the provider of the main organizational framework-the European Organization for Experimental Photogrammetric Research (OEEPE) which is the research platform of national mapping agencies and other institutions regarding technology developments to optimise the use of core data in a geoinformation infrastructure context [C6869]

"L- and P-band for surface parameter estimation"

This work presents a first qualitative and quantitative comparison of fully polarimetric SAR data at L- and P-band with respect to surface parameter estimation. The potential combination of these two frequencies in order to obtain more robust estimates and/or to extend the validity range of the inversion algorithms is investigated based on experimental data acquired by DLR's airborne SAR system [C6870]

"Undergraduate research on remote sensing at Colorado State University"

First Page of the Article [C6871]

"Undergraduate research on remote sensing at Colorado State University"

Colorado State University-CHILL (CSU-CHILL) radar is a state of the art polarization diversity/agile radar system primarily used for research and education in radar technology and atmospheric remote sensing. This paper briefly describes the undergraduate research activities on remote sensing during the summer, associated with CSU-CHILL. The CSU-CHILL radar is a state of the art dual polarized Doppler research radar located outside of Greeley, CO, about 30 miles from the CSU campus. Characteristics of the CSU-CHILL radar are given. The radar has two transmitters and receivers to enable simultaneous sampling of both H and V channels in a pulse to pulse switching of polarization states or transmission of arbitrary polarization state. The two receiver system allows for simultaneous measurements of co-polar and cross-polar backscattered signals [C6872]

"A preliminary evaluation of the absolute backscatter calibration of the ERS-1 altimeter using a passive technique"

This paper focuses on the determination of receiver gain and offset of the ERS-1 radar altimeter, operated in listen-only mode over few orbits. The determination is carried out by examining the receiver response over different types of earth surfaces against concurrent measurements of other radiometers and an ocean emission model. The results are discussed, and it is shown how this technique can be refined to support the determination of the absolute backscattering coefficient, if the transmitted power and the antenna characteristics are known [C6873]

"The SIVAM airborne SAR system"

In response to the significant task of mapping and monitoring the Amazon region, the System for Vigilance of the Amazon (SIVAM) program was initiated by the Brazilian government. One of the key elements of SIVAM is a group of three remote sensing aircraft, each equipped with a multi-mode synthetic aperture radar as the prime sensor. The SARs are extremely flexible and provide: multi-channel fully polarimetric SAR mapping modes, cross-track interferometric SAR modes, spotlight SAR, and wide area surveillance with ground moving target indicator (GMTI) capability [C6874]

"Deriving forest characteristics using polarimetric InSAR measurements and models"

We report on a range of experiments designed to address previous shortcomings in microwave imaging of forests, by exploiting more sophisticated radar measurements and bringing physical models to bear. The experiments are based around a set of high-resolution airborne X- and L-band polarimetric interferometric radar acquisitions of Thetford forest, a managed plantation in the UK. The information content of the interferometric coherence, scattering phase centres and backscatter coefficients at different wavelengths and polarisations with respect to canopy structure is examined and compared with outputs from a coherent microwave scattering model to support interpretation of the data. The results suggest that improved resolution and interferometric information are important in retrieving biophysical parameters of interest to the forestry and carbon modelling communities [C6875]

"Remotely sensed and geophysical data for nondestructive archaeological prospection"

Remotely sensed and geophysical data can be effectively integrated through the use of geographical information

systems (GIS). The role of GIS in the accurate mapping of an area of archaeological interest, prerequisite for a devising and effective excavation strategy, is well established. Multitemporal aerial photos at different scales and high-resolution magnetic data were acquired over the ancient Greek colony of Metaponto in Southern Italy (7thC. BC). Aerial photos were converted to digital form and georeferenced using a GIS. Magnetic data were interpolated and processed to produce raster images. Radar satellite imagery and magnetic and electric geophysical data were acquired over the Eolic town of Kyme (Turkey), along the Aegean coast. All data were integrated and analyzed in the GIS environment to infer the buried archaeological features. For each site, a final digital map of the archaeological structures and relevant landforms was produced [C6876]

"Combined active and passive remote sensing of the properties of cirrus clouds"

Since October 1987, a uniquely extensive high cloud dataset has been collected from the University of Utah Facility for Atmospheric Remote Sensing (FARS). The measurements, which currently total over 3000-h of ruby (0.694 μm) lidar data, have been directed toward (i) basic cloud physics research, (ii) improving satellite-based and GCM cloud property predictions by providing climatologically representative local cloud statistics, and (iii) creating parameterizations of the mean cirrus cloud radiative properties [C6877]

"Monitoring wetland extent and dynamics in the Cat Tien National Park, Vietnam, using space-based radar remote sensing"

A range of spaceborne radar images are acquired over a tropical catchment containing a large floodplain wetland in Cat Tien National Park, Vietnam. The images, which are a combination of ERS and JERS SAR over the period 1992 to 2000, are focussed on the wet season in each year while more frequent sampling is available throughout 1999-2000. These data are being used to delineate the area of the wetland and, by superimposing on a digital elevation model, the volume of water in the wetland at the time of each image acquisition. This provides temporal estimates of maximum flood extent since 1992 and for 1999-2000 the seasonal variation in wetland extent (i.e. the hydroperiod). The remote sensing derived estimates are compared with meteorological records for the area, and with limited in-situ measurements of water depth. The work is extended to include JERS acquisitions, in order to (i) extend the record of wetland extent, and (ii) compare estimates of wetland extent acquired with C-band and L-band sensors [C6878]

"Radar imagery for environmental geology study of coastal zones in southern Italy"

Summary form only given, as follows. The high spatial resolution of fine beam Radarsat imagery makes it suitable for detailed analysis of coastal zones. For this study three SAR images were acquired in different seasons and a stereoscopic pair was acquired with different incidence angles. The images were visually and automatically interpreted to derive the geological, geomorphologic and hydrogeologic setting of the Ionic coastal zone of Salento Peninsula (southern Italy). Mesozoic age limestone underlying calcarenite, sand and clay of Cenozoic-Quaternary age characterize the geological setting of the study area. The structural-geological setting largely determines the morphology of coastal areas, the erosion-accumulation processes and the groundwater flow patterns. Several coastal environment types can be recognized in this area with different geomorphologic setting and dynamic evolution trend, such as cliffs, sandy beaches, rocky low coasts, gravel bays, coastal dunes, coastal lakes and wetlands. The sea level changes in recent times have produced a general geomorphologic instability in the coastal zones, confirmed by active erosion and accumulation processes. A texture classification of the radar images was carried out in order to produce a land use map of the study area. This map provides useful information about underlying geology and geomorphologic setting, besides giving a comprehensive view of the anthropic activities that can interfere with natural processes. The radar stereoscopic imagery acquired in the F2 and F4 far beam mode was visually interpreted using a mirror stereoscope. The 3D view considerably improves the reconnaissance of geological structures and landforms characterizing the study area. The stereo pair was also interpreted to analyze the geomorphology of the coastal line, and local erosion and accumulation processes. The results highlighted the fact that the coast is mainly affected by erosion, with local high regression rate. These destructive processes affect both high cliff coast and sand beaches with coastal dunes. Besides their stereoscopic vision, these images were used for radargrammetric measurement of topographic surfaces. The DEM was calculated by means of a fully digital radargrammetric process based on an automatic pixel matching on both images for parallax measurement. Several DEMs were produced using the original and filtered images in order to evaluate the influence of speckle on the results. The accuracy of the radargrammetric DEMs was assessed by comparing them to a DEM interpolated from the official contour map at scale 1:50000. The difference between the elevation measured by radargrammetry and the topomap data was calculated on each pixel to produce error maps. The mean values of the error (generally below 2 m) are satisfactory, while their standard deviation (about 15-20 m) is slightly high considering the flat morphology of the study area. In this study, fine resolution radar images were interpreted using different approaches. The results obtained testify that these imagery- single, stereo pairs and multitemporal-provide a large amount of information

on several environmental variables that are essential for producing a global model of coastal zones [C6879]

"Field experiments synchronous with SRTM flights"

A national coordinated program was evolved to utilise SRTM data for applications to Earth sciences, hydrology and technology development. The project was sponsored by Department of Science and Technology, Government of India. Fourteen test sites covering the above themes spread all over India were selected for conducting synchronous field experiments. About 52 corner reflectors (CR) were fabricated with two sizes (1.2 meters and 1.6 meters shortest length) and installed in the fields by the respective groups according to the installation parameters given by DLR, Germany. The CRs and GPS data will be useful for calibration of the SAR system and validation of DEM products. This paper gives the details of the field campaign [C6880]

"Automatic weather station (AWS) lidar"

A ground based, autonomous, low power atmospheric lidar instrument is being developed at NASA Goddard Space Flight Center. We report on the design and anticipated performance of the proposed instrument and show data from two prototype lidar instruments previously deployed to Antarctica [C6881]

"SIRAL, a high spatial resolution radar altimeter for the Cryosat mission"

SIRAL (SAR Interferometer Radar Altimeter) is the new spaceborne altimeter designed for CryoSat mission. This ESA mission, planned for 2004, will be used to estimate-on a global scale- the fluctuations in mass of sea-ice and land-ice. The novelty of SIRAL concept with respect to conventional pulse-limited altimeter, is the implementation of Doppler processing for along-track resolution enhancement and also of interferometry, used to locate the echo in the across-track direction. The innovative technical features of SIRAL are presented hereafter with regards to the function requirements and also the expected performance [C6882]

"Correction of residual motion errors in airborne repeat-pass interferometry"

The usage of airborne repeat-pass single-baseline interferometry at longer wavelengths, like the L- and P-bands, is starting to be an established technique for parameter inversion studies, as well as for coherence analysis. The main limitation for a wider applicability of such data is the presence of small uncompensated motion errors, which appear as low-frequency phase modulations in the image data. Airborne repeat-pass data are therefore not useful for applications which depend on large-scale spatial or multiple-image phase relations. This includes important tasks like multi-baseline parameter inversion techniques, differential interferometry as well as high precision DEM generation. In this paper we address the effect of residual motion compensation errors in repeat-pass interferometry and propose a new technique to minimize their influence on the interferometric phase [C6883]

"Polarimetric detectors of extended targets for ship detection in SAR images"

This paper deals with polarimetric detection of ships in SAR images of medium/high resolution (about meters). The aim is to develop detection techniques able to exploit the polarimetric information in order to improve the detection capability of ships or generally man-made targets modelled as extended targets (i.e. occupying multiple pixels). Both a decentralized and a centralized approach are considered for the fusion of the polarimetric information and their performance are characterized [C6884]

"Large aperture scanning lidar based on holographic optical elements"

We have developed simplified conical scanning telescopes using Holographic Optical Elements (HOEs) to reduce the size, mass, angular momentum, and cost of scanning lidar systems. This technology enables wide-angle scanning and three-dimensional measurements of atmospheric backscatter when used in airborne instruments, and high temporal resolution observations of atmospheric dynamic structure, including wind profiles from ground-based facilities [C6885]

"A synthetic moving target generator for calibration of Radarsat 2 Moving-Object Detection Experiment (MODEX)"

The Moving-Object Detection Experiment (MODEX) of the Radarsat 2 platform will allow object motion extraction and measurement by partitioning the radar antenna into fore and aft apertures. Accurate extraction of object motion requires compensation to produce two equivalent radar channels. Calibration of MODEX signals is best accomplished by a transponder that receives and measures the signal transmitted by the satellite and uses the captured radar waveform to generate moving point-target signals with precisely known properties. We are

proposing to use a computed approach to implement a synthetic target generator (STG) as a transponder for the motion calibration of Radarsat 2 MODEX. With this approach, the incoming pulses are digitized, manipulated using a fast digital signal processor (DSP) to synthesize signals simulating moving point-targets, and then converted back to analog for transmission. This paper reviews theoretical considerations for the synthesis of moving-object signals, demonstrates the concepts with simulations, and discusses implementation issues [C6886]

"Validation of grid-based surface reconstruction techniques applied to digital elevation models including the Shuttle Radar Topographic Mission"

For the suitability towards the reconstruction of geomorphological sound surfaces using digital elevation models different methods as a weighted neighborhood member procedure, a ordinary kriging procedure, a gradient spline technique and a new modification of heat flow equation were tested. Round-off effects and effects of local noise-signal ratio were investigated [C6887]

"Modelling returns from urban manufacts: simulation results for finite trihedrals"

Simulation results obtained by means of our polarimetric model for dielectric trihedral corner reflectors are presented in this paper. The model takes into account the dimensions of the reflecting surfaces, their dielectric properties and roughness, and evaluates contributions of coherent and diffuse scattering. The simulation has been carried out choosing values of input parameters able to describe an urban environment [C6888]

"Soil moisture retrieval using SAR data and a priori roughness information"

In this paper, two model-based methods for soil moisture retrieval from SAR measurements are described. The performances of the two methods are compared using, simulated L-band data obtained by exploiting the integral equation model (IEM). The first method is based on a previously developed soil moisture retrieval algorithm. It estimates the soil moisture content by approximating the IEM inverse function using a neural network approach. The second method is an iterative technique which adopts a searching strategy by using the IEM direct model. The two methods are also compared when using a priori information, such as the roughness state of the bare soil surfaces [C6889]

"The Polarization Diversity Lidar: a dual-wavelength, high-resolution, scanning lidar for cloud and aerosol research"

The unique cloud and aerosol research capabilities of the Polarization Diversity Lidar system are described, and outstanding data display examples will be illustrated [C6890]

"Automated sea ice classification using spaceborne polarimetric SAR data"

This paper discusses the capability of spaceborne polarimetric C-band SAR data for sea ice detection and classification. Unsupervised classification using polarimetric decomposition and the complex Wishart classifier was performed on SIR-C data acquired off the coast of Newfoundland in April 1994. The algorithm is used for sea ice applications for the first time, and appears promising. In addition to polarimetric classification, three of the measured features were found to have ice edge detection capability: HV-intensity, HH/VV-ratio and anisotropy. These features show a clear separation between sea ice and open water and simple thresholds can be applied [C6891]

"Origin and correction of phase errors in airborne repeat-pass SAR interferometry"

Airborne SAR surveys are often subject to severe motion errors. As the different tracks of a repeat-pass interferometric data set are acquired successively, any residual motion error has strong influences on the accuracy of the derived interferometric phase. In this paper we analyze the different error sources and present suitable compensation methods. Interferometric data acquired in L-band by the DLR's E-SAR system are used for quantitative analysis and for the demonstration of the proposed correction methods [C6892]

"Thin linear features extraction in SAR images by fusion of amplitude and coherence information"

In this paper, we propose a new method to extract thin linear decorrelated features in SAR interferometric images by fusing the information provided by the amplitude and the coherence. A first detection is the result of an unsupervised classification performed on the coherence image, where linear features correspond to dark areas (low coherence) and non-linear features to brighter areas. This approximate location of the linear features is further refined by using edge information extracted in the amplitude data by two measures: the coefficient of

variation (CV) and the ratio of local means (RLM). A precise detection is then performed by using the results of coherence classification and the fusion of the two previous measures. The method has been applied on ERS SAR images from the western part of Cameroon to extract thin river networks in mangrove areas. The goal is to update-or create geographical maps [C6893]

"SAR processing algorithms in the KSPT ENVISAT ASAR processor"

This paper describes the algorithms used in the KSPT ENVISAT ASAR processor. The KSPT ASAR processor is required to process data from image (IM) mode, alternating polarization (AP) mode and wide swath (WS) mode. Three different processing algorithms are used for processing the different modes. For IM mode the processor is using the Extended Exact Transfer Function (EETF) algorithm, for AP mode the burst-EETF algorithm and for WS a modified phase preserving SPECAN algorithm. The algorithms have been selected to get optimal image quality for the different modes [C6894]

"Moving target detection by along-track interferometry"

In this paper we consider the detection of a moving point target using along-track (AT) InSAR systems. We consider two cases: conventionally and one bit coded raw data. The performance of the system is evaluated by comparing the probabilities of false alarm and detection [C6895]

"Exotic forest clear-fell mapping from the New Zealand PACRIM-2 mission"

The all weather imaging ability of SAR has real benefits in maintaining detailed forest inventories.. However, previous work has indicated that even clear-fell detection is not always straightforward using C-band radar. Backscatter from bare ground can vary considerably with environmental conditions. This paper takes an initial look at the PACRIM-2 study of Kaingaroa Forest which aims to better understand these problems and provide solutions. While bare ground and even tree species can be distinguished visually, the detailed analysis of the statistics still indicate difficulties and not all the results are consistent with a previous study. An anomalous dip in the near-range C-band vertical response has been noted, which may be affecting the statistics. A change in the polarization response was seen for two artificially wetted areas, which may help define better classification strategies [C6896]

"InSAR analysis of Miyake-jima volcano with Radarsat images"

A volcanic island, Miyake-jima, has erupted since the end of June 2000. Fifteen Radarsat images of the island are analyzed and eight fine interferograms are produced with a newly developed enhance filter although the island is covered with vegetation. Eleven GPS stations were set since 1998 in the island, but most of them stopped working mainly because of failure of the electric power supply. Differential SAR interferometry could detect crustal deformation in space continuously and is the only way to monitor crustal deformation caused by the volcanic activity. Orbital base lines of pairs of SAR images are corrected using GPS data [C6897]

"Interferometric performance estimation for the interferometric Cartwheel in combination with a transmitting SAR-satellite"

Presents the results of a preliminary interferometric performance estimation for the bistatic Cartwheel/ASAR combination. The interferometric baselines are investigated and a first estimation for the achievable interferometric height performance is given [C6898]

"Fusion of multitemporal contextual information by neural networks for multisensor image classification"

The analysis of a multitemporal sequence of images of a given site makes it possible to exploit temporal information in addition to spectral and spatial information, and therefore represents a way to improve the accuracy with respect to the non-contextual single-time classification. The proposed contextual multitemporal classification scheme consists of two stages of multilayer perceptron (MLP) neural networks for each single-time image of the multitemporal sequence. The first stage is a one-hidden layer MLP whose rôle is to estimate, for each pixel, the single-time posterior probability of each class, given the feature vector. These probability estimates represent spectral information; in addition, they are utilized to generate a non-contextual classification map. The neighboring class labels of a given pixel in the non-contextual classification map are exploited to extract spatial information, while temporal information is deduced from the non-contextual maps produced by the remaining single-time images in the multitemporal sequence. Spatial and temporal contextual information together with spectral information serve as inputs for the second stage network of the classification scheme where the fusion takes place. As the network configuration can influence the classification performances, three

MLP-based configurations are investigated. Experimental results on a multitemporal data set consisting of two multisensor (Landsat TM and ERS-1 SAR) images are presented. The performances of the proposed methods are discussed and compared with those obtained by a reference classifier based on the Markov random fields fusion approach in terms of classification accuracy. The results show that the proposed fusion approach based on neural networks may represent an interesting solution to the problem of multitemporal contextual fusion [C6899]

"Airborne remote sensing without ground control"

Describes how position and orientation measurement systems are used to directly georeference airborne imagery data, and presents the accuracies that are attainable for the final mapping products. The Applanix Position and Orientation System for Airborne Vehicles (POS/AV™) has been used successfully since 1994 to georeference airborne data collected from multispectral and hyperspectral scanners, LIDARs, and film and digital cameras. The POS/AV™ uses integrated inertial/GPS technology to directly compute the position and orientation of the airborne sensor with respect to the local mapping frame. A description of the POS/AV™ system is given, along with an overview of the integrated inertial/GPS processing. An error analysis for the airborne direct georeferencing technique is then presented. Firstly, theoretical analysis is used to determine the attainable positioning accuracy of ground objects using only camera position, attitude, and image data, without ground control. Besides theoretical error analysis, a practical error analysis was done to present actual results using only the POS data plus digital imagery without ground control except for QA/QC. The results show that the use of POS/AV™ enables a variety of mapping products to be generated from airborne navigation and imagery data without the use of ground control [C6900]

"Polarimetric observations of wave breaking induced by ship wakes"

Describes two experiments conducted using the DSTO mobile high resolution radar facility to observe wave breaking events induced by ship wakes. In the first experiment high resolution polarimetric range profiles of the wake produced by a displacement hull vessel were recorded at X and Ku band frequencies. Periodic transient enhancements were observed, generated by wave breaking events precipitated by the superposition of the dominant wake components with the crests of the incoming swell. In order to identify the induced wave breaking events unambiguously, the measurements were carried out for ship headings directly into and directly opposed to the prevailing waves. Clear confirmation of the proposed mechanism was thus demonstrated. The second experiment employed a planing hull vessel. Because of the high speed of this ship, the measurement geometry was changed to set one of the diverging wake arms perpendicular to the radar beam. High resolution polarimetric range profiles were then recorded at X and Ku band frequencies [C6901]

"3D scene modeling from data fusion"

We proposed in this paper a key approach for remote sensing data fusion for the purpose of three dimensional (3D) modeling. A 3D digital elevation model (DEM) is a full description of the scene, including 3D geometric representation and 2D radiometric classification. In this context the purpose of fusion is to provide a more reliable and more accurate model than single data would provide. We give thereafter the main principles of the approach. The application is on Poyang lake, in the Jiangxi province of China. This is an ongoing project [C6902]

"Polarimetric properties of boreal forest in L- and C-band SAR images"

In this study the usability of L- and C-band SAR polarimetry in boreal forest remote sensing is examined and discussed. The influence of snow cover, weather conditions, forest type and several other aspects to forest backscattering in L- and C-bands is investigated by using multitemporal polarimetric images [C6903]

"Seasonal variations of ERS Tandem coherence values over a mixed temperate forest"

The present study aims to evaluate the relevance of Tandem ERS-1/2 coherence values for monitoring temporal and structural changes in a mixed temperate forest ecosystem. The analysis of the decorrelation factors show very interesting results we attempt to understand thanks to a coherent model [C6904]

"Radar remote sensing of mangroves: results and perspectives"

This paper gives an overview of our work conducted since 1993 and based on the analysis of AIRSAR data over a variety of mangrove forests. The effects of canopy structure on the polarimetric radar response of mangrove forests are analyzed from both an experimental and a theoretical point of view. Particularly, two mangrove stands of equal biomass but with great differences in their structural characteristics are also studied. Quantitative estimation of mangrove parameters is then discussed [C6905]

"Improving the focusing properties of SAR processors for wide-band and wide-beam low frequency imaging"

An increasing amount of interest has been evolved in VHF/UHF SAR applications. These radars have proven to be a very powerful method for underground and obscured object detection as well as for parameter retrieval purposes. For new upcoming applications, high-resolution VHF/UHF SAR imaging is an important task but cannot be achieved easily with conventional SAR processing techniques. A new algorithm is presented in this paper, which modifies the azimuth compression step of the extended chirp scaling (ECS) algorithm [Moreira et al. 1996]. It provides high azimuth resolution also for high squint or wide swath. Additionally, the effect of strong motion errors in wide-beam azimuth processing is analysed and discussed, using simulated data as well as data collected by the airborne experimental SAR system of DLR (E-SAR) in P-band. In this context, a sub-aperture approach for motion error compensation in wide-beam azimuth processing is also presented [C6906]

"Pre-formation SAR to SAR image registration"

A critical step in the formation of multi-pass IFSAR and CCD products involves the registration to subpixel scales of two complex SAR images. This is usually performed as a two step process where correspondences between the images are determined followed by a warping of the imagery. Since more information is available in the phase history data (PHD) it might be expected that improved registration results could be achieved. This paper investigates a number of registration approaches in the PHD and shows that the techniques are equivalent to each other and to registration in the image domain. It is also demonstrated that processing in the PHD, although potentially minimizing the impact of numerical errors from resampling introduces complexity when estimating local registration estimates and has difficulty in regions that decorrelate [C6907]

"Phase analysis for the limitations of the tomographic paradigm on a 3D scene"

The tomographic paradigm argues that the demodulated pulses from a spotlight mode SAR system trace a 2D slice of the 3D Fourier transform of the complex surface reflectivity. This paper derives the phase errors that result from imaging a 3D surface from a non planar collection geometry and shows how correct projection to the true surface can eliminate many of the errors. The response from an ideal scatterer is derived and then approximated to simplify the expression into a manageable and meaningful form and so that insight can be gained into the artifacts produced. The theory indicates that warping an image by distorting the final image to correct for layover doesn't eliminate the second order blurring terms produced by the relief and that both the layover and these blurring affects can be properly eliminated through correct projection to the real ground plane [C6908]

"The use of realistic aerosol models to limit the range of aerosol possibilities in deriving aerosol scatter"

The lidar equation is given by $E(r, \lambda) = C(\lambda) \sigma_s(r, \lambda) P(180, r, \lambda) T(r, \lambda)^2 / 4\pi r^2$ (equation 1). $E(r, \lambda)$ is the energy received at a distance r , $C(\lambda)$ is the lidar calibration factor accounting for the laser power and detector efficiency, $\sigma_s(r, \lambda)$ is the combined aerosol and molecular scattering coefficient (in m^{-1}), $P(180, r, \lambda)$ is the weighted aerosol-molecular phase function at the backscattering angle of 180 degrees, and $T(r, \lambda)$ is the two way transmission due to aerosol and molecular extinction. If the aerosol type is known at each distance then the aerosol phase function can be calculated and a forward stepping approach can be implemented to derive the aerosol extinction coefficient at each range. Typically the aerosol type is not known and various methods have been used to constrain Eq. 1. Here we investigate the use of multi-wavelength lidar measurements to derive the aerosol phase function as a function of distance. As aerosol extinction at several wavelengths is not sufficient to constrain the aerosol type for large marine aerosols, we use a set of realistic aerosol models to limit the range of aerosol size distribution possibilities. For this paper we also limit ourselves to clean marine conditions where the aerosols are non-absorbing. The most common lidar wavelengths (from an NdYag laser) include 355, 532, and 1064 nm [C6909]

"Speckle noise removal in SAR image based on SOT structure in wavelet domain"

The Spatial-orientated tree (SOT) structure plays a very important role in wavelet-based image compression. Both the Embedded Zero-tree Wavelet (EZW) and the Set Partitioning in Hierarchical Trees (SPIHT) coding schemes utilize the parent-children relationship in SOT for image compression. The SOT is a very efficient data structure to be used for investigation of spatial correlations among wavelet coefficients at different resolutions. However, to the best knowledge of the authors, the SOT has not been widely used in noise suppression or image enhancement. This paper addresses this application and presents a novel denoising algorithm that utilizes the SOT to normalize the wavelet coefficients at different resolutions and remove the signal-dependence of the

speckles before applying the thresholding scheme [C6910]

"Mapping the Antarctic ice sheet margin and grounding zone for change detection"

We have undertaken mapping of the ice sheet margin and grounding zone in East Antarctica using Landsat TM and ERS SAR images in order to establish an accurate baseline for the detection of future change. As part of this work we have implemented a computer-aided edge-following algorithm to provide an objective and consistent mechanism for analysis of different images. Accurate geocoding of the images is achieved with sparsely distributed ground control points and a transformation of the images which preserves their inherent geometric properties and internal positioning accuracy. An initial comparison with published maps has identified significant changes in several large ice shelves [C6911]

"The spatial variability of summer sea ice in the Amundsen Sea seen from MODIS, RADARSAT SCANSAR and LANDSAT 7 ETM+ images"

The summer sea ice extent, concentration and zonation in the Southern Ocean is investigated using three new satellite sensors. They are the MODerate resolution Imaging Spectroradiometer (MODIS) on the first NASA Earth Observing System (EOS) satellite, Terra, the synthetic aperture radar (SAR) on the first Canadian Space Agency Radarsat satellite, and the Enhanced Thematic Mapper Plus (ETM+) on the NASA Landsat 7 satellite. A large number of images of these satellite sensors were acquired in February and March 2000, when a sea ice field campaign was conducted aboard the U.S. research vessel Nathaniel B. Palmer. MODIS images acquired under clear sky conditions provide regional information of the spatial variability of the austral sea ice cover. Mosaics of Radarsat images present complementary information under various weather conditions and fill the MODIS information gap caused by cloudiness. ETM+ images give detailed information of the characteristics of individual ice zones, including the landfast, coastal polynyas, pack ice, and pancake and cake ice zones [C6912]

"SARfari: a tool for analyzing Arctic hydrology using space-borne SAR"

Some of the problems with analyzing SAR imagery for Earth-surface change-detection are discussed, along with solutions for hydrological applications. These involve analysis of long time-series of terrain corrected scenes. Examples of such analyses are given for watersheds in Alaska and Siberia [C6913]

"Combining SAR and AVHRR to understand sea ice dynamics in the seasonal and perennial ice zones of the Beaufort and Chukchi seas"

In this paper, we discuss the use of three data analysis techniques for understanding sea ice dynamics at the regional scale during the Surface Heat Budget of the Arctic (SHEBA) Experiment in the winter of 1998. The satellite data consist of SAR and AVHRR, and the techniques used include: 1) hue-intensity saturation (HIS); 2) Radarsat Geophysical Processor System (RGPS) ice tracking; 3) measurements of sea ice deformation in the seasonal ice zone (SIZ) and the perennial ice zone (PIZ) of the Beaufort and Chukchi seas. We then discuss the results of data analyses using these techniques and the importance of the observations in understanding the behavior of the SIZ and PIZ, and the implications these observations have for understanding and modeling ice dynamics in this region [C6914]

"DInSAR applications to landslide studies"

Operational monitoring of slope instabilities by SAR interferometry poses a number of challenges due to the limited spatial extent of the landsliding areas and the rainy conditions usually associated with mass movement events. In this work, we present applications of DInSAR techniques to the assessment of the stability of landslide-prone areas. A long-term analysis over single, stable scatterers can be attempted, in order to overcome the intrinsic low-coherence conditions associated with landslide sites. The technique, known as the permanent scatterers approach, has been shown to give excellent results over areas with high densities of man-made targets. In this work, some aspects of the PS processing are reviewed and possible improvements are proposed to bring the method to give reliable results over sites with low urbanization such as the rural settings associated with landslide-prone areas in Southern Italy [C6915]

"First P-band results using the GeoSAR mapping system"

GeoSAR is a program to develop a dual frequency airborne radar interferometric mapping instrument designed to meet the mapping needs of a variety of users in government and private industry. Program participants are the Jet Propulsion Laboratory (JPL), Calgis, Inc., and the California Department of Conservation with funding provided initially by DARPA and currently by the National Imagery and Mapping Agency. Begun to address the critical mapping needs of the California Department of Conservation to map seismic and landslide hazards

throughout the state, GeoSAR is currently undergoing tests of the X-band and P-band radars designed to measure the terrain elevation at the top and bottom of the vegetation canopy. Maps created with the GeoSAR data will be used to assess potential geologic/seismic hazard (such as landslides), classify land cover, map farmlands and urbanization, and manage forest harvests. This system is expected to be fully operational in 2002. In this paper we describe an experiment conducted at California's Latour State Demonstration Forest located near the city of Redding. This experiment marks the first operation of the-P-band radar in a vegetated area [C6916]

"Repeat pass SAR interferometry at VHF band"

The South African SAR system (SASAR) has flown a number of repeat pass interferometry flights, and this paper reports on the results achieved to date with the system. The flight geometry, data acquisition and processing are described, and examples of interferograms are shown. This paper also shows simulations of fringe patterns obtained from an interferogram simulator developed in the UCT Radar Remote Sensing Group. The simulated fringes obtained from a DEM are compared to those obtained from the real SAR data [C6917]

"Effect of the ionosphere on P-band spaceborne SAR images"

Radar backscatter measurements have proven to be positively correlated with above ground biomass and this correlation increases with the wavelength. Biomass retrieval algorithms have been developed for airborne P-band data collected over both boreal and tropical forests. Radar measurements are insensitive to cloud cover and can be operated during day and night. Hence a space-borne radar system, operating at low frequency, will permit the measurement, mapping, and understanding of these parameters with a spatial and temporal resolution suitable for modeling ecosystem processes at regional, continental, and global scales. Based on experience with airborne campaigns, a polarimetric low frequency or P-band SAR has been shown to be the most appropriate instrument to this purpose. One of the disadvantages of the P-band is that in this frequency band ionospheric distortion of the images is expected to be high. A quantitative estimation of the ionospheric influences on P-band imagery needs to be derived, which can lead to orbit parameters, which minimizes the impact of the ionosphere on biomass measurements [C6918]

"Performance of the CARABAS-II VHF-band synthetic aperture radar"

CARABAS-II is an airborne SAR operating in the 20-90 MHz band. The low operating frequency enables detection of concealed objects in dense forests as well as mapping of forest stem volume. A number of calibration experiments have recently been conducted to evaluate system performance. In this paper, we report on some of the results from the analysis. Spatial resolution, measured using 5-m trihedrals, is typically 2.5 m in both slant range and azimuth. The right-left ambiguity ratio, measured using 5-m trihedrals on both sides of the flight track, is about 10 dB for a single antenna element on receive. The noise level varies in the images and includes both multiplicative (integrated sidelobe ratio, right-left ambiguity ratio) and additive (radio-frequency interference, receiver noise) terms. Analysis of images from a recent campaign in northern Sweden shows that the additive noise term is less than -20 dB (noise-equivalent β°) for slant ranges less than 14 km [C6919]

"Support vector machine classification of land cover: application to polarimetric SAR data"

Support vector machines (SVMs) have much attention as a promising approach to pattern recognition. They are able to handle linearly nonseparable problems by combining the maximal margin strategy with the kernel method. This paper addresses a novel SVM-based classification scheme of land cover from polarimetric synthetic aperture radar (SAR) data. The SVMs are successfully applied to the feature vectors which consist of several polarimetric features or the texture measure, and perform efficient image classification. Some important properties of SVMs, for example the relation between the number of support vectors and classification accuracy, are also discussed [C6920]

"Remote Minefield Detection System (REMIDS): a UK programme for airborne minefield detection"

The UK Remote Minefield Detection System (REMIDS) Technology Demonstration Programme (TDP) is nearing the end of a five year programme that has developed emerging remote sensing technologies into an integrated system to demonstrate a capability for the reliable detection of minefields and mined areas from an airborne platform. The multi-sensor system demonstrator is being managed by DERA on behalf of the UK MoD. A novel Ultra Wide Band Synthetic Aperture Radar (UWB SAR) and a full Stokes Vector Time-parallel Polarimetric IR camera (IRPC) have been developed and a commercial VIS-NIR hyperspectral sensor is being considered for inclusion in the final system trials. While the UWB SAR is the lead sensor, with a capability for foliage penetration and target identification, confirmation and additional target discrimination is provided by polarimetric IR imaging to give a 24 hr capability. A ground station processor, based on COTS systems, has been developed

to fuse all sensor outputs in a decision level process through a variety of target detection and identification algorithms. Probabilistic analysis is used on the resulting outputs to define the extent of a minefield to the system operator. In this paper we report on the development of the REMIDS programme by DERA from inception through to sensor trials, providing an overview of the sensor technologies developed and a discussion of the preliminary results [C6921]

"CloudSat and the EOS constellation"

CloudSat is a multi-satellite satellite experiment designed to utilize the opportunity provided by the EOS constellation to deliver, as-directly as possible, information relevant for assessing the way cloud processes are parameterized in global weather prediction and climate models. In this way, CloudSat will provide a means for the critical evaluation of model prediction of clouds. The prime source of this information is to be extracted from vertical profiles of radar reflectivity obtained with the CloudSat 94 GHz nadir pointing radar. When this information is augmented by other measurements of the constellation, a rich data source for studying clouds, precipitation and the interaction of cloud processes with aerosol can be expected. There remain a number of key challenges for optimally extracting the important information from the suite of constellation measurements. Included in these challenges is the need both to understand the disparate nature of the information content contained in multi-sensor data and develop a retrieval framework that optimizes this information content [C6922]

"Multifrequency radar backscattering from wheat canopy in the light of theory and experiments"

A discrete volume scattering model based on a distorted Born approximation was validated with the experimental data from a multi-frequency scatterometer. The influence of the ground interface has been found important for high wavelength bands while as for bands with low wavelength, the soil contribution is negligible under vegetated conditions. It could be concluded both from the experimental and simulation results that low frequency radars (L-band) are most suitable for soil moisture determination and the soil moisture determination gets difficult with the high frequency radars (X-band) which are suitable for wheat growth monitoring [C6923]

"Various approaches for soil moisture estimates using remote sensing"

Three approaches using optical and microwave remotely sensed data were considered for soil moisture assessment. The first was based on NOAA/AVHRR images and meteorological data, the second on synergy of NOAA and ERS-2.SAR data, and the third one on the ERS-2 SAR and JERS SAR data. For the test area the classification of crop type has been carried out using Thematic Mapper images [C6924]

"High resolution (metric) SAR microsatellite, based on the CNES MYRIADE bus"

A significant reduction of observation satellite size (and cost) has been achieved over the years. Have we reached the limit? How can we go further? Those questions are all the more relevant as one of the future challenges in spaceborne SAR is likely to be the near real time imaging (less than 30 or 60 minutes delay). not only in military but also in civilian studies, which automatically requires a large number of satellites in orbit. In SAR, unlike in the optical, the barriers cannot be only technological, there is a matter of the physics and of the wavelength which makes the SAR antenna area a tight constraint. Increasing the frequency beyond the X band is of poor benefit since it jeopardises the all weather capability of radar. CNES is exploring the capability of an SAR microsat based on the CNES bus product line currently in development and called MYRIADE (<120 kg satellite mass). The core mission objective is high resolution (1 or 2 meters) in the X band. Such resolution achievement under the limited mass and power budget requires significant trade-offs against other performance areas (swath, incidence domain, working duty cycle), however these operational limitations of each satellite can be circumvented by the high cost saving and the resulting affordability of a large constellation format. The current studies are aimed at identifying new SAR mission rationales that the micro-satellite concept may open. up and at identifying the technological constraints and development needs. The relevant technological areas are antennas (parabolic reflector or electronic reflect array, fixed or deployable), small TWTA, ultra-capacitor (to concentrate energy from battery into high power bursts for payload), low mass data handling and telemetry. This paper presents the status of the analyses and tradeoffs at the early phase of the study [C6925]

"Bayesian-hierarchical SAR classifier"

This research combines three existing statistical tools (optimal Bayesian techniques, maximum entropy density estimation, and hierarchical classification techniques) to develop a practical, robust technique for classifying short vegetation, which we call the Bayesian-hierarchical classifier. We apply this technique to real SAR data, using it to identify five types of short vegetation. It yields high accuracies across an entire growing season, despite the natural fluctuations of vegetation dielectric constant and structural characteristics due to changes in each plant type as it matures. We also show the results of two existing classification techniques, the ISOCCLUS

unsupervised clustering technique, and a simple maximum likelihood estimator with Gaussian assumptions, on the same data set used to develop the Bayesian-hierarchical classifier. All classifications and comparisons are done on the basis of independent testing and training data, an important criterion to ensure accurate evaluation under real world conditions. The Bayesian-hierarchical classifier has an average accuracy of 95% on the diagonals of the confusion matrix, improving over the other techniques by between 10-20% [C6926]

"Estimation of sea-ice SAR clutter statistics from Pearson's system of distributions"

SAR images can be used to help ship routing in sea-ice conditions. In this study, we focus on the Antarctic region where no multi-year ice nor big ice floes are to be found. As a matter of fact, each clutter obeys a backscattering mechanism that induces a specific pixel distribution and our attempt is to identify automatically the correct distribution for each ice type. The problem is that of generalized mixture estimation and unsupervised image classification. In this work, we modelled the mixture with distributions from Pearson's system. Parameter estimation is realized according to the ICE algorithm in the context of hidden Markov chains. The results obtained from Pearson's system are compared to ones obtained with a classical mixture of Gaussian distributions [C6927]

"Acquisition of sensing data on a reconfigurable platform"

Recent developments in wireless networking and re-configurable computing are making real-time processing of remotely sensed data and real-time information dissemination feasible. In this paper we describe the development of a single card reconfigurable hardware system that allows for both real-time acquisition and processing of radar polarimetric data. The proposed approach was developed after examining the architecture and implementation of several current data acquisition systems. Upon project completion it will be possible to support the acquisition, processing, bulk hard-disk data storage and Ethernet transfer of radar polarimetric data. This work will be particularly useful in supporting real-time operation due to speed improvements gained from reconfigurable devices [C6928]

"Design status of a combined Ka-band altimeter/radiometer"

In preparation of the post ENVISAT and Jason-2 altimetry missions, Alcatel has completed a phase A study for CNES on a new class of altimeter. A major objective is to propose a combined altimeter and radiometer at minimum cost, size and power consumption compatible with a micro satellite (<100 kg class). The micro-satellite(s) would be used to improve the spatial/temporal sampling of the ocean which is not sufficient for current and future oceanographic missions. The Ka-band (35 GHz) is more interesting than the Ku-band for the altimeter since it improves the link budget and allows larger bandwidth (500 MHz) and pulse repetition frequency (4 kHz). From the scientific point of view, Ka-band altimeter data would give access to a different part of the sea surface roughness spectrum and thus would complement the C+Ku measurements available from other altimeters. The microwave radiometer, used for wet path delay correction, is a dual-frequency instrument (23.8 & 36.8 GHz). The proposed architecture for the Ka-band altimeter is based on the classical deramp technique for pulse compression and it takes benefits of Alcatel and CNES experience from the realisations of Poseidon 1 & 2. The radiometer is of the total power type and is based on direct detection. The altimeter and the radiometer share the same antenna. In parallel of the phase A, breadboarding activities have been started under development in Alcatel on CNES contracts: the transmit power module (2W SSPA) composed of a medium level amplifier, a divider, two high power amplifiers and a combiner.-the signal generator unit (500 MHz bandwidth chirp) [C6929]

"VHF radar mapping of forest biomass in Panama"

In 1998 a VHF (80-116 MHz) synthetic aperture radar (BioSAR) mounted on NASA's C-130 aircraft collected data over a series of Smithsonian Tropical Research Institute (STRI) test sites along the Panama Canal Zone in the Republic of Panama. A biomass surface map of the area was generated by interpolating between BioSAR measurement points for a set of parallel flight lines. Accuracy testing showed that there was good agreement ($\pm 10\%$) between the sensor-derived estimates of above ground biomass and the field data [C6930]

"HF radar wind measurement over the Eastern China Sea"

HF radar can be employed to measure sea surface state parameters such as waveheight, wind field and surface current velocity. This paper describes the application of the high frequency ground wave radar OSMAR2000 developed by Wuhan University in remote sensing the surface condition over the East China Sea in October 2000. The preliminary wind field estimated from the collected data is outlined and compared with the ship-recorded results. The range for wind direction sensing is up to 180 or 220 km, wind speed can be provided out to a range of 80 or 120 km. The mean difference of wind direction is 20° and wind speed is measured to within

0.6 m/s; the agreements are fairly good. The feasibility of the inversion algorithm and ocean state real-time sensing capability of OSMAR2000 are demonstrated [C6931]

"Estimation of radio refractivity structure using radar clutter"

Describes the estimation of low-altitude atmospheric refractivity from observations of radar sea clutter. Both surface and evaporation ducts are considered. The intended use of the technique is to provide near-real-time estimation of ducting effects for naval forces, which is important for radar performance prediction. For surface duct inversions, the authors use the Simulated Annealing/Genetic Algorithm (SAGA) general purpose inversion code. SAGA is configured to use an embedded parabolic equation electromagnetic propagation model, a four-parameter model for atmospheric refractivity, and a linear least-squares objective function. The mismatch between (a) the optimal replica field and the observed clutter and (b) the inferred refractivity profile and the range-dependent refractivity structure obtained by in situ measurements, is discussed. The inference of evaporation duct heights is simpler than the inference of surface duct parameters and has already been presented in the open literature. The material presented is an update on the performance of the algorithm based on at-sea testing [C6932]

"A quantitative comparison of soil moisture inversion algorithms"

This paper compares the performance of four bare surface radar soil moisture inversion algorithms in the presence of measurement errors. The particular errors considered include calibration errors, system thermal noise, local topography and vegetation cover [C6933]

"Low-cost, low-power nanosecond pulse radar for industrial applications with mm accuracy"

A low-cost, low-power radar for the near-range is proposed, which employs nanosecond pulses. The proposed pulse radar consists of state-the-art SiGe components for generation of the nanosecond pulse in the 5.8 GHz ISM-band. Developing the low-cost, low-power radar in an ISM-band results in an unrestricted measurement system worldwide. It is even possible to use the ISM-band radar outside any metal surroundings in a free environment. As the main target area of this low-cost, low-power radar is level measurement in the industrial field, galvanic isolation between measurement system and sensor is needed to avoid any restriction in measurement applications. A solution is presented for separation of radar and sensor. Experimental results shows good agreement with the theory. Experimental verification of the realised pulse radar under lab conditions shows that an accuracy of better 10 mm can be obtained over a distance of 10 m [C6934]

"Effectiveness of spatial-temporal collocated microwave scatterometric and vertical-horizontal polarized radiometric images in sea surface monitoring"

A concept for combining of data of scatterometric and dual polarization radiometer observations is presented. Microwave, combined active-passive method for detection and identification of sea surface anomalous formations (signatures) is described, originated due to separate changes of such parameters as: the wind speed, the sea state in the form of swell or long wave spectrum characteristics, air and water temperatures, characteristics of foam formations, etc. A block diagram of combined radar-radiometer detector-identifier is described, as well as the samples of sea surface radar-radiometer images are presented [C6935]

"The Northern Gulf of Mexico Littoral Initiative"

The Northern Gulf of Mexico Littoral Initiative (NGLI) is a multi-agency program established through a partnership between the Commander, Naval Meteorology and Oceanography Command (COMNAVMETOCCOM) and the Environmental Protection Agency's Gulf of Mexico Program Office. The goal of NGLI is to become a sustained comprehensive nowcasting/forecasting system for the coastal areas of Mississippi, Louisiana, and Alabama that will use model forecasts and observational data for military training and coastal resource management. The program integrates a reliable and timely meteorological and oceanographic modeling scheme, combining three-dimensional circulation, sediment transport, and atmosphere and wave models with in situ and remotely sensed observations via an extensive data distribution network that is available to a wide range of users in near-real time through an interactive website. The Naval Oceanographic Office, who manages the program for COMNAVMETOCCOM, has chosen the Mississippi Bight as an ideal test bed to economically examine new modeling and observational technologies before they are applied to littoral areas of military interest. NGLI directly addresses the Navy's requirement to project oceanographic information from deepwater environments shoreward into hostile littoral areas. Model nowcasts and forecasts are being applied to the ocean littoral environment by cascading information from large ocean basin models to shallow-water models. NGLI plans to support military training exercises performed by Special Boat Unit 22, stationed at Stennis Space Center, MS. Lessons learned within this "natural laboratory" also provide civil authorities with the means to consider the environmental

stresses (sediment transport modifications, increased pollution, etc.) caused by growth in hotel and casino developments, population, and industry. The NGLI modeling system will aid in ensuring the quality of shellfish harvests, one of the area's largest industries. NGLI utilizes a variety of oceanographic technologies for in situ observations. Measurements consist of both moored upward-looking and buoy downward-looking acoustic Doppler current profiler observations telemetered in near-real time; buoy meteorological observations; surface drifters; and survey-collected profiles of temperature, salinity, oxygen, current velocity, optical parameters, and sediment data. Remotely sensed observations include surface currents from Coastal Ocean Dynamics Applications Radar, Sea-viewing Wide Field-of-view Sensor, Geostationary Operational Environmental Satellite, and Advanced Very High Resolution Radiometer imagery, satellite altimetry, gravimetric geoid studies, and Global Positioning System technology to determine sea surface height. Information generated from observational data and model output is deposited into a large data distribution system, consisting of data archives, data exchange and networking systems, and web site maintenance. This infrastructure provides NGLI data access not only to the U.S. Navy, but also to the area's resource managers, conservationists, educational institutions, and the entire Gulf Coast community [C6936]

"A multi-agency solution for coastal surveys-SHOALS in the Pacific"

In late boreal summer 2000 and into early spring 2001 an ambitious multi-agency plan was put in motion to survey ten Pacific islands ranging from the Hawaiian Island group to Guam and the Commonwealth of the Northern Mariana Islands (CNMI). Encompassing a span of nearly 4000 miles, approximately 1100 square miles of shallow coastal ocean was mapped from 50 m deep to 50 m above the high water mark. The foundation for this project was an existing partnership between the US Navy and the US Army Corps of Engineers (USACE) that operates the Scanning Hydrographic Operational Airborne Lidar Survey (SHOALS) system through the Joint Airborne Lidar Bathymetry Technical Center of Expertise (JALBTCX). As the only operational lidar bathymetry system in the USA, and one of only four in the world, SHOALS' availability to rapidly and safely survey shallow water areas is at a premium. By including the requirements of the US Geological Survey (USGS) and the National Oceanic and Atmospheric Administration (NOAA) National Ocean Service (NOS), along with those of the Navy and USACE, it became possible for all agencies to benefit from a Navy-sponsored deployment of this highly specialized, but flexible technology. Expanding the project allowed each agency to contribute in its own specific area of expertise. This paper presents the data collected in Hawaii and demonstrates how multi-agency relationships can be optimized through a flexible technology, such as airborne lidar, to concurrently satisfy a wide variety of requirements. These include tactical charting, safety of navigation, coral reef mapping, environmental assessment, shoreline dynamics and coastal engineering [C6937]

"On the distribution of small-scale roughness at the edges of monomolecular surface films"

The authors have carried out wind-wave tank measurements of wave slopes, radar backscattering, and video image intensity, while the water surface was covered with small patches of surface-active material. Their results show that, at low wind speed, the slick patches consist of regions of different damping behavior caused by the freshly spread slick. By analyzing the radar Doppler shifts they could show that the distribution of bound and freely propagating waves along a slick patch strongly varies. Since the video camera is less sensitive to the observed small-scale features they support the use of such devices for automated slick detection [C6938]

"Prediction of chaotic time series based on wavelet neural network"

Wavelet neural network possesses the best function approximation ability, that is to say it has the ability to identify the model. Because the constricting model algorithm is different from common artificial neural network BP algorithm, it can effectively overcome intrinsic defect of common artificial neural network. Therefore the better prediction effect can be reached effectively. The paper gives a method of prediction model of chaotic time series based on wavelet neural network that enables prediction model to have not only wavelet good approximation property, but also neural network self-learning adaptive quality. The authors make use the method to predict sea clutter data [C6939]

"Is SAR capable of mapping small-scale spatial patterns of soil moisture?"

We assess the potential for measuring spatial patterns of soil moisture using SAR at spatial resolutions down to 15 m. Highly detailed ground data on soil moisture and dielectric constant were collected in the 10.5 ha Tarrawarra experimental catchment in south-eastern Australia. C-band SAR measurements by ERS-1, ERS-2 and AirSAR provided no useful information on the spatial moisture pattern. Empirical comparisons suggest that L and P-band AirSAR data contain useful information on the soil moisture pattern, but this could not be extracted using a semi-empirical inversion algorithm. The spatial average moisture was successfully obtained from the L-band AirSAR data [C6940]

"A combined speckle noise reduction and, compression of SAR images using a multiwavelet based method to improve codec performance"

SAR images are corrupted by multiplicative noise (speckle) which limits the performance of the classical coder/decoder (codec) in the spatial domain. Our objective is to give an evaluation of the efficiency of a multiwavelet transform coding algorithm. We use the additional degree of freedom offered by multiwavelets to fine tune the number of vanishing moments and the approximation order of their basis functions. Once the multiwavelet transform is performed, we apply an optimal bit allocation scheme on the subbands data using a set of vector quantizers. The quantization of the high frequencies multiwavelets coefficients may be thought of as a hard thresholding algorithm. A measure of the equivalent number of looks is performed in the reconstructed SAR image in order to evaluate the impact of the codec in the noise reduction process. We compare our method with classical algorithm (baseline scalar wavelet transform followed by an optimal scalar quantization). The codec achieves comparable SNR, but performs surprising speckle noise reduction. Some results are presented with ERS-PRI images of Cameroon which can be compressed at 20: 1 while still remaining of sufficient quality for visual interpretation, segmentation and land use monitoring [C6941]

"Despeckle-based SAR image compression"

SAR images suffer from speckle noise that degrades image quality. Speckle removal is to be applied when signatures such as edges and fields have to be extracted from the image; speckle removal is also needed for image compression as such noise increases image entropy. Nevertheless, most lossy compression schemes act as low pass filters that do not fit multiplicative noise reduction. In order to build a compression scheme that takes into consideration statistics of SAR images, a well known reflectivity estimator is integrated into an image compression strategy, so that image compression artifacts may be viewed as an adaptive despeckled filter instead of a simple low-pass filter. The compression method has been developed with the most efficient tools dedicated for image compression, that suit the JPEG 2000 norm, such as multi-resolution analysis achieved by wavelet transform, optimal scalar quantization adjusted with a distortion-rate constraint and an arithmetic encoder. It yields a compression algorithm that acts in a similar way to the Lee filter. A theoretical analysis is also applied on the multi-wavelet transform in order to take into consideration scene correlation in the speckle removal filter. Some results are presented on ERS PRI images compressed at a factor of $\eta = 20: 1$ [C6942]

"A new approach based on network theory to locate phase unwrapping unreliable results"

Two-dimensional phase unwrapping (PU) is always affected by errors. In this paper we propose and implement a new method that locates the large and small-scale PU errors. In addition, by using ground control points, we eliminate the large-scale errors. The method is tested on the real and simulated SAR interferometric data. Results of the tests indicate a high efficiency of the proposed method [C6943]

"System and estimation problems for multibaseline InSAR imaging of multiple layovered reflectors"

In the recent years there has been growing interest in exploiting the advanced multibaseline operation of synthetic aperture radar interferometry (InSAR) to solve layover effects that can degrade conventional InSAR imagery. In this work we consider detailed modelling of this problem including speckle noise for extended targets, application of several non-parametric and parametric spatial spectral estimation methods to multibaseline layover solution, and system trade-offs analysis. Corresponding statistical accuracy of estimated heights is investigated by simulation [C6944]

"Observations over Australia of plumes from distant biomass-burning sources using remote sensing and airborne techniques"

Although the free troposphere in the Southern Hemisphere has often been considered to contain very low concentrations of aerosols, significant enhancements in the aerosol loading have been reported on several occasions during the last three decades. This paper reports on the results of two recent experiments in which significant increases in the loading of aerosols and trace gases were observed over southern Australia. The Mildura Aerosol Tropospheric Experiment (MATE 98) and an experiment conducted during SAFARI 2000 used a ground-based lidar and a combination of instruments mounted on balloons and aircraft to measure increased concentrations of aerosols and trace gases. Back-trajectory analyses show that these plumes did not originate from the Australian continent, but are likely to have come from southern Africa or South America [C6945]

"Spaceborne lidar calibration from cirrus and molecular backscatter returns"

In order to make optimal quantitative use of multiwavelength spaceborne lidar data it is essential that the lidar be

well calibrated. Due to system gain/efficiency changes that can be expected to occur during the course of a shuttle or satellite mission, it is essential to employ a calibration approach that can be implemented on-orbit, preferably repeatable at least a few times per orbit. For wavelengths less than about 550 nm, in situ calibration can be accomplished via normalization to high altitude, nearly molecular scattering regions. However, for longer wavelengths beyond about 800 nm, particularly the popular Nd:YAG fundamental wavelength at 1064 nm, the Rayleigh normalization approach becomes questionable due to both an inherently weaker signal and a stronger, variable and somewhat unknown aerosol scattering contribution. For lidars operating at both longer and shorter wavelengths, a viable approach is to retrieve the longer wavelength calibrations ratioed to the shorter wavelength calibrations via comparisons of spectral backscatter from known/quantifiable scatterers. Cirrus clouds are good for this purpose because they occur at high altitudes with significant frequency and provide strong, nearly spectrally flat backscatter. This paper presents the cirrus spectral backscatter ratio calibration approach, including results obtained from case studies of lidar data collected during the LITE shuttle mission. Attention is focused on developing a simple, autonomous approach applicable to satellite lidar missions such as PICASO-CENA [C6946]

"Calibration of forest chemistry for hyperspectral analysis"

A primary advantage of hyperspectral sensors is the ability to provide measurements of canopy chemistry. Canopy chemistry can be used to estimate new and old foliage, detect damage, identify trees under stress, and map chemical distributions in the forests. We have begun a new EO-1 project, Evaluation and Validation of EO-1 for Sustainable Development of forests (EVEOSD). NASA's EO-1 satellite was successfully launched on November 21, 2000. In preparation for airborne and spaceborne data collection and calibration, we collected in September 2000 foliar canopy and ground cover chemistry samples from 54 plots distributed across the Greater Victoria Watershed (GVWD) test site. Treetop samples were collected from helicopters. Differential GPS was used to provide sample positioning to within 1 m. The foliar samples were divided into new and old foliage. Organic and inorganic chemistry analyses were done. Spectral calibration samples were collected over ground targets, over stacks of foliar samples, and over ground vegetation. Landsat-7 and Radarsat data were collected at the same time. The chemistry samples were placed into a database and integrated with GIS files of topography and forest cover. We obtained 1 m aerial orthophotography that allowed us to investigate the spectral components making up the Landsat-7 and EO-1 pixels [C6947]

"Lidar aerosol ratio: measurements and models"

Lidar offers an effective means for monitoring and characterizing global aerosol properties. While relative backscatter maps provided by spaceborne lidar measurements such as those obtained with LITE are valuable for delineating global aerosol structural features, obtaining more quantitative information needed for assessing aerosol radiative effects, namely, retrieval of aerosol extinction and backscatter, requires more information/constraints than what is provided by simple, single-direction lidar soundings. The aerosol extinction-to-backscatter ratio, or lidar aerosol ratio, S_a , is a key parameter which, if known, permits retrieval of aerosol backscatter and extinction profiles from the lidar measurements. This paper assesses S_a determinations obtained from a number of lidar, nephelometer and solar radiometer/sky radiance observations. Results of modeling studies to relate different aerosol models to various ranges of S_a values are also considered. The goal is to establish an S_a climatology that can be used to aid aerosol retrievals from satellite lidar observations such as those to be provided by GLAS and PICASO-CENA [C6948]

"First retrievals of the physical thickness and optical depth of dense clouds with off-beam/multiple-scattering lidar"

Cloud lidar data from NASA's Lidar-Inspace Technology Experiment (LITE) mission and from LANL's new Wide-Angle Imaging Lidar (WAIL) prototype show that the multiple-scattering theory of off-beam lidar readily explains the observations, as long as internal stratification of cloud density is accounted for. At the same time, predictions for spatial and temporal statistics of the signals are used to infer the optical depth and the physical thickness of the clouds being probed [C6949]

"Surface current observations by HF radar during EEGLE 2000"

HF radar has become an important tool for mapping surface currents in the coastal ocean. However, its use over fresh water has been limited due to much higher propagation loss and smaller wave heights on fresh water lakes. During the Episodic Events Great Lakes Experiment (EEGLE) two multifrequency coastal radars (MCRs), operating between 4.8 MHz and 21.8 MHz, were installed on the southeast shore of the lake, together with an air-sea measurement buoy. Data from the February-April 2000 observations demonstrate HF radar performance characteristics over fresh water as well as characteristics of the surface flow in the lake during periods of

moderate to high winds and waves. In early April an episodic event occurred in which strong northerly winds blew down Lake Michigan driving currents down the western shore of the lake past Racine, Wisconsin and Chicago, Illinois and around the southern lake shore to the southeastern shore of the lake. Sediments are resuspended during such an event, putting a variety of pollutants in the water column. These suspended sediments are clearly shown in visible light images from the NOAA-14 satellite. HF radar and buoy measurements of an episodic resuspension event are presented. They show a southward surface current flow at the beginning of the event and then a reversal of the near-shore current as the event progresses and the aforementioned currents move around the bottom of Lake Michigan and reach the St. Joseph, Michigan area. These observations show the interplay of large scale currents from the south and local wind driven currents

[C6950]

"RADARSAT-1 image quality/five years of achievement"

RADARSAT-1, the first Canadian SAR remote sensing satellite, was launched on November 4, 1995. After commissioning, it was put into routine operations on April 1, 1996. In September 1997, RADARSAT-1 underwent a major configuration change to accommodate the Antarctic Mapping Mission (AMM-a joint mission by Canada and USA aimed at completing high-resolution mapping of Antarctica) for a period of about five weeks. Significant effort continues to be expended in the provision of high quality products to users generated by the Canadian Data Processing Facility (CDPF). The image quality measurement results indicate that the RADARSAT-1 system is meeting and exceeding its performance specification and that image quality is maintained. This paper will describe the overall process of data acquisition, data analysis and re calibration for image quality maintenance

[C6951]

"A geosynchronous synthetic aperture radar; for tectonic mapping, disaster management and measurements of vegetation and soil moisture"

A geosynchronous synthetic aperture radar (SAR) with an orbit inclination of 50-65° can provide daily coverage of all of North and South America. Longitudinally, the width of the mapped area would be on the order of $\pm 50^\circ$ at the Equator, somewhat more at the most northern/southern latitudes. Within the area mapped, very good temporal coverage can be obtained-up to several mappings during the 12 hours per day where the satellite is in the "right" hemisphere. This would be a key capability in relation to disaster management, tectonic mapping and modeling, vegetation and soil moisture mapping, and for operational and semi-operational requirements. A constellation of geosynchronous satellites could provide global coverage [C6952]

"Radarsat-1 Hurricane Watch"

Radarsat-1 ScanSAR wide mode images of Atlantic basin hurricanes have been acquired over two hurricane seasons through the Canadian Space Agency's Disaster Watch program. These images provide a high-resolution view of these intense storms and new insights into their morphology. A new result is recognition of the widespread presence of boundary layer rolls in these storms. In 2001, "Hurricane Watch" will focus on obtaining contemporaneous aircraft-based turbulence measurements at Radarsat-1 pass times [C6953]

"Geological applications of RADARSAT-1: a review"

Recent results have shown that RADARSAT-1 images have provided geologists with useful information. for mapping structure, geomorphology and rock units. This paper discusses the role of multi-incidence RADARSAT and data fusion techniques for geological mapping. The results of several case studies, the guidelines for the selection-of the various RADARSAT-1 incidence angles for geological applications, and the use of stereo RADARSAT and visualization techniques for geohazard characterization, are presented [C6954]

"A geosynchronous lidar system for atmospheric winds and moisture measurements"

An observing system comprised of two lidars in geosynchronous orbit would enable the synoptic and meso-scale measurement of atmospheric winds and moisture, both of which are key first-order variables of the Earth's weather equation. Simultaneous measurement of these parameters at fast revisit rates promises large advancements in our weather prediction skills. Such capabilities would be unprecedented and (a) yield greatly improved and finer resolution initial conditions for models, (b) make existing costly and cumbersome measurement approaches obsolete, and (c) obviate the use of numerical techniques needed to correct data obtained using present observing systems. Additionally, simultaneous synoptic wind and moisture observations would lead to improvements in model parameterizations, and in our knowledge of small-scale weather processes. Technology and science data product assessments are ongoing [C6955]

"Cross-calibration experiment of airborne L-band polarimetric SAR"

Cross-calibration experiment of airborne L-band SAR systems, the JPL's AIRSAR and the NASDA/CRL's PI-SAR, was conducted on the Tottori sand dune. This experiment forms a part of PacificRim-2 campaign from July to October in 2000. Both AIRSAR and PI-SAR acquired the data over the test site within two hours on October 4, 2000. The track altitudes of airplanes were about 8000 m. Four rectangle trihedral corner reflectors with 80 cm of leg-length were deployed in order to derive absolute calibration coefficients. We also deployed four dihedral corner reflectors with different rotation angles for polarimetric calibration purpose. This report describes the results of calibration experiment for JPL's AIRSAR and NASDA/CRL's PI-SAR conducted on Tottori sand dune. Since the AIRSAR data has not been available yet, this report concentrates on the calibration of our PI-SAR system. The distortion matrices for both transmitting and receiving system can be calculated by using the data containing one trihedral reflector and two dihedral reflectors with different rotation angles. Gain balance between HH and VV was not good in this time, because the PI-SAR had some hardware degradation. The absolute calibration coefficient for HH channel has the almost same value as the previous calibration experiment in 1999. However, we found that the VV channel had been degraded more than 3 dB. The improvements of gain balance and cross-talk between H and V channels were confirmed after the calibration using the extracted distortion matrices [C6956]

"A new method for a posteriori polarimetric SAR calibration"

Fully polarimetric SAR data analysis has found wide application for terrain classification, land-use, soil moisture and ground cover classification. Critical to all analyses and applications is accurate calibration of the relative amplitudes of and phases between the various polarimetric channels. Here we develop a "minimalist" approach to polarimetric calibration, wherein only the weakest of constraints, reciprocity, is initially imposed upon the data. Additional parameters are self-consistently estimated from the data. In this manner channel imbalances and cross-talk are estimated without unduly biasing the resulting polarimetric information [C6957]

"The future of instrument technology for space-based remote sensing for NASA's Earth Science Enterprise"

The vision of the Earth Science Enterprise (ESE) of the National Aeronautics and Space Administration (NASA) established a variety of science challenges for the next 25 years, relating to predictions of weather, climate, and foreseeable changes in the Earth's environment. In this paper, we discuss the attendant needs for space-based remote sensing technologies. In addition, we suggest some strategies for deploying the necessary assets [C6958]

"Ship-sea contrast optimization when using polarimetric SARs"

The polarization information was investigated in Touzi (2000) for ship detection using calibrated polarimetric Convair-580 SAR data that were collected within the incidence angle range of 45° to 70°. It was shown that at operational satellite SAR incidence angles (lower than 60°), there is a significant improvement of ship-sea contrast when the full polarimetric information is used instead of the information provided by the (scalar) one channel polarization (HH, VV, or HV). In this paper, the investigation is extended to lower incidence angles, and the robustness of the polarimetric discriminators used for ship enhancement, is assessed at various wind conditions (7, 14 and 20 knots). Polarization channel phase information is also investigated. It is shown that the information contained in the HH-VV channel phase difference, looks to be very promising for ship enhancement, mainly when a dual-polarized SAR is used [C6959]

"Mapping seasonal vegetation changes with multi-temporal radar segmentation"

The wet/dry cycle particular to the Northern Australian climate creates a distinctively harsh environment for the vegetation species present. At a particular location a species adapted to immersion in water may flourish whilst the site is inundated but as the water dries up will be replaced by a species capable of surviving in the drier conditions. In this way particular species continually replace one another as the cycle progresses. For this highly complex environment single date image classification does not do justice to the constantly changing patchwork of vegetation as the drying cycle progresses. As moisture is a major determinant of the dielectric properties of most non-metallic materials, and vegetation in particular, any change with time may be mapped. A multi temporal approach to the situation is well suited to highlight not only the changes in vegetation community between seasons, but also that occurring between years. A region of the South Alligator River floodplain, within Kakadu National Park was surveyed to ascertain if these changes could be accurately mapped. Analysis of three multi temporal radar images obtained by Radarsat during the period of 1998-1999 were co-registered and subjected to GMRFM segmentation. The results of this segmentation were then used in a statistical clustering algorithm in order to regroup spatially separate segments into a smaller number of classes. Subsequent air photo

interpretation and ground truth information have shown that the technique is invaluable in determining the timing and location of ecological classes in a highly variable climate [C6960]

"RADARSAT-2 calibration: proposed targets and techniques"

RADARSAT-2 is an advanced synthetic aperture radar satellite scheduled for launch in 2003. The satellite will be equipped with an active phased array antenna which will be used to provide a wide variety of beams and modes, including all the beams and modes of RADARSAT-1 and additional Ultra-fine resolution, dual and quad-polarimetric modes. The large number and variety of modes presents a major calibration challenge and, because the satellite is intended for operational use, efficient means for achieving and maintaining this calibration are essential. This paper identifies the three principal types of target which are planned for use in achieving radiometric, polarimetric, geo-location, and other types of calibration for RADARSAT-2, and describes how the data will be analyzed to generate the required calibration information [C6961]

"Preparing for operational use of RADARSAT-2 data at the Canadian Ice Service"

As one of the world's largest operational users of RADARSAT-1 data, the Canadian Ice Service (CIS) is looking forward to the future launch of RADARSAT-2. The RADARSAT-2 mission, including both the Space and Ground segments, promises several technical enhancements beyond RADARSAT-1, which should be beneficial to the CIS. Towards that end and to prepare for operational use of the data, the CIS has been working closely with the Canadian Space Agency (CSA) and MacDonald Detwiler (MDA), particularly on the Ground Segment, to ensure that the RADARSAT-2 system will best meet our operational needs. Additionally, the CIS is investigating the operational utility to be gained from some of the advanced capabilities of the SAR sensor, specifically the selective single-, dual-, and quad-polarization modes. In this paper we briefly examine, from an operational perspective, various elements and enhancements of the RADARSAT-2 Space and Ground segments, and issues concerning data usage to be addressed in order to maximize the operational utility of RADARSAT-2 data at the CIS [C6962]

"Calibration of an across track interferometric P-band SAR"

The techniques for interferometric calibration of the GeoSAR P-band system are discussed. These techniques are demonstrated using preliminary GeoSAR data [C6963]

"The RADARSAT-2/3 topographic mission"

The RADARSAT-2 Synthetic Aperture Radar (SAR) satellite currently under development is jointly funded by the Canadian government and MacDonald Detwiler. RADARSAT-2 will further Canada's world-leading position in the world of synthetic aperture radar Earth observation, and provide an enormous opportunity for growth in technical expertise and environmental, agricultural, and commercial applications. Plans are now in preparation for the development of a RADARSAT-3 satellite to be operated interferometrically in tandem with RADARSAT-2 to provide very high precision global topographical data. This paper will describe the mission concept, explain the key characteristics of the two satellites, and discuss some of the design and operational issues which have been studied. The system concept potentially includes both Bistatic and "Pursuit Monostatic" operation of the two radars, and both options will be described [C6964]

"Applications potential of planned C-band SAR satellites: leading to RADARSAT-2"

To date, satellite SAR data for civilian purposes, have been routinely available from single channel, i.e., single frequency and single polarization, radar systems. In the near future, we expect satellite SAR systems with enhanced capabilities in terms of polarization, frequency, spatial resolution, spatial coverage and temporal resolution. In this paper, we discuss the increase in applications potential resulting from the progress in SAR technology, in particular in C-band systems. The application fields discussed include agriculture, forestry, geology, hydrology, oceans, and sea ice. Most applications are anticipated to benefit from the upcoming availability of cross-polarized C-band data. Likewise the introduction of fully polarimetric C-band satellite SAR systems is expected to improve the overall application potential [C6965]

"Evolution of Canadian Earth observation from RADARSAT-1 to RADARSAT-2"

Earth observation is identified as a major component of the Canadian Space Program. Canada introduced itself into space Earth observation market with the launch of RADARSAT-1 operations five years ago. Since then RADARSAT-1 has been providing data for operational needs and commercial services worldwide. The Canadian government through the Canadian Space Agency is committed to synthetic aperture radar (SAR) data continuity and technology improvement for better data services. The government also encourages an increased role of the

private sector in space Earth observation, comparable to space telecommunications. RADARSAT-2 is the product of this new government approach. RADARSAT-2 will maintain all the existing RADARSAT-1 SAR imaging capabilities and will in addition provide multi-polarization polarimetry, very high resolution, and left- and right-looking modes to make it the remote sensing data source of choice [C6966]

"Radarsat-1 for sea ice monitoring in Canada-an operational success story"

Monitoring of sea ice in Canada's Arctic was one of the prime motivations for the development of an all-weather, active remote sensing satellite by the Canadian government. The Canadian Ice Service (CIS) has been an active participant in the Radarsat-1 program since its inception, and throughout the research, development, and operational phases. The CIS now critically relies on Radarsat-1 to provide operational ice reconnaissance over a seasonal ice cover of approximately 2 million km² [C6967]

"New modes and techniques of the RADARSAT-2 SAR"

The RADARSAT-2 system currently under development is required to generate a much wider range of data products than any other preceding civilian satellite SAR. In addition to the single polarization Standard, Fine Resolution, Wide Swath, ScanSAR and Extended Coverage Beams of RADARSAT-1, the new mission requirements include Quad-Polarization and UltraFine Resolution modes, and selectable single and dual-polarization options for the heritage beams. The radar is also required to operate in experimental modes to provide data for detection of moving objects. To support this mission, a significantly more technologically advanced instrument has been designed, with a number of extra degrees of freedom in its operation. This paper describes some key features in the design of the instrument, and explains how they will be used in generating the new types of data [C6968]

"Mapping recent lava flows with Radarsat-1 imagery"

The sensitivity of radar imagers towards surface roughness and moisture can be used for mapping rock, soil and vegetation. High-resolution Radarsat-1 data were used to map successive lava flows of the Hekla volcano. The volcano erupted in early 2000. It was monitored throughout the eruptive activity using Radarsat-1 Fine beam images. The Radarsat-1 images were compared with those retrieved from the archive, which had been acquired immediately before the event in the course of Radarsat-1 Background Mission and Disaster Watch Program. Radarsat-1 images were interpreted based on the radar tone and texture as a function of the state of lava solidification, and it was possible to distinguish between lava flows of different stages of the eruptive activity. Using the same tonal and textural the interpretations, an attempt was made to trace the past history of the Hekla volcano. Successive lava flows were delineated and are shown on the image map. The study demonstrates the effectiveness of Radarsat-1 fine resolution imagery for lithological mapping and the usefulness of Radarsat-1 data archives that are being built as a result of the satellite's various baseline acquisitions [C6969]

"Development of polarization selective corner reflectors and its experiment for calibration of airborne polarimetric synthetic aperture radar"

As a part of polarimetric calibration efforts of CRL/NASDA airborne synthetic aperture radar system (Pi-SAR), we have developed corner reflectors to reflect a specific polarization channel. They include a 45° rotated dihedral, a 22.5° rotated dihedral, and a dihedral made of thin wires placed in the direction of polarization to be reflected, horizontal (H) or vertical (V). The wire-aligned dihedral we proposed has a thin dielectric frame to hold the wires, requiring no base material. In October 2000 we made a polarimetric calibration experiment of the X-band synthetic aperture radar, a part of the Pi-SAR. Those polarization selective dihedrals, together with conventional trihedrals, were deployed in the experiment. Preliminary results of the image data analysis showed that they were of practical use for polarimetric calibration, while there were some errors in reflected power probably due to their structure and their misalignment. It also showed that the corner reflectors were useful to determine phase calibration coefficients that is phase imbalances between polarimetric channels in the radar hardware [C6970]

"Radar image studies of scattering from random rough surfaces"

In this paper electromagnetic scattering from deterministic rough surfaces is described through analysis of radar images. Backscatter results are considered for 1-D random rough surfaces which satisfy an impedance boundary condition (IBC). Radar images of single realizations of random surfaces are formed through back-projection tomography. Detailed investigations of the images are also provided to clarify major and secondary scattering events, angular dependencies, and polarization effects, and a ray tracing analysis is performed to predict multiple scattering images. For an ocean-like surface, effects of surface length scale components are discussed [C6971]

"Application of remote sensing data for oil spill monitoring in the Guanabara Bay, Rio de Janeiro, Brazil"

This paper describes the application of remote sensing data for oil spill monitoring in the Guanabara Bay, Rio de Janeiro, Brazil. During the emergency, Landsat-5/TM (Thematic Mapper) and Radarsat-1 data were acquired to monitor the location of the spill and its movement. Image classification procedures have been utilized to highlight oil-covered areas on the water surface. Ambiguities in the oil detection were resolved with the aid of ancillary information in a GIS (geographic information system) environment. The results obtained helped PETROBRAS to optimize the emergency response procedures and subsequent cleaning efforts [C6972]

"Model-based estimation of forest canopy parameters using polarimetric and interferometric SAR"

Synthetic aperture radar (SAR), interferometric SAR (INSAR), and polarimetric INSAR (POLINSAR) have been shown to be sensitive to various biophysical forest canopy parameters. The two general classes of models employed in parameter extraction are random-media and structure-based. Since the quality of canopy parameter retrieval depends on the attributes of the forward-scattering models that are inverted, we review the general characteristics of each type of model. The random-media models invoke simplifying assumptions, such as independent scattering statistics, to yield analytical expressions. Some of the central assumptions, however, do not hold as resolution increases. Structure-based models can be used in these high-resolution scenarios. We are developing a new structure-based wideband SAR/INSAR/POLINSAR model to explore the effects of increasing resolution on POLINSAR observables. A simple example of a structure-based SAR simulator is presented [C6973]

"Near-field 2-D and 3-D radar imaging using a chirp scaling algorithm"

A new chirp scaling algorithm (CSA) has been formulated and tested. This method yields more accurate results when applied to configurations with high coherent integration angles and high bandwidth-to-center-frequency ratios than the original CSA. Moreover, it has been extended to the three-dimensional case when a planar synthetic aperture is employed. The formulation of the new method is justified in this work. In addition, an algorithm version adapted to stepped-frequency radars has been developed. Finally, this technique is implemented and successfully tested with numerical simulations and real data obtained with a ground-based system [C6974]

"Continuous strife for better coverage and more details in ocean surface winds measurements-from Midori and ADEOS-2 to GCOM"

The series of joint U.S.-Japan spaceborne scatterometer missions to provide continuous measurements of ocean wind vectors is reviewed. Examples of the scientific impact of the continuous effort in improving spatial resolution and coverage are provided. The plan for future missions is reviewed [C6975]

"Visible and microwave signatures of river plumes in microtidal seas"

We give examples of the use of satellite and hyperspectral data to retrieve characteristics of solid suspended matter in the Rhone and Ebro river plumes, on particular concerning stratification. We also show that dynamical features of the Rhone river plume (its frontal boundaries) can be observed on ERS radar images. Preliminary modeling results are presented [C6976]

"Current structure off the North Spanish coast observed by HF radar"

The objective of the European Radar Ocean Sensing (EuroROSE) project is to develop a radar based ocean monitoring system in support of safe navigation in port approach areas and otherwise densely operated sea areas. Radar measured data are assimilated into a fine gridded numerical model with the aim of predicting, for a few hours, currents and waves. A demonstration of this system was carried out off the North Spanish coast from October to November 2000. The area selected covers the approach to the harbour of Gijon. Two HF radars WERA (Wellen Radar) of the University of Hamburg were deployed. WERA, operated at 27.65 MHz, measures surface currents within an area of about 40 by 40 km with a spatial resolution of about 1 km and with a temporal sampling of 20 min. The Spanish measurement network consists of different types of wave bouys. Currents have not been recorded in the area under consideration. For the first time, the maps of surface current, acquired during the EuroROSE Gijon experiment, show the high spatial and temporal variability off the North Spanish coast. This paper presents first experimental results with emphasis on the dynamics of the coastal current. Depending on the wind situation, up to two coastal jets with a chain of eddies in between has been observed [C6977]

"Accuracy of rain rate retrieval from dual-frequency precipitation radar data"

This paper outlines the principles and issues of dual-frequency algorithms to estimate the raindrop size distribution parameters from a space-borne radar system that is planned to be flown on the Global Precipitation Mission's "core" spacecraft [C6978]

"Variability in the evolution of the Chesapeake Bay outflow plume front as observed with a real aperture radar"

In this paper, time sequences of radar imagery are presented that illustrate the spatial and temporal evolution of the Chesapeake Bay outflow plume front. These images were collected in May 1997 and May 1999 during parts 2 and 5 of the Chesapeake Bay Outflow Plume Experiment (COPE2 and COPE5, respectively). The COPE5 data set features an image sequence that spans nearly ten hours during the early-flood to maximum-ebb portion of the semidiurnal tidal cycle. The frontal evolution shown in this continuous image sequence shows a striking resemblance to that implied by a "composite" sequence from COPE2, formed by combining data from two separate flights flown on two consecutive days, indicating a high degree of reproducibility in the frontal evolution [C6979]

"Polarimetric SAR processing using the polar decomposition of the scattering matrix"

The concept of scattering is one of the mechanisms that polarimetry seeks to express through data. A multiplicative decomposition of the scattering matrix is proposed in order to try to separate different kind of scattering and the applicability to polarimetric SAR images is investigated [C6980]

"INSAR activities in central Asia using mobile SAR receiving station"

From March 7th 1999 till July 2nd 1999 an INSAR campaign of GFZ/DLR with a mobile receiving station was established at Kitab in Uzbekistan. The mobile ground station contains three subsystems: receiving system, SAR processing system and INSAR processing system. Everyday more than 10 scenes of the received SAR raw data were processed to single look complex image data, then the corresponding interferograms from tandem pair as well as differential interferograms can be produced. Besides receiving and archiving the ERS-1/2 radar data, the task of the campaign is to test a simultaneous SAR- and INSAR-Processing of the ERS1/2 data in field. The aim of the processing in field is to demonstrate and enable near-real-time SAR-Interferometry. In this paper some preliminary results of the campaign in the selected test area of Fergana-Valley and Urumqi are presented [C6981]

"Interferometric calibration for DEM enhancing and system characterization in single pass SAR interferometry"

In this paper the comparison between different methods to calibrate a digital elevation map (DEM) generated from airborne differential SAR interferometry will be presented. The traditional methods applied phase ramp corrections along the swath derived from the errors in some ground control points (GCP) to improve the DEM. A more advanced technique is proposed based on the sensitivity equations, which are derived by differentiating the basic location equations with respect to the different parameters of the error model. The behavior of the different techniques have been tested with both synthetic and real interferometric SAR data [C6982]

"Segmentation of polarimetric SAR images"

In this paper, we proposed a new polarimetric SAR segmentation scheme based on the effect of speckle filtering for initial segmentation. We also incorporate a technique to preserve the scattering mechanism for pixels in each class [C6983]

"Segmentation and labeling of polarimetric SAR data: can wavelets help?"

In this paper we report about a novel approach to segmentation and thematic labeling of SAR polarimetric data. A pre-processing phase based on a wavelet frame that works as a differential operator generates piece-wise smooth approximations of the covariance matrix power term images. This step matches the signal characteristics with the requirements of well proven and computationally robust clustering algorithms of the Bayesian MAP, hard or soft labeling, and contextual type. Segments defined in this first phase are then used to estimate polarimetric quantities such as the Cloude's and Pottier's target decomposition parameters. The advantage over methods that use local statistics in a moving window is that the variance of the estimators decreases with the segment size, good accuracy can be obtained without sacrificing spatial resolution, and errors due to the signal discontinuities are avoided. The passage is then made from pixel based clustering to segment wise thematic classification. To

the purpose reference feature vectors based on ground truth are needed, and segments are reassigned to the thematic labels. The per-segment feature vectors, including averages of polarimetric, radiometric quantities, or texture measures, can also be exploited to derive biophysical parameters and qualify additionally the classification categories. The proposed approach seems to be appealing because it can tackle under a unified framework resting on solid mathematical foundations-such as Bayesian inference and wavelet theory-different data sources (microwave and optical) and different thematic contexts [C6984]

"Modelling of interferometric phase for forested areas"

We present a coherent model to study radar backscattering by forested areas. This full wave model is based on complex summation of fields radiated by all forest contributors (leaves, branches, trunks, soil) at the observer locations. This fully coherent model uses outputs of a coupled incoherent one, which alleviates the computational effort. The models are described and the Fontainebleau forest briefly presented. We display the center phase height derived from interferometric complex coherence simulations using ground truth descriptions. The influence of parameters like frequency and polarisation is investigated [C6985]

"Interferometric Cartwheel payload: development status and current issues"

The CNES interferometric cartwheel (ICW) system is based on a microsatellite constellation placed close enough to a conventional SAR radar to take opportunity from its Earth surface illumination. The microsatellite relative positions in time are such that at any moment, a vertical or an horizontal baseline may be constituted from a selection among the satellites for interferometric purposes. Due to the simultaneous acquisition of radar echoes on the various microsatellites, the expected performances are optimal with regard to time decorrelation effects. The microsatellite context will also allow for an overall cost optimization, these two points justifying the concept potential interest. A first application is expected to be launched by 2005, as a companion mission to the ASAR C-band synthetic aperture radar onboard the ESA ENVISAT satellite. This paper is focused on the microsatellite payload, which consists in a passive receiver, decomposed in: (i) a reflector based antenna sub-system, (ii) a RF analog receiver, (iii) a digital sub-system performing signal digitization, pre-processing, compression, and storing, (iv) a telemetry module, (v) a GPS receiver. The current interest for the ICW concept, and the existence of various possible missions in cooperation with SAR satellites, operating in L, C, and possibly X band has led to a search for genericity in the payload design, allowing it to evolve easily from a system concept to another. Special emphasis is given here on this genericity issue, and on Alcatel's direct heritage for the payload development [C6986]

"Quantitative intercomparison of polarimetric ground radar and TRMM PR observations"

The Tropical Rainfall Measuring Mission (TRMM) Precipitation Radar (PR) is a spaceborne radar operating in a nearly circular orbit at 350 km altitude with 35 degrees inclination and period of about 91.5 minutes. Simultaneous comparisons of radar observations were made between the National Center for Atmospheric Research (NCAR) S-POL radar and TRMM PR during the TEXas and FLorida UNderflights (TEFLUN-B) campaign that took place near Melbourne, FL in 1998, and the Large Biosphere-Atmosphere experiment in Amazonia (LBA) near Ji-Parana, Brazil in 1999. Though direct intercomparison between space and ground radar observations is, in principle, straight forward, differences in viewing aspects between space and Earth point observations, propagation frequencies, resolution volume size and time synchronization mismatch between instrument measurements can contribute, in a significant way, to intercomparison errors and should be taken into account. Vertical profile of polarimetric radar variables, namely, reflectivity (Z_h), differential reflectivity (Z_{dr}), specific differential phase (K_{dp}), cross-correlation coefficient (ρ_{co}) and linear depolarization ratio (LDR) are used to describe the precipitation characteristics through the TRMM PR beam. These observations are, in turn, used to determine the type of hydrometeor along the PR beam using a fuzzy-logic technique [C6987]

"InSAR phase unwrapping: a Bayesian approach"

The paper proposes a Bayesian approach to absolute phase (not simply modulo- 2π) estimation in interferometric aperture radar (InSAR). The observation density is 2π -periodic and accounts for the interferometric pair decorrelation and the system noise; the a priori probability of the absolute phase is modeled by a compound Gauss Markov random field (CGMRF). To compute the absolute phase estimate we propose an iterative scheme aiming at the computation of the maximum a posteriori probability (MAP) estimate. Each iteration embodies a discrete optimization step (Z-step), implemented by network programming techniques, and an iterative conditional modes (ICM) step (pi-step). According to the terms Z-step and pi-step, we term our algorithm ZpiM, where the letter M stands for maximization. Experimental results, comparing the proposed algorithm with classical approaches, illustrate the effectiveness of the ZpiM algorithm [C6988]

"Co-registration-geometrical analysis and verification for SAR interferometry under SRTM data conditions"

This paper describes a method that helps to guarantee and verify the accuracy of the co-registration module of an interferometric system. As an example, SRTM mission conditions and data are used. Geometrical predictions are derived for azimuth and range. Finally, the verification approach is shown by comparing theoretical expectations for range co-registration parameters with actual measurements from the data. Potential further applications are Radarsat repeat pass interferometry and may arise with the ENVISAT/Cartwheel configuration [C6989]

"Technologies for the next generation of spaceborne precipitation radars"

The precipitation radar (PR) aboard the Tropical Rainfall Measuring Mission (TRMM) has demonstrated the feasibility of measuring rainfall from space. A concept for the next step, the Second Generation Precipitation Radar (PR-2), has been developed. The PR-2 will yield improved capabilities and substantially reduced system mass compared to the TRMM PR. However, implementation of the PR-2 concept depends upon the development of several technologies including membrane antennas with inflatable structure, Ka-band phased arrays and real time digital pulse compression. Development is currently underway in these areas. This paper surveys the technologies for the PR-2 and describes developments in each aforementioned area [C6990]

"The 94-GHz cloud profiling radar for the CloudSat mission"

The CloudSat Mission is a new international satellite mission to acquire a global data set of vertical atmospheric cloud structure and its variability. Such data set is expected to provide crucial input to the studies of cloud physics, radiation budget, water distribution in the atmosphere, and to the numerical weather prediction models. The key science instrument aboard the CloudSat satellite is the Cloud Profiling Radar (CPR). CPR is a 94-GHz nadir-looking radar that measures the power backscattered by clouds as a function of distance from the radar. This sensor is expected to provide cloud measurements at a 500-m vertical resolution and a 1.5-km horizontal resolution. CPR will operate in a short-pulse mode and will yield measurements at a minimum detectable sensitivity of -28 dBZ. In this paper, we will present the system design and the expected performance of this instrument, as well as the state-of-the art millimeter-wave technologies employed by this instrument [C6991]

"Advanced design concepts for a SeaWinds scatterometer follow-on mission"

The SeaWinds wind scatterometer was first launched in June of 1999, and has contributed significantly to the study of global climate phenomena and to the fidelity of operational weather forecasting. A second SeaWinds instrument is planned to be launched aboard the Japanese ADEOS-II platform in late 2001, and operate until mid-decade. To extend the important Ku-Band scatterometer data base to the end of the decade and beyond, a follow-on system to the SeaWinds series of scatterometers is being developed. The goals for this system are to continue the core Ku-Band backscatter measurement, to further improve spacecraft accommodation constraints so as to be easily operated on a variety of platforms, and-where possible under existing cost constraints-improve wind retrieval performance. It is shown that a system, which meets these objectives, can be achieved by the addition of polarimetric measurement capability to the existing SeaWinds approach. Polarimetric scatterometry is demonstrated to improve wind measurement performance without impacting instrument complexity or cost, and has the long term potential to further ease spacecraft accommodation requirements [C6992]

"SeaWinds: the QuikSCAT wind scatterometer"

The QuikSCAT wind scatterometer, named SeaWinds, is a scanning, pencil-beam, microwave radar that was designed to measure global ocean surface winds from space. Originally planned for flight aboard the National Space Development Agency of Japan (NASDA) Advanced Earth Observing Satellite II (ADEOS-II) spacecraft, SeaWinds was expected to continue the series of Ku-band scatterometer data initiated by the NASA Scatterometer (NSCAT). Unfortunately, the failure of NSCAT's host spacecraft, ADEOS-I, prematurely ended NSCAT's mission and created a data gap. The QuikSCAT mission was rapidly developed to fill in the data gap between NSCAT on ADEOS-I and SeaWinds on ADEOS-II. A scatterometer nearly identical to SeaWinds was quickly assembled and launched on June 19, 1999 aboard the QuikSCAT spacecraft. In this paper, we describe the QuikSCAT mission, outline the key design features of the SeaWinds scatterometer, and mention some of the current and emerging science applications [C6993]

"Synthetic aperture sonar-the modern method of underwater remote sensing"

Synthetic aperture processing-the coherent combination of data from multiple returns-has revolutionized radar imaging over the past 35 years. Sonar is in the early stages of the same revolution. Synthetic aperture sonar

(SAS) data can be processed into images with resolution independent of range. Additionally, within diffraction limits, the resolution is frequency independent. Such characteristics make SAS a useful tool for applications such as bottom searching and mapping, mine hunting, or submarine detection, for near ranges (~50 m), mid-ranges (several hundreds of meters), and far ranges (several tens of kilometers) respectively. We have SAS-processed data collected by eleven different hardware suites at frequencies ranging from 240 kHz down to 600 Hz; physical array sizes ranging from half a meter to 256 meters; and with range-independent azimuthal resolutions ranging from 2.5 cm at 50 m for the high frequency systems to ~6 m resolution at 26 km for the lowest frequency system. Our results demonstrate that phase coherence can be maintained in spite of severe vehicle motion, medium fluctuations, and multipath propagation. For instance, we imaged the interior structure of a sunken airplane at 350 m and at 1,000 m with similar cross-range resolution, despite the rays having suffered a bottom bounce on both the transmit and return paths for the 1,000 m range data. The same imaging technology is applicable to cross-track interferometry (for resolving vertical features), bottom penetrating sonar, and wideband waveforms [C6994]

"Concurrent storm damage data collection by high altitude airborne IFSAR"

This paper discusses the use of high altitude airborne interferometric synthetic aperture radar (IFSAR) operations for concurrent severe storm damage data collection. The primary storm damage observable is changes in surface topography induced by storm effects. The surface topography in the form of a digital surface matrix (DSM) derived from concurrent IFSAR operations is compared to an archived DSM collected prior to the storm. Information on storm damage is developed from analysis of DSM changes. Combined with a-priori photo and radar imagery, the technique provides means for detection, location, quantification and characterization of storm damage. The paper discusses limitations to the concept due primarily to radar signal propagation effects. Results of simulations of IFSAR measured surface topography are presented [C6995]

"A 94 GHz spaceborne cloud profiling radar antenna system"

The CloudSat spacecraft, scheduled to launch in 2003, will carry a 94 GHz cloud profiling radar. The electrical design of its antenna system has been completed and is presented here. It consists of a quasi-optical transmission line that performs signal relaying and duplexing (using a Faraday rotator), and a collimating antenna that provides the required gain and spatial resolution. A shaped open Cassegrain collimating antenna is used because of its clear aperture, which allows for accurate electrical modeling, good performance, and significant reduction in implementation time and cost. The complete antenna system (horns to free space) has a worst case predicted gain of 63.1 dBi (59% efficiency) and exceeds the sidelobe envelope requirement of 50 dB below the peak gain at angles from boresight greater than 7 degrees [C6996]

"Pattern synthesis for TechSat21-a distributed spacebased radar system"

The TechSat21 space-based radar employs a cluster of free-floating satellites, each of which transmits its own orthogonal signal and receives all reflected signals. The satellites operate coherently at X-band. The cluster forms essentially a multi-element interferometer with a concomitant large number of grating lobes and significant ground clutter. A novel technique for pattern synthesis in angle-frequency space is proposed, which exploits the double periodicities of the grating lobes in the angular domain and of the radar pulses in the frequency domain, and allows substantial gains in clutter suppression. Gains from 7 to 17 dB relative to the normal random, sparse array appear feasible [C6997]

"Dual frequency synthetic aperture radar (SAR) mission for monitoring Earth"

Advances in spaceborne Synthetic Aperture Radar (SAR) remote sensing technology make it possible to acquire global-scale data sets that provide unique information about the Earth's continually changing surface characteristics. Short duration missions such as the Spaceborne Imaging Radar-C (SIR-C) and the Shuttle Radar Topography Mission (SRTM) have established the vast potential of SAR for expanding our knowledge of Earth. A long-duration (>5 year) free-flying SAR mission is essential to routinely provide valuable information about the dynamic characteristics of our planet. The SAR mission concept, consists of a dual frequency, polarimetric, interferometric system that has broad scientific, environmental preservation, operational, and commercial utility. A feature that greatly reduces the potential for tasking conflicts is the instrument's ability to operate both frequencies independently and simultaneously. The implementation approach includes an innovative government-industry collaboration that has the potential to lead to the creation of new information industries, in a manner similar to the Internet, Global Positioning Satellite (GPS) and commercial space telecommunications [C6998]

"A spaceborne L-band radiometer-radar concept for land and ocean surface monitoring"

An L-band radiometer-radar concept has been studied for spaceborne remote sensing of land surface soil moisture, freeze-thaw state, and ocean surface salinity. The integrated design provides simultaneous passive and active measurements with potential for enhanced geophysical retrieval accuracy and spatial resolution. The design takes advantage of cost savings achievable using shared subsystems and hardware. The baseline system concept has been evaluated to determine the feasibility of the technical approach and as a point of departure for system trade-offs. The unique features of this concept are the integration of the radiometer and radar sensors, the use of a deployable-mesh conically scanned reflector antenna, and the use of unfocused synthetic aperture radar (SAR) processing. Taken together, these features represent a significant departure from conventional radiometer, scatterometer, and SAR approaches. The conical wide-swath scan is a desirable feature that provides constant incidence angle and antenna pattern characteristics across the swath, simplified data processing (passive and active), and frequent global sampling. The concept is targeted for a low-cost, short-development-cycle mission, suitable for NASA's Earth System Science Pathfinder (ESSP) series [C6999]

"Segmenting polarimetric SAR images using robust competitive clustering"

POLSAR (POLarimetric Synthetic Aperture Radar) images have great potential for land-use management, provided that the images can be efficiently segmented. This paper describes the application of the Robust Competitive Agglomeration (RCA) clustering algorithm to POLSAR images to segment the images. Examples are presented and future efforts are discussed [C7000]

"A new independent component analysis (ICA) method and its application to SAR images"

A novel independent component analysis (ICA) method is proposed that makes use of higher order statistics. We name it joint cumulant ICA (JC-ICA) algorithm. It can be implemented efficiently by a neural network. Its application in synthetic aperture radar (SAR) is discussed. The results show its potential usage in image processing problems [C7001]

"Cloud radar activities at the Institute of Radio Astronomy of the NAS of Ukraine"

A review of recent activities undertaken at the Institute of Radio Astronomy of the National Academy of Sciences of Ukraine for the development of cloud radars is presented. Design approaches to the development of coherent radar systems operating at the frequencies of 36 GHz and 95 GHz are discussed. Examples of cloud radars developed at the Institute are presented [C7002]

"Fourth International Kharkov Symposium 'Physics and Engineering of Millimeter and Sub-Millimeter Waves'. Symposium Proceedings (Cat. No.01EX429)"

The following topics are dealt with: EM theory; numerical simulation; atomic functions, wavelets and fractals; wave phenomena in finite-size semiconductors and solid-state structures; high-temperature superconductors; low-temperature superconductors; wave propagation and radar; remote sensing; vacuum electronics, gyrotrons and FELs [C7003]

"Refractivity estimation from radar clutter by sequential importance sampling with a Markov model for microwave propagation"

This paper addresses the problem of estimating range-varying parameters of the height-dependent index of refraction over the sea surface in order to predict ducted microwave propagation loss. Refractivity estimation is performed using a Markov model for microwave radar clutter returns from the sea surface. Specifically, the parabolic approximation for numerical solution of the wave equation is used to formulate the problem within a nonlinear recursive Bayesian state estimation framework. Solution for the conditional expectation of range-varying refractivity, given log-amplitude clutter versus range data, is achieved using a sequential importance sampling technique. Simulation results are presented which demonstrate the ability of this approach to synoptically estimate range-varying refractivity parameters by "through-the-sensor" remote sensing [C7004]

"The SRTM sub-arcsecond metrology camera"

To achieve the necessary interferometric baseline for the recent Shuttle Radar Topography Mission (SRTM), an outboard radar antenna was deployed using a 60 meter mast from a main radar antenna in the shuttle payload bay. The mast had dominant flexible modes around 0.1 Hz with tip displacements on the order of several centimeters in response to shuttle thrusters. Continuous knowledge of the mast tip position to submillimeter accuracy and antenna orientation to an accuracy of 100 arcseconds (1.6 sigma) was necessary to meet the fundamental SRTM requirements. The selected approach involved an optical metrology camera which tracked three LED targets located on the outboard antenna structure. The metrology camera was required to generate

target centroid coordinates (in CCD frame) with a relative accuracy of 0.8 arcsec, 1 sigma. This paper provides a description of the metrology camera, the process used to prepare it for flight on SRTM, the LED target development effort, test and alignment issues, and the observed in-flight performance [C7005]

"Estimating road networks using archived GMTI data"

It is increasingly accepted that accurate maps of road networks can make a critical difference in enabling accurate tracking of ground movers using GMTI radar data, especially when sensor resources are limited. However, road maps are often incomplete and inaccurate to such an extent that their utility is eliminated or greatly reduced. At the same time, users of GMTI data have noted in heavily trafficked areas that the road networks are readily apparent on positional displays of GMTI data. This has led to the notion of estimating the road networks using GMTI data, an idea, which is operationally appealing given that the data, can be collected over a time period of several days to several months. This paper addresses one of the fundamental issues of estimating road networks from GMTI data. We derive a methodology for estimating a road network that views the road in a fundamentally different way than has been the case in previous approaches to this problem. The methodology is motivated by the stochastic models typically employed to model target trajectories as indexed by time, which we modify to come up with a stochastic model for the road trajectory which is indexed by arc-length. We apply this new method and compare it to a recently presented method that views the road as fundamentally composed of segments and vertices, and show using a limited data set that the stochastic estimation approach seems to offer much better performance [C7006]

"Robotic Antarctic meteorite search: outcomes"

Automation of the search for and classification of Antarctic meteorites offers a unique case for early demonstration of robotics in a scenario analogous to geological exploratory missions to other planets and to the Earth's extremes. Moreover, the discovery of new meteorite samples is of great value because meteorites are the only significant source of extraterrestrial material available to scientists. In this paper we focus on the primary outcomes and technical lessons learned from the first field demonstration of autonomous search and in situ classification of Antarctic meteorites by a robot. Using a novel autonomous control architecture, specialized science sensing, combined manipulation and visual servoing, and Bayesian classification, the Nomad robot classified five indigenous meteorites during an expedition to the remote site of Elephant Moraine in January 2000. Nomad's expedition proved the rudiments of science autonomy and exemplified the merits of machine learning techniques for autonomous geological classification in real-world settings. On the other hand, the expedition showcased the difficulty in executing reliable robotic deployment of science sensors and a limited performance in the speed and coverage of autonomous search. [C7007]

"Automated planning for the Modified Antarctic Mapping Mission"

The RadarSAT Modified Antarctic Mapping Mission (MAMM) ran from September to November 2000. The MAMM mission consisted of over 2400 synthetic aperture radar (SAR) data takes over Antarctica that had to satisfy coverage and other scientific criteria while obeying tight resource and operational constraints. Developing these plans is a time and knowledge intensive effort. It required over a work-year to manually develop a comparable plan for AMM-1, the precursor mission to MAMM. This paper describes the automated mission planning system for MAMM, which dramatically reduced mission planning costs to just a few work-weeks, and enabled rapid generation of "what-if" scenarios for evaluating mission-design trades. This latter capability informed several critical design decisions and was instrumental in accurately costing the mission. This paper describes the mission, the planning problem, the system architecture, the planning challenges involved, and the impact of the automated planning system on planning and operating the mission [C7008]

"The computer replacement program for the joint surveillance target attack radar system"

This paper presents development and testing results of the Computer Replacement Program (CRP) for the Joint Surveillance Target Attack Radar System (Joint STARS). Joint STARS, which consists of a modified Boeing 707-300 (E-8C) developed by Northrop Grumman and Common Ground Stations developed by Motorola, provides theater commanders near real-time surveillance and attack support information on moving and stationary targets. Diminishing manufacturing sources and an emphasis on life-cycle cost reduction required a modernization program that took maximum advantage of commercial equipment. The primary program objectives were maximizing marketplace support, reducing life-cycle costs and facilitating cyclic upgrades. CRP implemented this via a commercial off-the-shelf-based open architecture. The Computer Replacement Program met all its development objectives and will be fielded on the entire 15-aircraft Joint STARS fleet. Lessons learned included applying innovative acquisition processes in an open architecture, adapting to processes while under schedule pressure, ensuring early operational tester involvement, and estimating laboratory and ground testing in addition

to flight-testing. The views expressed in this paper are those of the authors and do not represent views of the U.S. government or their contractors [C7009]

"Detecting a step pattern of change in multitemporal SAR images"

We address the problem of deriving adequate detection and classification schemes to fully exploit the information available in a sequence of SAR images. In particular we address the case of detecting a step reflectivity change pattern against a constant pattern. We propose two different techniques, based on a maximum likelihood approach, that make different use of prior knowledge on the searched pattern. They process the whole sequence to achieve optimal discrimination capability between regions affected and not affected by a step change. The first technique assumes a complete knowledge of the pattern of change, while the second one is based on the assumption of totally unknown pattern. A fully analytical expression of the detection performance of both techniques is obtained, which shows the large improvement achievable using longer sequences instead of only two images. The practical effectiveness of the technique on real data is shown by applying the detector for unknown step pattern to a sequence of 10 ERS-1 SAR images of forest and agricultural areas, which is also used to validate the theoretical results [C7010]

"Application of array processing techniques to multibaseline InSAR for layover solution"

Synthetic aperture radar interferometry (InSAR) is a modern technique to derive digital height maps of the land surface from SAR images. In recent years there has been great interest in exploiting the advanced multibaseline operation for solving layover effects that can degrade SAR and InSAR imagery. We consider detailed modelling of this problem including speckle noise for extended targets, application of several nonparametric and parametric spectral estimation methods to multibaseline layover solution, and performance analysis. The problem of layover solution is formulated as the estimation of a multi-component signal composed by multiple cisoids corrupted by complex multiplicative Gaussian noise and additive white Gaussian thermal noise. Beamforming, Capon's, High-Order Yule-Walker, MUSIC, Min-Norm, and ESPRIT spatial spectral estimators are applied to this interferometric problem, and an extensive simulated performance comparison is carried out in terms of statistical accuracy and resolution [C7011]

"On CFAR detection of oil slicks on the ocean surface by a multifrequency and/or multipolarization SAR"

This paper addresses detection of oil spills on the sea surface as viewed by multifrequency and/or multipolarimetric synthetic aperture radars. We propose a two-stage processor: the first stage is a conventional detector designed to operate in a Gaussian environment; its detections are fed to a second stage designed to discriminate between candidate oil spills and templates of dark areas due to different phenomena, based upon different multifrequency and/or polarimetric signatures. Remarkably, the second stage possesses the constant false alarm rate property with respect to all of the unknown statistics of slick-free returns [C7012]

"A general signal processing algorithm for MTI with multiple receive apertures"

Moving target indication (MTI) is demonstrated for general antenna arrays, especially sparse 3D arrays. The framework for space-time adaptive processing (STAP) is generalized to include frequency (fast-time) data and array elements offset in cross track dimensions. The degrees of freedom (rank) needed to represent clutter are derived for general systems. The clutter rank compared to the number of independent samples collected by a radar determine whether MTI is achievable. The optimum detector and the minimum norm eigen canceler (MNE) are implemented through simulation to demonstrate effective clutter cancellation [C7013]

"A cluster-based geophysical template matching system"

There has been increased interest in the use of sensing devices in the detection and classification of subsurface objects, particularly for the purpose of eradicating Unexploded Ordnance (UXO) from military sites. The Geophysical Template Matching System (GTMS) is a cluster-based framework for the storage and analysis of spatial data sets derived from scanning subsurface objects using geophysical sensing devices. Current approaches to the UXO detection and classification problem have met with limited success. The template matching approach employs libraries of templates extracted from known objects. Coarse grain parallel processing techniques are used to speed up the matching algorithms with fine grain parallelism also planned. The user interface is via the World Wide Web providing interaction, a graphical user interface and convenient access from remote locations [C7014]

"Smart sensing for mine detection studies with IR cameras"

Because of the high risks involved, it is necessary to conduct mine detection remotely. By making use of infrared (IR) cameras, scattered mines can be detected from remote locations. In the case of mines buried in the ground, detection is possible if the peripheral temperature difference is large enough between the ground and mine weapon. As one of the world's advanced nations in sensor technology, Japan should promote surveys and studies for detecting mines safely by using its advanced remote sensing technologies. [C7015]

"A digital signal processor for Doppler radar sensing of vital signs"

A voltage waveform signal containing respiration and heartbeat signatures is low-pass filtered (0.7 Hz) for the respiration and band-pass filtered (1.0-3.0 Hz) for the heart signal. The autocorrelation function is used to calculate the rate per minute for each of these signals. To make the processor more robust, several signal processing techniques are applied. One of these techniques, a method commonly used on audio signals for formant removal, is called center clipping. Another technique is the use of a Hanning window. To reverse the distinct shape left by the Hanning window an "undo" window is applied. The processor is programmed in LabVIEW. [C7016]

"Development of antenna-source system for generation of high-power electromagnetic pulses"

High-power electromagnetic pulse sources are of interest for a variety of applications such as transient radar and remote sensing. For such investigations, a simple, mobile and robust source system has been developed at DSTO. It comprises a pulsed resonant transformer, a spark-gap switch, and a modified biconical antenna. The antenna is charged to a high voltage, in the order of hundreds of kV, by the transformer and then is shorted at the bicone centre by the spark gap switch. The charge energy stored in the antenna then oscillates at the resonant frequency of the system and produces high-power electromagnetic pulses. In this paper we describe the system design, present results of measurements and numerical simulations, and discuss areas for further improvements in energy transfer efficiency and power output. [C7017]

"Combination of multiple classifiers by fuzzy integrals: an application to synthetic aperture radar (SAR) data"

In this work, the results obtained in the classification of a multi-source-multi-temporal remote sensed data set by means of a distributed neuro-fuzzy system are compared with the results of a traditional centralized neural classification system, based on a single multilayer perceptron (MLP) neural network module. The distributed system is composed by a set of neural classifiers, whose partial results were combined with both Sugeno and Choquet fuzzy integrals. Two classification experiments were carried out with the distributed system. In the first experiment, each neural module of the distributed system used the same learning rule but was trained with a subset of the input features, i.e., a specific spectral band. In the second experiment, the neural modules of the system were trained with the same complete set of input features available for each training pixel, but consisted of MLP networks characterized by different specific topologies or different neural algorithms. The results show that larger improvements can be obtained by combining more independent classifiers. The Choquet fuzzy integral provided better performance than Sugeno fuzzy integral. The centralized system, based on a single MLP module, provided the best classification performance. [C7018]

"Ultra-wideband P-3 and CARABAS II foliage attenuation and backscatter analysis"

Two-way foliage attenuation measurements from UHF and VHF SAR images collected from several USA forests and an empirical model of two-way attenuation versus center frequency are presented. Comparisons of UHF and VHF clutter backscatter coefficient distributions are made for different forest areas and terrain slopes. UHF two-way attenuation and backscatter coefficient statistics are presented for different polarization channels [C7019]

"Sensor integration in airborne mapping"

The rapid technological developments of the 90s have completely redefined the mapping practice. In less than a decade, digital techniques have come to outnumber traditional analog data acquisition and processing methods. Supported by unprecedented demand for large-volume, accurate spatial data, these new digital techniques emerged as dominant mapping technologies by the end of the decade. Two key components of this emerging technology are the electronic sensor-based digital camera and GPS/INS-based direct platform orientation. In fact, these new platform orientation systems are rapidly becoming a core component of modern airborne mapping and remote sensing systems [C7020]

"Applications using a low-cost baseband pulsed microwave radar sensor"

This paper presents several measurement applications using a low-cost baseband pulsed microwave radar

sensor. The sensor transmits and receives Gaussian pulses having a full width half maximum of 150 ps and peak amplitude of 7 V via two ultrawide band antennas in a bistatic configuration. Time-domain scattering and ranging measurements of metallic plates and cylinders in addition to fluid volume gauging were performed. Target range was calculated by applying the time-of-flight concept. Range uncertainty was less than 6 mm. For a pulse repetition frequency of 5 MHz, an upper limit on the power spectral density (PSD) of the radiated pulses was calculated. The PSD upper limit had a peak of -74 dBm/Hz at a frequency of 1.5 GHz [C7021]

"Multiprocessor digital signal processing on Earth orbiting scatterometers"

The implementation of a Multi Digital Signal Processor for radar return analysis on a Ku-Band Earth orbiting scatterometer is discussed. Historically, radar signal processing on scatterometers has been implemented with discrete components, Field Programmable Gate Arrays (FPGA) and Application Specific Integrated Circuits (ASIC). These methods are expensive due to long development times, expensive tools, and their lack of modularity. The system presented in this paper uses a radiation tolerant, space qualified version of a commercial general purpose DSP (ADSP-21020) to perform the radar signal processing functions. This approach allows the use of development tools such as compilers, libraries, evaluation boards and emulators. The presented system uses multiple processors interconnected with IEEE-1355 high-speed links to provide the computational power necessary. Operating systems such as Virtuoso provide core capabilities to facilitate scalability, which is important to accommodate changes in functional or performance requirements that inevitably occur late in the development cycle, or even on orbit. A testbed was assembled using a combination of commercial DSP hardware and spaceflight components to evaluate the proposed multiprocessing approaches. Test results of real-time radar echo processing are presented, as well as proposed designs for future investigation [C7022]

"Opportunity of reduction of objects visibility using diffraction-reflecting coverings in conditions of application laser detection systems"

We consider a single-channel locator without accumulation of an uninterrupted signal, this is, actually, close enough to a real situation, when the target is immobile and the value of Doppler shift of frequency is given, as far as it is determined by the rate of the movement of the receiving system. Further we use the characteristics of the laser heterodyne locator produced by Rockwell, which has the parameters close to the heterodyne locators of MTL complexes as an example [C7023]

"Estimating wind speed in lower atmosphere wind profiler based on genetic algorithms"

A lower atmosphere wind profiler, which is a pulse Doppler radar is a useful operation tool which can provide unattended and continuous observation of wind profiles. Since the observed signals are usually degraded by ground clutters which are overlapped with the wind signal it is necessary to develop a method to estimate the wind signal from the observed signals. We propose to use a genetic algorithm to resolve the overlapped signals [C7024]

"Processing of multi-aperture SAR to produce fine-resolution images of arbitrarily large extent"

The spatial extent that can be accurately imaged by a synthetic aperture radar (SAR) is unfortunately limited. This restriction results from the fact that the number of independent pixel estimates produced by a SAR is constrained by the number of independent measurements that it collects. The solution is to increase the number of independent sensor measurements, without modifying sensor resolution. This can be accomplished by subdividing the SAR aperture into an array of receiver elements, each with a coherent receiver. This sensor collects information over both time and space, and thus space-time processing must be implemented. Three SAR processors are evaluated: a correlation processor, a maximum likelihood estimator, and a minimum mean-squared error estimator. Simulations demonstrate that all three processors can create fine resolution SAR images over an arbitrarily large area, provided that the number of array elements is sufficiently large. Additionally, it is shown that the ML and MMSE processors provide quality SAR images from a sparse receiver array, such as those produced by a "formation-flying" collection of radar satellites [C7025]

"Characterization of C-band and X-band InSAR data for 3D urban analysis"

We compare C and X-band SAR measurements over the same urban area to understand which kind of information they are able to provide and which are the differences and similarities of the data sets. In particular, we consider data recorded over Los Angeles by the C-band NASA/JPL AIRSAR system and by the X-band Intermap Star-3i system. We analyze for both data sets the original range measurements as reconstructed after the phase unwrapping procedure, the bare earth topography that we were able to retrieve, and the 3D shapes of some of the buildings in the UCLA campus area. Our results show that, despite the lower resolution, AIRSAR data are still able to provide interesting views of an urban environment. The better ground resolution of the X-

band system allows us to perform slightly better building analysis and extraction. Both systems suffer from large data drop out regions that prevent the original data from being immediately useful. However, it is still possible to extract the terrain height to some extent by means of a filtering procedure and to deduce built structure characteristics if suitable ad hoc algorithms are introduced [C7026]

"The characteristics of rainfall and melting layer in Singapore: experimental results from radar and ground instruments"

The radio frequencies used by current and future satellite communications systems have been gradually shifted towards higher bands due to a rapidly increasing demand for bandwidth. At higher frequencies, such as Ku-band systems, which have been deployed widely in most of the Asian countries, rain-induced attenuation can severely affect the availability of the Earth-satellite communications service. In particular, tropical regions have posed extra difficulties in predicting attenuation due to the lack of understanding of tropical precipitation and climate, e.g., rainfall intensity and rainfall heights. Moreover, millimetre wave specific attenuation is very dependent on raindrop size distributions. In addition, total path integrated attenuation on satellite paths depends on the maximum height of rainfall. To explore these uncertainties, the Radio Communications Research Unit (RCRU) at Rutherford Appleton Laboratory (RAL) installed a tropical rain radar in 1998. We aim to study the characteristics of tropical rainfall and predict attenuation by utilising data gathered by rain radar, distrometer and a ground-based beacon receiver. Moreover, this radar has been involved with the ongoing Tropical Rainfall Measurement Mission (TRMM) and EuroTRMM projects to improve our understanding of the characteristics of tropical rainfall [C7027]

"Eleventh International Conference on Antennas and Propagation (IEE Conf. Publ.No.480)"

First Page of the Article [C7028]

"Data aggregation approach to multisensor radar imaging"

By integrating two developed optimization methods for optimal data aggregation modifications can also be proposed that involve a priori calibration information both on the systems' resolution and relative noise levels in the acquired images. In view of this, some previously developed fusion schemes, in which the weights were proposed to be selected proportionally to the width of the PSF and signal-to-noise ratio (i.e. inversely proportional to the relative noise intensities) could be referred to as suboptimal versions of the developed regularization-based aggregation approach [C7029]

"A microwave radio for Doppler radar sensing of vital signs"

A microwave radio for Doppler radar sensing of vital signs is described. This radio was developed using custom DCS1800/PCS1900 base station RFICs. It transmits a single tone signal, demodulates the reflected signal, and outputs a baseband signal. If the object that reflects the signal has periodic motion, the magnitude of the baseband output signal is directly proportional to the periodic displacement of the object. When the signal is reflected off a person's chest, this radio with appropriate baseband filters can detect heart and respiration rates from a distance as large as one meter from the target [C7030]

"Development of a helicopter obstacle detection and air data system"

This paper describes a sensor that provides the combination of obstacle detection, air data and wind velocity. This laser-based sensor, the Multi-Mode InfraRed Radar (MMIRR), has been under development for two years. An early prototype test flown in an Army helicopter in December 1999 validated the ability of the underlying technology to detect wires and measure True Airspeed (TAS) and wind velocity. This paper discusses: the results of the first demonstration flight; the technology program that reduced the technical risks in the laser, optics, scanner and signal processing areas; the technical hurdles, the tradeoffs and the resulting improvements in sensor performance; the results of tests of the improved MMIRR model that had a finer range resolution, wider field of view and an attitude-stabilized scanner. The projected performance and physical characteristics of a producible and affordable MMIRR product capable of providing obstacle detection and air data to helicopter pilots in the near future is provided [C7031]

"Continuous monitoring of atmosphere by compact automated lidar"

The development of a diode pumped solid state laser has made possible to construct a compact lidar system. A portable automated lidar was investigated to make possible continuous monitoring of the air pollution and radiative properties of atmosphere, which is prospective for the practical operation and a lidar monitoring network formation [C7032]

"K-band direct detect MMIC Si micromachined radiometer"

This paper describes the design of a K-Band direct detect MMIC radiometer using bulk micromachining techniques to create the conformal package, interconnecting structures and CPW-fed slot-coupled patch antenna array. Parylene encapsulation is used following die-attach and wire bonding. Also, a unique on-board calibration technique using an MHEMT based cold/warm noise source offers an alternative to other forms of calibration of radiometers and radar receivers. Experimental results are given for the 20.7 GHz radiometer printed on high-resistivity silicon [C7033]

"A low-cost solution for obtaining remote sensing images"

This paper presents a low-cost system based on kites to obtain remote sensing images. These low altitude images have interesting properties to application on areas with high rates of cloud cover or precision agriculture [C7034]

"System measurement of antennas"

Antenna measurements are typically performed at a component level establishing the gain, pattern, polarization, and impedance characteristics. Clearly, the need for these measurements continues, but additional antenna-related measurements are required in system applications to verify compliance with system requirements. The trend of integrating antennas with system electronics also requires such characterizations to evaluate antenna system performance since an antenna port per se for measurement does not exist. Examples of antenna-related system measurements are described [C7035]

"Ground penetrating radar imaging of buried metallic objects"

During the past decade there has been considerable research on ground penetrating radar (GPR) tomography for detecting objects such as pipes, cables, mines and barrels buried under the surface of the Earth. While the earlier researches were all based on the assumption of a homogeneous background for simplicity, the planar air-soil interface has also been taken into account in two recently developed algorithms (see Hansen, T.B. and Meincke Johansen, P., IEEE Trans. Geosci. Remote Sensing, vol.38, no.1, 2000; Meincke, P., IEEE AP-S International Symposium, 2001). We address a general formulation for GPR imaging of buried 3D metallic objects within the physical optics (PO) approximation which also highlights the analytical background behind the success of methods employed by Hansen and Meincke Johansen and Meincke in identifying high contrast scatterers [C7036]

"Development of antenna-source system for high-power electromagnetic pulse generation"

Summary form only given, as follows. High-power electromagnetic pulse sources are of interest for a variety of applications such as transient radar and remote sensing. For such investigation, a simple, mobile and robust source system has been developed at DSTO. It comprises a pulsed resonant transformer, a spark-gap switch, and a modified biconical antenna. The antenna is charged to a high voltage, in the order of hundreds of kV, by the transformer and then shorted at the bicone centre by the spark gap switch. The charge energy stored in the antenna then oscillates at the resonant frequency of the system and produces high-power electromagnetic pulses. In this paper we describe the system design, present results of measurements and numerical simulations, and discuss areas for further improvements in energy transfer efficiency and power output [C7037]

"IEEE Antennas and Propagation Society International Symposium. 2001 Digest. Held in conjunction with: USNC/URSI National Radio Science Meeting (Cat. No.01CH37229)"

The following topics are dealt with: FDTD theory; broadband microstrip antennas; antenna applications for mobile communications; reconfigurable antennas; FEM; electromagnetic theory; medical imaging and treatment with microwaves; RF coil design for high field MRI; electromagnetic education; mobile antennas; radio propagation theory; microstrip antennas; random media and rough surfaces; reflector antennas; diverse waveguiding structures; antenna measurements and calibration; EM health effects of cellular phone radiation; array design; mutual coupling; multiband antennas; electromagnetic scattering; conformal antennas; time domain antennas; wideband array antennas; photonic bandgap structures; higher-order basis function methods; integral equation techniques; inverse scattering; lens antennas; multiresolution methods; fractal antennas; finite element methods; PCS antennas; CPW feeds; circularly polarized microstrip antennas; aperture-coupled microstrip antennas; fixed beam microstrip arrays; RF MEMS; antenna arrays; rough surface scattering; remote sensing; fast multipole methods; phased arrays; adaptive arrays; dual band antennas; spiral antennas; antenna theory; radar imaging; frequency selective surfaces; patch antennas; complex media; time domain theory; helical antennas; slotted

antennas; genetic algorithms; RCS calculations; active microstrip phased arrays; wavelets [C7038]

"Development of a two-color dual-polarization pulsed bistatic lidar for measuring water cloud droplet size"

A new bistatic lidar is being developed for measuring water cloud particle size. The system employs a pulsed two-color Nd:YAG laser and a receiver with a polarization analyzer located at a suitable scattering angle to measure water cloud droplet size [C7039]

"Super-resolution ocean surface current algorithm based on MUSIC for OSMAR2000"

Owing to the decametric wavelength, a large aperture antenna array is needed for high frequency (HF) ground radar to obtain high angular resolution with conventional beam forming (CBF); for the case of a compact antenna or small aperture array, spatial super-resolution algorithms are used to get satisfactory angular resolution. Wuhan University's ocean state measuring and analyzing radar (OSMAR2000) is expected to real-time extract ocean surface current, wave and surface wind information at medium-range and long-range. To obtain long-range (i.e. 200 km) current mapping, the radar frequency must be selected in the lower region of the HF band, e.g. 7.5 MHz. Digital beam forming (DBF) is applied with the 120 m-long phased array to determine the bearings of the sea echo with 15° resolution for wave and wind extraction. The angular resolution is, however, too coarse for current mapping, especially when the ocean current detection range is as far as 200 km. Consequently, a super-resolution ocean surface current algorithm based on multiple signal classification (MUSIC) is developed for OSMAR2000. The relative theory basis, processing procedure and preprocessing and postprocessing associated with the algorithm are given. The comparison of OSMAR2000 measurements with the measurements from a current meter and the Seasonde system shows the ocean surface current algorithm based on MUSIC for OSMAR2000 can meet the requirements of the project contract successfully [C7040]

"Direction of arrival estimation using super-resolution algorithm"

The angular resolution of conventional antenna is limited by the antenna mainlobe beamwidth. To reduce the antenna mainlobe beamwidth by conventional approach requires either using larger antenna or operating at a higher frequency. Both approaches may be undesirable for the application of airborne radar systems. This report suggests using a sensor array to perform space-time processing to enhance the angular resolution of antenna. By using the eigenanalysis method, the time sequence of sensor array outputs are decomposed into the signal and noise subspace and noise only subspace. The two subspaces are orthogonal to each other. Using the generalized MULTiple Signal Classification (MUSIC) method, closed spaced targets within the antenna mainlobe may be resolved. The theoretical background is discussed in this report. Computer simulation results are presented to verify the super resolution capability of this signal processing algorithm [C7041]

"Detection of the number of signals in super-resolution ocean surface current algorithm for OSMAR2000"

Super-resolution ocean surface current algorithm based on MULTiple Signal Classification (MUSIC) is used for current mapping of Wuhan University's ocean state measuring and analyzing radar (OSMAR2000), in which MUSIC is applied to estimate the bearings of the first-order sea echo signals. The premise of MUSIC processing is that the number of signals is known in advance. In fact, the number of signals is unknown, and needs to be estimated from received data. In the case of discrete targets, the problem can be perfectly solved using information theoretic criteria such as the Akaike Information Criterion (AIC) or the Minimum Description Length (MDL) criterion. However, these criteria are proved unsuccessful for sea echo signals both in simulation and in actual application, since sea surface is essentially a continuum. Therefore, an ad hoc method of detection of number of signals, a bit different from the existent methods, is developed for the current algorithm of OSMAR2000. The underlying idea is to determine the number of signals based on the variance of MUSIC spectra structure under different candidate number of signals [C7042]

"Multifrequency HF radar observations of surface currents: measurements from different systems and environments"

The authors present three aspects of current HF radar research. First, they examine the consistency of measurements by HF ground wave radars with different designs, but operating on the same physical principles. This is done using data from the commercially available SeaSonde (Codar Ocean Systems) and from the Multifrequency Coastal Radar (MCR), which is a research system. Data from the two systems are compared for co-located units at Santa Cruz and Moss Landing CA on Monterey Bay. They conclude that the two systems make current-vector-field measurements that are consistent to an accuracy of better than 10 cm/s and that the

data from two such systems can be integrated to form reliable composite current maps. Second, they present results from an air-sea interaction investigation using the MCR systems on Monterey Bay during 1997 and 2000. We show that near surface currents are correlated with the wind with correlation coefficients 0.6 and are rotated 35 to 45° with respect to the wind in the sense of the Ekman spiral. They also show results of near shore observations on Lake Michigan during the EEGLE campaign of 2000. These measurements show the capability of HF radars to operate over fresh water [C7043]

"U.S. CELRAP laser radar design considerations"

In the U.S. CELRAP laser radar program, an eyesafe laser radar has been designed and built using designator-class laser technology and linear multiple channel detector arrays. Functions include obstacle detection, target profiling, and range mapping [C7044]

"Iterative correction of multiple-scattering effects in Mie-scattering lidar signals"

This paper describes an iterative method for extracting single-scattering contributions in the retrieval of aerosol extinction profiles from lidar signals. The iterative procedure is formulated by use of the lidar solution with introducing a multiple-scattering ratio as a correction factor, which is calculated by the Monte Carlo method. The iterative method is applied to an experimental signal observed by a multi-wavelength lidar [C7045]

"DIAL measurement of daytime variations of vertical tropospheric O₃ concentration profiles"

DIAL measurement of vertical daytime O₃ concentration profiles was performed. The DIAL system linearity was checked using O₃S-value profiles. In the winter season, O₃ concentration is variable between 50-270 ppb [C7046]

"UV Rayleigh lidar system for accurate temperature profiling of the troposphere"

A compact and efficient ultraviolet lidar system is designed and developed to measure the temperature profile in the troposphere. The Doppler broadened Rayleigh-Brillouin scattering is detected with two etalon filters. The Mie scattering noise effect is reduced by a proper signal processing method. High temperature sensitivity is expected in this scheme [C7047]

"Development of ISS/JEM-borne coherent Doppler lidar"

Development of a space-borne coherent Doppler lidar (CDL) for the Japanese Experiment Module (JEM) of the International Space Station (ISS) is now under way in CRL. Objective of the CDL with an eye-safe solid state laser is the demonstration of effectiveness of global wind profiling [C7048]

"Linearized multi-frequency inversion of ground penetrating radar data"

Although inverse scattering methods have reached a level of considerable sophistication in the past decades, their testing and verification remains predominantly numerical. By inverse scattering methods we understand those mathematical techniques that go beyond the trivial time-domain backpropagation or frequency-domain migration algorithms (sometimes called SAR imaging). The present study is concerned with the application of such inverse scattering methods to a practical problem of landmine detection using commercial ground penetrating radar (GPR) equipment. In particular, we investigate the performance of the so-called linearized inversion, i.e. the one where the description of the scattering process is subject to the Born approximation [C7049]

"Superactive pump-and-probe LIDAR technology: biophysical insight into aquatic remote sensing"

Summary form only given. An advanced pump-and-probe (P&P) airborne LIDAR technology for remote monitoring of aquatic photosynthesis and complimentary environmental variables has been recently developed at Wallops Flight Facility (NASA Goddard Space Flight Center). The P&P LIDAR provides remote measurement of important phytoplankton photosynthetic characteristics, such as the functional absorption cross-section of photosystem II (PSII), PSII photochemical quantum yield, and PSII turnover time. In addition, the rate parameters of singlet-singlet and singlet-triplet quenching and carotenoid triplet lifetime are measured. A set of 'conventional' LIDAR characteristics, such as chlorophyll (Chl), phycoerythrin and dissolved organic matter fluorescence, as well as water Raman scattering are simultaneously retrieved for detailed characterization of the surveyed area. The utilization of an airplane as a platform allows the remote acquisition of unique biophysical and environmental data over large aquatic areas at synoptic space/time scales. The P&P LIDAR can be efficiently used in studies of regulatory mechanisms of biological "carbon pump" in the ocean and ocean responses to environmental

changes, as well as for improved validation of satellite data and monitoring coastal processes and special events (phytoplankton blooms, nutrient deficiency, tidal mixing, floods, etc.) [C7050]

"Short range spectral lidar using mid-infrared semiconductor laser with code-division multiplexing technique"

Summary form only given. A short-range spectral lidar based on the code-division multiplexing (CDM) architecture using mid-infrared Sb semiconductor lasers for remote sensing has been demonstrated with near detector-limited performance. The system principle is similar to optical-CDMA for communications and applicable to any number of wavelengths, but was demonstrated with two wavelengths similarly to conventional DIAL (Powers et al, Appl. Opt. vol. 39, pp. 1440-1448, 2000; McRae and Kulp, Appl. Opt. vol. 32, pp. 4037-4050, 1993). An experiment using <20-mW transmitter average power could detect an open-air acetylene gas leak from 10 m away with dynamic, random, noncooperative backscatters. We believe this is among the first demonstrations of this semiconductor spectral lidar with orthogonal CDM architecture, as well as the first demonstration of mid-IR Sb lasers used in open path, noncooperative target remote sensing [C7051]

"Laser remote sensing for characterization of planetary boundary layer properties"

The lowest layer of the atmosphere is, due to the friction of the moving air masses with the earth surface, very turbulent. The mixing of exhaust fumes and dust and a lot of chemical reactions take place. For that reason, 3D data of trace gas concentrations as well as aerosol properties and parameters of the dynamics are absolutely necessary for the understanding of the processes, model initialization, evaluation and pollution prediction. Laser remote sensing is one of the favorite methods to get measurement of time series with a reasonable resolution in time and space. However, the fast dynamic causes problems in the evaluation of laser remote sensing signals. Elastic backscattering, which is normally used as a signal source for differential absorption measurements, also uses Rayleigh scattering and scattering on aerosols. The backscatter intensity depending on aerosols varies significantly in time. For differential absorption lidar (DIAL) measurements in particular, we must average some hundreds or thousands of shots to get an adequate signal to noise ratio. The influence of short time fluctuations to the average causes major problems in the retrieval of trace gas concentration profiles, and we lose information about short time fluctuations and dynamics. To overcome these problems, we decided to combine fast sampled elastic scattering signals and averaged Raman signals to bring out the dynamics, aerosol size distribution, the extinction and the ozone concentration [C7052]

"Holographic Raman and Rayleigh lidar"

Summary form only given. Thermometric lidar systems exploiting either Raman or Rayleigh scattering have been operating for many years. In the majority of these systems, the critical components of the return signal are isolated using conventional multilayer filters. In the case of Raman lidar, the filters are used to isolate two discrete parts of the rotational Raman scattering (RRS) spectrum. Since the spectrum shape is temperature dependent, the relative photon count through each filter gives a measure of the temperature of the air molecules. This method, however, suffers from inaccuracies due to unknowns in the filter profile and central wavelength due to thermal effects. This, along with the low throughput of the required ultra-narrowband filters has restricted the range and accuracy of these systems. In our system, a holographic optical element (HOE) has been constructed, which simultaneously disperses and focuses the backscattered light. Individual lines of the nitrogen RRS spectrum can be extracted with high efficiency making it possible to obtain more accurate temperatures, at much higher altitudes than previously possible. Furthermore, with the simple addition of another collection fiber, the Rayleigh signal can be extracted for temperature measurements at much higher altitudes [C7053]

"Millimeter wave and infrared electronics for investigations of acoustic-electromagnetic phenomena due to activity of Popocatepetl volcano"

The report is devoted to millimeter and sub millimeter electronics intended for research of acoustic-electromagnetic phenomena caused by Popocatepetl volcano (Mexico). The main purpose is to present different types of sensors, one of them is based on a red and infra red silicon detector (avalanche photodiode with separated regions of absorption and multiplication). This sensor guarantees both a good sensibility and a wide range of sensing in infra red range. It has the advantage of a realization as a planar array. For millimeter and sub millimeter radar measurements, using a modulator based on the surface oriented p-i-n structure with "deep" junctions is possible. For the remote measurements of basic meteorological parameters and chemical state by means of radio brightness temperatures (radiometer systems), a low noise receiver based on a dielectric waveguides and Schottky diodes cooled by means of cryoelectronic elements can be used [C7054]

"Experimental study of spectra and X- and Ka-band backscattering from the rain agitated water surface"

On the basis of experimental research the shape of the spectra of rain agitated water surface was qualified. It was shown that for frequencies above 15 to 20 Hz the spectral density decreases more slowly than in the lower frequency areas. This spectrum area corresponds to the backscattering of the cm and mm radiowaves at low grazing angles. The quantity estimation of the RCS of agitated. surface was found for the single drops and for the artificial rain. On that basis the decision was made that, at low grazing angles the main effect in backscattering comes from the stalk and crown in place of splash at impact point, but at high grazing angles, the main effect is backscattering by the ring waves [C7055]

"Experimental research of the spectral, polarizing and azimuthal features of the S-, Ka- and V-band backscattering by the water and petroleum surfaces"

The local monitoring of marine water area contaminations by ground allocation radar will be an actual problem for some considerable time due to the growth in the incidence of such contaminations. Besides this area, the research can be relevant to satellite remote sensing of a marine surface and for studying the hydrodynamic processes in the upper layers of ocean. In this context, the authors present experimental research of the spectral, polarizing and azimuthal features of the S-, Ka- and V-band backscattering by water and petroleum surfaces. The instrumentation and experimental techniques are discussed, while the results of processing experimental data are given [C7056]

"Model of drop canting in microwave remote sensing of rain"

Doppler-polarimetric remote sensing techniques are powerful tools in microwave remote sensing of atmosphere. Combination of polarization. diversity with Doppler measurements opens new possibilities for research microphysics and dynamic processes in clouds and precipitation. Series of new sophisticated models, which relate atmospheric processes with behavior of scatterers' should be developed for radar data interpretation. It is especially important for mm-band facilities because of their sensitivity to small particles. The calculations and measurements have shown that small particles contribute significantly to the scattered signal from. rain at wavelength of 8 mm and especially of 4 mm and less. That is why well-known Marshall-Palmer drops size distribution for rain, which is usually used to estimate radar reflectivity in X-band, can lead to errors in mm-band because it exaggerates strongly the number of small particles. This simple example clearly shows that one must be very careful when applying known initial models for mm-band modeling, simulation or data interpretation. In this paper, describing rain drop size distribution $N(D)$, we use a very flexible gamma-distribution [C7057]

"mm-band radar image filtering with texture information preservation"

Studies the texture preserving properties for different simple basic filters (of DPF and NSF types) in order to provide a possibility of using one of them in the filtering scheme for texture region processing. These properties have been analyzed both quantitatively and visually. The filters analyzed were the following: the noise suppressing filters (NSFs)-mean, median, and Lpqfilters; the detail preserving filters (DPFs)-the standard sigma filter and the local statistical Lee filter [C7058]

"A narrow band fiber Bragg grating filter for lidar receivers"

.Summary form only given. For a space-based water vapor differential absorption lidar (DIAL) system there is a need for improved optical receiver filters especially for daytime operation to reject background radiation on the detector. Present dielectric interference filters have transmission bandwidths of approximately 1 nm and are not tunable. To achieve good system performance the daytime filter bandwidth should be 10 pm a factor of about 100 narrower than interference filters. Unless a better filter can be found, future space based DIAL systems may only be able to operate at night. Fortunately a new technology has emerged that could allow very narrow bandwidth filters to be made in optical fibers. These Bragg gratings have been applied to the communications industry at the 1.55-micron wavelength, but there is evidence that the same technology will work at the 946 nm wavelength of interest to water vapor DIAL receivers. The paper discuss research on the testing of a new optical receiver using an ultra-narrow fiber Bragg grating optical filter at 946 nm for potential use on space borne lidar [C7059]

"Despeckling SAR images using wavelets and a new class of adaptive shrinkage estimators"

We propose an efficient and fast wavelet based technique for speckle removal from SAR images. It relies on realistic distributions of the wavelet coefficients which represent mainly speckle noise on the one hand and those

that represent the useful signal corrupted by speckle on the other. We propose analytic models for these distributions, and compute their parameters automatically from a given SAR image. The resulting algorithm strongly suppresses speckle, while preserving image details and sharpness [C7060]

"Gabor vs. GMRF features for SAR imagery classification"

A comparison of the ability to discriminate among distinct regions in synthetic aperture radar (SAR) imagery using textural features based on two different methods is presented. Features are generated from Gauss Markov random field (GMRF) model parameters and from Gabor convolution energies. The discrimination ability is evaluated in terms of misclassification errors resulting from tests performed on a patchwork of different MSTAR clutter regions [C7061]

"Rain clouds tracking with radar image processing based on morphological skeleton matching"

The aim of this study is to perform a short term forecasting of dynamic radar clutter evolution (shape and position). This dynamic clutter, like thunderstorms, can be tracked by means of adapted algorithms based on the matching of the morphological skeleton polygonal approximation by relaxation labeling processes. The efficiency of our methods is demonstrated on meteorological radar images. The objective of this application is dedicated to civil traffic regulation according to severe atmospheric phenomenon, as described in Monnier & al. (1997). Through radar environment assessment, we observe radar clutter, like precipitation, submitted to very complex deformations that cannot be modeled easily. In Barbaresco (1999), we proposed a method based on morphological skeleton deformation to forecast the fluid topological evolution. This method allows management of very complex shapes evolution thanks to polygonal approximation of the skeletons and matching of their closed couple of elements by the relaxation algorithm. The skeleton simplifies shape analysis and deformation but also distinguishes clutter displacement and articulated deformation by skeleton matching from homothetic deformation (inflation and deflation) by medial axis (radius of maximal disks contained in the shape) tracking [C7062]

"Simulation of radar echo from a ship in ocean clutter using the GFBM/SAA method"

A hybrid approach of the generalized forward-backward method (GFBM) with the spectral accelerate algorithm (SAA) and Monte Carlo method is developed. It is applied to numerical simulation of angular radar echo from a rough sea surface with a ship presence as TE or TM tapered waves are incident upon it. Due to the high efficiency of the GFBM/SAA, radar echo at low grazing angle (LGA) can be also calculated. Numerical simulations show the functional dependence upon polarization, observation angle, sea surface wind speeds, ship location and other parameters [C7063]

"3D regularized velocity from 3D Doppler radial velocity"

The availability of sequences of 3D Doppler radial velocity datasets provides sufficient information to estimate the 3D velocity of Doppler storms. We present a regularization framework for computing the 3D velocity field of storms from the underlying 3D radial velocities via an intermediate least squares computation. We obtain very realistic Doppler velocities, which can be used to estimate and predict the motion of Doppler storms. Such information is fundamental in the tracking of Doppler storms over time [C7064]

"Extraction of forest attribute information using multisensor data fusion techniques: a case study for a test site on Vancouver Island, British Columbia"

The use of multisensor and multitemporal remotely sensed data is important for the extraction of forest attribute information for Canada's 418 million km² of forests. Hyperspectral data can provide vegetation signatures for forest attributes and canopy chemistry. Hyperspatial data can be used for individual tree recognition. Data from P-band synthetic aperture radar (SAR) have yielded accurate timber volume information in experiments involving managed plantations. We present the results of a study undertaken to assess forest attribute determination over the Greater Victoria Watershed District (GVWD) test site on Vancouver Island, BC, Canada from the following airborne and satellite sensors: Multi-detector Electro-optical Imaging Scanner (MEIS), Airborne Visible Infrared Imaging Spectrometer (AVIRIS), AirSAR and LANDSAT-7. GIS information and field data from field spectrometers are used for validation and calibration of AVIRIS and LANDSAT-7 ETM+ data. Inventory information (e.g. stem density, biomass) for our plots is known as a result of both field sampling and data fusion of GIS and high spatial resolution MEIS data. Segmentation techniques are applied to identify spatially homogeneous objects for quantification of forest attributes [C7065]

"30-mJ, 30-Hz, and 300-nm ultraviolet laser source generated by a frequency-tripled Ti:sapphire laser [Cfor DIAL]"

Summary form only given. A compact, frequency-tripled, and 30-Hz Ti:sapphire laser at 900 nm has been developed. The laser provides more than 30-mJ ultraviolet output pulse energy at 300 nm and will be used in an airborne ozone differential absorption lidar [C7066]

"Two and three dimensional images of shallow geological structures"

The purposes of imaging are to gain some understanding of what a ground probing radar (GPR) image would look like, to facilitate interpretation and to test signal and image processing techniques. An interesting structure is the buried valley aquifer due to its potential for storing groundwater. This is investigated by simulation using ray tracing for two dimensional images and facet modelling for three dimensional images [C7067]

"Comparison of PCA and ICA based clutter reduction in GPR systems for anti-personal landmine detection"

This paper presents statistical signal processing approaches for clutter reduction in stepped-frequency ground penetrating radar (SF-GPR) data. In particular, we suggest clutter/signal separation techniques based on principal and independent component analysis (PCA/ICA). The approaches are successfully evaluated and compared on a real SF-GPR time-series. Field-test data are acquired using a monostatic S-band rectangular waveguide antenna [C7068]

"Multi-polarization SAR data for operational ice monitoring"

The launch of Envisat-ASAR, RADARSAT-2 and ALOS-PALSAR will offer operational polarization-diverse SAR data for the first time. A series of example data sets from aircraft and SIR-C are examined to evaluate the operational potential of these future systems. The primary operational advantage of multi-polarization data will be improved ice-water discrimination at low incidence angles, although the expected noise-floor of the satellite systems may limit their utility for discrimination of new ice types [C7069]

"Multi-polarization C-band SAR signatures of arctic sea ice"

The Advanced Synthetic Aperture Radar (ASAR) is scheduled to be launched on the ENVISAT satellite in summer 2001. For Arctic-sea ice mapping using future ASAR data, we carry out a study of multiple polarization C-band SAR signatures of various sea ice types. We present polarimetric SAR data acquired over sea ice acquired by the Jet Propulsion Laboratory polarimetric AIRSAR system on the NASA DC-8 aircraft over sea ice regions in the Beaufort Sea and the Bering Sea. We use a physical sea ice model to study polarimetric scattering signatures of sea ice. The results also provides useful information to the future RADARSAT-2 multi-polarization SAR for sea ice mapping [C7070]

"Independent component analysis for sea ice SAR image classification"

Independent component analysis (ICA) is used to compute sets of basis vectors for image data, i.e. for small randomly selected image windows. From these basis vectors a smaller set is selected to be used in classifying sea ice SAR images. A SAR image window is classified based on its projection to the selected basis vectors [C7071]

"Seasonal sea ice studies in the Kara Sea region using satellite radar data"

Synthetic aperture radar images from ERS and Radarsat, as well as Okean Side-Looking Radar and passive microwave data, are used to study a number of different sea ice processes and signatures in the Russian Arctic coastal region, especially in the Kara Sea region where the seasonal ice cover is a dominant feature. This paper is focused on sea ice processes observed from sequence of SAR images, such as fast-ice and coastal polynyas, ice drift through straits, ice formation and motion in response to ocean and atmospheric forcing. Repeated SAR images obtained roughly every 3 days, combined with wind and temperature data, are used to describe the advance and retreat of coastal polynyas in southern Kara Sea during a winter season [C7072]

"Bathymetric effects on a tropical cyclone wave field at landfall"

On 26 August 1998, the NASA Scanning Radar Altimeter (SRA) flew on a NOAA hurricane research aircraft to document the directional wave spectrum as Hurricane Bonnie was making landfall near Wilmington, NC, SRA measurements in deep ocean two days earlier provided a basis of comparison for the bathymetric effects at landfall. The open ocean wave heights indicated that Hurricane Bonnie would have produced waves of 11 m height on the shore had there not been wave damping by the continental shelf. The bathymetry distributed the dissipation process across the shelf so that wavelength and height were reduced gradually. The wave height 5

km from shore was about 4 m [C7073]

"On the radar imaging of the sea frontal zone: "CoastWatch-95" experiment and its analysis"

A new model of radar imaging of ocean fronts is presented. Along with Bragg scattering the radar part of the model accounts for scattering from breaking waves. The Impact of sea front on wind waves results from both surface current and varying wind forcing adjusted to sea temperature. The model results are compared with field "CoastWatch-95" observations [C7074]

"Analysis of oceanic long wave refraction at the Gulf Stream boundary using RADARSAT synthetic aperture radar during Hurricane Bonnie"

In this study, we analyze the Gulf Stream's effect on the refraction of ocean waves observed in data obtained from the RADARSAT synthetic aperture radar (SAR). The ocean waves observed on this SAR image have very long wavelengths and are mainly generated by Hurricane Bonnie which was located to the east of the Gulf Stream when the SAR image was taken. 256 by 256 pixel sub-images are extracted from the SAR image, and the SAR image spectrum is calculated from these sub-images. The SAR image spectrum should represent the directional ocean wave spectrum in this case, because the dominant wavelength is very long at about 400 m. A wave-current interaction model is used to simulate the wave refraction and reflection at the Gulf Stream boundary. We find that wave refraction is the dominant mechanism at the Gulf Stream boundary for these very long oceanic waves, while wave reflection is not a dominant factor. The waves turn about 15 degrees from their original direction [C7075]

"A proposal of measuring ocean wavelengths by satellite altimeters"

This paper presents methods for estimating the ocean wavelength in satellite altimetry and discusses the possibility of detecting the ocean wavelength. Numerical analyses show that there exists a relation between the significant wavelength and the pulse-to-pulse correlation coefficient [C7076]

"Global tracking of swell with complex ERS-2 wave mode data"

Complex synthetic aperture radar (SAR) data acquired by the European remote sensing satellite ERS-2 are used to analyze the propagation of swell on a global basis. The study is based on complex SAR wave mode imageries, which were processed from ERS-2 SAR raw data using the DLR BSAR processor. Complex imageries allow to apply the so called cross spectra technique globally for the first time. In contrast to conventional SAR intensity images, cross spectra provide information on ocean wave propagation without 180° ambiguity. A test data set of three weeks of complex imageries (≈36000) is used to measure ocean swell. Distribution of swell is studied based on maps showing swell direction, wave height and wavelength. Temporal swell dynamics is analyzed using data acquisitions with small spatial distance and a time gap of ≈12 h. Apart from providing information on ocean swell the study is a preparation for the coming ENVISAT era where cross spectra will be a standard product of the European Space Agency (ESA) [C7077]

"Study of sea ice in North Water Polynya using multi-sensor spaceborne data"

The North Water Polynya (NOW) is the largest and perhaps most active polynya in the Arctic region. A study of sea ice distribution and surface properties was conducted using multi sensor satellite remote sensing data in conjunction with surface measurements during an expedition in April/May 1998. The study utilized a data fusion technique which co-locates observations from three sensors: SSM/I, AVHRR and Radarsat SAR to explore spatial and temporal statistics of sea ice in the polynya. Results show that thin ice (less than 15 cm thickness) occupied 35% of the polynya (during the study period). Ice surface temperature and surface albedo varied significantly in the middle of the polynya and were related to ice types (identified in the fine-resolution Radarsat images). Ice concentration calculation from SSM/I brightness temperature was verified against Radarsat visual observations. The mean concentration was 0.65 and it constituted mostly thin ice types [C7078]

"Improving soil moisture retrieval by incorporating a priori information on roughness parameters"

In this paper we examine the influence of a priori information on the roughness characteristics of agricultural fields within the context of soil moisture retrieval using SAR. Laser profile data from several European in-situ measurement campaigns is put together and typical distributions for 3 tillage types-seedbed, harrowed and ploughed-determined. In a subsequent step the information content and the retrieval uncertainties before and after a priori roughness information has been introduced into the inversion procedure is determined using a Bayesian approach [C7079]

"Backscattering model validity across large footprints for global scatterometer applications"

Medium to low resolution (1-50 km) active microwave sensors such as spaceborne scatterometers and wide-swath mode SAR have great potential as tools for long term monitoring over land and ice. Their large area coverage and low cost make them ideal for measuring mesoscale land surface changes. One approach to the interpretation of such data is to employ a modeling approach whereby the backscatter model can be inverted to estimate some representative surface parameters. However, to optimize this method it is necessary to use scattering models that are applicable to large (> 1 km) footprints that inevitably contain a range of surface characteristics. This paper investigates the validity of a number of surface scattering models for such a task. The investigation is carried out both from a theoretical modeling approach as well as through comparison to real data from the ERS scatterometer over non-vegetated areas. Modified models that incorporate surface heterogeneity through probability distributions are also introduced. It will be shown that the ERS scatterometer data are better represented using these modified models than the standard theoretical models. Good results are also obtained using the semi-empirical model by Oh et al. that seems to incorporate for the target heterogeneity [C7080]

"Observations of sea surface mean square slope during the Southern Ocean Waves Experiment"

Registered ocean wave topography and backscattered power data at 36 GHz were collected off the coast of Tasmania under a wide range of wind and sea conditions, from quiescent to gale force winds with 9 m wave height. Collection altitude varied from 35 m to 1.4 km, allowing determination of the sea surface mean squared slope (mss), the directional wave spectrum, and mss variation with respect to wind and wave parameters [C7081]

"A multistaged approach to mapping soil salinity in a tropical coastal environment using airborne SAR and Landsat TM data"

This paper provides a methodology to map soil salinity and a recent saline intrusion in the coastal fringe of Kakadu National Park, Australia. A model inversion from AirSAR data to map soil salinity on the bare and partially vegetated floodplain was used. This algorithm has been developed by combining the small perturbation model and the Dubois model to extract the imaginary part of the dielectric constant as an improved indicator of salinity. A vegetation correction to the combined model has been developed to allow salinity extraction from floodplain areas with moderate vegetation cover. Recent saline intrusion areas are often characterised by stands of dead Melaleuca (paper bark trees). These are unsuitable for the inversion algorithms due to pronounced corner reflector effects on the radar. These areas were identified with high accuracy using a supervised classification on a fused AirSAR/TM image. The resulting map provides salinity levels for most of the floodplain and clearly identifies recent saltwater intrusion [C7082]

"Canal and river tests of a RiverSonde streamflow measurement system"

Results of field tests of a RiverSonde streamflow radar are compared with in-situ current measurements at a canal and a river in central California during June, 2000. Typical water velocity in the middle of the canal was about 0.45 m s⁻¹ and 0.30 m s⁻¹ at the edges. Velocity in the river was about 20% lower with similar cross-channel variation. Differences between the RiverSonde and in-situ velocities were 6-18% of the mean flow, with similar differences among the various in-situ velocities. In addition to the surface velocities, the total volume flow was estimated based on the in-situ depth measurements. Volume flow for the canal was about 37 m³ s⁻¹ and for the river was about 64 m³ s⁻¹, with differences between the various radar and in-situ techniques of less than 10% [C7083]

"Planar domain indices: a method for measuring a quality of a single component in two-component pixels"

A method is presented that reduces the difficulty of measuring a particular quality of one component in a multi-component element. The planar domain index design requires two measurements: that of a signal sensitive to the desired quality of the target component and another signal sensitive to the component's weight or relative proportion to the whole. The quality signal and component weight signal form the two dimensions of a plane, and the maximum and minimum possible values for each signal define the boundaries of a domain within this plane. The position of a coordinate pair within the domain can then be correlated to the quality being measured, independent of the component's proportion to the whole. Examples given involve mixed vegetation and soil targets, with vegetation indices used to measure the component weight. Quality signals of the example applications include canopy minus air temperature as a measure of evapotranspiration, a normalized difference of near infrared and far red wavelengths as a measure of chlorophyll content, and differential synthetic aperture radar (SAR) for measuring near-surface soil moisture [C7084]

"Interactions between multi-frequency microwave backscatters and rice canopy variables"

Microwave backscatter coefficients at all combinations of five frequencies (Ka, Ku, X, C, and L), all polarizations (HH, VH, HV, and VV) and four incident angles (25°, 35°, 45°, and 55°) have been collected on nearly a daily basis before transplanting to after the harvesting period of the rice paddy. Analysis based on a backscattering model clearly showed unique interactions between each microwave backscattering signature and vegetation variables such as LAI, biomass, and grain yield [C7085]

"An electromagnetic model for scattering from buildings"

In this paper, a geometric and electromagnetic model of a typical element of urban structure is presented, in order to analytically evaluate its electromagnetic return to an active microwave sensor. This model can be used to understand what information on geometric and dielectric properties of buildings can be extracted from microwave remote sensing data [C7086]

"Analytical investigation of urban SAR features having a group of corner reflectors"

Many man-made structures found in urban areas respond in predictable manners and appear as dominantly bright features within SAR images. In this paper the role of electromagnetic phenomena in SAR environment is analyzed. We present several SAR simulation results performed on multiple arbitrary building structures. The simulated results, which are tabulated on various cases, may be utilized to benefit urban planners or image interpreters by providing clues to relate target reflectivity and their average height distribution in urban SAR imagery [C7087]

"Improved texture recognition of SAR sea ice imagery by data fusion of MRF features with traditional methods"

Image texture interpretation is an important aspect of the computer-assisted discrimination of SAR sea ice imagery. Co-occurrence probabilities are the most common approach to solve this problem. However, other texture feature extraction methods exist that have not been fully studied for their ability to interpret SAR sea ice imagery. Gabor filters and Markov random fields (MRF) are two such methods considered. Classification and significance level testing shows that co-occurrence probabilities classify the data with the highest classification rate, with Gabor filters a close second. MRF results significantly lag Gabor and co-occurrence results. However, the MRF features are uncorrelated with respect to co-occurrence and Gabor features. The fused co-occurrence/MRF feature set achieves higher performance [C7088]

"Polarimetric and interferometric SAR calibration verification methods"

It is necessary to calibrate SAR data in order to use the data for science applications. When both polarimetric and interferometric data are collected simultaneously, these SAR data can be used for cross-calibration and verification. The frequency of polarimetric and interferometric data does not have to be the same for this purpose. For example, the NASA/JPL AIRSAR system can acquire C-band interferometric data and L-band polarimetric data simultaneously. The radiometric calibration of polarimetric data can be improved using the local slope information obtained from SAR interferometry. The accuracy of geophysical parameter estimation may be enhanced using true incidence angles derived from SAR interferometry. The calibration of interferometric SAR data can be verified by examining interferometric correlation coefficients. Both azimuth and range slopes estimated from an interferometric SAR DEM can be used to examine the polarization calibration accuracy. In this paper, we show several examples of cross-calibration verification between polarimetric and interferometric SAR data [C7089]

"Forest height mapping using space-borne polarimetric SAR interferometry"

In this paper we generate a statistical significance test for a 2-level coherent mixture model of interferometric radar scattering from forested terrain. We test the model against SIR-C L-band data and show that the assumption of a random volume scattering model for vegetation is fully justified for L-band remote sensing of forested areas. This has important implications for the design of future spaceborne radar sensors aimed at forest mapping applications [C7090]

"Long-term subsidence monitoring of urban areas using differential interferometric SAR techniques"

Subsidence monitoring of areas affected by low velocity displacements is an extremely useful application of SAR (synthetic aperture radar) techniques. However, the required long time-baselines reduce the quality of the information stored in differential interferograms, adding difficulties to their processing. Typical characteristics of

these interferograms are the presence of coherent areas that correspond to urban zones and totally incoherent areas of vegetation. A partial reconstruction of the subsidence map can be achieved by means of DInSAR (differential interferometric SAR) techniques based on the processing of coherent patches. On the other hand, PS (permanent scatterers) techniques can deal with incoherent areas, generating subsidence information of the whole image. A comparison of both techniques using ERS data is presented in this paper [C7091]

"Polarimetric SAR interferometry for forest canopy analysis by using the super-resolution method"

In this paper, we propose an polarimetric SAR interferometry technique for interferometric phase extraction of each local scatterer of the forest region. The proposed method formulated for local scattering center extraction is based on the ESPRIT algorithm which is known for high-resolution capability of closely located incidences. The method shows high-resolution performance when local scattered waves are uncorrelated and have different polarization characteristics. Using the method, the number of dominant local scattered waves and their interferometric phases in each image patch can be estimated directly. Validity of the algorithm is demonstrated by using examples derived from SIR-C data [C7092]

"Recent advances in extra-wide-band multi-modal POL-IN-SAR imaging"

Radar polarimetry, radar interferometry and polarimetric SAR interferometry present the current culmination in 'microwave remote sensing' technology, but we still need to progress very considerably in order to reach the limits of physical realizability. Whereas with radar polarimetry the textural fine-structure, target orientation, symmetries and material constituents can be recovered with considerable improvement above that of standard 'amplitude-only' radar; with radar interferometry the spatial (in depth) structure can be explored. With polarimetric interferometric synthetic aperture radar (POL-IN-SAR) imaging, it is possible to recover such co-registered textural and spatial information from POL-IN-SAR digital image data sets simultaneously, including the extraction of digital elevation maps (DEM) from either repeated-pass polarimetric (scattering matrix) or interferometric (dual antenna) SAR systems. Simultaneous polarimetric-plus-interferometric SAR imaging offers the additional benefit of obtaining co-registered textural-plus-spatial three-dimensional POL-IN-DEM information, which when applied to repeat-pass image-overlay interferometry provides differential background validation and environmental stress-change information with highly improved accuracies. Then, by either designing multiple dual polarization antenna POL-IN-SAR systems or by applying advanced POL-IN-SAR image compression techniques, will result in 'POL-arimetric TOMO-graphic' (multi-interferometric) SAR or POL-TOMO-SAR imaging. By advancing these EWB-D-POLIN/TOMO-SAR imaging modes, we are slowly but steadily approaching the ultimate goal of eventually realizing air-borne and space-borne 'geo-environmental background validation, stress assessment, and stress-change monitoring of the terrestrial and planetary covers' [C7093]

"Advanced algorithms for QuikScat and SeaWinds/AMSR"

QuikScat is providing scientists and weather forecasters with an unprecedented view of ocean winds at a 25-km resolution. With a typical accuracy of 1 m/s in speed and 15° in direction, the retrieved wind vectors are being used for a number of important oceanographic and air/sea interaction studies. We present work on a QuikScat wind-vector retrieval algorithm that contains a number of advanced features, including: an updated geophysical model function (Ku-2001), a fully integrated stand-alone rain flag, and the capability to retrieve winds up to 70 m/s. In addition, the QuikScat data processing is done in parallel with our near-real-time operational data processing for SSM/I and TMI. In this way, an additional rain flag as well as a sea-ice flag (both based on the SSM/I and TMI observations) can be appended to the QuikScat wind vectors. We present results of two studies: (1) the capability for QuikScat to measure very high winds (>30 m/s) and (2) comparisons between scatterometer and radiometer wind speed retrievals (i.e. QuikScat versus TMI). These investigations are leading towards a combined SeaWinds-AMSR algorithm for ADEOS-2, which will ingest both scatterometer and radiometer observations to obtain more accurate wind vectors and sea-surface temperatures [C7094]

"Development of a SeaWinds wind product for weather forecasting"

SeaWinds data are provided by the Jet Propulsion Laboratory (JPL) at 25-km resolution, whereas most numerical weather prediction (NWP) models use observations at least a 100-km density. We have developed a QuikSCAT wind product at a coarser resolution than the JPL product in order to achieve a more appropriate information content for assimilation in NWP models. This product includes quality control, wind retrieval, and ambiguity removal [C7095]

"QuikSCAT geophysical model function for hurricane wind and rain"

The SeaWinds scatterometer on the QuikSCAT spacecraft has been operating since August 1999 to provide global mapping of ocean winds. The ocean surface winds from the QuikSCAT scatterometer have been shown to

be accurate, except for precipitating and extreme high wind conditions. It is known that the QuikSCAT scatterometer winds typically underestimate the strength of tropical cyclones and overestimate the wind speed for low to moderate wind speeds (3-10 m/s) under rainy conditions. We examined collocated QuikSCAT radar data and SSM/I rain rate to assess the effects of rain. It is shown that the QuikSCAT σ_0 s increase with increasing rain rate for low and moderate wind speeds (<15 m/s) and has an opposite trend for hurricane force winds (>32 m/s). It is also shown that the QuikSCAT σ_0 modulation by the wind direction is reduced by the rain. The results are consistent with the existing QuikSCAT wind speed biases and characteristics of wind direction solutions at the presence of rain. Our results suggest that the rain rate can be introduced as an additional modeling parameter for the Ku-band scatterometer model function to reduce the wind retrieval bias resulting from the rain for adverse weather conditions [C7096]

"Evaluation of wind vectors observed by QuikSCAT/SeaWinds using ocean buoy data"

Wind vectors observed by QuikSCAT/SeaWinds are compared with wind and wave data from offshore moored buoys. Effects of oceanographic and atmospheric parameters on the scatterometry are also assessed by using the buoy data. The QuikSCAT/SeaWinds Standard Wind Data Products (Level 2B) were collocated with the Japan Meteorological Agency (JMA), National Data Buoy Center (NDBC), and Tropical Atmosphere Ocean (TAO) buoys. Only buoys located offshore and in deep water were selected. Temporal difference and spatial separation between the QuikSCAT/SeaWinds and buoy observations were limited to less than 30 min and 25 km. Wind speeds measured by the buoys at various height above the sea surface were corrected to equivalent neutral winds at a height of 10 m. Wind speeds and directions observed by QuikSCAT/SeaWinds agree well with the buoy data. Root-mean-squared differences of the wind speed and direction are 1.02 m/s and 22° , respectively. Dependencies of wind speed residuals on oceanographic and atmospheric parameters observed by buoys are examined using the collocated data. Weak positive correlation of the wind speed residuals with the significant wave height is found, although no significant dependence on the sea surface temperature and atmospheric stability is discernible [C7097]

"Estimation of alpine permafrost surface deformation using InSAR data"

The detection of an active rock glacier and the quantification of the observed surface movement as well as its temporal change using the D-InSAR method are presented. An average deformation rate of -7.7 mm/35 days in the radar line-of-sight, in the summer of 1992, was estimated. Whereas, the corresponding geodetic measurement, vertical component of 3D flow velocity, was about -8.0 mm/35 days. Additionally, the spatial distribution of the rock glacier surface deformation derived from the D-InSAR data matches the photogrammetric and geodetic generated results to a very high degree [C7098]

"Multiplicative and product model constraints upon speckle filtering of SAR images"

Speckle filter performances depend strongly on the speckle and scene models used as the basis for filter development. These models that incorporate implicitly certain assumptions on speckle, scene and observed signals, were generally adopted and used without any justification. In this study, the multiplicative and the product speckle models, which have been used as the basis for the development of the most well known filters, are analyzed. Their implicit assumptions are discussed with regards to the stationarity-nonstationarity of speckle, observed and scene signals. Two categories of speckle filters are distinguished as a function of the stationarity-nonstationary assumption on speckle random variations. The various approximate models used for the multiplicative speckle noise model are then assessed as functions of speckle and scene characteristics. The S. N. Madsen method (1987) was extended to the various models to derive the requirements on scene signal variations for the validity of the multiplicative stationary speckle model, and the product model which forces speckle to be a nonstationary process [C7099]

"Soft morphology and Bayesian reconstruction for SAR image filtering"

In this paper we present a morphological operator based on the statistical generalization of soft morphological operators. We are showing that the proposed operator can assume the behaviour of several morphological and linear filters depending on the parameter setting. In this paper, we are showing the application of the proposed operator to SAR images and we are presenting a comparison with the results obtained with the Lee filter [C7100]

"Bayesian fusion of active and passive microwave data for estimating bare soil water content"

Evaluates an approach to improve the estimation of soil moisture from remotely sensed data. We focus on two types of sensors: a radiometer and a scatterometer operating at a frequency of 4.6 GHz, which both observe the same portion of the Earth surface. Active and passive microwave systems are sensitive to changes in the dielectric properties of the soil and surface morphological properties. Indeed they show complementary

capabilities useful for the quantification of these soil parameters. In this context, a retrieval algorithm based on a Bayesian approach has been developed. Our analysis indicates that an improvement in soil moisture estimation accuracy can be obtained when passive radiometric measurements and active radar data are fused with respect to the estimation from a single source. The evaluated soil moisture values show a reasonable agreement in comparison with in situ measurements [C7101]

"Markovian methods for SAR image processing"

This article aims at illustrating the generality and the powerfulness of Bayesian and specially Markovian frameworks for different remote sensing applications and in particular for SAR (synthetic aperture radar) image processing. Indeed, the Markovian model is a very convenient way to introduce prior knowledge on the problem to solve. It will first be evoked with examples on the pixel level like filtering, segmentation and classification. Then higher level applications, like object recognition, and global image interpretation will be developed [C7102]

"Diurnal cycle of oceanic precipitation from microwave radiometry"

We examine the spatial and temporal distribution of the diurnal cycles derived from seasonal averages of 1° latitude by 1° longitude grids based on measurements of the TRMM Precipitation Radar. Afternoon maxima are found overland and nocturnal to early morning maxima are observed over the oceans. Regions of land-sea breeze are also delineated. The diurnal amplitudes are comparable to if not larger than the daily means [C7103]

"A climatology of tropical instability waves using the ERS-1 and -2 scatterometers"

The strong coupling of the atmospheric boundary layer to oceanic tropical instability waves (TIW) results in a signature of these waves in the surface wind field. Surface winds derived from the ERS-1 and -2 scatterometers enable the development of a climatology of these waves. Although the sparsity of this data introduces sampling errors, the waves are clearly visible when they are present and their phase speeds are clearly discernible. The ERS-1 and -2 scatterometers have been in operation since 1991, and therefore provide us with a look at these waves on annual and interannual time scales. Here ERS-1 and -2 data are analyzed in conjunction with sea surface temperatures (SST) illuminating the behavior of TIWs. On annual time-scales, the waves regularly appear in May at about 95°W and propagate westward along the SST front that marks the northern edge of the Pacific SST cold tongue. The western-most extent of these waves varies considerably from year to year as does the cold tongue. On the interannual time scale, TIW activity is strongest during the cold phase of the ENSO cycle (La Nina) when the cold tongue is most pronounced; the waves are nonexistent during the warm phase of ENSO (El Nino) when the SST front is weak [C7104]

"Discrimination between low metal content mine and non-mine-targets using polarimetric ultra-wide-band radar"

In this paper we show that wide band radar polarimetry can be used for discrimination between surface laid AP mine and non-mine targets. To do this we employ two types of coherent radar decomposition theorem applied to wide band chamber measurement data from the European Microwave Scattering Laboratory (EMSL). Our main conclusion is that radar polarimetry should be further investigated as an important way to secure low false alarm rate from radar sensors in stand off mine detection [C7105]

"WEMSAR-wind energy mapping using synthetic aperture radar"

Satellite-measured wind speed data may offer new possibilities for off-shore wind resource assessment. Currently a minimum of one year wind observations at meteorological masts positioned in the sea or at the coastline are used in atmospheric models at local and regional scale to predict the off-shore wind resources. Satellite SAR imagery from the ERS satellites provide ocean wind speed maps at a local scale of 400 m spatial resolution covering areas of 100 km \times 100 km as snap-shots several times a month. New SAR systems (Radarsat, Envisat) will increase the spatial and temporal data coverage at lower cost. The SAR wind speed maps may provide new and useful information relevant for planning optimal siting of off-shore wind parks. A possible future application is thus to use satellite data in combination with numerical modeling in order to get a better indication of where to place a test site [C7106]

"Effective depth of HF current measurements: observations from COPE-3"

Comparison of HF radar measurements of ocean surface current with those from moored acoustic Doppler current profilers (ADCPs) during the third Chesapeake Bay Outflow Plume Experiment during October and November 1997 suggests that the effective depth of the HF radar measurements is between $(2k)^{-1}$ and $1.4(2k)^{-1}$, where k is the ocean wavenumber which is in Bragg resonance with the HF wavelength. This is consistent with

the analysis of Stewart and Joy [1974] who estimated an effective depth of $(2k-1)$ for a linear current profile [C7107]

"SAR interferometry confirms the present land stability of Venice"

The city of Venice is very vulnerable to loss in land elevation as a result of subsidence and eustasy because of its small elevation above sea level. The alarm of the scientific community related to this persistent problem is increasing because of the forecasts of sea level rise caused by global warming. In order to evaluate the present relative settlement of Venice, a study has been performed by combining high precision levelling surveys and SAR interferometry. The analysis points out at an unprecedented detail the present ground stability of the city [C7108]

"The effect of polar format resampling on uncompensated motion phase errors and the phase gradient autofocus algorithm"

The phase gradient algorithm (PGA) is an autofocus technique applied after SAR image formation for correcting uncompensated motion phase errors. A crucial aspect of the algorithm is the assumed phase error model used to describe the motion errors in the phase history data. In this paper it is shown that the Polar Format Algorithm (PFA) image formation processor introduces a distortion to the phase error that is not considered in the PGA formulation. It is shown that the PFA distortions degrade the point target response in the PGA image output and act as a source of relative phase errors in repeat pass SAR interferometry applications [C7109]

"Spaceborne X-band small SAR system model design and its imaging performance characteristics"

In this paper, the spaceborne SAR system is designed with the key performance parameters for the given mission and system requirements characterized by the small satellite system. Based on the various SAR imaging modes and the SAR system requirement model, the X-band SAR payload and ground reception/processing subsystems are designed and the major results are presented with the key performance characteristics [C7110]

"Spatially adaptive radar speckle reduction using wavelet denoising and Markov random fields"

In this paper, we develop a speckle reduction algorithm by fusing the wavelet Bayesian denoising technique with Markov-random-fields-based image regularization. Wavelet coefficients are modeled independently and identically by a two-state Gaussian mixture model, while their spatial dependence is characterized by a Markov random field imposed on the hidden state of Gaussian mixtures. The EM (expectation-maximization) algorithm is used to estimate hyperparameters which specify the mixture model, and simulated annealing is implemented to optimize the state configuration. The noise-free wavelet coefficients are finally estimated by a shrinkage function based on local weighted averaging of the Bayesian estimator. Experimental results show that the proposed method outperforms standard wavelet denoising techniques in terms of MSE measure. It also achieves better performance than the refined Lee filter in the case of low noise levels [C7111]

"A maximum likelihood approach for detecting a step pattern of change and locating the transition instant in a sequence of multitemporal SAR images"

In this work we derive two different detectors that fully exploit the information available in a multitemporal sequence of M SAR images with regions possibly affected by step changes in reflectivity, with unknown transition instant. These detectors process the whole sequence using a maximum likelihood approach to: (i) locate the transition instant, and (ii) discriminate between regions affected and not affected by a step change. The KSP-detector assumes that the two mean RCS levels are known, while the USP-detector assumes that the two mean RCS levels are unknown. Two different approximations for the probability of correctly locating the transition instant for the KSP-detector are considered, thus obtaining two analytical performance expressions. The practical effectiveness of the technique is shown by applying the USP-detector to a sequence of 10 ERS-1 SAR images of forest and agricultural areas [C7112]

"Motion compensation for ultra wide band SAR"

The character of ultra wide band (UWB) synthetic aperture radar (SAR) data acquired from an airborne platform invalidates most conventional SAR batch processing algorithms. This paper describes an algorithm that combines wavenumber domain processing with a procedure that enables motion compensation to be applied as a function of target range and azimuth angle. First, data are processed with nominal motion compensation applied, partially focusing the image, then the motion compensation of individual subpatches is refined. The results show that the proposed algorithm is effective in compensating for deviations from a straight flight path, from both a performance and a computational efficiency point of view [C7113]

"Object based analysis of polarimetric SAR data in alpha-entropy-anisotropy decomposition using fuzzy classification by eCognition"

Polarimetric SAR data possess a high potential for classification of the Earth surface. Various publications demonstrate detailed analysis of soil and vegetation properties and characteristics of man made structures on selected examples. To ensure wider application of these developments, integration in commercial systems should be studied. In a first approach, the object based image analysis eCognition is employed on alpha, entropy and anisotropy and the span of fully polarimetric L-band SAR data of the German airborne sensor, E-SAR. We show that by using eCognition land cover classes can be conveniently assigned to the scattering classes and ambiguities can be resolved by geometric and context object features [C7114]

"Applying polarimetric interferometric methods to invert vegetation parameters from SAR-data"

In this paper the use of polarimetric interferometric SAR data for extracting vegetation parameters is studied. For this purpose an inversion algorithm is performed with indoor polarimetric interferometric SAR measurements by applying a simplified scattering model. The performance of the inversion algorithm is investigated by varying the carrier frequency of the PolInSAR system used to acquire the measurement data and by varying the polarimetric base. The results are presented and analyzed concerning the feasibility of the extracted parameters. Additionally sensitivity analysis of the algorithm are undertaken to investigate the stability of the output parameters with respect to initial conditions and inversion progression [C7115]

"The latest development of high resolution imaging for forward looking SAR with multiple receiving antennas"

The paper provides some new developments based on the azimuth synthetic and compressing method to achieve a high azimuth resolution and unambiguous image for forward-looking SAR (F-SAR) with multiple receiving antennas. The first point of the new development is addressed on how to select and optimize the reference functions for azimuth compression. The second new point is addressed on how to configure the parameters such as wavelength and the distances between the receiving antennas. And the effect of these parameters to the practical implementation of F-SAR system will be also discussed. The third point is addressed on the methods to fuse the data from different receiving antennas for solving the left/right azimuth ambiguity [C7116]

"Tree height estimation using an airborne L-band polarimetric interferometric SAR"

Interferometric phase difference among the SAR and trees, composed of trunks, branches, and canopies, provides an information related to trees heights and structures at a given polarization. Vertical polarization (like) is sensitive on the vertical structure and the horizontal pot. (like) for the horizontal one. Cross pol. is sensitive to the inclined branches (inclined cylinder depolarizes the incoming signal). Thus, combination of the polarization based phase measurement might give tree height distribution and the structures when a scattering model that simulates electromagnetic signal interaction with the trees is used. Interferometric sensitivity to the height decreases with slant range and signal to noise ratio and increases with the baseline and the spaceborne sensor has some difficulty. Thus, we used the NASDA-CRL's airborne L-band Polarimetric Interferometric Synthetic Aperture Radar (PISAR), and its acquired polarimetric SAR interferometry datasets. Test site was the Tottori Dune and its surrounding area, where pine trees were planted and the characteristics were well known. Coherence and the phase differences obtained by the interferometric analysis were evaluated. As a result, we could estimate the tree height distribution if the polarimetric SAR images (co-pol and cross-pot) are acquired with larger baselines and smaller slant ranges. Quantitative evaluation is required to relate the phase center differences and the tree types and the polarization combinations [C7117]

"Smoothing speckled SAR images by using maximum homogeneous region filters: an improved approach"

Because the speckle phenomenon corrupts the visibility of SAR images, many techniques have been proposed to improve the data. In this paper, we present an improved first step in the filtering process by using adaptively tailored windows in order to select maximum homogeneous regions. This selection is based on a classical growing region method tuned by the variations of the local estimate of the equivalent number of looks L : dealing with an analytical expression for the variance of L -estimator, the proposed segmentation seems to be more realistic than the initial method [C7118]

"Pulse versus stepped frequency continuous wave modulation for ground penetrating radar"

There has often been debate concerning the relative merits of pulsed ("carrier-less") and stepped frequency continuous wave (SFCW) radars used in ground penetrating radar (GPR) applications. It is sometimes claimed that SFCW has poor time sidelobe performance. In this paper we tease out the definition of resolution and bandwidth, and show that both systems have equivalent resolution and time sidelobe performance if the spectral shapes are properly defined [C7119]

"Application of an optical electric field sensor array for direction of arrival estimation in a borehole"

Dipole array antennas with optical modulators are applied to directional borehole radar. Experimental results of 2-D source location are shown. In the experiments, two dipole antennas are set in a borehole as receivers, and a transmitter is located 0.9 m apart from the borehole. The 2-D MUSIC algorithm modified for array type radar in a borehole is applied to the measured data to estimate the location. Method of moment was used to model the antenna [C7120]

"Quantifying riparian vegetation and stream bank form through the use of airborne laser scanning and digital video data"

A methodology for a cost-effective and detailed assessment of the riparian zone of segments (~30 km) of the Brisbane River and Lockyer Creek in Queensland, Australia is described. Digital terrain models (DTMs) of the stream banks as well as detailed maps of the riparian vegetation type and structure were produced using airborne laser scanner and digital video data. The methodology is applicable to almost any stream or river system worldwide. DTMs of the river banks and adjacent land approximately 100 m from the waters edge were produced from the laser scanner data with an accuracy of 30 cm or better for 80% of the data. Open areas with little understorey or grass cover tended to be accurate to approximately 10 cm. Vegetation maps at a scale of approximately 1:4,000 were produced. Each clump of shrubs or small trees as well as larger individual trees were delineated and attributed with species, weed infestation levels, height and foliage projected cover (FPC) values. The vegetation mapping was completed through classification of the laser data and manual interpretation of the video imagery supported by field verification. The accuracy of the floristic components of the vegetation map is estimated to be approaching 100% although validation has not yet been completed. The spatial accuracy of vegetation polygons delineated is approximately one meter. The laser data as captured for this project allows for maps to be produced at a scale of 1:1000 [C7121]

"Assessment of the coastal maritime environment with airborne mid-wave infrared imagery"

Images acquired with an airborne mid-wave infrared camera over the Netherlands North Sea coast are presented. A number of features are tentatively attributed to a non-thermal origin, and identified as sea bottom topography, current fronts, and tidal channels. Parallels with radar imaging are drawn [C7122]

"Non-iterative GPR imaging through a non-planar air-ground interface"

It is often advantageous to acquire pulse-echo ground penetrating radar (GPR) measurements from antennas that are offset from a non-planar air-ground interface by a non-negligible distance, either because the ground surface is rough, or because measurements must be collected remotely. To compensate for a non-planar air-ground interface, a modification of the plane-to-plane backpropagation algorithm is formulated for surface variations that are relatively smooth with respect to the radar waveform wavelengths. To facilitate this method, a technique for inferring the surface topography from the radar returns is developed. Finally, examples are given to demonstrate the improvement offered over other non-iterative imaging techniques [C7123]

"Simulation of wind speed retrievals from an orbiting bistatic GPS receiver"

Monte Carlo simulations were performed to predict the statistical errors in satellite based wind speed measurements using bistatic GPS signals. A scattering model based upon geometric optics and empirical ocean surface slope variances was used to simulate the mean post-correlation waveform. Synthetic Rayleigh scattered and thermal noise signals were generated. Batches of between 50 and 1000 independent samples were used in these simulations. The surface resolution was set to a radius of approximately 50 km through selection of range and Doppler bins [C7124]

"Textural method to evaluate speckle noise filters based on AR-2D models using P-band radar data"

The performance evaluation of some speckle reduction filters for synthetic aperture radar images is addressed in this work. The criteria used to evaluate the filters performance are based on the improvement of signal to noise ratio and its ability to preserve textural features. The former is achieved through equivalent number of looks

(ENL) computation, while the latter is analyzed by Euclidean distance between AR-2D models, which are estimated from several samples of three land cover classes [C7125]

"Simulation and design of ground-penetrating radar for Mars exploration"

Over the past few years, the interest in exploring Mars has grown, with several missions in the planning stages for the next decade. One motivating theme is the potential of discovering substantial subsurface aqueous reservoirs. This paper outlines the simulation and development of a lightweight, low-power, ground-penetrating radar system intended for the subsurface exploration of Mars [C7126]

"Student Reflected GPS Experiment (SuRGE)"

SuRGE is a low-Earth orbit satellite proposed for an 8-month mission to establish the possibility of spaceborne bistatic GPS remote sensing of ocean surface wind speed/direction, sea surface elevation and soil moisture. Equipped with two GPS reflection instruments and three downward-looking antennas, SuRGE is optimized to validate this measurement technology. Through a nadir facing high-gain (~ 20 db) antenna, a delay and Doppler mapping receiver will continuously record and process GPS reflections. Using this same antenna an analog translator will capture GPS reflections, downconvert the signals and rebroadcast them to properly equipped ground stations where the data can be post-processed to also retrieve the ocean and land surface properties [C7127]

"Synthetic aperture radar for woodland biomass estimation in Australia: an overview"

In response to Australia's requirement for spatial information on greenhouse gas emissions from land use change and forestry, the past and present use and future potential of synthetic aperture radar (SAR) data for quantifying woodland biomass is reviewed [C7128]

"Sub-surface imaging by combining airborne SAR and GPR: application to water detection in arid zones"

We investigate the penetration capabilities of microwaves, particularly L-band, for the mapping of sub-surface moisture. The experiment site is the Pyla dune, a bare sandy area allowing high signal penetration and presenting large subsurface wet structures (paleosols) at varying depths. The SAR penetration depth is estimated by inverting a scattering model for which the sub-surface structure geometric and dielectric properties are determined by the GPR data analysis. We observed a specific phase difference between HH and VV channels, due to a wet layer covered by dry sand. Our results suggest that airborne radar systems in a lower frequency range (P-band) should be able to detect sub-surface moisture down to at least ten meters [C7129]

"Imaging and inversion of buried objects using GPR"

The problem of detection of a buried object is formulated as an electromagnetic inverse scattering problem, using algorithms of increasing complexity. Our first approach consists of a back-projection of the measured data and this imaging algorithm enables the location of the suspicious areas, where further investigation is needed. The second approach is effective inversion, where a domain of interest is selected and an effective permittivity and conductivity inside the domain is computed using either a linear or a nonlinear optimization scheme. In our third approach we aim to invert the spatial distribution of the permittivity and conductivity inside the domain of interest. We employ either a linearized inversion scheme based on the Born approximation or a full non-linearized inverse method based on the contrast source inversion (CSI) method [C7130]

"PacRIM II: a review of AirSAR operations and system performance"

NASA's AirSAR instrument has long been a heavily utilized resource in the international remote sensing community, including, most recently, the very successful PACRIM II mission. In this paper we briefly review the AirSAR system, its expected performance, and quality of data obtained during that mission. We discuss the system hardware calibration methodologies, and present quantitative performance values of radar backscatter and interferometric height errors (random and systematic) from PACRIM II calibration data. We also summarize the various anomalies experienced during the PACRIM II mission, their potential impacts on data quality, and possible solutions to those problems. Finally, in light of these assessments, we discuss near term system enhancements, and expected performance improvements for future AirSAR missions. In particular, we present a redesigned data acquisition system that promises to improve data reliability and system flexibility while increasing data-throughput. One distinct advantage of this system is it will allow us to collect wide-swath high-bandwidth data thereby making data collection more efficient when high bandwidth area imagery is required [C7131]

"An overview of the PACRIM 2000 Airborne Synthetic Aperture Radar (AIRSAR) mission in the Pacific, Australia and Asian region"

PACRIM 2 is a NASA-Australia sponsored science program whose primary purpose is to advance the development and use of polarimetric and interferometric radar in Pacific Rim countries including island nations of the South Pacific, New Zealand, Australia, Papua New Guinea, Indonesia, Malaysia, Cambodia, Philippines, Taiwan, South Korea, Japan and the United States. The deployment of AIRSAR on board NASA's DC-8 research aircraft has provided an opportunity to investigators with diverse backgrounds to collect, analyze and apply state-of-the-art data for Earth science studies in preparation for datasets likely to become available in the near future from satellite and commercial airborne systems [C7132]

"A second order backscatter model for wheat canopies. Formulation and comparison with data"

This paper describes a theoretical study on radar backscatter from a wheat canopy, based on experimental data. The objective is to interpret C-band SAR data provided by ERS and RADARSAT, and the forthcoming ENVISAT. Data from four ERS overpasses during the growth season are interpreted in a first step using 1st order coherent modelling. For fully-developed wheat stands, however, this type of modelling fails to correctly estimate the attenuation of the incident wave within the canopy, resulting in a predicted backscattering coefficient one order of magnitude lower than that observed by SAR system. The main reason for these observed discrepancies between theory and observation is shown to be the assumption of a sparse scatterers in the original model, a condition which does not apply to fully-grown wheat canopies. Accordingly we trace an outline of future modeling work that will be carried out to tackle this problem [C7133]

"Development of multistage procedures for quantifying the biomass, structure and community composition of Australian woodlands using polarimetric radar and optical data"

Focusing on woodlands in Queensland, Australia, this paper outlines a multi-stage approach to quantifying and scaling-up field-based measurements of vegetation structure, biomass and community composition to the landscape. The approach utilises remotely sensed data from a range of instruments (including SAR, hyperspectral and lidar) operating at different spatial and spectral resolutions. The research is anticipated to benefit the calculation of greenhouse gas emissions, conservation of biodiversity, and sustainable utilisation of woodlands in Australia [C7134]

"A vegetation map of the Central Congo basin derived from microwave and optical remote sensing data using a variable resolution classification approach"

A vegetation map of the Central Congo basin was derived from observations performed by several imaging orbital instruments. These are the synthetic aperture radars on board the ESA ERS and the NASDA JERS-1 satellites (C-band and L-band), and the imaging spectrometer VEGETATION on board SPOT 4. The different properties of the composite microwave and optical observations are exploited in a complementary way to achieve the intended thematic goal. In particular the secondary forest formation that cannot be mapped consistently by the radar instruments, is captured by the optical observations. Information fusion is achieved at the level of the classification maps derived independently from the microwave and the optical instruments. The derived classification product is a data structure (dubbed VARMAP) composed of elementary variable size cells holding class labels. The VARMAP supports the generation of thematic products at different scales according to the end use. The paper touches upon some of the challenging issues that arise in the compilation of wide area multi-resolution thematic products, with emphasis on the classification methodology and in particular on novel non-contextual and contextual clustering techniques. The thematic products cover an area of approximately 576 million square kilometres, while keeping a resolution of 200 m for most of the thematic classes. It constitutes therefore an invaluable source of ecological information both for global change studies and for the sustainable management of local resources [C7135]

"Bistatic scattering measurements using near-field scanning"

Accurate characterization of bistatic scattering responses of targets is of practical importance for a number of military and remote sensing applications. In this paper a novel approach for efficient and accurate bistatic scattering pattern measurement of point and distributed targets using a near-field system is demonstrated. This system is equipped with a relatively large XY-table (3 m⁴3 m) and makes use of an HP 8720D vector network analyzer as its transmitter, receiver, and signal processing units. The near-field probe of this system is dual polarized to facilitate polarimetric bistatic scattering measurements. Issues such as calibration procedure for removing systematic errors such as channel imbalances, probe cross-talk, and characterization of radiometric

calibration constants are discussed. Finally the feasibility and the accuracy of the proposed method are demonstrated by measuring the bistatic scattering of point and distributed targets with known bistatic RCS and scattering coefficient and comparing the measured results with the theoretical one [C7136]

"High-resolution tropical forest mapping of the Amazon basin: a novel classification approach for the GRFM radar mosaic"

The high resolution (100 m) Global Rain Forest Mapping (GRFM) radar mosaics, providing a spatially continuous coverage of entire ecosystems, pave the way to improved estimates of bio-physical parameters related to the tropical vegetation. A new classification scheme for producing a high-resolution regional scale forest/non-forest thematic map of the Amazon is proposed. First, a new wavelet multi-resolution decomposition/reconstruction technique is employed to generate an edge-preserving piecewise constant approximation of the original radar image. Second, a two-stage hybrid learning Nearest Multiple-Prototype (NMP) classifier is applied to the reconstructed radar image. The NMP first stage employs a near-optimal vector quantization algorithm called Enhanced Linde-Buzo-Gray (ELBG). During the training phase, ELBG employs only 1% of the whole data set. At the second stage of NMP, vector prototypes are combined into land cover classes of interest by an expert photo-interpreter. In the pattern recognition phase, each pixel is labeled according to the minimum-distance-to-prototype criterion. Experimental results are reported for a thematic problem involving classes: primary forest, degraded forest, non-forest, and water bodies. Validation is performed using land cover maps provided by the Tropical Rain Forest Information Center (TRIFIC) over three test sites featuring different forest cover disturbance patterns. Main results are that the proposed classifier (i) provides a classification accuracy of 87% in forest/non-forest mapping, (ii) is capable of generalizing over the entire data set, and (iii) requires minor user interaction. It is concluded that the proposed approach responds adequately to the requirements of regional scale high-resolution vegetation mapping [C7137]

"The data processing and calibration of the AIRSAR PacRim II mission"

In this paper, we present the results of raw echo data analysis with data error recovery, data processing, and the calibration results of the Jet Propulsion Laboratory's airborne synthetic aperture radar (AIRSAR) for the Pacific Rim II mission. We also present the key elements of the calibration techniques for both polarimetric SAR (POLSAR) and cross-track interferometric SAR (TOPSAR) processed with the AIRSAR Integrated Processor [C7138]

"The fusion of polarimetric AirSAR data with digital aerial photography to improve aquatic macrophyte classification in a tropical reservoir"

Previous attempts to map wetland environments in northern Australia using optical satellite sensors have highlighted the difficulties in mapping the vegetation in these systems using remotely sensed data. Recently, more promising results have been achieved through the use of polarimetric AirSAR obtained during the 1996 PACRIM campaign. The mapping has been conducted on a tropical floodplain containing a reservoir, Fogg Dam, that is characterised by a permanent water supply. A maximum likelihood supervised classification was implemented on four data sets: CIR photography; a Cloude decomposed 9 band AirSAR image; the optimum 3 band combination Cloude decomposed image; and the fused data. The macrophyte classification was improved when utilising AirSAR data, with the 3 band decomposed image yielding the most accurate results [C7139]

"Land cover discrimination in a wetland environment using TopSAR data"

A long-term monitoring system based on remote sensing techniques is currently being developed for the Mary River Catchment in the Northern Territory, Australia. Two of the major environmental issues in this area are saltwater intrusion and weed infestation. An intensive ground based monitoring program provides in situ data for sites in a variety of wetland habitats. TopSAR data have been acquired for the catchment during the PACRIM 2000 campaign to investigate the potential of SAR data for the long term monitoring of this environment. In this paper, the results of a preliminary investigation of the use of TopSAR data in a wetland environment are presented. A land cover classification was derived using a previously developed methodology. This involves the correction of TopSAR data for variation in incidence angle and a maximum likelihood classification based on training areas. The separability of the major land cover classes in this environment, especially weed species was assessed against available ground data with encouraging results. Additionally, the digital elevation data derived from the C-band interferometry are evaluated for their relative accuracy in this environment in comparison to survey data [C7140]

"Investigation of the April 2000 forest fire in Kangwon Province, Korea, using RADARSAT data"

A series of forest fires in Kangwon Province in April 2000 was one of the most serious ones in Korea in recent years. A set of multi-temporal RADARSAT data was used to identify the burned area from the undamaged background forest. First, the backscattering coefficient (σ_0) of SAR image was computed and examined. Depending on the slope of the scattering surface, σ_0 changes slightly (1~3 dB) in burnt areas, and there are consistent trends in the front- and back-slopes. Secondly, multitemporal texture analysis of the RADARSAT data was carried out using Markov random field models. The lognormal multiplicative autoregressive random field (MAR) model was employed to determine the textural attributes of the SAR image. The contextual fusion of multi-temporal changes in textures was evaluated using the fuzzy concept. The performance of texture analysis alone could not give a clear result, but the contextual fusion clarified the severely burned areas [C7141]

"Investigation of ocean waves and currents with PacRim along-track interferometry (ATI)"

The investigation of ocean surface waves and current velocity using conventional synthetic aperture radar techniques is not an easy task. Recently, airborne along-track interferometric synthetic aperture radars (AT-INSARs) have been developed, which employ two antennas, which are physically separated along the platform flight path (along track) direction. The two complex images received from two antennas are combined interferometrically into a single complex ATI image. The phase of the resulting complex image is proportional to the radial component of the ocean surface scatterers velocity. This velocity is the sum of the orbital motion of water particles from the swell, phase velocity of the Bragg waves, and ocean currents. We have tested and investigated the ATI data which was collected by the PacRim-I AIRSAR experiment over the Kohala coast, on the northwest shore of the big island of Hawaii. We investigated the ocean wave and current features and have retrieved dominant ocean wave spectrum. This research is a part of the PACRIM-II ATI related research off Ulsan study area, Korea [C7142]

"Biophysical forest type characterisation in the Colombian Amazon by airborne polarimetric SAR"

Fully polarimetric C-, L- and P- band data were collected by NASA's AirSAR system at the Araracuara test site, a well-surveyed forest reserve in the centre of the Colombian Amazon. The area is characterised by a high diversity of forest types, soil types and flooding conditions. A polarimetric classification technique is used to assess AirSAR's potential for forest structural type mapping and, indirectly, forest biophysical characterisation. Field observations were made at 23 0.1 ha plots to obtain additional quantitative descriptions on forest structure and ground surface conditions, but also to assess the suitability of existing map legends for SAR mapping. It could be shown that a new type of legend leads to physically better interpretable results. A method based on iterated conditional modes is introduced and is shown to yield radar-derived maps with a high level of agreement with existing maps, as well as with the ground observations. The following results may indicate the high level of accuracy obtained: 15 classes can be differentiated, the average radar map agreement ranges from 68-94% (depending on the type of map and approach) and for only a few classes the agreement is less than 70%. The relation between physical forest structure and polarimetric signal properties is studied explicitly using polarimetric decomposition. A new method is introduced based on the decomposition of polarimetric coherence, instead of power. It is based on simple physical descriptions of the wave-object interaction. The accuracy of the complex coherence estimation derived from the complex Wishart distribution. Thus several interesting physical relations between polarimetric signal and forest structure can be revealed. The physical limitations of this technique and its relation with sample size are indicated [C7143]

"Volcano and natural hazard studies from the PacRim 2000 deployment to the W. Pacific"

The 2000 deployment of the NASA DC-8 aircraft to the western Pacific collected large amounts of data of great value to both volcanological and natural hazards research. While data processing is still in its early phase, it is clear that many new analyses in the region will soon be possible. Both the TOPSAR interferometric radar and the MASTER hyperspectral imager are expected to provide significant new insights into numerous targets. This paper reviews some of the science objectives of the deployment, and presents some first-results for selected targets [C7144]

"Comparison of forest parameter estimation techniques using SAR data"

It is important to monitor forests in order to understand the impacts of global climate changes on terrestrial ecosystems. To characterize forest changes, it is useful to parameterize a forest using several parameters, such as biomass, basal area, tree density, tree height, and trunk diameter. These parameters are not independent and some of them are related by allometric equations. Remote sensing data can be used for estimating some forest parameters and others may be retrieved using allometric equations. Many researchers reported algorithms to estimate forest parameters using polarimetric SAR data. However, these algorithms cannot be applied to all types of forests without additional information on the forest type and environmental conditions since radar

measurements depend on the tree structure, incidence angle, and environmental conditions. The backscattering cross section also saturates as forest parameters, such as biomass and the tree height, increase. Forest parameters also have been estimated using SAR interferometry. Specifically, the interferometric correlation coefficient has been used to estimate the angular range of volume scattering. In this paper, we compare and contrast polarimetric and interferometric approaches to understand their advantages and limitations using NASA/JPL AIRSAR data [C7145]

"PACRIM-II AIRSAR/MASTER experiment in Korean (an overview)"

The advantages of the synthetic aperture radar (SAR) have been well known among remote sensing data users since the launching of SEASAT in 1978. However, one of the major limiting factors has been the limited spectral resolution with only a single frequency and single polarization data, even from the most sophisticated space-borne SAR systems today. The AIRSAR system, developed by NASA (JPL) in the late 1980s and became fully operation in 1990, has been a unique and valuable tool for the investigators interested in multiple frequency fully polarimetric SAR experiments. The PACRIM-I experiment in selected Pacific Rim countries in 1996 was a great success and the current PACRIM-II is the successor of PACRIM-I. In view of the new space-borne SAR systems: ENVISAT (ESA) ALOS (Japan) and RADARSAT-II (Canadian Space Agency) planned for launching in the 2002 and 2003 time frames, are all polarimetric SAR systems, and it is not only timely but also essential for any remote sensing community to develop polarimetric SAR application capabilities. The Korean participants in PACRIM-II include both the AIRSAR research teams and MASTER hyperspectral research team. The main objectives of the Korean participation in PACRIM-II include establishment of scientific and engineering knowledge base for the polarimetric SAR technology, training of qualified graduate students, and developments of new polarimetric SAR applications. Science and engineering disciplines participating in the Korean PACRIM-II experiment included agriculture, archeology, land use, forestry, geography, geology, geohydrology, coastal science, oceanography, environmental applications, natural disaster monitoring and disaster management [C7146]

"Combination of two airborne SAR observations (PacRim2 over Japan)"

Two airborne SAR systems observed jointly over Japan in October 2000. JPL's AIRSAR system flew over Japan in the NASA's Pacific Rim Campaign 2000 (PacRim2). At the same time, the Japanese airborne SAR system (Pi-SAR) has observed the same test area. We are aiming at technical and application objectives. The objective of the joint flight includes cross comparison of the capabilities between two systems. Cross calibration of the L-band between Pi-SAR and AIRSAR at the Tottori sand-dune with corner-reflectors. Various applications such as forestry, vegetation, urban environment, volcano, and oceanography using four-band full-polarimetry are possible to investigate using combination of Pi-SAR and AIRSAR data. Digital elevations derived from interferometry of both systems are compared to investigate the errors by influence of penetration depth. Ground-based experiments for this purpose were carried out at the same time in many areas of Japan [C7147]

"On the combination of active and passive measurements in the study of clouds and precipitation"

Presents an approach that combines millimetric radar measurements and radiometer measurements for deriving the water contents of clouds and precipitation and does so within the context of the CloudSat satellite mission [C7148]

"CloudSat radar instrument design and development status"

The Cloud Profiling Radar is the key science instrument for the CloudSat Mission to acquire a global data set of vertical atmospheric cloud structure and its variability. CPR is a 94-GHz nadir-looking radar that measures the power backscattered by clouds as a function of distance from the radar. This sensor is expected to provide cloud measurements at a 500-m vertical resolution and a 1.5-km horizontal resolution. CPR will operate in a short-pulse mode and will yield measurements at a minimum detectable sensitivity of -28 dBZ [C7149]

"Multi-frequency radar Doppler spectrum measurements of cirrus clouds"

Improved remote sensing of cirrus cloud particle size and ice mass content is important for validating and improving cloud microphysical models used in climate research. Previous radar studies have shown that cloud particle size can be derived from non-Rayleigh scattering effects at 95 GHz (W-band) using dual-frequency radar. Typically, non-Rayleigh scattering is quantified by comparing 95 GHz Doppler spectra moments to those collected at a second lower frequency such as 35 GHz (Ka-band). The ratio of 95 GHz reflectivity to that at the lower frequency is referred to as the dual wavelength ratio (DWR). Scattering models relate DWR to median volume diameter or some other characteristic size parameter. However, analysis of full Doppler spectrum measurements collected at 33 GHz and 95 GHz reveals additional information from which vertical air motion and

parameters of the particle size-velocity relationship can be retrieved. During 2000, the U.S. Department of Energy Atmospheric Radiation (DOE-ARM) Program sponsored the 2000 Cloud Intensive Operations Period (2000 Cloud IOP). A number of unique remote and in situ sensors participated in the IOP, including the University of Massachusetts dual-frequency Cloud Profiling Radar System (CPRS). CPRS operates simultaneously at 33 GHz and 95 GHz through a single one-metre-diameter dielectric lens antenna, which ensures beam co-location. Both the Ka-band and W-band recorded fast Fourier transform measurements of the full Doppler spectrum at vertical incidence [C7150]

"X-SAR/SRTM instrument phase error calibration"

Before starting the operational processing of all the acquired X-SAR interferometric SAR data from the SRTM mission, the calibration of deterministic phase errors as far as possible is necessary. Besides the phase errors caused by the shuttle and mast dynamic variations and the position and attitude inaccuracy, there are phase errors originating from the radar instrument itself that may be compensated. Temperature variations and radar parameter changes like gain settings are the major contributors to these phase errors. During the mission we monitored and recorded telemetry data indicating periodic temperature variation along with the orbit, during a data-take and from mission day one to the end. Temperature variations in microwave devices and cables cause a phase variation, which contributes to the overall phase error and degrades the accuracy of the interferometric height measurement. The phase errors have been measured directly, like for the long mast cables, or derived from the calibration tone phase analysis or simply by correcting the known phase to temperature characterization values of the microwave parts with the measured mission temperature data. The lessons learned from that mission and the results of the analysis and the improvement of the height accuracy is presented in this paper [C7151]

"SRTM C-band topographic data: quality assessments and calibration activities"

In February 2000 the Shuttle Radar Topography Mission (SRTM) mapped the topography of the world's landmasses between $\pm 60^\circ$ using radar interferometry. The radar instrument, designed for global coverage, is a two-aperture C-band interferometer, comprising a modified SIR-C C-band system and an added receive antenna mounted at the end of a 60 m deployable boom. Full coverage of the Earth was possible in the 10 day mission by operating the radar in two two-beam ScanSAR modes, one with vertical polarization, and the other with horizontal polarization. The four beams together covered about a 225 km ground swath. An additional X-band interferometer was also flown on the shuttle, with a narrower swath. One of the key components of the interferometer was the Attitude and Orbit Determination Avionics (AODA), comprising a suite of instruments to measure the shuttle position and attitude and the boom tip location relative to the shuttle. Absolute position information was determined from two GPS receivers located on the deployed radar antenna structure. Attitude information was derived from a combination of star tracker and IRU measurements. The boom tip location was determined with an optical target tracker, which measured the angles to several targets located on the tip structure, and an electronic ranging device used to measure the distance to the boom tip [C7152]

"A multi-scale perspective of TRMM-LBA convection"

This study presents an overview of Amazonian convection from the perspective of both ground and satellite instrumentation, with particular emphasis on radar observations of two MCSs (mesoscale convective systems) that occurred during the TRMM-LBA field campaign. The MCSs formed in different meteorological regimes, based on profiles of atmospheric wind and thermodynamic data. The radar analyses show that the MCSs were distinct in terms of kinematic and microphysical characteristics. These observations suggest that the easterly and westerly wind regimes in the southwest Amazon region produce convection with different vertical structure characteristics, similar to regimes elsewhere in the global tropics (e.g., maritime continent) [C7153]

"Tropical Rainfall Measuring Mission algorithm consistency studies"

Results are presented from analysis of the Tropical Rainfall Measuring Mission (TRMM) data from two perspectives: instrument/algorithm consistency checks and comparisons of precipitation retrievals between instruments. The instruments specific to this study are the Precipitation Radar (PR) and the TRMM Microwave Imager (TMI) [C7154]

"Spaceborne radar measurements of vertical rainfall velocity: the non-uniform beam filling considerations"

In this paper, the characteristics of the Doppler power spectrum observed by a spaceborne precipitation radar, under non uniform beam filling (NUBF) conditions is presented, and the expected performance of some standard Doppler estimators and that of a new inversion technique are investigated and compared [C7155]

"Planning for Global Precipitation Measurement"

The Tropical Rainfall Measuring Mission (TRMM) has demonstrated the importance of rain measurements for both the science and the meteorological communities. The National Aeronautics and Space Administration (NASA) has established a Pre-Formulation Office to initiate the planning for Global Precipitation Measurement (GPM), a follow-on to TRMM. GPM is envisioned as a multi-satellite constellation using passive and active microwave sensors to take rainfall measurements every few hours on a global basis. This paper discusses the programmatic status of GPM, and opportunities for international partnership arrangements. In addition, the top-level science requirements as currently identified, and concepts under consideration for obtaining the desired measurements, are briefly discussed. Finally, ground data processing and distribution, and an overview of instrument concepts is addressed [C7156]

"Profiling atmospheric graupel, snow and ice using TRMM's PR and TMI"

Of TRMM's three instantaneous algorithms, the radar-only and combined radar-radiometer algorithms currently produce profiles of liquid rain only. These two algorithms do not attempt to estimate the graupel, snow or other ice distributions. This severely limits their usefulness in estimating the underlying latent heating due to the precipitation. While the radiometer algorithm does produce estimates of liquid rain and undifferentiated solid ice, it does so at a much coarser resolution than the other two and accounts for only a small fraction of the available data. In order to improve the accuracy of TRMM's current estimates of the vertical distribution of the various hydrometeor species, we have refined the combined algorithm to expand its scope and estimate graupel, snow and ice profiles along with the current rain-only estimates, at the resolution of the TRMM radar. The associated uncertainties are automatically quantified and should allow TRMM to produce robust latent heating estimates that have unprecedented accuracy [C7157]

"Monitoring forest dynamics using multi-sensor data in Northeastern China"

To monitor the dynamics of the forests in the vast Northeastern China region, we are developing an operational forest monitoring system using satellite remote sensing data. The major components of this system will include both standard and enhanced methodologies for forest cover mapping and change detection within a geographic information system (GIS) database. To rapidly assess forest conditions over the large geographical expanses in Northeast China, Moderate Resolution Imaging Spectroradiometer (MODIS) data are first used to detect areas of change at the macro scale. Once identified, fine resolution Landsat 7 ETM+, and SAR data, are used to generate fine resolution, micro-scale forest maps to characterize the nature/cause of the change(s). This paper describes the project and presents preliminary results in forest classification and change detection in this region [C7158]

"The use of SRTM data for visualizing the mid-upper reaches of Yangtze River area and dynamic monitoring of land cover changes"

The Mid-Upper Reach section of the Yangtze River in China has the most spectacular landscape in the world, where the Three Gorges is famed for its beautiful scenery and one of the largest hydrological dam projects in the world. In the past, the destruction of natural ecological environment, such as excessive deforestation, resulted in heavy soil erosion and unprecedented floods in 1998. In 1999, however, the central government of China has launched a national-wide project for developing the western part of China. Returning farmland and deforested land to forest and grassland is the main theme of the project. The SRTM data could provide high precision topographic data for visualizing the Mid- and Upper Reaches of the Yangtze River and dynamic monitoring of land-cover changes. We intend to use SRTM data by integrating them with other source remote sensing data for visualization. By using a software package "World Construction Set", a 3D digital "Yangtze River" could be constructed for visualization. The land-cover changes due to the Three Gorge hydrological engineering, deforestation and ecological reconstruction can then be analyzed according to multi-source remotely sensed data [C7159]

"Forest biometrics from ERS and JERS in Michigan"

Operational forest information gathering in the US is moving fast toward the increased use of remote sensing data for a broad variety of applications in the private and public forestry sector. To achieve the best information extraction from remotely sensed data the focus needs to be on combining the strength of active and passive sensor systems. While optical data have demonstrated strength, e.g., in forest species distinction and forest health monitoring questions, the structural composition of forests can be better detected with radar data. The excellent correlation of the radar signals with forest biophysical parameters has been demonstrated through

multi-frequency and multi-polarimetric AIRSAR and SIR-C/X-SAR data and lead to significant knowledge about the specifications for the design of future SAR missions for natural resources mapping and monitoring. To test the capabilities of current SAR missions which provide global coverage, i.e. ERS, JERS and Radarsat, we conducted an intensive study with multi-seasonal ERS and JERS data in the Raco test site in the Upper Peninsula of Michigan. The Raco test site was a SIR-C ecological supersite and intensive ground campaigns were conducted over the course of five years where more than 80 stands were repeatedly sampled, with fixed plots leading to an unprecedented set of ground truth data for research with the SIR-C data. This paper discusses the results of studies on forest parameter retrieval (basal area, height, stem density, biomass) with ERS-1 Cvv and JERS-1 Lhh data for upland pines (jack pine, red pine, white pine). Statistical models (log-log) were generated to measure the correlation between the various forest biophysical parameters and the radar backscatter [C7160]

"Inventory of forest biomass in Brazilian Amazon: a local approach using airborne P-band SAR data"

The objective of this study is to explore the use of airborne P-band SAR polarimetric data, to stratify biomass by primary and secondary vegetation typology. To ensure that different landscapes of Amazon upland forest are represented, a test-site located in the lower Rio Tapajos region, Par  State, was selected. The backscatter signals derived from the complex image of the P-band SAR were correlated with field data obtained from a forest inventory, for different physiognomic-structural aspects of the tropical rainforest. The estimation of above-ground biomass for these forest types was modeled by DBH and total height measurements, including the use of general allometric equations. Statistical regression models were applied to establish the relationship between biomass and radar data at HH, HV and VV polarization. The overall objective of this P-band experiment is to improve the regional monitoring process of biomass dynamics as well as landscape changes, due to human action [C7161]

"Synthetic aperture radar for AGB estimation in Australia's woodlands"

Multi-temporal spatial datasets quantifying above ground biomass (AGB) are required for calculating national, regional and global carbon budgets, due to the large extent and rapidly changing nature of woodlands in Australia. This paper provides an overview of procedures for quantifying and scaling-up estimates of total AGB and component biomass from the tree to the landscape using remote sensing data and focusing on woodlands in Queensland [C7162]

"SRTM X-SAR calibration results"

The paper presents the results of the Shuttle Radar Topography Mission (SRTM) X-band calibration at DLR as of April 2001, the time of writing. While some areas may be subject to further improvement, the overall image will not change significantly. We summarize the various calibration issues, the methods applied and the results obtained. Addressed topics are: Timing calibration, SNR and coherence, motion analysis and instrument phase errors. The qualitative and quantitative effects of the distortions above on the DEM quality are discussed [C7163]

"SRTM/X-SAR: products and processing facility"

The Shuttle Radar Topography Mission SRTM mapped the Earth's surface in two frequencies-C-band and X-band. This paper presents the SRTM/X-SAR products, the processing and archiving facility as well as the procedures on how the products will be made available. The raw data volume stored online within the robot archive of DLR's Remote Sensing Data Center (DM) will be about four TBytes. The processing of this amount of data requires the use of high performance parallel computers scheduled and supervised by a new control and information system. The DEM production line is split into three subsystems: the scanning and screening, the SAR as well as interferometric processing and finally the elevation derivation and mosaicking procedure. An online catalogue accessible via web browser provides all information required for a product selection [C7164]

"SRTM-Mission-cross comparison of X and C band data properties"

In February 2000 the Shuttle Radar Topography Mission (SRTM) mapped large areas of the global landmass using two radar systems operating simultaneously in X- and C-band. The radar mapping instrument consisted of modified versions of the SIR-C C-band and X-band radars flown on the shuttle in 1994. Modifications included a 60 m retractable boom, with C-band and X-band receive-only antennas attached to the boom's end. High accuracy metrology systems were added to measure the shuttle position and attitude, and the position of the boom antennas. The dual apertures at each band form radar interferometers suitable for making high accuracy topographic maps of the Earth. The C-band data set is being processed by JPL for the archives of the US National Imaging and Mapping Agency (NIMA) and the National Aeronautics and Space Administration (NASA).

The X-band data set is processed and distributed at DLR Germany. This paper compares the specific properties of the X- and C-band data sets with respect to global coverage, height accuracy, sensor specific errors, product definition, product format and availability [C7165]

"Topographic change on volcanoes from SRTM and other interferometric radars"

Data from the Shuttle Radar Topographic Mission (SRTM) will permit extensive analysis of volcanoes and volcanic processes in many parts of the world that are infrequently studied by field volcanologists. In preparation for the release of the SRTM data, we have been conducting several studies of volcanoes using digital elevation data collected either from airborne interferometric radars (the TOPSAR and Star-3i systems) or from repeat-pass radar interferometry from the ERS-2 spacecraft. We report here on our results from these preparatory studies in the Philippines, Java and the Galapagos Islands, and suggest how SRTM observations will enhance future work in these areas [C7166]

"A comparison of US Geological Survey seamless elevation models with Shuttle Radar Topography Mission data"

Elevation models produced from Shuttle Radar Topography Mission (SRTM) data will be the most comprehensive, consistently processed, highest resolution topographic dataset ever produced for the Earth's land surface. Many applications that currently use elevation data will benefit from the increased availability of data with higher accuracy, quality, and resolution, especially in poorly mapped areas of the globe. SRTM data will be produced as seamless data, thereby avoiding many of the problems inherent in existing multi-source topographic databases. Serving as precursors to SRTM datasets, the US Geological Survey (USGS) has produced and is distributing seamless elevation datasets that facilitate scientific use of elevation data over large areas. GTOPO30 is a global elevation model with a 30 arc-second resolution (approximately 1-kilometer). The National Elevation Dataset (NED) covers the United States at a resolution of 1 arc-second (approximately 30-meters). Due to their seamless format and broad area coverage, both GTOPO30 and NED represent an advance in the usability of elevation data, but each still includes artifacts from the highly variable source data used to produce them. The consistent source data and processing approach for SRTM data will result in elevation products that will be a significant addition to the current availability of seamless datasets, specifically for many areas outside the US [C7167]

"Radar image study of ocean breaking waves"

In this paper a radar image study of electromagnetic scattering from one dimensional ocean breaking waves is described. Backscatter results are considered for 1-D surfaces which satisfy an impedance boundary condition (IBC). Radar images of single ocean breaking wave profiles are formed through back-projection tomography. Detailed investigations of the images are also provided to clarify major and secondary scattering events as well as the polarization dependence. A ray tracing analysis is performed to predict possible multiple scattering images [C7168]

"A pod-based dual-beam interferometric radar for ocean surface current vector mapping"

The University of Massachusetts is developing a dual-beam along-track interferometer with the objective of obtaining two components of surface velocity sufficient to yield a current vector estimate with a single aircraft pass. The instrument consists of a C-band chirp radar transmitter and a pair of along-track interferometers multiplexed into a common dual-channel receiver. The interferometers are squinted respectively forward and aft of cross-track. An FPGA-based data acquisition system permits real-time pulse integration, and a combined GPS/INS system is incorporated to provide velocity and attitude information. Current plans call for the instrument to be housed in a pod suitable for mounting on the inboard wing pylons of NOAA WP-3D research aircraft with network communication to an operator inside the aircraft [C7169]

"The potential of SAR interferometry for oceanographic measurements: a review"

In this presentation, the basic physics that governs the use of SAR interferometry for the collection of oceanographic measurements is reviewed using the results of previous measurement campaigns as a guide. This review sets the stage for more specific discussions of the usefulness of INSAR ocean measurements to be presented in other talks in the session on 'SAR interferometry for oceanic applications' [C7170]

"Multibaseline ATI-SAR for robust ocean surface velocity estimation in presence of bimodal Doppler spectrum"

Advanced multibaseline along-track synthetic aperture radar interferometry (ATI-SAR) offers the new functionality

of resolution in the Doppler shift domain. This paper investigates the possibility of exploiting multibaseline Doppler resolution capability to produce estimates of ocean surface velocity that are robust to possible bimodal spectra of speckle, arising when both advancing and receding Bragg waves contribute to radar scattering. Bias and inflated variance for unexpected dual Bragg components in conventional ATI are analyzed. Four methods are proposed and analyzed to process multibaseline data for robust estimation, based on Fourier transform or on modern adaptive Capon's filtering. Simulated results show that this multibaseline technique can be effective to produce accurate estimates in the presence of bimodal spectra [C7171]

"Possibilities and limitations of current measurements by airborne and spaceborne along-track interferometric SAR"

With the development of reliable and computationally efficient data processing algorithms and a growing demand for high-resolution synoptic current measurements, along-track synthetic aperture radar interferometry (ATI) is becoming an attractive new technique for oceanic and coastal applications. After a number of successful experiments with airborne interferometric radars, the development of concepts for satellite-based ATI systems has started. We review findings of several authors working in this field, present results of a previous experiment in the German Bight, and discuss possibilities and limitations of current measurements by ATI from space [C7172]

"Initiating the ALOS Kyoto & Carbon Initiative"

The ALOS Kyoto & Carbon Initiative is an international endeavour initialized by NASDA, with the main objective to support information needs raised by the UNFCCC Kyoto Protocol and by the international global carbon cycle science community, by provision of systematic, consistent, repetitive and regional scale data of the global forest cover. Of central importance for the Initiative is a Dedicated Data Acquisition Strategy for the polarimetric Phased Array L-band Synthetic Aperture Radar (PALSAR) sensor onboard the Advanced Land Observation Satellite (ALOS) satellite, which, as a major project output, is foreseen to result in an extensive data archive with consistent time series of dual-polarization (HH/HV) PALSAR data over any given land area on the Earth. Tentative plans for derived data products include regional scale image mosaics, maps of annual forest change, wetland flood distribution/duration, and rice cultivation [C7173]

"Validation of SeaWinds on QuikSCAT cell location"

Increased interest in high resolution ocean wind measurements, as well as excellent past performance, has led to the development of enhanced resolution applications of SeaWinds on QuikSCAT scatterometer data. An essential requirement of this development is the validation of the cell location accuracy-the latitude and longitude of each measurement. This paper discusses two methods of validating measurement location accuracy. One method entails analysis of normalized backscatter coefficients over specific land/ocean boundaries. This method has proven accurate for nominal resolution; it is refined for increasing resolution. Another technique employs the QuikSCAT Calibration Ground Station (CGS). Telemetry-reported cell location is compared to the known location of the CGS. Calibration of measurement location using these techniques reveals the limits of SeaWinds pointing accuracy and precision [C7174]

"A new airborne Earth observing system and its applications"

A new airborne Earth observing system has been developed in China directed by the Expert Group for Information Acquisition and Processing Technology, Hi-tech Research and Development Program of China during the period from 1996 to 2000. The system is composed of 5 remote sensing sensors, including a 128-band modular imaging spectrometer with high spectral resolution, 244-band hyperspectral imaging spectrometer, an area array CCD digital camera with high spatial resolution, a 3 D imager with real time imaging capability, and an L-band SAR with 3m resolution. These sensors are installed onto different aircraft according to their performance, therefore, forming a set of distributive airborne Earth observing system. Since 1998, demonstrative applications study using the system has been conducted, and remote sensing imagery over 10 test sites have been acquired. These data after processing and analysis have achieved very satisfactory application results in rice classification, urban planning, water pollution and desertification monitoring, natural hazards monitoring, mineral exploration and other fields. These demonstrate the roles and application potentials of the new airborne system for Earth observation [C7175]

"Calibration of an airborne along-track interferometric SAR system for accurate measurement of velocities"

One of the applications of synthetic aperture radar in oceanography is the study of ocean surface currents by

airborne along-track interferometric SAR (along-track INSAR, ATI). There is undoubted evidence that ATI enables studies of moving processes and can give an estimate of target velocities. This paper discusses experimental and theoretical concepts for processing ATI data very accurately. Furthermore, it shows that the proposed remote sensing technique for accurate measurement of ATI phase generated from ocean surface currents is promising in terms of accuracy and spatial resolution [C7176]

"The CryoSat Earth Explorer Opportunity Mission-system calibration and mission performance"

The CryoSat Earth Explorer Opportunity Mission will allow an accurate determination of the marine and land ice mass fluxes at a global scale. This paper gives a brief overview on the CryoSat mission and describes the CryoSat. system calibration. Special attention is given to the calibration of the interferometric baseline attitude, which is a novelty with respect to conventional radar altimeter external calibration. The impact of the calibration accuracy on the overall mission performance is shown [C7177]

"Characteristic structures of Typhoon Jelawat observed by OSMI,. TRMM/PR and QuikSCAT"

Typhoon Jelawat, which formed over the tropical Pacific Ocean on August 1, 2000 and made landfall over China on August 10, 2000, was observed by the Korea Multi-purpose Satellite (KOMPSAT-1) Ocean Scanning Multispectral Imager (OSMI), Tropical Rainfall Measuring Mission (TRMM)/Precipitation Radar (PR) and Quick Scatterometer (QuikSCAT). In spite of discontinuous observation, important mesoscale features of the typhoon depending on life cycle were detected prominently. It is possible to distinguish on the OSMI photograph between the eye-wall convection and the stratiform and other convective clouds near the center of Typhoon Jelawat. The TRMM/PR observations show quite clearly the eye-wall convection, stratiform regions, and convective bands. The vertical cross section of rainfall in the genesis stage of Typhoon Jelawat exhibits a circular ring of intense convection surrounding the eye. The mature stage of Typhoon Jelawat consists of a strong rotational circulation with clouds which are well organized about a center of low pressure. The OSMI, TRMM/PR and QuikSCAT measurements presented here agree qualitatively with each other and provide a wealth of information on the structure of Typhoon Jelawat [C7178]

"Gridded hourly text products: a TRMM data reduction approach"

The quantity of satellite observations available for the study of global precipitation is both a blessing and a curse. The sheer volume and complexity of many of the data products makes it difficult for many researchers to use. This paper describes one approach that TRMM used to reduce the volume and complexity of data [C7179]

"Iterative 2D hydrometeor profile retrievals using radar and wideband radiometer observations"

By combining active radar and passive radiometers, the opportunities to accurately estimate hydrometeor and cloud characteristics improve. The authors present a retrieval algorithm that determines an appropriate, though not necessarily unique, estimate of the hydrometeor profiles associated with anvil, convective-and quasistratiform clouds whose forward calculations match the observations within specified error thresholds. These thresholds might be reduced with algorithm improvements. The high frequencies help define the frozen particle size distributions [C7180]

"The continuous tracking of reflectivity data from multi-platform observations using genetic algorithm"

The Tropical Rainfall Measuring Mission (TRMM) satellite was launched with the first space-borne Precipitation Radar (PR) to collect accurate precipitation measurements. To validate the space data set, well-instrumented and calibrated ground validation (GV) sites are established. The paper is a first attempt to merging rainfall estimates from space-borne and ground based radars. We describe a technique to forecast bogus PR data that occurred before and after the passage of the PR over a GV site. Several simulations are performed at 10-minute intervals of GV reflectivity data at Melbourne, Florida on March 9, 1998 from 8:00 am to 9:00 am to track continuously PR reflectivity which overpass the GV site at 8:30 am. We apply genetic algorithms (GAs) to find the needed transformations to produce a time series of PR reflectivity data. The transformations include translation and rotation. By registering the PR original data following the transformed results, the new PR data are presented 20 minutes before and after the overpass. Finally, the statistic analyses are used to compare the relationship between these different sources of reflectivity. The increased correlation between GV and bogus PR reflectivity data demonstrated the potential use of GAs in merging multi-platform remote sensing data [C7181]

"Variability of rain profiles and its impact on microwave precipitation remote sensing as inferred from TRMM PR and TMI"

This paper presents the characteristics of tropical rain profiles observed by the Precipitation Radar (PR) on TRMM satellite. Data for the entire year of 1998 were used in the analysis. The investigation focuses on the following questions: (1) given a surface rainfall rate, what are the typical rain profiles for different cloud and surface types? (2) Given the same surface rainfall rate, what is the variability of tropical rain profiles? How does it affect the microwave brightness temperatures? (3) How is the difference among rain profiles related to cloud development? The objectives of the study are both for better understanding the precipitation physics and for improving microwave remote sensing techniques [C7182]

"First results on ocean wave imaging from the Shuttle Radar Topography Mission"

The paper is a short summary on measurements of directional wave spectra during the Shuttle Radar Topography Mission (SRTM) in Feb. 2000 and mainly demonstrates the possibility to retrieve information on significant wave height and direction of ocean waves. Further information will be available after the data are phase calibrated and delivered to users [C7183]

"Joint along-across track interferometry of ocean waves"

In the framework of the EuroROSE project high resolution ocean wave, wind and current fields were measured at the North Coast of Spain by simultaneous data acquisitions of spaceborne, airborne, and in situ instruments. The objective of the project was to provide a guidance system for ships entering the harbour of Gijon, by monitoring and forecasting wind, waves and currents. This paper presents first results of a new airborne three antenna interferometric synthetic aperture radar (InSAR) system which provides information on both sea surface elevation and motion. The system transmits and receives signals with a combination of three antennas, whereby two are placed along flight direction and the third in across flight direction. This configuration allows, for the first time, to acquire along and across track InSAR data simultaneously. The system was flown in different flight patterns with simultaneous measurements of directional wave spectra, wind and currents fields taken by the HF-radar WERA, the radar based wave monitoring system WaMoSII, the ERS-2 SAR and a waverider buoy [C7184]

"Doppler polarimetry of high resolution radar sea clutter"

The non-stationary nature of high resolution grazing angle X-band radar backscatter of the sea surface is investigated. The temporal behavior is modeled as resulting from a fast and a slow process, and statistical parameters are derived for both processes separately. It is found that the fast process is consistent with an underlying complex Gaussian process, independent of polarization or range resolution, while the slow process is responsible for the spiky nature of the HH backscatter [C7185]

"Optical and physical characterization of European and Indo-Asian pollution plumes with six-wavelength aerosol lidar"

Optical and physical particle properties of two typical pollution plumes emitted from the European continent during the Aerosol Characterization Experiment ACE 2, and from the Indo-Asian continent during INDOEX are characterized from six-wavelength lidar observations. In both cases effective radii were 0.1-0.25 μm . Complex refractive indices were $<1.6-0.0075i$ for the measurement during ACE 2. values $>1.6-0.01i$ were obtained for the INDOEX case. Accordingly the single scattering albedo was 0.95-1.0 at 532 nm in the first case, but 0.8-0.93 in the second case [C7186]

"IGARSS 2001. Scanning the Present and Resolving the Future. Proceedings. IEEE 2001 International Geoscience and Remote Sensing Symposium (Cat. No.01CH37217)"

The following topics were dealt with: soil moisture remote sensing; archaeology; global clouds and aerosols; remote sensing; data compression and coding; SAR; floods and disasters; Antarctica; Arctic; classification, labelling and inference; visualization; advanced sensors and measurement techniques; missions and programs; skin sea surface temperature; agriculture, coastal lakes and rivers; hyperspectral environment; geoscience; Global Change Observation Mission; environmental degradation and Earth systems; student prize paper competition; processing and analysis methods; interferometry; Africa; Radarsat 1; sensor calibration; oceans; Australian applications; aquatic and submerged ecosystems; hyperspectral and multispectral mineral exploration; advanced lidar systems; Tropical Rainfall Mapping Mission; clouds and precipitation data fusion; thermal remote sensing; biophysical modelling; Shuttle Radar Topography Mission; forestry; fires; passive remote sensing; state communities; active remote sensing; snow; local communities; geospatial data fusion; multisource vision; knowledge based systems and unmixing; tropospheric refractivity estimation; radar polarimetry; ocean color; sea ice, snow and glaciers; short wind waves; topography, DTM and cartography; arid zone; rangelands; lidar technology; ozone; clouds and precipitation; inverse problems; spaceborne scatterometers; differential SAR

interferometry; antipersonnel landmine detection and classification; landcover change; air-sea interaction; knowledge based systems and unmixing; Bayesian techniques; data formats, archiving and retrieval; EOS-Terra mission; ocean waves; agriculture; salinity; urban studies; hydrology; soils; geoscience; atmosphere; climate; large scale thematic products; emission and scattering; image processing and enhancement; GPS reflection; electromagnetics; AIRSAR and PACRIM; synthetic aperture techniques; processing systems; policy, education and societal issues; GPR; ocean winds; disaster assessment; target detection; environmental degradation; coastal landscapes and fisheries; biophysical modelling; neural networks, expert system systems; inverse problems [C7187]

"Performance of a 1319 nm laser radar using RF pulse compression"

Spaceborne lidars have been shown to provide data on surface elevation, vegetation canopy heights, and aerosol characteristics. Satellites carrying lidars for measuring ice sheet surface elevation and vegetation canopy heights are scheduled to be launched in the next few years. To achieve the necessary resolution and sensitivity, lidars on these satellites will use short duration, high peak power transmit pulses. Because of their high peak power, these lidars must be operated with a low pulse repetition frequency (PRF). The high peak power operation results in limited lidar lifetime and the low PRF provides insufficient spatial samples along the satellite track. To overcome these limitations of high peak power systems, at the University of Kansas we have developed a low peak power laser radar using modern RF techniques and fiber-optic technologies developed in support of the communication industry. We used RF pulse compression to achieve the sensitivity needed for spaceborne applications and have increased the PRF to provide more dense sampling. We have developed and reported preliminary results of a fiber-optic-based, laser radar that applies RF pulse compression and digital signal processing techniques to improve receiver sensitivity and range measurement capabilities. With our improved super-heterodyne receiver, we have achieved receiver sensitivities below -100 dBm with transmit pulses with 40 μ s duration, 260 MHz bandwidth, and a 4 kHz PRF. These parameters are sufficient for altimeter operation from a satellite. We have modified the receiver architecture, performed detailed system simulations, developed a new data acquisition system, and conducted laboratory tests to verify simulation results. We present the system design, results of performance analyses and tests. We also show details on the two-stage down-conversion receiver with envelope detection and present issues concerning telescope-to-optical fiber coupling [C7188]

"Estimating vegetation cover and soil roughness in semi-arid regions from multitemporal dual-frequency SAR data"

An experiment aimed at evaluating the potential of synthetic aperture radar (SAR) in monitoring hydrological parameters in semi-desert areas was carried out within the framework of the EC project FLAUBERT (FLood in Arid Units By Earth Remote Techniques). In spite of the very low changes in space and time, the analysis of backscattering and interferometric coherence showed the capability of SAR to separate a few land classes and to point out yearly variations due to vegetation cycles [C7189]

"The measurement of salinity from space: sensor concept"

Salinity in the open ocean is important for understanding ocean dynamics and for modeling energy exchange with the atmosphere. The potential exists for obtaining global coverage of sea surface salinity using a microwave sensor in space operating at L-band (1.4 GHz). Work is currently underway at NASA's Goddard Space Flight Center and the Jet Propulsion Laboratory to define a sensor to make this measurement from space. The goal is to achieve spatial resolution on the order of 100 km with a revisit time of 14 days or less and a calibration accuracy equivalent to 0.2 psu. It is planned to combine the radiometer with a radar to help correct for surface roughness. It is believed that such a sensor system can be developed within the confines of a future Earth Sensor System Pathfinder (ESSP) mission [C7190]

"Use of airborne scanning lidar and large scale photography within a strategic forest inventory and monitoring framework"

Australia has approximately 160 million hectares of forest and woodland, 70% of which is under private ownership. Increasing commitments in relation to climate change and sustainable forest management, particularly in the private sector, is creating an environment where rapid, cost-effective assessment and monitoring of forests is becoming critical. Using an example from Injune, central Queensland, this paper provides an overview of the potential use of both airborne scanning lidar and large scale photography as sampling tools. The capability of these sensors for extending and optimising ground-truth data and, in turn, maximising the potential of other forms of remote sensing through improved calibration and validation, is outlined [C7191]

"DTM extraction in urban areas: a detailed comparison of methodologies, algorithms and results"

In this paper we propose a comparison of the most important digital terrain model extraction techniques proposed in urban environments. In particular, we focus here on those based on digital signal processing applied to LIDAR data and on stereo photogrammetry. To this aim, we start from a data set composed by LIDAR and photo acquisitions over the town of Pavia, Northern Italy, and apply suitable DTM algorithms. Our investigation aims to provide a way to exploit both data sets. We were able to provide a complete DTM of Pavia with a very small degradation of the original measurements, as shown by a comparison with extremely precise ground control points [C7192]

"Estimating snow accumulation on Greenland from SSM/I radiometer data"

This paper discusses a new method for determining snow accumulation on the Greenland ice sheet using passive radiometer data. The algorithm exploits high spatial correlation observed in brightness temperatures for adjacent pixels from SSM/I data to iteratively remove the effect of surface temperature and emissivity variation. This processed data reveals an exponential change in brightness temperature with time, with the time constant of this exponential proportional to the accumulation rate. Representative accumulation rates obtained using the method are shown to agree well with existing accumulation maps [C7193]

"A study of Greenland ice sheet elevation change by using satellite altimeter data"

ERS-1 satellite radar altimeter measurements show that from 1992 to 1996 the average Greenland ice sheet elevation change is -1.7 ± 0.6 cm/year. The spatial distribution of ice sheet elevation change reveals its relationship with the areas of maximum and minimum accumulation rates, the boundaries of drainage basins and snow and snow-firn zones. The elevation reduction is typical of the coastal regions where the phenomenon of climate warming can be revealed most evidently. It is shown that utilization in ice sheet elevation change studies the ERS altimeter ocean-mode data is not warrantable. Different threshold retracking corrections should be applied for various ice sheet areas. Similar features in the spatial distribution of the Greenland ice sheet elevation change derived from ERS-1 and Seasat 4 Geosat are observed [C7194]

"Multi-annual changes in microwave backscatter over the Greenland ice sheet"

Changes in the location of key ice facies/zones on the Greenland ice sheet are considered key indicators of global climate change. Microwave scatterometers are effective tools for monitoring these changes. Measurements for three Ku-band scatterometers, SASS (1978), NSCAT (1996), and SeaWinds (1999-present), span a 23-year period. While the ERS scatterometer (C-band) offers a continuous 9-year dataset (1992-2000). Using the SIR algorithm to produce σ^0 images, the measurements made by these sensors over Greenland are compared. We find an increase in σ^0 along the southern border between the dry snow zone and percolation zone, and a decrease for C-band measurements along the northern portions of this boundary [C7195]

"Applications of airborne LiDAR mapping in glacierised mountainous terrain"

Discusses logistics and applications of the first complete airborne scanning LiDAR survey of a glacierised mountain basin. The survey was conducted over a 2546 km area with ground height variation from 1800 m asl to 3400 m asl. The resolution of survey points on the ground varied from 1 per sq metre to around 1 per 4 sq metres, depending on elevation. Correspondence from swath to swath is very good despite the extreme nature of the topography and individual ground laser heights are accurate to within 20 cm. Glaciological applications for the high-resolution digital elevation data are outlined. Special attention is paid to radiation loading model-scaling issues [C7196]

"A novel high resolution, wide swath SAR system"

A novel SAR system architecture is presented. It allows to combine a high azimuth resolution with a wide imaged swath width. The architecture and the required on board signal processing is described. Finally two examples systems and their image performance are presented [C7197]

"Case-study on the use of microwave sensors for cloud detection over Tuscany"

The present work empirically deals with the challenging problem of the integration of data obtained from passive and active microwave sources, in order to develop procedures to suitably calibrate and validate satellite-based passive microwave rainfall algorithms by means of multiparameter radar information over midlatitude areas. In particular it addresses the problems due to the time interval between radar and radiometer acquisitions and to the different view geometry of the sensors. A statistical image processing technique is utilised in order to

navigate data, reducing effects due to cloud shape change and motion during the time lag. Results show that time lag and geometry differences effects reduction can significantly improve correlation allowing to better investigate the inner cloud structure [C7198]

"Millimeter-wave observations of precipitation using AMSU on the NOAA-15 satellite"

Promising agreement over land and sea has been obtained between NEXRAD 3-GHz radar observations of precipitation rate and retrievals based on simultaneous passive observations at 50-191 GHz from the Advanced Microwave Sounding Unit (AMSU) on the NOAA-15 meteorological satellite. This paper extends prior work by increasing the number of inputs into the feed-forward neural network used for estimating precipitation. It also is based on a much larger and more representative training and evaluation data set that spans rain rates up to 80 mm/h and incorporates 22 rainy orbits distributed over a year [C7199]

"Shallow sea tides estimated using T/P data and adjoint assimilation model"

Shallow sea tide estimated using TOPEX/Poseidon (T/P) data is presented. Twenty-one tidal constituents including shallow sea constituents MN4, M4, MS4, 2MS6, and M6 are estimated along the T/P track. A time-domain adjoint assimilation model was used in order to give the tide in Bohai Sea and Yellow Sea [C7200]

"Statistical sensitivity analysis of a vegetation canopy microwave scattering model based on an experiment design method"

A sensitivity analysis (SA) based on an experimental design is used to locate the most relevant input parameters of the scattering model MIMICS. The study relies on experimental data acquired during an active truck-mounted microwave experiment in the framework of the French ERABLE project. The results of SA corroborate the experimental ones and enable us to propose a hierarchical classification of the input parameters in terms of their relevance [C7201]

"Two-dimensional rain mapping using transmissions from geostationary satellites"

This paper proposes a rain mapping method using a computerized tomography (CT) technique. Since satellite transmissions at Ku-band frequency suffer from attenuation due to intervening rain. The propagation data along several paths toward satellites geostationed at different longitudes are analyzed to reconstruct the two-dimensional rain distribution by a CT technique. A brief description is given on the approach and the results of simple numerical tests are described to show the feasibility of the proposed method [C7202]

"Lidar ozone measurements in the marine and terrestrial atmosphere from the ground to the tropopause"

A conventional differential-absorption lidar and a Raman lidar have been used for ozone concentration profiling. Measurements over land show such unusual phenomena as a nighttime ozone maximum over Munich, a mass of ozone creeping up a valley to the top of Mount Schauinsland, and a polar stratospheric cloud as far south its Geesthacht, located 54°N, with corresponding reduction of the ozone columnar density. Ozone along a 30°W transect over the Atlantic Ocean is correlated with wind speed when the wind blows from the continents, but anticorrelated when the air masses are essentially oceanic in origin. A conspicuous absence of ozone in cirrus clouds needs further investigation as to whether the effect is advective or reactive in nature; for this purpose a new technique is proposed [C7203]

"Laser altimetry and lidar from ICESat/GLAS"

In December 2001, a spaceborne laser altimeter will be launched into a near-polar, near-circular orbit to measure changes in polar ice-sheet topography, as well as along-track land and ocean topography. The ice-sheet measurements will address fundamental questions about the growth or shrinkage of the polar ice-sheets and their contribution to current and future global sea level rise or fall. The measurements, which also include cloud heights, will be made using a 1064 nm laser pulse. An atmospheric channel, using a 532 nm pulse, will measure aerosol vertical profiles and other atmospheric properties [C7204]

"Lidar applications in regional air quality studies"

During air quality studies in the United States, NOAA's Environmental Technology Laboratory (ETL) deployed three lidars to improve characterization of the regional environment. An airborne ozone DIAL system mapped out 3-dimensional profiles of ozone and aerosol, enabling tracking of urban plumes, identification of the residual layer, and specification of ozone production efficiency and dispersion associated with power plant plumes. At

surface sites, Doppler and ozone DIAL systems characterized the time evolution of wind profiles, turbulence, vertical mixing, horizontal transport from low level flows, and effects of transient events such as gust front passages. The lidar information greatly complemented observations from airborne and surface in situ sensors, and will be critical for improving understanding and modeling of regional air quality events [C7205]

"A next-generation ground-based sensor for tropospheric ozone"

Excessive concentrations of ground-level ozone present a public health hazard in polluted environments. The Environmental Protection Agency currently rates air quality problems in several metropolitan areas in the United States as either serious or severe. These cities are required to have plans in place for improving air quality. In general, they also attempt to forecast peak ground-level ozone concentrations at the start of each day during the summer months. Air quality improvement strategies and daily forecasts are based on models in which both the science and the input data are very limited. The models are three-dimensional, but conventional ground-based ozone monitoring networks are only two-dimensional. For this reason, we are developing an unattended ozone lidar to be manufactured in multiple units and deployed at several locations throughout a metropolitan region. The lidars will add the third dimension to the data and enable researchers to fully understand ground level ozone concentrations. In this paper we describe the design considerations for the lidars [C7206]

"An airborne radar system for high-resolution mapping of internal layers"

Accumulation rate is a key variable in assessing the mass balance of polar ice sheets. An improved knowledge of the mass balance of polar ice sheets is needed to determine their role in current and future sea level rise. Existing accumulation maps, derived from sparsely distributed ice cores and pits, contain accumulation rate errors as large as 20% in certain areas. Remote sensing methods to complement and supplement in situ measurements are required to generate improved accumulation maps. For this reason we have been investigating the use of high-resolution radars for mapping of near-surface internal layers and generating continuous profiles of the dated layers in the ice sheet (isochrones). We successfully mapped isochrones within 2 m of those in an ice core up to a depth of 280 m at the North Greenland Ice core Project (NGRIP) ice camp during the 1998 and 1999 field seasons using a 170-2,000 MHz frequency modulated continuous wave (FM-CW) radar. We described the system and reported results of our experiments in previous IGARSS meetings [Kanagaratnam et al. 1999, 2000]. Recently we performed detailed analysis of the data collected from these experiments and determined the frequency response of reflections from the internal layers. The results showed the optimum frequency range for monitoring near-surface layers is between 500 and 1000 MHz. Based on these results we are developing a 600-900 MHz coherent airborne radar for high-resolution mapping of the internal layers in the Greenland ice sheet. We designed this system to operate in different modes: simple pulse, chirped pulse, step-frequency, and FM-CW. We have also developed a digital data acquisition system to collect and process data. We designed this system such that it can operate in an undersampling mode to digitize the received signal directly without down conversion. In this paper we present results of data analysis and detailed design of the airborne radar [C7207]

"Multiscale adaptive estimation for fusing interferometric radar and laser altimeter data"

Interferometric synthetic aperture radar (INSAR) data are fused with laser altimeter (LIDAR) data to produce improved estimates of bare-surface topography and vegetation heights. The data from both sensors are first transformed into estimates of surface elevations and vegetation heights to obtain linear measurement-state relations. A spatially-adaptive multiscale estimation framework is then used to combine the data, which were acquired at different resolutions. The estimation is performed in scale and space via a set of Kalman filters. It yields better error characteristics than the nonadaptive multiscale filter and accommodates non-stationarity in the image data [C7208]

"Fuzzy pyramidal joint classification of SIR-C and AIRSAR data"

In this paper, we exploit the possibility to have SAR data with different ground resolution to characterize different fusion methodologies. We consider fuzzy algorithms, based on the fuzzy-c-means procedure, and applied to a data set of AIRSAR and SIR C-band SAR images. First, we consider a pyramidal approach, starting from coarse data analysis and using the higher details to add precision to the classification map. Then, a spatial enhancement algorithm has been implemented to provide a guess of the details of the coarse resolution data. The second approach allows obtaining better classification results as long as we consider only the soil classes that it is possible to identify in both the low and high resolution data. No serious advantage is instead found for the investigated procedure when a more detailed classification map is searched [C7209]

"Estimating forest variables from fusion of SAR and TM data and analytical scattering and

reflectance models"

A method for simultaneous integration of synthetic aperture radar (SAR) and optical remote sensing data in an estimation algorithm is presented which results in estimates of foliage mass over a larger range of values and more accurately than would be possible with either data type alone. The improved estimates are expected to result in more accurate calculation of ecosystem exchange from biogeochemistry models. The solution uses simplified closed-form models of scattering and reflectance derived from more complicated numerical models in a nonlinear estimation algorithm. Results are compared with available field measurements for 25 reference plots. A thorough error analysis is carried out to characterize the statistical accuracy of the estimation results with respect to errors in the microwave scattering and optical reflectance models. The foliage mass data are ultimately to be used to derive leaf area index (LAI), an essential driving variable for forest process models [C7210]

"Estimating refractivity from land clutter: another look at a simple approach"

In a previous report, two methods of estimating refractivity from land clutter were discussed where one of the methods used a parabolic equation (PE) algorithm combined with a least squares technique, and the other used a ray trace algorithm combined with a rank correlation scheme (Barrios 2000). Based on simulations alone, both of these methods were fairly successful in estimating a tri-linear representation of a radiosonde-measured refractivity profile over two mixed land-sea paths. However, each method appears to favor a certain type of land topography. The PE/least-squares method performed well over land paths characterized by steep peaks and valleys and the ray trace/correlation method performed well over land paths which were not sharply varying in elevation. This latter method offers a more attractive alternative to the conventional least-squares technique because of its execution speed and simplicity, therefore we take a more extensive look at this technique [C7211]

"Island wake impact on evaporation duct height and sea clutter in the lee of Kauai"

Perturbed flow over and around an island can produce leeside vortices and a long wake region of reduced wind speed and altered thermodynamic structure that impacts the evaporation duct height field and directional wave spectra, both of which impact radar sea clutter returns. In this paper, predicted radar clutter is constructed by using evaporation duct height and wind fields from a mesoscale model along with appropriate sea clutter and electromagnetic propagation models. This predicted radar clutter is compared to shipboard observations of radar clutter taken off the leeward side of Kauai, in December 1999 [C7212]

"Compensation of forest canopy effects in the estimation of snow covered area from SAR data"

As spaceborne SAR is used for monitoring the snow cover during the spring melt period, temporal changes in backscattering properties of forest cover disturb the quantitative estimation of snow covered area (SCA). This paper introduces an algorithm that eliminates the related disturbances in SCA estimation. The algorithm is developed based on the Helsinki University of Technology (HUT) forest backscattering model. An extensive multitemporal ERS-2 C-band SAR data set from Northern Finland is used for validating the backscattering model and for testing the SCA estimation algorithm. Comparison of SCA estimation results with available ground truth data for SCA indicates a good performance and a significant improvement when compared with the estimates produced by commonly used linear interpolation algorithms [C7213]

"Identification of the tropical forest in Brazilian Amazon based on the DEM difference from P and X bands interferometric data"

In this paper the difference between digital elevation models, derived from P and X bands interferometric data, is used as a main information to identify land cover classes. The radar data used in this work were collected on September of 2000 over Tapajos National Forest, which is a region of Brazilian Amazon, Para State. The SAR images were acquired from an airborne polarimetric system, AeS-1, that could provide P and X bands interferometric data. During the radar mission ground survey was carried out, and the georeferenced information about the forest typology were acquired, and used as a support for the thematic identification and calibration of the remoted sensing data. The X-band DEM was generated using one-pass interferometric data and the P-band DEM was generated using two-pass interferometric data. The grid of the DEMs has a spatial resolution of 2.5 meters. Images from P and X bands and coherence maps were also used in order to improve the classification. Supervised and unsupervised classifications techniques are used and their results are shown [C7214]

"Snow signature with the ERS2 radar altimeter"

Radar altimeter data from ERS2 satellite have been processed across The Northern Great Plains of U.S for an entire snow season and compared to in-situ measurements. We show that cover strongly decreases the variability and the intensity of the backscattering coefficient. The decrease in backscatter can be related to snow

depth [C7215]

"Fusion of SAR and SPOT image data for crop mapping"

This paper describes image processing and fusion for land cover mapping focusing on mapping agricultural crops. To achieve a frequent update of crop maps, classification and segmentation algorithms were applied to 13 test cases. Reference data for classification were available from 302 crop fields, and reference data for segmentation from vector data of field boundaries. The reference vector dataset was enhanced by means of visual image interpretation. Radiometric accuracy of segmentation results was evaluated using ratio images. These studies show synergy of radar and optical imagery, with dependence on the sequence of pre-processing and processing techniques in the mapping procedure. Classification accuracy of crop maps based on synthetic aperture radar (SAR), visible-infrared (VIR) and fused imagery reached 82%, 92% and 76% respectively. We conclude that majority based object classification does not improve significantly the overall accuracy. Subsets resulting from the optimum index factor (OIF) algorithm proved slightly better than principal component analysis (PCA) fusion and intensity-hue-saturation (IHS) colour transformation proved worse [C7216]

"Cluster-based feature extraction and data fusion in the wavelet domain"

This paper concentrates on a linear feature extraction method for neural network classifiers. The considered feature extraction method is based on discrete wavelet transformations (DWTs) and a cluster-based procedure, i.e., cluster-based feature extraction of the wavelet coefficients of remote sensing and geographic data is considered. The cluster-based feature extraction is a preprocessing routine that computes feature-vectors to group the wavelet coefficients in an unsupervised way. These feature-vectors are then used as a mask or a filter for the selection of representative wavelet coefficients that are used to train the neural network classifiers. In experiments, the proposed feature extraction methods performed well in neural networks classifications of multisource remote sensing and geographic data [C7217]

"A numerical simulation of estimating snow wetness with ASAR"

In hydrological investigations, modeling and forecasting of snow melt runoff requires timely information about snow properties and their spatial variability. The liquid water content in snow pack is an important parameter. A fully polarimetric C-band synthetic aperture radar (SAR) has the capability to estimate the free liquid water content-snow wetness-in the top layer of a snow pack quantitatively as demonstrated in Shi and Dozier 1995). The objective of this study is to develop an algorithm under the configuration of ASAR's C-band dual-copolarization measurements, e.g., HH and VV polarization. We have established a model-simulated C-band data-base by using multi-scattering model. The data-base covers the most possible wet snow physical properties and surface roughness conditions. Using this data-base, an inversion algorithm has been developed for using C-band dual-copolarization measurements. The newly developed algorithm mainly involved two steps: 1) decomposition of the surface and volume scattering signals, and 2) then using each scattering component to estimate snow wetness [C7218]

"Estimation of snow hydrological parameters using single-parameter, multi-temporal SAR images"

The objective of this study is to develop an algorithm for estimating snow parameter distributions using multi-temporal synthetic aperture radar (SAR) data and a numerical scattering model. Simultaneous Radarsat SAR observations were carried out during the two winter seasons. The study area is a part of the Hokuriku District of Japan that is well known for having wet snow from the beginning of the winter season. We compared the results of simulated backscattering coefficients with the ground-truth data and observed backscattering coefficients. Since the agreement was good, we demonstrated the possibility of estimating roughness distributions of soil surface using images acquired just before the snowfall with an assumption. Furthermore, we estimated the distributions of snow depth and roughness using images after a snowfall and estimated soil roughness distributions [C7219]

"The depolarization of radar backscatter from rough surfaces due to surface roughness and slopes"

In this study, the depolarization of radar backscatter from rough surfaces is investigated. Short scale surface roughness and long scale surface slopes are shown to contribute towards the depolarization of the co-polarized and cross-polarized components. The study investigates the effects of both these surface parameters on the correlation between the different polarizations. The calculations show that the copolarized coherence, ρ_{hhvv} , is most sensitive to changes in roughness and the circularly polarized coherence, ρ_{rlll} , is sensitive to long scale surface slopes. Results appear to be consistent with measurements from controlled laboratory measurements of backscatter from rough surfaces [C7220]

"Ocean surface salinity remote sensing with the JPL Passive/Active L-/S-band (PALS) microwave instrument"

Describes the measurements acquired by the aircraft Passive/Active L-/S-band (PALS) instrument from two field campaigns in 1999 and 2000. These measurements were in support of the development of ocean surface salinity remote sensing techniques for the future Aquarius space mission. The 2000 measurements demonstrated the aircraft radiometer stability of ± 0.3 K over time periods of 30 minutes with a salinity measurement accuracy of 0.2 PSS (Practical Salinity Scale or parts per thousand) [C7221]

"Optimal polarimetric decomposition variables-non-linear dimensionality reduction"

Polarimetric SAR image analysis often depends upon proper identification of the relevant degrees of freedom for the problem at hand. Employing physical models of particular scattering processes simplifies identification of the appropriate polarimetric variables. Determining how well variables chosen on the basis of a particular model describe the region of applicability of that model is difficult. Here we attempt in a model independent manner to identify "optimal" variables to both segment an image and highlight the variation within each segment. The method presently employed is non-linear dimensionality reduction [C7222]

"Maximum a posteriori refractivity estimation from radar clutter using a Markov model for microwave propagation"

This paper addresses the problem of estimating range-varying parameters of the height-dependent index of refraction over the sea surface in order to predict ducted microwave propagation loss. Refractivity estimation is performed using a Markov model for microwave radar clutter returns from the sea surface. Specifically, the parabolic approximation for numerical solution of the wave equation is used to formulate the problem within a non-linear recursive Bayesian state estimation framework. Solution for the maximum a posteriori (MAP) sequence of range-varying refractivity parameters, given log-amplitude clutter versus range data, is achieved using a technique based on the Viterbi algorithm. Simulation and real data results based on experiments performed off Wallops Island, Virginia are presented which quantify the technique's ability to predict propagation loss at 3 GHz [C7223]

"A new method for characterizing depolarization effects in radar and optical remote sensing"

In this paper we consider a new approach to the parameterization of depolarization effects in electromagnetic scattering. We define a unitary reduction operator, which is used to generate an $N-1$ dimensional representation of depolarization in an N dimensional scattering problem. We illustrate the application of this technique to polarimetric radar backscatter from random media with various symmetries [C7224]

"Remote sensing of surface roughness using polarimetric SAR data"

The circular polarization coherence, $pRLL$, is investigated in this paper as a measure of terrain surface roughness. The studies utilized data collected 1) from dielectric surfaces in an anechoic chamber and, 2) from a larger desert test site using P-, L-, and C-band NASA/JPL AIRSAR data. These experimental results, and supporting theory, indicate a sensitive decorrelation of $|pRLL|$ with increasing surface roughness k_s . Practical measurement issues and a performance comparison relative to the polarimetric anisotropy A are discussed [C7225]

"Interpreting off-diagonal terms in polarimetric coherency matrix"

This paper addresses interpretation of off-diagonal terms in the coherency matrix of polarimetric SAR data. The off-diagonal terms, especially the correlations between copolarization and cross-polarization are frequently ignored in many studies. We will show that this misconception will introduce errors, especially when imaging rugged terrain areas [C7226]

"Target-aided compression of SAR imagery for transmission over noisy wireless channels"

We present a target-aided, error-resilient system for coding synthetic aperture radar (SAR) imagery, whereby regions of interest and background information are coded independently of each other. A multiresolution constant-false-alarm-rate (CFAR) detection scheme is utilized to discriminate between target regions and natural clutter. Based upon the detected target regions, we apply less compression to targets, and more compression to background data. This methodology preserves relevant features of targets for further analysis, and preserves the background only to the extent of providing contextual information. The resilience to channel errors is obtained

without the use of channel coding or error concealment techniques. The robust nature of the coder eliminates the appearance of impulsive channel-error-induced artifacts in the decoded imagery, while increasing the security level of the encoded bit stream. The proposed coder is evaluated in terms of target detection performance on the decoded SAR image for a wide variety of channel conditions and encoding bit rates. The resulting system dramatically reduces the bandwidth requirements of the digital SAR imagery, and is shown to provide outstanding performance in adverse channel conditions. [C7227]

СПИСОК ЛИТЕРАТУРЫ

- C5963.** Csatho B. Investigating long-term behavior of Greenland outlet glaciers using high resolution satellite imagery. / Csatho B., Schenk T., Sung Woong Shin, van der Veen C.J. // 2002. IGARSS '02. 2002 IEEE International Geoscience and Remote Sensing Symposium. 24-28 June 2002. - Vol. 2. - P. 1047-1050. ↑
- C5964.** Kanagaratnam P. A wideband radar for mapping internal layers in the polar icesheets for estimating accumulation rate. / Kanagaratnam P., Gogineni S., Plummer T., Parthasarathy B. // 2002. IGARSS '02. 2002 IEEE International Geoscience and Remote Sensing Symposium. 24-28 June 2002. - Vol. 2. - P. 1051-1053. ↑
- C5965.** Qong M. A new scattering enhancement scheme for polarimetric SAR images based on covariance matrix. 2002. IGARSS '02. 2002 IEEE International Geoscience and Remote Sensing Symposium. 2002. - Vol. 2. - P. 1023-1025. ↑
- C5966.** Kasilingam D. A technique for removing vegetation bias from polarimetric SAR interferometry. / Kasilingam D., Nomula M., Cloude S. // 2002. IGARSS '02. 2002 IEEE International Geoscience and Remote Sensing Symposium. 2002. - Vol. 2. - P. 1017-1019. ↑
- C5967.** Tabb M. An extended model for characterizing vegetation canopies using polarimetric SAR interferometry. / Tabb M., Flynn T., Carande R. // 2002. IGARSS '02. 2002 IEEE International Geoscience and Remote Sensing Symposium. 2002. - Vol. 2. - P. 1020-1022. ↑
- C5968.** McNeill S.J. Forest biomass estimation in New Zealand using full-polarisation SAR imagery. / McNeill S.J., Belliss S.E. // 2002. IGARSS '02. 2002 IEEE International Geoscience and Remote Sensing Symposium. 24-28 June 2002. - Vol. 2. - P. 1079-1081. ↑
- C5969.** Alpers W. Generation of secondary internal waves by the interaction of internal solitary waves with an underwater bank. / Alpers W., Vlasenko V. // 2002. IGARSS '02. 2002 IEEE International Geoscience and Remote Sensing Symposium. 24-28 June 2002. - Vol. 2. - P. 1105-1107. ↑
- C5970.** Guoqing Sun. Characterization of forest recovery from fire using Landsat and SAR data. / Guoqing Sun, Rocchio L., Masek J., Williams D., Ranson K.J. // 2002. IGARSS '02. 2002 IEEE International Geoscience and Remote Sensing Symposium. 24-28 June 2002. - Vol. 2. - P. 1076-1078. ↑
- C5971.** Mohr J.J. Glacier surface velocity measurements from radar interferometry and the principle of mass conservation. / Mohr J.J., Reeh N. // 2002. IGARSS '02. 2002 IEEE International Geoscience and Remote Sensing Symposium. 24-28 June 2002. - Vol. 2. - P. 1054-1056. ↑
- C5972.** Pietroniro A. A multi-sensor remote sensing approach for monitoring large wetland complexes in northern Canada. / Pietroniro A., Toyra J. // 2002. IGARSS '02. 2002 IEEE International Geoscience and Remote Sensing Symposium. 24-28 June 2002. - Vol. 2. - P. 1069-1072. ↑
- C5973.** Romeiser R. Interpretation of convection cell signatures in radar images of the Greenland Sea. / Romeiser R., Ufermann S., Rubino A., Androssov A., Kern S., Mitnik L. // 2002. IGARSS '02. 2002 IEEE International Geoscience and Remote Sensing Symposium. 2002. - Vol. 2. - P. 943-945. ↑
- C5974.** Ge Chen. Identification of swell zones in the ocean: a remote sensing approach. / Ge Chen, Jun Ma. // 2002. IGARSS '02. 2002 IEEE International Geoscience and Remote Sensing Symposium. 2002. - Vol. 2. - P. 946-948. ↑
- C5975.** Keller M.R. Multiple sea spike definitions: reducing the clutter. / Keller M.R., Gotwols B.L., Chapman

R.D. // 2002. IGARSS '02. 2002 IEEE International Geoscience and Remote Sensing Symposium. 2002. - Vol. 2. - P. 940-942. ↑

C5976. Hoja D. Global analysis of ocean wave systems from SAR wave mode data. / Hoja D., Schulz-Stellenfleth J., Lehner S., König T. // 2002. IGARSS '02. 2002 IEEE International Geoscience and Remote Sensing Symposium. 24-28 June 2002. - Vol. 2. - P. 934-936. ↑

C5977. Hwang P.A. Ambient and breaking roughness of the ocean surface. 2002. IGARSS '02. 2002 IEEE International Geoscience and Remote Sensing Symposium. 2002. - Vol. 2. - P. 937-939. ↑

C5978. Skriver H. Polarimetric segmentation using Wishart test statistic. / Skriver H., Schou J., Nielsen A.A., Conradsen K. // 2002. IGARSS '02. 2002 IEEE International Geoscience and Remote Sensing Symposium. 24-28 June 2002. - Vol. 2. - P. 1011-1013. ↑

C5979. Brandfass M. Generation of bald Earth digital elevation models as applied to polarimetric SAR interferometry. 2002. IGARSS '02. 2002 IEEE International Geoscience and Remote Sensing Symposium. 2002. - Vol. 2. - P. 1014-1016. ↑

C5980. Santos J.R. Estimation of basal area from Amazon tropical rain forest using airborne P-band SAR data. / Santos J.R., Araujo L.S., Dutra L.V., Freitas C.C., Mura J.C., Gama F.F. // 2002. IGARSS '02. 2002 IEEE International Geoscience and Remote Sensing Symposium. 2002. - Vol. 2. - P. 1008-1010. ↑

C5981. Caves R. Topographic performance evaluation of the RADARSAT-2/3 tandem mission. / Caves R., Luscombe A.P., Lee P.F., James K. // 2002. IGARSS '02. 2002 IEEE International Geoscience and Remote Sensing Symposium. 24-28 June 2002. - Vol. 2. - P. 961-963. ↑

C5982. Jolly G.W. A Canadian spaceborne hyperspectral mission. / Jolly G.W., Rowlands N., Staenz K., Hollinger A. // 2002. IGARSS '02. 2002 IEEE International Geoscience and Remote Sensing Symposium. 24-28 June 2002. - Vol. 2. - P. 967-969. ↑

C5983. Randall L. Estimation of land cover and biomass change from remotely sensed data. / Randall L., Lee A., Austin J., Barson M. // 2002. IGARSS '02. 2002 IEEE International Geoscience and Remote Sensing Symposium. 24-28 June 2002. - Vol. 2. - P. 1213-1215. ↑

C5984. Colesanti C. Ground deformation monitoring exploiting SAR permanent scatterers. / Colesanti C., Locatelli R., Novali F. // 2002. IGARSS '02. 2002 IEEE International Geoscience and Remote Sensing Symposium. 24-28 June 2002. - Vol. 2. - P. 1219-1221. ↑

C5985. Townsend P.A. Assessing flooding and vegetation structure in forested wetlands using Radarsat SAR imagery. / Townsend P.A., Foster J.R. // 2002. IGARSS '02. 2002 IEEE International Geoscience and Remote Sensing Symposium. 24-28 June 2002. - Vol. 2. - P. 1171-1173. ↑

C5986. Rubinstein I.G. Seasonal and spatial variability of surface hydraulic properties. / Rubinstein I.G., Fernandes R., Corner B. // 2002. IGARSS '02. 2002 IEEE International Geoscience and Remote Sensing Symposium. 24-28 June 2002. - Vol. 2. - P. 1161-1164. ↑

C5987. Pierdicca N. Inversion of surface scattering models: comparing criteria and algorithms to estimate bare soil parameters. / Pierdicca N., Castracane P., Ciotti P. // 2002. IGARSS '02. 2002 IEEE International Geoscience and Remote Sensing Symposium. 24-28 June 2002. - Vol. 2. - P. 1165-1167. ↑

C5988. Crosetto M. Quantitative subsidence monitoring using SAR interferometry. / Crosetto M., Crippa B., Barzaghi R. // 2002. IGARSS '02. 2002 IEEE International Geoscience and Remote Sensing Symposium. 24-28 June 2002. - Vol. 2. - P. 1231-1233. ↑

C5989. Colesanti C. Full exploitation of the ERS archive: multi data set permanent scatterers analysis. / Colesanti C., Ferretti A., Prati C., Rocca F. // 2002. IGARSS '02. 2002 IEEE International Geoscience and Remote Sensing Symposium. 24-28 June 2002. - Vol. 2. - P. 1234-1236. ↑

C5990. van der Kooij M. Results of processing and analysis of large volumes of repeat-pass InSAR data of Vancouver and Mount Meager (B.C.). / van der Kooij M., Lambert A. // 2002. IGARSS '02. 2002 IEEE International Geoscience and Remote Sensing Symposium. 24-28 June 2002. - Vol. 2. - P. 1228-1230. ↑

- C5991.** Le Mouelic S. Ground uplift in the city of Paris (France) revealed by satellite radar interferometry. / Le Mouelic S., Raucoules D., Carnec C., King C., Adragna F. // 2002. IGARSS '02. 2002 IEEE International Geoscience and Remote Sensing Symposium. 24-28 June 2002. - Vol. 2. - P. 1222-1224. ↑
- C5992.** Raucoules D. Urban subsidence in the city of Prato (Italy) monitored by satellite radar interferometry. / Raucoules D., Le Mouelic S., Carnec C., King C. // 2002. IGARSS '02. 2002 IEEE International Geoscience and Remote Sensing Symposium. 24-28 June 2002. - Vol. 2. - P. 1225-1227. ↑
- C5993.** Cumming I. Polarmetric SAR data compression using wavelet packets in a block coding scheme. / Cumming I., Wang J. // 2002. IGARSS '02. 2002 IEEE International Geoscience and Remote Sensing Symposium. 24-28 June 2002. - Vol. 2. - P. 1126-1128. ↑
- C5994.** Magli E. Wavelet-based compression of SAR raw data. / Magli E., Olmo G., Penna B. // 2002. IGARSS '02. 2002 IEEE International Geoscience and Remote Sensing Symposium. 24-28 June 2002. - Vol. 2. - P. 1129-1131. ↑
- C5995.** Berizzi F. Fractal behavior of sea SAR ERS-1 images. / Berizzi F., Gamba P., Garzelli A., Bertini G., Dell'Acqua F. // 2002. IGARSS '02. 2002 IEEE International Geoscience and Remote Sensing Symposium. 24-28 June 2002. - Vol. 2. - P. 1114-1116. ↑
- C5996.** Gade M. Remotely sensing bound and free small-scale waves at the edges of monomolecular surface films in a wind-wave tank. / Gade M., Lange P.A., Huhnerfuss H. // 2002. IGARSS '02. 2002 IEEE International Geoscience and Remote Sensing Symposium. 24-28 June 2002. - Vol. 2. - P. 1108-1110. ↑
- C5997.** Ermakov S.A. Wave tank studies of radar Doppler shifts in the presence of surfactant films on the water surface. / Ermakov S.A., Sergievskaya I.A., Shchegol'kov Yu.B., Scott J.C., Stapleton N.R. // 2002. IGARSS '02. 2002 IEEE International Geoscience and Remote Sensing Symposium. 24-28 June 2002. - Vol. 2. - P. 1111-1113. ↑
- C5998.** Karna J.-P. Assimilation of SAR data to operational hydrological runoff and snow melt forecasting model. / Karna J.-P., Pulliainen J., Huttunen M., Koskinen J. // 2002. IGARSS '02. 2002 IEEE International Geoscience and Remote Sensing Symposium. 24-28 June 2002. - Vol. 2. - P. 1146-1148. ↑
- C5999.** Borgeaud M. Analysis of detailed in-situ soil measurements with ERS C-band radar backscattering data. / Borgeaud M., Davidson M., Attema E., Louis J., Dente L., Floury N., Tell B.R. // 2002. IGARSS '02. 2002 IEEE International Geoscience and Remote Sensing Symposium. 24-28 June 2002. - Vol. 2. - P. 1158-1160. ↑
- C6000.** Scipal K. Comparison of Ku-and C-band backscatter time series over land. / Scipal K., Wagner W., Kidd R., Ringelmann N. // 2002. IGARSS '02. 2002 IEEE International Geoscience and Remote Sensing Symposium. 24-28 June 2002. - Vol. 2. - P. 1143-1145. ↑
- C6001.** Magli E. Predictive coding of SAR phase history data. / Magli E., Olmo G. // 2002. IGARSS '02. 2002 IEEE International Geoscience and Remote Sensing Symposium. 24-28 June 2002. - Vol. 2. - P. 1132-1134. ↑
- C6002.** Algra T. Data compression for operational SAR missions using entropy-constrained block adaptive quantisation. 2002. IGARSS '02. 2002 IEEE International Geoscience and Remote Sensing Symposium. 24-28 June 2002. - Vol. 2. - P. 1135-1139. ↑
- C6003.** Helz R.T. Satellite imagery for volcanic hazards mitigation. / Helz R.T., Ellrod G.A., Wadge G. // 2002. IGARSS '02. 2002 IEEE International Geoscience and Remote Sensing Symposium. 2002. - Vol. 2. - P. 757-758. ↑
- C6004.** Bertoia C. Earth observation for ice hazard support. / Bertoia C., Manore M., Seymour P., Benner D., Ramsay B. // 2002. IGARSS '02. 2002 IEEE International Geoscience and Remote Sensing Symposium. 2002. - Vol. 2. - P. 759-761. ↑
- C6005.** Long D.G. High resolution wind retrieval from SeaWinds. 2002. IGARSS '02. 2002 IEEE International Geoscience and Remote Sensing Symposium. 2002. - Vol. 2. - P. 751-753. ↑
- C6006.** Connor L.N. Buoy validation of ocean surface wind estimates from the TRMM precipitation radar. / Connor L.N., Chang P.S. // 2002. IGARSS '02. 2002 IEEE International Geoscience and Remote Sensing Symposium. 2002. - Vol. 2. - P. 745-747. ↑

- C6007.** Li Li. Detecting ocean surface winds using TRMM precipitation radar. / Li Li, Im E., Connor L.N., Chang P.S. // 2002. IGARSS '02. 2002 IEEE International Geoscience and Remote Sensing Symposium. 2002. - Vol. 2. - P. 748-750. ↑
- C6008.** Berkun A.C. An advanced FPGA-based processor and controller for the Next-Generation Precipitation Radar. / Berkun A.C., Fischman M.A., Im E. // 2002. IGARSS '02. 2002 IEEE International Geoscience and Remote Sensing Symposium. 24-28 June 2002. - Vol. 2. - P. 780-782. ↑
- C6009.** Mette T. Forest biomass estimation using polarimetric SAR interferometry. / Mette T., Papathanassiou K.P., Hajnsek I., Zimmermann R. // 2002. IGARSS '02. 2002 IEEE International Geoscience and Remote Sensing Symposium. 2002. - Vol. 2. - P. 817-819. ↑
- C6010.** Calvary P. Preliminary design of the SWIMSAT radar for the measurement of ocean wave spectra. / Calvary P., Phalippou L., Thouvenot E., Hauser D. // 2002. IGARSS '02. 2002 IEEE International Geoscience and Remote Sensing Symposium. 24-28 June 2002. - Vol. 2. - P. 777-779. ↑
- C6011.** Singhroy V. Earth observation for landslide assessment. / Singhroy V., Ohkura H., Glenn N. // 2002. IGARSS '02. 2002 IEEE International Geoscience and Remote Sensing Symposium. 2002. - Vol. 2. - P. 765-767. ↑
- C6012.** Carayon G. Poseidon 2 radar altimeter design and in flight preliminary performances. / Carayon G., Steunou N., Courriere J.-L., Thibaut P. // 2002. IGARSS '02. 2002 IEEE International Geoscience and Remote Sensing Symposium. 24-28 June 2002. - Vol. 2. - P. 774-776. ↑
- C6013.** McCoy R.P. Upcoming naval space missions for remote sensing of the oceans, atmosphere and space. 2002. IGARSS '02. 2002 IEEE International Geoscience and Remote Sensing Symposium. 2002. - Vol. 2. - P. 702-704. ↑
- C6014.** Jeremy M.L. Results from the Crusade ship detection trial: polarimetric SAR. / Jeremy M.L., Geling G., Rey M. // 2002. IGARSS '02. 2002 IEEE International Geoscience and Remote Sensing Symposium. 2002. - Vol. 2. - P. 711-713. ↑
- C6015.** Stacy N.J.S. The Global Hawk UAV Australian deployment: imaging radar sensor modifications and employment for maritime surveillance. / Stacy N.J.S., Craig D.W., Staromlynska J., Smith R.B. // 2002. IGARSS '02. 2002 IEEE International Geoscience and Remote Sensing Symposium. 2002. - Vol. 2. - P. 699-701. ↑
- C6016.** Suess H. Possible military requirements and applications of active and passive imaging sensors at micro- and millimeterwave frequencies. / Suess H., Schroeder R., Peichl M., Neff T. // 2002. IGARSS '02. 2002 IEEE International Geoscience and Remote Sensing Symposium. 24-28 June 2002. - Vol. 2. - {no data available}. ↑
- C6017.** Van Woert M.L. U.S. Navy operational sea ice remote sensing. 2002. IGARSS '02. 2002 IEEE International Geoscience and Remote Sensing Symposium. 24-28 June 2002. - Vol. 2. - P. 696-698. ↑
- C6018.** Smith D.K. Detection and characterization of diurnal winds using QuikScat data. / Smith D.K., Wentz F.J., Mears C.A. // 2002. IGARSS '02. 2002 IEEE International Geoscience and Remote Sensing Symposium. 2002. - Vol. 2. - P. 735-737. ↑
- C6019.** {no data available}. The ocean surface wind direction signal in passive microwave brightness temperatures. 2002. IGARSS '02. 2002 IEEE International Geoscience and Remote Sensing Symposium. 2002. - Vol. 2. - P. 738-740. ↑
- C6020.** Jelenak Z. The accuracy of high resolution winds from QuikSCAT. / Jelenak Z., Connor L.N., Chang P.S. // 2002. IGARSS '02. 2002 IEEE International Geoscience and Remote Sensing Symposium. 2002. - Vol. 2. - P. 732-734. ↑
- C6021.** Pichel W.G. NOAA CoastWatch RADARSAT-1 SAR coastal monitoring applications demonstrations. / Pichel W.G., Clemente-Colon P., Friedman K.S., Xiaofeng Li, Tseng W., Monaldo F., Beal R., Wackerman C.C. // 2002. IGARSS '02. 2002 IEEE International Geoscience and Remote Sensing Symposium. 24-28 June 2002. - Vol. 2. - P. 714-716. ↑
- C6022.** Woodhouse I.H. Improving the visualisation of polarimetric response in SAR imagery from pixels to

images. / Woodhouse I.H., Turner D., Laidlaw D.H. // 2002. IGARSS '02. 2002 IEEE International Geoscience and Remote Sensing Symposium. 2002. - Vol. 2. - P. 726-728. ↑

C6023. Werner C. SAR geocoding and multi-sensor image registration. / Werner C., Strozzi T., Wegmuller U., Wiesmann A. // 2002. IGARSS '02. 2002 IEEE International Geoscience and Remote Sensing Symposium. 24-28 June 2002. - Vol. 2. - P. 902-904. ↑

C6024. Pellizzeri T.M. A new maximum likelihood classification technique for multitemporal SAR and multiband optical images. / Pellizzeri T.M., Lombardo P., Oliver C.J. // 2002. IGARSS '02. 2002 IEEE International Geoscience and Remote Sensing Symposium. 2002. - Vol. 2. - P. 908-910. ↑

C6025. Churchill S. An outline of fusion and sensor combinational methodologies for disparate, sparse multi-sensor networks for detecting icebergs. / Churchill S., Randell C., Gill E., Power D. // 2002. IGARSS '02. 2002 IEEE International Geoscience and Remote Sensing Symposium. 2002. - Vol. 2. - P. 899-901. ↑

C6026. Satake M. Range antenna pattern measurements of airborne SAR system with arrayed corner reflectors. / Satake M., Umehara T., Maeno H., Uratsuka S., Nakayama H. // 2002. IGARSS '02. 2002 IEEE International Geoscience and Remote Sensing Symposium. 2002. - Vol. 2. - P. 859-861. ↑

C6027. De Grandi G.F. Cornerstones and epilogue of the GRFM Africa project: a gallery of regional scale vegetation maps. / De Grandi G.F., Mayaux P., Malingreau J.P., Baraldi A., Simard M., Saatchi S. // 2002. IGARSS '02. 2002 IEEE International Geoscience and Remote Sensing Symposium. 2002. - Vol. 2. - P. 893-895. ↑

C6028. Niedermeier A. Ocean wave groupiness from ERS-1/2 and ENVISAT imageries. / Niedermeier A., Schulz-Stellenfleth J., Nieto Borge J.C., Lehner S., Dankert H. // 2002. IGARSS '02. 2002 IEEE International Geoscience and Remote Sensing Symposium. 2002. - Vol. 2. - P. 928-930. ↑

C6029. Duk-jin Kim. Remote sensing of ocean waves and currents using NASA (JPL) AIRSAR along-track interferometry (ATI). / Duk-jin Kim, Moon W.M., Imel D.A., Moller D. // 2002. IGARSS '02. 2002 IEEE International Geoscience and Remote Sensing Symposium. 2002. - Vol. 2. - P. 931-933. ↑

C6030. Schulz-Stellenfleth J. Use of the coherence of synthetic aperture radar cross spectra for ocean wave measurements. / Schulz-Stellenfleth J., Lehner S., Hoja D. // 2002. IGARSS '02. 2002 IEEE International Geoscience and Remote Sensing Symposium. 2002. - Vol. 2. - P. 925-927. ↑

C6031. Loghmari M.A. Mixed pixel decomposition of satellite images based on source separation method. / Loghmari M.A., Naceur M.S., Boussema M.R. // 2002. IGARSS '02. 2002 IEEE International Geoscience and Remote Sensing Symposium. 24-28 June 2002. - Vol. 2. - P. 914-916. ↑

C6032. Sletten M.A. Radar investigations of breaking water waves at low grazing angles with simultaneous high-speed optical imagery. / Sletten M.A., Liu X., Duncan J.H., West J.C. // 2002. IGARSS '02. 2002 IEEE International Geoscience and Remote Sensing Symposium. 2002. - Vol. 2. - P. 922-924. ↑

C6033. Yamada H. Interferometric phase and coherence of forest estimated by ESPRIT-based polarimetric SAR interferometry. / Yamada H., Sato K., Yamaguchi Y., Boerner W.-M. // 2002. IGARSS '02. 2002 IEEE International Geoscience and Remote Sensing Symposium. 24-28 June 2002. - Vol. 2. - P. 829-831. ↑

C6034. Jong-Sen Lee. Speckle filtering of polarimetric SAR interferometry data. / Jong-Sen Lee, Cloude S.R., Papathanassiou K., Grunes M.R., Ainsworth T.L., Schuler D.L. // 2002. IGARSS '02. 2002 IEEE International Geoscience and Remote Sensing Symposium. 24-28 June 2002. - Vol. 2. - P. 832-834. ↑

C6035. Papathanassiou K.P. Interferometric SAR polarimetry using a passive polarimetric microsatellite concept. / Papathanassiou K.P., Hajnsek L., Moreira A., Cloude S.R. // 2002. IGARSS '02. 2002 IEEE International Geoscience and Remote Sensing Symposium. 24-28 June 2002. - Vol. 2. - P. 826-828. ↑

C6036. Woodhouse I.H. Polarimetric interferometry in the Glen Affric project: results & conclusions. / Woodhouse I.H., Cloude S., Papathanassiou K., Hope J., Suarez J., Osborne P., Wright G. // 2002. IGARSS '02. 2002 IEEE International Geoscience and Remote Sensing Symposium. 2002. - Vol. 2. - P. 820-822. ↑

C6037. Stebler O. Forward and inverse modelling of multi-baseline L-band Pol-InSAR E-SAR data. / Stebler O., Meier E., Nuesch D. // 2002. IGARSS '02. 2002 IEEE International Geoscience and Remote Sensing

Symposium. 2002. - Vol. 2. - P. 823-825. ↑

C6038. Franceschetti G. A 2-D Fourier domain approach for spotlight SAR raw signal simulation of extended scenes. / Franceschetti G., Iodice A., Riccio D., Ruello G. // 2002. IGARSS '02. 2002 IEEE International Geoscience and Remote Sensing Symposium. 24-28 June 2002. - Vol. 2. - P. 853-855. ↑

C6039. Masayuki M. An advanced airborne real-time SAR processing system. / Masayuki M., Hidefumi N., Hiroshi S., Minoru M., Hitoshi N. // 2002. IGARSS '02. 2002 IEEE International Geoscience and Remote Sensing Symposium. 24-28 June 2002. - Vol. 2. - P. 856-858. ↑

C6040. Le Vine D.M. ESTAR experience with RFI at L-band and implications for future passive microwave remote sensing from space. 2002. IGARSS '02. 2002 IEEE International Geoscience and Remote Sensing Symposium. 24-28 June 2002. - Vol. 2. - P. 847-849. ↑

C6041. Martinez C.L. Polarimetric and interferometric noise modelling. / Martinez C.L., Papathanassiou K.P., Canovas X.F. // 2002. IGARSS '02. 2002 IEEE International Geoscience and Remote Sensing Symposium. 24-28 June 2002. - Vol. 2. - P. 835-837. ↑

C6042. Cloude S.R. Robust parameter estimation using dual baseline polarimetric SAR interferometry. 2002. IGARSS '02. 2002 IEEE International Geoscience and Remote Sensing Symposium. 24-28 June 2002. - Vol. 2. - P. 838-840. ↑

C6043. Cui T.J. The inversion of subsurface VETEM data-theory and practice. / Cui T.J., Chew W.C., Aydinler A.A., Wright D.L., Smith D.V. // 2002. IGARSS '02. 2002 IEEE International Geoscience and Remote Sensing Symposium. 24-28 June 2002. - Vol. 3. - P. 1566-1568. ↑

C6044. Chi-Chih Chen. Advanced classification of buried UXO using a broadband, fully polarimetric ground penetrating radar. / Chi-Chih Chen, Higgins M.B., O'Neill K. // 2002. IGARSS '02. 2002 IEEE International Geoscience and Remote Sensing Symposium. 2002. - Vol. 3. - P. 1569-1571. ↑

C6045. Sun K. Treatment of broadband and multi-object electromagnetic induction scattering using high frequency approximations. / Sun K., O'Neill K., Shubitidze F., Paulsen K.D. // 2002. IGARSS '02. 2002 IEEE International Geoscience and Remote Sensing Symposium. 24-28 June 2002. - Vol. 3. - P. 1546-1549. ↑

C6046. Shao Yun. Study on complex dielectric properties of saline soils. / Shao Yun, Guo Huadong, Hu Qingrong, Lu Yuan, Dong Qing, Han Chunming. // 2002. IGARSS '02. 2002 IEEE International Geoscience and Remote Sensing Symposium. 24-28 June 2002. - Vol. 3. - P. 1541-1541b. ↑

C6047. Shubitidze F. Application of broadband EMI responses to infer buried object's aspect ratio. / Shubitidze F., O'Neill K., Sun K., Shamatava I. // 2002. IGARSS '02. 2002 IEEE International Geoscience and Remote Sensing Symposium. 24-28 June 2002. - Vol. 3. - P. 1542-1545. ↑

C6048. Sukhacheva L.L. Multiyear remotely sensed data in support of monitoring, management and protection of the eastern Gulf of Finland coastal zone. / Sukhacheva L.L., Bychkova L.A., Victorov S.V. // 2002. IGARSS '02. 2002 IEEE International Geoscience and Remote Sensing Symposium. 2002. - Vol. 3. - P. 1585-1587. ↑

C6049. Joong-Sun Won. Control factors of spectral reflectance in tidal flat: a case study in the Gomso Bay, Korea. / Joong-Sun Won, Joo-Hyung Ryu. // 2002. IGARSS '02. 2002 IEEE International Geoscience and Remote Sensing Symposium. 2002. - Vol. 3. - P. 1588-1590. ↑

C6050. Ufermann S. The role of synergy in developing a marine SAR analysis and interpretation system. / Ufermann S., Robinson I.S., da Silva J.C.B., Johannessen J.A. // 2002. IGARSS '02. 2002 IEEE International Geoscience and Remote Sensing Symposium. 2002. - Vol. 3. - P. 1582-1584. ↑

C6051. Kwan-Ho Lee. A numerical study of the effects of realistic GPR antennas on the scattering characteristics from unexploded ordnances. / Kwan-Ho Lee, Chi-Chih Chen, Lee R. // 2002. IGARSS '02. 2002 IEEE International Geoscience and Remote Sensing Symposium. 2002. - Vol. 3. - P. 1572-1574. ↑

C6052. Changbao Zhou. The dynamic monitoring and management of coastal zone with SAR remote sensing and fractal approach. / Changbao Zhou, Weigen Huang, Jingsong Yang, Bin Fu, Dongling Li, Qinmei Xiao, Huaguo Zhang. // 2002. IGARSS '02. 2002 IEEE International Geoscience and Remote Sensing Symposium. 2002. - Vol. 3. - P. 1579-1581. ↑

- C6053.** Long D.G. The Scatterometer Climate Record Pathfinder. / Long D.G., Drinkwater M., Holt B. // 2002. IGARSS '02. 2002 IEEE International Geoscience and Remote Sensing Symposium. 2002. - Vol. 3. - P. 1509-1511. ↑
- C6054.** Gutierrez S. Computer vision applications to the study of sea-ice motion in Antarctica. / Gutierrez S., Long D.G. // 2002. IGARSS '02. 2002 IEEE International Geoscience and Remote Sensing Symposium. 2002. - Vol. 3. - P. 1512-1514. ↑
- C6055.** Hong-Gyoo Sohn. Accurate classification of water area with fusion of RADARSAT and SPOT satellite imagery. / Hong-Gyoo Sohn, Yeong-Sun Song, Hwan-Hee Yoo, Bock-Mo Yeu. // 2002. IGARSS '02. 2002 IEEE International Geoscience and Remote Sensing Symposium. 2002. - Vol. 3. - P. 1503-1505. ↑
- C6056.** Henry J.-B. Earth observation and case-based systems for flood risk management. / Henry J.-B., Fellah K., Clandillon S., Allenbach B., De Fraipont P. // 2002. IGARSS '02. 2002 IEEE International Geoscience and Remote Sensing Symposium. 24-28 June 2002. - Vol. 3. - P. 1496-1498. ↑
- C6057.** Galantowicz J.F. High-resolution flood mapping from low-resolution passive microwave data. 2002. IGARSS '02. 2002 IEEE International Geoscience and Remote Sensing Symposium. 2002. - Vol. 3. - P. 1499-1502. ↑
- C6058.** Karvonen J. An iterative incidence angle normalization algorithm for sea ice SAR images. / Karvonen J., Simila M., Makynen M. // 2002. IGARSS '02. 2002 IEEE International Geoscience and Remote Sensing Symposium. 24-28 June 2002. - Vol. 3. - P. 1524-1527. ↑
- C6059.** Sokol J. Polarimetric C-band observations of soil moisture for pasture fields. / Sokol J., Pultz T.J., Deschamps A., Jobin D. // 2002. IGARSS '02. 2002 IEEE International Geoscience and Remote Sensing Symposium. 24-28 June 2002. - Vol. 3. - P. 1532-1534. ↑
- C6060.** Scheuchl B. Model-based classification of polarimetric SAR sea ice data. / Scheuchl B., Hajnsek I., Cumming I.G. // 2002. IGARSS '02. 2002 IEEE International Geoscience and Remote Sensing Symposium. 24-28 June 2002. - Vol. 3. - P. 1521-1523. ↑
- C6061.** Konig T. Extracting sea ice parameters from SAR imagettes. / Konig T., Niedermeier A., Lehner S. // 2002. IGARSS '02. 2002 IEEE International Geoscience and Remote Sensing Symposium. 2002. - Vol. 3. - P. 1515-1517. ↑
- C6062.** Makynen M. Incidence angle dependence of the mean C-band HH-polarization backscattering signatures of the Baltic Sea ice. / Makynen M., Manninen T., Simila M., Karvonen J., Hallikainen M. // 2002. IGARSS '02. 2002 IEEE International Geoscience and Remote Sensing Symposium. 2002. - Vol. 3. - P. 1518-1520. ↑
- C6063.** Dubois-Fernandez P. The ONERA RAMSES SAR system. / Dubois-Fernandez P., du Plessis O.R., le Coz D., Dupas J., Vaizan B., Dupuis X., Cantalloube H., Coulombeix C., Titin-Schnaider C., Dreuillet P., Boutry J.M., Canny J.P., Kaisersmertz L., Peyret J., Martineau P., Chanteclerc M., Pastore L., Bruyant J.P. // 2002. IGARSS '02. 2002 IEEE International Geoscience and Remote Sensing Symposium. 24-28 June 2002. - Vol. 3. - P. 1723-1725. ↑
- C6064.** Yu Yong. A phase unwrapping method based on minimum cost flows method in irregular network. / Yu Yong, Wang Chao, Zhang Hong, Liu Zhi, Gao Xin. // 2002. IGARSS '02. 2002 IEEE International Geoscience and Remote Sensing Symposium. 24-28 June 2002. - Vol. 3. - P. 1726-1728. ↑
- C6065.** Uratsuka S. High-resolution dual-bands interferometric and polarimetric airborne SAR (Pi-SAR) and its applications. / Uratsuka S., Satake M., Kobayashi T., Umehara T., Nadai A., Maeno H., Masuko H., Shimada M. // 2002. IGARSS '02. 2002 IEEE International Geoscience and Remote Sensing Symposium. 24-28 June 2002. - Vol. 3. - P. 1720-1722. ↑
- C6066.** Schimpf H. MEMPHIS-a fully polarimetric experimental radar. / Schimpf H., Essen H., Boehmsdorff S., Brehm T. // 2002. IGARSS '02. 2002 IEEE International Geoscience and Remote Sensing Symposium. 24-28 June 2002. - Vol. 3. - P. 1714-1716. ↑
- C6067.** Greidanus H. Coastal imagery from the polarimetric airborne SAR PHARUS. / Greidanus H., Otten M.P.G. // 2002. IGARSS '02. 2002 IEEE International Geoscience and Remote Sensing Symposium. 24-28 June

2002. - Vol. 3. - P. 1717-1719. ↑

C6068. Achan K. Phase unwrapping by minimizing Kikuchi free energy. / Achan K., Frey B., Koetter R., Munson D. // 2002. IGARSS '02. 2002 IEEE International Geoscience and Remote Sensing Symposium. 24-28 June 2002. - Vol. 3. - P. 1738-1740. ↑

C6069. Costantini M. A three-dimensional phase unwrapping algorithm for processing of multitemporal SAR interferometric measurements. / Costantini M., Malvarosa F., Minati F., Pietranera L., Milillo G. // 2002. IGARSS '02. 2002 IEEE International Geoscience and Remote Sensing Symposium. 24-28 June 2002. - Vol. 3. - P. 1741-1743. ↑

C6070. Sikaneta I. Parameter estimation for the phase statistics in interferometric SAR. / Sikaneta I., Gierull C. // 2002. IGARSS '02. 2002 IEEE International Geoscience and Remote Sensing Symposium. 24-28 June 2002. - Vol. 3. - P. 1735-1737. ↑

C6071. Refice A. Use of scaling information for stochastic atmospheric absolute phase screen retrieval. / Refice A., Bovenga F., Stramaglia S., Conte D. // 2002. IGARSS '02. 2002 IEEE International Geoscience and Remote Sensing Symposium. 24-28 June 2002. - Vol. 3. - P. 1729-1731. ↑

C6072. Ferraiuolo G. Maximum a posteriori height estimation in InSAR imaging. / Ferraiuolo G., Pascazio V., Schirinzi G. // 2002. IGARSS '02. 2002 IEEE International Geoscience and Remote Sensing Symposium. 24-28 June 2002. - Vol. 3. - P. 1732-1734. ↑

C6073. Arini N.S. Post-segmentation feature-based classification of synthetic aperture radar data. 2002. IGARSS '02. 2002 IEEE International Geoscience and Remote Sensing Symposium. 24-28 June 2002. - Vol. 3. - P. 1615-1617. ↑

C6074. Gasiewski A.J. Impacts of mobile radar and telecommunications systems on Earth remote sensing in the 22-27 GHz range. / Gasiewski A.J., Ruf C.S., Younis M., Wesbeck W. // 2002. IGARSS '02. 2002 IEEE International Geoscience and Remote Sensing Symposium. 24-28 June 2002. - Vol. 3. - P. 1679-1681. ↑

C6075. Horn G.D. Segmentation and classification of multitemporal data: methodology and results of a modified Gaussian Markov random field model classification system. / Horn G.D., Milne A.K. // 2002. IGARSS '02. 2002 IEEE International Geoscience and Remote Sensing Symposium. 2002. - Vol. 3. - P. 1609-1611. ↑

C6076. Plant W.J. Shoaling waves produced by offshore winds. / Plant W.J., Keller W.C., Hayes K. // 2002. IGARSS '02. 2002 IEEE International Geoscience and Remote Sensing Symposium. 2002. - Vol. 3. - P. 1597-1599. ↑

C6077. Azevedo A. Possible generation sites of internal solitary waves observed by ERS SAR in the central region of the Bay of Biscay. / Azevedo A., da Silva J.C.B., New A.L. // 2002. IGARSS '02. 2002 IEEE International Geoscience and Remote Sensing Symposium. 2002. - Vol. 3. - P. 1600-1602. ↑

C6078. Hoffmann K. DOSAR: a multifrequency polarimetric and interferometric airborne SAR-system. / Hoffmann K., Fischer P. // 2002. IGARSS '02. 2002 IEEE International Geoscience and Remote Sensing Symposium. 24-28 June 2002. - Vol. 3. - P. 1708-1710. ↑

C6079. Christensen E.L. EMISAR: a dual-frequency, polarimetric airborne SAR. / Christensen E.L., Dall J. // 2002. IGARSS '02. 2002 IEEE International Geoscience and Remote Sensing Symposium. 24-28 June 2002. - Vol. 3. - P. 1711-1713. ↑

C6080. Hawkins R.K. The SAR-580 facility-system update. / Hawkins R.K., Brown C.E., Murnaghan K.P., Gibson J.R., Alexander A., Marois R. // 2002. IGARSS '02. 2002 IEEE International Geoscience and Remote Sensing Symposium. 24-28 June 2002. - Vol. 3. - P. 1705-1707. ↑

C6081. Ender J.H.G. Multi-channel SAR/MTI system development at FGAN: from AER to PAMIR. / Ender J.H.G., Berens P., Brenner A.R., Rossing L., Skupin U. // 2002. IGARSS '02. 2002 IEEE International Geoscience and Remote Sensing Symposium. 24-28 June 2002. - Vol. 3. - P. 1697-1701. ↑

C6082. Yunling Lou. Review of the NASA/JPL airborne synthetic aperture radar system. 2002. IGARSS '02. 2002 IEEE International Geoscience and Remote Sensing Symposium. 24-28 June 2002. - Vol. 3. - P. 1702-1704. ↑

- C6083.** Bhogal A.S. Automated methods for atmospheric correction and fusion of multispectral satellite data for national monitoring. / Bhogal A.S., Goodenough D.G., Chen H., Hobart G., Rancourt B., Murdoch M., Love J., Dyk A. // 2002. IGARSS '02. 2002 IEEE International Geoscience and Remote Sensing Symposium. 2002. - Vol. 3. - P. 1316-1319. ↑
- C6084.** Ali M.A. Automatic registration of SAR and visible band remote sensing images. / Ali M.A., Clausi D.A. // 2002. IGARSS '02. 2002 IEEE International Geoscience and Remote Sensing Symposium. 2002. - Vol. 3. - P. 1331-1333. ↑
- C6085.** Garrison J.L. Model function development for GPS reflection measurements. / Garrison J.L., Bertuccelli L. // 2002. IGARSS '02. 2002 IEEE International Geoscience and Remote Sensing Symposium. 24-28 June 2002. - Vol. 2. - P. 1293-1295. ↑
- C6086.** Tatarskii V.I. Fresnel approximation for wave scattering in a random medium. 2002. IGARSS '02. 2002 IEEE International Geoscience and Remote Sensing Symposium. 24-28 June 2002. - Vol. 2. - P. 1272-1274. ↑
- C6087.** Thompson D.R. Surface roughness estimation from GPS sea reflections. / Thompson D.R., Linstrom L.A., Gasparovic R.F., Elfouhaily T.M. // 2002. IGARSS '02. 2002 IEEE International Geoscience and Remote Sensing Symposium. 24-28 June 2002. - Vol. 2. - P. 1278-1280. ↑
- C6088.** Raney R.K. Bistatic WITEX: an innovative constellation of radar altimeter satellites. / Raney R.K., Porter D.L., Monaldo F.M. // 2002. IGARSS '02. 2002 IEEE International Geoscience and Remote Sensing Symposium. 24-28 June 2002. - Vol. 3. - {no data available}. ↑
- C6089.** Pampaloni P. HYDRO-POL-a spaceborne polarimetric radar-radiometer for land hydrology and ocean salinity. / Pampaloni P., Decarolis G., Entekhabi D., Ferrazzoli P., Kim Y., Pasquariello G., Pierdicca N., Posa F., Zecchetto S., Zelli C., Castracane P., De Biasio F., Desantis G., Guerriero L., Macelloni G., Njoku E., Notarnicola C., Mattia F., Paloscia S., Satalino G. // 2002. IGARSS '02. 2002 IEEE International Geoscience and Remote Sensing Symposium. 24-28 June 2002. - Vol. 3. - P. 1358-1360. ↑
- C6090.** Vincent P. ALTIKA3: a high-resolution ocean topography mission. / Vincent P., Thouvenot E., Steunou N., Verron J., Bahurel P., Le Provost C., Le Traon P.Y., Caubet E., Phalippou L. // 2002. IGARSS '02. 2002 IEEE International Geoscience and Remote Sensing Symposium. 24-28 June 2002. - Vol. 3. - P. 1352-1354. ↑
- C6091.** Abdelfattah R. Interferometric SAR image coregistration based on the Fourier-Mellin invariant descriptor. / Abdelfattah R., Nicolas J.M., Tupin F. // 2002. IGARSS '02. 2002 IEEE International Geoscience and Remote Sensing Symposium. 24-28 June 2002. - Vol. 3. - P. 1334-1336. ↑
- C6092.** Giancaspro A. SAR images co-registration parallel implementation. / Giancaspro A., Candela L., Lopint E., Lore V.A., Milillo G. // 2002. IGARSS '02. 2002 IEEE International Geoscience and Remote Sensing Symposium. 2002. - Vol. 3. - P. 1337-1339. ↑
- C6093.** Usai S. A least-squares approach for long-term monitoring of deformations with differential SAR interferometry. 2002. IGARSS '02. 2002 IEEE International Geoscience and Remote Sensing Symposium. 24-28 June 2002. - Vol. 2. - P. 1247-1250. ↑
- C6094.** Iodice A. Forward-backward iterative method for scattering by dielectric fractal surfaces. 2002. IGARSS '02. 2002 IEEE International Geoscience and Remote Sensing Symposium. 24-28 June 2002. - Vol. 2. - P. 1254-1256. ↑
- C6095.** Ye Xia. Differential SAR interferometry using corner reflectors. / Ye Xia, Kaufmann H., Xiaofang Guo. // 2002. IGARSS '02. 2002 IEEE International Geoscience and Remote Sensing Symposium. 24-28 June 2002. - Vol. 2. - P. 1243-1246. ↑
- C6096.** Mora O. A new algorithm for monitoring localized deformation phenomena based on small baseline differential SAR interferograms. / Mora O., Lanari R., Mallorqui J.J., Berardino P., Sansosti E. // 2002. IGARSS '02. 2002 IEEE International Geoscience and Remote Sensing Symposium. 24-28 June 2002. - Vol. 2. - P. 1237-1239. ↑
- C6097.** Inglada J. Blind source separation applied to multitemporal series of differential SAR interferograms. / Inglada J., Adragna F. // 2002. IGARSS '02. 2002 IEEE International Geoscience and Remote Sensing Symposium. 24-28 June 2002. - Vol. 2. - P. 1240-1242. ↑

- C6098.** Zribi M. Backscattering behavior of a cloddy soil surface. / Zribi M., Dechambre M. // 2002. IGARSS '02. 2002 IEEE International Geoscience and Remote Sensing Symposium. 24-28 June 2002. - Vol. 2. - P. 1266-1268. ↑
- C6099.** West J.C. Diffractive analysis of backscatter from wave-crest-like objects. 2002. IGARSS '02. 2002 IEEE International Geoscience and Remote Sensing Symposium. 24-28 June 2002. - Vol. 2. - P. 1269-1271. ↑
- C6100.** Plant W.J. Bound wave effects in microwave and acoustic backscatter from rough water surfaces. / Plant W.J., Dahl P., Geovanangeli J.-P., Branger H. // 2002. IGARSS '02. 2002 IEEE International Geoscience and Remote Sensing Symposium. 24-28 June 2002. - Vol. 2. - P. 1263-1265. ↑
- C6101.** Qin Li. Numerical study of frequency and polarimetric dependence of the emissivities and backscattering coefficients of soil based on three dimensional Monte-Carlo simulation of Maxwell equations. / Qin Li, Lin Zhou, Chan C.H., Chen K.S. // 2002. IGARSS '02. 2002 IEEE International Geoscience and Remote Sensing Symposium. 24-28 June 2002. - Vol. 2. - P. 1257-1259. ↑
- C6102.** Gilbert M.S. Implementation of the higher order small slope approximation for scattering from a Gaussian rough surface. / Gilbert M.S., Johnson J.T. // 2002. IGARSS '02. 2002 IEEE International Geoscience and Remote Sensing Symposium. 24-28 June 2002. - Vol. 2. - P. 1260-1262. ↑
- C6103.** van der Sanden J.J. RADARSAT-2; are its technical capabilities expected to provide potential for remote sensing applications ?. / van der Sanden J.J., Budkewitsch P., Flett D.G., Gray A.L., Hawkins R.K., Landry R., Lukowski T.I., McNairn H., Pultz T.J., Singhroy V., Sokol J., Toutin T., Touzi R., Vachon P.W. // 2002. IGARSS '02. 2002 IEEE International Geoscience and Remote Sensing Symposium. 2002. - Vol. 3. - P. 1468-1470. ↑
- C6104.** McNairn H. The sensitivity of C-band polarimetric SAR to crop condition. / McNairn H., Decker V., Murnaghan K. // 2002. IGARSS '02. 2002 IEEE International Geoscience and Remote Sensing Symposium. 24-28 June 2002. - Vol. 3. - P. 1471-1473. ↑
- C6105.** Thompson A.A. RADARSAT-2 antenna calibration using Ground Receivers/Transmitters. / Thompson A.A., Racine D., Luscombe A.P. // 2002. IGARSS '02. 2002 IEEE International Geoscience and Remote Sensing Symposium. 2002. - Vol. 3. - P. 1465-1467. ↑
- C6106.** Chowdhury M.S. Shape preserving edge enhancement in remote sensing imagery. / Chowdhury M.S., Clausi D.A. // 2002. IGARSS '02. 2002 IEEE International Geoscience and Remote Sensing Symposium. 2002. - Vol. 3. - P. 1450-1452. ↑
- C6107.** Brule L. RADARSAT-2 program update. / Brule L., Baeggli H. // 2002. IGARSS '02. 2002 IEEE International Geoscience and Remote Sensing Symposium. 2002. - Vol. 3. - P. 1462-1464. ↑
- C6108.** Madsen S.N. Radar options for global earthquake monitoring. / Madsen S.N., Chen C., Edelstein W. // 2002. IGARSS '02. 2002 IEEE International Geoscience and Remote Sensing Symposium. 2002. - Vol. 3. - P. 1483-1485. ↑
- C6109.** Wright C.W. Realtime storm surge measurement with a scanning radar altimeter. / Wright C.W., Walsh E.J., Krabill W.B., Vandemark D., Garcia A.W., Black P.G., Marks F.D. Jr., Luetlich R.A. Jr. // 2002. IGARSS '02. 2002 IEEE International Geoscience and Remote Sensing Symposium. 2002. - Vol. 3. - P. 1492-1495. ↑
- C6110.** Farhat M. InSAR end-to-end simulation environment. / Farhat M., Lauzon F., Trudeau A., Fiset R. // 2002. IGARSS '02. 2002 IEEE International Geoscience and Remote Sensing Symposium. 2002. - Vol. 3. - P. 1480-1482. ↑
- C6111.** Staples G.C. Turning the scientifically possible into the operationally practical: RADARSAT-2 polarimetry applications. / Staples G.C., Hornsby J. // 2002. IGARSS '02. 2002 IEEE International Geoscience and Remote Sensing Symposium. 2002. - Vol. 3. - P. 1474-1476. ↑
- C6112.** Girard R. The RADARSAT-2&3 topographic mission: an overview. / Girard R., Lee P.F., James K. // 2002. IGARSS '02. 2002 IEEE International Geoscience and Remote Sensing Symposium. 2002. - Vol. 3. - P. 1477-1479. ↑
- C6113.** Reagan J.A. LITE aerosol retrievals revisited in support of CALIPSO and GLAS. / Reagan J.A., Wang

X., Fang H. // 2002. IGARSS '02. 2002 IEEE International Geoscience and Remote Sensing Symposium. 2002. - Vol. 3. - P. 1379-1381. ↑

C6114. Spinhirne J. High pulse repetition rate, eye safe, visible wavelength lidar systems: Design, results and potential. / Spinhirne J., Berkoff T., Welton E., Campbell J. // 2002. IGARSS '02. 2002 IEEE International Geoscience and Remote Sensing Symposium. 2002. - Vol. 3. - P. 1382-1383. ↑

C6115. Palm S.P. An overview of the GLAS real-time atmospheric processing algorithms and results from the analysis of simulated GLAS data sets. / Palm S.P., Hart B., Hlavka D., Spinhirne J., Mahesh A., Welton E.J. // 2002. IGARSS '02. 2002 IEEE International Geoscience and Remote Sensing Symposium. 2002. - Vol. 3. - P. 1376-1378. ↑

C6116. Bidwell S.W. Plans for Global Precipitation Measurement ground validation. / Bidwell S.W., Yuter S., Adams W.J., Everett D.F., Flaming G.M., Smith E.A. // 2002. IGARSS '02. 2002 IEEE International Geoscience and Remote Sensing Symposium. 2002. - Vol. 3. - P. 1370-1372. ↑

C6117. Hlavka D.L. Cloud Physics Lidar optical measurements during the SAFARI-2000 field campaign. / Hlavka D.L., McGill M., Hart W.D., Spinhirne J.D. // 2002. IGARSS '02. 2002 IEEE International Geoscience and Remote Sensing Symposium. 2002. - Vol. 3. - P. 1373-1375. ↑

C6118. Pultz T.J. Temporal soil moisture estimation of pastures from Radarsat data for applications in watershed modelling. / Pultz T.J., Sokol J., Deschamps A., Jobin D. // 2002. IGARSS '02. 2002 IEEE International Geoscience and Remote Sensing Symposium. 24-28 June 2002. - Vol. 3. - P. 1402-1404. ↑

C6119. Fletcher N.D. Minimum distance texture classification of SAR images using wavelet packets. / Fletcher N.D., Evans A.N. // 2002. IGARSS '02. 2002 IEEE International Geoscience and Remote Sensing Symposium. 2002. - Vol. 3. - P. 1438-1440. ↑

C6120. Scipal K. The global soil moisture archive 1992-2000 from ERS scatterometer data: first results. / Scipal K., Wagner W., Trommler M., Naumann K. // 2002. IGARSS '02. 2002 IEEE International Geoscience and Remote Sensing Symposium. 24-28 June 2002. - Vol. 3. - P. 1399-1401. ↑

C6121. Weed C.A. Classification of LIDAR data using a lower envelope follower and gradient-based operator. / Weed C.A., Crawford M.M., Neuenschwander A.L., Gutierrez R. // 2002. IGARSS '02. 2002 IEEE International Geoscience and Remote Sensing Symposium. 24-28 June 2002. - Vol. 3. - P. 1384-1386. ↑

C6122. Sun G. Modeling lidar and radar returns of forest canopies for data fusion. / Sun G., Ranson K.J. // 2002. IGARSS '02. 2002 IEEE International Geoscience and Remote Sensing Symposium. 24-28 June 2002. - Vol. 3. - P. 1387-1389. ↑

C6123. Malnes E. Mapping of snow covered area with Radarsat in Norway. / Malnes E., Guneriusson T. // 2002. IGARSS '02. 2002 IEEE International Geoscience and Remote Sensing Symposium. 2002. - Vol. 1. - P. 683-685. ↑

C6124. Horn G.D. Monitoring seasonal dynamics of Northern Australian wetlands with multitemporal Radarsat data. / Horn G.D., Milne A.K. // 2002. IGARSS '02. 2002 IEEE International Geoscience and Remote Sensing Symposium. 2002. - Vol. 1. - P. 137-139. ↑

C6125. Srivastava S.K. RADARSAT-1 image quality/continuing success in extended mission. / Srivastava S.K., Le Dantec P., Banik B.T., Shepherd N., Gray R., Hawkins R.K., Murnaghan K.P. // 2002. IGARSS '02. 2002 IEEE International Geoscience and Remote Sensing Symposium. 24-28 June 2002. - Vol. 1. - P. 140-142. ↑

C6126. Abbott K. Use of RADARSAT-1 images to map forest fuel moisture over boreal forests. / Abbott K., Leblon B., Staples G., Alexander M.E., MacLean D. // 2002. IGARSS '02. 2002 IEEE International Geoscience and Remote Sensing Symposium. 2002. - Vol. 1. - P. 134-136. ↑

C6127. Raymond C.A. Understanding and responding to earthquake hazards. / Raymond C.A., Lundgren P.R., Madsen S.N., Rundle J.B. // 2002. IGARSS '02. 2002 IEEE International Geoscience and Remote Sensing Symposium. 2002. - Vol. 1. - P. 128-130. ↑

C6128. Mahmood A. RADARSAT-1 Background Mission global coverage. 2002. IGARSS '02. 2002 IEEE International Geoscience and Remote Sensing Symposium. 2002. - Vol. 1. - P. 131-133. ↑

- C6129.** Bast D.C. RADARSAT ScanSAR roll angle estimation. / Bast D.C., Cumming I.G. // 2002. IGARSS '02. 2002 IEEE International Geoscience and Remote Sensing Symposium. 2002. - Vol. 1. - P. 152-154. ↑
- C6130.** Breit H. SRTM X-SAR DEM of Europe-Results and algorithmic improvements. / Breit H., Knopfle W., Adam N., Eineder M., Suchandt S., Rabus B. // 2002. IGARSS '02. 2002 IEEE International Geoscience and Remote Sensing Symposium. 24-28 June 2002. - Vol. 1. - P. 155-157. ↑
- C6131.** Labelle-Hamer N. RADARSAT Geophysical Processor System: 2 years of production. / Labelle-Hamer N., Kwok R., Cunningham G., Moore C., Barker E. Jr. // 2002. IGARSS '02. 2002 IEEE International Geoscience and Remote Sensing Symposium. 2002. - Vol. 1. - P. 149-151. ↑
- C6132.** Staples G. The use of RADARSAT-1 SAR data for operational wind field retrieval. / Staples G., Mendoza A. // 2002. IGARSS '02. 2002 IEEE International Geoscience and Remote Sensing Symposium. 2002. - Vol. 1. - P. 143-145. ↑
- C6133.** Peterson I.K. Validation of sea ice signatures in radarsat ScanSAR imagery for the Gulf of St. Lawrence. / Peterson I.K., Prinsenberg S.J., Holladay J.S., Lalumiere L.A. // 2002. IGARSS '02. 2002 IEEE International Geoscience and Remote Sensing Symposium. 2002. - Vol. 1. - P. 146-148. ↑
- C6134.** Hellwich O. Sensor and data fusion contest: test imagery to compare and combine airborne SAR and optical sensors for mapping. / Hellwich O., Reigber A., Lehmann H. // 2002. IGARSS '02. 2002 IEEE International Geoscience and Remote Sensing Symposium. 2002. - Vol. 1. - P. 82-84. ↑
- C6135.** Dell'Acqua F. Extraction and fusion of street networks from fine resolution SAR data. / Dell'Acqua F., Gamba P., Lisini G. // 2002. IGARSS '02. 2002 IEEE International Geoscience and Remote Sensing Symposium. 2002. - Vol. 1. - P. 89-91. ↑
- C6136.** Stancu S. Improving feature extraction in satellite SAR images by an interactive fuzzy fusion of multi-temporal data. / Stancu S., Bujor F.T., Trouve E., Mauris G., Bolon P., Rudant J.P. // 2002. IGARSS '02. 2002 IEEE International Geoscience and Remote Sensing Symposium. 2002. - Vol. 1. - P. 75-78. ↑
- C6137.** Yanovsky F.J. Radar estimation of turbulence eddy dissipation rate in rain. / Yanovsky F.J., Prokopenko I.G., Prokopenko K.I., Russchenberg H.W.J., Ligthart L.P. // 2002. IGARSS '02. 2002 IEEE International Geoscience and Remote Sensing Symposium. 2002. - Vol. 1. - P. 63-65. ↑
- C6138.** Slatton K.C. Multiscale fusion of INSAR data for improved topographic mapping. / Slatton K.C., Crawford M., Teng L. // 2002. IGARSS '02. 2002 IEEE International Geoscience and Remote Sensing Symposium. 2002. - Vol. 1. - P. 69-71. ↑
- C6139.** Sveinsson J.R. Double density wavelet transformation for speckle reduction of SAR images. / Sveinsson J.R., Benediktsson J.A. // 2002. IGARSS '02. 2002 IEEE International Geoscience and Remote Sensing Symposium. 2002. - Vol. 1. - P. 113-115. ↑
- C6140.** Schwartz G. Elimination of false positives in vessels detection and identification by remote sensing. / Schwartz G., Alvarez M., Varfis A., Kourti N. // 2002. IGARSS '02. 2002 IEEE International Geoscience and Remote Sensing Symposium. 2002. - Vol. 1. - P. 116-118. ↑
- C6141.** Sciotti M. Ship wake detection in SAR images: a segmentation-based approach. / Sciotti M., Capecchi G., Lombardo P. // 2002. IGARSS '02. 2002 IEEE International Geoscience and Remote Sensing Symposium. 2002. - Vol. 1. - P. 110-112. ↑
- C6142.** Inglada J. Similarity measures for multisensor remote sensing images. 2002. IGARSS '02. 2002 IEEE International Geoscience and Remote Sensing Symposium. 2002. - Vol. 1. - P. 104-106. ↑
- C6143.** Lampropoulos G.A. Detection of targets from electro-optical and SAR data using chaotic predictors and optimal CFAR detectors. / Lampropoulos G.A., Gigli G., Seigny L., Beaudoin A., Secker J. // 2002. IGARSS '02. 2002 IEEE International Geoscience and Remote Sensing Symposium. 2002. - Vol. 1. - P. 107-109. ↑
- C6144.** van der Kooij M. The application of satellite radar interferometry to subsidence monitoring in the Belridge and Lost Hills fields, California. / van der Kooij M., Mayer D. // 2002. IGARSS '02. 2002 IEEE International Geoscience and Remote Sensing Symposium. 2002. - Vol. 1. - P. 201-202. ↑

- C6145.** Dehls J.F. Ground deformation monitoring in the Ranafjord area of Norway by means of the permanent scatterers technique. / Dehls J.F., Basilico M., Colesanti C. // 2002. IGARSS '02. 2002 IEEE International Geoscience and Remote Sensing Symposium. 2002. - Vol. 1. - P. 203-207. ↑
- C6146.** Nagler T. Analysis of landslides in Alpine areas by means of SAR interferometry. / Nagler T., Rott H., Kamelger A. // 2002. IGARSS '02. 2002 IEEE International Geoscience and Remote Sensing Symposium. 2002. - Vol. 1. - P. 198-200. ↑
- C6147.** Zhong Lu. Interferometric synthetic aperture radar studies of Alaska volcanoes. / Zhong Lu, Wicks C. Jr., Power J., Dzurisin D., Thatcher W., Masterlark T. // 2002. IGARSS '02. 2002 IEEE International Geoscience and Remote Sensing Symposium. 2002. - Vol. 1. - P. 191-194. ↑
- C6148.** Grunsky E.C. The use of multi-beam RADARSAT-1 satellite imagery for terrain mapping. 2002. IGARSS '02. 2002 IEEE International Geoscience and Remote Sensing Symposium. 2002. - Vol. 1. - P. 195-197. ↑
- C6149.** Flaming G.M. Requirements for Global Precipitation Measurement. 2002. IGARSS '02. 2002 IEEE International Geoscience and Remote Sensing Symposium. 2002. - Vol. 1. - P. 269-271. ↑
- C6150.** Meneghini R. Integral equations for a dual-wavelength radar. / Meneghini R., Liang Liao, Iguchi T. // 2002. IGARSS '02. 2002 IEEE International Geoscience and Remote Sensing Symposium. 2002. - Vol. 1. - P. 272-274. ↑
- C6151.** Yackel J.J. Validation of a snow water equivalence algorithm over landfast first-year sea ice using RADARSAT-1. / Yackel J.J., Barber D.G. // 2002. IGARSS '02. 2002 IEEE International Geoscience and Remote Sensing Symposium. 2002. - Vol. 1. - P. 234-236. ↑
- C6152.** Fortin J.-P. New developments and results for snowcover monitoring using RADARSAT and VEGETATION data and the HYDROTEL hydrological model. / Fortin J.-P., Bernier M., Savary S., El Battay A., Khaldoune J. // 2002. IGARSS '02. 2002 IEEE International Geoscience and Remote Sensing Symposium. 2002. - Vol. 1. - P. 223-226. ↑
- C6153.** Bernier M. Radiometric correction of RADARSAT-1 images for mapping the snow water equivalent (SWE) in a mountainous environment. / Bernier M., Gauthier Y., Briand P., Coulombe-Simoneau J., Hurley J., Weber F. // 2002. IGARSS '02. 2002 IEEE International Geoscience and Remote Sensing Symposium. 2002. - Vol. 1. - P. 227-230. ↑
- C6154.** Sarabandi K. Calibration and validation of the Shuttle Radar Topography Mission height data for southeastern Michigan. / Sarabandi K., Brown C.G., Pierce L., Zahn D., Azadegan R., Buell K., Casciato M., Koh I., Lawrence D., Park M. // 2002. IGARSS '02. 2002 IEEE International Geoscience and Remote Sensing Symposium. 2002. - Vol. 1. - P. 167-169. ↑
- C6155.** Dall J. Interferometric calibration with natural distributed targets. / Dall J., Christensen E.L. // 2002. IGARSS '02. 2002 IEEE International Geoscience and Remote Sensing Symposium. 2002. - Vol. 1. - P. 170-172. ↑
- C6156.** Eineder M. Filtering of interferometric SRTM X-SAR data. / Eineder M., Rabus B., Holzner J., Suchandt S., Knopfle W. // 2002. IGARSS '02. 2002 IEEE International Geoscience and Remote Sensing Symposium. 2002. - Vol. 1. - P. 164-166. ↑
- C6157.** Romeiser R. Demonstration of current measurements from space by along-track SAR interferometry with SRTM data. / Romeiser R., Breit H., Eineder M., Runge H. // 2002. IGARSS '02. 2002 IEEE International Geoscience and Remote Sensing Symposium. 2002. - Vol. 1. - P. 158-160. ↑
- C6158.** Knedlik S. Baseline estimation and prediction referring to the SRTM. / Knedlik S., Loffeld O. // 2002. IGARSS '02. 2002 IEEE International Geoscience and Remote Sensing Symposium. 2002. - Vol. 1. - P. 161-163. ↑
- C6159.** Fornaro G. Range resolution limits in multi-pass SAR data processing. / Fornaro G., Pascasio V., Schirizzi G. // 2002. IGARSS '02. 2002 IEEE International Geoscience and Remote Sensing Symposium. 2002. - Vol. 1. - P. 182-184. ↑

C6160. Singhroy V. Characterization of landslide deposits using SAR images. / Singhroy V., Molch K., Bulmer M. // 2002. IGARSS '02. 2002 IEEE International Geoscience and Remote Sensing Symposium. 2002. - Vol. 1. - P. 185-187. ↑

C6161. Preiss M. Space variant filtering of polar format spotlight SAR images for wavefront curvature correction and interferometric processing. / Preiss M., Gray D., Stacy N. // 2002. IGARSS '02. 2002 IEEE International Geoscience and Remote Sensing Symposium. 2002. - Vol. 1. - P. 179-181. ↑

C6162. Scheiber R. Interferometric multi-look techniques for SAR data. / Scheiber R., Bothale V.M. // 2002. IGARSS '02. 2002 IEEE International Geoscience and Remote Sensing Symposium. 2002. - Vol. 1. - P. 173-175. ↑

C6163. Berardino P. Multi-pass synthetic aperture radar for 3-D focusing. / Berardino P., Fornaro G., Lanari R., Sansosti E., Serafino F., Soldovieri F. // 2002. IGARSS '02. 2002 IEEE International Geoscience and Remote Sensing Symposium. 2002. - Vol. 1. - P. 176-178. ↑

C6164. Avgerinos E. Towards evolutionary optimisation for high resolution bathymetry from sidescan sonars. / Avgerinos E., Zalzal A.M.S., Zografos G. // 2002. CEC '02. Proceedings of the 2002 Congress on Evolutionary Computation. - Honolulu, HI, 2002. - Vol. 2. - P. 1244-1249. ↑

C6165. Chapursky V.V. Subsurface radar examination of an airstrip. / Chapursky V.V., Ivashov S.I., Razevig V.V., Sheyko A.P., Vasilyev I.A., Pomozov V.V., Semeikin N.P., Desmond D.J. // 2002. Digest of Papers. 2002 IEEE Conference on Ultra Wideband Systems and Technologies. 2002. - P. 181-185. ↑

C6166. Manik H. Combined underwater acoustic and radar instruments for assessing fish near seabed and mapping seabed. / Manik H., Furusawa M. // 2002. Proceedings of the 2002 International Symposium on Underwater Technology. 2002. - P. 131-134. ↑

C6167. Droitcour A.D. 0.25 μ m CMOS and BiCMOS single-chip direct-conversion Doppler radars for remote sensing of vital signs. / Droitcour A.D., Boric-Lubecke O., Lubecke V.M., Jenshan Lin. // 2002. Digest of Technical Papers. ISSCC. 2002 IEEE International Solid-State Circuits Conference. - San Francisco, CA, 2002. - Vol. 1. - P. 348-349. ↑

C6168. Droitcour A.D. 0.25 μ m CMOS and BiCMOS single-chip direct-conversion doppler radar for remote sensing of vital signs. / Droitcour A.D., Boric-Lubecke O., Lubecke V.M., Jenshan Lin. // 2002. Digest of Technical Papers. ISSCC. 2002 IEEE International Solid-State Circuits Conference. 2002. - Vol. 2. - P. 278-505. ↑

C6169. Lubecke V. A compact low-cost add-on module for Doppler radar sensing of vital signs using a wireless communications terminal. / Lubecke V., Boric-Lubecke O., Beck E. // 2002 IEEE MTT-S International Microwave Symposium Digest. - Seattle, WA, 2002. - Vol. 3. - P. 1767-1770. ↑

C6170. Tessmann A. A 94 GHz single-chip FMCW radar module for commercial sensor applications. / Tessmann A., Kudzusz S., Feltgen T., Riessle M., Sklarczyk C., Haydl W.H. // 2002 IEEE MTT-S International Microwave Symposium Digest. - Seattle, WA, 2002. - Vol. 3. - P. 1851-1854. ↑

C6171. Brown E.R. Remote detection of bioparticles in the THz region. / Brown E.R., Woolard D.L., Samuels A.C., Globus T., Gelmont B. // 2002 IEEE MTT-S International Microwave Symposium Digest. - Seattle, WA, 2002. - Vol. 3. - P. 1591-1594. ↑

C6172. Lohmeier S.P. Development of an ultra-wideband radar system for vehicle detection at railway crossings. / Lohmeier S.P., Rajaraman R., Ramasami V.C. // 2002. Digest of Papers. 2002 IEEE Conference on Ultra Wideband Systems and Technologies. 2002. - P. 207-211. ↑

C6173. Bujor F.T. An interactive fuzzy fusion system applied to change detection in SAR images. / Bujor F.T., Valet L., Trouve E., Mauris G., Bolon Ph. // 2002. FUZZ-IEEE'02. Proceedings of the 2002 IEEE International Conference on Fuzzy Systems. - Honolulu, HI, 2002. - Vol. 2. - P. 932-937. ↑

C6174. Lopez Dekker P. Entropy based phase calibration of antenna arrays for digital beamforming remote sensing radars. / Lopez Dekker P., Farquharson G., Frasier S.J. // 2002. Proceedings of the IEEE Radar Conference. 2002. - P. 445-452. ↑

C6175. Aubry W.M. Airborne sensor concept to image shallow-buried targets. / Aubry W.M., Bonneau R.J.,

Brown R.D., Lynch E.D., Wicks M.C., Schneible R.A., George A.D., Krumme M.A. // 2002. Proceedings of the IEEE Radar Conference. 2002. - P. 233-236. ↑

C6176. Yang Zhen. Application of polarimetric synthetic aperture radar interferometry for land cover classification. / Yang Zhen, Yang Ruliang. // 2002. Proceedings of the IEEE Radar Conference. 2002. - P. 459-463. ↑

C6177. Kanagaratnam P. A High-Resolution Airborne Radar System for Near Surface Mapping of Internal Layers to Estimate Accumulation Rate. / Kanagaratnam P., Parthasarathy B., Plummer T., Akins T., Braaten D., Gogineni S.P. // 2002. 32nd European Microwave Conference. - Milan, Italy, 23-26 Sept. 2002. - P. 1-4. ↑

C6178. Jun-Yi Xu. A new solution to polarimetric radar discrimination problem. / Jun-Yi Xu, Jian Yang, Ying-Ning Peng, Chao Wang. // 2002. Proceedings of the IEEE Radar Conference. 2002. - P. 484-487. ↑

C6179. Danly B.G. Gyro-amplifiers for high power millimeter wave radar. 2002. IVEC 2002. Third IEEE International Vacuum Electronics Conference. 2002. - P. 361-362. ↑

C6180. Geiko L.G. Laser frequency converters for Universal Lidar system. / Geiko L.G., Andreev Yu.M., Geiko P.P. // 2002. SIBEDM 2002. The IEEE-Siberian Conference on Electron Devices and Materials. - Tomsk, 2002. - P. 28-31. ↑

C6181. Lombardo P. Optimal classification of polarimetric SAR images using segmentation. / Lombardo P., Oliver C.J. // 2002. Proceedings of the IEEE Radar Conference. 2002. - P. 8-13. ↑

C6182. Stosic D.K. Radar breadboard for DSP scatterometer. / Stosic D.K., Lux J.P. // 2002. Proceedings of the IEEE Radar Conference. 2002. - P. 168-175. ↑

C6183. Ivashov S.I. Subsurface radar investigation of arched wall aperture. / Ivashov S.I., Razevig V.V., Sheyko A.P., Vasilyev I.A., Desmond D.J. // 2002. Proceedings of the IEEE Radar Conference. 2002. - P. 125-128. ↑

C6184. Shostak A.C. Influence of two media interface on the frequency characteristics of a two dipole antenna system. / Shostak A.C., Zagoskin V.V., Lighthart L.P., Iljushenko V.N., Duma R., Yarovoy A.G. // 2002. MIKON-2002. 14th International Conference on Microwaves, Radar and Wireless Communications. 2002. - Vol. 3. - P. 854-857. ↑

C6185. Dawood M. Specular multipath analysis for a coherent ultrawideband random noise radar. / Dawood M., Narayanan R.M. // 2002. IEEE Antennas and Propagation Society International Symposium. 2002. - Vol. 3. - P. 368-371. ↑

C6186. Yanovsky F.J. Airborne weather radar as an instrument for automatic mapping. / Yanovsky F.J., Belkin V.V., Dzyubenko V.P. // 2002. MIKON-2002. 14th International Conference on Microwaves, Radar and Wireless Communications. 2002. - Vol. 2. - P. 704-707. ↑

C6187. Kozlov A.I. Statistical modeling of scattering matrix elements. / Kozlov A.I., Logvin A.I., Lighthart L.P. // 2002. MIKON-2002. 14th International Conference on Microwaves, Radar and Wireless Communications. 2002. - Vol. 2. - P. 673-676. ↑

C6188. Logvin A.I. Methods for solving inverse problems in radar remote sensing. / Logvin A.I., Lighthart L.P., Kozlov A.I. // 2002. MIKON-2002. 14th International Conference on Microwaves, Radar and Wireless Communications. 2002. - Vol. 2. - P. 681-685. ↑

C6189. {no data available}. 2002 IEEE International Geoscience and Remote Sensing Symposium. 24th Canadian Symposium on Remote Sensing. Proceedings (Cat. No.02CH37380). 2002. IGARSS '02. 2002 IEEE International Geoscience and Remote Sensing Symposium. 24-28 June 2002. - Vol. 1. - {no data available}. ↑

C6190. Shimoda H. GCOM mission concept. 2002. IGARSS '02. 2002 IEEE International Geoscience and Remote Sensing Symposium. 2002. - Vol. 1. - P. 3-5. ↑

C6191. Ismail N.H. Mapping of land mines using air borne radars. / Ismail N.H., Khairallah H.N., Metwally M.A. // 2002. (NRSC 2002). Proceedings of the Nineteenth National Radio Science Conference. 2002. - P. 592-598. ↑

- C6192.** Bonneau R.J. A wavelet galerkin scattering approach for improved radar detection models. 2002. IEEE Antennas and Propagation Society International Symposium. 2002. - Vol. 3. - P. 636. ↑
- C6193.** Kacelenga R. Voting fusion adaptation for landmine detection. / Kacelenga R., Erickson D., Palmer D. // 2002. Proceedings of the Fifth International Conference on Information Fusion. 2002. - Vol. 1. - P. 333-340. ↑
- C6194.** Ya-Qiu Jin. The Mueller matrix solution for polarimetric scattering from inhomogeneous random media of non-spherical scatterers under a pulse incidence. / Ya-Qiu Jin, Mei Chang. // 2002. IEEE Antennas and Propagation Society International Symposium. 2002. - Vol. 2. - P. 110-113. ↑
- C6195.** Barkeshli K. The synthesis of offset dual reflector antennas by genetic algorithms. / Barkeshli K., Mazlumi F., Azadegan R. // 2002. IEEE Antennas and Propagation Society International Symposium. 2002. - Vol. 1. - P. 670-673. ↑
- C6196.** Brunham K. A study of bit planes for the compression of raw synthetic aperture radar data. / Brunham K., El Boustani A., Kinsner W. // 2002. IEEE CCECE 2002. Canadian Conference on Electrical and Computer Engineering. 2002. - Vol. 1. - P. 347-352. ↑
- C6197.** {no data available}. IEEE CCECE2002. Canadian Conference on Electrical and Computer Engineering. Conference Proceedings (Cat. No.02CH37373). 2002. IEEE CCECE 2002. Canadian Conference on Electrical and Computer Engineering. 2002. - Vol. 2. - {no data available}. ↑
- C6198.** Tyurin S.V. Research of possible improvement of lidar potential performance. / Tyurin S.V., Bykov M.M., Romanyuk V.A., Shurygin S.V. // 2002. Proceedings of LFNМ 2002. International Workshop on 4thLaser and Fiber-Optical Networks Modeling. 2002. - P. 262-265. ↑
- C6199.** Ligthart L.P. Classification of objects by radar remote sensing. / Ligthart L.P., Logvin A.I., Kozlov A.I. // 2002. MIKON-2002. 14th International Conference on Microwaves, Radar and Wireless Communications. 2002. - Vol. 1. - P. 159-163. ↑
- C6200.** Karnychev V. Determination of polarization invariants of asymmetric scattering matrix. / Karnychev V., Ligthart L., Khlusov V., Sharygin G. // 2002. MIKON-2002. 14th International Conference on Microwaves, Radar and Wireless Communications. 2002. - Vol. 2. - P. 572-575. ↑
- C6201.** Chao-Hsiung Tseng. Frequency-swept microwave imaging using multi-source illumination. / Chao-Hsiung Tseng, Tah-Hsiung Chu. // 2002. IEEE Antennas and Propagation Society International Symposium. 2002. - Vol. 4. - P. 330-333. ↑
- C6202.** Meincke P. Accurate antenna models in ground penetrating radar diffraction tomography. / Meincke P., Kim O. // 2002. IEEE Antennas and Propagation Society International Symposium. 2002. - Vol. 4. - P. 306-309. ↑
- C6203.** Franceschetti G. Modelling and simulating SAR raw signals of oil-covered sea. / Franceschetti G., Iodice A., Riccio D., Ruello G. // 2002. IEEE Antennas and Propagation Society International Symposium. 2002. - Vol. 4. - P. 310-313. ↑
- C6204.** Gurgel K.-W. The role of HF radar within operational forecasting systems of the ocean. / Gurgel K.-W., Essen H.-H., Schlick T. // 2002. IGARSS '02. 2002 IEEE International Geoscience and Remote Sensing Symposium. 2002. - Vol. 1. - P. 512-514. ↑
- C6205.** Wyatt L.R. The availability and accuracy of HF radar wave measurements. / Wyatt L.R., Green J.J. // 2002. IGARSS '02. 2002 IEEE International Geoscience and Remote Sensing Symposium. 2002. - Vol. 1. - P. 515-517. ↑
- C6206.** Pal M. A comparison of decision tree and backpropagation neural network classifiers for land use classification. / Pal M., Mather P.M. // 2002. IGARSS '02. 2002 IEEE International Geoscience and Remote Sensing Symposium. 2002. - Vol. 1. - P. 503-505. ↑
- C6207.** Niemann K.O. Evaluation of RADARSAT-1 for monitoring and mapping land use/land cover in Thailand. / Niemann K.O., Filion R., Flaherty M., Steckler C. // 2002. IGARSS '02. 2002 IEEE International Geoscience and Remote Sensing Symposium. 24-28 June 2002. - Vol. 1. - P. 484-486. ↑
- C6208.** Gamba P. On the optimisation of RBF-based radar rainmap prediction. / Gamba P., Dell'Acqua F. //

2002. IGARSS '02. 2002 IEEE International Geoscience and Remote Sensing Symposium. 2002. - Vol. 1. - P. 491-493. ↑

C6209. Zink M. Calibration and early results of the ASAR on ENVISAT. / Zink M., Torres R., Buck C.H., Rosich B., Closa J. // 2002. IGARSS '02. 2002 IEEE International Geoscience and Remote Sensing Symposium. 2002. - Vol. 1. - P. 596-598. ↑

C6210. Roca M. RA-2/MWR in-flight performance-preliminary results. / Roca M., Laxon S., Zelli C., Martini A., Celani C., Guijarro J., Femenias P. // 2002. IGARSS '02. 2002 IEEE International Geoscience and Remote Sensing Symposium. 2002. - Vol. 1. - P. 611-613. ↑

C6211. Davis A.B. Active optical remote sensing of dense clouds with diffusing light: early results, present implementations, and the challenges ahead. / Davis A.B., Love S.P., Cahalan R.F., McGill M.J., Winker D.M. // 2002. IGARSS '02. 2002 IEEE International Geoscience and Remote Sensing Symposium. 2002. - Vol. 1. - P. 545-547. ↑

C6212. Hickey K. Some fundamental statistics associated with ocean surface current measurement using a dual station, long-range, high-frequency ground wave radar system. / Hickey K., Gill E., Walsh J. // 2002. IGARSS '02. 2002 IEEE International Geoscience and Remote Sensing Symposium. 2002. - Vol. 1. - P. 518-520. ↑

C6213. Gill E.W. A perspective on two decades of fundamental and applied research in electromagnetic scattering and high frequency ground wave radar on the Canadian East Coast. / Gill E.W., Walsh J. // 2002. IGARSS '02. 2002 IEEE International Geoscience and Remote Sensing Symposium. 2002. - Vol. 1. - P. 521-523. ↑

C6214. Chen F.W. Global millimeter-wave observations of precipitation using AMSU on the NOAA-15 satellite. / Chen F.W., Staelin D.H. // 2002. IGARSS '02. 2002 IEEE International Geoscience and Remote Sensing Symposium. 2002. - Vol. 1. - P. 460-462. ↑

C6215. Lawrence D.E. Elastic-wave scattering from a solid circular cylinder embedded in an elastic half-space. / Lawrence D.E., Sarabandi K. // 2002. IGARSS '02. 2002 IEEE International Geoscience and Remote Sensing Symposium. 2002. - Vol. 1. - P. 463-465. ↑

C6216. Mojarrabi B. Power budget study for passive target detection and imaging using secondary applications of GPS signals in bistatic radar systems. / Mojarrabi B., Homer J., Kubik K., Longstaff I.D. // 2002. IGARSS '02. 2002 IEEE International Geoscience and Remote Sensing Symposium. 2002. - Vol. 1. - P. 449-451. ↑

C6217. Lewis G. Bistatic radar scattering experiments of parallel wire grids. / Lewis G., Fortuny-Guasch J., Sieber A. // 2002. IGARSS '02. 2002 IEEE International Geoscience and Remote Sensing Symposium. 2002. - Vol. 1. - P. 444-446. ↑

C6218. Ferrazzoli P. Could bistatic observations contribute to forest biomass monitoring?. / Ferrazzoli P., Guerriero L., Solimini D. // 2002. IGARSS '02. 2002 IEEE International Geoscience and Remote Sensing Symposium. 2002. - Vol. 1. - P. 447-448. ↑

C6219. Yun Shao. Analysis of temporal backscatter of rice: A comparison of RADARSAT observations with modeling results. / Yun Shao, Jingjuan Liao, Xiangtao Fan, Yonghong Wang. // 2002. IGARSS '02. 2002 IEEE International Geoscience and Remote Sensing Symposium. 2002. - Vol. 1. - P. 478-480. ↑

C6220. Del Frate F. Wheat cycle monitoring using radar data and a neural network trained by a model. / Del Frate F., Ferrazzoli P., Guerriero L., Strozzi T., Wegmuller U., Cookmartin G., Quegan S. // 2002. IGARSS '02. 2002 IEEE International Geoscience and Remote Sensing Symposium. 2002. - Vol. 1. - P. 481-483. ↑

C6221. Ouchi K. Automatic rice-crop mapping using maximum likelihood SAR segmentation and Gaussian expectation maximisation. / Ouchi K., Davidson G., Saito G., Ishitsuka N., Mohri N., Uratsuka S. // 2002. IGARSS '02. 2002 IEEE International Geoscience and Remote Sensing Symposium. 2002. - Vol. 1. - P. 475-477. ↑

C6222. Brown C.G. Physics-based simulation of high-resolution polarimetric SAR images of forested areas. / Brown C.G., Sarabandi K., Gilgenbach M. // 2002. IGARSS '02. 2002 IEEE International Geoscience and Remote Sensing Symposium. 2002. - Vol. 1. - P. 466-468. ↑

- C6223.** Arakelyan A.A. Joint application of altimeter and radiometer data for sea surface microwave signatures' detection and classification. / Arakelyan A.A., Hambaryan A.K., Arakelyan A.K. // 2002. IGARSS '02. 2002 IEEE International Geoscience and Remote Sensing Symposium. 24-28 June 2002. - Vol. 1. - P. 472-474. ↑
- C6224.** Bennaceur L. A study of radar backscattering on multi-scale bi-dimensional rough surfaces. / Bennaceur L., Belhadj Z., Boussema M.R. // 2002. IGARSS '02. 2002 IEEE International Geoscience and Remote Sensing Symposium. 2002. - Vol. 1. - P. 659-661. ↑
- C6225.** Mametsa H.J. Application of IEM and radiative transfer formulations for bistatic scattering of rough surfaces. / Mametsa H.J., Koudogbo F., Combes P.F. // 2002. IGARSS '02. 2002 IEEE International Geoscience and Remote Sensing Symposium. 2002. - Vol. 1. - P. 662-664. ↑
- C6226.** Yunhua Zhang. Electromagnetic field simulation of target detection by high-resolution radar. / Yunhua Zhang, Weng Cho Chew, Tie Jun Cui. // 2002. IGARSS '02. 2002 IEEE International Geoscience and Remote Sensing Symposium. 2002. - Vol. 1. - P. 656-658. ↑
- C6227.** Krieger G. Performance analysis for bistatic interferometric SAR configurations. / Krieger G., Wendler M., Fiedler H., Mittermayer J., Moreira A. // 2002. IGARSS '02. 2002 IEEE International Geoscience and Remote Sensing Symposium. 2002. - Vol. 1. - P. 650-652. ↑
- C6228.** Pan G. Comparison of microwave scattering models for leaf. / Pan G., Narayanan R.M. // 2002. IGARSS '02. 2002 IEEE International Geoscience and Remote Sensing Symposium. 2002. - Vol. 1. - P. 653-655. ↑
- C6229.** Aguttes J.P. New designs or modes for flexible space borne SAR. 2002. IGARSS '02. 2002 IEEE International Geoscience and Remote Sensing Symposium. 2002. - Vol. 1. - P. 674-676. ↑
- C6230.** Younis M. An evaluation of performance parameters of reconfigurable SAR systems. / Younis M., Fischer C., Wiesbeck W. // 2002. IGARSS '02. 2002 IEEE International Geoscience and Remote Sensing Symposium. 2002. - Vol. 1. - P. 677-679. ↑
- C6231.** Hoeg F. SAR++: a multi-channel scalable and reconfigurable SAR system. / Hoeg F., Christensen E.L. // 2002. IGARSS '02. 2002 IEEE International Geoscience and Remote Sensing Symposium. 2002. - Vol. 1. - P. 671-673. ↑
- C6232.** Goodman N.A. Synthetic aperture characterization of radar satellite constellations. / Goodman N.A., Stiles J.M. // 2002. IGARSS '02. 2002 IEEE International Geoscience and Remote Sensing Symposium. 2002. - Vol. 1. - P. 665-667. ↑
- C6233.** Soumekh M. Multi-channel airborne radar. 2002. IGARSS '02. 2002 IEEE International Geoscience and Remote Sensing Symposium. 2002. - Vol. 1. - P. 668-670. ↑
- C6234.** Souyris J.-C. Polarimetry based on one transmitting and two receiving polarizations: the $\pi/4$ mode. / Souyris J.-C., Mingot S. // 2002. IGARSS '02. 2002 IEEE International Geoscience and Remote Sensing Symposium. 24-28 June 2002. - Vol. 1. - P. 629-631. ↑
- C6235.** Shimada M. Incidence angle dependence of the L-band POL-IN-SAR sensitivity at forestry region-ALOS PALSAR study using the Pi-SAR. / Shimada M., Tadono T., Rosenqvist A., Shakil A. // 2002. IGARSS '02. 2002 IEEE International Geoscience and Remote Sensing Symposium. 24-28 June 2002. - Vol. 1. - P. 632-634. ↑
- C6236.** Ainsworth T.L. Eigenvector analysis of polarimetric SAR data. / Ainsworth T.L., Cloude S.R., Lee J.S. // 2002. IGARSS '02. 2002 IEEE International Geoscience and Remote Sensing Symposium. 2002. - Vol. 1. - P. 626-628. ↑
- C6237.** Horstmann J. A new method for radiometric calibration of spaceborne SAR and its global monitoring. / Horstmann J., Lehner S. // 2002. IGARSS '02. 2002 IEEE International Geoscience and Remote Sensing Symposium. 2002. - Vol. 1. - P. 620-622. ↑
- C6238.** De Grandi G.F. Multi-resolution analysis of polarimetric SAR data using wavelets. / De Grandi G.F., Lee J.S., Schuler D.L., Siqueira P., Ainsworth T., Simard M. // 2002. IGARSS '02. 2002 IEEE International Geoscience and Remote Sensing Symposium. 2002. - Vol. 1. - P. 623-625. ↑

- C6239.** Yunjin Kim. On the relationship between polarimetric parameters and soil moisture. / Yunjin Kim, van Zyl J. // 2002. IGARSS '02. 2002 IEEE International Geoscience and Remote Sensing Symposium. 2002. - Vol. 1. - P. 644-646. ↑
- C6240.** Jiancheng Shi. Estimate relative soil moisture change with multi-temporal L-band radar measurements. / Jiancheng Shi, Kunshan Chen, Van Zyl J., Yunjin Kim, Eni, Njoku G. // 2002. IGARSS '02. 2002 IEEE International Geoscience and Remote Sensing Symposium. 24-28 June 2002. - Vol. 1. - P. 647-649. ↑
- C6241.** Cloude S.R. A new parameter for soil moisture estimation. / Cloude S.R., Corr D.G. // 2002. IGARSS '02. 2002 IEEE International Geoscience and Remote Sensing Symposium. 2002. - Vol. 1. - P. 641-643. ↑
- C6242.** Ferro-Famil L. Classification and interpretation of polarimetric interferometric SAR data. / Ferro-Famil L., Pottier E., Lee J.S. // 2002. IGARSS '02. 2002 IEEE International Geoscience and Remote Sensing Symposium. 2002. - Vol. 1. - P. 635-637. ↑
- C6243.** Schuler D.L. Polarimetric SAR measurements of slope distribution and coherence changes due to internal waves and current fronts. / Schuler D.L., Kasilingam D., Lee J.S., Jansen R.W., De Grandi G. // 2002. IGARSS '02. 2002 IEEE International Geoscience and Remote Sensing Symposium. 2002. - Vol. 1. - P. 638-640. ↑
- C6244.** Jie Cheng. Model-based principal component techniques for detection of buried landmines in multiframe synthetic aperture radar images. / Jie Cheng, Miller E. // 2002. IGARSS '02. 2002 IEEE International Geoscience and Remote Sensing Symposium. 2002. - Vol. 1. - P. 334-336. ↑
- C6245.** Xiaoyin Xu. Optimization of migration method to locate buried object in lossy medium. / Xiaoyin Xu, Miller E.L. // 2002. IGARSS '02. 2002 IEEE International Geoscience and Remote Sensing Symposium. 2002. - Vol. 1. - P. 337-339. ↑
- C6246.** Fischer C. Multistatic GPR data acquisition and imaging. / Fischer C., Younis M., Wiesbeck W. // 2002. IGARSS '02. 2002 IEEE International Geoscience and Remote Sensing Symposium. 2002. - Vol. 1. - P. 328-330. ↑
- C6247.** Hua Xie. Despeckling SAR images using a low-complexity wavelet denoising process. / Hua Xie, Pierce L.E., Ulaby F.T. // 2002. IGARSS '02. 2002 IEEE International Geoscience and Remote Sensing Symposium. 2002. - Vol. 1. - P. 321-324. ↑
- C6248.** Johnson P.W. Stand off detection of buried anti-personnel landmines. 2002. IGARSS '02. 2002 IEEE International Geoscience and Remote Sensing Symposium. 2002. - Vol. 1. - P. 325-327. ↑
- C6249.** Sato T. A super-resolution locationing algorithm for ultra-wideband phased-array radars. / Sato T., Horita S. // 2002. IGARSS '02. 2002 IEEE International Geoscience and Remote Sensing Symposium. 2002. - Vol. 1. - P. 348-350. ↑
- C6250.** Schoeberl M.R. The afternoon constellation: a formation of Earth observing systems for the atmosphere and hydrosphere. 2002. IGARSS '02. 2002 IEEE International Geoscience and Remote Sensing Symposium. 2002. - Vol. 1. - P. 354-356. ↑
- C6251.** Sato M. Ground water migration monitoring by GPR. / Sato M., Lu Q. // 2002. IGARSS '02. 2002 IEEE International Geoscience and Remote Sensing Symposium. 2002. - Vol. 1. - P. 345-347. ↑
- C6252.** Coatanhay A. Optimized GPR signal deconvolution using an adaptative conjugate gradient method. 2002. IGARSS '02. 2002 IEEE International Geoscience and Remote Sensing Symposium. 2002. - Vol. 1. - P. 340-341. ↑
- C6253.** Yapar A. On the use of surface impedance in the detection of buried objects. / Yapar A., Sahinturk H. // 2002. IGARSS '02. 2002 IEEE International Geoscience and Remote Sensing Symposium. 2002. - Vol. 1. - P. 342-344. ↑
- C6254.** Villa J.M. Performance of scanning millimeter-wave radar in a tropical environment. / Villa J.M., Cruz-Pol S.L., Sekelsky S.M. // 2002. IGARSS '02. 2002 IEEE International Geoscience and Remote Sensing Symposium. 2002. - Vol. 1. - P. 284-286. ↑

- C6255.** Kwiatkowski J. Estimating TRMM spacecraft attitude errors using the precipitation radar. / Kwiatkowski J., Stout J., Bilanow S. // 2002. IGARSS '02. 2002 IEEE International Geoscience and Remote Sensing Symposium. 2002. - Vol. 1. - P. 287-289. ↑
- C6256.** Im E. Rainfall observations by the airborne dual-frequency precipitation radar during CAMEX-4. / Im E., Durden S.L., Sadowy G., Li L. // 2002. IGARSS '02. 2002 IEEE International Geoscience and Remote Sensing Symposium. 2002. - Vol. 1. - P. 281-283. ↑
- C6257.** Gorgucci E. Polarimetric radar rainfall algorithms at S and X bands. / Gorgucci E., Chandrasekar V., Bringi V.N. // 2002. IGARSS '02. 2002 IEEE International Geoscience and Remote Sensing Symposium. 2002. - Vol. 1. - P. 275-277. ↑
- C6258.** Liang Liao. Bright-band modeling of air/space-borne microwave radars. / Liang Liao, Meneghini R., Iguchi T. // 2002. IGARSS '02. 2002 IEEE International Geoscience and Remote Sensing Symposium. 2002. - Vol. 1. - P. 278-280. ↑
- C6259.** Ulfarsson M.O. Speckle reduction of SAR images in the curvelet domain. / Ulfarsson M.O., Sveinsson J.R., Benediktsson J.A. // 2002. IGARSS '02. 2002 IEEE International Geoscience and Remote Sensing Symposium. 2002. - Vol. 1. - P. 315-317. ↑
- C6260.** Aiazzi B. Heterogeneity-sensitive adaptive speckle reduction in a translation-invariant wavelet domain. / Aiazzi B., Alparone L., Argenti F., Baronti S. // 2002. IGARSS '02. 2002 IEEE International Geoscience and Remote Sensing Symposium. 2002. - Vol. 1. - P. 318-320. ↑
- C6261.** Zrnic D.S. Enhanced polarimetric radar signatures above the melting level in a supercell storm. / Zrnic D.S., Loney M.L., Straka J.M., Ryzhkov A.V. // 2002. IGARSS '02. 2002 IEEE International Geoscience and Remote Sensing Symposium. 2002. - Vol. 1. - P. 296-298. ↑
- C6262.** Bolen S. Evaluation of TRMM PR attenuation correction using ground radar estimations of the raindrop size distribution along the PR beam. / Bolen S., Chandrasekar V. // 2002. IGARSS '02. 2002 IEEE International Geoscience and Remote Sensing Symposium. 2002. - Vol. 1. - P. 290-292. ↑
- C6263.** Fukatsu H. Global mapping of attenuation at X-band and higher frequencies. / Fukatsu H., Chandrasekar V. // 2002. IGARSS '02. 2002 IEEE International Geoscience and Remote Sensing Symposium. 2002. - Vol. 1. - P. 293-295. ↑
- C6264.** Yamaguchi Y. L-band polarimetric AIR/Pi-SAR images around Niigata City. / Yamaguchi Y., Kimura K., Yamada H., Uratsuka S., Boerner W.-M. // 2002. IGARSS '02. 2002 IEEE International Geoscience and Remote Sensing Symposium. 24-28 June 2002. - Vol. 1. - P. 423-425. ↑
- C6265.** Allain S. Extraction of surface parameters from multi-frequency and polarimetric SAR data. / Allain S., Ferro-Famil L., Pottier E., Hajnsek I. // 2002. IGARSS '02. 2002 IEEE International Geoscience and Remote Sensing Symposium. 2002. - Vol. 1. - P. 426-428. ↑
- C6266.** Hajnsek I. Surface parameter estimation using interferometric and polarimetric SAR. / Hajnsek I., Papathanassiou K.P., Moreira A., Cloude S.R. // 2002. IGARSS '02. 2002 IEEE International Geoscience and Remote Sensing Symposium. 2002. - Vol. 1. - P. 420-422. ↑
- C6267.** Touzi R. Characterization of symmetric scattering using polarimetric SARs. / Touzi R., Charbonneau F. // 2002. IGARSS '02. 2002 IEEE International Geoscience and Remote Sensing Symposium. 2002. - Vol. 1. - P. 414-416. ↑
- C6268.** Ferro-Famil L. Scene characterization using sub-aperture polarimetric SAR data analysis. / Ferro-Famil L., Reigber A., Pottier E., Boerner W.M. // 2002. IGARSS '02. 2002 IEEE International Geoscience and Remote Sensing Symposium. 2002. - Vol. 1. - P. 417-419. ↑
- C6269.** Homer J. Passive bistatic radar sensing with LEOS based transmitters. / Homer J., Kubik K., Mojarrabi B., Longstaff I.D., Donskoi E., Cherniakov M. // 2002. IGARSS '02. 2002 IEEE International Geoscience and Remote Sensing Symposium. 2002. - Vol. 1. - P. 438-440. ↑
- C6270.** Fung A.K. A comparison between IEM-based surface bistatic scattering models. / Fung A.K., Liu W.Y., Chen K.S. // 2002. IGARSS '02. 2002 IEEE International Geoscience and Remote Sensing Symposium. 2002. -

Vol. 1. - P. 441-443. ↑

C6271. Amiot T. The interferometric cartwheel: a multi-purpose formation of passive radar microsatellites. / Amiot T., Douchin F., Thouvenot E., Souyris J.C., Cugny B. // 2002. IGARSS '02. 2002 IEEE International Geoscience and Remote Sensing Symposium. 24-28 June 2002. - Vol. 1. - P. 435-437. ↑

C6272. Morris J. Polarimetric mapping of ship wakes. / Morris J., Anderson S., Parfitt A. // 2002. IGARSS '02. 2002 IEEE International Geoscience and Remote Sensing Symposium. 2002. - Vol. 1. - P. 429-431. ↑

C6273. Kasilingam D. Modulation of polarimetric coherence by ocean features. / Kasilingam D., Schuler D., Jong-Sen Lee, Malhotra S. // 2002. IGARSS '02. 2002 IEEE International Geoscience and Remote Sensing Symposium. 2002. - Vol. 1. - P. 432-434. ↑

C6274. Kimura H. Feasibility study on polarimetric use and calibration of ALOS/PALSAR. / Kimura H., Mizuno T. // 2002. IGARSS '02. 2002 IEEE International Geoscience and Remote Sensing Symposium. 2002. - Vol. 1. - P. 387-389. ↑

C6275. Fujita M. Development of a retrodirective PARC for ALOS/PALSAR calibration. 2002. IGARSS '02. 2002 IEEE International Geoscience and Remote Sensing Symposium. 2002. - Vol. 1. - P. 390-392. ↑

C6276. Shimada A. Calibration and validation of PALSAR. / Shimada A., Tadono T., Matsuoka M. // 2002. IGARSS '02. 2002 IEEE International Geoscience and Remote Sensing Symposium. 2002. - Vol. 1. - P. 393-395. ↑

C6277. Lansing F. Needs for communications and onboard processing in the vision era. / Lansing F., Lemmerman L., Walton A., Bothwell G., Bhasin K., Prescott G. // 2002. IGARSS '02. 2002 IEEE International Geoscience and Remote Sensing Symposium. 2002. - Vol. 1. - P. 375-377. ↑

C6278. Yamaguchi Y. ALOS-PALSAR image simulation in various polarization bases. / Yamaguchi Y., Kimura K., Kakizaki S., Yamada H. // 2002. IGARSS '02. 2002 IEEE International Geoscience and Remote Sensing Symposium. 2002. - Vol. 1. - P. 381-383. ↑

C6279. Boerner W.-M. Advances in extra wide-band multi-modal air/space-borne radar polarimetry, POL-IN-SAR imaging and its applications. / Boerner W.-M., Cloude S.R., Jong-Sen Lee, Papathanassiou K.P., Lukowski T.I. // 2002. IGARSS '02. 2002 IEEE International Geoscience and Remote Sensing Symposium. 2002. - Vol. 1. - P. 408-410. ↑

C6280. Cloude S.R. Helicity in radar remote sensing. 2002. IGARSS '02. 2002 IEEE International Geoscience and Remote Sensing Symposium. 2002. - Vol. 1. - P. 411-413. ↑

C6281. Cho K. Preparation of multi-stage remote sensing for monitoring sea ice in the Okhotsk Sea with ALOS sensors. / Cho K., Nakayama M., Shimoda H., Uratsuka S., Enomoto H., Honda Y. // 2002. IGARSS '02. 2002 IEEE International Geoscience and Remote Sensing Symposium. 2002. - Vol. 1. - P. 402-404. ↑

C6282. Guo Huadong. Study of environmental issues with ALOS PALSAR data. / Guo Huadong, Wang Changlin. // 2002. IGARSS '02. 2002 IEEE International Geoscience and Remote Sensing Symposium. 2002. - Vol. 1. - P. 396-398. ↑

C6283. Kawamura H. Study on air-sea-land interaction in the coastal seas using ALOS data. 2002. IGARSS '02. 2002 IEEE International Geoscience and Remote Sensing Symposium. 2002. - Vol. 1. - P. 399-401. ↑

C6284. Gao Xin. Anisotropic diffusion filtering and phase unwrapping for interferometric SAR. / Gao Xin, Wang Chao, Zhang Hong. // 2002. IGARSS '02. 2002 IEEE International Geoscience and Remote Sensing Symposium. 24-28 June 2002. - Vol. 3. - P. 1744-1746. ↑

C6285. Bachmann T.M. PURSUIT: an automatic classification tool for remote sensing data. / Bachmann T.M., Bettenhausen M.H. // 2002. IGARSS '02. 2002 IEEE International Geoscience and Remote Sensing Symposium. 2002. - Vol. 6. - P. 3360-3362. ↑

C6286. Berizzi F. A spectral analysis algorithm for the estimation of sea SAR image fractal dimension. / Berizzi F., Garzelli A., Mese E.D., Condello R. // 2002. IGARSS '02. 2002 IEEE International Geoscience and Remote Sensing Symposium. 2002. - Vol. 6. - P. 3366-3368. ↑

- C6287.** Friedman K.S. GoMEx-an experimental GIS system for the Gulf of Mexico region using SAR and additional satellite and ancillary data. / Friedman K.S., Pichel W.G., Clemente-Colon P., Xiaofeng Li. // 2002. IGARSS '02. 2002 IEEE International Geoscience and Remote Sensing Symposium. 2002. - Vol. 6. - P. 3343-3345. ↑
- C6288.** Sahyun Hong. Data fusion of multiple polarimetric SAR images using discrete wavelet transform (DWT). / Sahyun Hong, Moon W.M., Hong-Yul Paik, Gi-Hyuk Choi. // 2002. IGARSS '02. 2002 IEEE International Geoscience and Remote Sensing Symposium. 2002. - Vol. 6. - P. 3323-3325. ↑
- C6289.** Deschamps A. Geospatial data integration for applications in flood prediction and management in the Red River Basin. / Deschamps A., Greenlee D., Pultz T.J., Saper R. // 2002. IGARSS '02. 2002 IEEE International Geoscience and Remote Sensing Symposium. 2002. - Vol. 6. - P. 3338-3340. ↑
- C6290.** Toutin T. Path processing and block bundle adjustment with RADARSAT-1 SAR images. / Toutin T., Carbonneau Y., Chenier R. // 2002. IGARSS '02. 2002 IEEE International Geoscience and Remote Sensing Symposium. 2002. - Vol. 6. - P. 3432-3434. ↑
- C6291.** Xiaoyin Xu. Adaptive difference of Gaussians to improve subsurface imagery. / Xiaoyin Xu, Miller E.L. // 2002. IGARSS '02. 2002 IEEE International Geoscience and Remote Sensing Symposium. 24-28 June 2002. - Vol. 6. - P. 3441-3443. ↑
- C6292.** Sakurai-Amano T. Automatic extraction of rivers in tropical rain forests from JERS-1 SAR images using spectral and spatial information. / Sakurai-Amano T., Onuki S., Takagi M. // 2002. IGARSS '02. 2002 IEEE International Geoscience and Remote Sensing Symposium. 2002. - Vol. 6. - P. 3429-3431. ↑
- C6293.** Gigli G. A new maximum likelihood generalized gamma CFAR detector. / Gigli G., Lampropoulos G.A. // 2002. IGARSS '02. 2002 IEEE International Geoscience and Remote Sensing Symposium. 24-28 June 2002. - Vol. 6. - P. 3399-3401. ↑
- C6294.** Han Chunming. A new multiscale edge detection technique [for synthetic aperture radar images]. / Han Chunming, Guo Huadong, Wang Changlin, Tan Qulin. // 2002. IGARSS '02. 2002 IEEE International Geoscience and Remote Sensing Symposium. 2002. - Vol. 6. - P. 3402-3404. ↑
- C6295.** Buckley J.R. Environmental change detection in prairie landscapes with simulated Radarsat 2 imagery. 2002. IGARSS '02. 2002 IEEE International Geoscience and Remote Sensing Symposium. 2002. - Vol. 6. - P. 3255-3257. ↑
- C6296.** Xulong Peng. Land cover classification using RADARSAT data in a mountainous area of southern Argentina. / Xulong Peng, Jinfei Wang, Raed M., Gari J. // 2002. IGARSS '02. 2002 IEEE International Geoscience and Remote Sensing Symposium. 2002. - Vol. 6. - P. 3270-3272. ↑
- C6297.** Cuccoli F. Monostatic CW radar system for microwave attenuation measurements for atmospheric water vapor estimate. / Cuccoli F., Facheris L. // 2002. IGARSS '02. 2002 IEEE International Geoscience and Remote Sensing Symposium. 2002. - Vol. 6. - P. 3215-3217. ↑
- C6298.** Yang Zhen. Feasibility study of using small satellite synthetic aperture radar for global 3D imaging. / Yang Zhen, Ruliang Y. // 2002. IGARSS '02. 2002 IEEE International Geoscience and Remote Sensing Symposium. 2002. - Vol. 6. - P. 3162-3164. ↑
- C6299.** Giancaspro A. COSMO-SkyMed SAR processing parallel implementation. / Giancaspro A., Candela L., Lopinto E., Lore V.A., Milillo G. // 2002. IGARSS '02. 2002 IEEE International Geoscience and Remote Sensing Symposium. 2002. - Vol. 6. - P. 3165-3166. ↑
- C6300.** Gleich D. Fuzzy coded space frequency quantization. / Gleich D., Planinsic P., Cucej Z. // 2002. IGARSS '02. 2002 IEEE International Geoscience and Remote Sensing Symposium. 2002. - Vol. 6. - P. 3308-3310. ↑
- C6301.** Cagnazzo M. The advantage of segmentation in SAR image compression. / Cagnazzo M., Poggi G., Verdoliva L. // 2002. IGARSS '02. 2002 IEEE International Geoscience and Remote Sensing Symposium. 2002. - Vol. 6. - P. 3320-3322. ↑
- C6302.** Hardin P.J. Examining vegetation phenological change in South America using reconstructed

SeaWinds data: grasslands and savanna. / Hardin P.J., Jackson M.W. // 2002. IGARSS '02. 2002 IEEE International Geoscience and Remote Sensing Symposium. 2002. - Vol. 6. - P. 3296-3298. ↑

C6303. Tae Hee Lee. Lineament extraction from Landsat TM, JERS-1 SAR, and DEM for geological applications. / Tae Hee Lee, Moon W.M. // 2002. IGARSS '02. 2002 IEEE International Geoscience and Remote Sensing Symposium. 2002. - Vol. 6. - P. 3276-3278. ↑

C6304. Takeuchi S. Monitoring of forest fire damage by using JERS-1 InSAR. / Takeuchi S., Yamada S. // 2002. IGARSS '02. 2002 IEEE International Geoscience and Remote Sensing Symposium. 2002. - Vol. 6. - P. 3290-3292. ↑

C6305. ZhaoHui Zhang. A new method for SAR speckle reduction. / ZhaoHui Zhang, Prinnet V., SongDe Ma. // 2002. IGARSS '02. 2002 IEEE International Geoscience and Remote Sensing Symposium. 24-28 June 2002. - Vol. 6. - P. 3450-3452. ↑

C6306. Sai B. Characterization of local 3D rough surfaces using UWB near-range phase-based GPR signatures from wide-beamwidth antennas. / Sai B., Ligthart L.P. // 2002. IGARSS '02. 2002 IEEE International Geoscience and Remote Sensing Symposium. 24-28 June 2002. - Vol. 6. - P. 3582-3584. ↑

C6307. Xiaoyin Xu. On the use of contrast stretch and adaptive filter to enhance ground penetrating radar imagery. / Xiaoyin Xu, Miller E.L. // 2002. IGARSS '02. 2002 IEEE International Geoscience and Remote Sensing Symposium. 24-28 June 2002. - Vol. 6. - P. 3585-3587. ↑

C6308. Leuschen C. Field experiments of a surface-penetrating radar for Mars. / Leuschen C., Kanagaratnam P., Yoshikawa K., Arcone S., Gogineni P. // 2002. IGARSS '02. 2002 IEEE International Geoscience and Remote Sensing Symposium. 24-28 June 2002. - Vol. 6. - P. 3579-3581. ↑

C6309. Mironov V.L. Generalized refractive mixing dielectric model for moist soils. / Mironov V.L., Dobson M.C., Kaupp V.H., Komarov S.A., Kleshchenko V.N. // 2002. IGARSS '02. 2002 IEEE International Geoscience and Remote Sensing Symposium. 24-28 June 2002. - Vol. 6. - P. 3556-3558. ↑

C6310. Ya-Qiu Jin. The Mueller matrix solution for polarimetric scattering from inhomogeneous random media of non-spherical scatterers under a pulse incidence. / Ya-Qiu Jin, Mei Chang. // 2002. IGARSS '02. 2002 IEEE International Geoscience and Remote Sensing Symposium. 24-28 June 2002. - Vol. 6. - P. 3567-3569. ↑

C6311. Muramoto K. Measurement of snowfall parameters by radar and optical lidar. / Muramoto K., Servomaa H., Kubo M., Ebisu S., Shiina T. // 2002. IGARSS '02. 2002 IEEE International Geoscience and Remote Sensing Symposium. 24-28 June 2002. - Vol. 6. - P. 3599-3601. ↑

C6312. Rall J.A.R. Automated Geophysical Observatory (AGO) Lidar-post Antarctic deployment performance. / Rall J.A.R., Cavanaugh J., Campbell J., Abshire J.B., Spinhirne J.D. // 2002. IGARSS '02. 2002 IEEE International Geoscience and Remote Sensing Symposium. 24-28 June 2002. - Vol. 6. - P. 3602-3604. ↑

C6313. Lewis K. Development of a 3-D scanning 1.5 μm portable aerosol lidar. / Lewis K., Wei Gong, Temple D.A., Omar A.H., Mangana J. // 2002. IGARSS '02. 2002 IEEE International Geoscience and Remote Sensing Symposium. 24-28 June 2002. - Vol. 6. - P. 3595-3598. ↑

C6314. Allen C. Test results from a 1319-nm laser radar with RF pulse compression. / Allen C., Chong S.K., Cobanoglu Y., Gogineni S. // 2002. IGARSS '02. 2002 IEEE International Geoscience and Remote Sensing Symposium. 24-28 June 2002. - Vol. 6. - P. 3588-3590. ↑

C6315. Filin S. Establishing analytical criteria for selection of sites for calibration of spaceborne laser altimeters. 2002. IGARSS '02. 2002 IEEE International Geoscience and Remote Sensing Symposium. 24-28 June 2002. - Vol. 6. - P. 3591-3594. ↑

C6316. Ma Debao. The relative and absolute geometric algorithm for the ERS baseline estimation. / Ma Debao, Li Wugao, Wang Fuming. // 2002. IGARSS '02. 2002 IEEE International Geoscience and Remote Sensing Symposium. 24-28 June 2002. - Vol. 6. - P. 3462-3464. ↑

C6317. Yue Huanyin. SAR interferogram MAP filtering based on stationary wavelet transform. / Yue Huanyin, Guo Huadong, Wang Changlin. // 2002. IGARSS '02. 2002 IEEE International Geoscience and Remote Sensing Symposium. 24-28 June 2002. - Vol. 6. - P. 3465-3467. ↑

- C6318.** Ma Debao. A piece-wise polynomial fitting method to filter the interferogram phase noise [InSAR]. / Ma Debao, Liu Ming, Deng Yi-qun, Lin Yi. // 2002. IGARSS '02. 2002 IEEE International Geoscience and Remote Sensing Symposium. 24-28 June 2002. - Vol. 6. - P. 3459-3461. ↑
- C6319.** Ciuc M. Amplitude-driven coherence filtering in complex interferograms. / Ciuc M., Trouve E., Bolon P., Buzuloiu V. // 2002. IGARSS '02. 2002 IEEE International Geoscience and Remote Sensing Symposium. 24-28 June 2002. - Vol. 6. - P. 3453-3455. ↑
- C6320.** Gens R. The Alaska DEM project: repeat-geometry approach for generating accurate InSAR DEMs. / Gens R., Jirousek M., Guritz R., Conner J. // 2002. IGARSS '02. 2002 IEEE International Geoscience and Remote Sensing Symposium. 24-28 June 2002. - Vol. 6. - P. 3456-3458. ↑
- C6321.** Nadir Arslan A. Scattering from wet snow by applying strong fluctuation theory. / Nadir Arslan A., Wang Huining, Koskinen J., Pulliainen J., Hallikainen M. // 2002. IGARSS '02. 2002 IEEE International Geoscience and Remote Sensing Symposium. 24-28 June 2002. - Vol. 6. - P. 3539-3541. ↑
- C6322.** Takumi I. Estimation of EM radiation source in ELF band. / Takumi I., Saito S., Shimura A., Hata M., Yasukawa H. // 2002. IGARSS '02. 2002 IEEE International Geoscience and Remote Sensing Symposium. 24-28 June 2002. - Vol. 6. - P. 3551-3553. ↑
- C6323.** Xie Wenhan. The application of analysis techniques based on DEM and GIS in airborne radar signal simulation. / Xie Wenhan, Lu Jian, Miao Yumei. // 2002. IGARSS '02. 2002 IEEE International Geoscience and Remote Sensing Symposium. 24-28 June 2002. - Vol. 6. - P. 3531-3534. ↑
- C6324.** Hosokawa M. Polarimetric SAR data classification method using the self-organizing map. / Hosokawa M., Hoshi T. // 2002. IGARSS '02. 2002 IEEE International Geoscience and Remote Sensing Symposium. 24-28 June 2002. - Vol. 6. - P. 3468-3470. ↑
- C6325.** Wanyu Li. Rainfall estimation from vertical profiles of reflectivity using neural networks. / Wanyu Li, Chandrasekar V. // 2002. IGARSS '02. 2002 IEEE International Geoscience and Remote Sensing Symposium. 24-28 June 2002. - Vol. 6. - P. 3477-3479. ↑
- C6326.** Gauthier E. Left- and right-looking RADARSAT-2 data for mosaics of ancient supercontinents. / Gauthier E., Budkewitsch P., D'Iorio M., de Miranda F.P. // 2002. IGARSS '02. 2002 IEEE International Geoscience and Remote Sensing Symposium. 2002. - Vol. 6. - P. 3142-3144. ↑
- C6327.** Ouchi K. Comparison of SAR and optical images of the rainforests of Borneo, Malaysia with field data. / Ouchi K., Ipor I.B. // 2002. IGARSS '02. 2002 IEEE International Geoscience and Remote Sensing Symposium. 2002. - Vol. 5. - P. 2905-2907. ↑
- C6328.** Vierling L.A. Relationships among airborne scanning LiDAR, high resolution multispectral imagery, and ground-based inventory data in a ponderosa pine forest. / Vierling L.A., Rowell E., Xuexia Chen, Dykstra D., Vierling K. // 2002. IGARSS '02. 2002 IEEE International Geoscience and Remote Sensing Symposium. 2002. - Vol. 5. - P. 2912-2914. ↑
- C6329.** Eriksson L.E.B. Multi-temporal JERS coherence for observation of Siberian forest. / Eriksson L.E.B., Schmullius C., Riedel T., Wiesmann A. // 2002. IGARSS '02. 2002 IEEE International Geoscience and Remote Sensing Symposium. 2002. - Vol. 5. - P. 2896-2898. ↑
- C6330.** Cunjian Yang. Rapidly assessing the flood disaster by using remote sensing and GIS. / Cunjian Yang, He Huang, Yiming Wei, Hong Zhu, Jieming Zhuo. // 2002. IGARSS '02. 2002 IEEE International Geoscience and Remote Sensing Symposium. 2002. - Vol. 5. - P. 2880-2882. ↑
- C6331.** Deslandes S. The wetland conservation atlas of the St. Lawrence valley produced from decision tree classifications of RADARSAT and Landsat images. / Deslandes S., Grenier M., Belanger L., Lacroix G., Zingraff V. // 2002. IGARSS '02. 2002 IEEE International Geoscience and Remote Sensing Symposium. 2002. - Vol. 5. - P. 2893-2895. ↑
- C6332.** Tadono T. Development of an algorithm for estimating snow hydrological parameters in wet snow regions using combined C- and L-band satellite-based SAR data. / Tadono T., Fukami K., Shi J. // 2002. IGARSS '02. 2002 IEEE International Geoscience and Remote Sensing Symposium. 2002. - Vol. 5. - P. 2930-2932. ↑

- C6333.** Lariviere J.M. Application of RADARSAT-1 in mineral potential evaluation, Lac Grandin area, NWT: identifying geologic features/processes associated with mineralization. / Lariviere J.M., Molch K., Singhroy V. // 2002. IGARSS '02. 2002 IEEE International Geoscience and Remote Sensing Symposium. 2002. - Vol. 5. - P. 2936-2938. ↑
- C6334.** Farina P. Estimating the morphological changes in fluvial beds by means of differential SAR interferometry. / Farina P., Leva D., Nico G., Moretti S., Rinaldi M., Tarchi D. // 2002. IGARSS '02. 2002 IEEE International Geoscience and Remote Sensing Symposium. 2002. - Vol. 5. - P. 2924-2926. ↑
- C6335.** Casagli N. Monitoring the Tessina landslide by a ground-based SAR interferometer and assessment of the system accuracy. / Casagli N., Farina P., Leva D., Nico G., Tarchi D. // 2002. IGARSS '02. 2002 IEEE International Geoscience and Remote Sensing Symposium. 2002. - Vol. 5. - P. 2915-2917. ↑
- C6336.** Rodriguez K.M. Classification of landslide surfaces using fully polarimetric SAR: examples from Taiwan. / Rodriguez K.M., Weissel J.K., Kim Y. // 2002. IGARSS '02. 2002 IEEE International Geoscience and Remote Sensing Symposium. 2002. - Vol. 5. - P. 2918-2920. ↑
- C6337.** Ryzhkov A. Using multiparameter data to calibrate polarimetric weather radars in the presence of a partial beam blockage. / Ryzhkov A., Giangrande S., Zrnic D. // 2002. IGARSS '02. 2002 IEEE International Geoscience and Remote Sensing Symposium. 2002. - Vol. 5. - P. 2832-2834. ↑
- C6338.** Yanovsky F.J. Recognition of hail areas with polarimetric radar by the method of potential functions. / Yanovsky F.J., Sinitsyn R.B., Braun I.M. // 2002. IGARSS '02. 2002 IEEE International Geoscience and Remote Sensing Symposium. 2002. - Vol. 5. - P. 2835-2837. ↑
- C6339.** Majurec N. Triple-wavelength radar for cloud and precipitation microphysics research. / Majurec N., Sekelsky S.M., Schaubert D.H., Hong Y., Rutledge S.A., Stephens G.L., Heymsfield A. // 2002. IGARSS '02. 2002 IEEE International Geoscience and Remote Sensing Symposium. 2002. - Vol. 5. - P. 2826-2828. ↑
- C6340.** Del Frate F. Ground-based radiometric retrieval of cloud liquid. / Del Frate F., Schiavon G., Solimini D., Simpson P.M., Brand E.C., Wrench C.L. // 2002. IGARSS '02. 2002 IEEE International Geoscience and Remote Sensing Symposium. 2002. - Vol. 5. - P. 2820-2822. ↑
- C6341.** Gojara K. Cross-calibration of ground and space radar. / Gojara K., Chandrasekar V. // 2002. IGARSS '02. 2002 IEEE International Geoscience and Remote Sensing Symposium. 2002. - Vol. 5. - P. 2823-2825. ↑
- C6342.** Kuehn S. Efficient flood monitoring based on RADARSAT-1 images data and information fusion with object-oriented technology. / Kuehn S., Benz U., Hurley J. // 2002. IGARSS '02. 2002 IEEE International Geoscience and Remote Sensing Symposium. 2002. - Vol. 5. - P. 2862-2864. ↑
- C6343.** Yamada Y. Detection of flood damaged areas in the entire Chao Phraya River Basin from JERS-1/SAR images with a help of spatial information. / Yamada Y., Sakurai-Amano T., Takagi M. // 2002. IGARSS '02. 2002 IEEE International Geoscience and Remote Sensing Symposium. 2002. - Vol. 5. - P. 2877-2879. ↑
- C6344.** Ito Y. Damage estimation model using temporal coherence ratio. / Ito Y., Hosokawa M. // 2002. IGARSS '02. 2002 IEEE International Geoscience and Remote Sensing Symposium. 2002. - Vol. 5. - P. 2859-2861. ↑
- C6345.** Donato T.F. A comparative analysis of Landsat TM and radarsat SAR signatures in restricted tidal channels. / Donato T.F., Lyzenga D.R., Xiao-Hai Yan. // 2002. IGARSS '02. 2002 IEEE International Geoscience and Remote Sensing Symposium. 2002. - Vol. 5. - P. 2841-2843. ↑
- C6346.** Marghany M. Polarised TOPSAR operational model of internal wave generation mechanism. 2002. IGARSS '02. 2002 IEEE International Geoscience and Remote Sensing Symposium. 2002. - Vol. 5. - P. 2847-2849. ↑
- C6347.** Bulatov M.G. Microwave, optical and IR combined studies of the sea surface perturbations caused by underwater gas bubble plume. / Bulatov M.G., Kravtsov Yu.A., Raev M.D., Repina I.A., Skvortsov E.I. // 2002. IGARSS '02. 2002 IEEE International Geoscience and Remote Sensing Symposium. 2002. - Vol. 5. - P. 2983-2985. ↑
- C6348.** Hogda K.A. Use of Radarsat F5 images for detection and positioning of fish cages. / Hogda K.A.,

Malnes E. // 2002. IGARSS '02. 2002 IEEE International Geoscience and Remote Sensing Symposium. 2002. - Vol. 5. - P. 3047-3049. ↑

C6349. Chao Wang. Joint field experiment of microwave and visible sensors for bare soil and vegetation and preliminary analysis. / Chao Wang, Weiguo Zhang, Hong Zhang, Ziqi Guo, Jianjun Ge, Kai Zhao, Baojiang Liu, Hang Dong. // 2002. IGARSS '02. 2002 IEEE International Geoscience and Remote Sensing Symposium. 2002. - Vol. 5. - P. 3062-3064. ↑

C6350. Qiyao Yu. SAR sea-ice texture classification using discrete wavelet transform based methods. / Qiyao Yu, Moloney C., Williams F.M. // 2002. IGARSS '02. 2002 IEEE International Geoscience and Remote Sensing Symposium. 2002. - Vol. 5. - P. 3041-3043. ↑

C6351. Garcia E. A comparison of sea ice field observations in the Barents Sea marginal ice zone with satellite SAR data. / Garcia E., Maksym T., Simard M., Dierking W., Van Woert M., Nghiem S.V., St Germain K. // 2002. IGARSS '02. 2002 IEEE International Geoscience and Remote Sensing Symposium. 2002. - Vol. 5. - P. 3035-3037. ↑

C6352. Kaleschke L. ERS-2 SAR image analysis for sea ice classification in the marginal ice zone. / Kaleschke L., Kern S. // 2002. IGARSS '02. 2002 IEEE International Geoscience and Remote Sensing Symposium. 2002. - Vol. 5. - P. 3038-3040. ↑

C6353. Pierdicca N. Passive calibration of the backscattering coefficient of the ENVISAT RA-2: evaluation of radiative models for sea and land. / Pierdicca N., Castracane P., Pulvirenti L., Greco B., Ferrazzoli P., Guerriero L., Schiavon G., Ciotti P., Marzano F.S., Bernardini L., Basili P., Bonafoni S., Mattioli V. // 2002. IGARSS '02. 2002 IEEE International Geoscience and Remote Sensing Symposium. 2002. - Vol. 6. - P. 3105-3107. ↑

C6354. Leshkevich G.A. Radar remote sensing of Great Lakes ice cover. / Leshkevich G.A., Nghiem S.V. // 2002. IGARSS '02. 2002 IEEE International Geoscience and Remote Sensing Symposium. 2002. - Vol. 6. - P. 3132 vol.6. ↑

C6355. Rostan F. The CryoSat space segment: definition, design and predicted performance. / Rostan F., Mallow U. // 2002. IGARSS '02. 2002 IEEE International Geoscience and Remote Sensing Symposium. 2002. - Vol. 6. - P. 3102-3104. ↑

C6356. Zhen Li. Measuring soil moisture change with vegetation cover using passive and active microwave data. / Zhen Li, Jiancheng Shi, Huadong Guo. // 2002. IGARSS '02. 2002 IEEE International Geoscience and Remote Sensing Symposium. 2002. - Vol. 5. - P. 3071-3073. ↑

C6357. Lentz H. Concept and realization of an Airborne SAR/Interferometric Radar Altimeter System (ASIRAS). / Lentz H., Braun H.-M., Younis M., Fischer C., Wiesbeck W., Mavrocordatos C. // 2002. IGARSS '02. 2002 IEEE International Geoscience and Remote Sensing Symposium. 2002. - Vol. 6. - P. 3099-3101. ↑

C6358. Dong Qing. South China Sea internal wave analysis using radar imagery. / Dong Qing, Guo Huadong, Zhou Chenghu, Shao Yun, Wang Changlin, Li Zhen. // 2002. IGARSS '02. 2002 IEEE International Geoscience and Remote Sensing Symposium. 2002. - Vol. 5. - P. 3008-3010. ↑

















C6359. Hayslip A.R. Further numerical studies of backscattering from time evolving non-linear sea surfaces. / Hayslip A.R., Johnson J.T., Baker G.R. // 2002. IGARSS '02. 2002 IEEE International Geoscience and Remote Sensing Symposium. 2002. - Vol. 5. - P. 3011-3013. ↑

C6360. Lavrova O.Yu. SAR manifestations of sea fronts and vortex streets in the Bering Strait. / Lavrova O.Yu., Bocharova T.Yu., Sabinin K.D. // 2002. IGARSS '02. 2002 IEEE International Geoscience and Remote Sensing Symposium. 2002. - Vol. 5. - P. 2997-2999. ↑

C6361. Ermakov S.A. Anormal Doppler shifts of radar signals backscattered from marine slicks. / Ermakov S.A., Sergievskaya I.A., Shchegolkov Yu.B., Kijashko S.V., Scott J.C., Stapleton N.R. // 2002. IGARSS '02. 2002 IEEE International Geoscience and Remote Sensing Symposium. 2002. - Vol. 5. - P. 2986-2988. ↑

C6362. Horie H. The property of sea surface scattering in millimeter wave \$satellite-borne cloud profiling radar calibration. / Horie H., Kuoriwa H., Ohno Y., Okamoto H., Kumagai H. // 2002. IGARSS '02. 2002 IEEE International Geoscience and Remote Sensing Symposium. 2002. - Vol. 5. - P. 2989-2990. ↑

- C6363.** Ballantyne J. A multidecadal study of the number of Antarctic icebergs using scatterometer data. / Ballantyne J., Long D.G. // 2002. IGARSS '02. 2002 IEEE International Geoscience and Remote Sensing Symposium. 2002. - Vol. 5. - P. 3029-3031. ↑
- C6364.** De Abreu R. Evaluating the use of QuikSCAT data for operational sea ice monitoring. / De Abreu R., Wilson K., Arkett M., Langlois D. // 2002. IGARSS '02. 2002 IEEE International Geoscience and Remote Sensing Symposium. 2002. - Vol. 5. - P. 3032-3033. ↑
- C6365.** Rouveure R. A microwave sensor for agricultural implements. / Rouveure R., Monod M.-O., Faure P., Chanet M. // 2002. IGARSS '02. 2002 IEEE International Geoscience and Remote Sensing Symposium. 2002. - Vol. 5. - P. 3020-3022. ↑
- C6366.** Horstmann J. Global ocean wind fields from SAR data using scatterometer models and neural networks. / Horstmann J., Lehner S. // 2002. IGARSS '02. 2002 IEEE International Geoscience and Remote Sensing Symposium. 2002. - Vol. 5. - P. 3014-3016. ↑
- C6367.** Nekrassov A. Measurement of the sea surface wind vector by an airborne altimeter. 2002. IGARSS '02. 2002 IEEE International Geoscience and Remote Sensing Symposium. 2002. - Vol. 5. - P. 3017-3019. ↑
- C6368.** Shelekhov A.P. Method of spectral function in the problem of Doppler lidar sensing in the stratified atmosphere. 2002. IGARSS '02. 2002 IEEE International Geoscience and Remote Sensing Symposium. 24-28 June 2002. - Vol. 6. - P. 3605-3607. ↑
- C6369.** Martins M.P. Texture feature neural classifier for remote sensing image retrieval systems. / Martins M.P., Frutuoso Guimaraes L.N., Maria Garcia Fonseca L. // 2002. Proceedings. XV Brazilian Symposium on Computer Graphics and Image Processing. 2002. - P. 90-96. ↑
- C6370.** Costa R.C.S. Linear features detection in SAR images for urban analysis. / Costa R.C.S., Medeiros F.N.S. // 2002. Proceedings. XV Brazilian Symposium on Computer Graphics and Image Processing. 2002. - P. 401. ↑
- C6371.** Nagao T. Recognition of drift ice using synthetic aperture radar images. / Nagao T., Mitsukura Y., Fukumi M., Akamatsu N. // SICE 2002. Proceedings of the 41st SICE Annual Conference. 5-7 Aug. 2002. - Vol. 3. - P. 1618-1621. ↑
- C6372.** Lerkvaranyu S. Automatic indexing system for atmospheric laser radar data. / Lerkvaranyu S., Miyanaga Y., Dehghan K., Cheevasuvit F., Mizutani K. // 2002. APCCAS '02. 2002 Asia-Pacific Conference on Circuits and Systems. 2002. - Vol. 2. - P. 237-240. ↑
- C6373.** Kaba M. Microwave photonic source for coherent Doppler LIDAR system operating at 1550 nm. / Kaba M., Mollier J.-C. // 2002. International Topical Meeting on Microwave Photonics. 5-8 Nov. 2002. - P. 277-280. ↑
- C6374.** Yilong Lu. Low frequency radar phenomenology study in equatorial vegetation \$preliminary results. / Yilong Lu, Yuping Cheng, Weixian Liu, Heong Wann Seah, Hian Lim Chan, Ling Chiat Tai, Lesturgie M., Borderies P., Guern R. // RADAR 2002. 15-17 Oct. 2002. - P. 70-74. ↑
- C6375.** Kelly F.J. An HF-radar test deployment amidst an ADCP array on the West Florida Shelf. / Kelly F.J., Bonner J.S., Perez J.C., Adams J.S., Prouty D., Trujillo D., Weisberg R.H., Luther M.E., He R., Cole R., Donovan J., Merz C.R. // OCEANS '02 MTS/IEEE. 29-31 Oct. 2002. - Vol. 2. - P. 692-698. ↑
- C6376.** Anderson S.J. Robust mapping of tropical cyclone wave fields using HF skywave radar. / Anderson S.J., Abramovich Y.I., Skinner A.I. // RADAR 2002. 15-17 Oct. 2002. - P. 47-50. ↑
- C6377.** Cherniakov M. Space-surface bistatic synthetic aperture radar-prospective and problems. RADAR 2002. 15-17 Oct. 2002. - P. 22-25. ↑
- C6378.** Wozencraft J.M. Complete coastal mapping with airborne lidar. OCEANS '02 MTS/IEEE. 29-31 Oct. 2002. - Vol. 2. - P. 1194-1198. ↑
- C6379.** Danly B.G. WARLOC: a high-power millimeter-wave radar. / Danly B.G., Cheung J., Gregers-Hansen V., Linde G., Ngo M. // 2002. Conference Digest. Twenty Seventh International Conference on Infrared and Millimeter Waves. 2002. - P. 233-234. ↑

- C6380.** Zahran O. Comparison between surface impulse ground penetrating radar signals and ultrasonic time-of-flight diffraction signals. / Zahran O., Shihab S., Al-Nuaimy W. // 2002.7th IEEE High Frequency Postgraduate Student Colloquium. 2002. - P. 7 
- C6381.** Brown E.R. Toward the detection of bioparticles by radar in the THz region. / Brown E.R., Woolard D.L., Samuels A.C., Globus T., Gelmont B. // 2002. Conference Digest. Twenty Seventh International Conference on Infrared and Millimeter Waves. 2002. - P. PI3-PI4. 
- C6382.** Young S.D. Real-time integrity monitoring of stored geo-spatial data using forward-looking remote sensing technology [aircraft navigation/displays]. / Young S.D., Harrah S.D., de Haag M.U. // 2002. Proceedings. The 21st Digital Avionics Systems Conference. 2002. - Vol. 2. - P. 11D1-1-11D1-10-1. 
- C6383.** Martone P.J. Helicopter in-flight tracking system (HITS) for the Gulf of Mexico. / Martone P.J., Daskalakis A.C. // 2002. Proceedings. The 21st Digital Avionics Systems Conference. 27-31 Oct. 2002. - Vol. 1. - P. 3E3-1-3E3-11-1. 
- C6384.** Palto A.A. Parameters optimization for synthesizing aperture method at practical use of continuous radiation underground radar. 2002. MMET '02. 2002 International Conference on Mathematical Methods in Electromagnetic Theory. 10-13 Sept. 2002. - Vol. 1. - P. 302-304. 
- C6385.** {no data available}. Conference Proceedings. 2002 International Conference on Mathematical Methods in Electromagnetic Theory. MMET '02 (Cat. No.02EX554). 2002. MMET '02. 2002 International Conference on Mathematical Methods in Electromagnetic Theory. 10-13 Sept. 2002. - Vol. 2. - {no data available}. 
- C6386.** Nagao T. Drift ice recognition using remote sensing data by neural networks. / Nagao T., Mitsukura Y., Fukumi M., Akamatsu N. // 2002. ICONIP '02. Proceedings of the 9th International Conference on Neural Information Processing. 18-22 Nov. 2002. - Vol. 2. - P. 645-649. 
- C6387.** Prokopenko I. Nonparametric algorithm for a detection of random process disorder in the signals of radar remote sensing. / Prokopenko I., Prokopenko K. // 2002. MMET '02. 2002 International Conference on Mathematical Methods in Electromagnetic Theory. 10-13 Sept. 2002. - Vol. 1. - P. 278-280. 
- C6388.** Yanovsky F.J. Doppler-polarimetric retrieval of rain rate and turbulence intensity in precipitation. 2002. MMET '02. 2002 International Conference on Mathematical Methods in Electromagnetic Theory. 10-13 Sept. 2002. - Vol. 1. - P. 281-286. 
- C6389.** Jones W.L. Combined active and passive microwave sensing of ocean surface wind vector from TRMM. / Jones W.L., Soisuvann S., Jun Park, Adams I., Kasparis T. // OCEANS '02 MTS/IEEE. 29-31 Oct. 2002. - Vol. 4. - P. 1981-1986. 
- C6390.** Zhiqun Yang. Delay compensation of stretching signal in OTHR. / Zhiqun Yang, Jinlin Ni, Guosui Liu. // 2002 6th International Conference on Signal Processing. 26-30 Aug. 2002. - Vol. 2. - P. 1461-1464. 
- C6391.** Bratsolis E. Despeckling and detection of high reflectance regions from SAR images. / Bratsolis E., Sigelle M. // 2002 6th International Conference on Signal Processing. 26-30 Aug. 2002. - Vol. 2. - P. 1407-1410. 
- C6392.** Xiaowei Li. A novel speckle filtering technique for SAR image. / Xiaowei Li, Hong Sun, Xin Xu. // 2002 6th International Conference on Signal Processing. 26-30 Aug. 2002. - Vol. 1. - P. 788-791. 
- C6393.** Bangolae S.L. TCP-friendly congestion control mechanism for an UDP-based high speed radar application and characterization of fairness. / Bangolae S.L., Jayasumana A.P., Chandrasekar V. // 2002. ICCS 2002. The 8th International Conference on Communication Systems. 25-28 Nov. 2002. - Vol. 1. - P. 164-168. 
- C6394.** Bonneau R. An architecture for sensor data fusion target tracking. / Bonneau R., Perretta J., Rahn B., Barnell M. // 2002. Proceedings. 31st Applied Imagery Pattern Recognition Workshop. 16-17 Oct. 2002. - P. 189-192. 
- C6395.** Davidson G. Performance evaluation of maximum likelihood SAR segmentation for multi-temporal rice crop mapping. / Davidson G., Ouchi K., Saito G., Ishitsuka N., Mohri K., Uratsuka S. // RADAR 2002. 15-17 Oct. 2002. - P. 390-394. 
- C6396.** Kwag Y.K. Radar payload design and its performance characteristics for spaceborne small platform

remote sensing system. RADAR 2002. 15-17 Oct. 2002. - P. 385-389. ↑

C6397. Pastore L. Evaluation of P-band foliage penetration through polarimetric high resolution SAR imaging with the RAMSES radar. / Pastore L., Cantalloube H., Priou A., Dreuillet Ph. // RADAR 2002. 15-17 Oct. 2002. - P. 516-520. ↑

C6398. Yadin E. Modern synthetic aperture radar systems. 2002. The 22nd Convention of Electrical and Electronics Engineers in Israel. 1 Dec. 2002. - P. 333-335. ↑

C6399. Fusco A. Statistical modeling of multipolarization and multifrequency SAR images of the sea surface. / Fusco A., Galdi C., Ricci G., Tesauro M. // RADAR 2002. 15-17 Oct. 2002. - P. 557-561. ↑

C6400. {no data available}. Oceans 2002 Conference and Exhibition. Conference Proceedings (Cat. No.02CH37362). OCEANS '02 MTS/IEEE. 29-31 Oct. 2002. - Vol. 3. - {no data available}. ↑

C6401. Dae-Won Do. A resolution enhancement method for SAR images with adaptive speckle reduction. / Dae-Won Do, Byung-Woo Yoon, Woo-Jin Song. // 2002. IEEE ICIT '02. 2002 IEEE International Conference on Industrial Technology. 11-14 Dec. 2002. - Vol. 2. - P. 961-964. ↑

C6402. Glenn S.M. The New Jersey Shelf Observing System. / Glenn S.M., Schofield O.M.E. // OCEANS '02 MTS/IEEE. 29-31 Oct. 2002. - Vol. 3. - P. 1680-1687. ↑

C6403. Adams I.S. Improved hurricane wind speed algorithm for the seawinds satellite scatterometer. / Adams I.S., Jones W.L., Park J.D., Kasparis T., Chen S.S., Tenerelli J.E. // OCEANS '02 MTS/IEEE. 29-31 Oct. 2002. - Vol. 4. - P. 1973-1980. ↑

C6404. Dehouck A. Measuring sea surface salinity from an airborne SAR in the Gironde region, France. / Dehouck A., Dupuis H., Gohin F., Chapron B., Reul N., Jegou A.M., Garello R. // OCEANS '02 MTS/IEEE. 29-31 Oct. 2002. - Vol. 4. - P. 1962-1967. ↑

C6405. Anxue J. A 3-D imaging method using cross-traverse data for ground-penetrating radar. / Anxue J., Yansheng J., Wenbing W. // 2002. Proceedings. ICMMT 2002. 2002 3rd International Conference on Microwave and Millimeter Wave Technology. 17-19 Aug. 2002. - P. 476-479. ↑

C6406. Su Fulin. An algorithm of bridge detection in radar sensing images based on fractal. / Su Fulin, Zhu Yong, Ge Hongtao. // 2002. Proceedings. ICMMT 2002. 2002 3rd International Conference on Microwave and Millimeter Wave Technology. 17-19 Aug. 2002. - P. 410-413. ↑

C6407. Lu Xiaode. Analyzing on phase error for single pass interferometric SAR. / Lu Xiaode, Song Fuming, Song Jiajun. // 2002. Proceedings. ICMMT 2002. 2002 3rd International Conference on Microwave and Millimeter Wave Technology. 17-19 Aug. 2002. - P. 489-492. ↑

C6408. Jasiunas M.D. Image fusion for uninhabited airborne vehicles. / Jasiunas M.D., Kearney D.A., Hopf J., Wigley G.B. // 2002. (FPT). Proceedings. 2002 IEEE International Conference on Field-Programmable Technology. 16-18 Dec. 2002. - P. 348-351. ↑

C6409. Ya-Qiu Jin. Polarimetric scattering from inhomogeneous random media under a pulse incidence. / Ya-Qiu Jin, Mei Chang. // 2002. Proceedings. ICMMT 2002. 2002 3rd International Conference on Microwave and Millimeter Wave Technology. 17-19 Aug. 2002. - P. 611-613. ↑

C6410. Borghys D. Edge and line detection in polarimetric SAR images. / Borghys D., Lacroix V., Perneel C. // 2002. Proceedings. 16th International Conference on Pattern Recognition. 2002. - Vol. 2. - P. 921-924. ↑

C6411. Zhang Xiaohui. Design on return signal simulator of scatterometer and method of generating its signal. / Zhang Xiaohui, Guo Wei, Liu Heguang. // 2002. IGARSS '02. 2002 IEEE International Geoscience and Remote Sensing Symposium. 24-28 June 2002. - Vol. 6. - P. 3668-3670. ↑

C6412. Yuping Cheng. A super resolution SAR imaging method based on CSA. / Yuping Cheng, Yilong Lu, Zhiping Lin. // 2002. IGARSS '02. 2002 IEEE International Geoscience and Remote Sensing Symposium. 24-28 June 2002. - Vol. 6. - P. 3671-3673. ↑

C6413. Wei G. Development of return signal simulator for Chinese satellite altimeter test and calibration. / Wei

G., Xiaohui Z., Heguang L. // 2002. IGARSS '02. 2002 IEEE International Geoscience and Remote Sensing Symposium. 24-28 June 2002. - Vol. 6. - P. 3658-3660. ↑

C6414. Ke Xu. The design of China spaceborne radar altimeter control system. / Ke Xu, Jingshan Jiang, Heguang Liu. // 2002. IGARSS '02. 2002 IEEE International Geoscience and Remote Sensing Symposium. 24-28 June 2002. - Vol. 6. - P. 3652-3654. ↑

C6415. Bovenga F. Automated calibration of multi-temporal ERS SAR data. / Bovenga F., Refice A., Nutricato R., Pasquariello G., De Carolis G. // 2002. IGARSS '02. 2002 IEEE International Geoscience and Remote Sensing Symposium. 24-28 June 2002. - Vol. 6. - P. 3655-3657. ↑

C6416. Goddard J.W.F. Ground-based aviation weather radar research at the Rutherford Appleton Laboratory and University College London. / Goddard J.W.F., Eastment J.D., Bradford W.J., Woodbridge K. // IEE Aviation Surveillance Systems (Ref. No. 2002/054). 23 Jan. 2002. - P. 6/1. ↑

C6417. Wei Gong. A portable eye-safe scanning aerosol lidar of the Hampton University Center for Lidar and Atmospheric Sciences Students. / Wei Gong, Temple D.A., Omar A., Mangana J., Khin Maung Maung, Bailey S., Harper D., Battle R., Futrell A., Haughton L., Johnson D., Lewis K., Gile C., Davis J., Williams L., Chyba T.H., Richter D.A., Higdon N.S. // 2002. CLEO '02. Technical Digest. Summaries of Papers Presented at the Lasers and Electro-Optics. 2002. - P. 218-219. ↑

C6418. Chitroub S. Unsupervised learning rules for POLSAR images analysis. / Chitroub S., Houacine A., Sansal B. // 2002. Proceedings of the 2002 12th IEEE Workshop on Neural Networks for Signal Processing. 2002. - P. 567-576. ↑

C6419. Li Haiying. Analysis of radial velocity effect on synthetic range profile of stepped-frequency waveform. / Li Haiying, Yang Ruliang. // 2002. IGARSS '02. 2002 IEEE International Geoscience and Remote Sensing Symposium. 24-28 June 2002. - Vol. 6. - P. 3689-3691. ↑

C6420. Lohmeier S.P. Development of an ultra-wideband radar system for vehicle detection at railway crossings. / Lohmeier S.P., Rajaraman R., Ramasami V.C. // 2002. IGARSS '02. 2002 IEEE International Geoscience and Remote Sensing Symposium. 24-28 June 2002. - Vol. 6. - P. 3692-3694. ↑

C6421. Dutra L.V. Assessment of digital elevation models obtained in Brazilian Amazon based on P and X band airborne interferometric data. / Dutra L.V., Elmiro M.T., Soares B.S., Mura F.J.C., Santos J.R., Freitas C.C., Araujo L.S., de Albuquerque P.C.G., Vieira P.R., Gama F.F. // 2002. IGARSS '02. 2002 IEEE International Geoscience and Remote Sensing Symposium. 24-28 June 2002. - Vol. 6. - P. 3617-3619. ↑

C6422. Markham K.J. A comparison of radar altimetry and repeat pass interferometry as methods of producing digital terrain elevation models. / Markham K.J., Morris W.A. // 2002. IGARSS '02. 2002 IEEE International Geoscience and Remote Sensing Symposium. 24-28 June 2002. - Vol. 6. - P. 3620-3622. ↑

C6423. Berardino P. Evidence for a peculiar style of ground deformation at Vesuvius volcano revealed by 10 years of ERS mission. / Berardino P., Bequignon J., Borgstrom S., De Natale G., Capuano P., Fornaro G., Lanari R., Pingue F., Ricciardi G.P., Sansosti E., Troise C. // 2002. IGARSS '02. 2002 IEEE International Geoscience and Remote Sensing Symposium. 24-28 June 2002. - Vol. 6. - P. 3614-3616. ↑

C6424. Yang P. The enhancement of lidar backscattering by horizontally oriented ice crystal plates in cirrus clouds. / Yang P., Hu Y.X., Zhao J., Winker D.M., Hstetler C.A., Baum B.A., Tsay S.-C., Gao B.-C., Mishchenko M.I. // 2002. IGARSS '02. 2002 IEEE International Geoscience and Remote Sensing Symposium. 24-28 June 2002. - Vol. 6. - P. 3608-3610. ↑

C6425. Younan N.H. DTM error minimization via adaptive smoothing [LIDAR forest measurements]. / Younan N.H., Lee H.S., King R.L. // 2002. IGARSS '02. 2002 IEEE International Geoscience and Remote Sensing Symposium. 24-28 June 2002. - Vol. 6. - P. 3611-3613. ↑

C6426. Klugmann D. A monostatic solid state W-band FM-CW Doppler profiler. 2002. IGARSS '02. 2002 IEEE International Geoscience and Remote Sensing Symposium. 24-28 June 2002. - Vol. 6. - P. 3646-3648. ↑

C6427. Weiss M. Motion compensation of wideband synthetic aperture radar with a new transponder technique. / Weiss M., Berens P. // 2002. IGARSS '02. 2002 IEEE International Geoscience and Remote Sensing Symposium. 24-28 June 2002. - Vol. 6. - P. 3649-3651. ↑

- C6428.** Strozzi T. Alpine landslide periodical survey. / Strozzi T., Wegmuller U., Werner C., Wiesmann A. // 2002. IGARSS '02. 2002 IEEE International Geoscience and Remote Sensing Symposium. 24-28 June 2002. - Vol. 6. - P. 3629-3631. ↑
- C6429.** Migliaccio M. Coherence loss minimization in SAR interferometric registration. / Migliaccio M., Bruno F. // 2002. IGARSS '02. 2002 IEEE International Geoscience and Remote Sensing Symposium. 24-28 June 2002. - Vol. 6. - P. 3623-3625. ↑
- C6430.** Nutricato R. Optimum interpolation and resampling for PSC identification. / Nutricato R., Bovenga F., Refice A. // 2002. IGARSS '02. 2002 IEEE International Geoscience and Remote Sensing Symposium. 24-28 June 2002. - Vol. 6. - P. 3626-3628. ↑
- C6431.** Afzal R.S. Solid-state lasers for space-based applications. 2002. CLEO '02. Technical Digest. Summaries of Papers Presented at the Lasers and Electro-Optics. 2002. - P. 425 vol.1. ↑
- C6432.** Lohmeier S.P. An ultra-wideband radar for vehicle detection in railroad crossings. / Lohmeier S.P., Rajaraman R., Ramasami V.C. // 2002. Proceedings of IEEE Sensors. 2002. - Vol. 2. - P. 1762-1766. ↑
- C6433.** Oscar V.-C. Fusion of radiometry and textural information for SIR-C image classification. / Oscar V.-C., Xavier D., Josiane Z., Nicolas B. // Image Processing. 2002. Proceedings. 2002 International Conference on. 2002. - Vol. 3. - P. III-109-III-112-109. ↑
- C6434.** Brooker G. A robust mm wave radar sensor for underground applications. 2002. ICARCV 2002. 7th International Conference on Control, Automation, Robotics and Vision. 2-5 Dec. 2002. - Vol. 1. - P. 1-6. ↑
- C6435.** Davis J.C. Developing a remote staring sensor for optimizing successful boost phase intercept. / Davis J.C., Lisowski J.J. // 2002. IEEE Aerospace Conference Proceedings. 2002. - Vol. 4. - P. 4-1649-4-1661-1649. ↑
- C6436.** Clark D.J. Testbed for development of a DSP-based signal processing subsystem for an earth-orbiting radar scatterometer. / Clark D.J., Lux J.P., Shirbacheh N. // 2002. IEEE Aerospace Conference Proceedings. 2002. - Vol. 4. - P. 4-1881-4-1890-1881. ↑
- C6437.** Xiaoyin Xu. Entropy optimized contrast stretch to enhance remote sensing imagery. / Xiaoyin Xu, Miller E.L. // 2002. Proceedings. 16th International Conference on Pattern Recognition. 2002. - Vol. 3. - P. 915-918. ↑
- C6438.** Riviere D. Relational graph labelling using learning techniques and Markov random fields. / Riviere D., Mangin J.-F., Martinez J.-M., Tupin F., Papadopoulos-Orfanos D., Frouin V. // 2002. Proceedings. 16th International Conference on Pattern Recognition. 2002. - Vol. 2. - P. 172-175. ↑
- C6439.** Krishnamoorthy P. Robust detection of buildings in digital surface models. / Krishnamoorthy P., Boyer K.L., Flynn P.J. // 2002. Proceedings. 16th International Conference on Pattern Recognition. 2002. - Vol. 1. - P. 159-163. ↑
- C6440.** Lei Ying. An iterative dynamic programming approach to 2-D phase unwrapping. / Lei Ying, Frey B.J., Koetter R., Munson D.C. Jr. // Image Processing. 2002. Proceedings. 2002 International Conference on. 2002. - Vol. 3. - P. 469-471. ↑
- C6441.** Liming Lu. A target detection method in range-Doppler domain from SAR echo data. / Liming Lu, Runsheng Wang, Wugao Li. // 2002. Proceedings. 16th International Conference on Pattern Recognition. 2002. - Vol. 1. - P. 91-94. ↑
- C6442.** Stalio R. Technological spin-offs of the PMST program of the Italian. Space agency (ASI). / Stalio R., Svelto F., Bonifazi C., D'Aversa E., Di Pippo S., Musso C., Zoffoli S., Salotti L., Bignami G.F. // 2002. IEEE Aerospace Conference Proceedings. 2002. - Vol. 2. - P. 2-583-2-589-583. ↑
- C6443.** D'Errico M. The BISSAT mission: A bistatic SAR operating in formation with COSMO/SkyMed X-band radar. / D'Errico M., Moccia A. // 2002. IEEE Aerospace Conference Proceedings. 2002. - Vol. 2. - P. 2-809-2-818-809. ↑
- C6444.** Coyle D.B. Design and performance of the vegetation canopy Lidar (VCL) laser transmitter. / Coyle D.B., Kay R.B., Lindauer S.J. // 2002. IEEE Aerospace Conference Proceedings. 2002. - Vol. 3. - P. 3-1457-3-

1464-1457. ↑

C6445. Heine F. Seed laser for space borne LIDAR applications. / Heine F., Salheiser H., Seel S., Schwander T., Smutny B. // 2002. CLEO '02. Technical Digest. Summaries of Papers Presented at the Lasers and Electro-Optics. 2002. - P. 425-426. ↑

C6446. Xiaoli Sun. Performance of a breadboard lidar receiver at 1570 nm for remotely sensing atmospheric CO2 concentration. / Xiaoli Sun, Abshire J.B. // 2002. CLEO '02. Technical Digest. Summaries of Papers Presented at the Lasers and Electro-Optics. 2002. - P. 648-649. ↑

C6447. Johnson W.T.K. The Europa Orbiter radar sounder: Innovative radar design for a challenging mission. / Johnson W.T.K., Jordan R., Safaeinili A. // 2002. IEEE Aerospace Conference Proceedings. 2002. - Vol. 1. - P. 1-189-1-194-189. ↑

C6448. Tacconi G. Subsurface water search by TEM [on Mars]. / Tacconi G., Pagnan S., Filippini R., Ottonello C. // 2002. IEEE Aerospace Conference Proceedings. 2002. - Vol. 1. - P. 1-417-1-426-417. ↑

C6449. Kobrick M. Mapping the world in 3-D. 2002. IEEE Aerospace Conference Proceedings. 2002. - Vol. 1. - P. 1-13 vol.1. ↑

C6450. Pollard B.D. The wide swath ocean altimeter: radar interferometry for global ocean mapping with centimetric accuracy. / Pollard B.D., Rodriguez E., Veilleux L., Akins T., Brown P., Kitiyakara A., Zawadski M., Dathanasombat S., Prata A. Jr. // 2002. IEEE Aerospace Conference Proceedings. 2002. - Vol. 2. - P. 2-1007-2-1020-1007. ↑

C6451. Stosic D.K. Ku-band receiver and transmitter for breadboard DSP scatterometer. / Stosic D.K., Lux J.P. // 2002. IEEE Aerospace Conference Proceedings. 2002. - Vol. 2. - P. 2-1023-2-1030-1023. ↑

C6452. Aydin K. Identification of cloud ice crystals using a 95 GHz polarimetric radar. / Aydin K., Singh J. // 2002. IGARSS '02. 2002 IEEE International Geoscience and Remote Sensing Symposium. 2002. - Vol. 5. - P. 2814-2816. ↑

C6453. Sai B. Detection and imaging of small buried 3D non-metallic objects with multistatic phase-based GPR signatures. / Sai B., Ligthart L.P. // 2002. IGARSS '02. 2002 IEEE International Geoscience and Remote Sensing Symposium. 24-28 June 2002. - Vol. 4. - P. 1988-1990. ↑

C6454. Leucci G. Integration of high resolution optical satellite imagery and geophysical survey for archaeological prospection in Hierapolis (Turkey). / Leucci G., Negri S., Ricchetti E. // 2002. IGARSS '02. 2002 IEEE International Geoscience and Remote Sensing Symposium. 24-28 June 2002. - Vol. 4. - P. 1991-1993. ↑

C6455. Millet F. Refining electromagnetic bias estimation [sea surface height measurement]. / Millet F., Warnick K., Arnold D. // 2002. IGARSS '02. 2002 IEEE International Geoscience and Remote Sensing Symposium. 24-28 June 2002. - Vol. 4. - P. 1980-1982. ↑

C6456. Zecchetto S. Wind field retrieval from SAR images using the continuous wavelet transform. / Zecchetto S., De Biasio R. // 2002. IGARSS '02. 2002 IEEE International Geoscience and Remote Sensing Symposium. 24-28 June 2002. - Vol. 4. - P. 1974-1976. ↑

C6457. Draper D.W. Evidence of a threshold wind speed in tower-mounted scatterometer data. / Draper D.W., Long D.G. // 2002. IGARSS '02. 2002 IEEE International Geoscience and Remote Sensing Symposium. 24-28 June 2002. - Vol. 4. - P. 1977-1979. ↑

C6458. Kelley O.A. Variations in the convective rain fraction observed by the Tropical Rainfall Measuring Mission (TRMM) Precipitation Radar (PR). / Kelley O.A., Stout J., Kwiatkowski J., Bacmeister J. // 2002. IGARSS '02. 2002 IEEE International Geoscience and Remote Sensing Symposium. 2002. - Vol. 4. - P. 2012-2016. ↑

C6459. Thome K. Cirrus spectral optical depths retrieved from solar transmittance measurements. / Thome K., Kuester M., Reagan J. // 2002. IGARSS '02. 2002 IEEE International Geoscience and Remote Sensing Symposium. 2002. - Vol. 4. - P. 2017-2019. ↑

C6460. Daisley S.E.A. Relationships between rainfall rate, attenuation, and reflectivity at 14 and 35 GHz frequencies. / Daisley S.E.A., Aydin K. // 2002. IGARSS '02. 2002 IEEE International Geoscience and Remote

Sensing Symposium. 2002. - Vol. 4. - P. 2009-2011. ↑

C6461. Crooks W.T. SAR observations of dryland moisture-towards monitoring outbreak areas of the Brown Locust in South Africa. / Crooks W.T., Archer D.J. // 2002. IGARSS '02. 2002 IEEE International Geoscience and Remote Sensing Symposium. 24-28 June 2002. - Vol. 4. - P. 1994-1996. ↑

C6462. Sandholt I. The use of ERS2 SAR for assessment of changes in dry herbaceous biomass. / Sandholt I., Moller Sorensen J., Rasmussen K., Ka A. // 2002. IGARSS '02. 2002 IEEE International Geoscience and Remote Sensing Symposium. 2002. - Vol. 4. - P. 2003-2005. ↑

C6463. Franceschetti G. An analytical and numerical framework for interpretation of SAR images of urban areas. / Franceschetti G., Iodice A., Riccio D., Ruello G. // 2002. IGARSS '02. 2002 IEEE International Geoscience and Remote Sensing Symposium. 24-28 June 2002. - Vol. 3. - P. 1926-1928. ↑

C6464. Tonboe R. Monitoring of new-ice in Greenland waters. / Tonboe R., Ezraty R.E. // 2002. IGARSS '02. 2002 IEEE International Geoscience and Remote Sensing Symposium. 24-28 June 2002. - Vol. 3. - P. 1932-1934. ↑

C6465. Jun-Yi Xu. Using cross-entropy for polarimetric SAR image classification. / Jun-Yi Xu, Jian Yang, Ying-Ning Peng, Chao Wang. // 2002. IGARSS '02. 2002 IEEE International Geoscience and Remote Sensing Symposium. 24-28 June 2002. - Vol. 3. - P. 1917-1919. ↑

C6466. Sciotti M. Exploiting the polarimetric information for the detection of ship targets in non-homogeneous SAR images. / Sciotti M., Pastina D., Lombardo P. // 2002. IGARSS '02. 2002 IEEE International Geoscience and Remote Sensing Symposium. 24-28 June 2002. - Vol. 3. - P. 1911-1913. ↑

C6467. Scheuchl B. Sea ice classification using multi-frequency polarimetric SAR data. / Scheuchl B., Hajnsek I., Cumming I. // 2002. IGARSS '02. 2002 IEEE International Geoscience and Remote Sensing Symposium. 24-28 June 2002. - Vol. 3. - P. 1914-1916. ↑

C6468. Chang Benyi. The principles of positioning with space-borne SAR images. / Chang Benyi, Fang Yong. // 2002. IGARSS '02. 2002 IEEE International Geoscience and Remote Sensing Symposium. 2002. - Vol. 4. - P. 1950-1952. ↑

C6469. Fujita M. Land use classification of SIR-C imagery based on a published database of multi-polarization backscattering. / Fujita M., Tamura D. // 2002. IGARSS '02. 2002 IEEE International Geoscience and Remote Sensing Symposium. 24-28 June 2002. - Vol. 4. - P. 1956-1958. ↑

C6470. Aiazzi B. Nonparametric classification of SAR data based on a modified iterated nearest-mean reclustering of pixel features. / Aiazzi B., Alparone L., Baronti S., Bianchini M., Macelloni G., Paloscia S. // 2002. IGARSS '02. 2002 IEEE International Geoscience and Remote Sensing Symposium. 2002. - Vol. 4. - P. 1947-1949. ↑

C6471. Kern S. Two ice concentration algorithms benefitting from 85 GHz Special Sensor Microwave/Imager data: a comparison. / Kern S., Kaleschke L. // 2002. IGARSS '02. 2002 IEEE International Geoscience and Remote Sensing Symposium. 24-28 June 2002. - Vol. 3. - P. 1938-1940. ↑

C6472. Jong-Sun Hwang. Microwave sensing implied sea ice distribution in the Weddell Sea, Antarctica. / Jong-Sun Hwang, Kyung Duck Min, Jeong Woo Kim, Sungmin Hong, Hoil Yoon. // 2002. IGARSS '02. 2002 IEEE International Geoscience and Remote Sensing Symposium. 24-28 June 2002. - Vol. 3. - P. 1941-1943. ↑

C6473. Marghany M. Radarsat Lagrangian flow effects on oil spill spreading. 2002. IGARSS '02. 2002 IEEE International Geoscience and Remote Sensing Symposium. 2002. - Vol. 4. - P. 2023-2025. ↑

C6474. Dankert H. Ocean wind fields retrieved from radar-image sequences. / Dankert H., Horstmann J., Koch W., Rosenthal W. // 2002. IGARSS '02. 2002 IEEE International Geoscience and Remote Sensing Symposium. 24-28 June 2002. - Vol. 4. - P. 2150-2152. ↑

C6475. Jelenak Z. A study of surface winds in tropical storms using modified near real-time processing of QuikSCAT measurements. / Jelenak Z., Connor L.N., Chang P.S. // 2002. IGARSS '02. 2002 IEEE International Geoscience and Remote Sensing Symposium. 24-28 June 2002. - Vol. 4. - P. 2153-2155. ↑

- C6476.** Ivanov L.M. Nowcast of surface currents from blending HF radar: inverse model, application to Monterey Bay. / Ivanov L.M., Melnichenko O.V. // 2002. IGARSS '02. 2002 IEEE International Geoscience and Remote Sensing Symposium. 24-28 June 2002. - Vol. 4. - P. 2138-2140. ↑
- C6477.** Hughes W. Ocean current estimation using ScanSAR data. / Hughes W., van der Kooij M.W.A. // 2002. IGARSS '02. 2002 IEEE International Geoscience and Remote Sensing Symposium. 24-28 June 2002. - Vol. 4. - P. 2132-2134. ↑
- C6478.** Hutt D. Capability of Radarsat-1 for estimation of ocean surface current on the Scotian Shelf. / Hutt D., Stockhausen J., Osler J., Mosher D. // 2002. IGARSS '02. 2002 IEEE International Geoscience and Remote Sensing Symposium. 24-28 June 2002. - Vol. 4. - P. 2135-2137. ↑
- C6479.** Haldermnn A.F.C. Mars meter-scale roughness: Goldstone Solar System Radar delay-Doppler database. / Haldermnn A.F.C., Jurgens R.F., Slade M.A. // 2002. IGARSS '02. 2002 IEEE International Geoscience and Remote Sensing Symposium. 24-28 June 2002. - Vol. 4. - P. 2169 vol.4. ↑
- C6480.** Maksym T. Sea ice microstructural characteristics in the Barents Sea in autumn: relevance to microwave remote sensing. / Maksym T., Van Woert M., Dierking W., Nghiem S.V. // 2002. IGARSS '02. 2002 IEEE International Geoscience and Remote Sensing Symposium. 24-28 June 2002. - Vol. 4. - P. 2176-2178. ↑
- C6481.** Biccari D. Venus radar for subsurface and ionosphere sounding (VENSIS). / Biccari D., Gurnett D., Johnson W., Huff R., Marinangeli L., Jordan R., Nielsen E., Ori G.G., Picardi G., Plaut J., Provvedi F., Seu R., Zampolini E. // 2002. IGARSS '02. 2002 IEEE International Geoscience and Remote Sensing Symposium. 24-28 June 2002. - Vol. 4. - P. 2162-2165. ↑
- C6482.** Schulz-Stellenfleth J. A parametric scheme for ocean wave spectra retrieval from complex SAR data using prior information. / Schulz-Stellenfleth J., Lehner S., Hoja D., Koenig T. // 2002. IGARSS '02. 2002 IEEE International Geoscience and Remote Sensing Symposium. 24-28 June 2002. - Vol. 4. - P. 2156-2158. ↑
- C6483.** Biccari D. Mars high resolution Shallow Radar (SHARAD) for the MRO 2005 mission. / Biccari D., Picardi G., Seu R. // 2002. IGARSS '02. 2002 IEEE International Geoscience and Remote Sensing Symposium. 24-28 June 2002. - Vol. 4. - P. 2159-2161. ↑
- C6484.** KelIndorfer J.M. Forest parameter retrieval with JPL Airsar P-, L- and C-band data: a plot level analysis for slash pine stands in Georgia. / KelIndorfer J.M., Dobson M.C., Clutter M., Vona J., Triplett G. // 2002. IGARSS '02. 2002 IEEE International Geoscience and Remote Sensing Symposium. 2002. - Vol. 4. - P. 2066-2068. ↑
- C6485.** Pierce L. Regrowth biomass estimation in the amazon using JERS-1/RADARSAT SAR composites. / Pierce L., Pan Liang, Dobson M.C. // 2002. IGARSS '02. 2002 IEEE International Geoscience and Remote Sensing Symposium. 24-28 June 2002. - Vol. 4. - P. 2075-2077. ↑
- C6486.** da Costa Freitas C. Assessment of operational radar satellite for monitoring land cover change in Amazonia. / da Costa Freitas C., Silva-Junior L.W.P., Dutra L.V. // 2002. IGARSS '02. 2002 IEEE International Geoscience and Remote Sensing Symposium. 24-28 June 2002. - Vol. 4. - P. 2063-2065. ↑
- C6487.** Matsuoka M. Application of the damage detection method using SAR intensity images to recent earthquakes. / Matsuoka M., Yamazaki F. // 2002. IGARSS '02. 2002 IEEE International Geoscience and Remote Sensing Symposium. 2002. - Vol. 4. - P. 2042-2044. ↑
- C6488.** Yonezawa C. Urban damage detection using decorrelation of SAR interferometric data. / Yonezawa C., Tomiyama N., Takeuchi S. // 2002. IGARSS '02. 2002 IEEE International Geoscience and Remote Sensing Symposium. 2002. - Vol. 4. - P. 2051-2053. ↑
- C6489.** Pack J.D. Greenland snowmelt estimation using multi-spectral passive and active microwave observations. / Pack J.D., Jensen M.A. // 2002. IGARSS '02. 2002 IEEE International Geoscience and Remote Sensing Symposium. 2002. - Vol. 4. - P. 2106-2108. ↑
- C6490.** Kourti N. Integrating active and passive satellite-based technologies to improve European fisheries monitoring and control. / Kourti N., Schwartz G., Shepherd I. // 2002. IGARSS '02. 2002 IEEE International Geoscience and Remote Sensing Symposium. 2002. - Vol. 4. - P. 2126-2128. ↑

- C6491.** Xiao Cheng. Interferometry SAR in Antarctic Grove Mountains. / Xiao Cheng, Chunxia Zhou, Qulin Tan, Guanhua Xu, Yun Shao. // 2002. IGARSS '02. 2002 IEEE International Geoscience and Remote Sensing Symposium. 2002. - Vol. 4. - P. 2100-2102. ↑
- C6492.** Ranson K.J. Utility of SARs for mapping forest disturbance in Siberia. / Ranson K.J., Sun G., Kovacs K., Kharuk V.I. // 2002. IGARSS '02. 2002 IEEE International Geoscience and Remote Sensing Symposium. 24-28 June 2002. - Vol. 4. - P. 2081-2083. ↑
- C6493.** Smith G. Forest stem volume estimation using high-resolution lidar and SAR data. / Smith G., Persson A., Hohmgren J., Hallberg B., Fransson J.E.S., Ulander L.M.H. // 2002. IGARSS '02. 2002 IEEE International Geoscience and Remote Sensing Symposium. 24-28 June 2002. - Vol. 4. - P. 2084-2086. ↑
- C6494.** Flynn T. Direct estimation of vegetation parameters from covariance data in polarimetric SAR interferometry. / Flynn T., Tabb M., Carande R. // 2002. IGARSS '02. 2002 IEEE International Geoscience and Remote Sensing Symposium. 24-28 June 2002. - Vol. 3. - P. 1908-1910. ↑
- C6495.** Pulliainen J. Estimation of boreal forest biomass from multi-temporal INSAR data by inverting an empirical backscattering-coherence model. / Pulliainen J., Engdahl M., Hallikainen A. // 2002. IGARSS '02. 2002 IEEE International Geoscience and Remote Sensing Symposium. 24-28 June 2002. - Vol. 3. - P. 1786-1788. ↑
- C6496.** Delbart N. Forest biomass retrieval using L-band polarimetric measurements. / Delbart N., Melon P., Florsch G., Le Toan T., Martinez J.-M. // 2002. IGARSS '02. 2002 IEEE International Geoscience and Remote Sensing Symposium. 24-28 June 2002. - Vol. 3. - P. 1789-1791. ↑
- C6497.** Lee A. Evaluating integrated multi-scale frameworks for strategic forest inventory and monitoring in Australian heterogenous woodlands. / Lee A., Tickle P.K., Austint J., Witte C., Lucas R.M., Jones K., Denham R., Davey S. // 2002. IGARSS '02. 2002 IEEE International Geoscience and Remote Sensing Symposium. 24-28 June 2002. - Vol. 3. - P. 1783-1785. ↑
- C6498.** Chen W. Improving temporal and spatial consistency of forest biomass data by integrating forest yield tables and satellite radar data. / Chen W., Cihlar J., Pavlic G., Zhang Q., Fernandes R., Wang S., Kerr J., Ung C.H., Price D.T., Moghaddam M., McDonald K. // 2002. IGARSS '02. 2002 IEEE International Geoscience and Remote Sensing Symposium. 24-28 June 2002. - Vol. 3. - P. 1777-1779. ↑
- C6499.** Stephen H. Multi-spectral analysis of the Amazon basin using SeaWinds, ERS, Seasat scatterometers, TRMM-PR and SSM/I. / Stephen H., Long D.G. // 2002. IGARSS '02. 2002 IEEE International Geoscience and Remote Sensing Symposium. 24-28 June 2002. - Vol. 3. - P. 1780-1782. ↑
- C6500.** Lohmeier S.P. Adaptive FIR filtering of range sidelobes for air and spaceborne rain mapping. 2002. IGARSS '02. 2002 IEEE International Geoscience and Remote Sensing Symposium. 24-28 June 2002. - Vol. 3. - P. 1801-1803. ↑
- C6501.** Ebuchi N. Probability distribution of surface wave slope derived using Sun glitter images from geostationary meteorological satellite and surface vector winds from scatterometers. 2002. IGARSS '02. 2002 IEEE International Geoscience and Remote Sensing Symposium. 24-28 June 2002. - Vol. 3. - P. 1813-1815. ↑
- C6502.** Coltuc D. A mean based algorithm for the multi-temporal SAR image filtering. / Coltuc D., Becker J.-M., Radescu R. // 2002. IGARSS '02. 2002 IEEE International Geoscience and Remote Sensing Symposium. 24-28 June 2002. - Vol. 3. - P. 1798-1800. ↑
- C6503.** Fransson J.E.S. Detection of thinning cuttings using CARABAS-II VHF SAR data. / Fransson J.E.S., Magnusson M., Gustavsson A., Smith G., Ulander L.M.H., Walter F. // 2002. IGARSS '02. 2002 IEEE International Geoscience and Remote Sensing Symposium. 24-28 June 2002. - Vol. 3. - P. 1792-1794. ↑
- C6504.** Romshoo S.A. Peatland ecosystem characterization employing L-band SAR. / Romshoo S.A., Shimada M., Igarashi T. // 2002. IGARSS '02. 2002 IEEE International Geoscience and Remote Sensing Symposium. 24-28 June 2002. - Vol. 3. - P. 1795-1797. ↑
- C6505.** Forsberg R. Airborne lidar measurements for Cryosat validation. / Forsberg R., Keller K., Jacobsen S.M. // 2002. IGARSS '02. 2002 IEEE International Geoscience and Remote Sensing Symposium. 24-28 June 2002. - Vol. 3. - P. 1756-1758. ↑

- C6506.** Francis C.R. Design of the CryoSat system. 2002. IGARSS '02. 2002 IEEE International Geoscience and Remote Sensing Symposium. 24-28 June 2002. - Vol. 3. - P. 1759-1761. ↑
- C6507.** Haas C. Validation of CryoSat sea-ice products: instruments and methods. 2002. IGARSS '02. 2002 IEEE International Geoscience and Remote Sensing Symposium. 24-28 June 2002. - Vol. 3. - P. 1753-1755. ↑
- C6508.** Linlin Ge. Tropospheric heterogeneities corrections in differential radar interferometry. / Linlin Ge, Tsujii T., Rizos C. // 2002. IGARSS '02. 2002 IEEE International Geoscience and Remote Sensing Symposium. 24-28 June 2002. - Vol. 3. - P. 1747-1749. ↑
- C6509.** Wingham D.J. CryoSat: a mission to determine fluctuations in the Earth's ice fields. 2002. IGARSS '02. 2002 IEEE International Geoscience and Remote Sensing Symposium. 24-28 June 2002. - Vol. 3. - P. 1750-1752. ↑
- C6510.** Pierce L.E. Fusion of optical and SAR data for forestry applications in the Sierra Nevada of California. / Pierce L.E., Walker W.S., Dobson M.C., Hunsaker C.T., Fites-Kaufman J.A., Dubayah R. // 2002. IGARSS '02. 2002 IEEE International Geoscience and Remote Sensing Symposium. 24-28 June 2002. - Vol. 3. - P. 1771-1773. ↑
- C6511.** Steinmeier C. The evaluation of different sensors and techniques for the detection of storm damages in forests. / Steinmeier C., Schwarz M., Holecz F., Stebler O., Wagner S. // 2002. IGARSS '02. 2002 IEEE International Geoscience and Remote Sensing Symposium. 24-28 June 2002. - Vol. 3. - P. 1774-1776. ↑
- C6512.** Rey L. SIRAL: the radar altimeter for CryoSat mission, under development. / Rey L., de Chateau-Thierry P., Phalippou L., Mavrocordatos C., Francis R. // 2002. IGARSS '02. 2002 IEEE International Geoscience and Remote Sensing Symposium. 24-28 June 2002. - Vol. 3. - P. 1768-1770. ↑
- C6513.** Cullen R.A. CryoSat level 1b processing algorithms and simulation results. / Cullen R.A., Wingham D.J. // 2002. IGARSS '02. 2002 IEEE International Geoscience and Remote Sensing Symposium. 24-28 June 2002. - Vol. 3. - P. 1762-1764. ↑
- C6514.** Raney R.K. An airborne CryoSat prototype: the D2P radar altimeter. / Raney R.K., Jensen J.R. // 2002. IGARSS '02. 2002 IEEE International Geoscience and Remote Sensing Symposium. 24-28 June 2002. - Vol. 3. - P. 1765-1767. ↑
- C6515.** Jones W.L. Validation of QuikSCAT Radiometer rain rates using the TRMM microwave radiometer. / Jones W.L., Ahmad K., Jun-Dong Park, Kasparis T., Zec J. // 2002. IGARSS '02. 2002 IEEE International Geoscience and Remote Sensing Symposium. 24-28 June 2002. - Vol. 3. - P. 1816-1818. ↑
- C6516.** Sikora T.D. Wind-direction dependence of quasi-2D SAR signatures. / Sikora T.D., Young G.S. // 2002. IGARSS '02. 2002 IEEE International Geoscience and Remote Sensing Symposium. 24-28 June 2002. - Vol. 3. - P. 1887-1889. ↑
- C6517.** Xiaofeng Li. SAR and MODIS images of atmospheric solitary waves generated by upstream blocking in flow over St. Lawrence Island Bering Sea. / Xiaofeng Li, Clemente-Colon P., Pichel W.G., Friedman K. // 2002. IGARSS '02. 2002 IEEE International Geoscience and Remote Sensing Symposium. 24-28 June 2002. - Vol. 3. - P. 1890-1892. ↑
- C6518.** Kawamura H. L-band SAR wind-retrieval model function and its application for studies of coastal surface winds and wind waves. / Kawamura H., Shimada T., Shimada M., Kortcheva A., Watabe I. // 2002. IGARSS '02. 2002 IEEE International Geoscience and Remote Sensing Symposium. 24-28 June 2002. - Vol. 3. - P. 1884-1886. ↑
- C6519.** Horstmann J. High resolution wind fields retrieved from SAR in comparison to numerical models. / Horstmann J., Koch W., Lehner S. // 2002. IGARSS '02. 2002 IEEE International Geoscience and Remote Sensing Symposium. 24-28 June 2002. - Vol. 3. - P. 1877-1879. ↑
- C6520.** Monaldo F. Implications of QuikSCAT and RADARSAT wind comparisons for SAR wind speed model functions. / Monaldo F., Thompson D. // 2002. IGARSS '02. 2002 IEEE International Geoscience and Remote Sensing Symposium. 24-28 June 2002. - Vol. 3. - P. 1881-1883. ↑
- C6521.** Trizna D. Results of a bistatic HF radar surface wave sea scatter experiment. / Trizna D., Gordon J. //

2002. IGARSS '02. 2002 IEEE International Geoscience and Remote Sensing Symposium. 24-28 June 2002. - Vol. 3. - P. 1902-1904. ↑

C6522. Yanovsky F.J. Phenomenological models of Doppler-polarimetric microwave remote sensing of clouds and precipitation. 2002. IGARSS '02. 2002 IEEE International Geoscience and Remote Sensing Symposium. 24-28 June 2002. - Vol. 3. - P. 1905-1907. ↑

C6523. Vesecky J.F. Measurement of wind speed and direction using multifrequency HF radar. / Vesecky J.F., Drake J., Teague C.C., Ludwig F.L., Davidson K., Paduan J. // 2002. IGARSS '02. 2002 IEEE International Geoscience and Remote Sensing Symposium. 24-28 June 2002. - Vol. 3. - P. 1899-1901. ↑

C6524. Lehner S. Detection of extreme waves using synthetic aperture radar images. / Lehner S., Schulz-Stellenfleth J., Niedermeier A. // 2002. IGARSS '02. 2002 IEEE International Geoscience and Remote Sensing Symposium. 24-28 June 2002. - Vol. 3. - P. 1893-1895. ↑

C6525. Teague C.C. Root-MUSIC direction finding applied to multifrequency coastal radar. 2002. IGARSS '02. 2002 IEEE International Geoscience and Remote Sensing Symposium. 24-28 June 2002. - Vol. 3. - P. 1896-1898. ↑

C6526. Dankert H. Detection of extreme waves using radar-image sequences. / Dankert H., Horstmann J., Rosenthal W. // 2002. IGARSS '02. 2002 IEEE International Geoscience and Remote Sensing Symposium. 24-28 June 2002. - Vol. 3. - P. 1831-1833. ↑

C6527. Ge Chen. Systematic discrepancies between altimeter and scatterometer wind speed measurements. / Ge Chen, Yong Han, Chaoyang Fang, Lixin Fang. // 2002. IGARSS '02. 2002 IEEE International Geoscience and Remote Sensing Symposium. 24-28 June 2002. - Vol. 3. - P. 1834-1836. ↑

C6528. Draper D.W. Simulation of SeaWinds measurements in the presence of rain using collocated TRMM PR data. / Draper D.W., Long D.G. // 2002. IGARSS '02. 2002 IEEE International Geoscience and Remote Sensing Symposium. 24-28 June 2002. - Vol. 3. - P. 1828-1830. ↑

C6529. Romeiser R. Validation of current and bathymetry measurements in the German Bight by airborne along-track interferometric SAR. / Romeiser R., Seibt-Winckler A., Heineke M., Eppel D. // 2002. IGARSS '02. 2002 IEEE International Geoscience and Remote Sensing Symposium. 24-28 June 2002. - Vol. 3. - P. 1822-1824. ↑

C6530. Schlick T. W-band radar backscattering at low grazing angles measured in a wave tank at various wind speeds. / Schlick T., Gade M., Essen H.-H., Gurgel K.-W., Lange P.A. // 2002. IGARSS '02. 2002 IEEE International Geoscience and Remote Sensing Symposium. 24-28 June 2002. - Vol. 3. - P. 1825-1827. ↑

C6531. Marzano F.S. Inversion techniques for ground-based microwave radiometric retrieval of precipitation columnar contents and path attenuation. / Marzano F.S., Fionda E., Ciotti P., Consalvi F. // 2002. IGARSS '02. 2002 IEEE International Geoscience and Remote Sensing Symposium. 24-28 June 2002. - Vol. 3. - P. 1869-1871. ↑

C6532. Walsh E.J. Rain rate measurement with an airborne scanning radar altimeter. / Walsh E.J., Wright C.W., Vandemark D., Bliven L.F., Uhlhorn E., Black P.G., Marks F.D. Jr. // 2002. IGARSS '02. 2002 IEEE International Geoscience and Remote Sensing Symposium. 24-28 June 2002. - Vol. 3. - P. 1875-1876. ↑

C6533. Klein A. Rain rate retrieval using airborne imaging radiometry during CAMEX3/TEFLUN-B. / Klein A., Gasiewski A.J., Yevgrafov A., Leuskiy V., Corbella I. // 2002. IGARSS '02. 2002 IEEE International Geoscience and Remote Sensing Symposium. 24-28 June 2002. - Vol. 3. - P. 1863-1865. ↑

C6534. Connor L.N. Measurement of the ocean surface in low to moderate winds at C-band. / Connor L.N., Chang P.S. // 2002. IGARSS '02. 2002 IEEE International Geoscience and Remote Sensing Symposium. 24-28 June 2002. - Vol. 3. - P. 1837-1838. ↑

C6535. Rincon R.F. Study of the variability in the rain drop size distribution over a 2.3 km path. / Rincon R.F., Lang R., Meneghini R., Bidwell S., Tokay A. // 2002. IGARSS '02. 2002 IEEE International Geoscience and Remote Sensing Symposium. 24-28 June 2002. - Vol. 3. - P. 1857-1859. ↑

C6536. Nedeltchev N.M. Polarimetric remote sensing of sea ice-from theory to practice. / Nedeltchev N.M.,

Peuch J.C., Baudrand H. // 2002. IGARSS '02. 2002 IEEE International Geoscience and Remote Sensing Symposium. 24-28 June 2002. - Vol. 4. - P. 2182-2184. ↑

C6537. Roman-Nieves J.I. High altitude compact solid state 95 GHz cloud radar. / Roman-Nieves J.I., Sekelsky S.M., Carswell J.R., Bolton W.R., Tooman T.P. // 2002. IGARSS '02. 2002 IEEE International Geoscience and Remote Sensing Symposium. 2002. - Vol. 5. - P. 2672-2674. ↑

C6538. Songxin Tan. A multiwavelength airborne polarimetric lidar for vegetation remote sensing: instrumentation and preliminary test results. / Songxin Tan, Narayanan R.M. // 2002. IGARSS '02. 2002 IEEE International Geoscience and Remote Sensing Symposium. 2002. - Vol. 5. - P. 2675-2677. ↑

C6539. Narayanan R. An airborne low-cost SAR for remote sensing: hardware design and development. / Narayanan R., Cantu P.C., Xiaojian Xu. // 2002. IGARSS '02. 2002 IEEE International Geoscience and Remote Sensing Symposium. 2002. - Vol. 5. - P. 2669-2671. ↑

C6540. Jie Lu. Research on ground based microwave signature measurement technology for spaceborne SAR applications. / Jie Lu, Ji Wu, Bo Sun, Suyun Zhu, Weixiong Luo. // 2002. IGARSS '02. 2002 IEEE International Geoscience and Remote Sensing Symposium. 2002. - Vol. 5. - P. 2663-2665. ↑

C6541. Sato M. Polarimetric borehole radar and its applications. / Sato M., Abe T. // 2002. IGARSS '02. 2002 IEEE International Geoscience and Remote Sensing Symposium. 2002. - Vol. 5. - P. 2666-2668. ↑

C6542. Wang C.K. Using SHOALS LIDAR system to detect bottom material change. / Wang C.K., Philpot W.D. // 2002. IGARSS '02. 2002 IEEE International Geoscience and Remote Sensing Symposium. 2002. - Vol. 5. - P. 2690-2692. ↑

C6543. Berardino P. Differential SAR interferometry for the study of slope instability at Maratea, Italy. / Berardino P., Costantini M., Franceschetti G., Iodice A., Pietranera L., Rizzo V. // 2002. IGARSS '02. 2002 IEEE International Geoscience and Remote Sensing Symposium. 2002. - Vol. 5. - P. 2693-2695. ↑

C6544. Dobler J.T. Doppler lidar using aerosol backscatter and a frequency agile laser transmitter for profiling atmospheric winds in the planetary boundary layer. / Dobler J.T., Gentry B.M., Reagan J.A. // 2002. IGARSS '02. 2002 IEEE International Geoscience and Remote Sensing Symposium. 2002. - Vol. 5. - P. 2687-2689. ↑

C6545. Dehai Zhang. An airborne multi-mode microwave sensor and flight experiments. / Dehai Zhang, Jingshang Jiang, Zhenfan Zheng, Shuanrong Wang, Huguang Liu, Bo Sun, Ke Xu, Shengwei Zhang. // 2002. IGARSS '02. 2002 IEEE International Geoscience and Remote Sensing Symposium. 2002. - Vol. 5. - P. 2681-2683. ↑

C6546. Zhu Suyun. JZM-Ku1 pulse-modulated scanning air-borne scatterometer. / Zhu Suyun, Jiang Changhong, Sun Bo. // 2002. IGARSS '02. 2002 IEEE International Geoscience and Remote Sensing Symposium. 2002. - Vol. 5. - P. 2684-2686. ↑

C6547. Jingjuan Liao. Modeling of microwave dielectric properties of rice growth stages in Zhaoqing test site of Southern China. / Jingjuan Liao, Huadong Guo, Yun Shao. // 2002. IGARSS '02. 2002 IEEE International Geoscience and Remote Sensing Symposium. 2002. - Vol. 5. - P. 2620-2622. ↑

C6548. Moccia A. BISSAT: a bistatic SAR for Earth observation. / Moccia A., Rufino G., D'Errico M., Alberti G., Salzillo G. // 2002. IGARSS '02. 2002 IEEE International Geoscience and Remote Sensing Symposium. 2002. - Vol. 5. - P. 2628-2630. ↑

C6549. Jianjun Guo. Frequency dependence of scattering by dense media of small particles based on Monte Carlo simulation of Maxwell's equations. / Jianjun Guo, Leung Tsang, Chang A.T.C., Kung-Hau Ding, Chi-Te Chen. // 2002. IGARSS '02. 2002 IEEE International Geoscience and Remote Sensing Symposium. 2002. - Vol. 5. - P. 2617-2619. ↑

C6550. Zhang Hong. Polarimetric SAR interferometry for vegetable vertical structure parameters extraction. / Zhang Hong, Wang Chao, Liu Zhi. // 2002. IGARSS '02. 2002 IEEE International Geoscience and Remote Sensing Symposium. 2002. - Vol. 5. - P. 2611-2613. ↑

C6551. Takumi I. Clustering of EM radiation source based on eigenvector. / Takumi I., Murakami S., Shimura A., Hata M., Yasukawa H. // 2002. IGARSS '02. 2002 IEEE International Geoscience and Remote Sensing Symposium. 2002. - Vol. 5. - P. 2604-2606. ↑

Symposium. 2002. - Vol. 5. - P. 2614-2616. ↑

C6552. Baghdadi N. An empirical calibration of the integral equation model based on SAR data and soil parameters measurements. / Baghdadi N., King C., Bonnifait A. // 2002. IGARSS '02. 2002 IEEE International Geoscience and Remote Sensing Symposium. 2002. - Vol. 5. - P. 2646-2650. ↑

C6553. Komarov S.A. SAR polarimetry for permafrost active layer freeze/thaw processes. / Komarov S.A., Mironov V.L., Li S. // 2002. IGARSS '02. 2002 IEEE International Geoscience and Remote Sensing Symposium. 2002. - Vol. 5. - P. 2654-2656. ↑

C6554. Zhang-anxue. Estimation of the object depth accurately with GPR. / Zhang-anxue, Jiang-yansheng, Wang-wenbing. // 2002. IGARSS '02. 2002 IEEE International Geoscience and Remote Sensing Symposium. 2002. - Vol. 5. - P. 2643-2645. ↑

C6555. El-Ocla H. Analysis of backscattering enhancement for partially convex targets in random media for plane and beam wave incidences. / El-Ocla H., Tateiba M. // 2002. IGARSS '02. 2002 IEEE International Geoscience and Remote Sensing Symposium. 2002. - Vol. 5. - P. 2634-2636. ↑

C6556. Macelloni G. Scattering from randomly distributed dielectric cylinders: experiment and modeling results. / Macelloni G., Marliani F., Nesti G., Paloscia S., Pampaloni P., Poggi P., Ruisi R., Bruscalgioni P. // 2002. IGARSS '02. 2002 IEEE International Geoscience and Remote Sensing Symposium. 2002. - Vol. 5. - P. 2637-2639. ↑

C6557. Mora O. Generation of deformation maps at low resolution using differential interferometric SAR data. / Mora O., Mallorqui J.J., Duro J. // 2002. IGARSS '02. 2002 IEEE International Geoscience and Remote Sensing Symposium. 2002. - Vol. 5. - P. 2696-2698. ↑

C6558. Rodriguez D. High performance artificial SAR raw data generation algorithms for remote-sensed imaging applications. / Rodriguez D., Rueda D., Nava H., Quinchanegua A. // 2002. IGARSS '02. 2002 IEEE International Geoscience and Remote Sensing Symposium. 2002. - Vol. 5. - P. 2747-2749. ↑

C6559. Simon-Klar C. A multi DSP board for real time SAR processing using the HiPAR-DSP 16. / Simon-Klar C., Friebe L., Kloos H., Lieske H., Hinrichs W., Pirsch P. // 2002. IGARSS '02. 2002 IEEE International Geoscience and Remote Sensing Symposium. 2002. - Vol. 5. - P. 2750-2752. ↑

C6560. Nicoll J. Pre-processing compensation for saturation power loss in SAR data. / Nicoll J., Gens R., Denny P. // 2002. IGARSS '02. 2002 IEEE International Geoscience and Remote Sensing Symposium. 2002. - Vol. 5. - P. 2744-2746. ↑

C6561. Axelsson S.R.J. SAR/MTI radar mapping from ships and ground based vehicles. 2002. IGARSS '02. 2002 IEEE International Geoscience and Remote Sensing Symposium. 2002. - Vol. 5. - P. 2738-2741. ↑

C6562. Goriachkin O.V. Techniques of blind SAR processing: theory and practical applications. / Goriachkin O.V., Klovsky D.D. // 2002. IGARSS '02. 2002 IEEE International Geoscience and Remote Sensing Symposium. 2002. - Vol. 5. - P. 2742-2743. ↑

C6563. Stephen H. Azimuth modulation of backscatter from SeaWinds and ERS scatterometers over the Saharo-Arabian deserts. / Stephen H., Long D.G. // 2002. IGARSS '02. 2002 IEEE International Geoscience and Remote Sensing Symposium. 2002. - Vol. 5. - P. 2808-2810. ↑

C6564. Helmis C.G. A study of low level jet characteristics using a sodar-RASS profiling system. / Helmis C.G., Halios Ch.H., Asimakopoulos D.N. // 2002. IGARSS '02. 2002 IEEE International Geoscience and Remote Sensing Symposium. 2002. - Vol. 5. - P. 2811-2813. ↑

C6565. Verdone G.R. Processing algorithms for COSMO-SkyMed SAR sensor. / Verdone G.R., Viggiano R., Lopinto E., Millillo G., Candela L., Lombardi N., Giannini V. // 2002. IGARSS '02. 2002 IEEE International Geoscience and Remote Sensing Symposium. 2002. - Vol. 5. - P. 2771-2774. ↑

C6566. Zhang Q. ISAR imaging in strong ground clutter by using a new stepped-frequency signal mode. / Zhang Q., Yeo T.S., Du G. // 2002. IGARSS '02. 2002 IEEE International Geoscience and Remote Sensing Symposium. 2002. - Vol. 5. - P. 2753-2755. ↑

- C6567.** Schubert A. Robustness of wavelet-based stereo matching for variable acquisition geometries using simulated SAR images. / Schubert A., Small D., Meier E., Nuesch D. // 2002. IGARSS '02. 2002 IEEE International Geoscience and Remote Sensing Symposium. 2002. - Vol. 5. - P. 2759-2761. ↑
- C6568.** Ya-Qiu Jin. Polarimetric scattering indexes and information entropy of the SAR imagery for surface classification. / Ya-Qiu Jin, Fei Chen. // 2002. IGARSS '02. 2002 IEEE International Geoscience and Remote Sensing Symposium. 2002. - Vol. 5. - P. 2708-2710. ↑
- C6569.** Mallorqui J.J. Simulation of polarimetric SAR vessel signatures for satellite fisheries monitoring. / Mallorqui J.J., Rius J.M., Bara M. // 2002. IGARSS '02. 2002 IEEE International Geoscience and Remote Sensing Symposium. 2002. - Vol. 5. - P. 2711-2713. ↑
- C6570.** Xinwu Li. Generation and error analysis of DEM using spaceborne polarimetric SAR interferometry data. / Xinwu Li, Huadong Guo, Changlin Wang, Zhen Li, Jingjuan Liao. // 2002. IGARSS '02. 2002 IEEE International Geoscience and Remote Sensing Symposium. 2002. - Vol. 5. - P. 2705-2707. ↑
- C6571.** Kun Tao. Quantitative assessment of interferometric SAR images registration accuracy. / Kun Tao, Yang Ruliang. // 2002. IGARSS '02. 2002 IEEE International Geoscience and Remote Sensing Symposium. 2002. - Vol. 5. - P. 2699-2701. ↑
- C6572.** Miyawaki M. The DEM generation of a volcano using airborne SAR interferometry. / Miyawaki M., Murata M., Sato J., Koarai M., Mizuno T., Watanabe N., Iida Y., Yamada Y., Tsuda Y. // 2002. IGARSS '02. 2002 IEEE International Geoscience and Remote Sensing Symposium. 2002. - Vol. 5. - P. 2702-2704. ↑
- C6573.** Markham K.J. Digital terrain elevation models produced using radar altimetry and GPS data. / Markham K.J., Morris W.A. // 2002. IGARSS '02. 2002 IEEE International Geoscience and Remote Sensing Symposium. 2002. - Vol. 5. - P. 2723-2725. ↑
- C6574.** Albright W. Empirical determination of thermal noise levels in synthetic aperture radar. / Albright W., Nicoll J. // 2002. IGARSS '02. 2002 IEEE International Geoscience and Remote Sensing Symposium. 2002. - Vol. 5. - P. 2729-2731. ↑
- C6575.** Jeremy M.L. Velocity estimates from fully polarimetric SAR. 2002. IGARSS '02. 2002 IEEE International Geoscience and Remote Sensing Symposium. 2002. - Vol. 5. - P. 2720-2722. ↑
- C6576.** Riedel T. Seasonal and diurnal changes of polarimetric parameters from crops derived by the Cloude decomposition theorem at L-band. / Riedel T., Liebeskind P., Schmullius C.C. // 2002. IGARSS '02. 2002 IEEE International Geoscience and Remote Sensing Symposium. 2002. - Vol. 5. - P. 2714-2716. ↑
- C6577.** Turner D. A synoptic visualisation of fully polarimetric SAR data-an annotated example icon. / Turner D., Woodhouse I.H., Laidlaw D.H. // 2002. IGARSS '02. 2002 IEEE International Geoscience and Remote Sensing Symposium. 2002. - Vol. 5. - P. 2717-2719. ↑
- C6578.** Tupin F. Matching criteria for radargrammetry. / Tupin F., Nicolas J.-M. // 2002. IGARSS '02. 2002 IEEE International Geoscience and Remote Sensing Symposium. 2002. - Vol. 5. - P. 2608-2610. ↑
- C6579.** Filippini R. Mars electromagnetic environment: insights from field analysis at Earth analogs. / Filippini R., Marcialis R., Ottonello C., Pagnan S. // 2002. IGARSS '02. 2002 IEEE International Geoscience and Remote Sensing Symposium. 24-28 June 2002. - Vol. 4. - P. 2340-2342. ↑
- C6580.** Fukui Y. A study on the surface temperature distribution and the urban structure in Tokyo with ASTER and LIDAR data. / Fukui Y., Hirose Y., Mushiake N. // 2002. IGARSS '02. 2002 IEEE International Geoscience and Remote Sensing Symposium. 24-28 June 2002. - Vol. 4. - P. 2343-2345. ↑
- C6581.** Pichel W.G. Ocean Observer SAR requirements and instrument characteristics. / Pichel W.G., McGuire J., Cunningham J.D., Gerber A., Huneycutt B., Holt B., Sandwell D.T. // 2002. IGARSS '02. 2002 IEEE International Geoscience and Remote Sensing Symposium. 2002. - Vol. 4. - P. 2296-2298. ↑
- C6582.** Wegmuller U. ENVISAT ASAR in disaster management and humanitarian relief. / Wegmuller U., Wiesmann A., Strozzi T., Werner C. // 2002. IGARSS '02. 2002 IEEE International Geoscience and Remote Sensing Symposium. 24-28 June 2002. - Vol. 4. - P. 2282-2284. ↑

- C6583.** Williams L. An aerosol lidar model program used for the Center for Lidar and Atmospheric Sciences Students lidar system. / Williams L., Wei Gong, Temple D.A., Omar A.H., Mangana J. // 2002. IGARSS '02. 2002 IEEE International Geoscience and Remote Sensing Symposium. 2002. - Vol. 4. - P. 2291-2295. ↑
- C6584.** Coltuc D. On the homomorphic filtering by channels' summation. / Coltuc D., Radescu R. // 2002. IGARSS '02. 2002 IEEE International Geoscience and Remote Sensing Symposium. 24-28 June 2002. - Vol. 4. - P. 2456-2458. ↑
- C6585.** Fedorov D. System for automatic registration of remote sensing images. / Fedorov D., Fonseca L.M.G., Kenney C., Manjunath B.S. // 2002. IGARSS '02. 2002 IEEE International Geoscience and Remote Sensing Symposium. 24-28 June 2002. - Vol. 4. - P. 2459-2461. ↑
- C6586.** Felton M. Polar Stratospheric Cloud (PSC) classification using LIDAR measurements from the recent SAGE III Ozone Loss and Validation Experiment (SOLVE). / Felton M., Omar A.H. // 2002. IGARSS '02. 2002 IEEE International Geoscience and Remote Sensing Symposium. 24-28 June 2002. - Vol. 4. - P. 2407-2410. ↑
- C6587.** Takeuchi S. Comparison of InSAR capability for land subsidence detection between C-band and L-band SAR. / Takeuchi S., Yamada S. // 2002. IGARSS '02. 2002 IEEE International Geoscience and Remote Sensing Symposium. 24-28 June 2002. - Vol. 4. - P. 2379-2381. ↑
- C6588.** Othman M.T. Microwave and optical remote sensing study of Boone County, Missouri. / Othman M.T., Legarsky J.J., Davis C.H. // 2002. IGARSS '02. 2002 IEEE International Geoscience and Remote Sensing Symposium. 24-28 June 2002. - Vol. 4. - P. 2404-2406. ↑
- C6589.** Romshoo S.A. C-band radar for soil moisture estimation under agricultural conditions. / Romshoo S.A., Taikan O., Katumi M. // 2002. IGARSS '02. 2002 IEEE International Geoscience and Remote Sensing Symposium. 2002. - Vol. 4. - P. 2217-2219. ↑
- C6590.** Sprintsin M. Estimation of soil water content in the Negev Desert open areas using archived ERS SAR images. / Sprintsin M., Blumberg D.G., Asher J.B., Daniels J., Linetsky M. // 2002. IGARSS '02. 2002 IEEE International Geoscience and Remote Sensing Symposium. 2002. - Vol. 4. - P. 2220-2222. ↑
- C6591.** Hogda K.A. Synthetic aperture radar for DEM generation in snow-covered mountain terrain. / Hogda K.A., Guneriusson T., Lauknes I. // 2002. IGARSS '02. 2002 IEEE International Geoscience and Remote Sensing Symposium. 2002. - Vol. 4. - P. 2193-2195. ↑
- C6592.** Scheuchl B. Potential of RADARSAT-2 for sea ice classification. / Scheuchl B., Cumming I.G. // 2002. IGARSS '02. 2002 IEEE International Geoscience and Remote Sensing Symposium. 2002. - Vol. 4. - P. 2185-2187. ↑
- C6593.** Braaten D. Radar measurements of ice sheet thickness of outlet glaciers in Greenland. / Braaten D., Gogineni S. // 2002. IGARSS '02. 2002 IEEE International Geoscience and Remote Sensing Symposium. 2002. - Vol. 4. - P. 2188-2189. ↑
- C6594.** Lane K. RADARSAT-1 synthetic aperture radar iceberg detection performance ADRO-2 A223. / Lane K., Power D., Chakraborty I., Youden J., Randell C., McClintock J., Flett D. // 2002. IGARSS '02. 2002 IEEE International Geoscience and Remote Sensing Symposium. 2002. - Vol. 4. - P. 2273-2275. ↑
- C6595.** Puestow T.M. Third party encroachment monitoring using RADARSAT-1, IKONOS, EROS-A1 and simulated RADARSAT-2 imagery. / Puestow T.M., Lane K., McHugh S., Power D., Randell C.J., Howell C. // 2002. IGARSS '02. 2002 IEEE International Geoscience and Remote Sensing Symposium. 2002. - Vol. 4. - P. 2276-2278. ↑
- C6596.** Durand P. An update in the evolution of Radarsat1 azimuth Doppler for differential interferometry purposes. / Durand P., van der Kooij M., Adragna F. // 2002. IGARSS '02. 2002 IEEE International Geoscience and Remote Sensing Symposium. 2002. - Vol. 4. - P. 2270-2272. ↑
- C6597.** Zribi M. A new empirical model to inverse soil moisture and roughness using two radar configurations. / Zribi M., Dechambre M. // 2002. IGARSS '02. 2002 IEEE International Geoscience and Remote Sensing Symposium. 2002. - Vol. 4. - P. 2223-2225. ↑
- C6598.** Lebel D. Moose Mountain Virtual Explorer: A learning and ground-truthing tool to explore high-

resolution remote sensing and geoscience data in mountainous area. / Lebel D., Kirkwood D., Molard P., Pouliot J., Morin A., Deblonde C. // 2002. IGARSS '02. 2002 IEEE International Geoscience and Remote Sensing Symposium. 2002. - Vol. 4. - P. 2257-2259. ↑

C6599. Fonseca L.M.G. Automatic registration of radar imagery. / Fonseca L.M.G., Costa M.H.M., Castellari S.P. // 2002. IGARSS '02. 2002 IEEE International Geoscience and Remote Sensing Symposium. 24-28 June 2002. - Vol. 4. - P. 2465-2467. ↑

C6600. Guifu Zhang. Range interferometry technique to determine radial wind. / Guifu Zhang, Doviak R.J., Vivekanandan J. // 2002. IGARSS '02. 2002 IEEE International Geoscience and Remote Sensing Symposium. 24-28 June 2002. - Vol. 4. - P. 2549-2552. ↑

C6601. Beaulieu J.-M. Hierarchical segmentation of polarimetric SAR images. / Beaulieu J.-M., Touzi R. // 2002. IGARSS '02. 2002 IEEE International Geoscience and Remote Sensing Symposium. 2002. - Vol. 5. - P. 2590-2592. ↑

C6602. Small D. Phase noise countermeasures for synthetic interferogram generation. / Small D., Meier E., Nuesch D. // 2002. IGARSS '02. 2002 IEEE International Geoscience and Remote Sensing Symposium. 24-28 June 2002. - Vol. 4. - P. 2546-2548. ↑

C6603. Ma Debao. The new curvature methods of image fine registration for synthetic aperture radar interferometry. / Ma Debao, Lu Yinghua, Liu Jianhua. // 2002. IGARSS '02. 2002 IEEE International Geoscience and Remote Sensing Symposium. 24-28 June 2002. - Vol. 4. - P. 2540-2542. ↑

C6604. Meyer F. Determination of the rheology of Arctic glaciers using multi-temporal ERS1/2 SAR interferograms combined in a least squares adjustment. / Meyer F., Hellwich O. // 2002. IGARSS '02. 2002 IEEE International Geoscience and Remote Sensing Symposium. 24-28 June 2002. - Vol. 4. - P. 2543-2545. ↑

C6605. Lee K.Y. Land cover classification of polarimetric synthetic aperture radar (POLSAR) data based on scattering mechanisms and complex Wishart distribution. / Lee K.Y., Soo Chin Liew, Leong Keong Kwoh. // 2002. IGARSS '02. 2002 IEEE International Geoscience and Remote Sensing Symposium. 2002. - Vol. 5. - P. 2602-2604. ↑

C6606. Sang-Eun Park. Polarimetric target decomposition and physical interpretation of NASA (JPL) AIRSAR data in mountainous terrain. / Sang-Eun Park, Moon W.M. // 2002. IGARSS '02. 2002 IEEE International Geoscience and Remote Sensing Symposium. 2002. - Vol. 5. - P. 2605-2607. ↑

C6607. Fukuda S. Unsupervised approach for polarimetric SAR image classification using support vector machines. / Fukuda S., Katagiri R., Hirokawa H. // 2002. IGARSS '02. 2002 IEEE International Geoscience and Remote Sensing Symposium. 2002. - Vol. 5. - P. 2599-2601. ↑

C6608. Macri Pellizzeri T. Multiband SAR classification using contextual analysis: annealing segmentation vs. a neural kernel-based approach. / Macri Pellizzeri T., Dell'Acqua F., Gamba P., Lombardo P., Mazzola D. // 2002. IGARSS '02. 2002 IEEE International Geoscience and Remote Sensing Symposium. 2002. - Vol. 5. - P. 2593-2595. ↑

C6609. Flynn T. Coherence region shape extraction for vegetation parameter estimation in polarimetric SAR interferometry. / Flynn T., Tabb M., Carande R. // 2002. IGARSS '02. 2002 IEEE International Geoscience and Remote Sensing Symposium. 2002. - Vol. 5. - P. 2596-2598. ↑

C6610. Oller G. SAR image matching using the edge strength map. / Oller G., Marthon P., Denise L. // 2002. IGARSS '02. 2002 IEEE International Geoscience and Remote Sensing Symposium. 24-28 June 2002. - Vol. 4. - P. 2495-2497. ↑

C6611. Ouchi K. Simulation on the extraction of ships' images embedded in speckle using cross-correlation of multilook SAR images and applications to Radarsat data. / Ouchi K., Yaguchi H. // 2002. IGARSS '02. 2002 IEEE International Geoscience and Remote Sensing Symposium. 24-28 June 2002. - Vol. 4. - P. 2498-2500. ↑

C6612. Nicolas J.M. Gamma mixture modeled with "second kind statistics": application to SAR image processing. / Nicolas J.M., Tupin F. // 2002. IGARSS '02. 2002 IEEE International Geoscience and Remote Sensing Symposium. 24-28 June 2002. - Vol. 4. - P. 2489-2491. ↑

- C6613.** Han Chumning. Edge preservation evaluation of digital speckle filters. / Han Chumning, Guo Huadong, Wang Changlin. // 2002. IGARSS '02. 2002 IEEE International Geoscience and Remote Sensing Symposium. 24-28 June 2002. - Vol. 4. - P. 2471-2473. ↑
- C6614.** Muller H.-R. From Gaussian to inverse Gaussian statistics in SAR imagery. / Muller H.-R., Horn R., Moreira A. // 2002. IGARSS '02. 2002 IEEE International Geoscience and Remote Sensing Symposium. 24-28 June 2002. - Vol. 4. - P. 2486-2488. ↑
- C6615.** Ferraiuolo G. MAP-MRF filtering of SAR interferometric phase fields. / Ferraiuolo G., Poggi G. // 2002. IGARSS '02. 2002 IEEE International Geoscience and Remote Sensing Symposium. 24-28 June 2002. - Vol. 4. - P. 2534-2536. ↑
- C6616.** Xinwu Li. Phase unwrapping of SAR interferogram based on dyadic wavelets. / Xinwu Li, Huadong Guo, Changlin Wang, Zhen Li, Jingjuan Liao. // 2002. IGARSS '02. 2002 IEEE International Geoscience and Remote Sensing Symposium. 24-28 June 2002. - Vol. 4. - P. 2537-2539. ↑
- C6617.** Schultz D.C. Balancing rewrapping error and smoothness in two dimensional phase unwrapping problems. / Schultz D.C., Koetter R., Frey B.J., Munson D.C. Jr. // 2002. IGARSS '02. 2002 IEEE International Geoscience and Remote Sensing Symposium. 24-28 June 2002. - Vol. 4. - P. 2507-2509. ↑
- C6618.** Rodriguez D. Signal operator cores for SAR real time processing hardware. / Rodriguez D., Quinchanequa A., Nava H. // 2002. IGARSS '02. 2002 IEEE International Geoscience and Remote Sensing Symposium. 24-28 June 2002. - Vol. 4. - P. 2501-2503. ↑
- C6619.** Sadjadi F. Image classification in complex spaces. 2002. IGARSS '02. 2002 IEEE International Geoscience and Remote Sensing Symposium. 24-28 June 2002. - Vol. 4. - P. 2504-2506. ↑
- C6620.** Inglada J. Automatic multi-sensor image registration by edge matching using genetic algorithms. / Inglada J., Adragna F. // 2001. IGARSS '01. IEEE 2001 International Geoscience and Remote Sensing Symposium. - Sydney, NSW, 2001. - Vol. 5. - P. 2313-2315. ↑
- C6621.** Friebe L. A compact real-time SAR processing system using the highly parallel HiPAR-DSP 16. / Friebe L., Kloos H., Wittenburg J.P., Hinrichs W., Lieske H., Klar C., Pirsch P. // 2001. IGARSS '01. IEEE 2001 International Geoscience and Remote Sensing Symposium. - Sydney, NSW, 2001. - Vol. 5. - P. 2307-2309. ↑
- C6622.** Pastina D. Super-resolution of polarimetric SAR images of a ship. / Pastina D., Lombardo P., Farina A., Daddi P. // 2001. IGARSS '01. IEEE 2001 International Geoscience and Remote Sensing Symposium. - Sydney, NSW, 2001. - Vol. 5. - P. 2343-2345. ↑
- C6623.** Lee W.K. Reduction of cardinal effects in SAR imagery of densely populated urban areas by suppressing strong multiple returns. 2001. IGARSS '01. IEEE 2001 International Geoscience and Remote Sensing Symposium. - Sydney, NSW, 2001. - Vol. 5. - P. 2328-2330. ↑
- C6624.** Franco J.A. SAR images filtering and segmentation: a multiresolution and contextual approach. / Franco J.A., Moctezuma M., Barilla M.E., Escalante B., Parmiggiani F. // 2001. IGARSS '01. IEEE 2001 International Geoscience and Remote Sensing Symposium. - Sydney, NSW, 2001. - Vol. 5. - P. 2304-2306. ↑
- C6625.** Erer I. Superresolution ISAR imaging by 2-D complex asymmetric half-plane lattice predictors. / Erer I., Kartal M., Kayran A.H. // 2001. IGARSS '01. IEEE 2001 International Geoscience and Remote Sensing Symposium. - Sydney, NSW, 2001. - Vol. 5. - P. 2268-2270. ↑
- C6626.** Takeuchi S. A comparative study of coherence information by L-band and C-band SAR for detecting deforestation in tropical rain forest. / Takeuchi S., Suga Y., Yoshimura M. // 2001. IGARSS '01. IEEE 2001 International Geoscience and Remote Sensing Symposium. - Sydney, NSW, 2001. - Vol. 5. - P. 2259-2261. ↑
- C6627.** Du Gan. A multifractal approach for auto-segmentation of SAR images. / Du Gan, Yeo Tat-Soon. // 2001. IGARSS '01. IEEE 2001 International Geoscience and Remote Sensing Symposium. - Sydney, NSW, 2001. - Vol. 5. - P. 2301-2303. ↑
- C6628.** Abdelfattah R. InSAR coherence estimation for temporal analysis and phase unwrapping applications. / Abdelfattah R., Nicolas J.M., Tupin F., Badredine B. // 2001. IGARSS '01. IEEE 2001 International Geoscience and Remote Sensing Symposium. - Sydney, NSW, 2001. - Vol. 5. - P. 2292-2294. ↑

- C6629.** Herold M. The effect of free vegetation water on the multi-frequency and polarimetric radar backscatter-first results from the TerraDew 2000 campaign. / Herold M., Pathe C., Schmullius C.C. // 2001. IGARSS '01. IEEE 2001 International Geoscience and Remote Sensing Symposium. - Sydney, NSW, 2001. - Vol. 5. - P. 2445-2447. ↑
- C6630.** de Badereau D. Radar remote sensing of a forest at VHF frequencies: a two dimensional full wave approach. / de Badereau D., Roussel H., Tabbara W. // 2001. IGARSS '01. IEEE 2001 International Geoscience and Remote Sensing Symposium. - Sydney, NSW, 2001. - Vol. 5. - P. 2436-2438. ↑
- C6631.** Zecchetto S. Small scale properties of the radar backscatter from the sea surface at off nadir angles. / Zecchetto S., De Biasio F., Pierdicca N., Trivero P. // 2001. IGARSS '01. IEEE 2001 International Geoscience and Remote Sensing Symposium. - Sydney, NSW, 2001. - Vol. 5. - P. 2457-2459. ↑
- C6632.** West J.C. LGA scattering from measured breaking water waves: extension to jetting surfaces. / West J.C., Zhiqin Zhao, Xinan Liu, Duncan J.H. // 2001. IGARSS '01. IEEE 2001 International Geoscience and Remote Sensing Symposium. - Sydney, NSW, 2001. - Vol. 5. - P. 2454-2456. ↑
- C6633.** Berizzi F. Fractal and multifractal analysis of sea SAR clutter data. / Berizzi F., Gamba P., Garzelli A., Martorella M., Dell'Acqua F. // 2001. IGARSS '01. IEEE 2001 International Geoscience and Remote Sensing Symposium. - Sydney, NSW, 2001. - Vol. 5. - P. 2430-2432. ↑
- C6634.** Rodriguez K.M. Lava-flow textural trends using SAR: the Virunga Volcanic Chain, East Africa. / Rodriguez K.M., Weissel J.K., Menke W.H. // 2001. IGARSS '01. IEEE 2001 International Geoscience and Remote Sensing Symposium. - Sydney, NSW, 2001. - Vol. 5. - P. 2421-2423. ↑
- C6635.** Sveinsson J.R. Speckle reduction of SAR images in the complex wavelet domain. / Sveinsson J.R., Benediktsson J.A. // 2001. IGARSS '01. IEEE 2001 International Geoscience and Remote Sensing Symposium. - Sydney, NSW, 2001. - Vol. 5. - P. 2346-2348. ↑
- C6636.** Bourlier C. The Kirchhoff analysis from one- and two-dimensional random surface with the statistical shadowing function. / Bourlier C., Berginc G., Saillard J. // 2001. IGARSS '01. IEEE 2001 International Geoscience and Remote Sensing Symposium. - Sydney, NSW, 2001. - Vol. 5. - P. 2427-2429. ↑
- C6637.** Kim Sang-Wan. Application of differential SAR interferometry over the Baegdu stratovolcanic mountain. / Kim Sang-Wan, Joong-Sun Won, Jeong Woo Kim, Moon W.M. // 2001. IGARSS '01. IEEE 2001 International Geoscience and Remote Sensing Symposium. - Sydney, NSW, 2001. - Vol. 5. - P. 2424-2426. ↑
- C6638.** Zribi M. Estimation of spatial and temporal evolution of vegetation and surface moisture from ERS2 radar in a semi-arid region. / Zribi M., Le Hegarat-Masclé S., Taconet O., Vidal-Madjar D., Boussema M.R., Belhadj Z. // 2001. IGARSS '01. IEEE 2001 International Geoscience and Remote Sensing Symposium. - Sydney, NSW, 2001. - Vol. 5. - P. 2109-2111. ↑
- C6639.** Herold M. Multi-parameter airborne SAR remote sensing of soil moisture in agricultural area. / Herold M., Shi J., Schmullius C.C. // 2001. IGARSS '01. IEEE 2001 International Geoscience and Remote Sensing Symposium. - Sydney, NSW, 2001. - Vol. 5. - P. 2103-2105. ↑
- C6640.** Sakurai-Amano T. Detection of seasonal water level changes in Amazon forests from JERS-1 SAR images using isolated strong scatterers. / Sakurai-Amano T., Nakasugi K., Takagi M. // 2001. IGARSS '01. IEEE 2001 International Geoscience and Remote Sensing Symposium. - Sydney, NSW, 2001. - Vol. 5. - P. 2140-2142. ↑
- C6641.** Long Chiu. Applications of Tropical Rainfall Measuring Mission (TRMM) data. / Long Chiu, Serafino G., Teng W.L. // 2001. IGARSS '01. IEEE 2001 International Geoscience and Remote Sensing Symposium. - Sydney, NSW, 2001. - Vol. 5. - P. 2118-2120. ↑
- C6642.** Kwon E.Y. Retrieval of soil moisture content with the use of neural network-scattering model. / Kwon E.Y., Ryu D., Moon W.M., Lee K.K. // 2001. IGARSS '01. IEEE 2001 International Geoscience and Remote Sensing Symposium. - Sydney, NSW, 2001. - Vol. 5. - P. 2094-2096. ↑
- C6643.** Manandhar D. Vehicle-borne laser mapping system (VLMS) for 3-D GIS. / Manandhar D., Shibasaki R. // 2001. IGARSS '01. IEEE 2001 International Geoscience and Remote Sensing Symposium. - Sydney, NSW, 2001. - Vol. 5. - P. 2073-2075. ↑

- C6644.** Younan N.H. Extracting digital terrain models in forestry using lidar data. / Younan N.H., Lee H.S., Evans D.L., Eggleston N.T. // 2001. IGARSS '01. IEEE 2001 International Geoscience and Remote Sensing Symposium. - Sydney, NSW, 2001. - Vol. 5. - P. 2070-2072. ↑
- C6645.** Dechambre M. Backscattering behavior and simulation comparison over bare soil using helicopterborne radar data (the Alpilles-ReSeDA project). / Dechambre M., Zribi M., Ciarletti V. // 2001. IGARSS '01. IEEE 2001 International Geoscience and Remote Sensing Symposium. - Sydney, NSW, 2001. - Vol. 5. - P. 2082-2084. ↑
- C6646.** Desai A.S. GPR SAR simulation and image reconstruction. / Desai A.S., Wilkinson A.J., Inggs M.R. // 2001. IGARSS '01. IEEE 2001 International Geoscience and Remote Sensing Symposium. - Sydney, NSW, 2001. - Vol. 5. - P. 2076-2078. ↑
- C6647.** Wang Changlin. Dynamic monitoring of land cover changes in Yellow River delta of China using multi-sources remote sensing data. / Wang Changlin, Yang Hu, Fan Xiangtao, Shao Yun. // 2001. IGARSS '01. IEEE 2001 International Geoscience and Remote Sensing Symposium. - Sydney, NSW, 2001. - Vol. 5. - P. 2202-2204. ↑
- C6648.** Mitchell A. Integration of aerial photography, hyperspectral and SAR data for mangrove characterization. / Mitchell A., Lucas R.M. // 2001. IGARSS '01. IEEE 2001 International Geoscience and Remote Sensing Symposium. - Sydney, NSW, 2001. - Vol. 5. - P. 2193-2195. ↑
- C6649.** Marano S. Influence of the microscopic fractal dimension on the statistical characterization of natural surfaces. / Marano S., Percannella R., Restaino R., Tesauro M. // 2001. IGARSS '01. IEEE 2001 International Geoscience and Remote Sensing Symposium. - Sydney, NSW, 2001. - Vol. 5. - P. 2208-2211. ↑
- C6650.** Kenyi L.W. Mapping the African rift valley in northern Uganda with SAR interferometry. 2001. IGARSS '01. IEEE 2001 International Geoscience and Remote Sensing Symposium. - Sydney, NSW, 2001. - Vol. 5. - P. 2205-2207. ↑
- C6651.** Draper D.W. An advanced point-wise ambiguity selection algorithm: application to SeaWinds. / Draper D.W., Long D.G. // 2001. IGARSS '01. IEEE 2001 International Geoscience and Remote Sensing Symposium. - Sydney, NSW, 2001. - Vol. 5. - P. 2190-2192. ↑
- C6652.** Guifu Zhang. Sampling effects on radar measurements and rain rate estimation. / Guifu Zhang, Vivekanandan J., Brandes E. // 2001. IGARSS '01. IEEE 2001 International Geoscience and Remote Sensing Symposium. - Sydney, NSW, 2001. - Vol. 5. - P. 2165-2168. ↑
- C6653.** Sakurai-Amano T. Seasonal water level changes in tropical forests in New Guinea detected from JERS-1 SAR images. / Sakurai-Amano T., Yoshioka T., Takagi M. // 2001. IGARSS '01. IEEE 2001 International Geoscience and Remote Sensing Symposium. - Sydney, NSW, 2001. - Vol. 5. - P. 2143-2145. ↑
- C6654.** Long D.G. High resolution wind retrieval from SeaWinds. 2001. IGARSS '01. IEEE 2001 International Geoscience and Remote Sensing Symposium. - Sydney, NSW, 2001. - Vol. 5. - P. 2187-2189. ↑
- C6655.** Donato T.F. Temporal analysis of synthetic aperture radar signatures in a back bay-barrier island system. / Donato T.F., Bachmann C.M., Fusina R.A., Oertel G.F., Carlson C.R. // 2001. IGARSS '01. IEEE 2001 International Geoscience and Remote Sensing Symposium. - Sydney, NSW, 2001. - Vol. 5. - P. 2169-2171. ↑
- C6656.** Clemente-Colon P. Evolution of upwelling-associated biological features in the Middle Atlantic Bight as captured by SAR, SST, and ocean color sensors. 2001. IGARSS '01. IEEE 2001 International Geoscience and Remote Sensing Symposium. - Sydney, NSW, 2001. - Vol. 6. - P. 2616-2618. ↑
- C6657.** Ciccarelli F. Feature extraction in the Hankel transform domain. / Ciccarelli F., Di Bisceglie M., Galdi C. // 2001. IGARSS '01. IEEE 2001 International Geoscience and Remote Sensing Symposium. - Sydney, NSW, 2001. - Vol. 6. - P. 2613-2615. ↑
- C6658.** Coltuc D. Bias correction and speckle reduction in time-space filtering of multi-temporal SAR images. / Coltuc D., Trouve E., Bolon Ph. // 2001. IGARSS '01. IEEE 2001 International Geoscience and Remote Sensing Symposium. - Sydney, NSW, 2001. - Vol. 6. - P. 2625-2627. ↑
- C6659.** Colesanti C. Comparing GPS, optical leveling and permanent scatterers. / Colesanti C., Ferretti A.,

Prati C., Rocca F. // 2001. IGARSS '01. IEEE 2001 International Geoscience and Remote Sensing Symposium. - Sydney, NSW, 2001. - Vol. 6. - P. 2622-2624. ↑

C6660. Chia-Tang Chen. Applications of AIRSAR data acquired during PACRIM-II in Taiwan. / Chia-Tang Chen, Chen K.S., Wang C.T., Liang L.S. // 2001. IGARSS '01. IEEE 2001 International Geoscience and Remote Sensing Symposium. - Sydney, NSW, 2001. - Vol. 6. - P. 2610-2612. ↑

C6661. Bujor F.T. Data fusion approach for change detection in multi-temporal ERS-SAR images. / Bujor F.T., Valet L., Trouwv E., Mauris G., Classeau N., Rudant J.P. // 2001. IGARSS '01. IEEE 2001 International Geoscience and Remote Sensing Symposium. - Sydney, NSW, 2001. - Vol. 6. - P. 2590-2592. ↑

C6662. Brule L. RADARSAT-2 mission update. / Brule L., Baeggli H. // 2001. IGARSS '01. IEEE 2001 International Geoscience and Remote Sensing Symposium. - Sydney, NSW, 2001. - Vol. 6. - P. 2581-2583. ↑

C6663. Chandrasekar V. Development of a virtual radar environment. / Chandrasekar V., Brunkow D., Jayasumana A.P., Bolen S. // 2001. IGARSS '01. IEEE 2001 International Geoscience and Remote Sensing Symposium. - Sydney, NSW, 2001. - Vol. 6. - P. 2599-2601. ↑

C6664. Caves R.G. Applications of RADARSAT-2-polarimetric data. / Caves R.G., Scheuchl B., Staples G. // 2001. IGARSS '01. IEEE 2001 International Geoscience and Remote Sensing Symposium. - Sydney, NSW, 2001. - Vol. 6. - P. 2596-2598. ↑

C6665. Di Bisceglie M. CFAR detection of extended objects in high resolution SAR images. / Di Bisceglie M., Galdi C. // 2001. IGARSS '01. IEEE 2001 International Geoscience and Remote Sensing Symposium. - Sydney, NSW, 2001. - Vol. 6. - P. 2674-2676. ↑

C6666. de Oliveira Andrade N.S. Evaluation of the potential cartographic accuracy of Radarsat and JERS-1 data. / de Oliveira Andrade N.S., Alves D.S. // 2001. IGARSS '01. IEEE 2001 International Geoscience and Remote Sensing Symposium. - Sydney, NSW, 2001. - Vol. 6. - P. 2662-2664. ↑

C6667. Eldhuset K. Ultra high resolution spaceborne SAR processing with EETF4. 2001. IGARSS '01. IEEE 2001 International Geoscience and Remote Sensing Symposium. - Sydney, NSW, 2001. - Vol. 6. - P. 2689-2691. ↑

C6668. Di Bisceglie M. Stochastic modelling of atmospheric effects in SAR differential interferometry. / Di Bisceglie M., Fusco A., Galdi C., Sansosti E. // 2001. IGARSS '01. IEEE 2001 International Geoscience and Remote Sensing Symposium. - Sydney, NSW, 2001. - Vol. 6. - P. 2677-2679. ↑

C6669. Cumming I. Model-based Doppler estimation for frame-based SAR processing. 2001. IGARSS '01. IEEE 2001 International Geoscience and Remote Sensing Symposium. - Sydney, NSW, 2001. - Vol. 6. - P. 2645-2647. ↑

C6670. Costantini M. A space-time analysis technique for monitoring terrain displacements from SAR differential interferometric measurements. / Costantini M., Malvarosa F., Minati F., Pietranera L., Giammarioli V., Jahjah M. // 2001. IGARSS '01. IEEE 2001 International Geoscience and Remote Sensing Symposium. - Sydney, NSW, 2001. - Vol. 6. - P. 2634-2636. ↑

C6671. Conradsen K. Change detection in polarimetric SAR data and the complex Wishart distribution. / Conradsen K., Aasbjerg Nielsen A., Schou J., Skriver H. // 2001. IGARSS '01. IEEE 2001 International Geoscience and Remote Sensing Symposium. - Sydney, NSW, 2001. - Vol. 6. - P. 2628-2630. ↑


C6672. Cruz Pol S.L. Multidimensional cloud images retrieval from dual-frequency millimeter-wave radar. / Cruz Pol S.L., Colon Diaz N., Sekelsky S. // 2001. IGARSS '01. IEEE 2001 International Geoscience and Remote Sensing Symposium. - Sydney, NSW, 2001. - Vol. 6. - P. 2642-2644. ↑


C6673. Costantini M. Analysis and correction of artifacts on differential SAR interferometry for the study of subsidence phenomena. / Costantini M., Lombardo P., Malvarosa F., Minati F., Pastina D., Pietranera L. // 2001. IGARSS '01. IEEE 2001 International Geoscience and Remote Sensing Symposium. - Sydney, NSW, 2001. - Vol. 6. - P. 2637-2639. ↑


C6674. Al-Sowayan S. Convective/stratiform classification from TRMM Precipitation Radar. / Al-Sowayan S., Chandrasekar V. // 2001. IGARSS '01. IEEE 2001 International Geoscience and Remote Sensing Symposium. -





Sydney, NSW, 2001. - Vol. 6. - P. 2507-2509. 


C6675. Allievi J. Automation of the DEM reconstruction from ERS Tandem pairs. / Allievi J., Ferretti A., Prati C., Ratti R., Rocca F. // 2001. IGARSS '01. IEEE 2001 International Geoscience and Remote Sensing Symposium. - Sydney, NSW, 2001. - Vol. 6. - P. 2504-2506. 


C6676. Aquilino E. On the relationship between the Mueller and the scattering matrices. / Aquilino E., Alvarez J.L., Chandra M., Migliaccio M. // 2001. IGARSS '01. IEEE 2001 International Geoscience and Remote Sensing Symposium. - Sydney, NSW, 2001. - Vol. 6. - P. 2516-2518. 


C6677. Amarouche L. A new estimator of the sea state bias using a three frequency radar altimeter. / Amarouche L., Thouvenor E., Chapron B., Zanife O.-Z. // 2001. IGARSS '01. IEEE 2001 International Geoscience and Remote Sensing Symposium. - Sydney, NSW, 2001. - Vol. 6. - P. 2510-2512. 


C6678. Abuzar M. Integrating multi-source remote sensing data for soil mapping in Victoria. / Abuzar M., Ryan S. // 2001. IGARSS '01. IEEE 2001 International Geoscience and Remote Sensing Symposium. - Sydney, NSW, 2001. - Vol. 6. - P. 2495-2497. 


C6679. Classeau N. View of French Guyana by ERS SAR presented on an interactive CD-ROM. / Classeau N., Rudant J.P., Trebossen H. // 2001. IGARSS '01. IEEE 2001 International Geoscience and Remote Sensing Symposium. - Sydney, NSW, 2001. - Vol. 5. - P. 2466-2468. 


C6680. Zribi M. Influence of stone cover over bare soil on backscattering. / Zribi M., Adar E., Garcia J.C., Ciarletti V., Macelloni G., Acquid N. // 2001. IGARSS '01. IEEE 2001 International Geoscience and Remote Sensing Symposium. - Sydney, NSW, 2001. - Vol. 5. - P. 2460-2462. 


C6681. Abeynayake C. A Kalman filter-based approach to detect landmines from metal detector data. / Abeynayake C., Chant I. // 2001. IGARSS '01. IEEE 2001 International Geoscience and Remote Sensing Symposium. - Sydney, NSW, 2001. - Vol. 6. - P. 2492-2494. 


C6682. Gunther H. EuroROSE: a project to support shipping in port approaches. / Gunther H., Gurgel K.W., Breivik O., Guddal J., Wyatt L.R., Nieto Borge J.C. // 2001. IGARSS '01. IEEE 2001 International Geoscience and Remote Sensing Symposium. - Sydney, NSW, 2001. - Vol. 5. - P. 2474-2476. 


C6683. Biccari D. Mars surface models and subsurface detection performance in MARSIS. / Biccari D., Picardi G., Seu R., Melacci P.T. // 2001. IGARSS '01. IEEE 2001 International Geoscience and Remote Sensing Symposium. - Sydney, NSW, 2001. - Vol. 6. - P. 2560-2562. 


C6684. Biccari D. Adaptive compensation of Mars ionosphere dispersion in the MARSIS experiment. / Biccari D., Picardi G., Seu R. // 2001. IGARSS '01. IEEE 2001 International Geoscience and Remote Sensing Symposium. - Sydney, NSW, 2001. - Vol. 6. - P. 2557-2559. 

C6685. Brandfass M. Polarimetric SAR interferometry as applied to fully polarimetric rain forest data. / Brandfass M., Hofmann C., Mura J.C., Papathanassiou K.P. // 2001. IGARSS '01. IEEE 2001 International Geoscience and Remote Sensing Symposium. - Sydney, NSW, 2001. - Vol. 6. - P. 2575-2577. 

C6686. Bradley C.J. A performance analysis of several bistatic calibration techniques. / Bradley C.J., Collins P.J., Terzuoli A.J. Jr., Temple M.A., Wilson K.S., Fortuny J., Lewis G. // 2001. IGARSS '01. IEEE 2001 International Geoscience and Remote Sensing Symposium. - Sydney, NSW, 2001. - Vol. 6. - P. 2572-2574. 

C6687. Berardino P. ERS-1/2 SAR and IFSAR for Antarctica. / Berardino P., Marrazzo M., Migliaccio M., Lanari R. // 2001. IGARSS '01. IEEE 2001 International Geoscience and Remote Sensing Symposium. - Sydney, NSW, 2001. - Vol. 6. - P. 2554-2556. 

C6688. Balan P. An adaptive filter for removal of noise in interferometrically derived digital elevation models. / Balan P., Mather P.M. // 2001. IGARSS '01. IEEE 2001 International Geoscience and Remote Sensing Symposium. - Sydney, NSW, 2001. - Vol. 6. - P. 2529-2531. 

C6689. Arbesser-Rastburg B. Electromagnetic aspects for sub-surface sounding of planets. / Arbesser-Rastburg B., Flouy N. // 2001. IGARSS '01. IEEE 2001 International Geoscience and Remote Sensing Symposium. - Sydney, NSW, 2001. - Vol. 6. - P. 2519-2521. 

C6690. Berardino P. A new approach for analyzing the temporal evolution of Earth surface deformations based

on the combination of DIFSAR interferograms. / Berardino P., Fornaro G., Fusco A., Galluzzo D., Lanari R., Sansosti E., Usai S. // 2001. IGARSS '01. IEEE 2001 International Geoscience and Remote Sensing Symposium. - Sydney, NSW, 2001. - Vol. 6. - P. 2551-2553. ↑

C6691. Bara A. A mosaic technique for the generation of wide-area DEMs with interferometric SAR data. / Bara A., Andreu J., Scheiber R., Horn R., Broquetas A. // 2001. IGARSS '01. IEEE 2001 International Geoscience and Remote Sensing Symposium. - Sydney, NSW, 2001. - Vol. 6. - P. 2532-2534. ↑

C6692. Inggs M.R. Borehole Interferometric SAR: A preliminary study. / Inggs M.R., Mukhopadhyay P.K., Wilkinson A.J. // 2001. IGARSS '01. IEEE 2001 International Geoscience and Remote Sensing Symposium. - Sydney, NSW, 2001. - Vol. 5. - P. 2064-2066. ↑

C6693. Lai K. A super-fast scanning technique study for an on-airport weather radar. / Lai K., Longstaff D., Callaghan G. // 2001. IGARSS '01. IEEE 2001 International Geoscience and Remote Sensing Symposium. - Sydney, NSW, 2001. - Vol. 4. - P. 1714-1715. ↑

C6694. Junho Choi. Localization of target tracking and navigation by correcting atmospheric effects. / Junho Choi, Sung Kwak. // 2001. IGARSS '01. IEEE 2001 International Geoscience and Remote Sensing Symposium. - Sydney, NSW, 2001. - Vol. 4. - P. 1711-1713. ↑

C6695. Buckley J.R. Can geometric optics fully describe radar images of the sea surface at grazing incidence? . 2001. IGARSS '01. IEEE 2001 International Geoscience and Remote Sensing Symposium. - Sydney, NSW, 2001. - Vol. 4. - P. 1732-1734. ↑

C6696. Berizzi F. On the fractal behavior of SAR images of ocean sea surface. / Berizzi F., Dell'Acqua F., Gamba P., Garzelli A., Martorella M. // 2001. IGARSS '01. IEEE 2001 International Geoscience and Remote Sensing Symposium. - Sydney, NSW, 2001. - Vol. 4. - P. 1729-1731. ↑

C6697. Ge Chen. Observing abnormal wind features of the tropical Pacific Ocean during the 1997-98 El Nino. / Ge Chen, Chaoyang Fang, Lixin Fang. // 2001. IGARSS '01. IEEE 2001 International Geoscience and Remote Sensing Symposium. - Sydney, NSW, 2001. - Vol. 4. - P. 1699-1701. ↑

C6698. Cloude S.R. The Glen Affric project: forest mapping using polarimetric radar interferometry. / Cloude S.R., Papathanassiou K.P., Woodhouse I., Hope J., Suarez Minguez J.C., Osborne P., Wright G. // 2001. IGARSS '01. IEEE 2001 International Geoscience and Remote Sensing Symposium. - Sydney, NSW, 2001. - Vol. 4. - P. 1642-1644. ↑

C6699. Fiset R. A low-cost polarimetric response tool using spreadsheets. / Fiset R., Farhat M. // 2001. IGARSS '01. IEEE 2001 International Geoscience and Remote Sensing Symposium. - Sydney, NSW, 2001. - Vol. 4. - P. 1625-1627. ↑

C6700. Moghaddam M. Estimation of comprehensive forest variable sets from multiparameter SAR data over a large area with diverse species. 2001. IGARSS '01. IEEE 2001 International Geoscience and Remote Sensing Symposium. - Sydney, NSW, 2001. - Vol. 4. - P. 1660-1662. ↑

C6701. Gustavsson A. A pilot experiment for stem volume retrieval based on VHF SAR data. / Gustavsson A., Walter F., Ulander L.M.H., Fransson J.E.S., Frolind P.-O., Jonsson T., Larsson B., Smith G., Stenstrom G. // 2001. IGARSS '01. IEEE 2001 International Geoscience and Remote Sensing Symposium. - Sydney, NSW, 2001. - Vol. 4. - P. 1651-1653. ↑

C6702. Niedermeier A. Monitoring big river estuaries using SAR images. / Niedermeier A., Lehner S., van der Sanden J. // 2001. IGARSS '01. IEEE 2001 International Geoscience and Remote Sensing Symposium. - Sydney, NSW, 2001. - Vol. 4. - P. 1756-1758. ↑

C6703. Jeong Woo Kim. Wavenumber correlation analysis of Topex/Poseidon and tide-gauge sea surface heights in the East Sea (Japan Sea). / Jeong Woo Kim, Joon Woo Lee, Kyung Duk Min, Joong-Sun Won, Jong-Sun Hwang, Sung-Chul Kang. // 2001. IGARSS '01. IEEE 2001 International Geoscience and Remote Sensing Symposium. - Sydney, NSW, 2001. - Vol. 4. - P. 1750-1752. ↑

C6704. Franceschetti G. Simulation of SAR raw signal relevant to oil slicks in ocean scenes. / Franceschetti G., Iodice A., Riccio D., Ruello G. // 2001. IGARSS '01. IEEE 2001 International Geoscience and Remote Sensing Symposium. - Sydney, NSW, 2001. - Vol. 4. - P. 1764-1766. ↑

- C6705.** Monaldo F.M. Comparison of RADARSAT SAR-derived wind speeds with buoy and QuikSCAT measurements. / Monaldo F.M., Thompson D.R., Pichel W.G., Clemente-Colon P. // 2001. IGARSS '01. IEEE 2001 International Geoscience and Remote Sensing Symposium. - Sydney, NSW, 2001. - Vol. 4. - P. 1759-1760. ↑
- C6706.** Horstmann J. Coastal high resolution wind fields retrieved from RADARSAT-1 ScanSAR. / Horstmann J., Koch W., Lehner S., Tonboe R. // 2001. IGARSS '01. IEEE 2001 International Geoscience and Remote Sensing Symposium. - Sydney, NSW, 2001. - Vol. 4. - P. 1747-1749. ↑
- C6707.** Ming-Xia He. The relationship between time series sea surface slope and El Nino event from satellite altimetry: a potential indicator. / Ming-Xia He, Rui Chen, Lei Guan, Mingqiang Fang. // 2001. IGARSS '01. IEEE 2001 International Geoscience and Remote Sensing Symposium. - Sydney, NSW, 2001. - Vol. 4. - P. 1738-1740. ↑
- C6708.** Ge Chen. Structures of marine wind variability at four selected sites derived from TOPEX altimeter data. / Ge Chen, Chaoyang Fang, Lixin Fang. // 2001. IGARSS '01. IEEE 2001 International Geoscience and Remote Sensing Symposium. - Sydney, NSW, 2001. - Vol. 4. - P. 1735-1737. ↑
- C6709.** Ermakov S.A. Wave tank modelling of strong modulation of radar backscatter due to long waves. / Ermakov S.A., Sergievskaya I.A., Shchegolkov Yu.B., Scott J.C., Stapleton N.R. // 2001. IGARSS '01. IEEE 2001 International Geoscience and Remote Sensing Symposium. - Sydney, NSW, 2001. - Vol. 4. - P. 1744-1746. ↑
- C6710.** Qing Dong. The scattering polarimetric response contrast between two wind-generated rough sea surfaces. / Qing Dong, Huadong Guo, Changlin Wang. // 2001. IGARSS '01. IEEE 2001 International Geoscience and Remote Sensing Symposium. - Sydney, NSW, 2001. - Vol. 4. - P. 1741-1743. ↑
- C6711.** Sato T. Precise orbit determination of meteors using a radar and an optical sensor. / Sato T., Nishimura K., Nakamura T. // 2001. IGARSS '01. IEEE 2001 International Geoscience and Remote Sensing Symposium. - Sydney, NSW, 2001. - Vol. 4. - P. 1575-1577. ↑
- C6712.** Dall J. Multiplier-free filters for wideband SAR. / Dall J., Christensen E.L. // 2001. IGARSS '01. IEEE 2001 International Geoscience and Remote Sensing Symposium. - Sydney, NSW, 2001. - Vol. 4. - P. 1568-1570. ↑
- C6713.** Yoho P. Improved timing calibration of QuikSCAT. / Yoho P., Long D.G. // 2001. IGARSS '01. IEEE 2001 International Geoscience and Remote Sensing Symposium. - Sydney, NSW, 2001. - Vol. 4. - P. 1591-1593. ↑
- C6714.** Magruder L.A. Pointing angle and timing calibration/validation of the Geoscience Laser Altimeter with a ground-based detection system. / Magruder L.A., Schutz B.E., Silverberg E.C. // 2001. IGARSS '01. IEEE 2001 International Geoscience and Remote Sensing Symposium. - Sydney, NSW, 2001. - Vol. 4. - P. 1584-1587. ↑
- C6715.** Perona G. Observations from space of meteorological fields on the scale of numerical weather forecasting models. / Perona G., Notarpietro R., Gabella M., Speranza A. // 2001. IGARSS '01. IEEE 2001 International Geoscience and Remote Sensing Symposium. - Sydney, NSW, 2001. - Vol. 4. - P. 1565-1567. ↑
- C6716.** Horstmann J. Global wind speed retrieval from complex SAR data using scatterometer models and neural networks. / Horstmann J., Lehner S., Schiller H. // 2001. IGARSS '01. IEEE 2001 International Geoscience and Remote Sensing Symposium. - Sydney, NSW, 2001. - Vol. 3. - P. 1553-1555. ↑
- C6717.** Onana V.P. Coastline detection in SAR images using texture analysis in textural or geometrical multi-resolution. / Onana V.P., Mvogo Ngono J., Trebossen H., Rudant J.P., Tonye E. // 2001. IGARSS '01. IEEE 2001 International Geoscience and Remote Sensing Symposium. - Sydney, NSW, 2001. - Vol. 3. - P. 1549-1551. ↑
- C6718.** Pospelov N.N. Polarimetric measurements of microwave emission from capillary waves. / Pospelov N.N., Kuzmin A.V., Trokhimovski Y.G. // 2001. IGARSS '01. IEEE 2001 International Geoscience and Remote Sensing Symposium. - Sydney, NSW, 2001. - Vol. 3. - P. 1561-1563. ↑
- C6719.** Yueh S.H. Polarimetric radar remote sensing of ocean surface wind. / Yueh S.H., Wilson W.J., Dinardo S. // 2001. IGARSS '01. IEEE 2001 International Geoscience and Remote Sensing Symposium. - Sydney, NSW, 2001. - Vol. 3. - P. 1557-1559. ↑

- C6720.** Goodman N.A. The information content of multiple receive aperture SAR systems. / Goodman N.A., Stiles J.M. // 2001. IGARSS '01. IEEE 2001 International Geoscience and Remote Sensing Symposium. - Sydney, NSW, 2001. - Vol. 4. - P. 1614-1616. ↑
- C6721.** Marques P.A.C. Velocity estimation of fast moving targets using undersampled SAR raw-data. / Marques P.A.C., Dias J.M.B. // 2001. IGARSS '01. IEEE 2001 International Geoscience and Remote Sensing Symposium. - Sydney, NSW, 2001. - Vol. 4. - P. 1610-1613. ↑
- C6722.** Poh Lian Choong. Statistical properties of L-band sea clutter measured with a polarimetric synthetic aperture radar. 2001. IGARSS '01. IEEE 2001 International Geoscience and Remote Sensing Symposium. - Sydney, NSW, 2001. - Vol. 4. - P. 1622-1624. ↑
- C6723.** Wang Yiding. Application of inverse chirp-z transform in wideband radar. / Wang Yiding, Wu Yirong, Hong Jun. // 2001. IGARSS '01. IEEE 2001 International Geoscience and Remote Sensing Symposium. - Sydney, NSW, 2001. - Vol. 4. - P. 1617-1619. ↑
- C6724.** Iwamoto M. A novel algorithm for reconstructing three-dimensional target shapes using sequential radar images. / Iwamoto M., Kirimoto T. // 2001. IGARSS '01. IEEE 2001 International Geoscience and Remote Sensing Symposium. - Sydney, NSW, 2001. - Vol. 4. - P. 1607-1609. ↑
- C6725.** Boerner E. SARIS: synthetic aperture radar instrument simulator. / Boerner E., Uhlmann F.H., Grafmueller B., Zahn R., Braumann H. // 2001. IGARSS '01. IEEE 2001 International Geoscience and Remote Sensing Symposium. - Sydney, NSW, 2001. - Vol. 4. - P. 1598-1600. ↑
- C6726.** Axelsson S.R.J. On the performance of curved SAR-mapping. 2001. IGARSS '01. IEEE 2001 International Geoscience and Remote Sensing Symposium. - Sydney, NSW, 2001. - Vol. 4. - P. 1594-1597. ↑
- C6727.** Hobbs B.G. Estimating X-band synthetic aperture radar detection of objects obscured by foliage using the DSTO Ingara airborne imaging radar. / Hobbs B.G., Stacy N.J.S. // 2001. IGARSS '01. IEEE 2001 International Geoscience and Remote Sensing Symposium. - Sydney, NSW, 2001. - Vol. 4. - P. 1604-1606. ↑
- C6728.** Callow H.J. Autofocus of multi-band, shallow-water synthetic aperture sonar imagery using shear-averaging. / Callow H.J., Hayes M.P., Gough P.T. // 2001. IGARSS '01. IEEE 2001 International Geoscience and Remote Sensing Symposium. - Sydney, NSW, 2001. - Vol. 4. - P. 1601-1603. ↑
- C6729.** Sobjaerg S.S. 2 GHz self-aligning tandem A/D converter for SAR. / Sobjaerg S.S., Christensen E.L. // 2001. IGARSS '01. IEEE 2001 International Geoscience and Remote Sensing Symposium. - Sydney, NSW, 2001. - Vol. 5. - P. 2028-2030. ↑
- C6730.** Phalippou L. Overview of the performances and tracking design of the SIRAL altimeter for the CryoSat mission. / Phalippou L., Rey L., de Chateau-Thierry P. // 2001. IGARSS '01. IEEE 2001 International Geoscience and Remote Sensing Symposium. - Sydney, NSW, 2001. - Vol. 5. - P. 2025-2027. ↑
- C6731.** Adam N. SRTM X-SAR motion compensation: concept and first assessment of the interferometric observation geometry. / Adam N., Eineder M., Breit H. // 2001. IGARSS '01. IEEE 2001 International Geoscience and Remote Sensing Symposium. - Sydney, NSW, 2001. - Vol. 5. - P. 2034-2036. ↑
- C6732.** Zahn R. SAR instrument using stable active front-end technologies. / Zahn R., Braumann H., Braubach H. // 2001. IGARSS '01. IEEE 2001 International Geoscience and Remote Sensing Symposium. - Sydney, NSW, 2001. - Vol. 5. - P. 2031-2033. ↑
- C6733.** Angelis C.F. ERS-1 multitemporal backscatter analysis of different types of land cover in Brazilian Amazonia. / Angelis C.F., Freitas C.C., Dutra L.V., Valeriano D.M. // 2001. IGARSS '01. IEEE 2001 International Geoscience and Remote Sensing Symposium. - Sydney, NSW, 2001. - Vol. 5. - P. 2019-2021. ↑
- C6734.** Axelsson S.R.J. Suppressed ambiguity in range by phase-coded waveforms. 2001. IGARSS '01. IEEE 2001 International Geoscience and Remote Sensing Symposium. - Sydney, NSW, 2001. - Vol. 5. - P. 2006-2009. ↑
- C6735.** Axelsson S.R.J. Noise radar for range/Doppler processing and digital beamforming using binary ADC. 2001. IGARSS '01. IEEE 2001 International Geoscience and Remote Sensing Symposium. - Sydney, NSW, 2001. - Vol. 5. - P. 2001-2005. ↑

- C6736.** Castells A. A high-resolution Imaging Wind and Rain Airborne Profiler for tropical cyclones. / Castells A., Carswell J.R., Chang P.S. // 2001. IGARSS '01. IEEE 2001 International Geoscience and Remote Sensing Symposium. - Sydney, NSW, 2001. - Vol. 5. - P. 2013-2015. ↑
- C6737.** Millikin R.L. Use of an adapted marine radar for the short-range detection and tracking of small birds in flight. / Millikin R.L., Buckley J.R. // 2001. IGARSS '01. IEEE 2001 International Geoscience and Remote Sensing Symposium. - Sydney, NSW, 2001. - Vol. 5. - P. 2010-2012. ↑
- C6738.** Doyle G.S. Major conclusions relating to the Katse Dam differential InSAR study. / Doyle G.S., Wilkinson A.J., Inggis M.R. // 2001. IGARSS '01. IEEE 2001 International Geoscience and Remote Sensing Symposium. - Sydney, NSW, 2001. - Vol. 5. - P. 2055-2057. ↑
- C6739.** Shimada M. Correction of atmospheric excess path delay appeared in repeat-pass SAR interferometry using objective analysis data. / Shimada M., Minamisawa M., Isoguchi O. // 2001. IGARSS '01. IEEE 2001 International Geoscience and Remote Sensing Symposium. - Sydney, NSW, 2001. - Vol. 5. - P. 2052-2054. ↑
- C6740.** Yue Huanyin. A SAR interferogram filter based on the empirical mode decomposition method. / Yue Huanyin, Guo Huadong, Han Chunming, Li Xinwu, Wang Changlin. // 2001. IGARSS '01. IEEE 2001 International Geoscience and Remote Sensing Symposium. - Sydney, NSW, 2001. - Vol. 5. - P. 2061-2063. ↑
- C6741.** Ashok A. Topographic mapping with multiple antenna SAR interferometry: a Bayesian model-based approach. / Ashok A., Wilkinson A.J. // 2001. IGARSS '01. IEEE 2001 International Geoscience and Remote Sensing Symposium. - Sydney, NSW, 2001. - Vol. 5. - P. 2058-2060. ↑
- C6742.** Kimura H. Effect of tropospheric range delay corrections on differential SAR interferograms. / Kimura H., Kinoshita H. // 2001. IGARSS '01. IEEE 2001 International Geoscience and Remote Sensing Symposium. - Sydney, NSW, 2001. - Vol. 5. - P. 2049-2051. ↑
- C6743.** Eineder N. Interferometric DEMs in rugged terrain. 2001. IGARSS '01. IEEE 2001 International Geoscience and Remote Sensing Symposium. - Sydney, NSW, 2001. - Vol. 5. - P. 2040-2042. ↑
- C6744.** Doyle G.S. Satellite radar interferometry reveals mining induced seismic deformation in South Africa. / Doyle G.S., Stow R.J., Inggis M.R. // 2001. IGARSS '01. IEEE 2001 International Geoscience and Remote Sensing Symposium. - Sydney, NSW, 2001. - Vol. 5. - P. 2037-2039. ↑
- C6745.** Lou Y. Progress report on the NASA/JPL airborne synthetic aperture radar system. / Lou Y., Imel D.A., Chu A., Miller T.W., Moller D., Skotnicki W. // 2001. IGARSS '01. IEEE 2001 International Geoscience and Remote Sensing Symposium. - Sydney, NSW, 2001. - Vol. 5. - P. 2046-2048. ↑
- C6746.** Hubig M. MCF-homomorphisms of cost functions for minimum cost flow InSAR phase unwrapping. / Hubig M., Adam N., Suchandt S. // 2001. IGARSS '01. IEEE 2001 International Geoscience and Remote Sensing Symposium. - Sydney, NSW, 2001. - Vol. 5. - P. 2043-2045. ↑
- C6747.** Friedman K.S. Validation of a CFAR vessel detection algorithm using known vessel locations. / Friedman K.S., Wackerman C., Funk F., Pichel W.G., Clemente-Colon P., Xiaofeng Li. // 2001. IGARSS '01. IEEE 2001 International Geoscience and Remote Sensing Symposium. - Sydney, NSW, 2001. - Vol. 4. - P. 1804-1806. ↑
- C6748.** Shusun Li. Derivation of spatial distribution of snow precipitation using interferometric SAR technique. / Shusun Li, Sturm M. // 2001. IGARSS '01. IEEE 2001 International Geoscience and Remote Sensing Symposium. - Sydney, NSW, 2001. - Vol. 4. - P. 1795-1797. ↑
- C6749.** Maki M. Volcanic ash size distribution determined by weather radar. / Maki M., Doviak R.J. // 2001. IGARSS '01. IEEE 2001 International Geoscience and Remote Sensing Symposium. - Sydney, NSW, 2001. - Vol. 4. - P. 1810-1811. ↑
- C6750.** Iehara M. Detection of ships using cross-correlation of split-look SAR images. / Iehara M., Ouchi K., Takami I., Morimura K., Kumano S. // 2001. IGARSS '01. IEEE 2001 International Geoscience and Remote Sensing Symposium. - Sydney, NSW, 2001. - Vol. 4. - P. 1807-1809. ↑
- C6751.** Jeong Woo Kim. Satellite altimetry-implied sea ice distribution in the Weddell Sea, Antarctica. / Jeong Woo Kim, Sungmin Hong, Dong-Cheon Lee, Chang-Ki Hong. // 2001. IGARSS '01. IEEE 2001 International

Geoscience and Remote Sensing Symposium. - Sydney, NSW, 2001. - Vol. 4. - P. 1792-1794. ↑

C6752. Zaugg D.A. Snow and ice characterization studies using a radar altimeter. / Zaugg D.A., Jensen M.A. // 2001. IGARSS '01. IEEE 2001 International Geoscience and Remote Sensing Symposium. - Sydney, NSW, 2001. - Vol. 4. - P. 1773-1775. ↑

C6753. Lehner S. Global distribution of sea surface features from SAR wave mode data. / Lehner S., Schulz-Stellenfleth J., Niedermeier A., Horstmann J. // 2001. IGARSS '01. IEEE 2001 International Geoscience and Remote Sensing Symposium. - Sydney, NSW, 2001. - Vol. 4. - P. 1767-1769. ↑

C6754. Ashcraft I.S. Azimuth variation in microwave backscatter over the Greenland Ice Sheet. / Ashcraft I.S., Long D.G. // 2001. IGARSS '01. IEEE 2001 International Geoscience and Remote Sensing Symposium. - Sydney, NSW, 2001. - Vol. 4. - P. 1779-1781. ↑

C6755. Zecchetto S. On shape, orientation and structure of atmospheric cells inside wind rolls in SAR images. / Zecchetto S., De Biasio F. // 2001. IGARSS '01. IEEE 2001 International Geoscience and Remote Sensing Symposium. - Sydney, NSW, 2001. - Vol. 4. - P. 1776-1778. ↑

C6756. Fujii K. Reconstruction of 3D urban model using range image and aerial image. / Fujii K., Arikawa T. // 2001. IGARSS '01. IEEE 2001 International Geoscience and Remote Sensing Symposium. - Sydney, NSW, 2001. - Vol. 4. - P. 1928-1932. ↑

C6757. Benz U. OSCAR-object oriented segmentation and classification of advanced radar allow automated information extraction. / Benz U., Baatz M., Schreier G. // 2001. IGARSS '01. IEEE 2001 International Geoscience and Remote Sensing Symposium. - Sydney, NSW, 2001. - Vol. 4. - P. 1913-1915. ↑

C6758. Kise W. Case-based lightning flash forecast support system taking account of range of thundercloud. / Kise W., Mitsuishi A., Kosuge Y. // SICE 2001. Proceedings of the 40th SICE Annual Conference. International Session Papers. - Nagoya, 2001. - P. 84-89. ↑

C6759. Shiina T. Measurement of Z-R relations using a small Doppler radar and image data of snow particles. / Shiina T., Muramoto K. // 2001. IGARSS '01. IEEE 2001 International Geoscience and Remote Sensing Symposium. - Sydney, NSW, 2001. - Vol. 4. - P. 1993-1995. ↑

C6760. Freitas C.C. The use of airborne P-band radar data for land use and land cover mapping in Brazilian Amazonia. / Freitas C.C., Sant'Anna S.J.S., Soler L.S., Santos J.R., Dutra L.V., de Araujo L.S., Mura J.C., Hernandez Filho P. // 2001. IGARSS '01. IEEE 2001 International Geoscience and Remote Sensing Symposium. - Sydney, NSW, 2001. - Vol. 4. - P. 1889-1891. ↑

C6761. Inggs M.R. Parallel SAR processor using PVM on a Beowulf cluster. / Inggs M.R., Bennett T.G. // 2001. IGARSS '01. IEEE 2001 International Geoscience and Remote Sensing Symposium. - Sydney, NSW, 2001. - Vol. 4. - P. 1850-1852. ↑

C6762. Ouchi K. Non-uniform azimuth image shift caused by the pitching motion of ships observed in Radarsat images. / Ouchi K., Iehara M., Takami I., Morimura K., Kumano S. // 2001. IGARSS '01. IEEE 2001 International Geoscience and Remote Sensing Symposium. - Sydney, NSW, 2001. - Vol. 4. - P. 1815-1817. ↑

C6763. Yue B. Sea ice segmentation using Markov random fields. / Yue B., Clausi D.A. // 2001. IGARSS '01. IEEE 2001 International Geoscience and Remote Sensing Symposium. - Sydney, NSW, 2001. - Vol. 4. - P. 1877-1879. ↑

C6764. Bachmann C.M. Effects of time series imagery on automated classification of coastal wetland environments using projection pursuit methods. / Bachmann C.M., Fusina R.A., Donato T.F. // 2001. IGARSS '01. IEEE 2001 International Geoscience and Remote Sensing Symposium. - Sydney, NSW, 2001. - Vol. 4. - P. 1868-1870. ↑

C6765. Ewe H.T. A comparison study of the surface scattering models and numerical model. / Ewe H.T., Johnson J.T., Chen K.S. // 2001. IGARSS '01. IEEE 2001 International Geoscience and Remote Sensing Symposium. - Sydney, NSW, 2001. - Vol. 6. - P. 2692-2694. ↑

C6766. Zanife O.Z. Performances of the POSEIDON-1 radar altimeter. / Zanife O.Z., Thibaut P., Vincent P., Bonhoutre B., Thouvenot E., Dorandeu J., Le Traon P.Y., Picot N., Escudier P., Cugny B., Ralzonville P., Dorrer

M. // 2001. IGARSS '01. IEEE 2001 International Geoscience and Remote Sensing Symposium. - Sydney, NSW, 2001. - Vol. 7. - P. 3309-3313. ↑

C6767. Yang Jingsong. Simulation study on optimal conditions for internal wave observation by SAR. / Yang Jingsong, Huang Weigen, Zhou Changbao, Xiao Qingmei. // 2001. IGARSS '01. IEEE 2001 International Geoscience and Remote Sensing Symposium. - Sydney, NSW, 2001. - Vol. 7. - P. 3288-3290. ↑

C6768. Zang Jingfa. Application of recent satellite remote sensing technology in earthquake disaster reduction. / Zang Jingfa, Xie Li-li. // 2001. IGARSS '01. IEEE 2001 International Geoscience and Remote Sensing Symposium. - Sydney, NSW, 2001. - Vol. 7. - P. 3319-3321. ↑

C6769. Zhang Hong. The seismic fault parameters retrieval of Zhangbei earthquake. / Zhang Hong, Wang Chao, Liu Zhi, Tang Yixian. // 2001. IGARSS '01. IEEE 2001 International Geoscience and Remote Sensing Symposium. - Sydney, NSW, 2001. - Vol. 7. - P. 3315-3317. ↑

C6770. Yang Jingsong. Depth and amplitude estimation of internal waves from SAR imagery. / Yang Jingsong, Huang Weigen, Zhou Changbao, Hsu Mingkuang, Xiao Qingmei. // 2001. IGARSS '01. IEEE 2001 International Geoscience and Remote Sensing Symposium. - Sydney, NSW, 2001. - Vol. 7. - P. 3285-3287. ↑

C6771. Ji Wu. Study on soil moisture with ground-based scatterometer and IEM model. / Ji Wu, Liwei Wang, Wei Zhang, Fung A.K., Bo Sun, Suyun Zhu. // 2001. IGARSS '01. IEEE 2001 International Geoscience and Remote Sensing Symposium. - Sydney, NSW, 2001. - Vol. 7. - P. 3271-3273. ↑

C6772. Wiesmann A. Potential and methodology of satellite based SAR for hazard mapping. / Wiesmann A., Wegmuller U., Honikel M., Strozzi T., Werner C.L. // 2001. IGARSS '01. IEEE 2001 International Geoscience and Remote Sensing Symposium. - Sydney, NSW, 2001. - Vol. 7. - P. 3262-3264. ↑

C6773. Yamada Y. Detection of flood-inundated area and relation between the area and micro-geomorphology using SAR and GIS. 2001. IGARSS '01. IEEE 2001 International Geoscience and Remote Sensing Symposium. - Sydney, NSW, 2001. - Vol. 7. - P. 3282-3284. ↑

C6774. Gang Xu. Radar rainfall estimation from vertical reflectivity profile using neural network. / Gang Xu, Chandrasekar V. // 2001. IGARSS '01. IEEE 2001 International Geoscience and Remote Sensing Symposium. - Sydney, NSW, 2001. - Vol. 7. - P. 3280-3281. ↑

C6775. Yang Cunjian. Extracting the flood extent from satellite SAR image with the support of topographic data. / Yang Cunjian, Wei yiming, Wang Siyuan, Zhang Zengxiang, Huang Shifeng. // 2001. Proceedings. ICII 2001-Beijing. 2001 International Conferences on Info-tech and Info-net. - Beijing, 2001. - Vol. 1. - P. 87-92. ↑

C6776. Nie Hong-feng. The application of SLAR image in surveying fossil river course. / Nie Hong-feng, Diao Shu-juan. // 2001. Proceedings. ICII 2001-Beijing. 2001 International Conferences on Info-tech and Info-net. - Beijing, 2001. - Vol. 1. - P. 76-80. ↑

C6777. Jie Yang. Extraction of DEM from single SAR based on radargrammetry. / Jie Yang, Mingsheng Liao, DaoSheng Du. // 2001. Proceedings. ICII 2001-Beijing. 2001 International Conferences on Info-tech and Info-net. - Beijing, 2001. - Vol. 1. - P. 212-217. ↑

C6778. Hongwei Zheng. SAR ocean wave imaging spectra simulation. / Hongwei Zheng, I-Fan Shen. // 2001. Proceedings. ICII 2001-Beijing. 2001 International Conferences on Info-tech and Info-net. - Beijing, 2001. - Vol. 1. - P. 206-211. ↑

C6779. Xiaoge Zhu. Data fusion of multi-sensor for petroleum geological exploration. / Xiaoge Zhu, Lipu Yin. // 2001. Proceedings. ICII 2001-Beijing. 2001 International Conferences on Info-tech and Info-net. - Beijing, 2001. - Vol. 1. - P. 70-75. ↑

C6780. Zuffada C. The collection of GPS signal scattered off a wind-driven ocean with a down-looking GPS receiver: polarization properties versus wind speed and direction. / Zuffada C., Fung A., Okolicanyi M., Huang E., Parker J. // 2001. IGARSS '01. IEEE 2001 International Geoscience and Remote Sensing Symposium. - Sydney, NSW, 2001. - Vol. 7. - P. 3335-3337. ↑

C6781. Zuffada C. Coherence time and statistical properties of the GPS signal scattered off the ocean surface and their impact on the accuracy of remote sensing of sea surface topography and winds. / Zuffada C.,

Zavorotny V. // 2001. IGARSS '01. IEEE 2001 International Geoscience and Remote Sensing Symposium. - Sydney, NSW, 2001. - Vol. 7. - P. 3332-3334. ↑

C6782. Huang Xianfang. Remote sensing technique and prognosis of sandstone type uranium deposit. / Huang Xianfang, Huang Shutao, Fang Maolong, He Jianguo, Xuan Yanxiu. // 2001. Proceedings. ICII 2001-Beijing. 2001 International Conferences on Info-tech and Info-net. - Beijing, 2001. - Vol. 1. - P. 64-69. ↑

C6783. Feng Wenhao. The scanning mathematic models of a sensor with three freedoms of rotation. / Feng Wenhao, Fan Qibin, Li Xin. // 2001. Proceedings. ICII 2001-Beijing. 2001 International Conferences on Info-tech and Info-net. - Beijing, 2001. - Vol. 1. - P. 18-24. ↑

C6784. Suess H. Investigations on anti-personnel mine detection using microwave radiometers. / Suess H., Peichl M., Zeiler M., Dill S. // 2001. IGARSS '01. IEEE 2001 International Geoscience and Remote Sensing Symposium. - Sydney, NSW, 2001. - Vol. 7. - P. 3178-3181. ↑

C6785. Stebler O. Multi-baseline airborne Pol-InSAR measurements for the estimation of scattering processes within vegetation media. / Stebler O., Meier E., Nuesch D. // 2001. IGARSS '01. IEEE 2001 International Geoscience and Remote Sensing Symposium. - Sydney, NSW, 2001. - Vol. 7. - P. 3172-3174. ↑

C6786. Thibaut P. The Poseidon-2 altimeter simulator of performances. / Thibaut P., Steunou N., Zanife O.Z., Carayon G., Thouvenot E. // 2001. IGARSS '01. IEEE 2001 International Geoscience and Remote Sensing Symposium. - Sydney, NSW, 2001. - Vol. 7. - P. 3212-3214. ↑

C6787. Tabb M. Robust inversion of vegetation structure parameters from low-frequency, polarimetric interferometric SAR. / Tabb M., Carande R. // 2001. IGARSS '01. IEEE 2001 International Geoscience and Remote Sensing Symposium. - Sydney, NSW, 2001. - Vol. 7. - P. 3188-3190. ↑

C6788. Sproule D. Barrier Reef Airborne Gravity Survey (BRAGS'99). / Sproule D., Kearsley A.H.W., Olesen A., Forsberg R. // 2001. IGARSS '01. IEEE 2001 International Geoscience and Remote Sensing Symposium. - Sydney, NSW, 2001. - Vol. 7. - P. 3166-3168. ↑

C6789. Small D. Efficient geolocation and image simulation for extended SAR strip maps. / Small D., Meier E., Nuesch D. // 2001. IGARSS '01. IEEE 2001 International Geoscience and Remote Sensing Symposium. - Sydney, NSW, 2001. - Vol. 7. - P. 3152-3154. ↑

C6790. Skriver H. Polarimetric edge detector based on the complex Wishart distribution. / Skriver H., Schou J., Nielsen A.A., Conradsen K. // 2001. IGARSS '01. IEEE 2001 International Geoscience and Remote Sensing Symposium. - Sydney, NSW, 2001. - Vol. 7. - P. 3149-3151. ↑

C6791. Soussi B. Validation of the ENVISAT RA2/MWR Level 2 ocean reference processor using real TOPEX data. / Soussi B., Zanifei O.Z., Dumont J.P., Benveniste J., Levrier G. // 2001. IGARSS '01. IEEE 2001 International Geoscience and Remote Sensing Symposium. - Sydney, NSW, 2001. - Vol. 7. - P. 3161-3165. ↑

C6792. Smith G. CARABAS measurements of coniferous forest stem volume on sloping terrain. / Smith G., Ulander L.M.H., Fransson J.E.S., Walter F. // 2001. IGARSS '01. IEEE 2001 International Geoscience and Remote Sensing Symposium. - Sydney, NSW, 2001. - Vol. 7. - P. 3155-3157. ↑

C6793. Weissman D.E. Polarimetric radiometer sensing of sea surface winds using SHOWEX data to determine the Stokes harmonic coefficients. / Weissman D.E., Plant W.J., Keller W.C., Irisov V.G. // 2001. IGARSS '01. IEEE 2001 International Geoscience and Remote Sensing Symposium. - Sydney, NSW, 2001. - Vol. 7. - P. 3252-3254. ↑

C6794. Wang Chao. ERS differential SAR interferometry for urban subsidence monitoring of Suzhou, Eastern China. / Wang Chao, Zhang Hong, Liu Zhi, Cheng Suozhong, Lu Guonian. // 2001. IGARSS '01. IEEE 2001 International Geoscience and Remote Sensing Symposium. - Sydney, NSW, 2001. - Vol. 7. - P. 3249-3251. ↑

C6795. Wiesbeck W. SDRS: software-defined radar sensors. 2001. IGARSS '01. IEEE 2001 International Geoscience and Remote Sensing Symposium. - Sydney, NSW, 2001. - Vol. 7. - P. 3259-3261. ↑

C6796. Werner C. Complimentary measurement of geophysical deformation using repeat-pass SAR. / Werner C., Strozzi T., Wiesmann A., Wegmuller U., Murray T., Pritchard H., Luckman A. // 2001. IGARSS '01. IEEE 2001 International Geoscience and Remote Sensing Symposium. - Sydney, NSW, 2001. - Vol. 7. - P. 3255-3258. ↑



- C6797.** Vesecky J.F. Air-sea interaction observed by HF radar on Monterey Bay. / Vesecky J.F., Fernandez Y., Davidson K., Paduan J., Teague C.C., Drake J., Plume M. // 2001. IGARSS '01. IEEE 2001 International Geoscience and Remote Sensing Symposium. - Sydney, NSW, 2001. - Vol. 7. - P. 3243-3245.
- C6798.** Titin-Schnaider C. Statistical and phenomenological recognition in polarimetric SAR imaging. 2001. IGARSS '01. IEEE 2001 International Geoscience and Remote Sensing Symposium. - Sydney, NSW, 2001. - Vol. 7. - P. 3221-3223.
- C6799.** Thiel C. Interpretation and analysis of polarimetric L-band E-SAR-data for the derivation of hydrologic land surface parameters. / Thiel C., Gruenler S., Herold M., Hochschild V., Jaeger G., Hellmann M. // 2001. IGARSS '01. IEEE 2001 International Geoscience and Remote Sensing Symposium. - Sydney, NSW, 2001. - Vol. 7. - P. 3215-3217.
- C6800.** Verlinde P. Preparing the Joint Multi-sensor Mine-signatures project database for data fusion. / Verlinde P., Acheroy M., Nesti G., Sieber A. // 2001. IGARSS '01. IEEE 2001 International Geoscience and Remote Sensing Symposium. - Sydney, NSW, 2001. - Vol. 7. - P. 3240-3242.
- C6801.** Trebossen H. Operational coastal map re-actualization by RADAR SAR images, examples in French Guiana, Mauritania and Cameroon. / Trebossen H., Rudant J.P., Classeau N., Fruneau B., Courel M.F., Trouve E., Deffontaines B., Mvogo J., Onana V. // 2001. IGARSS '01. IEEE 2001 International Geoscience and Remote Sensing Symposium. - Sydney, NSW, 2001. - Vol. 7. - P. 3224-3226.
- C6802.** Tupin F. Markov random fields for digital terrain model extraction. / Tupin F., Roux M. // IEEE/ISPRS Joint Workshop 2001 Remote Sensing and Data Fusion over Urban Areas. - Rome, 2001. - P. 95-99.
- C6803.** Nardinocchi C. Building extraction from LIDAR data. / Nardinocchi C., Scaioni M., Forlani G. // IEEE/ISPRS Joint Workshop 2001 Remote Sensing and Data Fusion over Urban Areas. - Rome, 2001. - P. 79-84.
- C6804.** Lombardo P. Classification of polarimetric SAR images of suburban areas using joint annealed segmentation and "H/A/ α " decomposition. / Lombardo P., Pellizzeri T.M., Tomasuolo A. // IEEE/ISPRS Joint Workshop 2001 Remote Sensing and Data Fusion over Urban Areas. - Rome, 2001. - P. 117-121.
- C6805.** Boehmsdorff S. Detection of urban areas in multispectral data. / Boehmsdorff S., Bers K., Brehm T., Essen H., Jager K. // IEEE/ISPRS Joint Workshop 2001 Remote Sensing and Data Fusion over Urban Areas. - Rome, 2001. - P. 100-104.
- C6806.** Haithcoat T.L. Building footprint extraction and 3-D reconstruction from LIDAR data. / Haithcoat T.L., Song W., Hipple J.D. // IEEE/ISPRS Joint Workshop 2001 Remote Sensing and Data Fusion over Urban Areas. - Rome, 2001. - P. 74-78.
- C6807.** Quartulli M. Bayesian model based city reconstruction from high resolution ISAR data. / Quartulli M., Datcu M. // IEEE/ISPRS Joint Workshop 2001 Remote Sensing and Data Fusion over Urban Areas. - Rome, 2001. - P. 58-63.
- C6808.** Costantini M. Optimal combination of multiple SAR differential interferometric measurements for monitoring terrain displacements. / Costantini M., Malvarosa F., Minati F., Pietranera L. // IEEE/ISPRS Joint Workshop 2001 Remote Sensing and Data Fusion over Urban Areas. - Rome, 2001. - P. 53-57.
- C6809.** Fanelli A. Analysis of coherence images over urban areas in the extraction of buildings heights. / Fanelli A., Ferri M., Santoro M., Vitale A. // IEEE/ISPRS Joint Workshop 2001 Remote Sensing and Data Fusion over Urban Areas. - Rome, 2001. - P. 69-73.
- C6810.** Stilla U. Potential and limits of InSAR data for the reconstruction of buildings. / Stilla U., Soergel U., Thoennessen U. // IEEE/ISPRS Joint Workshop 2001 Remote Sensing and Data Fusion over Urban Areas. - Rome, 2001. - P. 64-68.
- C6811.** Houshmand B. Interpretation of InSAR mapping for geometrical structures. / Houshmand B., Gamba P. // IEEE/ISPRS Joint Workshop 2001 Remote Sensing and Data Fusion over Urban Areas. - Rome, 2001. - P. 309-311.

- C6812.** Costantini M. Correction of artifacts on differential SAR interferometry for the study of subsidence phenomena in urban and suburban areas. / Costantini M., Lombardo P., Malvarosa F., Minati F., Pastina D., Pietranera L. // IEEE/ISPRS Joint Workshop 2001 Remote Sensing and Data Fusion over Urban Areas. - Rome, 2001. - P. 236-240. ↑
- C6813.** Salim T. Investigation of multirate techniques for digital generation of transmitter signals for TIGER radar. / Salim T., Devlin J., Whittington J. // 2001. IEEE INMIC 2001. Technology for the 21st Century. Proceedings. IEEE International Multi Topic Conference. 2001. - P. 16-22. ↑
- C6814.** Dell'Acqua F. Fully 3D and joint 2D/3D segmentation of InSAR data over urban environments. / Dell'Acqua F., Gamba P., Soergel U., Thoennessen U. // IEEE/ISPRS Joint Workshop 2001 Remote Sensing and Data Fusion over Urban Areas. - Rome, 2001. - P. 328-331. ↑
- C6815.** Dekker R.J. Texture analysis of urban areas in ERS SAR imagery for map updating. IEEE/ISPRS Joint Workshop 2001 Remote Sensing and Data Fusion over Urban Areas. - Rome, 2001. - P. 226-230. ↑
- C6816.** Dell'acqua F. Evaluation of COSMO/SkyMed SAR data for urban area characterization. / Dell'acqua F., Gamba P. // IEEE/ISPRS Joint Workshop 2001 Remote Sensing and Data Fusion over Urban Areas. - Rome, 2001. - P. 141-145. ↑
- C6817.** {no data available}. IEEE/ISPRS Joint Workshop on Remote Sensing and Data Fusion over Urban Areas (Cat. No.01EX482). IEEE/ISPRS Joint Workshop 2001 Remote Sensing and Data Fusion over Urban Areas. 2001. - {no data available}. ↑
- C6818.** Fatone L. Fusion of SAR/optical images to detect urban areas. / Fatone L., Maponi P., Zirilli F. // IEEE/ISPRS Joint Workshop 2001 Remote Sensing and Data Fusion over Urban Areas. - Rome, 2001. - P. 217-221. ↑
- C6819.** Al-Nuaimy W. Automatic mapping of linear structures in 3-dimensional space from ground-penetrating radar data. / Al-Nuaimy W., Hui Hai Lu, Shihab S., Eriksen A. // IEEE/ISPRS Joint Workshop 2001 Remote Sensing and Data Fusion over Urban Areas. - Rome, 2001. - P. 198-201. ↑
- C6820.** Andryukhin A.N. 3D surface-penetrating radar "Defectoscope". / Andryukhin A.N., Linnikov O.N., Trusov V.N., Surikov B.S., Sosulin Yu.G., Tolmazov B.B. // Proceedings Radar, 2001 CIE International Conference on. - Beijing, 2001. - P. 65-70. ↑
- C6821.** Gjessing D.T. Bistatic matched illumination radar involving synthetic aperture and synthetic pulse for signal to clutter enhancement and target characterization. / Gjessing D.T., Saebboe J. // Proceedings Radar, 2001 CIE International Conference on. - Beijing, 2001. - P. 20-24. ↑
- C6822.** Wu Xide. The influence of the lower atmospheric refraction on measurements of down-looking radar. / Wu Xide, Luo Xianyun, Kang Shifeng, Guo Li. // Proceedings Radar, 2001 CIE International Conference on. - Beijing, 2001. - P. 271-274. ↑
- C6823.** Li Jing. An analysis method research of radar measuring precision. / Li Jing, Li Yuan-Ping, Liu Jun, Hong Yu. // Proceedings Radar, 2001 CIE International Conference on. - Beijing, 2001. - P. 134-135. ↑
- C6824.** Farina A. Fusion of radar images: state of art and perspective. / Farina A., Morabito F.C., Serpico S., Simone G. // Proceedings Radar, 2001 CIE International Conference on. - Beijing, 2001. - P. 9-15. ↑
- C6825.** {no data available}. 2001 International Conferences on Info-Tech and Info-Net. Proceedings (Cat. No.01EX479). 2001. Proceedings. ICII 2001-Beijing. 2001 International Conferences on Info-tech and Info-net. 2001. - Vol. 4. - {no data available}. ↑
- C6826.** Miao Yumei. Research on GIS-oriented radar background clutter database. 2001. Proceedings. ICII 2001-Beijing. 2001 International Conferences on Info-tech and Info-net. - Beijing, 2001. - Vol. 1. - P. 233-237. ↑
- C6827.** Brown E.R. Remote detection of biomolecules in the THz region. / Brown E.R., Woolard D., Globus T., Gelmont B., Samuels A. // 2001 International Semiconductor Device Research Symposium. - Washington, DC, 2001. - P. 553. ↑
- C6828.** Ryzhakov V.V. Concurrent polarization operation mode of location system. / Ryzhakov V.V.,

Sukhanyuk A.M., Shoshin E.L. // Post-graduates and Young Scientists Modern Techniques and Technology, 2001. MTT 2001. Proceedings of the 7th International Scientific and Practical Conference of Students. - Tomsk, 2001. - P. 56-58. ↑

C6829. Franceschetti G. An electromagnetic model for SAR raw signal simulation of urban areas. / Franceschetti G., Iodice A., Riccio D., Ruello G. // IEEE/ISPRS Joint Workshop 2001 Remote Sensing and Data Fusion over Urban Areas. - Rome, 2001. - P. 10-14. ↑

C6830. Manandhar D. Vehicle-borne Laser Mapping System (VLMS)-a new observation system for 3-D mapping of urban areas. / Manandhar D., Shibasaki R. // IEEE/ISPRS Joint Workshop 2001 Remote Sensing and Data Fusion over Urban Areas. - Rome, 2001. - P. 5-9. ↑

C6831. Ferretti A. Radar permanent scatterers identification in urban areas: target characterization and sub-pixel analysis. / Ferretti A., Colesanti C., Prati C., Rocca F. // IEEE/ISPRS Joint Workshop 2001 Remote Sensing and Data Fusion over Urban Areas. - Rome, 2001. - P. 52. ↑

C6832. Datcu M. Scene understanding for settlements from metric resolution imagery. / Datcu M., Piardi A., Daschiel H., Quartulli M., Serpico S., Tupin F. // IEEE/ISPRS Joint Workshop 2001 Remote Sensing and Data Fusion over Urban Areas. - Rome, 2001. - P. 45. ↑

C6833. Chen K.S. Statistical characterization of scattering signals from vegetation at frequency above X-band by numerical simulations. / Chen K.S., Chih-Yuan Chu. // 2001. APMC 2001. 2001 Asia-Pacific Microwave Conference. - Taipei, Taiwan, 3-6 Dec. 2001. - Vol. 2. - P. 835-838. ↑

C6834. Werner M. Shuttle radar topography mission (SRTM): experience with the X-band SAR interferometer. Proceedings Radar, 2001 CIE International Conference on. - Beijing, 2001. - P. 634-638. ↑

C6835. Yamaguchi Y. Polarimetric classification of trees. / Yamaguchi Y., Murase M., Yamada H., Yang J. // Proceedings Radar, 2001 CIE International Conference on. - Beijing, 2001. - P. 440-443. ↑

C6836. Guo Yongmei. The geometric distortion correction in SAR motion compensation. / Guo Yongmei, Hong Wen, Mao Shiyi. // Proceedings Radar, 2001 CIE International Conference on. - Beijing, 2001. - P. 943-946. ↑

C6837. Xu Huaping. Analysis and simulation of spaceborne SAR interferometric baseline. / Xu Huaping, Zhou Yinqing, Li Chunsheng. // Proceedings Radar, 2001 CIE International Conference on. - Beijing, 2001. - P. 639-643. ↑

C6838. Siegmund R. Surface currents imaged with hybrid along and cross track interferometry. / Siegmund R., Mingquan Bao, Lehner S., Niedermeier A., Mayerle R. // 2001. IGARSS '01. IEEE 2001 International Geoscience and Remote Sensing Symposium. - Sydney, NSW, 2001. - Vol. 7. - P. 3146-3148. ↑

C6839. Koch A. Quality assessment of digital surface models derived from the Shuttle Radar Topography Mission (SRTM). / Koch A., Heipke C. // 2001. IGARSS '01. IEEE 2001 International Geoscience and Remote Sensing Symposium. - Sydney, NSW, 2001. - Vol. 6. - P. 2863-2865. ↑

C6840. Knobnob B. Synthetic aperture radar (SAR) images classification using speckle filtering and texture information. / Knobnob B., Thitimajshima P. // 2001. IGARSS '01. IEEE 2001 International Geoscience and Remote Sensing Symposium. - Sydney, NSW, 2001. - Vol. 6. - P. 2856-2858. ↑

C6841. Sanghoon Lee. Multi-sensor data classification in remote sensing using MRF regional growing algorithm. / Sanghoon Lee, Asook Suh, Myunghee Jung. // 2001. IGARSS '01. IEEE 2001 International Geoscience and Remote Sensing Symposium. - Sydney, NSW, 2001. - Vol. 6. - P. 2884-2886. ↑

C6842. Koskinen J.T. Snow monitoring using interferometric TOPSAR data. 2001. IGARSS '01. IEEE 2001 International Geoscience and Remote Sensing Symposium. - Sydney, NSW, 2001. - Vol. 6. - P. 2866-2868. ↑

C6843. Khenchaf A. The bistatic scattering from the natural rough surfaces in X and Ku bands. 2001. IGARSS '01. IEEE 2001 International Geoscience and Remote Sensing Symposium. - Sydney, NSW, 2001. - Vol. 6. - P. 2843-2845. ↑

C6844. Huber R. SAR interferogram phase filtering based on the Von Mises distribution. / Huber R., Dutra L.V., da Costa Freitas C. // 2001. IGARSS '01. IEEE 2001 International Geoscience and Remote Sensing

Symposium. - Sydney, NSW, 2001. - Vol. 6. - P. 2816-2818. ↑

C6845. Huber R. Road extraction from high-resolution airborne SAR using operator fusion. / Huber R., Lang K. // 2001. IGARSS '01. IEEE 2001 International Geoscience and Remote Sensing Symposium. - Sydney, NSW, 2001. - Vol. 6. - P. 2813-2815. ↑

C6846. Kampes B.M. Strategies for non-linear deformation estimation from interferometric stacks. / Kampes B.M., Hanssen R.F., Swart L.M.T. // 2001. IGARSS '01. IEEE 2001 International Geoscience and Remote Sensing Symposium. - Sydney, NSW, 2001. - Vol. 6. - P. 2828-2831. ↑

C6847. Imbo P. Wake detection in polarimetric SAR images. / Imbo P., Souyris J.-C., Y Jeremy M. // 2001. IGARSS '01. IEEE 2001 International Geoscience and Remote Sensing Symposium. - Sydney, NSW, 2001. - Vol. 6. - P. 2819-2821. ↑

C6848. Lombardo P. A new AR-based technique to exploit SAR image correlation properties for rain forest classification. / Lombardo P., Macri Pellizzeri T., Pastina A., Libranti A. // 2001. IGARSS '01. IEEE 2001 International Geoscience and Remote Sensing Symposium. - Sydney, NSW, 2001. - Vol. 6. - P. 2925-2927. ↑

C6849. Lombardo P. A joint classification technique based on multivariate annealing segmentation and "H/A/α_" decomposition for fully polarimetric SAR images of suburban areas. / Lombardo P., Macri Pellizzeri T., Tomasuolo A. // 2001. IGARSS '01. IEEE 2001 International Geoscience and Remote Sensing Symposium. - Sydney, NSW, 2001. - Vol. 6. - P. 2922-2924. ↑

C6850. Lytle V.I. Methods of estimating ridging of Antarctic sea ice. / Lytle V.I., Massom R.A., Worby A.P. // 2001. IGARSS '01. IEEE 2001 International Geoscience and Remote Sensing Symposium. - Sydney, NSW, 2001. - Vol. 6. - P. 2937-2938a. ↑

C6851. Lopez C. Noise filtering of SAR interferometric phase based on wavelet transform. / Lopez C., Fabregas X., Mallorqui J., Mora O., Chandra M. // 2001. IGARSS '01. IEEE 2001 International Geoscience and Remote Sensing Symposium. - Sydney, NSW, 2001. - Vol. 6. - P. 2928-2930. ↑

C6852. Liu Zhao. Application of InSAR on the research of Mani strong earthquake. / Liu Zhao, Zhang Jingfa. // 2001. IGARSS '01. IEEE 2001 International Geoscience and Remote Sensing Symposium. - Sydney, NSW, 2001. - Vol. 6. - P. 2919-2921. ↑

C6853. Licheri M. On the scattering from natural surfaces: the IEM and the improved IEM. / Licheri M., Flourey N., Borgeaud M., Migliaccio M. // 2001. IGARSS '01. IEEE 2001 International Geoscience and Remote Sensing Symposium. - Sydney, NSW, 2001. - Vol. 6. - P. 2911-2913. ↑

C6854. Zhen Li. SAR Interferometry coherence analysis for snow mapping. / Zhen Li, Huadong Guo, Xinwu Li, Changlin Wang. // 2001. IGARSS '01. IEEE 2001 International Geoscience and Remote Sensing Symposium. - Sydney, NSW, 2001. - Vol. 6. - P. 2905-2907. ↑

C6855. Liu W.Y. Another surface scattering model for bistatic scattering. / Liu W.Y., Fung A.K., Chen K.S. // 2001. IGARSS '01. IEEE 2001 International Geoscience and Remote Sensing Symposium. - Sydney, NSW, 2001. - Vol. 6. - P. 2916-2918. ↑

C6856. Lienert B. A 50 MHz logarithmic amplifier for use in lidar measurements. / Lienert B., Porter J., Ahlquist N., Harris D., Sharma S. // 2001. IGARSS '01. IEEE 2001 International Geoscience and Remote Sensing Symposium. - Sydney, NSW, 2001. - Vol. 6. - P. 2914-2915. ↑

C6857. Fransson J.E.S. Mapping of wind-thrown forests using CARABAS-II VHF SAR image data. / Fransson J.E.S., Gustavsson A., Ulander L.M.H., Walter F. // 2001. IGARSS '01. IEEE 2001 International Geoscience and Remote Sensing Symposium. - Sydney, NSW, 2001. - Vol. 6. - P. 2737-2739. ↑

C6858. Fornaro G. Resolution improvement via multipass SAR imaging. / Fornaro G., Pascazio V., Schirizzi G. // 2001. IGARSS '01. IEEE 2001 International Geoscience and Remote Sensing Symposium. - Sydney, NSW, 2001. - Vol. 6. - P. 2734-2736. ↑

C6859. Gleich D. Context based SAR data compression using fuzzy logic. / Gleich D., Planinsic P., Gergic B., Cucej Z. // 2001. IGARSS '01. IEEE 2001 International Geoscience and Remote Sensing Symposium. - Sydney, NSW, 2001. - Vol. 6. - P. 2753-2755. ↑

- C6860.** Gerstoft P. Refractivity-from-clutter using global environmental parameters. / Gerstoft P., Rogers L.T., Hodgkiss W.S., Rovner G. // 2001. IGARSS '01. IEEE 2001 International Geoscience and Remote Sensing Symposium. - Sydney, NSW, 2001. - Vol. 6. - P. 2746-2748. ↑
- C6861.** Fischer C. Multistatic GPR for antipersonnel mine detection. / Fischer C., Wiesbeck W. // 2001. IGARSS '01. IEEE 2001 International Geoscience and Remote Sensing Symposium. - Sydney, NSW, 2001. - Vol. 6. - P. 2721-2723. ↑
- C6862.** Fang Guangyou. Reconstruction parameters of underground objects based on FDTD and optimization method. 2001. IGARSS '01. IEEE 2001 International Geoscience and Remote Sensing Symposium. - Sydney, NSW, 2001. - Vol. 6. - P. 2698-2700. ↑
- C6863.** Fang Guangyou. Instantaneous parameters calculation and analysis of impulse ground penetrating radar (GPR) data. / Fang Guangyou, Pipan M. // 2001. IGARSS '01. IEEE 2001 International Geoscience and Remote Sensing Symposium. - Sydney, NSW, 2001. - Vol. 6. - P. 2695-2697. ↑
- C6864.** Ferro-Famil L. Unsupervised classification and analysis of natural scenes from polarimetric interferometric SAR data. / Ferro-Famil L., Pottier E., Lee J.S. // 2001. IGARSS '01. IEEE 2001 International Geoscience and Remote Sensing Symposium. - Sydney, NSW, 2001. - Vol. 6. - P. 2715-2717. ↑
- C6865.** Ferro-Famil L. Multi-baseline polarimetric SAR data classification using the complex Wishart distribution and principal component analysis. / Ferro-Famil L., Reigber A., Pottier E., Boerner W.M. // 2001. IGARSS '01. IEEE 2001 International Geoscience and Remote Sensing Symposium. - Sydney, NSW, 2001. - Vol. 6. - P. 2712-2714. ↑
- C6866.** Hellmann M. Fuzzy clustering and interpretation of fully polarimetric SAR data. / Hellmann M., Jager G., Pottier E. // 2001. IGARSS '01. IEEE 2001 International Geoscience and Remote Sensing Symposium. - Sydney, NSW, 2001. - Vol. 6. - P. 2790-2792. ↑
- C6867.** Hajnsek I. Removal of additive noise in polarimetric eigenvalue processing. / Hajnsek I., Papathanassiou K.P., Cloude S.R. // 2001. IGARSS '01. IEEE 2001 International Geoscience and Remote Sensing Symposium. - Sydney, NSW, 2001. - Vol. 6. - P. 2778-2780. ↑
- C6868.** Huang W.G. Shallow water bathymetric surveys by spaceborne synthetic aperture radar. / Huang W.G., Fu B., Zhou C.B., Yang J.S., Shi A.Q., Li D.L. // 2001. IGARSS '01. IEEE 2001 International Geoscience and Remote Sensing Symposium. - Sydney, NSW, 2001. - Vol. 6. - P. 2810-2812. ↑
- C6869.** Hellwich O. Sensor and data fusion contest: information for mapping from airborne SAR and optical imagery. / Hellwich O., Heipke C., Wessel B. // 2001. IGARSS '01. IEEE 2001 International Geoscience and Remote Sensing Symposium. - Sydney, NSW, 2001. - Vol. 6. - P. 2793-2795. ↑
- C6870.** Hajnsek I. L- and P-band for surface parameter estimation. / Hajnsek I., Papathanassiou K.P., Cloude S.R. // 2001. IGARSS '01. IEEE 2001 International Geoscience and Remote Sensing Symposium. - Sydney, NSW, 2001. - Vol. 6. - P. 2775-2777. ↑
- C6871.** Gojara K. Undergraduate research on remote sensing at Colorado State University. / Gojara K., Bolen S., Chandrasekar V. // 2001. IGARSS '01. IEEE 2001 International Geoscience and Remote Sensing Symposium. 2001. - Vol. 6. - P. 2757-2758. ↑
- C6872.** Gojara K. Undergraduate research on remote sensing at Colorado State University. / Gojara K., Bolen S., Chandrasekar V. // 2001. IGARSS '01. IEEE 2001 International Geoscience and Remote Sensing Symposium. - Sydney, NSW, 2001. - Vol. 6. - P. 2757-2758. ↑
- C6873.** Greco B. A preliminary evaluation of the absolute backscatter calibration of the ERS-1 altimeter using a passive technique. / Greco B., Castracane P., Pierdicca N., Martini A., Ciotti P., Marzano F.S. // 2001. IGARSS '01. IEEE 2001 International Geoscience and Remote Sensing Symposium. - Sydney, NSW, 2001. - Vol. 6. - P. 2772-2774. ↑
- C6874.** Goulding M.M. The SIVAM airborne SAR system. / Goulding M.M., Stevens D.R., Lim P.R. // 2001. IGARSS '01. IEEE 2001 International Geoscience and Remote Sensing Symposium. - Sydney, NSW, 2001. - Vol. 6. - P. 2763-2765. ↑

- C6875.** Saich P. Deriving forest characteristics using polarimetric InSAR measurements and models. / Saich P., Balzter H., Luckman A. // 2001. IGARSS '01. IEEE 2001 International Geoscience and Remote Sensing Symposium. - Sydney, NSW, 2001. - Vol. 7. - P. 3096-3098. ↑
- C6876.** Richetti E. Remotely sensed and geophysical data for nondestructive archaeological prospection. 2001. IGARSS '01. IEEE 2001 International Geoscience and Remote Sensing Symposium. - Sydney, NSW, 2001. - Vol. 7. - P. 3084-3086. ↑
- C6877.** Sassen K. Combined active and passive remote sensing of the properties of cirrus clouds. 2001. IGARSS '01. IEEE 2001 International Geoscience and Remote Sensing Symposium. - Sydney, NSW, 2001. - Vol. 7. - P. 3105-3107. ↑
- C6878.** Saich P. Monitoring wetland extent and dynamics in the Cat Tien National Park, Vietnam, using space-based radar remote sensing. / Saich P., Thompson S.R., Rebelo L.M. // 2001. IGARSS '01. IEEE 2001 International Geoscience and Remote Sensing Symposium. - Sydney, NSW, 2001. - Vol. 7. - P. 3099-3101. ↑
- C6879.** Ricchetti E. Radar imagery for environmental geology study of coastal zones in southern Italy. 2001. IGARSS '01. IEEE 2001 International Geoscience and Remote Sensing Symposium. - Sydney, NSW, 2001. - Vol. 7. - P. 3083 vol.7. ↑
- C6880.** Rao K.S. Field experiments synchronous with SRTM flights. / Rao K.S., Rao Y.S., Jayanand D., Prithviraj M. // 2001. IGARSS '01. IEEE 2001 International Geoscience and Remote Sensing Symposium. - Sydney, NSW, 2001. - Vol. 7. - P. 3071-3073. ↑
- C6881.** Rall J.A.R. Automatic weather station (AWS) lidar. / Rall J.A.R., Campbell J., Abshire J.B., Spinhirne J.D. // 2001. IGARSS '01. IEEE 2001 International Geoscience and Remote Sensing Symposium. - Sydney, NSW, 2001. - Vol. 7. - P. 3065-3067. ↑
- C6882.** Rey L. SIRAL, a high spatial resolution radar altimeter for the Cryosat mission. / Rey L., de Chateau-Thierry P., Phalippou L., Mavrocordatos C., Francis R. // 2001. IGARSS '01. IEEE 2001 International Geoscience and Remote Sensing Symposium. - Sydney, NSW, 2001. - Vol. 7. - P. 3080-3082. ↑
- C6883.** Reigber A. Correction of residual motion errors in airborne repeat-pass interferometry. / Reigber A., Papathanassiou K.P. // 2001. IGARSS '01. IEEE 2001 International Geoscience and Remote Sensing Symposium. - Sydney, NSW, 2001. - Vol. 7. - P. 3077-3079. ↑
- C6884.** Sciotti M. Polarimetric detectors of extended targets for ship detection in SAR images. / Sciotti M., Pastina D., Lombardo P. // 2001. IGARSS '01. IEEE 2001 International Geoscience and Remote Sensing Symposium. - Sydney, NSW, 2001. - Vol. 7. - P. 3132-3134. ↑
- C6885.** Schwemmer G. Large aperture scanning lidar based on holographic optical elements. / Schwemmer G., Miller D.O., Wilkerson T.D., Andrus I., Guerra D.V. // 2001. IGARSS '01. IEEE 2001 International Geoscience and Remote Sensing Symposium. - Sydney, NSW, 2001. - Vol. 7. - P. 3129-3131. ↑
- C6886.** Seigny P. A synthetic moving target generator for calibration of Radarsat 2 Moving-Object Detection Experiment (MODEX). / Seigny P., Livingstone C., Saper R. // 2001. IGARSS '01. IEEE 2001 International Geoscience and Remote Sensing Symposium. - Sydney, NSW, 2001. - Vol. 7. - P. 3141-3143. ↑
- C6887.** Selige T. Validation of grid-based surface reconstruction techniques applied to digital elevation models including the Shuttle Radar Topographic Mission. / Selige T., Ringeler A., Boehner J., Conrad O., Koethe R. // 2001. IGARSS '01. IEEE 2001 International Geoscience and Remote Sensing Symposium. - Sydney, NSW, 2001. - Vol. 7. - P. 3135-3137. ↑
- C6888.** Schiavon G. Modelling returns from urban manufacts: simulation results for finite trihedrals. / Schiavon G., Solimini D., Mandile A. // 2001. IGARSS '01. IEEE 2001 International Geoscience and Remote Sensing Symposium. - Sydney, NSW, 2001. - Vol. 7. - P. 3120-3122. ↑
- C6889.** Satalino G. Soil moisture retrieval using SAR data and a priori roughness information. / Satalino G., Pasquariello G., Mattia F., Davidson M., Le Toan T., Borgeaud M. // 2001. IGARSS '01. IEEE 2001 International Geoscience and Remote Sensing Symposium. - Sydney, NSW, 2001. - Vol. 7. - P. 3111-3113. ↑
- C6890.** Sassen K. The Polarization Diversity Lidar: a dual-wavelength, high-resolution, scanning lidar for cloud

and aerosol research. 2001. IGARSS '01. IEEE 2001 International Geoscience and Remote Sensing Symposium. - Sydney, NSW, 2001. - Vol. 7. - P. 3108-3110. ↑

C6891. Scheuchl B. Automated sea ice classification using spaceborne polarimetric SAR data. / Scheuchl B., Caves R., Cumming I., Staples G. // 2001. IGARSS '01. IEEE 2001 International Geoscience and Remote Sensing Symposium. - Sydney, NSW, 2001. - Vol. 7. - P. 3117-3119. ↑

C6892. Scheiber R. Origin and correction of phase errors in airborne repeat-pass SAR interferometry. / Scheiber R., Robert P. // 2001. IGARSS '01. IEEE 2001 International Geoscience and Remote Sensing Symposium. - Sydney, NSW, 2001. - Vol. 7. - P. 3114-3116. ↑

C6893. Onana V.P. Thin linear features extraction in SAR images by fusion of amplitude and coherence information. / Onana V.P., Trouve E., Mauris G., Rudant J.P., Tonye E. // 2001. IGARSS '01. IEEE 2001 International Geoscience and Remote Sensing Symposium. - Sydney, NSW, 2001. - Vol. 7. - P. 3012-3014. ↑

C6894. Olsen O.M. SAR processing algorithms in the KSPT ENVISAT ASAR processor. / Olsen O.M., Rasmussen G.L., Indregard M., Oynes F. // 2001. IGARSS '01. IEEE 2001 International Geoscience and Remote Sensing Symposium. - Sydney, NSW, 2001. - Vol. 7. - P. 3009-3011. ↑

C6895. Pascazio V. Moving target detection by along-track interferometry. / Pascazio V., Schirinzi G., Farina A. // 2001. IGARSS '01. IEEE 2001 International Geoscience and Remote Sensing Symposium. - Sydney, NSW, 2001. - Vol. 7. - P. 3024-3026. ↑

C6896. Pairman D. Exotic forest clear-fell mapping from the New Zealand PACRIM-2 mission. / Pairman D., McNeill S.J., McNab D., Belliss S.E. // 2001. IGARSS '01. IEEE 2001 International Geoscience and Remote Sensing Symposium. - Sydney, NSW, 2001. - Vol. 7. - P. 3018-3020. ↑

C6897. Ohkura H. InSAR analysis of Miyake-jima volcano with Radarsat images. / Ohkura H., Shimada M. // 2001. IGARSS '01. IEEE 2001 International Geoscience and Remote Sensing Symposium. - Sydney, NSW, 2001. - Vol. 7. - P. 3001-3005. ↑

C6898. Mittermayer J. Interferometric performance estimation for the interferometric Cartwheel in combination with a transmitting SAR-satellite. / Mittermayer J., Krieger G., Moreira A., Wendler M. // 2001. IGARSS '01. IEEE 2001 International Geoscience and Remote Sensing Symposium. - Sydney, NSW, 2001. - Vol. 7. - P. 2955-2957. ↑

C6899. Melgani F. Fusion of multitemporal contextual information by neural networks for multisensor image classification. / Melgani F., Serpico S.B., Vernazza G. // 2001. IGARSS '01. IEEE 2001 International Geoscience and Remote Sensing Symposium. - Sydney, NSW, 2001. - Vol. 7. - P. 2952-2954. ↑

C6900. Mostafa M. Airborne remote sensing without ground control. / Mostafa M., Hutton J. // 2001. IGARSS '01. IEEE 2001 International Geoscience and Remote Sensing Symposium. - Sydney, NSW, 2001. - Vol. 7. - P. 2961-2963. ↑

C6901. Morris J. Polarimetric observations of wave breaking induced by ship wakes. / Morris J., Anderson S., Parfitt A. // 2001. IGARSS '01. IEEE 2001 International Geoscience and Remote Sensing Symposium. - Sydney, NSW, 2001. - Vol. 7. - P. 2958-2960. ↑

C6902. Prinnet V. 3D scene modeling from data fusion. / Prinnet V., Feng Wang, ZhaoHui Zhang, Gang Wu. // 2001. IGARSS '01. IEEE 2001 International Geoscience and Remote Sensing Symposium. - Sydney, NSW, 2001. - Vol. 7. - P. 3053-3055. ↑

C6903. Praks J. Polarimetric properties of boreal forest in L- and C-band SAR images. / Praks J., Alasalmi H., Hallikainen M. // 2001. IGARSS '01. IEEE 2001 International Geoscience and Remote Sensing Symposium. - Sydney, NSW, 2001. - Vol. 7. - P. 3050-3052. ↑


C6904. Proisy C. Seasonal variations of ERS Tandem coherence values over a mixed temperate forest. / Proisy C., Mougin E., Martin E., Borderies P., Chenerie I., Thirion L. // 2001. IGARSS '01. IEEE 2001 International Geoscience and Remote Sensing Symposium. - Sydney, NSW, 2001. - Vol. 7. - P. 3059-3061. ↑


C6905. Proisy C. Radar remote sensing of mangroves: results and perspectives. / Proisy C., Mougin E. // 2001. IGARSS '01. IEEE 2001 International Geoscience and Remote Sensing Symposium. - Sydney, NSW, 2001. - Vol. 7. - P. 3062-3064. ↑


2001. - Vol. 7. - P. 3056-3058. 


C6906. Potsis A. Improving the focusing properties of SAR processors for wide-band and wide-beam low frequency imaging. / Potsis A., Reigber A., Mittermayer J., Moreira A., Uzunoglou N. // 2001. IGARSS '01. IEEE 2001 International Geoscience and Remote Sensing Symposium. - Sydney, NSW, 2001. - Vol. 7. - P. 3047-3049.





C6907. Payne T. Pre-formation SAR to SAR image registration. 2001. IGARSS '01. IEEE 2001 International Geoscience and Remote Sensing Symposium. - Sydney, NSW, 2001. - Vol. 7. - P. 3033-3035. 


C6908. Payne T. Phase analysis for the limitations of the tomographic paradigm on a 3D scene. 2001. IGARSS '01. IEEE 2001 International Geoscience and Remote Sensing Symposium. - Sydney, NSW, 2001. - Vol. 7. - P. 3030-3032. 


C6909. Porter J.N. The use of realistic aerosol models to limit the range of aerosol possibilities in deriving aerosol scatter. / Porter J.N., Lienert B.R., Sharma S.K. // 2001. IGARSS '01. IEEE 2001 International Geoscience and Remote Sensing Symposium. - Sydney, NSW, 2001. - Vol. 7. - P. 3045-3046. 


C6910. Cheng Peng. Speckle noise removal in SAR image based on SOT structure in wavelet domain. / Cheng Peng, Chan A. // 2001. IGARSS '01. IEEE 2001 International Geoscience and Remote Sensing Symposium. - Sydney, NSW, 2001. - Vol. 7. - P. 3039-3041. 

C6911. Young N.W. Mapping the Antarctic ice sheet margin and grounding zone for change detection. / Young N.W., Collings A.D., Gale T., Hyland G., Morffew M., Williams R. // 2001. IGARSS '01. IEEE 2001 International Geoscience and Remote Sensing Symposium. - Sydney, NSW, 2001. - Vol. 1. - P. 168-170. 

C6912. Shusun Li. The spatial variability of summer sea ice in the Amundsen Sea seen from MODIS, RADARSAT SCANSAR and LANDSAT 7 ETM+ images. / Shusun Li, Xiaobing Zhou, Morris K., Jeffries M. // 2001. IGARSS '01. IEEE 2001 International Geoscience and Remote Sensing Symposium. - Sydney, NSW, 2001. - Vol. 1. - P. 160-162. 


C6913. Nolan M. SARfari: a tool for analyzing Arctic hydrology using space-borne SAR. / Nolan M., Overduin P. // 2001. IGARSS '01. IEEE 2001 International Geoscience and Remote Sensing Symposium. - Sydney, NSW, 2001. - Vol. 1. - P. 184-186. 


C6914. McNutt S.L. Combining SAR and AVHRR to understand sea ice dynamics in the seasonal and perennial ice zones of the Beaufort and Chukchi seas. / McNutt S.L., Labelle-Hamer N., Overland J.E. // 2001. IGARSS '01. IEEE 2001 International Geoscience and Remote Sensing Symposium. - Sydney, NSW, 2001. - Vol. 1. - P. 177-180. 

C6915. Refice A. DInSAR applications to landslide studies. / Refice A., Bovenga F., Guerriero L., Wasowski J. // 2001. IGARSS '01. IEEE 2001 International Geoscience and Remote Sensing Symposium. - Sydney, NSW, 2001. - Vol. 1. - P. 144-146. 

C6916. Hensley S. First P-band results using the GeoSAR mapping system. / Hensley S., Chapin E., Freedman A., Le C., Madsen S., Michel T., Rodriguez E., Siqueira P., Wheeler K. // 2001. IGARSS '01. IEEE 2001 International Geoscience and Remote Sensing Symposium. - Sydney, NSW, 2001. - Vol. 1. - P. 126-128.



C6917. Wilkinson A.J. Repeat pass SAR interferometry at VHF band. / Wilkinson A.J., Lord R.T., Inggs M.R. // 2001. IGARSS '01. IEEE 2001 International Geoscience and Remote Sensing Symposium. - Sydney, NSW, 2001. - Vol. 1. - P. 123-125. 

C6918. Snoeij P. Effect of the ionosphere on P-band spaceborne SAR images. / Snoeij P., van der Valk N., Boom E., Hoekman D. // 2001. IGARSS '01. IEEE 2001 International Geoscience and Remote Sensing Symposium. - Sydney, NSW, 2001. - Vol. 1. - P. 132-134. 

C6919. Ulander L.M.H. Performance of the CARABAS-II VHF-band synthetic aperture radar. / Ulander L.M.H., Frolind P.-O., Gustavsson A., Hellsten H., Jonsson T., Larsson B., Stenstrom G. // 2001. IGARSS '01. IEEE 2001 International Geoscience and Remote Sensing Symposium. - Sydney, NSW, 2001. - Vol. 1. - P. 129-131.



C6920. Fukuda S. Support vector machine classification of land cover: application to polarimetric SAR data. /

Fukuda S., Hirose H. // 2001. IGARSS '01. IEEE 2001 International Geoscience and Remote Sensing Symposium. - Sydney, NSW, 2001. - Vol. 1. - P. 187-189. ↑

C6921. Poulter M.A. Remote Minefield Detection System (REMIDS): a UK programme for airborne minefield detection. / Poulter M.A., Tee H.S. // 2001. IGARSS '01. IEEE 2001 International Geoscience and Remote Sensing Symposium. - Sydney, NSW, 2001. - Vol. 1. - P. 243-245. ↑

C6922. Stephens G.L. CloudSat and the EOS constellation. 2001. IGARSS '01. IEEE 2001 International Geoscience and Remote Sensing Symposium. - Sydney, NSW, 2001. - Vol. 1. - P. 233-235. ↑

C6923. Romshoo S.A. Multifrequency radar backscattering from wheat canopy in the light of theory and experiments. 2001. IGARSS '01. IEEE 2001 International Geoscience and Remote Sensing Symposium. - Sydney, NSW, 2001. - Vol. 1. - P. 263-265. ↑

C6924. Dabrowska-Zielinska K. Various approaches for soil moisture estimates using remote sensing. / Dabrowska-Zielinska K., Inoue Y., Gruszczynska A., Kowalik W., Stankiewicz K. // 2001. IGARSS '01. IEEE 2001 International Geoscience and Remote Sensing Symposium. - Sydney, NSW, 2001. - Vol. 1. - P. 261-262. ↑

C6925. Aguttes J.P. High resolution (metric) SAR microsatellite, based on the CNES MYRIADE bus. 2001. IGARSS '01. IEEE 2001 International Geoscience and Remote Sensing Symposium. - Sydney, NSW, 2001. - Vol. 1. - P. 224-226. ↑

C6926. Kouskoulas Y. Bayesian-hierarchical SAR classifier. / Kouskoulas Y., Ulaby F.T., Pierce L. // 2001. IGARSS '01. IEEE 2001 International Geoscience and Remote Sensing Symposium. - Sydney, NSW, 2001. - Vol. 1. - P. 193-195. ↑

C6927. Derrode S. Estimation of sea-ice SAR clutter statistics from Pearson's system of distributions. / Derrode S., Mercier G., Le Caillec J.-M., Garelo R. // 2001. IGARSS '01. IEEE 2001 International Geoscience and Remote Sensing Symposium. - Sydney, NSW, 2001. - Vol. 1. - P. 190-192. ↑

C6928. Ramanathan A. Acquisition of sensing data on a reconfigurable platform. / Ramanathan A., Tessier R., McLaughlin D., Carswell J., Frasier S. // 2001. IGARSS '01. IEEE 2001 International Geoscience and Remote Sensing Symposium. - Sydney, NSW, 2001. - Vol. 1. - P. 222-223. ↑

C6929. Caubet E. Design status of a combined Ka-band altimeter/radiometer. / Caubet E., Pralippou L. // 2001. IGARSS '01. IEEE 2001 International Geoscience and Remote Sensing Symposium. - Sydney, NSW, 2001. - Vol. 1. - P. 219-221. ↑

C6930. Imhoff M.L. VHF radar mapping of forest biomass in Panama. / Imhoff M.L., Johnson P., Carson S., Lawrence W., Condit R., Stutzer D., Wright J. // 2001. IGARSS '01. IEEE 2001 International Geoscience and Remote Sensing Symposium. - Sydney, NSW, 2001. - Vol. 1. - P. 121-122. ↑

C6931. Huang Wei-min. HF radar wind measurement over the Eastern China Sea. / Huang Wei-min, Wu Shi-cai, Wen Bi-yang, Hou Jie-chang. // 2001. MTS/IEEE Conference and Exhibition OCEANS. - Honolulu, HI, 2001. - Vol. 1. - P. 642-645. ↑

C6932. Gerstoft P. Estimation of radio refractivity structure using radar clutter. / Gerstoft P., Rogers L.T., Wagner L.J., Hodgkiss W.S. // 2001. MTS/IEEE Conference and Exhibition OCEANS. - Honolulu, HI, 2001. - Vol. 1. - P. 636-641. ↑

C6933. van Zyl J.J. A quantitative comparison of soil moisture inversion algorithms. / van Zyl J.J., Yunjin Kim. // 2001. IGARSS '01. IEEE 2001 International Geoscience and Remote Sensing Symposium. - Sydney, NSW, 2001. - Vol. 1. - P. 37-39. ↑

C6934. Weiss M. Low-cost, low-power nanosecond pulse radar for industrial applications with mm accuracy. 2001 International Symposium on Electron Devices for Microwave and Optoelectronic Applications. - Vienna, 2001. - P. 199-204. ↑

C6935. Arakelyan A. Effectiveness of spatial-temporal collocated microwave scatterometric and vertical-horizontal polarized radiometric images in sea surface monitoring. / Arakelyan A., Hambaryan A.K., Arakelian A.K. // 2001. MTS/IEEE Conference and Exhibition OCEANS. - Honolulu, HI, 2001. - Vol. 4. - P. 2658-2665. ↑

- C6936.** Carroll S.N. The Northern Gulf of Mexico Littoral Initiative. / Carroll S.N., Szczechowski C. // 2001. MTS/IEEE Conference and Exhibition OCEANS. - Honolulu, HI, 2001. - Vol. 2. - P. 1311-1317. ↑
- C6937.** Ebrite S. A multi-agency solution for coastal surveys-SHOALS in the Pacific. / Ebrite S., Pope B., Lillycrop W.J. // 2001. MTS/IEEE Conference and Exhibition OCEANS. - Honolulu, HI, 2001. - Vol. 2. - P. 1204-1211. ↑
- C6938.** Gade M. On the distribution of small-scale roughness at the edges of monomolecular surface films. / Gade M., Lange P.A. // 2001. MTS/IEEE Conference and Exhibition OCEANS. - Honolulu, HI, 2001. - Vol. 4. - P. 2425-2431. ↑
- C6939.** Lan Gao. Prediction of chaotic time series based on wavelet neural network. / Lan Gao, Ling Lu, Zhijun Li. // 2001. MTS/IEEE Conference and Exhibition OCEANS. - Honolulu, HI, 2001. - Vol. 4. - P. 2046-2050. ↑
- C6940.** Western A. Is SAR capable of mapping small-scale spatial patterns of soil moisture?. / Western A., Sadek T., Li Wang, Grayson R., Tural H., Troch P. // 2001. IGARSS '01. IEEE 2001 International Geoscience and Remote Sensing Symposium. - Sydney, NSW, 2001. - Vol. 1. - P. 40-42. ↑
- C6941.** Mvogo J. A combined speckle noise reduction and, compression of SAR images using a multiwavelet based method to improve codec performance. / Mvogo J., Mercier G., Onana V.P., Rudant J.R., Tonye E., Trebossen H. // 2001. IGARSS '01. IEEE 2001 International Geoscience and Remote Sensing Symposium. - Sydney, NSW, 2001. - Vol. 1. - P. 103-105. ↑
- C6942.** Mercier G. Despeckle-based SAR image compression. 2001. IGARSS '01. IEEE 2001 International Geoscience and Remote Sensing Symposium. - Sydney, NSW, 2001. - Vol. 1. - P. 100-102. ↑
- C6943.** Galli L. A new approach based on network theory to locate phase unwrapping unreliable results. 2001. IGARSS '01. IEEE 2001 International Geoscience and Remote Sensing Symposium. - Sydney, NSW, 2001. - Vol. 1. - P. 118-120. ↑
- C6944.** Gini F. System and estimation problems for multibaseline InSAR imaging of multiple layovered reflectors. / Gini F., Lombardini F., Matteucci P., Verrazzani L. // 2001. IGARSS '01. IEEE 2001 International Geoscience and Remote Sensing Symposium. - Sydney, NSW, 2001. - Vol. 1. - P. 115-117. ↑
- C6945.** Young S.A. Observations over Australia of plumes from distant biomass-burning sources using remote sensing and airborne techniques. / Young S.A., Langenfelds R.L., Rosen J.M. // 2001. IGARSS '01. IEEE 2001 International Geoscience and Remote Sensing Symposium. - Sydney, NSW, 2001. - Vol. 1. - P. 88-90. ↑
- C6946.** Reagan J.A. Spaceborne lidar calibration from cirrus and molecular backscatter returns. / Reagan J.A., Wang X., Osborn M.T. // 2001. IGARSS '01. IEEE 2001 International Geoscience and Remote Sensing Symposium. - Sydney, NSW, 2001. - Vol. 1. - P. 64-66. ↑
- C6947.** Goodenough D.G. Calibration of forest chemistry for hyperspectral analysis. / Goodenough D.G., Bhogal A.S., Dyk A., Niemann O., Tian Han, Hao Chen, West C., Schmidt C. // 2001. IGARSS '01. IEEE 2001 International Geoscience and Remote Sensing Symposium. - Sydney, NSW, 2001. - Vol. 1. - P. 52-56. ↑
- C6948.** Reagan J.A. Lidar aerosol ratio: measurements and models. / Reagan J.A., Thome K.J., Powell D.M. // 2001. IGARSS '01. IEEE 2001 International Geoscience and Remote Sensing Symposium. - Sydney, NSW, 2001. - Vol. 1. - P. 84-87. ↑
- C6949.** Love S.P. First retrievals of the physical thickness and optical depth of dense clouds with off-beam/multiple-scattering lidar. / Love S.P., Davis A.B., Winker D.M., Cahalan R.F. // 2001. IGARSS '01. IEEE 2001 International Geoscience and Remote Sensing Symposium. - Sydney, NSW, 2001. - Vol. 1. - P. 67-71. ↑
- C6950.** Vesecky J.F. Surface current observations by HF radar during EEGLE 2000. / Vesecky J.F., Meadows L.A., Teague C.C., Hansen P., Plume M., Fernandez Y. // 2001. IGARSS '01. IEEE 2001 International Geoscience and Remote Sensing Symposium. - Sydney, NSW, 2001. - Vol. 1. - P. 272-274. ↑
- C6951.** Srivastava S.K. RADARSAT-1 image quality/five years of achievement. / Srivastava S.K., Banik B.T., Le Dantec P., Hawkins R.K., Lukowski T.I., Murnaghan K.P. // 2001. IGARSS '01. IEEE 2001 International Geoscience and Remote Sensing Symposium. - Sydney, NSW, 2001. - Vol. 1. - P. 465-467. ↑

- C6952.** Madsen S.N. A geosynchronous synthetic aperture radar; for tectonic mapping, disaster management and measurements of vegetation and soil moisture. / Madsen S.N., Edelstein W., DiDomenico L.D., LaBrecque J. // 2001. IGARSS '01. IEEE 2001 International Geoscience and Remote Sensing Symposium. - Sydney, NSW, 2001. - Vol. 1. - P. 447-449. ↑
- C6953.** Vachon P.W. Radarsat-1 Hurricane Watch. / Vachon P.W., Clemente-Colon P., Pichel W.G., Black P.G., Dodge P., Katsaros K.B., MacDonell K. // 2001. IGARSS '01. IEEE 2001 International Geoscience and Remote Sensing Symposium. - Sydney, NSW, 2001. - Vol. 1. - P. 471-473. ↑
- C6954.** Singhroy V.H. Geological applications of RADARSAT-1: a review. 2001. IGARSS '01. IEEE 2001 International Geoscience and Remote Sensing Symposium. - Sydney, NSW, 2001. - Vol. 1. - P. 468-470. ↑
- C6955.** Emmitt G.D. A geosynchronous lidar system for atmospheric winds and moisture measurements. 2001. IGARSS '01. IEEE 2001 International Geoscience and Remote Sensing Symposium. - Sydney, NSW, 2001. - Vol. 1. - P. 444-446. ↑
- C6956.** Wakabayashi H. Cross-calibration experiment of airborne L-band polarimetric SAR. / Wakabayashi H., Tadono T., Matsuoka M., Matsuoka T., Shimada M., Uratsuka S. // 2001. IGARSS '01. IEEE 2001 International Geoscience and Remote Sensing Symposium. - Sydney, NSW, 2001. - Vol. 1. - P. 423-425. ↑
- C6957.** Ainsworth T.L. A new method for a posteriori polarimetric SAR calibration. / Ainsworth T.L., Lee J.S. // 2001. IGARSS '01. IEEE 2001 International Geoscience and Remote Sensing Symposium. - Sydney, NSW, 2001. - Vol. 1. - P. 420-422. ↑
- C6958.** Peri F. Jr. The future of instrument technology for space-based remote sensing for NASA's Earth Science Enterprise. / Peri F. Jr., Hartley J.B., Duda J.L. // 2001. IGARSS '01. IEEE 2001 International Geoscience and Remote Sensing Symposium. - Sydney, NSW, 2001. - Vol. 1. - P. 432-435. ↑
- C6959.** Touzi R. Ship-sea contrast optimization when using polarimetric SARs. / Touzi R., Charbonneau F., Hawkins R.K., Murnaghan K., Kavoun X. // 2001. IGARSS '01. IEEE 2001 International Geoscience and Remote Sensing Symposium. - Sydney, NSW, 2001. - Vol. 1. - P. 426-428. ↑
- C6960.** Horn G. Mapping seasonal vegetation changes with multi-temporal radar segmentation. / Horn G., Milne A.K., Dong Y., Finlayson M. // 2001. IGARSS '01. IEEE 2001 International Geoscience and Remote Sensing Symposium. - Sydney, NSW, 2001. - Vol. 1. - P. 474-476. ↑
- C6961.** Luscombe A.P. RADARSAT-2 calibration: proposed targets and techniques. / Luscombe A.P., Thompson A. // 2001. IGARSS '01. IEEE 2001 International Geoscience and Remote Sensing Symposium. - Sydney, NSW, 2001. - Vol. 1. - P. 496-498. ↑
- C6962.** Flett D.G. Preparing for operational use of RADARSAT-2 data at the Canadian Ice Service. / Flett D.G., Manore M.J., Ramsay B.R., Falkingham J.C. // 2001. IGARSS '01. IEEE 2001 International Geoscience and Remote Sensing Symposium. - Sydney, NSW, 2001. - Vol. 1. - P. 493-495. ↑
- C6963.** Chapin E. Calibration of an across track interferometric P-band SAR. / Chapin E., Hensley S., Michel T.R. // 2001. IGARSS '01. IEEE 2001 International Geoscience and Remote Sensing Symposium. - Sydney, NSW, 2001. - Vol. 1. - P. 502-504. ↑
- C6964.** Lee P.F. The RADARSAT-2/3 topographic mission. / Lee P.F., James K. // 2001. IGARSS '01. IEEE 2001 International Geoscience and Remote Sensing Symposium. - Sydney, NSW, 2001. - Vol. 1. - P. 499-501. ↑
- C6965.** van der Sanden J.J. Applications potential of planned C-band SAR satellites: leading to RADARSAT-2. / van der Sanden J.J., Budkewitsch P., Flett D., Landry R., Lukowski T.I., McNairn H., Pultz T.J., Singhroy V., Sokol J., Touzi R., Vachon P.W. // 2001. IGARSS '01. IEEE 2001 International Geoscience and Remote Sensing Symposium. - Sydney, NSW, 2001. - Vol. 1. - P. 488-492. ↑
- C6966.** McGuire M.E. Evolution of Canadian Earth observation from RADARSAT-1 to RADARSAT-2. / McGuire M.E., Parashar S., Mahmood A., Brule L. // 2001. IGARSS '01. IEEE 2001 International Geoscience and Remote Sensing Symposium. - Sydney, NSW, 2001. - Vol. 1. - P. 480-481. ↑
- C6967.** Ramsay B. Radarsat-1 for sea ice monitoring in Canada-an operational success story. / Ramsay B., Flett D., Manore M., De Abreu R. // 2001. IGARSS '01. IEEE 2001 International Geoscience and Remote

Sensing Symposium. - Sydney, NSW, 2001. - Vol. 1. - P. 477-479. ↑

C6968. Thompson A.A. New modes and techniques of the RADARSAT-2 SAR. / Thompson A.A., Luscombe A.P., James K., Fox P. // 2001. IGARSS '01. IEEE 2001 International Geoscience and Remote Sensing Symposium. - Sydney, NSW, 2001. - Vol. 1. - P. 485-487. ↑

C6969. Mahmood A. Mapping recent lava flows with Radarsat-1 imagery. / Mahmood A., Giugni L.P. // 2001. IGARSS '01. IEEE 2001 International Geoscience and Remote Sensing Symposium. - Sydney, NSW, 2001. - Vol. 1. - P. 482-484. ↑

C6970. Satake M. Development of polarization selective corner reflectors and its experiment for calibration of airborne polarimetric synthetic aperture radar. / Satake M., Umehara T., Nadai A., Maeno H., Uratsuka S., Matsuoka T., Honma H. // 2001. IGARSS '01. IEEE 2001 International Geoscience and Remote Sensing Symposium. - Sydney, NSW, 2001. - Vol. 1. - P. 417-419. ↑

C6971. Hyunjun Kim. Radar image studies of scattering from random rough surfaces. / Hyunjun Kim, Johnson J.T. // 2001. IGARSS '01. IEEE 2001 International Geoscience and Remote Sensing Symposium. - Sydney, NSW, 2001. - Vol. 1. - P. 351-353. ↑

C6972. Bentz C. Application of remote sensing data for oil spill monitoring in the Guanabara Bay, Rio de Janeiro, Brazil. / Bentz C., Pellon de Miranda F. // 2001. IGARSS '01. IEEE 2001 International Geoscience and Remote Sensing Symposium. - Sydney, NSW, 2001. - Vol. 1. - P. 333-335. ↑

C6973. Brown C.G. Model-based estimation of forest canopy parameters using polarimetric and interferometric SAR. / Brown C.G., Sarabandi K. // 2001. IGARSS '01. IEEE 2001 International Geoscience and Remote Sensing Symposium. - Sydney, NSW, 2001. - Vol. 1. - P. 357-359. ↑

C6974. Gimeno E. Near-field 2-D and 3-D radar imaging using a chirp scaling algorithm. / Gimeno E., Lopez-Sanchez J.M. // 2001. IGARSS '01. IEEE 2001 International Geoscience and Remote Sensing Symposium. - Sydney, NSW, 2001. - Vol. 1. - P. 354-356. ↑

C6975. Liu W.T. Continuous strife for better coverage and more details in ocean surface winds measurements from Midori and ADEOS-2 to GCOM. / Liu W.T., Hua Hu, Wenqing Tang, Xiaosu Xie. // 2001. IGARSS '01. IEEE 2001 International Geoscience and Remote Sensing Symposium. - Sydney, NSW, 2001. - Vol. 1. - P. 322-324. ↑

C6976. Forget P. Visible and microwave signatures of river plumes in microtidal seas. / Forget P., Fraunie P., Ouillon S. // 2001. IGARSS '01. IEEE 2001 International Geoscience and Remote Sensing Symposium. - Sydney, NSW, 2001. - Vol. 1. - P. 278-280. ↑

C6977. Gurgel K.W. Current structure off the North Spanish coast observed by HF radar. / Gurgel K.W., Essen H.H., Schlick T. // 2001. IGARSS '01. IEEE 2001 International Geoscience and Remote Sensing Symposium. - Sydney, NSW, 2001. - Vol. 1. - P. 275-277. ↑


C6978. Iguchi T. Accuracy of rain rate retrieval from dual-frequency precipitation radar data. / Iguchi T., Hanado H., Kozu T. // 2001. IGARSS '01. IEEE 2001 International Geoscience and Remote Sensing Symposium. - Sydney, NSW, 2001. - Vol. 1. - P. 317-319. ↑


C6979. Sletten M.A. Variability in the evolution of the Chesapeake Bay outflow plume front as observed with a real aperture radar. / Sletten M.A., Twarog E., Xuehu Zhang, McLaughlin D.J. // 2001. IGARSS '01. IEEE 2001 International Geoscience and Remote Sensing Symposium. - Sydney, NSW, 2001. - Vol. 1. - P. 281-283. ↑


C6980. Carrea L. Polarimetric SAR processing using the polar decomposition of the scattering matrix. / Carrea L., Wanielik G. // 2001. IGARSS '01. IEEE 2001 International Geoscience and Remote Sensing Symposium. - Sydney, NSW, 2001. - Vol. 1. - P. 363-365. ↑


C6981. Xia Y. INSAR activities in central Asia using mobile SAR receiving station. 2001. IGARSS '01. IEEE 2001 International Geoscience and Remote Sensing Symposium. - Sydney, NSW, 2001. - Vol. 1. - P. 407-409. ↑


C6982. Mallorqui J.J. Interferometric calibration for DEM enhancing and system characterization in single pass SAR interferometry. / Mallorqui J.J., Rosado I., Bara M. // 2001. IGARSS '01. IEEE 2001 International
↑


Geoscience and Remote Sensing Symposium. - Sydney, NSW, 2001. - Vol. 1. - P. 404-406. 


C6983. Lee J.S. Segmentation of polarimetric SAR images. / Lee J.S., Grunes M.R., Pottier E., Ferro-Famil L. // 2001. IGARSS '01. IEEE 2001 International Geoscience and Remote Sensing Symposium. - Sydney, NSW, 2001. - Vol. 1. - P. 414-416. 


C6984. De Grandi G.F. Segmentation and labeling of polarimetric SAR data: can wavelets help?. / De Grandi G.F., Lee J.S., Siqueira R., Baraldi A., Simard M. // 2001. IGARSS '01. IEEE 2001 International Geoscience and Remote Sensing Symposium. - Sydney, NSW, 2001. - Vol. 1. - P. 410-413. 


C6985. Thirion L. Modelling of interferometric phase for forested areas. / Thirion L., Borderies P., Chenierie I., Mougin E., Proisy C. // 2001. IGARSS '01. IEEE 2001 International Geoscience and Remote Sensing Symposium. - Sydney, NSW, 2001. - Vol. 1. - P. 401-403. 


C6986. Martinerie F. Interferometric Cartwheel payload: development status and current issues. / Martinerie F., Ramongassie S., Deligny B., Thouvenot E., Massonnet D. // 2001. IGARSS '01. IEEE 2001 International Geoscience and Remote Sensing Symposium. - Sydney, NSW, 2001. - Vol. 1. - P. 390-392. 


C6987. Bolen S. Quantitative intercomparison of polarimetric ground radar and TRMM PR observations. / Bolen S., Chandraker V., Gorgucci E., Scarchilli G. // 2001. IGARSS '01. IEEE 2001 International Geoscience and Remote Sensing Symposium. - Sydney, NSW, 2001. - Vol. 1. - P. 375-377. 


C6988. Dias J.M.B. InSAR phase unwrapping: a Bayesian approach. / Dias J.M.B., Leitao J.M.N. // 2001. IGARSS '01. IEEE 2001 International Geoscience and Remote Sensing Symposium. - Sydney, NSW, 2001. - Vol. 1. - P. 396-400. 


C6989. Holzner J. Co-registration-geometrical analysis and verification for SAR interferometry under SRTM data conditions. / Holzner J., Suchandt S., Eineder M., Breit H., Adam N. // 2001. IGARSS '01. IEEE 2001 International Geoscience and Remote Sensing Symposium. - Sydney, NSW, 2001. - Vol. 1. - P. 393-395. 


C6990. Sadowy G. Technologies for the next generation of spaceborne precipitation radars. / Sadowy G., Berkun A., Durden S., Huang J., Im E., Lopez B., Lou M., Rahmat-Samii Y., Fan-Yun Liu, Rengarajan S. // IEEE Proceedings. Aerospace Conference, 2001. - Big Sky, MT, 2001. - Vol. 4. - P. 4/1811. 


C6991. Im E. The 94-GHz cloud profiling radar for the CloudSat mission. / Im E., Durden S.L., Chialin Wu, Livermore T.R. // IEEE Proceedings. Aerospace Conference, 2001. - Big Sky, MT, 2001. - Vol. 4. - P. 4/1803. 


C6992. Spencer M.W. Advanced design concepts for a SeaWinds scatterometer follow-on mission. / Spencer M.W., Huddleston J.N., Stiles B.W. // IEEE Proceedings. Aerospace Conference, 2001. - Big Sky, MT, 2001. - Vol. 4. - P. 4/1833. 


C6993. Huddleston J.N. SeaWinds: the QuikSCAT wind scatterometer. / Huddleston J.N., Spencer M.W. // IEEE Proceedings. Aerospace Conference, 2001. - Big Sky, MT, 2001. - Vol. 4. - P. 4/1825. 

C6994. Putney A. Synthetic aperture sonar-the modern method of underwater remote sensing. / Putney A., Chang E., Chatham R., Marx D., Nelson M., Warman L.K. // IEEE Proceedings. Aerospace Conference, 2001. - Big Sky, MT, 2001. - Vol. 4. - P. 4/1749. 

C6995. Malliot H.A. Concurrent storm damage data collection by high altitude airborne IFSAR. IEEE Proceedings. Aerospace Conference, 2001. - Big Sky, MT, 2001. - Vol. 2. - P. 2/695. 

C6996. Spitz S. A 94 GHz spaceborne cloud profiling radar antenna system. / Spitz S., Prata A. Jr., Harrell J., Perez R., Veruttipong W. // IEEE Proceedings. Aerospace Conference, 2001. - Big Sky, MT, 2001. - Vol. 2. - P. 2/685. 

C6997. Steyskal H. Pattern synthesis for TechSat21-a distributed spacebased radar system. / Steyskal H., Schindler J.K., Franchi P., Mailloux R.J. // IEEE Proceedings. Aerospace Conference, 2001. - Big Sky, MT, 2001. - Vol. 2. - P. 2/725. 

C6998. Hilland J. Dual frequency synthetic aperture radar (SAR) mission for monitoring Earth. / Hilland J., Bard S., Key R., Yunjin Kim, Vaze P., Huneycutt B. // IEEE Proceedings. Aerospace Conference, 2001. - Big Sky, MT, 2001. - Vol. 2. - P. 2/719. 

- C6999.** Njoku E. A spaceborne L-band radiometer-radar concept for land and ocean surface monitoring. / Njoku E., Yunjin Kim, Spencer M., Wu-Yang Tsai, Rahmat-Samii Y., Thomson M.W. // IEEE Proceedings. Aerospace Conference, 2001. - Big Sky, MT, 2001. - Vol. 4. - P. 4/1841. ↑
- C7000.** Kersten P.R. Segmenting polarimetric SAR images using robust competitive clustering. / Kersten P.R., Lee R.R.Y. // 2001. Joint 9th IFSA World Congress and 20th NAFIPS International Conference. - Vancouver, BC, 25-28 July 2001. - Vol. 2. - P. 1140-1144. ↑
- C7001.** Xiaohui Zhang. A new independent component analysis (ICA) method and its application to SAR images. / Xiaohui Zhang, Chen C.H. // 2001. Proceedings of the 2001 IEEE Signal Processing Society Workshop Neural Networks for Signal Processing XI. - North Falmouth, MA, 2001. - P. 283-292. ↑
- C7002.** Vavriv D.M. Cloud radar activities at the Institute of Radio Astronomy of the NAS of Ukraine. 2001. The Fourth International Kharkov Symposium on Physics and Engineering of Millimeter and Sub-Millimeter Waves. - Kharkov, 2001. - Vol. 1. - P. 85-89. ↑
- C7003.** {no data available}. Fourth International Kharkov Symposium 'Physics and Engineering of Millimeter and Sub-Millimeter Waves'. Symposium Proceedings (Cat. No.01EX429). 2001. The Fourth International Kharkov Symposium on Physics and Engineering of Millimeter and Sub-Millimeter Waves. 2001. - Vol. 1. - {no data available}. ↑
- C7004.** Vasudevan S. Refractivity estimation from radar clutter by sequential importance sampling with a Markov model for microwave propagation. / Vasudevan S., Krolik J.L. // 2001. Proceedings. (ICASSP '01). 2001 IEEE International Conference on Acoustics, Speech, and Signal Processing. - Salt Lake City, UT, 2001. - Vol. 5. - P. 2905-2908. ↑
- C7005.** Duren R.M. The SRTM sub-arcsecond metrology camera. / Duren R.M., Liebe C.C. // IEEE Proceedings. Aerospace Conference, 2001. - Big Sky, MT, 2001. - Vol. 4. - P. 4/2037. ↑
- C7006.** O'Neil S.D. Estimating road networks using archived GMTI data. IEEE Proceedings. Aerospace Conference, 2001. - Big Sky, MT, 2001. - Vol. 4. - P. 4/1865. ↑
- C7007.** Apostolopoulos D.S. Robotic Antarctic meteorite search: outcomes. / Apostolopoulos D.S., Pedersen L., Shamah B.N., Shillcutt K., Wagner M.D., Whittaker W.L. // 2001. Proceedings 2001 ICRA. IEEE International Conference on Robotics and Automation. 2001. - Vol. 4. - P. 4174-4179. ↑
- C7008.** Smith B.D. Automated planning for the Modified Antarctic Mapping Mission. / Smith B.D., Engelhardt B.E., Mutz D.H., Crawford J.P. // IEEE Proceedings. Aerospace Conference, 2001. - Big Sky, MT, 2001. - Vol. 1. - P. 1/151. ↑
- C7009.** Kish B.A. The computer replacement program for the joint surveillance target attack radar system. / Kish B.A., Gibboney W., Veth M., Moran M. // IEEE Proceedings. Aerospace Conference, 2001. - Big Sky, MT, 2001. - Vol. 5. - P. 2629-2638. ↑
- C7010.** Pellizzeri T.M. Detecting a step pattern of change in multitemporal SAR images. / Pellizzeri T.M., Lombardo P. // 2001. Proceedings of the 2001 IEEE Radar Conference. - Atlanta, GA, 2001. - P. 294-299. ↑
- C7011.** Lombardini F. Application of array processing techniques to multibaseline InSAR for layover solution. / Lombardini F., Gini F., Matteucci P. // 2001. Proceedings of the 2001 IEEE Radar Conference. - Atlanta, GA, 2001. - P. 210-215. ↑
- C7012.** De Maio A. On CFAR detection of oil slicks on the ocean surface by a multifrequency and/or multipolarization SAR. / De Maio A., Ricci G., Tesauro M. // 2001. Proceedings of the 2001 IEEE Radar Conference. - Atlanta, GA, 2001. - P. 351-356. ↑
- C7013.** Goodman N.A. A general signal processing algorithm for MTI with multiple receive apertures. / Goodman N.A., Stiles J.M. // 2001. Proceedings of the 2001 IEEE Radar Conference. - Atlanta, GA, 2001. - P. 315-320. ↑
- C7014.** Dunstan N. A cluster-based geophysical template matching system. / Dunstan N., Hodgson S. // 2001. ACSC 2001. Proceedings. 24th Australasian Computer Science Conference. - Gold Coast, Qld., 2001. - P. 54-59. ↑

- C7015.** Shimoi N. Smart sensing for mine detection studies with IR cameras. / Shimoi N., Takita Y., Nonami K., Wasaki K. // 2001. Proceedings 2001 IEEE International Symposium on Computational Intelligence in Robotics and Automation. 2001. - P. 356-361. ↑
- C7016.** Lohman B. A digital signal processor for Doppler radar sensing of vital signs. / Lohman B., Boric-Lubecke O., Lubecke V.M., Ong P.W., Sondhi M.M. // 2001. Proceedings of the 23rd Annual International Conference of the IEEE Engineering in Medicine and Biology Society. 2001. - Vol. 4. - P. 3359-3362. ↑
- C7017.** Hong K. Development of antenna-source system for generation of high-power electromagnetic pulses. / Hong K., Braidwood S. // 2001. PPPS-2001. Digest of Technical Papers Pulsed Power Plasma Science. 2001. - Vol. 1. - P. 203-206. ↑
- C7018.** Blonda P. Combination of multiple classifiers by fuzzy integrals: an application to synthetic aperture radar (SAR) data. / Blonda P., Tarantino C., D'Addabbo A., Satalino G., Pasquariello G. // 2001. The 10th IEEE International Conference on Fuzzy Systems. 2-5 Dec. 2001. - Vol. 2. - P. 944-947. ↑
- C7019.** Bessette L.A. Ultra-wideband P-3 and CARABAS II foliage attenuation and backscatter analysis. / Bessette L.A., Ayasli S. // 2001. Proceedings of the 2001 IEEE Radar Conference. - Atlanta, GA, 2001. - P. 357-362. ↑
- C7020.** Toth C.K. Sensor integration in airborne mapping. 2001. IMTC 2001. Proceedings of the 18th IEEE Instrumentation and Measurement Technology Conference. - Budapest, 2001. - Vol. 3. - P. 2000-2005. ↑
- C7021.** Duzdar A. Applications using a low-cost baseband pulsed microwave radar sensor. / Duzdar A., Kompa G. // 2001. IMTC 2001. Proceedings of the 18th IEEE Instrumentation and Measurement Technology Conference. - Budapest, 21-23 May 2001. - Vol. 1. - P. 239-243. ↑
- C7022.** Bachmann A. Multiprocessor digital signal processing on Earth orbiting scatterometers. / Bachmann A., Clark D., Lux J., Steme R. // IEEE Proceedings. Aerospace Conference, 2001. - Big Sky, MT, 2001. - Vol. 5. - P. 2241-2248. ↑
- C7023.** Dolya G.N. Opportunity of reduction of objects visibility using diffraction-reflecting coverings in conditions of application laser detection systems. / Dolya G.N., Katunin A.N., Moiseyeva G.A. // 2001. Proceedings of LFNМ 2001. 3rd International Workshop on Laser and Fiber-Optical Networks Modeling. - Kharkiv, 2001. - P. 136-139. ↑
- C7024.** Yen-Wei Chen. Estimating wind speed in lower atmosphere wind profiler based on genetic algorithms. / Yen-Wei Chen, Mendoza N., Uehara S., Nakao Z., Adachi T., Masuda Y. // 2001. IMTC 2001. Proceedings of the 18th IEEE Instrumentation and Measurement Technology Conference. - Budapest, 2001. - Vol. 2. - P. 1258-1263. ↑
- C7025.** Stiles J.M. Processing of multi-aperture SAR to produce fine-resolution images of arbitrarily large extent. / Stiles J.M., Goodman N. // 2001. Proceedings of the 2001 IEEE Radar Conference. - Atlanta, GA, 2001. - P. 451-456. ↑
- C7026.** Gamba P. Characterization of C-band and X-band InSAR data for 3D urban analysis. / Gamba P., Houshmand B. // 2001. Proceedings of the 2001 IEEE Radar Conference. - Atlanta, GA, 2001. - P. 415-420. ↑
- C7027.** Wilson C.L. The characteristics of rainfall and melting layer in Singapore: experimental results from radar and ground instruments. / Wilson C.L., Tan J. // 2001. Eleventh International Conference on (IEE Conf. Publ. No. 480) Antennas and Propagation. - Manchester, 2001. - Vol. 2. - P. 852-856. ↑
- C7028.** {no data available}. Eleventh International Conference on Antennas and Propagation (IEE Conf. Publ.No.480). 2001. Eleventh International Conference on (IEE Conf. Publ. No. 480) Antennas and Propagation. 17-20 April 2001. - Vol. 1. - {no data available}. ↑
- C7029.** Shkvarko Y. Data aggregation approach to multisensor radar imaging. / Shkvarko Y., Jaime-Rivas R. // 2001. The Fourth International Kharkov Symposium on Physics and Engineering of Millimeter and Sub-Millimeter Waves. - Kharkov, 2001. - Vol. 1. - P. 247-249. ↑
- C7030.** Droitcour A. A microwave radio for Doppler radar sensing of vital signs. / Droitcour A., Lubecke V., Jenshan Lin, Boric-Lubecke O. // 2001 IEEE MTT-S International Microwave Symposium Digest. - Phoenix, AZ,

2001. - Vol. 1. - P. 175-178. ↑

C7031. Mangogna A.J. Development of a helicopter obstacle detection and air data system. 2001. DASC. The 20th Conference Digital Avionics Systems. - Daytona Beach, FL, 14-18 Oct 2001. - Vol. 1. - P. 1A4/1. ↑

C7032. Takeuchi N. Continuous monitoring of atmosphere by compact automated lidar. 2001. CLEO/Pacific Rim 2001. The 4th Pacific Rim Conference on Lasers and Electro-Optics. - Chiba, 2001. - Vol. 1. - P. I-158-I-159-158. ↑

C7033. Smith M. K-band direct detect MMIC Si micromachined radiometer. / Smith M., Weller T., Culver J., Roeder B., Trent C., Naylor J. // 2001 IEEE MTT-S International Microwave Symposium Digest. - Phoenix, AZ, 2001. - Vol. 3. - P. 2255-2258. ↑

C7034. Marcos De Moraes R. A low-cost solution for obtaining remote sensing images. 2001 Proceedings of XIV Brazilian Symposium on Computer Graphics and Image Processing. - Florianopolis, Oct 2001. - P. 405. ↑

C7035. Dybdal R.B. System measurement of antennas. 2001. IEEE Antennas and Propagation Society International Symposium. - Boston, MA, 2001. - Vol. 4. - P. 616-619. ↑

C7036. Polat B. Ground penetrating radar imaging of buried metallic objects. / Polat B., Meincke P. // 2001. IEEE Antennas and Propagation Society International Symposium. - Boston, MA, 2001. - Vol. 4. - P. 264-267. ↑

C7037. Hong K.D. Development of antenna-source system for high-power electromagnetic pulse generation. / Hong K.D., Braidwood S.W. // 2001. IEEE Conference Record-Abstracts Pulsed Power Plasma Science. - Las Vegas, NV, 2001. - P. 250. ↑

C7038. {no data available}. IEEE Antennas and Propagation Society International Symposium. 2001 Digest. Held in conjunction with: USNC/URSI National Radio Science Meeting (Cat. No.01CH37229). 2001. IEEE Antennas and Propagation Society International Symposium. 2001. - Vol. 2. - {no data available}. ↑

C7039. Sugimoto N. Development of a two-color dual-polarization pulsed bistatic lidar for measuring water cloud droplet size. / Sugimoto N., Shimizu A., Matsui I. // 2001. CLEO/Pacific Rim 2001. The 4th Pacific Rim Conference on Lasers and Electro-Optics. - Chiba, 2001. - Vol. 1. - P. I-160-I-161-160. ↑

C7040. Yang Shaolin. Super-resolution ocean surface current algorithm based on MUSIC for OSMAR2000. / Yang Shaolin, Ke Hengyu, Hou Jiechang, Wu Shicai, Yang Zijie, Wen Biyang, Wu Xiongbin. // 2001. MTS/IEEE Conference and Exhibition OCEANS. - Honolulu, HI, 2001. - Vol. 2. - P. 930-941. ↑

C7041. Yi Xu. Direction of arrival estimation using super-resolution algorithm. / Yi Xu, Wei Feng Feng, Jun Yan Hao, Hwang H.K. // 2001. MTS/IEEE Conference and Exhibition OCEANS. - Honolulu, HI, 2001. - Vol. 2. - P. 749-755. ↑

C7042. Yang Shaolin. Detection of the number of signals in super-resolution ocean surface current algorithm for OSMAR2000. / Yang Shaolin, Ke Hengyu, Hou Jiechang, Wu Xiongbin, Tian Jiansheng, Wen Biyang. // 2001. MTS/IEEE Conference and Exhibition OCEANS. - Honolulu, HI, 2001. - Vol. 2. - P. 962-966. ↑

C7043. Vesecky J. Multifrequency HF radar observations of surface currents: measurements from different systems and environments. / Vesecky J., Drake J., Plume M., Teague C., Meadows L., Fernandez Y., Davidson K., Paduan J. // 2001. MTS/IEEE Conference and Exhibition OCEANS. - Honolulu, HI, 2001. - Vol. 2. - P. 942-948. ↑

C7044. Hutchinson J.A. U.S. CELRAP laser radar design considerations. / Hutchinson J.A., Trussell C.W., Allik T.H., Hamlin S.J. // 2001. CLEO/Pacific Rim 2001. The 4th Pacific Rim Conference on Lasers and Electro-Optics. - Chiba, 2001. - Vol. 1. - P. I-576-I-577-576. ↑

C7045. Widada W. Iterative correction of multiple-scattering effects in Mie-scattering lidar signals. / Widada W., Minomura M., Kuze H., Takeuchi N. // 2001. CLEO/Pacific Rim 2001. The 4th Pacific Rim Conference on Lasers and Electro-Optics. - Chiba, 2001. - Vol. 1. - P. I-166-I-167-166. ↑

C7046. Nianwen Cao. DIAL measurement of daytime variations of vertical tropospheric O₃ concentration profiles. / Nianwen Cao, Fukuchi T., Nayuki T., Fujii T., Nemoto K., Takeuchi N. // 2001. CLEO/Pacific Rim 2001. The 4th Pacific Rim Conference on Lasers and Electro-Optics. - Chiba, 2001. - Vol. 1. - P. I-164-I-165-164. ↑

- C7047.** Kobayashi T. UV Rayleigh lidar system for accurate temperature profiling of the troposphere. / Kobayashi T., Imaki M. // 2001. CLEO/Pacific Rim 2001. The 4th Pacific Rim Conference on Lasers and Electro-Optics. - Chiba, 2001. - Vol. 1. - P. I-174-I-175-174. ↑
- C7048.** Itabe T. Development of ISS/JEM-borne coherent Doppler lidar. / Itabe T., Mizutani K., Ishizu M., Ishii S., Asai K. // 2001. CLEO/Pacific Rim 2001. The 4th Pacific Rim Conference on Lasers and Electro-Optics. - Chiba, 2001. - Vol. 1. - P. I-168-I-169-168. ↑
- C7049.** Budko N.V. Linearized multi-frequency inversion of ground penetrating radar data. / Budko N.V., van den Berg P.M. // 2001. IEEE Antennas and Propagation Society International Symposium. - Boston, MA, 2001. - Vol. 4. - P. 256-259. ↑
- C7050.** Chekalyuk A.M. Superactive pump-and-probe LIDAR technology: biophysical insight into aquatic remote sensing. / Chekalyuk A.M., Hoge F.E., Swift R.N. // 2001. CLEO '01. Technical Digest. Summaries of papers presented at the Conference on Lasers and Electro-Optics. - Baltimore, MD, 2001. - P. 492-493. ↑
- C7051.** Morbi Z. Short range spectral lidar using mid-infrared semiconductor laser with code-division multiplexing technique. / Morbi Z., Ho D.B., Zhang H.-L., Ren H.-W., Le H.Q., Pei S.S. // 2001. CLEO '01. Technical Digest. Summaries of papers presented at the Conference on Lasers and Electro-Optics. - Baltimore, MD, 2001. - P. 491-492. ↑
- C7052.** Frey S. Laser remote sensing for characterization of planetary boundary layer properties. / Frey S., Geurts W., Woste L. // 2001. CLEO '01. Technical Digest. Summaries of papers presented at the Conference on Lasers and Electro-Optics. - Baltimore, MD, 2001. - P. 494. ↑
- C7053.** Andersen G. Holographic Raman and Rayleigh lidar. / Andersen G., Knize R.J., Dills A., Sawruk N., Ziarnick B. // 2001. CLEO '01. Technical Digest. Summaries of papers presented at the Conference on Lasers and Electro-Optics. - Baltimore, MD, 2001. - P. 493-494. ↑
- C7054.** Tecpoyotl-T M. Millimeter wave and infrared electronics for investigations of acoustic-electromagnetic phenomena due to activity of Popocatepetl volcano. / Tecpoyotl-T M., Solov'yev D., Grimalsky V., Torres-J A., De La Hidalgo-W J., Kishenko Ya. // 2001. The Fourth International Kharkov Symposium on Physics and Engineering of Millimeter and Sub-Millimeter Waves. - Kharkov, 2001. - Vol. 2. - P. 759-761. ↑
- C7055.** Kirichenko V.A. Experimental study of spectra and X- and Ka-band backscattering from the rain agitated water surface. / Kirichenko V.A., Logvinov Yu.F., Pedenko Yu.A., Razskazovsky V.B. // 2001. The Fourth International Kharkov Symposium on Physics and Engineering of Millimeter and Sub-Millimeter Waves. - Kharkov, 2001. - Vol. 1. - P. 423-425. ↑
- C7056.** Senko V.I. Experimental research of the spectral, polarizing and azimuthal features of the S-, Ka- and V-band backscattering by the water and petroleum surfaces. / Senko V.I., Uzlenkov A.V. // 2001. The Fourth International Kharkov Symposium on Physics and Engineering of Millimeter and Sub-Millimeter Waves. - Kharkov, 2001. - Vol. 1. - P. 408-410. ↑
- C7057.** Yanovsky F.J. Model of drop canting in microwave remote sensing of rain. / Yanovsky F.J., Russchenberg H.W.J., Ligthart L.P., Aver'yanova Yu.A. // 2001. The Fourth International Kharkov Symposium on Physics and Engineering of Millimeter and Sub-Millimeter Waves. - Kharkov, 2001. - Vol. 1. - P. 471-473. ↑
- C7058.** Lukin V. mm-band radar image filtering with texture information preservation. / Lukin V., Tsymbal O. // 2001. The Fourth International Kharkov Symposium on Physics and Engineering of Millimeter and Sub-Millimeter Waves. - Kharkov, 2001. - Vol. 1. - P. 435-437. ↑
- C7059.** De Young R.J. A narrow band fiber Bragg grating filter for lidar receivers. 2001. CLEO '01. Technical Digest. Summaries of papers presented at the Conference on Lasers and Electro-Optics. - Baltimore, MD, 2001. - P. 494-495. ↑
- C7060.** Pizurica A. Despeckling SAR images using wavelets and a new class of adaptive shrinkage estimators. / Pizurica A., Philips W., Lemahieu I., Acheroy M. // 2001. Proceedings. 2001 International Conference on Image Processing. - Thessaloniki, 7-10 Oct 2001. - Vol. 2. - P. 233-236. ↑
- C7061.** Torres-Torriti M. Gabor vs. GMRF features for SAR imagery classification. / Torres-Torriti M., Jouan A. // 2001. Proceedings. 2001 International Conference on Image Processing. - Thessaloniki, 2001. - Vol. 3. - P. ↑

1043-1046. ↑

C7062. Barbaresco F. Rain clouds tracking with radar image processing based on morphological skeleton matching. / Barbaresco F., Monnier B. // 2001. Proceedings. 2001 International Conference on Image Processing. - Thessaloniki, 2001. - Vol. 1. - P. 830-833. ↑

C7063. Ya-Qiu Jin. Simulation of radar echo from a ship in ocean clutter using the GFBM/SAA method. / Ya-Qiu Jin, Zhongxin Li. // 2001. IEEE Antennas and Propagation Society International Symposium. - Boston, MA, 2001. - Vol. 1. - P. 320-323. ↑

C7064. Chen X. 3D regularized velocity from 3D Doppler radial velocity. / Chen X., Barron J.L., Mercer R.E., Joe P. // 2001. Proceedings. 2001 International Conference on Image Processing. - Thessaloniki, 2001. - Vol. 3. - P. 664-667. ↑

C7065. Bhogall A.S.P. Extraction of forest attribute information using multisensor data fusion techniques: a case study for a test site on Vancouver Island, British Columbia. / Bhogall A.S.P., Goodenough D.G., Dyk A., Chen H., Niemann K.O., West C. // 2001. PACRIM. 2001 IEEE Pacific Rim Conference on Communications, Computers and signal Processing. - Victoria, BC, 2001. - Vol. 2. - P. 674-680. ↑

C7066. Songsheng Chen. 30-mJ, 30-Hz, and 300-nm ultraviolet laser source generated by a frequency-tripled Ti:sapphire laser [for DIAL]. / Songsheng Chen, Petway L.B., Meadows B.L., Elsayed K.A., Marsh W.D., Edwards W.C., Barnes J.C. // 2001. CLEO '01. Technical Digest. Summaries of papers presented at the Conference on Lasers and Electro-Optics. - Baltimore, MD, 2001. - P. 506. ↑

C7067. Elkhetali S. Two and three dimensional images of shallow geological structures. 2001. TELSIKS 2001. 5th International Conference on Telecommunications in Modern Satellite, Cable and Broadcasting Service. - Nis, 2001. - Vol. 2. - P. 434-435. ↑

C7068. Karlsen B. Comparison of PCA and ICA based clutter reduction in GPR systems for anti-personal landmine detection. / Karlsen B., Larsen J., Sorensen H.B.D., Jakobsen K.B. // 2001. Proceedings of the 11th IEEE Signal Processing Workshop on Statistical Signal Processing. 2001. - P. 146-149. ↑

C7069. Manore M.J. Multi-polarization SAR data for operational ice monitoring. / Manore M.J., Flett D.G., De Abreu R.A., Ramsay B.R., van der Sanden J.J. // 2001. IGARSS '01. IEEE 2001 International Geoscience and Remote Sensing Symposium. - Sydney, NSW, 2001. - Vol. 3. - P. 1246-1248. ↑

C7070. Nghiem S.V. Multi-polarization C-band SAR signatures of arctic sea ice. / Nghiem S.V., Bertoia C. // 2001. IGARSS '01. IEEE 2001 International Geoscience and Remote Sensing Symposium. - Sydney, NSW, 2001. - Vol. 3. - P. 1243-1245. ↑

C7071. Karvonen J. Independent component analysis for sea ice SAR image classification. / Karvonen J., Simila M. // 2001. IGARSS '01. IEEE 2001 International Geoscience and Remote Sensing Symposium. - Sydney, NSW, 2001. - Vol. 3. - P. 1255-1257. ↑

C7072. Johannessen O.M. Seasonal sea ice studies in the Kara Sea region using satellite radar data. / Johannessen O.M., Sandven S., Pettersson L.H., Lundhaug M., Dalen O., Alexandrov V.Yu. // 2001. IGARSS '01. IEEE 2001 International Geoscience and Remote Sensing Symposium. - Sydney, NSW, 2001. - Vol. 3. - P. 1252-1254. ↑

C7073. Wright C.W. Bathymetric effects on a tropical cyclone wave field at landfall. / Wright C.W., Walsh E.J., Vandemark D., Krabill W.B. // 2001. IGARSS '01. IEEE 2001 International Geoscience and Remote Sensing Symposium. - Sydney, NSW, 2001. - Vol. 3. - P. 1237-1239. ↑

C7074. Akimov D.B. On the radar imaging of the sea frontal zone: "CoastWatch-95" experiment and its analysis. / Akimov D.B., Johannessen O.M., Kudryavtsev V.N. // 2001. IGARSS '01. IEEE 2001 International Geoscience and Remote Sensing Symposium. - Sydney, NSW, 2001. - Vol. 3. - P. 1228-1230. ↑

C7075. Xiaofeng Li. Analysis of oceanic long wave refraction at the Gulf Stream boundary using RADARSAT synthetic aperture radar during Hurricane Bonnie. / Xiaofeng Li, Mingxia He, Pichel W.G., Kan Zeng, Friedman K.S., Clemente-Colon P., Laibu Wang, Chaofang Zhao. // 2001. IGARSS '01. IEEE 2001 International Geoscience and Remote Sensing Symposium. - Sydney, NSW, 2001. - Vol. 3. - P. 1225-1227. ↑

- C7076.** Fujisaki K. A proposal of measuring ocean wavelengths by satellite altimeters. / Fujisaki K., Tateiba M. // 2001. IGARSS '01. IEEE 2001 International Geoscience and Remote Sensing Symposium. - Sydney, NSW, 2001. - Vol. 3. - P. 1234-1236. ↑
- C7077.** Schulz-Stellenfleth J. Global tracking of swell with complex ERS-2 wave mode data. / Schulz-Stellenfleth J., Hoja D., Lehner S. // 2001. IGARSS '01. IEEE 2001 International Geoscience and Remote Sensing Symposium. - Sydney, NSW, 2001. - Vol. 3. - P. 1231-1233. ↑
- C7078.** Shokr M. Study of sea ice in North Water Polynya using multi-sensor spaceborne data. 2001. IGARSS '01. IEEE 2001 International Geoscience and Remote Sensing Symposium. - Sydney, NSW, 2001. - Vol. 3. - P. 1259-1261. ↑
- C7079.** Davidson M.W.J. Improving soil moisture retrieval by incorporating a priori information on roughness parameters. / Davidson M.W.J., Le Toan T., Mattia F., Satalino G., Verhoest N.E.C., Borgeaud M. // 2001. IGARSS '01. IEEE 2001 International Geoscience and Remote Sensing Symposium. - Sydney, NSW, 2001. - Vol. 3. - P. 1306-1308. ↑
- C7080.** Grippa M. Backscattering model validity across large footprints for global scatterometer applications. / Grippa M., Woodhouse I.H. // 2001. IGARSS '01. IEEE 2001 International Geoscience and Remote Sensing Symposium. - Sydney, NSW, 2001. - Vol. 3. - P. 1303-1305. ↑
- C7081.** Walsh E.J. Observations of sea surface mean square slope during the Southern Ocean Waves Experiment. / Walsh E.J., Vandemark D.C., Wright C.W., Banner M.L., Swift R.N., Scott J.F., Hines D.E., Jensen J., Lee S. // 2001. IGARSS '01. IEEE 2001 International Geoscience and Remote Sensing Symposium. - Sydney, NSW, 2001. - Vol. 3. - P. 1318-1320. ↑
- C7082.** Bell D. A multistaged approach to mapping soil salinity in a tropical coastal environment using airborne SAR and Landsat TM data. / Bell D., Menges C.H., Bartolo R.E., Ahmad W., VanZyl J.J. // 2001. IGARSS '01. IEEE 2001 International Geoscience and Remote Sensing Symposium. - Sydney, NSW, 2001. - Vol. 3. - P. 1309-1311. ↑
- C7083.** Teague C.C. Canal and river tests of a RiverSonde streamflow measurement system. / Teague C.C., Barrick D.E., Lilleboe P., Cheng R.T. // 2001. IGARSS '01. IEEE 2001 International Geoscience and Remote Sensing Symposium. - Sydney, NSW, 2001. - Vol. 3. - P. 1288-1290. ↑
- C7084.** Clarke T.R. Planar domain indices: a method for measuring a quality of a single component in two-component pixels. / Clarke T.R., Moran M.S., Barnes E.M., Pinter P.J. Jr., Qi J. // 2001. IGARSS '01. IEEE 2001 International Geoscience and Remote Sensing Symposium. - Sydney, NSW, 2001. - Vol. 3. - P. 1279-1281. ↑
- C7085.** Inoue Y. Interactions between multi-frequency microwave backscatters and rice canopy variables. / Inoue Y., Dabrowska-Zielinska K., Kurosu T., Maeno H., Uratsuka S., Kozu T. // 2001. IGARSS '01. IEEE 2001 International Geoscience and Remote Sensing Symposium. - Sydney, NSW, 2001. - Vol. 3. - P. 1270-1272. ↑
- C7086.** Franceschetti G. An electromagnetic model for scattering from buildings. / Franceschetti G., Lodice A., Riccio D. // 2001. IGARSS '01. IEEE 2001 International Geoscience and Remote Sensing Symposium. - Sydney, NSW, 2001. - Vol. 3. - P. 1285-1287. ↑
- C7087.** Lee W.K. Analytical investigation of urban SAR features having a group of corner reflectors. 2001. IGARSS '01. IEEE 2001 International Geoscience and Remote Sensing Symposium. - Sydney, NSW, 2001. - Vol. 3. - P. 1282-1284. ↑
- C7088.** Clausi D.A. Improved texture recognition of SAR sea ice imagery by data fusion of MRF features with traditional methods. 2001. IGARSS '01. IEEE 2001 International Geoscience and Remote Sensing Symposium. - Sydney, NSW, 2001. - Vol. 3. - P. 1170-1172. ↑
- C7089.** Yunjin Kim. Polarimetric and interferometric SAR calibration verification methods. / Yunjin Kim, van Zyl J. // 2001. IGARSS '01. IEEE 2001 International Geoscience and Remote Sensing Symposium. - Sydney, NSW, 2001. - Vol. 3. - P. 1098-1100. ↑
- C7090.** Isola M. Forest height mapping using space-borne polarimetric SAR interferometry. / Isola M., Cloude S.R. // 2001. IGARSS '01. IEEE 2001 International Geoscience and Remote Sensing Symposium. - Sydney, NSW, 2001. - Vol. 3. - P. 1095-1097. ↑

- C7091.** Mora O. Long-term subsidence monitoring of urban areas using differential interferometric SAR techniques. / Mora O., Mallorqui J.J., Duro J., Broquetas A. // 2001. IGARSS '01. IEEE 2001 International Geoscience and Remote Sensing Symposium. - Sydney, NSW, 2001. - Vol. 3. - P. 1104-1106. ↑
- C7092.** Yamada H. Polarimetric SAR interferometry for forest canopy analysis by using the super-resolution method. / Yamada H., Yamaguchi Y., Rodriguez E., Kim Y., Boerner W.M. // 2001. IGARSS '01. IEEE 2001 International Geoscience and Remote Sensing Symposium. - Sydney, NSW, 2001. - Vol. 3. - P. 1101-1103. ↑
- C7093.** Boernerl W.-M. Recent advances in extra-wide-band multi-modal POL-IN-SAR imaging. / Boernerl W.-M., Jong-Sen Lee. // 2001. IGARSS '01. IEEE 2001 International Geoscience and Remote Sensing Symposium. - Sydney, NSW, 2001. - Vol. 3. - P. 1092-1094. ↑
- C7094.** Wentz F.J. Advanced algorithms for QuikScat and SeaWinds/AMSR. / Wentz F.J., Smith D.K., Mears C.A., Gentemann C.L. // 2001. IGARSS '01. IEEE 2001 International Geoscience and Remote Sensing Symposium. - Sydney, NSW, 2001. - Vol. 3. - P. 1079-1081. ↑
- C7095.** Portabella M. Development of a SeaWinds wind product for weather forecasting. / Portabella M., Stoffelen A., de Vries J. // 2001. IGARSS '01. IEEE 2001 International Geoscience and Remote Sensing Symposium. - Sydney, NSW, 2001. - Vol. 3. - P. 1076-1078. ↑
- C7096.** Yueh S.H. QuikSCAT geophysical model function for hurricane wind and rain. / Yueh S.H., Stiles B., Wu-Yang Tsai, Hua Hu, Liu W.T. // 2001. IGARSS '01. IEEE 2001 International Geoscience and Remote Sensing Symposium. - Sydney, NSW, 2001. - Vol. 3. - P. 1089-1091. ↑
- C7097.** Ebuchi N. Evaluation of wind vectors observed by QuikSCAT/SeaWinds using ocean buoy data. 2001. IGARSS '01. IEEE 2001 International Geoscience and Remote Sensing Symposium. - Sydney, NSW, 2001. - Vol. 3. - P. 1082-1085. ↑
- C7098.** Kenyi L.W. Estimation of alpine permafrost surface deformation using InSAR data. / Kenyi L.W., Kaufmann V. // 2001. IGARSS '01. IEEE 2001 International Geoscience and Remote Sensing Symposium. - Sydney, NSW, 2001. - Vol. 3. - P. 1107-1109. ↑
- C7099.** Touzi R. Multiplicative and product model constraints upon speckle filtering of SAR images. 2001. IGARSS '01. IEEE 2001 International Geoscience and Remote Sensing Symposium. - Sydney, NSW, 2001. - Vol. 3. - P. 1161-1163. ↑
- C7100.** Stringa E. Soft morphology and Bayesian reconstruction for SAR image filtering. / Stringa E., Smits P.C. // 2001. IGARSS '01. IEEE 2001 International Geoscience and Remote Sensing Symposium. - Sydney, NSW, 2001. - Vol. 3. - P. 1158-1160. ↑
- C7101.** Notarnicola C. Bayesian fusion of active and passive microwave data for estimating bare soil water content. / Notarnicola C., Posa F. // 2001. IGARSS '01. IEEE 2001 International Geoscience and Remote Sensing Symposium. - Sydney, NSW, 2001. - Vol. 3. - P. 1167-1169. ↑
- C7102.** Tupin F. Markovian methods for SAR image processing. 2001. IGARSS '01. IEEE 2001 International Geoscience and Remote Sensing Symposium. - Sydney, NSW, 2001. - Vol. 3. - P. 1164-1166. ↑
- C7103.** Chiu L.S. Diurnal cycle of oceanic precipitation from microwave radiometry. / Chiu L.S., Chang A.T.-C. // 2001. IGARSS '01. IEEE 2001 International Geoscience and Remote Sensing Symposium. - Sydney, NSW, 2001. - Vol. 3. - P. 1140-1142. ↑
- C7104.** Contreras R.F. A climatology of tropical instability waves using the ERS-1 and -2 scatterometers. / Contreras R.F., Wallace J.M. // 2001. IGARSS '01. IEEE 2001 International Geoscience and Remote Sensing Symposium. - Sydney, NSW, 2001. - Vol. 3. - P. 1131-1133. ↑
- C7105.** Hellmann M. Discrimination between low metal content mine and non-mine-targets using polarimetric ultra-wide-band radar. / Hellmann M., Cloude S.R. // 2001. IGARSS '01. IEEE 2001 International Geoscience and Remote Sensing Symposium. - Sydney, NSW, 2001. - Vol. 3. - P. 1113-1115. ↑
- C7106.** Espedal H.A. WEMSAR-wind energy mapping using synthetic aperture radar. / Espedal H.A., Johannessen O.M., Furevik B., Sandven S., Hasager C.B., Christensen L.C., Gaudiosi G. // 2001. IGARSS '01. IEEE 2001 International Geoscience and Remote Sensing Symposium. - Sydney, NSW, 2001. - Vol. 3. - P.

1137-1139. ↑

C7107. Teague C.C. Effective depth of HF current measurements: observations from COPE-3. / Teague C.C., Vesecky J.F., Hallock Z.R. // 2001. IGARSS '01. IEEE 2001 International Geoscience and Remote Sensing Symposium. - Sydney, NSW, 2001. - Vol. 3. - P. 1134-1136. ↑

C7108. Strozzi T. SAR interferometry confirms the present land stability of Venice. / Strozzi T., Tosi L., Teatini P., Wegmuller U., Carbognin L., Werner C., Wiesmann A. // 2001. IGARSS '01. IEEE 2001 International Geoscience and Remote Sensing Symposium. - Sydney, NSW, 2001. - Vol. 3. - P. 1321-1323. ↑

C7109. Preiss M. The effect of polar format resampling on uncompensated motion phase errors and the phase gradient autofocus algorithm. / Preiss M., Gray D., Stacy N.J.S. // 2001. IGARSS '01. IEEE 2001 International Geoscience and Remote Sensing Symposium. - Sydney, NSW, 2001. - Vol. 3. - P. 1442-1444. ↑

C7110. Kwag Y.K. Spaceborne X-band small SAR system model design and its imaging performance characteristics. 2001. IGARSS '01. IEEE 2001 International Geoscience and Remote Sensing Symposium. - Sydney, NSW, 2001. - Vol. 3. - P. 1439-1441. ↑

C7111. Hua Xie. Spatially adaptive radar speckle reduction using wavelet denoising and Markov random fields. / Hua Xie, Pierce L.E., Ulaby F.T. // 2001. IGARSS '01. IEEE 2001 International Geoscience and Remote Sensing Symposium. - Sydney, NSW, 2001. - Vol. 3. - P. 1499-1502. ↑

C7112. Pellizzeri T.M. A maximum likelihood approach for detecting a step pattern of change and locating the transition instant in a sequence of multitemporal SAR images. / Pellizzeri T.M., Lombardo P. // 2001. IGARSS '01. IEEE 2001 International Geoscience and Remote Sensing Symposium. - Sydney, NSW, 2001. - Vol. 3. - P. 1484-1486. ↑

C7113. Madsen S.N. Motion compensation for ultra wide band SAR. 2001. IGARSS '01. IEEE 2001 International Geoscience and Remote Sensing Symposium. - Sydney, NSW, 2001. - Vol. 3. - P. 1436-1438. ↑

C7114. Benz U. Object based analysis of polarimetric SAR data in alpha-entropy-anisotropy decomposition using fuzzy classification by eCognition. / Benz U., Pottier E. // 2001. IGARSS '01. IEEE 2001 International Geoscience and Remote Sensing Symposium. - Sydney, NSW, 2001. - Vol. 3. - P. 1427-1429. ↑

C7115. Ulbricht A. Applying polarimetric interferometric methods to invert vegetation parameters from SAR-data. / Ulbricht A., Fabregas X., Sagues L. // 2001. IGARSS '01. IEEE 2001 International Geoscience and Remote Sensing Symposium. - Sydney, NSW, 2001. - Vol. 3. - P. 1424-1426. ↑

C7116. Shengli Dai. The latest development of high resolution imaging for forward looking SAR with multiple receiving antennas. / Shengli Dai, Min Liu, Yajun Sun, Wiesbeck W. // 2001. IGARSS '01. IEEE 2001 International Geoscience and Remote Sensing Symposium. - Sydney, NSW, 2001. - Vol. 3. - P. 1433-1435. ↑

C7117. Shimada M. Tree height estimation using an airborne L-band polarimetric interferometric SAR. / Shimada M., Muhtar Q., Tadono T., Wakabayashi H. // 2001. IGARSS '01. IEEE 2001 International Geoscience and Remote Sensing Symposium. - Sydney, NSW, 2001. - Vol. 3. - P. 1430-1432. ↑

C7118. Nicolas J.M. Smoothing speckled SAR images by using maximum homogeneous region filters: an improved approach. / Nicolas J.M., Tupin F., Maitre H. // 2001. IGARSS '01. IEEE 2001 International Geoscience and Remote Sensing Symposium. - Sydney, NSW, 2001. - Vol. 3. - P. 1503-1505. ↑

C7119. Langman A. Pulse versus stepped frequency continuous wave modulation for ground penetrating radar. / Langman A., Inggis M.R. // 2001. IGARSS '01. IEEE 2001 International Geoscience and Remote Sensing Symposium. - Sydney, NSW, 2001. - Vol. 3. - P. 1533-1535. ↑

C7120. Ebihara S. Application of an optical electric field sensor array for direction of arrival estimation in a borehole. / Ebihara S., Sato M. // 2001. IGARSS '01. IEEE 2001 International Geoscience and Remote Sensing Symposium. - Sydney, NSW, 2001. - Vol. 3. - P. 1530-1532. ↑

C7121. Witte C. Quantifying riparian vegetation and stream bank form through the use of airborne laser scanning and digital video data. / Witte C., Dowling R., Weller D., Denham R., Rowland T. // 2001. IGARSS '01. IEEE 2001 International Geoscience and Remote Sensing Symposium. - Sydney, NSW, 2001. - Vol. 3. - P. 1545-1548. ↑

- C7122.** Greidanus H. Assessment of the coastal maritime environment with airborne mid-wave infrared imagery. 2001. IGARSS '01. IEEE 2001 International Geoscience and Remote Sensing Symposium. - Sydney, NSW, 2001. - Vol. 3. - P. 1542-1544. ↑
- C7123.** Walker P.D. Non-iterative GPR imaging through a non-planar air-ground interface. / Walker P.D., Bell M.R. // 2001. IGARSS '01. IEEE 2001 International Geoscience and Remote Sensing Symposium. - Sydney, NSW, 2001. - Vol. 3. - P. 1527-1529. ↑
- C7124.** Garrison J.L. Simulation of wind speed retrievals from an orbiting bistatic GPS receiver. 2001. IGARSS '01. IEEE 2001 International Geoscience and Remote Sensing Symposium. - Sydney, NSW, 2001. - Vol. 3. - P. 1515-1517. ↑
- C7125.** Sant'Anna S.J.S. Textural method to evaluate speckle noise filters based on AR-2D models using P-band radar data. / Sant'Anna S.J.S., Freitas C.C., Fernandes D., Dutra L.V. // 2001. IGARSS '01. IEEE 2001 International Geoscience and Remote Sensing Symposium. - Sydney, NSW, 2001. - Vol. 3. - P. 1506-1508. ↑
- C7126.** Leuschen C.J. Simulation and design of ground-penetrating radar for Mars exploration. / Leuschen C.J., Gogineni S.P., Clifford S.M., Raney R.K. // 2001. IGARSS '01. IEEE 2001 International Geoscience and Remote Sensing Symposium. - Sydney, NSW, 2001. - Vol. 3. - P. 1524-1526. ↑
- C7127.** Emery W.J. Student Reflected GPS Experiment (SuRGE). / Emery W.J., Axelrad P., Nerem R.S., Masters D., Armatys M., Komjathy A. // 2001. IGARSS '01. IEEE 2001 International Geoscience and Remote Sensing Symposium. - Sydney, NSW, 2001. - Vol. 3. - P. 1518-1520. ↑
- C7128.** Lucas R.M. Synthetic aperture radar for woodland biomass estimation in Australia: an overview. / Lucas R.M., Milne A.K. // 2001. IGARSS '01. IEEE 2001 International Geoscience and Remote Sensing Symposium. - Sydney, NSW, 2001. - Vol. 3. - P. 1421-1423. ↑
- C7129.** Paillou P. Sub-surface imaging by combining airborne SAR and GPR: application to water detection in arid zones. / Paillou P., August-Bernex T., Grandjean G., Dreuillet P., Achache J. // 2001. IGARSS '01. IEEE 2001 International Geoscience and Remote Sensing Symposium. - Sydney, NSW, 2001. - Vol. 3. - P. 1384-1386. ↑
- C7130.** van den Berg P.M. Imaging and inversion of buried objects using GPR. / van den Berg P.M., Abubakar A., Budko N.V., Remis R.F. // 2001. IGARSS '01. IEEE 2001 International Geoscience and Remote Sensing Symposium. - Sydney, NSW, 2001. - Vol. 3. - P. 1377-1380. ↑
- C7131.** Moller D. PacRIM II: a review of AirSAR operations and system performance. / Moller D., Anhua Chu, Yunling Lou, Miller T., O'Leary E. // 2001. IGARSS '01. IEEE 2001 International Geoscience and Remote Sensing Symposium. - Sydney, NSW, 2001. - Vol. 3. - P. 1389-1391. ↑
- C7132.** Tapley I.J. An overview of the PACRIM 2000 Airborne Synthetic Aperture Radar (AIRSAR) mission in the Pacific, Australia and Asian region. / Tapley I.J., Milne A.K., O'Leary E. // 2001. IGARSS '01. IEEE 2001 International Geoscience and Remote Sensing Symposium. - Sydney, NSW, 2001. - Vol. 3. - P. 1387-1388. ↑
- C7133.** Picard G. A second order backscatter model for wheat canopies. Formulation and comparison with data. / Picard G., Le Toan T., Davidson M., Melon P. // 2001. IGARSS '01. IEEE 2001 International Geoscience and Remote Sensing Symposium. - Sydney, NSW, 2001. - Vol. 3. - P. 1368-1370. ↑
- C7134.** Lucas R.M. Development of multistage procedures for quantifying the biomass, structure and community composition of Australian woodlands using polarimetric radar and optical data. / Lucas R.M., Tickle P., Witte C., Milne A.K. // 2001. IGARSS '01. IEEE 2001 International Geoscience and Remote Sensing Symposium. - Sydney, NSW, 2001. - Vol. 3. - P. 1353-1355. ↑
- C7135.** De Grandi G.F. A vegetation map of the Central Congo basin derived from microwave and optical remote sensing data using a variable resolution classification approach. / De Grandi G.F., Mayaux P., Massart M., Baraldi A., Sgrenzaroli M. // 2001. IGARSS '01. IEEE 2001 International Geoscience and Remote Sensing Symposium. - Sydney, NSW, 2001. - Vol. 3. - P. 1350-1352. ↑
- C7136.** Sarabandi K. Bistatic scattering measurements using near-field scanning. / Sarabandi K., Zahn D. // 2001. IGARSS '01. IEEE 2001 International Geoscience and Remote Sensing Symposium. - Sydney, NSW, 2001. - Vol. 3. - P. 1359-1361. ↑

- C7137.** Sgrenzaroli M. High-resolution tropical forest mapping of the Amazon basin: a novel classification approach for the GRFM radar mosaic. / Sgrenzaroli M., Baraldi A., De Grandi G.F., Achard F., Eva H. // 2001. IGARSS '01. IEEE 2001 International Geoscience and Remote Sensing Symposium. - Sydney, NSW, 2001. - Vol. 3. - P. 1356-1358. ↑
- C7138.** Anhua Chu. The data processing and calibration of the AIRSAR PacRim II mission. / Anhua Chu, O'Leary E., Wayne Tung, Carrico L. // 2001. IGARSS '01. IEEE 2001 International Geoscience and Remote Sensing Symposium. - Sydney, NSW, 2001. - Vol. 3. - P. 1392-1394. ↑
- C7139.** Bartolo R.E. The fusion of polarimetric AirSAR data with digital aerial photography to improve aquatic macrophyte classification in a tropical reservoir. / Bartolo R.E., Forner J., Bell D., Menges C.H., Hill G.J.E. // 2001. IGARSS '01. IEEE 2001 International Geoscience and Remote Sensing Symposium. - Sydney, NSW, 2001. - Vol. 3. - P. 1412-1414. ↑
- C7140.** Menges C.H. Land cover discrimination in a wetland environment using TopSAR data. / Menges C.H., Bach C., Hosking J. // 2001. IGARSS '01. IEEE 2001 International Geoscience and Remote Sensing Symposium. - Sydney, NSW, 2001. - Vol. 3. - P. 1409-1411. ↑
- C7141.** Sang-Eun Park. Investigation of the April 2000 forest fire in Kangwon Province, Korea, using RADARSAT data. / Sang-Eun Park, Tae-Hee Lee, Seok-Young Hong, Moon W.M. // 2001. IGARSS '01. IEEE 2001 International Geoscience and Remote Sensing Symposium. - Sydney, NSW, 2001. - Vol. 3. - P. 1418-1420. ↑
- C7142.** Dukjin Kim. Investigation of ocean waves and currents with PacRim along-track interferometry (ATI). / Dukjin Kim, Moon W.M. // 2001. IGARSS '01. IEEE 2001 International Geoscience and Remote Sensing Symposium. - Sydney, NSW, 2001. - Vol. 3. - P. 1415-1417. ↑
- C7143.** Hoekman D.H. Biophysical forest type characterisation in the Colombian Amazon by airborne polarimetric SAR. / Hoekman D.H., Quinones M.J. // 2001. IGARSS '01. IEEE 2001 International Geoscience and Remote Sensing Symposium. - Sydney, NSW, 2001. - Vol. 3. - P. 1406-1408. ↑
- C7144.** Mouginis-Mark P.J. Volcano and natural hazard studies from the PacRim 2000 deployment to the W. Pacific. / Mouginis-Mark P.J., Garbeil H. // 2001. IGARSS '01. IEEE 2001 International Geoscience and Remote Sensing Symposium. - Sydney, NSW, 2001. - Vol. 3. - P. 1398-1399. ↑
- C7145.** Yunjin Kim. Comparison of forest parameter estimation techniques using SAR data. / Yunjin Kim, van Zyl J. // 2001. IGARSS '01. IEEE 2001 International Geoscience and Remote Sensing Symposium. - Sydney, NSW, 2001. - Vol. 3. - P. 1395-1397. ↑
- C7146.** Moon W.M. PACRIM-II AIRSAR/MASTER experiment in Korean (an overview). 2001. IGARSS '01. IEEE 2001 International Geoscience and Remote Sensing Symposium. - Sydney, NSW, 2001. - Vol. 3. - P. 1403-1405. ↑
- C7147.** Uratsuka E. Combination of two airborne SAR observations (PacRim2 over Japan). / Uratsuka E., Kobayashi T., Umehara T., Satake M., Nadai A., Maeno H., Matsuoka T., Masuko H., Wakabayashi H., Shimada M. // 2001. IGARSS '01. IEEE 2001 International Geoscience and Remote Sensing Symposium. - Sydney, NSW, 2001. - Vol. 3. - P. 1400-1402. ↑
- C7148.** Stephens G.L. On the combination of active and passive measurements in the study of clouds and precipitation. 2001. IGARSS '01. IEEE 2001 International Geoscience and Remote Sensing Symposium. - Sydney, NSW, 2001. - Vol. 2. - P. 694-696. ↑
- C7149.** Im E. CloudSat radar instrument design and development status. / Im E., Durden S.L., Li F.K., Chialin Wu, Haddad Z.S. // 2001. IGARSS '01. IEEE 2001 International Geoscience and Remote Sensing Symposium. - Sydney, NSW, 2001. - Vol. 2. - P. 691-693. ↑
- C7150.** Sekelsky S.M. Multi-frequency radar Doppler spectrum measurements of cirrus clouds. 2001. IGARSS '01. IEEE 2001 International Geoscience and Remote Sensing Symposium. - Sydney, NSW, 2001. - Vol. 2. - P. 697-699. ↑
- C7151.** Werner M. X-SAR/SRTM instrument phase error calibration. / Werner M., Haeusler M. // 2001. IGARSS '01. IEEE 2001 International Geoscience and Remote Sensing Symposium. - Sydney, NSW, 2001. -

Vol. 2. - P. 742-744. ↑

C7152. Rosen P.A. SRTM C-band topographic data: quality assessments and calibration activities. / Rosen P.A., Hensley S., Gurrola E., Rogez F., Chan S., Martin J., Rodriguez E. // 2001. IGARSS '01. IEEE 2001 International Geoscience and Remote Sensing Symposium. - Sydney, NSW, 2001. - Vol. 2. - P. 739-741. ↑

C7153. Cifelli R. A multi-scale perspective of TRMM-LBA convection. / Cifelli R., Petersen W.A., Carey L.D., Rutledge S.A. // 2001. IGARSS '01. IEEE 2001 International Geoscience and Remote Sensing Symposium. - Sydney, NSW, 2001. - Vol. 2. - P. 676-678. ↑

C7154. Kwiatkowski J. Tropical Rainfall Measuring Mission algorithm consistency studies. / Kwiatkowski J., Stout J. // 2001. IGARSS '01. IEEE 2001 International Geoscience and Remote Sensing Symposium. - Sydney, NSW, 2001. - Vol. 2. - P. 673-675. ↑

C7155. Tanelli S. Spaceborne radar measurements of vertical rainfall velocity: the non-uniform beam filling considerations. / Tanelli S., Im E., Durden S.L., Facheris L., Giuli D., Haddad Z.S., Smith E.A. // 2001. IGARSS '01. IEEE 2001 International Geoscience and Remote Sensing Symposium. - Sydney, NSW, 2001. - Vol. 2. - P. 679-681. ↑

C7156. Flaming G.M. Planning for Global Precipitation Measurement. / Flaming G.M., Adams W.J., Neeck S.P., Smith E.A. // 2001. IGARSS '01. IEEE 2001 International Geoscience and Remote Sensing Symposium. - Sydney, NSW, 2001. - Vol. 2. - P. 685-687. ↑

C7157. Meagher J.P. Profiling atmospheric graupel, snow and ice using TRMM's PR and TMI. / Meagher J.P., Haddad Z.S. // 2001. IGARSS '01. IEEE 2001 International Geoscience and Remote Sensing Symposium. - Sydney, NSW, 2001. - Vol. 2. - P. 682-684. ↑

C7158. Guoqing Sun. Monitoring forest dynamics using multi-sensor data in Northeastern China. / Guoqing Sun, Williams D., Xiwu Zhan, Zengyuan Li, Masek J., Ranson K.J., Rocchio L. // 2001. IGARSS '01. IEEE 2001 International Geoscience and Remote Sensing Symposium. - Sydney, NSW, 2001. - Vol. 2. - P. 768-770. ↑

C7159. Guo Huadong. The use of SRTM data for visualizing the mid-upper reaches of Yangtze River area and dynamic monitoring of land cover changes. / Guo Huadong, Wang Changlin. // 2001. IGARSS '01. IEEE 2001 International Geoscience and Remote Sensing Symposium. - Sydney, NSW, 2001. - Vol. 2. - P. 762-763. ↑

C7160. Kelldorfer J.M. Forest biometrics from ERS and JERS in Michigan. / Kelldorfer J.M., Dobson M.C., Pierce L.E. // 2001. IGARSS '01. IEEE 2001 International Geoscience and Remote Sensing Symposium. - Sydney, NSW, 2001. - Vol. 2. - P. 780-782. ↑

C7161. dos Santos J.R. Inventory of forest biomass in Brazilian Amazon: a local approach using airborne P-band SAR data. / dos Santos J.R., Araujo L.S., Freitas C.C., Sant'Anna S.J.S., Dutra L.V., Mura J.C., Gama F.F., Filho P.H. // 2001. IGARSS '01. IEEE 2001 International Geoscience and Remote Sensing Symposium. - Sydney, NSW, 2001. - Vol. 2. - P. 786-788. ↑

C7162. Cronin N.L.R. Synthetic aperture radar for AGB estimation in Australia's woodlands. / Cronin N.L.R., Lucas R.M., Witte C., Milne A.K., Hoffmann M.B. // 2001. IGARSS '01. IEEE 2001 International Geoscience and Remote Sensing Symposium. - Sydney, NSW, 2001. - Vol. 2. - P. 783-785. ↑

C7163. Eineder M. SRTM X-SAR calibration results. / Eineder M., Breit H., Adam N., Holzner J., Suchandt S., Rabus B. // 2001. IGARSS '01. IEEE 2001 International Geoscience and Remote Sensing Symposium. - Sydney, NSW, 2001. - Vol. 2. - P. 748-750. ↑

C7164. Roth A. SRTM/X-SAR: products and processing facility. / Roth A., Eineder A., Rabus B., Mikusch E., Schattler B. // 2001. IGARSS '01. IEEE 2001 International Geoscience and Remote Sensing Symposium. - Sydney, NSW, 2001. - Vol. 2. - P. 745-747. ↑

C7165. Rosen P. SRTM-Mission-cross comparison of X and C band data properties. / Rosen P., Eineder M., Rabus B., Gurrola E., Hensley S., Knoepfle W., Breit H., Roth A., Werner M. // 2001. IGARSS '01. IEEE 2001 International Geoscience and Remote Sensing Symposium. - Sydney, NSW, 2001. - Vol. 2. - P. 751-753. ↑

C7166. Mougini-Mark P.J. Topographic change on volcanoes from SRTM and other interferometric radars. / Mougini-Mark P.J., Rowland S.K., Garbeil H., Amelung F. // 2001. IGARSS '01. IEEE 2001 International

Geoscience and Remote Sensing Symposium. - Sydney, NSW, 2001. - Vol. 2. - P. 757-758. ↑

C7167. Gesch D. A comparison of US Geological Survey seamless elevation models with Shuttle Radar Topography Mission data. / Gesch D., Williams J., Miller W. // 2001. IGARSS '01. IEEE 2001 International Geoscience and Remote Sensing Symposium. - Sydney, NSW, 2001. - Vol. 2. - P. 754-756. ↑

C7168. Hyunjun Kim. Radar image study of ocean breaking waves. / Hyunjun Kim, Johnson J.T. // 2001. IGARSS '01. IEEE 2001 International Geoscience and Remote Sensing Symposium. - Sydney, NSW, 2001. - Vol. 1. - P. 567-569. ↑

C7169. Frasier S.J. A pod-based dual-beam interferometric radar for ocean surface current vector mapping. / Frasier S.J., Carswell J.R., Capdevila J. // 2001. IGARSS '01. IEEE 2001 International Geoscience and Remote Sensing Symposium. - Sydney, NSW, 2001. - Vol. 1. - P. 561-563. ↑

C7170. Thompson D.R. The potential of SAR interferometry for oceanographic measurements: a review. 2001. IGARSS '01. IEEE 2001 International Geoscience and Remote Sensing Symposium. - Sydney, NSW, 2001. - Vol. 1. - P. 573-574. ↑

C7171. Lombardini F. Multibaseline ATI-SAR for robust ocean surface velocity estimation in presence of bimodal Doppler spectrum. / Lombardini F., Gini F., Matteucci P. // 2001. IGARSS '01. IEEE 2001 International Geoscience and Remote Sensing Symposium. - Sydney, NSW, 2001. - Vol. 1. - P. 578-580. ↑

C7172. Romeiser R. Possibilities and limitations of current measurements by airborne and spaceborne along-track interferometric SAR. / Romeiser R., Hirsch O. // 2001. IGARSS '01. IEEE 2001 International Geoscience and Remote Sensing Symposium. - Sydney, NSW, 2001. - Vol. 1. - P. 575-577. ↑

C7173. Rosenqvist A. Initiating the ALOS Kyoto & Carbon Initiative. / Rosenqvist A., Ogawa T., Shimada M., Igarashi T. // 2001. IGARSS '01. IEEE 2001 International Geoscience and Remote Sensing Symposium. - Sydney, NSW, 2001. - Vol. 1. - P. 546-548. ↑

C7174. Yoho P. Validation of SeaWinds on QuikSCAT cell location. / Yoho P., Long D.G. // 2001. IGARSS '01. IEEE 2001 International Geoscience and Remote Sensing Symposium. - Sydney, NSW, 2001. - Vol. 1. - P. 508-510. ↑

C7175. Guo Huadong. A new airborne Earth observing system and its applications. / Guo Huadong, Xu Jianmin, Ni Guoqiang, Miao Jialing. // 2001. IGARSS '01. IEEE 2001 International Geoscience and Remote Sensing Symposium. - Sydney, NSW, 2001. - Vol. 1. - P. 549-551. ↑

C7176. Hirsch O. Calibration of an airborne along-track interferometric SAR system for accurate measurement of velocities. 2001. IGARSS '01. IEEE 2001 International Geoscience and Remote Sensing Symposium. - Sydney, NSW, 2001. - Vol. 1. - P. 558-560. ↑

C7177. Rostan F. The CryoSat Earth Explorer Opportunity Mission-system calibration and mission performance. / Rostan F., Mallow U. // 2001. IGARSS '01. IEEE 2001 International Geoscience and Remote Sensing Symposium. - Sydney, NSW, 2001. - Vol. 1. - P. 552-554. ↑

C7178. Hyo-Suk Lim. Characteristic structures of Typhoon Jelawat observed by OSMI,. TRMM/PR and QuikSCAT. / Hyo-Suk Lim, Gi-Hyuk Choi, Hong-Yul Paik. // 2001. IGARSS '01. IEEE 2001 International Geoscience and Remote Sensing Symposium. - Sydney, NSW, 2001. - Vol. 2. - P. 661-663. ↑

C7179. Stocker E.F. Gridded hourly text products: a TRMM data reduction approach. / Stocker E.F., Kwiatkowski J., Kelley O. // 2001. IGARSS '01. IEEE 2001 International Geoscience and Remote Sensing Symposium. - Sydney, NSW, 2001. - Vol. 2. - P. 658-660. ↑

C7180. Skofronick-Jackson G.M. Iterative 2D hydrometeor profile retrievals using radar and wideband radiometer observations. 2001. IGARSS '01. IEEE 2001 International Geoscience and Remote Sensing Symposium. - Sydney, NSW, 2001. - Vol. 2. - P. 664-666. ↑

C7181. Vongsaard J. The continuous tracking of reflectivity data from multi-platform observations using genetic algorithm. / Vongsaard J., Chiu L.S., El-Ghazawi T., Kafatos M., Yang R. // 2001. IGARSS '01. IEEE 2001 International Geoscience and Remote Sensing Symposium. - Sydney, NSW, 2001. - Vol. 2. - P. 669-671. ↑

↑

- C7182.** Guosheng Liu. Variability of rain profiles and its impact on microwave precipitation remote sensing as inferred from TRMM PR and TMI. / Guosheng Liu, Yunfei Fu. // 2001. IGARSS '01. IEEE 2001 International Geoscience and Remote Sensing Symposium. - Sydney, NSW, 2001. - Vol. 2. - P. 667-668. ↑
- C7183.** Bao M. First results on ocean wave imaging from the Shuttle Radar Topography Mission. / Bao M., Schulz-Stellenfleth J., Lehner S., Eineder M. // 2001. IGARSS '01. IEEE 2001 International Geoscience and Remote Sensing Symposium. - Sydney, NSW, 2001. - Vol. 1. - P. 584-586. ↑
- C7184.** Lehner S. Joint along-across track interferometry of ocean waves. / Lehner S., Gunther H., Horstmann J., Bao M., Schulz-Stellenfleth J. // 2001. IGARSS '01. IEEE 2001 International Geoscience and Remote Sensing Symposium. - Sydney, NSW, 2001. - Vol. 1. - P. 581-583. ↑
- C7185.** Greidanus H. Doppler polarimetry of high resolution radar sea clutter. / Greidanus H., Melief H.W., Hoogeboom P., van Genderen P. // 2001. IGARSS '01. IEEE 2001 International Geoscience and Remote Sensing Symposium. - Sydney, NSW, 2001. - Vol. 1. - P. 587-589. ↑
- C7186.** Muller D. Optical and physical characterization of European and Indo-Asian pollution plumes with six-wavelength aerosol lidar. / Muller D., Ansmann A., Franke K., Althausen D., Wandinger U. // 2001. IGARSS '01. IEEE 2001 International Geoscience and Remote Sensing Symposium. - Sydney, NSW, 2001. - Vol. 2. - P. 652-654. ↑
- C7187.** {no data available}. IGARSS 2001. Scanning the Present and Resolving the Future. Proceedings. IEEE 2001 International Geoscience and Remote Sensing Symposium (Cat. No.01CH37217). 2001. IGARSS '01. IEEE 2001 International Geoscience and Remote Sensing Symposium. 2001. - Vol. 2. - {no data available}. ↑
- C7188.** Allen C. Performance of a 1319 nm laser radar using RF pulse compression. / Allen C., Cobanoglu Y., Sekken Kenny Chong, Gogineni S. // 2001. IGARSS '01. IEEE 2001 International Geoscience and Remote Sensing Symposium. - Sydney, NSW, 2001. - Vol. 3. - P. 997-999. ↑
- C7189.** Paloscia S. Estimating vegetation cover and soil roughness in semi-arid regions from multitemporal dual-frequency SAR data. / Paloscia S., Bianchini M., Macelloni G., Pampaloni P., Santi E., Aqid N., Ouazar D., Zribi M. // 2001. IGARSS '01. IEEE 2001 International Geoscience and Remote Sensing Symposium. - Sydney, NSW, 2001. - Vol. 3. - P. 994-996. ↑
- C7190.** Le Vine D. The measurement of salinity from space: sensor concept. / Le Vine D., Koblinsky C., Pellerano F., Lagerloef G., Chao Y., Yueh S., Wilson W. // 2001. IGARSS '01. IEEE 2001 International Geoscience and Remote Sensing Symposium. - Sydney, NSW, 2001. - Vol. 3. - P. 1010-1012. ↑
- C7191.** Tickle P.K. Use of airborne scanning lidar and large scale photography within a strategic forest inventory and monitoring framework. / Tickle P.K., Witte C., Lee A., Lucas R.M., Jones K., Austin J. // 2001. IGARSS '01. IEEE 2001 International Geoscience and Remote Sensing Symposium. - Sydney, NSW, 2001. - Vol. 3. - P. 1000-1003. ↑
- C7192.** Casella V. DTM extraction in urban areas: a detailed comparison of methodologies, algorithms and results. / Casella V., Zampori B., Dell'Acqua F., Gamba P., Mainardi A. // 2001. IGARSS '01. IEEE 2001 International Geoscience and Remote Sensing Symposium. - Sydney, NSW, 2001. - Vol. 3. - P. 976-978. ↑
- C7193.** Pack J.D. Estimating snow accumulation on Greenland from SSM/I radiometer data. / Pack J.D., Jensen M.A. // 2001. IGARSS '01. IEEE 2001 International Geoscience and Remote Sensing Symposium. - Sydney, NSW, 2001. - Vol. 2. - P. 946-948. ↑
- C7194.** Khvorostovskiy K.S. A study of Greenland ice sheet elevation change by using satellite altimeter data. / Khvorostovskiy K.S., Bobylev L.P., Johannessen O.M. // 2001. IGARSS '01. IEEE 2001 International Geoscience and Remote Sensing Symposium. - Sydney, NSW, 2001. - Vol. 2. - P. 943-945. ↑
- C7195.** Ashcraft I.S. Multi-annual changes in microwave backscatter over the Greenland ice sheet. / Ashcraft I.S., Long D.G. // 2001. IGARSS '01. IEEE 2001 International Geoscience and Remote Sensing Symposium. - Sydney, NSW, 2001. - Vol. 2. - P. 958-960. ↑
- C7196.** Hopkinson C. Applications of airborne LiDAR mapping in glacierised mountainous terrain. / Hopkinson C., Demuth M., Sitar M., Chasmer L. // 2001. IGARSS '01. IEEE 2001 International Geoscience and Remote Sensing Symposium. - Sydney, NSW, 2001. - Vol. 2. - P. 949-951. ↑

- C7197.** Suess M. A novel high resolution, wide swath SAR system. / Suess M., Grafmueller B., Zahn R. // 2001. IGARSS '01. IEEE 2001 International Geoscience and Remote Sensing Symposium. - Sydney, NSW, 2001. - Vol. 3. - P. 1013-1015. ↑
- C7198.** Mazzetti P. Case-study on the use of microwave sensors for cloud detection over Tuscany. / Mazzetti P., Nativi S., Giuli D. // 2001. IGARSS '01. IEEE 2001 International Geoscience and Remote Sensing Symposium. - Sydney, NSW, 2001. - Vol. 3. - P. 1055-1057. ↑
- C7199.** Chen F.W. Millimeter-wave observations of precipitation using AMSU on the NOAA-15 satellite. / Chen F.W., Staelin D.H. // 2001. IGARSS '01. IEEE 2001 International Geoscience and Remote Sensing Symposium. - Sydney, NSW, 2001. - Vol. 3. - P. 1044-1045. ↑
- C7200.** Yijun He. Shallow sea tides estimated using T/P data and adjoint assimilation model. / Yijun He, Jinping Zhao, Xianqing Lu. // 2001. IGARSS '01. IEEE 2001 International Geoscience and Remote Sensing Symposium. - Sydney, NSW, 2001. - Vol. 3. - P. 1073-1075. ↑
- C7201.** Dechambre A. Statistical sensitivity analysis of a vegetation canopy microwave scattering model based on an experiment design method. / Dechambre A., Le Gac C. // 2001. IGARSS '01. IEEE 2001 International Geoscience and Remote Sensing Symposium. - Sydney, NSW, 2001. - Vol. 3. - P. 1070-1072. ↑
- C7202.** Fujita M. Two-dimensional rain mapping using transmissions from geostationary satellites. 2001. IGARSS '01. IEEE 2001 International Geoscience and Remote Sensing Symposium. - Sydney, NSW, 2001. - Vol. 3. - P. 1041-1043. ↑
- C7203.** Weitkamp C. Lidar ozone measurements in the marine and terrestrial atmosphere from the ground to the tropopause. / Weitkamp C., Baumgart R., Behrendt A., Bisling P., Glauer J., Goers U.-B., Kohler S., Lahmann W., Reichardt J. // 2001. IGARSS '01. IEEE 2001 International Geoscience and Remote Sensing Symposium. - Sydney, NSW, 2001. - Vol. 3. - P. 1023-1025. ↑
- C7204.** Schutz B.E. Laser altimetry and lidar from ICESat/GLAS. 2001. IGARSS '01. IEEE 2001 International Geoscience and Remote Sensing Symposium. - Sydney, NSW, 2001. - Vol. 3. - P. 1016-1019. ↑
- C7205.** Hardesty R.M. Lidar applications in regional air quality studies. / Hardesty R.M., Senff C.J., Banta R.M., Brewer W.A., Alvarez R.J. II, Darby L.S., Marchbanks R.D. // 2001. IGARSS '01. IEEE 2001 International Geoscience and Remote Sensing Symposium. - Sydney, NSW, 2001. - Vol. 3. - P. 1029-1031. ↑
- C7206.** Gimmestad G.G. A next-generation ground-based sensor for tropospheric ozone. / Gimmestad G.G., Patterson E.M., Roberts D.W., Stewart J.M., West L.L., Wood J.W. // 2001. IGARSS '01. IEEE 2001 International Geoscience and Remote Sensing Symposium. - Sydney, NSW, 2001. - Vol. 3. - P. 1026-1028. ↑
- C7207.** Kanagaratnam P. An airborne radar system for high-resolution mapping of internal layers. / Kanagaratnam P., Eakin R., Gogineni S.P. // 2001. IGARSS '01. IEEE 2001 International Geoscience and Remote Sensing Symposium. - Sydney, NSW, 2001. - Vol. 2. - P. 940-942. ↑
- C7208.** Slatton K.C. Multiscale adaptive estimation for fusing interferometric radar and laser altimeter data. / Slatton K.C., Crawford M., Evans B.L. // 2001. IGARSS '01. IEEE 2001 International Geoscience and Remote Sensing Symposium. - Sydney, NSW, 2001. - Vol. 2. - P. 879-881. ↑
- C7209.** Amici G. Fuzzy pyramidal joint classification of SIR-C and AIRSAR data. / Amici G., Cerutti D., Dell'Acqua F., Gamba P. // 2001. IGARSS '01. IEEE 2001 International Geoscience and Remote Sensing Symposium. - Sydney, NSW, 2001. - Vol. 2. - P. 876-878. ↑
- C7210.** Moghaddam M. Estimating forest variables from fusion of SAR and TM data and analytical scattering and reflectance models. / Moghaddam M., Dungan J.L. // 2001. IGARSS '01. IEEE 2001 International Geoscience and Remote Sensing Symposium. - Sydney, NSW, 2001. - Vol. 2. - P. 885-887. ↑
- C7211.** Barrios A.E. Estimating refractivity from land clutter: another look at a simple approach. 2001. IGARSS '01. IEEE 2001 International Geoscience and Remote Sensing Symposium. - Sydney, NSW, 2001. - Vol. 2. - P. 904-905. ↑
- C7212.** Wagner L.J. Island wake impact on evaporation duct height and sea clutter in the lee of Kauai. / Wagner L.J., Rogers L.T., Burk S.D., Haack T.A. // 2001. IGARSS '01. IEEE 2001 International Geoscience and Remote Sensing Symposium. - Sydney, NSW, 2001. - Vol. 2. - P. 906-908. ↑

Remote Sensing Symposium. - Sydney, NSW, 2001. - Vol. 2. - P. 901-903. ↑

C7213. Pulliainen J. Compensation of forest canopy effects in the estimation of snow covered area from SAR data. / Pulliainen J., Koskinen J., Hallikainen M. // 2001. IGARSS '01. IEEE 2001 International Geoscience and Remote Sensing Symposium. - Sydney, NSW, 2001. - Vol. 2. - P. 813-815. ↑

C7214. Mura J.C. Identification of the tropical forest in Brazilian Amazon based on the DEM difference from P and X bands interferometric data. / Mura J.C., Sant'Anna Bins L., Gama F.F., da Costa Freitas C., dos Santos J.R., Dutra L.V. // 2001. IGARSS '01. IEEE 2001 International Geoscience and Remote Sensing Symposium. - Sydney, NSW, 2001. - Vol. 2. - P. 789-791. ↑

C7215. Papa F. Snow signature with the ERS2 radar altimeter. / Papa F., Mognard N., Josberger E.D., Remy F. // 2001. IGARSS '01. IEEE 2001 International Geoscience and Remote Sensing Symposium. - Sydney, NSW, 2001. - Vol. 2. - P. 816-818. ↑

C7216. Feingersh T. Fusion of SAR and SPOT image data for crop mapping. / Feingersh T., Gorte B.G.H., Van Leeuwen H.J.C. // 2001. IGARSS '01. IEEE 2001 International Geoscience and Remote Sensing Symposium. - Sydney, NSW, 2001. - Vol. 2. - P. 873-875. ↑

C7217. Sveinsson J.R. Cluster-based feature extraction and data fusion in the wavelet domain. / Sveinsson J.R., Ulfarsson M.O., Benediktsson J.A. // 2001. IGARSS '01. IEEE 2001 International Geoscience and Remote Sensing Symposium. - Sydney, NSW, 2001. - Vol. 2. - P. 867-869. ↑

C7218. Jiancheng Shi. A numerical simulation of estimating snow wetness with ASAR. 2001. IGARSS '01. IEEE 2001 International Geoscience and Remote Sensing Symposium. - Sydney, NSW, 2001. - Vol. 2. - P. 922-924. ↑

C7219. Tadono T. Estimation of snow hydrological parameters using single-parameter, multi-temporal SAR images. / Tadono T., Fukami K., Shi J. // 2001. IGARSS '01. IEEE 2001 International Geoscience and Remote Sensing Symposium. - Sydney, NSW, 2001. - Vol. 2. - P. 919-921. ↑

C7220. Kasilingam D. The depolarization of radar backscatter from rough surfaces due to surface roughness and slopes. / Kasilingam D., Schuler D., Jong-Sen Lee. // 2001. IGARSS '01. IEEE 2001 International Geoscience and Remote Sensing Symposium. - Sydney, NSW, 2001. - Vol. 2. - P. 925-927. ↑

C7221. Wilson W.J. Ocean surface salinity remote sensing with the JPL Passive/Active L-/S-band (PALS) microwave instrument. / Wilson W.J., Yueh S.H., Li F.K., Dinardo S., Yi Chao, Koblinksky C., Lagerloef G., Howden S. // 2001. IGARSS '01. IEEE 2001 International Geoscience and Remote Sensing Symposium. - Sydney, NSW, 2001. - Vol. 2. - P. 937-939. ↑

C7222. Ainsworth T.L. Optimal polarimetric decomposition variables-non-linear dimensionality reduction. / Ainsworth T.L., Lee J.S. // 2001. IGARSS '01. IEEE 2001 International Geoscience and Remote Sensing Symposium. - Sydney, NSW, 2001. - Vol. 2. - P. 928-930. ↑

C7223. Anderson R. Maximum a posteriori refractivity estimation from radar clutter using a Markov model for microwave propagation. / Anderson R., Vasudevan S., Krolik J.L., Rogers L.T. // 2001. IGARSS '01. IEEE 2001 International Geoscience and Remote Sensing Symposium. - Sydney, NSW, 2001. - Vol. 2. - P. 906-909. ↑

C7224. Cloude S.R. A new method for characterizing depolarization effects in radar and optical remote sensing. 2001. IGARSS '01. IEEE 2001 International Geoscience and Remote Sensing Symposium. - Sydney, NSW, 2001. - Vol. 2. - P. 910-912. ↑

C7225. Schuler D.L. Remote sensing of surface roughness using polarimetric SAR data. / Schuler D.L., Lee J.S., Kasilingam D., Nesti G. // 2001. IGARSS '01. IEEE 2001 International Geoscience and Remote Sensing Symposium. - Sydney, NSW, 2001. - Vol. 2. - P. 916-918. ↑

C7226. Lee J.S. Interpreting off-diagonal terms in polarimetric coherency matrix. / Lee J.S., Ainsworth T.L., Schuler D.L., Kasilingam D., Boerner W.M. // 2001. IGARSS '01. IEEE 2001 International Geoscience and Remote Sensing Symposium. - Sydney, NSW, 2001. - Vol. 2. - P. 913-915. ↑

C7227. Bonneau R.J. Target-aided compression of SAR imagery for transmission over noisy wireless channels. / Bonneau R.J., Abousleman G.P. // 1993 IEEE International Conference on Acoustics, Speech, and

© В.И. Карнышев, 2011

Тематический реферативный сборник сгенерирован в автоматическом режиме
с использованием специализированного программного модуля (ПАО ТУСУР)